Approximate Global Convergence and Adaptivity for Coefficient Inverse Problems

Larisa Beilina • Michael Victor Klibanov

Approximate Global Convergence and Adaptivity for Coefficient Inverse Problems

Springer

Larisa Beilina
Department of Mathematical Sciences
Chalmers University of Technology
Gothenburg University
Gothenburg, Sweden

Michael Victor Klibanov
University of North Carolina
Charlotte, North Carolina, USA

ISBN 978-1-4419-7804-2 e-ISBN 978-1-4419-7805-9
DOI 10.1007/978-1-4419-7805-9
Springer New York Dordrecht Heidelberg London

Library of Congress Control Number: 2012931927

Printed on acid-free paper

Springer is part of Springer Science+Business Media (www.springer.com)

To our parents Yefrosiniya, Vladimir, Ada, and Victor

Preface

This book focuses on two new ideas of the authors: approximate global convergence and adaptive finite element method (FEM) for coefficient inverse problems (CIPs) for a hyperbolic partial differential equation (PDE). The first chapter might be used as an introductory course to the theory of ill-posed problems. In addition, a number of uniqueness theorems for CIPs are proved in this chapter via the method of Carleman estimates. The book features many recipes for numerical implementations of developed algorithms. Those readers who would wish to focus on numerical studies, might skip the reading of the convergence analysis. Naturally, those recipes are accompanied by many numerical examples. These examples address both synthetic (computational) and experimental data.

Two types of experimental data are studied: the data collected in a laboratory and the data collected in the field by a forward-looking radar of the US Army Research laboratory (ARL); see [126] for the description of this radar. In both cases, the most challenging case of *blind* experimental data is considered. Results of numerical testing for both synthetic and experimental data are in a good agreement with the convergence analysis. Results for ARL data address a real world problem of imaging of explosives using the data of the forward-looking radar of ARL.

Suppose that the propagation of a signal through a medium of interest is governed by a PDE. Assume that one wants to calculate a certain spatially distributed internal property of that medium using measurements of the output signal either at the entire boundary or at a part of the boundary of that medium. This property is usually described by a spatially dependent coefficient of that PDE. Thus, one arrives at a CIP for that PDE. This CIP is about the computation of that coefficient using those boundary measurements.

Having a good approximation for the coefficient of interest, one can visualize its spatial distribution. In other words, one can create an image of the interior of that medium. Hence, in simple terms, a CIP is a problem of "seeing through" the medium, i.e., this is the problem of imaging of the interior structure of that medium. Some examples of those properties of interest are spatially distributed dielectric permittivity, electric conductivity, and sound speed. It is clear from the above that CIPs have a broad range of applications in, for example, geophysics, imaging of land

mines, and, more generally, hidden explosives, geophysics, and medical imaging, etc. However, having said this, the next question is: *Given measurements of an output signal, how to actually calculate the unknown coefficient of interest?*

CIPs are both nonlinear and ill-posed. These two factors combined cause very substantial difficulties in the goal of addressing this question. The very first idea which comes in mind is to minimize a least squares objective functional and approximate solution this way. However, these functionals suffer from the phenomenon of local minima and ravines. Hence, any gradient-like technique of the minimization of such a functional will likely stop at such a point of a local minimum which is the closest one to the starting point of that iteration process. Because of the local minima problem, all conventional algorithms for CIPs are locally convergent ones. This means that their convergence can be rigorously guaranteed only if the starting point of iterations is sufficiently close to the exact solution. However, a knowledge of a sufficiently small neighborhood of the exact coefficient is a luxury in the majority of applications.

Therefore, it is important for many applications to develop such numerical methods which would provide good approximations for exact solutions of CIPs without any advanced knowledge of small neighborhoods of exact solutions. This goal is an enormously challenging one. Hence, to achieve it, one can work with some approximate mathematical models. Still, these models should be verified numerically. It is also desirable to verify those approximate mathematical models on experimental data, provided of course that such data are available (usually it is both hard and expensive to get experimental data). Thus, we use a new term for such numerical methods "approximate global convergence." Results of abovementioned testing on synthetic and experimental data validate approximate mathematical models.

The development of approximately globally convergent numerical methods for CIPs with single measurement data has started from the so-called convexification algorithm [101,102,157–160], which the authors consider as an approximately globally convergent method of the first generation. The book focuses on a substantially different approach, which can be regarded as the approximately globally convergent method of the second generation. This approach was developed by the authors in 2008–2011 [9, 24–29, 109, 114–117, 160].

Only the single measurement case is considered in this book. The term "single measurement" means that only a single position of the point source or a single direction of the incident plane wave is used to generate the data. This case is preferable in, for example, military applications in which one wants to minimize the number of measurements because of many dangers on the battlefield.

The main interest in computations of applied CIPs is an accurate imaging of both locations of small inclusions as well as values of unknown coefficients inside them. Those inclusions are embedded in an otherwise slowly changing background medium. This is because those inclusions are, for example, land mines, tumors, defects in materials, etc. It is important to accurately calculate values of unknown coefficients, because they can help to identify those inclusions. We do not separate

between inclusions and backgrounds. Rather we just calculate unknown coefficients. A different approach to the topic of imaging of small inclusions can be found in [4–6].

This book considers both two-dimensional and three-dimensional CIPs for an important hyperbolic PDE and addresses two questions which are the central ones for numerical treatments of those CIPs:

1. How to calculate a good approximation for the exact solution without an advanced knowledge of a small neighborhood of this solution?
2. How to refine that approximation?

The first question is addressed via a new approximately globally convergent numerical method of the authors. Corresponding approximate mathematical models basically amount to the truncation of a certain asymptotic series. The second question is addressed via a locally convergent adaptive finite element method (adaptivity). It is natural therefore that a two-stage numerical procedure is developed. On the first stage, the approximately globally convergent method provides a good approximation for the exact coefficient. On the second stage, this approximation is refined via the adaptivity. A detailed convergence analysis for both stages is an important part of this book.

The work on this book was generously supported by US Army Research Laboratory and US Army Research Office (ARO) grants W911NF-08-1-0470, W911NF-09-1-0409, and W911NF-11-1-0399, by National Institutes of Health (USA) grant 1R21NS052850-01A1, by Swedish Research Council, Swedish Foundation of Strategic Research, Gothenburg Mathematical Modeling Center and by Visby Program of Swedish Institute. We express our special gratitude to Dr. Joseph D. Myers, the Program Manager of the Numerical Analysis program of ARO.

Computations of Chaps. 3–5 and Sect. 6.8.5 were performed (1) on 16 parallel processors in NOTUR 2 production system of NTNU, Trondheim, Norway (67 IBM p575+16 way nodes, 1.9 GHz dual-core CPU, 2,464 GB memory) and (2) in a center for scientific and technical computing C3SE at Chalmers University and Gothenburg University, Gothenburg, Sweden. Computations of Chap. 6 with the only exception of Sect. 6.8.5 were performed computational facilities of the Department of Mathematics and Statistics of University of North Carolina at Charlotte, Charlotte, USA.

A number of our colleagues, who are listed below in the alphabetical order, have helped us in our work on this book. Dr. Mohammad Asadzadeh has collaborated with the first author on the development of the idea of using the adaptivity inside the approximately globally convergent method. This has resulted in the adaptive one-stage numerical procedure; see [9] and Sect. 4.17. Dr. Anatoly B. Bakushinsky has provided a significant input in our formulation of the definition of the approximate global convergence property and has also advised us many times on a number of issues of the theory of ill-posed problems; see [111] and Sect. 1.8. Dr. Christian Clason has collaborated with the first author on the subject of the application of the adaptivity technique to scanning acoustic microscopy; see [21] and Sect. 4.14.2.2. Drs. Michael A. Fiddy and John Schenk have collected experimental data in the

Microwave Laboratory of University of North Carolina at Charlotte; see Chap. 5 as well as [28, 109]. Dr. Irina Gainova has helped us with many technical issues related to the text of this book. Dr. Claes Johnson was Ph.D. advisor of the first author. He has presented to the first author the idea of the adaptivity for the CIPs, for the first time; see [16, 20] and Sects. 4.5 and 4.14. Dr. Mikhail Yu. Kokurin has collaborated with us on the topic of the accuracy improvement with mesh refinements in the adaptivity technique; see [29] as well as Sects. 1.9, 4.1.2, and 4.9. Drs. Andrey V. Kuzhuget and Natee Pantong have performed computations of the major part of results of Chap. 6; also see [114–117]. Drs. Lam Nguyen and Anders Sullivan from ARL have supplied us with experimental data collected by the forward-looking radar of ARL in the field, along with the permission to use these data in the current book; see Sect. 6.9 of Chap. 6. The corresponding joint work is [117]. Dr. Roman G. Novikov has given us a number of quite useful advises on some analytical and numerical issues. We sincerely appreciate a great help of all these individuals.

Gothenburg, Sweden — Larisa Beilina
Charlotte, North Carolina, USA — Michael Victor Klibanov

Contents

Chapter 1
Two Central Questions of This Book and an Introduction to the Theories of Ill-posed and Coefficient Inverse Problems

This is an introductory chapter. In Sect. 1.1, we outline two central questions discussed in this book. Sections 1.2–1.9 are introductory ones to the theory of ill-posed problems. In Sects. 1.10 and 1.11, we present main uniqueness results for coefficient inverse problems (CIPs) with the single measurement data. The material of this chapter might serve as an introductory course for theories of ill-posed and CIPs. We refer to books [7, 10, 41, 45, 48, 51, 54, 60, 65, 83, 84, 90, 93, 94, 102, 124, 138, 143, 144, 153, 154] where various Ill-Posed and CIPs were studied.

This book focuses on CIPs with single measurement time resolved data. "Single measurement" means that the data are generated by either a single location of the point source or a single direction of the incident plane wave. More generally, in the case of a CIP for a hyperbolic partial differential equation (PDE), "single measurement" means that only one pair of initial conditions is available, and in the case of a CIP for a parabolic PDE, only one initial condition is available. In other words, single measurement amounts to the minimal information content. The single measurement arrangement is the most suitable one for military applications. Indeed, because of various dangers on the battlefield, it is desirable to minimize the number of measurements in the military environment.

The single measurement case is the most economical way of data collection with the minimal available information. At the same time, because of the minimal information content, it is apparently more challenging than the multiple measurement case. At the time of the submission of this book the authors are unaware about other research groups working on non-local numerical methods for multidimensional CIPs with single measurement data.

CIPs with the data resulting from multiple measurements are also considered in the mathematical literature. These CIPs have applications in, for example, medical imaging and geophysics. In the case of multiple measurements, either the point source should run along a manifold or the direction of the incident plane wave should vary within a certain cone. We refer to, for example, [3, 35, 46, 63, 75, 82, 90, 92, 129–132] and references cited therein for some nonlocal algorithms for CIPs with multiple measurements.

L. Beilina and M.V. Klibanov, *Approximate Global Convergence and Adaptivity for Coefficient Inverse Problems*, DOI 10.1007/978-1-4419-7805-9_1,

CIPs have many applications, for example, geophysics, detection of explosives (e.g., land mines), and medical imaging of malignant tumors. Because of these applications, we focus our numerical studies on imaging of small sharp abnormalities embedded in an otherwise slowly changing background medium. We image both locations of these inclusions and values of the unknown coefficient inside them. However, we are not interested in imaging of slowly changing backgrounds. We point out to an important point: our algorithms, which address the first central question of this book, as well as those of the two-stage numerical procedure (Sect. 1.1), do not use a priori knowledge of the background medium. An application to the detection of explosives is addressed in Sect. 6.9 of Chap. 6 for the case of blind experimental data collected by a radar in the field.

1.1 Two Central Questions of This Book

Since the field of inverse problems is an applied one, it is important to develop numerical methods for these problems. The following are the two central questions which inevitably surface in the computational treatment of any CIP for a PDE:

The First Central Question. Consider a CIP and suppose that this problem has unique exact solution for noiseless data. Assume that we have a small noise in the data. Then the question is, *how to develop such a numerical method for this CIP, which would provide an approximate solution located in a sufficiently small neighborhood of that exact solution without any a priori knowledge of this neighborhood?* The most important point here is that this method should not rely on the assumption of a priori knowledge of that neighborhood. The second very important point is that the property of obtaining such an approximation should be rigorously guaranteed. However, since CIPs are enormously challenging ones, then one has no choice but to "allow" this rigorous guarantee to be within the framework of a certain reasonable approximate mathematical model. Numerical studies should confirm this property. It is also desirable to provide an addition confirmation for the case of experimental data.

The most challenging case of **blind** experimental data is especially persuasive one. Indeed, since results are unbiased in this case, then the success in the blind data case would mean an ultimate verification of that approximate mathematical model. Similarly, the ultimate verification of any Partial Differential Equation of Mathematical Physics is in experiments. Results for blind experimental data are described in Chap. 5 and Sect. 6.9 of this book.

The Second Central Question. Suppose that the approximate solution mentioned in the first central question is computed. The second central question is, *how to refine this solution*? Indeed, since an approximate mathematical model is used, then the room might be left for a refinement.

Roughly speaking, any numerical method addressing the first central question is called *globally convergent*. However, because of the abovementioned approximation, we use in this book the term *approximate global convergence*. A rigorous definition of this term is presented in Sect. 1.1.2. Still, a short term for the latter is *global convergence*.

It is well known that there are a number of numerical methods for one-dimensional CIPs which do not require a priori knowledge of a small neighborhood of the exact solution; see, for example, [40, 47, 51, 56, 90] and references cited therein. At the same time, the latter is not the case for multidimensional CIPs. In this book, we consider only multidimensional CIPs with the only exception of Sect. 6.9. Thus, below, the abbreviation "CIP" always means an n-D CIP ($n = 2, 3$).

Conventional numerical methods for CIPs, such as, for example, various versions of Newton and gradient methods, converge locally, i.e., they need to use a good approximation for the exact solution to start from; see, for example, books [10, 93] for these methods for ill-posed problems. However, in the case of CIPs, such an approximation is rarely available in applications. Nevertheless, locally convergent methods can well be used to address the second central question. Indeed, the *main input* which any locally convergent algorithm needs is a good approximation for the exact solution. This approximation would be used as the starting point for iterations.

The above two questions were addressed in a series of recent publications of the authors for 2D and 3D CIPs for a hyperbolic PDE [9, 24–29, 109, 114–117, 160]. In particular, numerical methods addressing first and second central questions were synthesized in these publications in a *two-stage numerical procedure*. On the first stage, a good approximation for the exact solution is obtained for a CIP via our approximately globally convergent algorithm. Hence, the first central question is addressed on the first stage. On the second stage, this approximation is taken as the starting point for iterations of a locally convergent adaptive finite element method (adaptivity). In other words, the second central question is addressed on the second stage.

Unlike traditional numerical methods for CIPs, our technique, which addresses the first central question, does not use least squares functionals. Rather, only the structure of the underlying PDE operator is used. Also, it does not use a knowledge of the background values of the unknown coefficient. The goal of this book is to present results of above cited publications of the authors in a concise way. In addition, some previous results of the authors are presented as well.

An approximately globally convergent numerical method, which is similar to the one of this book, was developed in parallel for the case of a CIP for an elliptic PDE:

$$\Delta u - a(x)\, u = -\delta(x - x_0), x \in \mathbb{R}^2,$$

with the point source $\{x_0\}$ running along a straight line. This CIP has direct applications in medical optical imaging. That effort was undertaken by a team of researchers from the University of Texas at Arlington in collaboration with the second author of this book [110, 135, 147, 149, 150]. However, a description of this effort is outside of the scope of the current book.

1.1.1 Why the Above Two Questions Are the Central Ones for Computations of CIPs

Consider a radiation propagating through a medium. Some examples of the radiation are electromagnetic (EM), acoustical, thermo, light, and nuclear. Usually, the propagation of a radiation is governed by a PDE. Suppose that one needs to figure out the spatial dependence of one of properties of that medium. That property of interest is described by one of coefficients of the governing PDE. Some examples of such properties are the spatially distributed dielectric constant, electric conductivity, speed of sound, and absorption coefficient of light. If one would approximately calculate the spatial distribution of the property of interest, then one would create an image of the interior of that medium.

An attractive goal is to image that property of interest without placing detectors inside the medium. The latter is called *noninvasive* imaging. To obtain a noninvasive image, one can place detectors at some positions either at the entire boundary of the medium or at a part of it. In the first case, one would have *complete data,* and one would have *incomplete data* in the second case. Quite often, detectors can be placed only rather far from the medium. The latter is the case in, for example, imaging of explosives. Detectors would measure the output radiation. That output signal should have some trace of the property of interest. Suppose that readings of those detectors are interpolated in one of standard ways over the surface where those detectors are placed. Then the resulting function represents a boundary condition for that PDE. This is an extra boundary condition, the one which is given in addition to the original boundary condition for that equation. We call this boundary condition *the measured data* or shortly *the data*. For example, if originally one has the Neumann boundary condition, then the additional one is the Dirichlet boundary condition. The idea is to compute that unknown coefficient of the governing PDE (i.e., the unknown property of ones interest) using this additional boundary condition. Hence, we arrive at a CIP for that PDE.

Therefore, a CIP for a PDE is the problem of the reconstruction of an unknown spatially dependent coefficient of that PDE, given an additional boundary condition. This boundary condition can be given either at the entire boundary or at its part, and it models measurements of the corresponding output signal propagating through the medium of interest. Thus, to find a good approximation of the target property, one should solve numerically that CIP using the measured data. Clearly, these data contain a noisy component, since noise is inevitable in any measurement.

It is well known that it is extremely hard to solve a CIP. First, an important theoretical question is far not easy to address. Namely, this is the question about the uniqueness of the solution of a CIP. It will be clear from the material of this chapter that the uniqueness is one of the central questions to address in order to justify numerical methods for CIPs. This is why many mathematicians work on proofs of uniqueness theorems for CIPs. At the same time, since the discipline of inverse problems is an applied one, it is insufficient only to prove a uniqueness theorem. Along with proofs of uniqueness results, an important question is to construct

reliable numerical methods. However, there are two main phenomena which cause huge challenges in the latter topic. These phenomena are the nonlinearity and the ill-posedness of CIPs combined. A problem is called *ill-posed* if small fluctuations of input data, which are inevitable in any experiment, can cause large fluctuations of resulting solutions. In other words this problem is unstable.

Here is a trivial example of the nonlinearity. Consider the Cauchy problem for the simplest ordinary differential equation:

$$y' = ay, y(0) = 1, \tag{1.1}$$

where $a = \text{const.} \neq 0$. The solution of the problem (1.1) is $y(t, a) = e^{at}$. Obviously, the function $y(t, a)$ depends nonlinearly on the coefficient a.

As to the numerical solution of a CIP, the first idea which naturally comes in mind is to construct a least squares cost functional and to minimize it then. It seems to be, on the first glance, that the point of the minimum of this functional should provide a good approximation for the exact solution. However, there are some serious problems associated with this idea. Indeed, because of the nonlinearity and the ill-posedness of CIPs, corresponding cost functionals usually suffer from the problem of multiple local minima and ravines; see, for example, [102] for some examples. Furthermore, there is no guarantee that a point of a global minimum is indeed close to the correct solution. Suppose, for example, that a cost functional has one hundred (100) points of local minima, one of them is a global one, the values of this functional at those points of local minima differ from each other by 0.5%, and the noise in the measured data is 5%. This might well happen when solving a 3D/2D CIP. Hence, there are no rigorous methods to decide which of these local minima is indeed close to the correct solution. Therefore, the idea of the minimization of the cost functional can work only in the case when a good first approximation for the exact solution is known in advance. However, the latter is a luxury in many applications.

A standard way to treat an ill-posed problem numerically is to minimize the Tikhonov regularization functional; see Sects. 1.7 and 1.8 below in this chapter for this functional. However, if the original problem is nonlinear, for example, a CIP, then this idea also cannot work in practical computations unless a good first approximation for the exact solution is available. In other words, one should know in advance such an approximation, which is located in the ε- neighborhood of the exact solution, where $\varepsilon > 0$ is sufficiently small. Indeed, the theory of the Tikhonov functional is based on the assumption that one can find a minimizing sequence, which ensures the convergence of the values of that functional to its infimum. However, the search of such a sequence can well face the abovementioned problem of local minima and ravines; see, for example, p. 3 of [93] for a similar observation.

Since the first central question is very challenging one to address, then it is hard to anticipate that it can be addressed without some approximations. In other words, a certain reasonable approximate mathematical model should likely be used. Because this model is not an exact one, it is likely that the above good approximation for the exact solution can be refined by one of locally convergent numerical methods. Thus, we arrive at the above second central question.

1.1.2 Approximate Global Convergence

Because of the approximate mathematical model mentioned both in the beginning of Sect. 1.1 and in the end of Sect. 1.1.1, we now discuss the notion of the global convergence. The common perception of the notion of a globally convergent numerical method is that this should be such an iterative algorithm which converges to the exact solution of a corresponding problem starting from an arbitrary point of a sufficiently large set. However, if thinking more carefully, all what one needs is to obtain a point in a sufficiently small neighborhood of the exact solution, provided that iterations would start not from an arbitrary point but rather from a prescribed and rather easily selected point. At the same time, the choice of that starting point should not be based on an a priori knowledge of a small neighborhood of the exact solution. In addition, one should have a rigorous guarantee of reaching that small neighborhood if starting from that selected point. Furthermore, it would be sufficient if that small neighborhood would be reached after a finite number of iterations. In other words, it is not necessary to consider infinitely many iterations, as it is usually done in the classical convergence analysis. On the other hand, since nonlinear problems are usually extremely challenging ones, some approximations should be allowed when developing such numerical methods. A valuable illustration of the idea of "allowed approximations" is the fifth Remark 1.1.2.1 below in this section. These thoughts have generated our definition of the approximate global convergence property.

Definition 1.1.2.1 (Approximate global convergence). Consider a nonlinear ill-posed problem P. Suppose that this problem has a unique solution $x^* \in B$ for the noiseless data y^*, where B is a Banach space with the norm $\|\cdot\|_B$. We call x^* "exact solution" or "correct solution." Suppose that a certain approximate mathematical model M_1 is proposed to solve the problem P numerically. Assume that, within the framework of the model M_1, this problem has unique exact solution $x^*_{M_1}$. Also, let one of assumptions of the model M_1 be that $x^*_{M_1} = x^*$. Consider an iterative numerical method for solving the problem P. Suppose that this method produces a sequence of points $\{x_n\}_{n=1}^N \subset B$, where $N \in [1, \infty)$. Let the number $\varepsilon \in (0, 1)$. We call this numerical method *approximately globally convergent of the level ε,* or shortly *globally convergent*, if, within the framework of the approximate model M_1, a theorem is proven, which guarantees that, without any a priori knowledge of a sufficiently small neighborhood of x^*, there exists a number $\overline{N} \in [1, N)$ such that

$$\|x_n - x^*\|_B \leq \varepsilon, \forall n \geq \overline{N}. \tag{1.2}$$

Suppose that iterations are stopped at a certain number $k \geq \overline{N}$. Then the point x_k is denoted as $x_k := x_{\text{glob}}$ and is called "the approximate solution resulting from this method."

This is our formal mathematical definition of the approximate global convergence property. However, since the approximate mathematical model M_1 is involved

in it, then a natural question can be raised about the validity of this model. This question can be addressed only via computational experiments. In fact, it is a success in computational experiments, which is the true key for the verification of the model M_1. In addition, it would be good to verify M_1 on experimental data. These thoughts lead to the following informal definition of the approximate global convergence property.

Definition 1.1.2.2 (informal definition of the approximate global convergence property). Consider a nonlinear ill-posed problem P. Suppose that this problem has a unique solution $x^* \in B$ for the noiseless data y^*, where B is a Banach space with the norm $\|\cdot\|_B$. Suppose that a certain approximate mathematical model M_1 is proposed to solve the problem P numerically. Assume that, within the framework of the model M_1, this problem has unique exact solution $x^*_{M_1}$. Also, let one of assumptions of the model M_1 be that $x^*_{M_1} = x^*$. Consider an iterative numerical method for solving the problem P. Suppose that this method produces a sequence of points $\{x_n\}_{n=1}^N \subset B$, where $N \in [1, \infty)$. Let the number $\varepsilon \in (0, 1)$. We call this numerical method *approximately globally convergent of the level ε,* or shortly *globally convergent*, if the following three conditions are satisfied:

1. Within the framework of the approximate model M_1, a theorem is proven, which claims that, without any knowledge of a sufficiently small neighborhood of x^*, there exists a number $\overline{N} \in [1, N)$ such that the inequality (1.2) is valid.
2. Numerical studies confirm that x_{glob} is indeed a sufficiently good approximation for the true exact solution x^*, where x_{glob} is introduced in Definition 1.1.2.1.
3. Testing of this numerical method on appropriate experimental data also demonstrates that iterative solutions provide a good approximation for the exact one (optional).

We consider the third condition as an optional one because it is sometimes both hard and expensive to obtain proper experimental data. Furthermore, these data might be suitable only for one version of that numerical method and not suitable for other versions. Nevertheless, we believe that good results obtained for experimental data provide an ultimate confirmation of the validity of the approximate mathematical model M_1.

Remarks 1.1.2.1. 1. We repeat that we have introduced these two definitions because of substantial challenges which one inevitably faces when attempting to construct reliable numerical methods for CIPs. Indeed, because of these challenges, it is unlikely that the desired good approximation for the exact solution would be obtained without a "price." This price is the approximate mathematical model M_1.

2. The *main requirement* of the above definitions is that this numerical method should provide a sufficiently good approximation for the exact solution x^* without any a priori knowledge of a sufficiently small neighborhood of x^*. Furthermore, it is important that one should have a rigorous guarantee of the latter, within the framework of the model M_1.

3. Unlike the classical convergence, these definitions only require that points $\{x_n\}_{n=1}^k$ belong to a small neighborhood of the exact solution x^*. However, the total number of iterations N can be finite in Definitions 1.1.2.1, 1.1.2.2. Such algorithms are not rare in the theory of Ill-Posed Problems. As two examples, we refer to Theorem 4.6 of [10] and Lemma 6.2 on page 156 of [65] for some other numerical methods with the property (1.2). Actually, (1.2) is sufficient, since one can apply a refinement procedure on the second stage, i.e. a procedure addressing The Second Central Question.
4. Therefore, the above definitions leave the room for a refinement of the approximate solution x_{glob} via a subsequent application of a locally convergent numerical method. The latter is exactly what the second central question is about.
5. As to the approximate mathematical model M_1, here is a good analogy. First of all, all equations of mathematical physics are approximate ones. More precisely, it is well known that the Huygens-Fresnel optics is not yet rigorously derived from the Maxwell equations. We now cite some relevant statements from Sect. 8.1 of the classical book of Born and Wolf [36]. "*Diffraction problems are amongst the most difficult ones encountered in optics. Solutions which, in some sense, can be regarded as rigorous are very rare in diffraction theory*." Next, "*because of mathematical difficulties, approximate models must be used in most cases of practical interest. Of these the theory of Huygens and Fresnel is by far the most powerful and is adequate for the treatment of the majority of problems encountered in instrumental optics.*" It is well known that the entire optical industry nowadays is based on the Huygens-Fresnel theory. Analogously, although the numerical method of this book works only with approximate models, its accurate numerical performance has been consistently demonstrated in [24–29, 109, 114–116], including the most challenging case of *blind* experimental data; see [109], Chap. 5, and Sect. 6.9.

Based on Definitions 1.1.2.1, 1.1.2.2, we address The First Central Question of this book via six steps listed below.

Step 1. A reasonable approximate mathematical model is proposed. The accuracy of this model cannot be rigorously estimated.

Step 2. A numerical method is developed, which works within the framework of this model.

Step 3. A theorem is proven, which guarantees that, within the framework of this model, the numerical method of Step 2 indeed reaches a sufficiently small neighborhood of the exact solution, as long as the error, both in the data and in some additional approximations is sufficiently small. It is a **crucial requirement** of our approach that this theorem should not rely neither on the assumption about a knowledge of any point in a small neighborhood of the exact solution nor on the assumption of a knowledge of the background medium inside the domain of interest.

Step 4. Testing of the numerical method of Step 2 on computationally simulated data.

Step 5. Testing of the numerical method of Step 2 on experimental data (if available). To have a truly unbiased case, the most challenging case of **blind** experimental data is preferable.

Step 6. Finally, if results of Step 4 and Step 5 are good ones, then we conclude that our approximate mathematical model is a valid one. However, if experimental data are unavailable, while results of Step 4 are good ones, then we still conclude that our approximate mathematical model is a valid one.

Step 6 is logical, because its condition is that the resulting numerical method is proved to be effective. It is sufficient to achieve that small neighborhood of the exact solution after a finite (rather than infinite) number of iterations. Next, because of approximations in the mathematical model, the resulting solution can be refined via a locally convergent numerical method, i.e. the Second Central Question should be addressed.

Therefore, the key philosophical focus of Definitions 1.1.2.1 and 1.1.2.2 is the point about natural assumptions/approximations which make the technique numerically efficient and, at the same time, independent on the availability of a good first guess.

The next definition is about a locally convergent numerical method for a nonlinear ill-posed problem. In this definition, we consider the Tikhonov functional which is introduced in Sect. 1.7. While sometimes the existence of a minimizer of the Tikhonov functional can be proved in an infinitely dimensional space, in a generic case of a nonlinear ill-posed problem, for example, CIP, this existence cannot be guaranteed; see Sects. 1.7.1 and 1.7.2. On the other hand, the existence of a minimizer for the classical Tikhonov regularization functional is guaranteed only in the case of a finite dimensional space (Sect. 1.8). This minimizer is called a *regularized solution* (in principle, one might have many minimizers). A good example of such a finite dimensional space is the space of piecewise linear finite elements. Furthermore, this is a natural space to use in practical computations, and we use it throughout this book.

Still, the resulting finite dimensional problem inherits the ill-posed nature of the original ill-posed problem. Thus, the Tikhonov regularization functional should be used in that finite dimensional space. At the same time, since a finite dimensional space is taken instead of an infinitely dimensional one, then this can be considered as an approximate mathematical model of the original ill-posed problem. Thus, the *approximate mathematical model* M_2 for an ill-posed problem P means that P is considered in a finite dimensional space.

Definition 1.1.2.3. Consider a nonlinear ill-posed problem P. Suppose that this problem has a exact unique solution $x^* \in B$ for the noiseless data y^*, where B is a Banach space. Consider the approximate mathematical model M_2 for the problem P. The model M_2 means the replacement of the infinitely dimensional space B with a finite dimensional Banach space B_k, $\dim B_k = k$. Assume that,

within the framework of the model M_2, the problem P has unique exact solution $x^*_{M_2} \in B_k$ and let one of assumptions of the model M_2 be that $x^*_{M_2} = x^*$. Let $G \subset B_k$ be an open bounded set. Let the small number $\delta > 0$ be the level of the error in the data and $\alpha = \alpha(\delta)$ be the regularization parameter depending on δ (Sect. 1.4). For the problem P, consider the Tikhonov functional defined in Sect. 1.7. Consider an iterative numerical method of the minimization of this functional on the set $\overline{G}$. Suppose that this method starts its iterations from the point x_0 and produces iterative solutions $\left\{x_n^\delta\right\}_{n=1}^\infty \subset \overline{G}$. Let $x_{\alpha(\delta)} \in \overline{G}$ be a minimizer of the Tikhonov functional with $\alpha = \alpha(\delta)$. Let $\delta_0, \rho \in (0,1)$ be two sufficiently small numbers. We call this method *locally convergent*, if the following two conditions are satisfied:

1. A theorem is proven, which ensures that if $\delta \in (0, \delta_0)$ and $\|x_0 - x^*\|_{B_k} \leq \rho$, then
$$\lim_{n\to\infty} \left\|x_n^\delta - x_{\alpha(\delta)}\right\|_{B_k} = 0, \ \forall \delta \in (0, \delta_0).$$
2. This theorem also claims that
$$\lim_{\delta\to 0} \left\|x_{\alpha(\delta)} - x^*\right\|_{B_k} = 0.$$

On the other hand, the global convergence in the classical sense intuitively means that, regardless on the absence of a good first approximation for the exact solution, the iterative solutions tend to the exact one, as long as certain parameters tend to their limiting values. This, as well as Definitions 1.1.2.1 and 1.1.2.3 lead to Definition 1.1.2.4. Prior this definition, we need to impose the Assumption 1.1.2. We impose this assumption only for the simplicity of the presentation. Note that Assumption 1.1.2 makes sense only if the two-stage numerical procedure mentioned in Sect. 1.1 is applied. However, if only the first stage is applied, then we do not need this assumption.

Assumption 1.1.2. Suppose that a nonlinear ill-posed problem P is the same in both Definitions 1.1.2.1 and 1.1.2.3. Suppose that the two-stage numerical procedure mentioned in Sect. 1.1 is applied. Then, we assume throughout the book that the finite dimensional space $B_k \subseteq B$ and that the exact solution x^* is the same for both mathematical models M_1, M_2 of these two stages.

Definition 1.1.2.4. Consider a nonlinear ill-posed problem. Let B and B_k be the Banach spaces, ε and ρ be the numbers of Definitions 1.1.2.1 and 1.1.2.3, respectively, and let $B_k \subseteq B$ and $\varepsilon \in (0, \rho]$. Consider a numerical procedure for this problem, which consists of the following two stages:

1. On the first stage, a numerical method satisfying conditions of Definitions 1.1.2.1 is applied, and it ends up with an element $x_{\text{glob}} \in B_k$ satisfying inequality (1.2).
2. On the second stage, a locally convergent numerical method satisfying conditions of Definition 1.1.2.3 is applied. This method takes $x_{\text{glob}} := x_0 \in B_k$ as the starting point for iterations.

Then, we call this two-stage numerical procedure *globally convergent in the classical sense within frameworks of the pair of approximate mathematical models* (M_1, M_2). In short, we call this procedure *globally convergent in the classical sense.*

Remarks 1.1.2.2. 1. The single most important point of Definition 1.1.2.4 is that the two-stage numerical procedure converges *globally* in the *classical* sense to the exact solution within the frameworks of the pair (M_1, M_2). In other words, it converges *regardless* on the availability of a good first guess for the exact solution.
2. The two-stage numerical procedure for CIPs which is developed in this book satisfies conditions of Definition 1.1.2.4.

1.1.3 Some Notations and Definitions

The theory of ill-posed problems addresses the following fundamental question: *How to obtain a good approximation for the solution of an ill-posed problem in a stable way?* Roughly speaking, a numerical method, which provides a stable and accurate solution of an ill-posed problem, is called the *regularization* method for this problem; see Sect. 1.7 for a rigorous definition. Foundations of the theory of ill-posed problems were established by three Russian mathematicians: Tikhonov [152–154], Lavrent'ev [122, 124], and Ivanov [85, 86] in the 1960s. The first foundational work was published by Tikhonov in 1943 [152].

We now briefly introduce some common notations which will be used throughout this book. These notations can be found in, for example, the textbook [127]. We work in this book only with real valued functions. Let $\Omega \subset \mathbb{R}^n$ be a bounded domain. We will always assume in our analytical derivations that its boundary $\partial\Omega \in C^3$, although we will work with piecewise smooth boundaries in numerical studies. This is one of natural discrepancies between the theory and its numerical implementation, which always exist in computations. Let $u(x)$, $x = (x_1, ..., x_n) \in \Omega$ be a k times continuously differentiable function defined in Ω. Denote

$$D^\alpha u = \frac{\partial^{|\alpha|} u}{\partial^{\alpha_1} x_1 \dots \partial^{\alpha_n} x_n}, \quad |\alpha| = \alpha_1 + \dots + \alpha_n,$$

the partial derivative of the order $|\alpha| \leq k$, where $\alpha = (\alpha_1, \dots, \alpha_n)$ is a multi-index with integers $\alpha_i \geq 0$. Denote $C^k\left(\overline{\Omega}\right)$ the Banach space of functions $u(x)$ which are continuous in the closure $\overline{\Omega}$ of the domain Ω together with their derivatives $D^\alpha u$, $|\alpha| \leq m$. The norm in this space is defined as

$$\|u\|_{C^k(\overline{\Omega})} = \sum_{|\alpha| \leq m} \sup_{x \in \Omega} |D^\alpha u(x)| < \infty.$$

By definition, $C^0\left(\overline{\Omega}\right) = C\left(\overline{\Omega}\right)$ is the space of functions continuous in $\overline{\Omega}$ with the norm

$$\|u\|_{C\left(\overline{\Omega}\right)} = \sup_{x\in\Omega} |u(x)|.$$

We also introduce Hölder spaces $C^{k+\alpha}\left(\overline{\Omega}\right)$ for any number $\alpha \in (0,1)$. The norm in this space is defined as

$$\|u\|_{C^{k+\alpha}\left(\overline{\Omega}\right)} := |u|_{k+\alpha} := \|u\|_{C^k\left(\overline{\Omega}\right)} + \sup_{x,y\in\Omega,\, x\neq y} \frac{|u(x)-u(y)|}{|x-y|^\alpha},$$

provided that the last term is finite. It is clear that if the function $u \in C^{k+1}\left(\overline{\Omega}\right)$, then $u \in C^{k+\alpha}\left(\overline{\Omega}\right), \forall \alpha \in (0,1)$, and:

$$|u|_{k+\alpha} \leq C\, \|u\|_{C^{k+1}\left(\overline{\Omega}\right)},\ \forall u \in C^{k+1}\left(\overline{\Omega}\right),$$

where $C = C(\Omega,\alpha) > 0$ is a constant independent on the function u. Sometimes, we also use the notion of Hölder spaces for infinite domains. Let D be such a domain. It is convenient for us to say that the function $u \in C^{k+\alpha}(D)$ if $u \in C^{k+\alpha}\left(\overline{\Omega}\right)$ for every bounded subdomain $\Omega \subset D$. Although sometimes people say that $u \in C^{k+\alpha}\left(\overline{D}\right)$ if the above Hölder norm in $\overline{D}$ is finite.

Consider the Sobolev space $H^k(\Omega)$ of all functions with the norm defined as

$$\|u\|^2_{H^k(\Omega)} = \sum_{|\alpha|\leq k} \int\limits_\Omega |D^\alpha u|^2 \,\mathrm{d}x < \infty,$$

where $D^\alpha u$ are weak derivatives of the function u. By the definition, $H^0(\Omega) = L_2(\Omega)$. It is well known that $H^k(\Omega)$ is a Hilbert space with the inner product defined as

$$(u,v)_{H^k(\Omega)} = \sum_{|\alpha|\leq k} \int\limits_\Omega D^\alpha u D^\alpha v \mathrm{d}x.$$

Let $T > 0$ and $\Gamma \subseteq \partial\Omega$ be a part of the boundary $\partial\Omega$ of the domain Ω. We will use the following notations throughout this book:

$$Q_T = \Omega \times (0,T),\ S_T = \partial\Omega \times (0,T),\ \Gamma_T = \Gamma \times (0,T),\ D_T^{n+1} = \mathbb{R}^n \times (0,T).$$

The space $C^{2k,k}\left(\overline{Q}_T\right)$ is defined as the set of all functions $u(x,t)$ having derivatives $D_x^\alpha D_t^\beta u \in C\left(\overline{Q}_T\right)$ with $|\alpha| + 2\beta \leq 2k$ and with the following norm:

$$\|u\|_{C^{2k,k}\left(\overline{Q}_T\right)} = \sum_{|\alpha|+2\beta\leq 2k} \max_{\overline{Q}_T} \left| D_x^\alpha D_t^\beta u(x,t) \right|.$$

The Hölder space $C^{2k+\alpha,k+\alpha/2}\left(\overline{Q}_T\right), \alpha \in (0,1)$ is defined similarly [120].

We now remind some definitions from the standard course of functional analysis.

Definition 1.1.3.1. Let B be a Banach space. The set $V \subset B$ is called *precompact* set if every sequence $\{x_n\}_{n=1}^{\infty} \subseteq V$ contains a fundamental subsequence (i.e., the Cauchy subsequence).

Although by the Cauchy criterion the subsequence of Definition 1.1.3.1 converges to a certain point, there is no guarantee that this point belongs to the set V. If we consider the closure of V, i.e., the set $\overline{V}$, then all limiting points of all convergent sequences in V would belong to V. Therefore, we arrive at Definition 1.1.3.2.

Definition 1.1.3.2. Let B be a Banach space. The set $V \subset B$ is called *compact* set if V is a closed set, $V = \overline{V}$, every sequence $\{x_n\}_{n=1}^{\infty} \subseteq V$ contains a fundamental subsequence, and the limiting point of this subsequence belongs to the set V.

Definition 1.1.3.3. Let B_1 and B_2 be two Banach spaces, $U \subseteq B_1$ be a set and $A : U \to B_2$ be a continuous operator. The operator A is called a *compact operator* or *completely continuous* operator if it maps any bounded subset $U' \subseteq U$ in a precompact set in B_2. Clearly, if U' is a closed set, then $A(U')$ is a compact set.

The following theorem is well known under the name of Ascoli-Archela theorem (More general formulations of this theorem can also be found).

Theorem 1.1.3.1. *The set of functions $\mathcal{M} \subset C\left(\overline{\Omega}\right)$ is a compact set if and only if it is uniformly bounded and equicontinuous. In other words, if the following two conditions are satisfied:*

1. There exists a constant $M > 0$ such that

$$\| f \|_{C\left(\overline{\Omega}\right)} \leq M, \ \forall f \in \mathcal{M}.$$

2. For any $\varepsilon > 0$, there exists $\delta = \delta(\varepsilon) > 0$ such that

$$|f(x) - f(y)| < \varepsilon, \quad \forall x, y \in \{|x - y| < \delta\} \cap \overline{\Omega}, \ \forall f \in \mathcal{M}.$$

In particular, because of some generalizations of this theorem, any bounded set in $C^k\left(\overline{\Omega}\right)$ (or $H^k(\Omega)$), $k \geq 1$ is a compact set in $C^p\left(\overline{\Omega}\right)$ (respectively $H^p(\Omega)$) for $p \in [0, k-1]$. We also remind one of the Sobolev embedding theorems for spaces $H^k(\Omega)$. Let $[n/2]$ be the least integer which does not exceed $n/2$.

Theorem 1.1.3.2 ([127]). *Suppose that $k > [n/2] + m$, the domain Ω is bounded and $\partial\Omega \in C^k$. Then $H^k(\Omega) \subset C^m\left(\overline{\Omega}\right)$ and $\| f \|_{C^m\left(\overline{\Omega}\right)} \leq C \| f \|_{H^k(\Omega)}, \forall f \in H^k(\Omega)$, where the constant $C = C(\Omega, k, m) > 0$ depends only on Ω, k, m. In addition, any bounded set in $H^k(\Omega)$ is a precompact set in $C^m\left(\overline{\Omega}\right)$.*

Theorem 1.1.3.2 actually claims that the space $H^k(\Omega)$ is compactly embedded in the space $C^m\left(\overline{\Omega}\right)$. "Compactly embedded" means that $\| f \|_{C^m\left(\overline{\Omega}\right)} \leq C \| f \|_{H^k(\Omega)}, \forall f \in H^k(\Omega)$, and any bounded set in $H^k(\Omega)$ is a precompact

set in $C^m\left(\overline{\Omega}\right)$. In other words, any sequence bounded in $H^k(\Omega)$ contains a subsequence, which converges in $C^m\left(\overline{\Omega}\right)$, although the limit of this subsequence does not necessarily belong to $H^k(\Omega)$.

1.2 Some Examples of Ill-posed Problems

Example 1 (J. Hadamard). We now describe the classical example of Hadamard; see, for example, [124]. Consider the Cauchy problem for the Laplace equation for the function $u(x, y)$:

$$\Delta u = 0, \quad x \in (0, \pi), \quad y > 0, \tag{1.3}$$

$$u(x, 0) = 0, u_y(x, 0) = \alpha \sin(nx), \tag{1.4}$$

where $n > 0$ is an integer. It is well known that the Cauchy problem for a general elliptic equation with "good" variable coefficients has at most one solution [102, 124] (although it might not have solutions at all). The unique solution of the problems (1.3) and (1.4) is

$$u(x, y) = \frac{\alpha}{n} \sinh(ny) \sin(nx). \tag{1.5}$$

Choose sufficiently small numbers $\varepsilon > 0, \alpha = \alpha(\varepsilon) > 0$ and a number $y := y_0 > 0$. Let in (1.5) $x \in (0, \pi)$. Since the function

$$\sinh(ny_0) = \frac{e^{ny_0}\left(1 + e^{-2ny_0}\right)}{2}$$

grows exponentially as $n \to \infty$, then it is clear from (1.5) that for any pair of reasonable functional spaces $C^k[0, \pi], L_2[0, \pi], H^k[0, \pi]$, etc., one can choose such two numbers $c > 0, n_0 > 0$ depending only on numbers ε, α, y_0 that

$$||\alpha \sin(nx)||_1 < \varepsilon, \quad \forall n \geq n_0,$$

$$\|u(x, y_0)\|_2 = \left|\left|\frac{\alpha}{n} \sinh(ny_0) \sin(nx)\right|\right|_2 > c, \quad \forall n \geq n_0,$$

where $\|\cdot\|_1$ is the norm in one of those spaces and $\|\cdot\|_2$ is the norm in another one.

The above example demonstrates that although both the Dirichlet and Neumann boundary data are small, any reasonable norm of the solution is still large. In other words, this is a manifestation of a high instability of this problem. Based on this example, Hadamard has concluded that it makes no sense to consider unstable problems. However, his conclusion was an exaggeration. Indeed, unstable problems

arise in many applications. Being inspired by applications to geophysics, Tikhonov has proposed in 1943 [152] the fundamental concept for solving unstable problems; see Sect. 1.3.

Example 2 (Differentiation of a Function Given with a Noise). The differentiation of functions given by analytic formulas is a trivial exercise. In the reality, however, functions are often measured in experiments. Since experimental data always contain noise, then measured functions are given with a noise. Quite often, it is necessary to differentiate these noisy functions. We demonstrate now that the problem of the differentiation of noisy functions is unstable. Suppose that the function $f(x), x \in [0,1]$ is given with a noise. In other words, suppose that instead of $f(x) \in C^1[0,1]$ the following function $f_\delta(x)$ is given:

$$f_\delta(x) = f(x) + \delta f(x), x \in [0,1],$$

where $\delta f(x)$ is the noisy component. Let $\delta > 0$ be a small parameter characterizing the level of noise. We assume that the noisy component is small, $\|\delta f\|_{C[0,1]} \leq \delta$. The problem of calculating the derivative $f'_\delta(x)$ is unstable. Indeed, let, for example,

$$\delta f(x) = \frac{\sin(n^2 x)}{n},$$

where $n > 0$ is a large integer. Then the $C[0,1]$-norm of the noisy component is small:

$$\|\delta f\|_{C[0,1]} \leq \frac{1}{n}.$$

However, the difference between derivatives of noisy and exact functions

$$f'_\delta(x) - f'(x) = n \cos n^2 x$$

is not small in any reasonable norm.

We now describe a simple regularization method of stable calculation of derivatives. The idea is that the step size h in the corresponding finite difference should be connected with the level of noise δ. Thus, h cannot be made arbitrary small, as it is the case of the classic definition of the derivative. We obviously have

$$f'_\delta(x) \approx \frac{f(x+h) - f(x)}{h} + \frac{\delta f(x+h) - \delta f(x)}{h}. \tag{1.6}$$

The first term in the right-hand side of (1.6) is close to the exact derivative $f'(x)$, if h is small enough. The second term, however, comes from the noise. Hence, we need to balance these two terms via an appropriate choice of $h = h(\delta)$. Obviously:

$$\left| f'_\delta(x) - \frac{f(x+h) - f(x)}{h} \right| \leq \frac{2\delta}{h}.$$

Hence, we should choose $h = h(\delta)$ such that

$$\lim_{\delta \to 0} \frac{2\delta}{h(\delta)} = 0.$$

For example, let $h(\delta) = \delta^{\mu}$, where $\mu \in (0,1)$. Then

$$\lim_{\delta \to 0} \left| f_{\delta}'(x) - \frac{f(x+h) - f(x)}{h} \right| \leq \lim_{\delta \to 0} \left(2\delta^{1-\mu} \right) = 0.$$

Hence, the problem becomes stable for this choice of the grid step size $h(\delta) = \delta^{\mu}$. This means that $h(\delta)$ is the regularization parameter here. There are many practical methods in the literature designed for stable differentiation. For example, one can approximate the function $f_{\delta}(x)$ via cubic B splines and differentiate this approximation then; see, for example, [73]. However, the number of these splines should not be too large; otherwise, the problem would become unstable. So the number of cubic B splines is the regularization parameter in this case, and its intuitive meaning is the same as the meaning of the number $1/h(\delta)$. A more detailed description of regularization methods for the differentiation procedure is outside of the scope of this book.

Let $\Omega \subset \mathbb{R}^n$ is a bounded domain and the function $K(x,y) \in C\left(\overline{\Omega} \times \overline{\Omega}\right)$. Recall that the equation

$$g(x) + \int_{\Omega} K(x,y)\, g(y)\, \mathrm{d}y = p(x), x \in \Omega, \tag{1.7}$$

where $p(x)$ is a bounded function, is called *integral equation of the second kind*. These equations are considered quite often in the classic theory of PDEs. The classical Fredholm theory works for these equations; see, for example, the textbook [127]. Next, let $\Omega' \subset \mathbb{R}^n$ be a bounded domain and the function $K(x,y) \in C\left(\overline{\Omega} \times \overline{\Omega}\right)$. Unlike (1.7), the equation

$$\int_{\Omega} K(x,y)\, g(y)\, \mathrm{d}y = p(x), x \in \Omega' \tag{1.8}$$

is called the integral equation of the first kind. The Fredholm theory does not work for such equations. The problem of solution of (1.8) is an ill-posed problem; see Example 3.

Example 3 (Integral Equation of the First Kind). Consider (1.8). The function $K(x,y)$ is called *kernel* of the integral operator. Equation (1.8) can be rewritten in the form

$$Kf = p, \tag{1.9}$$

where $K : C\left(\overline{\Omega}\right) \to C\left(\overline{\Omega'}\right)$ is the integral operator in (1.8). It is well known from the standard functional analysis course that K is a compact operator. We now

show that the problem (1.9) is ill-posed. Let $\Omega = (0,1)$, $\Omega' = (a,b)$. Replace the function f with the function $f_n(x) = f(x) + \sin nx$. Then

$$\int_0^1 K(x,y)\, f_n(y)\, \mathrm{d}y = g_n(x),\ x \in (0,1), \tag{1.10}$$

where $g_n(x) = p(x) + p_n(x)$ and

$$p_n(x) = \int_0^1 K(x,y) \sin ny \mathrm{d}y.$$

By the Lebesque lemma,

$$\lim_{n\to\infty} \|p_n\|_{C[a,b]} = 0.$$

However, it is clear that

$$\|f_n(x) - f(x)\|_{C[0,1]} = \|\sin nx\|_{C[0,1]}$$

is not small for large n.

Example 4 (The Case of a General Compact Operator). We now describe an example of a general ill-posed problem. Let H_1 and H_2 be two Hilbert spaces with $\dim H_1 = \dim H_2 = \infty$. We remind that a sphere in an infinitely dimensional Hilbert space is not a compact set. Indeed, although the orthonormal basis in this space belongs to the unit sphere, it does not contain a fundamental subsequence.

Theorem 1.2. *Let $G = \{\|x\|_{H_1} \le 1\} \subset H_1$. Let $A : G \to H_2$ be a compact operator and let $R(A) := A(G)$ be its range. Consider an arbitrary point $y_0 \in R(A)$. Let $\varepsilon > 0$ be a number and $U_\varepsilon(y_0) = \{y \in H_2 : \|y - y_0\|_{H_2} < \varepsilon\}$. Then there exists a point $y \in U_\varepsilon(y_0) \setminus R(A)$. If, in addition, the operator A is one-to-one, then the inverse operator $A^{-1} : R(A) \to G$ is not continuous. Hence, the problem of the solution of the equation*

$$A(x) = z, x \in G, z \in R(A) \tag{1.11}$$

is unstable, i.e., this is an ill-posed problem.

Proof. First, we prove the existence of a point $y \in U_\varepsilon(y_0) \setminus R(A)$. Assume to the contrary, i.e., assume that $U_\varepsilon(y_0) \subset R(A)$. Let $\{y_n\}_{n=1}^\infty \subset H_2$ be an orthonormal basis in H_2. Then the sequence

$$\left\{y_0 + \frac{\varepsilon}{2} y_n\right\}_{n=1}^\infty := \{z_n\}_{n=1}^\infty \subset \left\{\|y - y_0\| = \frac{\varepsilon}{2}\right\} \subset U_\varepsilon(y_0).$$

We have

$$\|z_n - z_m\|_{H_2} = \frac{\varepsilon}{\sqrt{2}}.$$

Hence, the sequence $\{z_n\}_{n=1}^{\infty}$ does not contain a fundamental subsequence. Therefore, $U_\varepsilon(y_0)$ is not a precompact set in H_2. On the other hand, since G is a closed bounded set and A is a compact operator, then $R(A)$ is a compact set. Hence, $U_\varepsilon(y_0)$ is a precompact set. We got a contradiction, which proves the first assertion of this lemma.

We now prove the second assertion. Assume to the contrary that the operator $A^{-1} : R(A) \to G$ is continuous. By the definition of the operator A, we have $A^{-1}(R(A)) = G$. Since $R(A)$ is a compact set in H_2, then the continuity of A^{-1} implies that G is a compact set in H_1, which is not true.

We now summarize some conclusions which follow from Theorem 1.2. By this theorem, the set $R(A)$ is not dense everywhere. Therefore, the question about the existence of the solution of either of (1.9) or (1.11) does not make an applied sense. Indeed, since the set $R(A)$ is not dense everywhere, then it is very hard to describe a set of values y belonging to this set. As an example, consider the case when the kernel $K(x,y) \in C([a,b] \times [0,1])$ in (1.10) is an analytic function of the real variable $x \in (a,b)$. Then the right hand side $p(x)$ of (1.8) should also be analytic with respect to $x \in (a,b)$. However, in applications, the function $p(x)$ is a result of measurements, it is given only at a number of discrete points and contains noise. Clearly, it is impossible to determine from this information whether the function $p(x)$ is analytic or not. Hence, we got the following important conclusion.

Conclusion. Assuming that conditions of Theorem 1.2 are satisfied, the problem of solving (1.11) is ill-posed in the following terms: (a) the proof of an existence theorem makes no applied sense, and (b) small fluctuations of the right hand side y can lead to large fluctuations of the solution x, i.e., the problem is unstable.

Example 5 (A Coefficient Inverse Problem (CIP)). Let the functions $a(x) \in C^\alpha(\mathbb{R}^n)$, $\alpha \in (0,1)$, and $a(x) = 0$ outside of the bounded domain $\Omega \subset \mathbb{R}^n$ with $\partial\Omega \in C^3$. Consider the following Cauchy problem:

$$u_t = \Delta u + a(x)u, \quad (x,t) \in D_T^{n+1}, \tag{1.12}$$

$$u(x,0) = f(x). \tag{1.13}$$

Here, the function $f(x) \in C^{2+\alpha}(\mathbb{R}^n)$ has a finite support in $\mathbb{R}^n$. Although less restrictive conditions on f can also be imposed, we are not doing this here for brevity; see details in the book [120]. Another option for the initial condition is

$$f(x) = \delta(x - x_0), \tag{1.14}$$

where the source position $x_0 \notin \overline{\Omega}$. Throughout the book, we will always assume that the source is located outside of the domain of interest Ω. The reason of doing this is that we do not want to work with singularities since CIPs are very complicated even without singularities. The second reason is that in the majority of applications, sources are indeed located outside of domains of interest; see Chaps. 5 and 6 for experimental data.

Statement of a Coefficient Inverse Problem. Assume that the function $a(x)$ is unknown inside the domain Ω. Determine this function for $x \in \Omega$ assuming that the following function $g(x,t)$ is known:

$$u|_{S_T} = g(x,t). \tag{1.15}$$

The function $g(x,t)$ is an additional boundary condition. This function can be interpreted as a result of measurements: One is measuring the function $u(x,t)$ at the boundary of the domain Ω in order to reconstruct the function $a(x)$ inside Ω. Indeed, if the coefficient $a(x)$ would be known in the entire space $\mathbb{R}^n$, then one would uniquely determine the function $u(x,t)$ in D_T^{n+1}. But since $a(x)$ is unknown, then the function $u|_{S_T}$ can be determined only via measurements. Note that since $a(x) = 0$ outside of Ω, then one can uniquely solve the following initial boundary value problem outside of Ω :

$$u_t = \Delta u, (x,t) \in (\mathbb{R}^n \setminus \Omega) \times (0,T),$$

$$u(x,0) = f(x), x \in \mathbb{R}^n \setminus \Omega,$$

$$u|_{S_T} = g(x,t).$$

Hence, one can uniquely determine the Neumann boundary condition for the function u at the boundary $\partial\Omega$, and we will use this consideration throughout this book. Thus, the following function $g_1(x,t)$ is known along with the function $g(x,t)$ in (1.15):

$$\partial_n u|_{S_T} = g_1(x,t).$$

This CIP has direct applications in imaging of the *turbid media* using light propagation [8, 76, 156]. In a turbid medium, photons of light, originated by a laser, propagate randomly in the diffuse manner. In other words, they experience many random scattering events. Two examples of turbid media are smog and flames in the air. The most popular example is the biological tissue, including human organs. Assuming that the diffusion coefficient $D = 1$, we obtain that in (1.12) the coefficient $a(x) = -\mu_a(x) \leq 0$, where $\mu_a(x)$ is the absorption coefficient of the medium. The case of smog and flames has military applications. Since $\mu_a(x) = \infty$ for any metallic target, then imaging small inhomogeneities with large values of the absorption coefficient might lead to detection of those targets. In the case of medical applications, high values of $\mu_a(x)$ usually correspond to malignant legions. Naturally, one is interested to image those legions noninvasively via solving a CIP.

Thus, in both applications, the main interest is in imaging of small sharp abnormalities, rather than in imaging of a slowly changing background function. Furthermore, to correctly identify those abnormalities, one needs to image with a good accuracy the value of the coefficient $\mu_a(x)$ within them. Naturally, in both applications, one should use the function (1.14) as the initial condition. In this case, x_0 is the location of the light source.

We now show that this CIP is an ill-posed problem. Let the function u_0 be the fundamental solution of the heat equation $u_{0t} = \Delta u_0$:

$$u_0(x,t) = \frac{1}{\left(2\sqrt{\pi t}\right)^n} \exp\left(-\frac{|x|^2}{4t}\right).$$

It is well known that the function u has the following integral representation [120]:

$$u(x,t) = \int\limits_{\mathbb{R}^n} u_0(x-\xi,t)\, f(\xi)\, d\xi + \int\limits_0^t \int\limits_\Omega u_0(x-\xi,t-\tau)\, a(\xi)\, u(\xi,\tau)\, d\tau. \tag{1.16}$$

Because of the presence of the integral

$$\int\limits_0^t (\cdot)\, d\tau,$$

(1.16) is a Volterra-like integral equation of the second kind. Hence, it can be solved as [120]:

$$u(x,t) = \int\limits_{\mathbb{R}^n} u_0(x-\xi,t)\, f(\xi)\, d\xi + \sum_{n=1}^{\infty} u_n(x,t), \tag{1.17}$$

$$u_n(x,t) = \int\limits_0^t \int\limits_\Omega u_0(x-\xi,t-\tau)\, a(\xi)\, u_{n-1}(\xi,\tau)\, d\tau.$$

One can prove that each function $u_n \in C^{2+\alpha,1+\alpha/2}\left(\overline{D}_T^{n+1}\right)$ and [120]

$$\left|D_x^\beta D_t^k u_n(x,t)\right| \le \frac{(Mt)^n}{n!}, \quad |\beta| + 2k \le 2, \tag{1.18}$$

where $M = \|a\|_{C^\alpha(\overline{\Omega})}$. In the case when $f = \delta(x - x_0)$, the first term in the right-hand side of (1.17) should be replaced with $u_0(x - x_0, t)$. Let $u_0^f(x,t)$ be the first term of the right-hand side of (1.17) and $v(x,t) = u(x,t) - u_0^f(x,t)$. Using (1.18), one can rewrite (1.17) as

$$v(x,t)=\int\limits_0^t\int\limits_\Omega u_0(x-\xi,t-\tau)\left(a(\xi)u_0^f(\xi,\tau)+P(a)(\xi,\tau)\right)\mathrm{d}\xi\mathrm{d}\tau, \quad (1.19)$$

where $P(a)$ is a nonlinear operator applied to the function a. It is clear from (1.17)–(1.19) that the operator $P: C^\alpha\left(\overline{\Omega}\right)\to C^{2+\alpha,1+\alpha/2}\left(\overline{Q}_T\right)$ is continuous. Setting in (1.19) $(x,t)\in S_T$, recalling (1.15), and denoting $\overline{g}(x,t)=g(x,t)-u_0^f(x,t)$, we obtain a nonlinear integral equation of the first kind with respect to the unknown coefficient $a(x)$:

$$\int\limits_0^t\int\limits_\Omega u_0(x-\xi,t-\tau)\left(u_0^f(\xi,\tau)a(\xi)+P(a)(\xi,\tau)\right)\mathrm{d}\xi\mathrm{d}\tau=\overline{g}(x,t),(x,t)\in S_T. \quad (1.20)$$

Let $A(a)$ be the operator in the left-hand side of (1.20). Let $H_1=L_2(\Omega)$ and $H_2=L_2(S_T)$. Consider now the set U of functions defined as

$$U=\left\{a: a\in C^\alpha\left(\overline{\Omega}\right), \|a\|_{C^\alpha\left(\overline{\Omega}\right)}\le M\right\}\subset H_1.$$

Since the $L_2(\Omega)$ norm is weaker than the $C^\alpha\left(\overline{\Omega}\right)$-norm, then U is a bounded set in H_1. Using (1.18) and Theorem 1.1, one can prove that $A: U\to C(S_T)$ is a compact operator. Since the norm in $L_2(S_T)$ is weaker than the norm in $C(S_T)$, then $A: U\to H_2$ is also a compact operator. Hence, Theorem 1.2 implies that the problem of solution of the equation

$$A(a)=g, a\in U\subset H_1, g\in H_2$$

is ill-posed in terms of the above conclusion.

1.3 The Foundational Theorem of A.N. Tikhonov

This theorem "restores" stability of unstable problems, provided that uniqueness theorems hold for such problems. The original motivation for this theorem came from the collaboration of Tikhonov with geophysicists. To his surprise, Tikhonov has learned that geophysicists successfully solve problems which are unstable from the mathematical standpoint. Naturally, Tikhonov was puzzled by this. This puzzle has prompted him to explain that "matter of fact" stability of unstable problems from the mathematical standpoint. He has observed that geophysicists have worked with rather simple models, which included only a few abnormalities. In addition, they knew very well ranges of parameters they have worked with. Also, they knew that the functions, which they have reconstructed from measured date, had only very few oscillations. In other words, they have reconstructed only rather simple media

structures. On the other hand, the Ascoli-Archela Theorem 1.1.3.1 basically requires a priori known upper bounds of both the function and its first derivatives. Clearly, there is a connection between the number of oscillations per a bounded set in $\mathbb{R}^n$ and the upper bound of the modulus of the gradient of the corresponding function. These observations have made Tikhonov to believe that actually geophysicists have worked with compact sets. This was the starting point for the formulation of the foundational Tikhonov theorem (below). In particular, this means that in an ill-posed problem, one should not expect to reconstruct a complicated fine structure of the medium of interest. Rather, one should expect to reconstruct rather simple features of this medium.

The key idea of Tikhonov was that to restore stability of an unstable problem, one should solve this problem on a compact set. The question is then whether it is reasonable to assume that the solution belongs to a specific compact set. The answer on this question lies in applications. Indeed, by, for example, Theorem 1.1.3.1, an example of a compact set in the space $C\left(\overline{\Omega}\right)$ is the set of all functions from $C^1\left(\overline{\Omega}\right)$ which are bounded together with the absolute values of their first derivatives by an a priori chosen constant. On the other hand, it is very often known in any specific application that functions of ones interest are bounded by a certain known constant. In addition, it is also known that those functions do not have too many oscillations, which is guaranteed by an a priori bound imposed on absolute values of their first derivatives. These bounds should be uniform for all functions under consideration. Similar arguments can be brought up in the case of other conventional functional spaces, like, for example, $C^k\left(\overline{\Omega}\right), H^k(\Omega)$. Another expression of these thoughts, which is often used in applications, is that the admissible range of parameters is known in advance. On the other hand, because of the compact set requirement of Theorem 1.3, the foundational Tikhonov theorem essentially requires a higher smoothness of sought for functions than one would originally expect. The latter is the true underlying reason why computed solutions of ill-posed problems usually look smoother than the original ones. In particular, sharp boundaries usually look as smooth ones.

Although the proof of Theorem 1.3 is short and simple, this result is one of only a few backbones of the entire theory of ill-posed problems.

Theorem 1.3 (Tikhonov [152], 1943). *Let B_1 and B_2 be two Banach spaces. Let $U \subset B_1$ be a compact set and $F : U \to B_2$ be a continuous operator. Assume that the operator F is one-to-one. Let $V = F(U)$. Then the inverse operator $F^{-1} : V \to U$ is continuous.*

Proof. Assume the opposite: that the operator F^{-1} is not continuous on the set V. Then, there exists a point $y_0 \in V$ and a number $\varepsilon > 0$ such that for any $\delta > 0$, there exists a point y_δ such that although $\|y_\delta - y_0\|_{B_2} < \delta$, still $\left\|F^{-1}(y_\delta) - F^{-1}(y_0)\right\|_{B_1} \geq \varepsilon$. Hence, there exists a sequence $\{\delta_n\}_{n=1}^{\infty}$, $\lim_{n\to\infty} \delta_n = 0^+$ and the corresponding sequence $\{y_n\}_{n=1}^{\infty} \subset V$ such that

$$\|y_{\delta_n} - y_0\|_{B_2} < \delta_n, \left\|F^{-1}(y_n) - F^{-1}(y_0)\right\|_{B_1} \geq \varepsilon. \tag{1.21}$$

Denote

$$x_n = F^{-1}(y_n), x_0 = F^{-1}(y_0). \tag{1.22}$$

Then

$$\|x_n - x_0\|_{B_1} \geq \varepsilon. \tag{1.23}$$

Since U is a compact set and all points $x_n \in U$, then one can extract a convergent subsequence $\{x_{n_k}\}_{k=1}^{\infty} \subseteq \{x_n\}_{n=1}^{\infty}$ from the sequence $\{x_n\}_{n=1}^{\infty}$. Let $\lim_{k\to\infty} x_{n_k} = \overline{x}$. Then $\overline{x} \in U$. Since $F\left(x_{n_k}\right) = y_{n_k}$ and the operator F is continuous, then by (1.21) and (1.22), $F(\overline{x}) = y_0 = F(x_0)$. Since the operator F is one-to one, we should have $\overline{x} = x_0$. However, by (1.23), $\|\overline{x} - x_0\|_{B_1} \geq \varepsilon$. We got a contradiction. □

1.4 Classical Correctness and Conditional Correctness

The notion of the classical correctness is called sometimes *correctness by Hadamard*.

Definition 1.4.1. Let B_1 and B_2 be two Banach spaces. Let $G \subseteq B_1$ be an open set and $F : G \to B_2$ be an operator. Consider the equation

$$F(x) = y, \ x \in G. \tag{1.24}$$

The problem of solution of (1.24) is called *well-posed by Hadamard,* or simply *well-posed,* or *classically well-posed* if the following three conditions are satisfied:

1. For any $y \in B_2$, there exists a solution $x = x(y)$ of (1.24) (existence theorem).
2. This solution is unique (uniqueness theorem).
3. The solution $x(y)$ depends continuously on y. In other words, the operator $F^{-1} : B_2 \to B_1$ is continuous.

Thus, the well-posedness by Hadamard means the existence of the solution of the operator equation (1.24) for any right-hand side y. This solution should be unique. In addition, it should depend on the data y continuously. All classical boundary value problems for PDEs, which are studied in the standard PDE course, satisfy these criteria and are, therefore, well-posed by Hadamard.

If (1.24) does not satisfy to at least one these three conditions, then the problem (1.24) is called *ill-posed*. The most pronounced feature of an ill-posed problem is its instability, i.e., small fluctuations of y can lead to large fluctuations of the solution x. The definition of the correctness by Tikhonov, or conditional correctness, reflects the above Theorems 1.2 and 1.3.

Since the experimental data are always given with a random noise, we need to introduce the notion of the error in the data. In practice, this error is always due to that random noise as well as due to an inevitable discrepancy between the mathematical model and the reality. However, we do not assume the randomness of

y in (1.24). Let $\delta > 0$ be a small number. We say that the right-hand side of (1.24) is given with an error of the level δ if $\|y^* - y\|_{B_2} \leq \delta$, where y^* is the exact value of y, which has no error.

Definition 1.4.2. Let B_1 and B_2 be two Banach spaces. Let $G \subset B_1$ be an a priori chosen set of the form $G = \overline{G}_1$, where G_1 is an open set in B_1. Let $F : G \to B_2$ be a continuous operator. Suppose that the right-hand side of (1.24) $y := y_\delta$ is given with an error of the level $\delta > 0$, where δ is a small number, $\|y^* - y_\delta\|_{B_2} \leq \delta$. Here, y^* is the ideal noiseless data y^*. The problem (1.24) is called *conditionally well-posed on the set* G, or *well-posed by Tikhonov* on the set G, if the following three conditions are satisfied:

1. It is a priori known that there exists an ideal solution $x^* = x^*(y^*) \in G$ of this problem for the ideal noiseless data y^*.
2. The operator $F : G \to B_2$ is one-to-one.
3. The inverse operator F^{-1} is continuous on the set $F(G)$.

Definition 1.4.3. The set G of Definition 1.4.2 is called *correctness set* for the problem (1.24).

We point out that, unlike the classical well-posedness, the conditional well-posedness, does not require the correctness set G to coincide with the entire Banach space B_1. Likewise, Definition 1.4.2 does not require a proof of an existence theorem, unlike the classical case. Indeed, it follows from Theorem 1.2 that it is hopeless to prove such a theorem for (1.11). In addition, such a result would not have a practical meaning. For comparison, recall that a significant part of the classical PDE theory is devoted to proofs of existence theorems, as it is required by the definition of the classical well-posedness. On the other hand, in the definition of the conditional well-posedness the existence is assumed a priori. Still, the existence is assumed not for every y in (1.24) but only for an *ideal*, noiseless $y := y^*$. The assumption of the existence of the ideal solution x^* is a very important notion of the theory of ill-posed problems. Neither the ideal right-hand side y^* nor the ideal solution x^* are never known in applications. This is because of the presence of the noise in any experiment. Still, this assumption is a quite reasonable one because actually, it tells one that the physical process is indeed in place and that the mathematical model, which is described by the operator F, governs this process accurately.

The second condition in Definition 1.4.2 means uniqueness theorem. Combined with Theorem 1.3, this condition emphasizes the importance of uniqueness theorems for the theory of ill-posed problems.

The third condition in Definition 1.4.2 means that the solution of the problem (1.24) is stable with respect to small fluctuations of the right-hand side y, as long as $x \in G$. This goes along well with Theorem 1.3. In other words, the third condition restores the most important feature: stability. The requirement that the correctness set $G \subset B_1$ is not conventionally used in the classical theory of PDEs. In other words, the requirement of x belonging to a "special" subset of B_1 is not imposed in classically well-posed problems.

Motivated by the above arguments, Tikhonov has introduced the Fundamental Concept of Tikhonov.

The Fundamental Concept of Tikhonov. This concept consists of the following three conditions which should be in place when solving the ill-posed problem (1.24):

1. One should a priori assume that there exists an ideal exact solution x^* of (1.24) for an ideal noiseless data y^*.
2. The correctness set G should be chosen a priori, meaning that some a priori bounds imposed on the solution x of (1.24) should be imposed.
3. To construct a stable numerical method for the problem (1.24), one should assume that there exists a family $\{y_\delta\}$ of right-hand sides of (1.24), where $\delta > 0$ is the level of the error in the data with $\|y^* - y_\delta\|_{B_2} \leq \delta$. Next, one should construct a family of approximate solutions $\{x_\delta\}$ of (1.24), where x_δ corresponds to y_δ. The family $\{x_\delta\}$ should be such that

$$\lim_{\delta \to 0^+} \|x_\delta - x^*\| = 0.$$

1.5 Quasi-solution

The concept of quasi-solutions was originally proposed by Ivanov [85]. It is designed to provide a rather general method for solving the ill-posed problem (1.24). This concept is actually a quite useful, as long as one is seeking a solution on a compact set. An example is when the solution is parametrized, i.e.,

$$x = \sum_{i=1}^{N} a_i \varphi_i,$$

where elements $\{\varphi_i\}$ are a part of an orthonormal basis in a Hilbert space, the number N is fixed, and coefficients $\{a_i\}_{n=1}^N$ are unknown. So, one is seeking numbers $\{a_i\}_{n=1}^N \subset G$, where $G \subset \mathbb{R}^N$ is a priori chosen closed bounded set. This set is called sometimes "the set of admissible parameters."

Since the right-hand side y of (1.24) is given with an error, Theorem 1.2 implies that it is unlikely that y belongs to the range of the operator F. Therefore, the following natural question can be raised about the usefulness of Theorem 1.3: *Since the right-hand side y of (1.24) most likely does not belong to the range $F(G)$ of the operator F, then what is the practical meaning of solving this equation on the compact set G, as required by Theorem 1.3?* The importance of the notion of quasi-solutions is that it addresses this question in a natural way.

Suppose that the problem (1.24) is conditionally well-posed and let $G \subset B_1$ be a compact set. Then, the set $F(G) \subset B_2$ is also a compact set. We have $\|y - y^*\|_{B_2} \leq \delta$. Consider the minimization problem

$$\min_G J(x), \text{ where } J(x) = ||F(x) - y||^2_{B_2}. \tag{1.25}$$

Since G is a compact set, then there exists a point $x = x(y_\delta) \in G$ at which the minimum in (1.25) is achieved. In fact, one can have many points $x(y_\delta)$. Nevertheless, it follows from Theorem 1.5 that they are located close to each other, as long as the number δ is sufficiently small.

Definition 1.5. Any point $x = x(y) \in G$ of the minimum of the functional $J(x)$ in (1.25) is called *quasi-solution* of equation in (1.24) on the compact set G.

A natural question is, *how far is the quasi-solution from the exact solution x^*?* Since by Theorem 1.3 the operator $F^{-1} : F(G) \to G$ is continuous and the set $F(G)$ is compact, then one of classical results of real analysis implies that there exists the modulus of the continuity $\omega_F(z)$ of the operator F^{-1} on the set $F(G)$. The function $\omega_F(z)$ satisfies the following four conditions:

1. $\omega_F(z)$ is defined for $z \geq 0$.
2. $\omega_F(z) > 0$ for $z > 0$, $\omega_F(0) = 0$, and $\lim_{z \to 0+} \omega_F(z) = 0$.
3. The function $\omega_F(z)$ is monotonically increasing for $z > 0$.
4. For any two points $y_1, y_2 \in F(G)$, the following estimate holds:

$$||F^{-1}(y_1) - F^{-1}(y_2)||_{B_1} \leq \omega_F(||y_1 - y_2)||_{B_2}).$$

The following theorem characterizes the accuracy of the quasi-solution:

Theorem 1.5. *Let B_1 and B_2 be two Banach spaces, $G \subset B_1$ be a compact set, and $F : G \to B_2$ be a continuous one-to-one operator. Consider (1.24). Suppose that its right-hand side $y := y_\delta$ is given with an error of the level $\delta > 0$, where δ is a small number, $\|y^* - y_\delta\|_{B_2} \leq \delta$. Here, y^* is the ideal noiseless data y^*. Let $x^* \in G$ be the ideal exact solution of (1.24) corresponding to the ideal data y^*, i.e., $F(x^*) = y^*$. Let x_δ^q be a quasi-solution of (1.24), i.e.,*

$$J(x_\delta^q) = \min_G ||F(x) - y_\delta||^2_{B_2}. \tag{1.26}$$

Let $\omega_F(z), z \geq 0$ be the modulus of the continuity of the operator $F^{-1} : F(G) \to G$ which exists by Theorem 1.3. Then the following error estimate holds

$$\left\| x_\delta^q - x^* \right\|_{B_1} \leq \omega_F(2\delta). \tag{1.27}$$

In other words, the problem of finding a quasi-solution is stable, and two quasi-solutions are close to each other as long as the error in the data is small.

Proof. Since $\|y^* - y_\delta\|_{B_2} \leq \delta$, then

$$J(x^*) = ||F(x^*) - y_\delta||^2_{B_2} = \|y^* - y_\delta\|^2_{B_2} \leq \delta^2.$$

Since the minimal value of the functional $J(x^*)$ is achieved at the point x_δ^q, then

$$J(x_\delta^q) \leq J(x^*) \leq \delta^2.$$

Hence, $||F(x_\delta^q) - y_\delta||_{B_2} \leq \delta$. Hence,

$$||F(x_\delta^q) - F(x^*)||_{B_2} \leq ||F(x_\delta^q) - y_\delta||_{B_2} + \|y_\delta - F(x^*)\|_{B_2}$$
$$= ||F(x_\delta^q) - y_\delta||_{B_2} + \|y_\delta - y^*\|_{B_2} \leq 2\delta.$$

Thus, we have obtained that $||F(x_\delta^q) - F(x^*)||_{B_2} \leq 2\delta$. Therefore, the definition of the modulus of the continuity of the operator F^{-1} implies (1.27). □

This theorem is very important for justifying the practical value of Theorem 1.3. Still, the notion of the quasi-solution has a drawback. This is because it is unclear how to actually find the target minimizer in practical computations. Indeed, to find it, one should minimize the functional $J(x)$ on the compact set G. The commonly acceptable minimization technique for any least squares functional is via searching points where the Frechét derivative of that functional equals zero. However, the well-known obstacle on this path is that this functional might have multiple local minima and ravines. Therefore, most likely, the norm of the Frechét derivative is sufficiently small at many points of, for example, a ravine. Thus, it is unclear how to practically select a quasi-solution. In other words, we come back again to the first central question of this book: *How to find a good approximation for the exact solution without an advanced knowledge of a small neighborhood of this solution?*

1.6 Regularization

To solve ill-posed problems, regularization methods should be used. In this section, we present main ideas of the regularization. Note that we do not assume in Definition 1.6 that the operator F is defined on a compact set.

Definition 1.6. Let B_1 and B_2 be two Banach spaces and $G \subset B_1$ be a set. Let the operator $F : G \to B_2$ be one-to-one. Consider the equation

$$F(x) = y. \tag{1.28}$$

Let y^* be the ideal noiseless right-hand side of (1.28) and x^* be the ideal noiseless solution corresponding to y^*, $F(x^*) = y^*$. Let $\delta_0 \in (0, 1)$ be a sufficiently small number. For every $\delta \in (0, \delta_0)$ denote

$$K_\delta(y^*) = \{z \in B_2 : \|z - y^*\|_{B_2} \leq \delta\}.$$

Let $\alpha > 0$ be a parameter and $R_\alpha : K_{\delta_0}(y^*) \to G$ be a continuous operator depending on the parameter α. The operator R_α is called the *regularization operator* for (1.28) if there exists a function $\alpha(\delta)$ defined for $\delta \in (0, \delta_0)$ such that

$$\lim_{\delta \to 0} \left\| R_{\alpha(\delta)}(y_\delta) - x^* \right\|_{B_1} = 0.$$

The parameter α is called the regularization parameter. The procedure of constructing the approximate solution $x_{\alpha(\delta)} = R_{\alpha(\delta)}(y_\delta)$ is called the *regularization procedure*, or simply *regularization*.

There might be several regularization procedures for the same problem. This is a simplified notion of the regularization. In our experience, in the case of CIPs, usually $\alpha(\delta)$ is a vector of regularization parameters, for example, the number of iterations, the truncation value of the parameter of the Laplace transform, and the number of finite elements. Since this vector has many coordinates, then its practical choice is usually quite time-consuming. This is because one should choose a proper combination of several components of the vector $\alpha(\delta)$.

The first example of the regularization was Example 2 of Sect. 1.6. We now present the second example. Consider the problem of the solution of the heat equation with the reversed time. Let the function $u(x,t)$ be the solution of the following problem:

$$\begin{aligned} u_t &= u_{xx},\ x \in (0,\pi),\ t \in (0,T), \\ u(x,T) &= y(x) \in L_2(0,\pi), \\ u(0,t) &= u(\pi,t) = 0. \end{aligned}$$

Uniqueness theorem for this and a more general problem is well known and can be found in, for example, the book [124]. Obviously, the solution of this problem, if it exists, is

$$u(x,t) = \sum_{n=1}^{\infty} y_n e^{n^2(T-t)} \sin nx, \tag{1.29}$$

$$y_n = \sqrt{\frac{2}{\pi}} \int_0^\pi y(x) \sin nx \, dx.$$

It is clear, however, that the Fourier series (1.29) converges a narrow class of functions $y(x)$. This is because the numbers $\{e^{n^2(T-t)}\}_{n=1}^{\infty}$ grow exponentially with n.

To regularize this problem, consider the following approximation for the function $u(x,t)$:

$$u_N(x,t) = \sum_{n=1}^{N} y_n e^{n^2(T-t)} \sin nx.$$

Here, $\alpha = 1/N$ is the regularization parameter. To show that this is indeed a regularization procedure in terms of Definition 1.6, we need to consider the following:

Inverse Problem. For each function $f \in L_2(0,\pi)$, consider the solution of the following initial boundary value problem

$$
\begin{aligned}
v_t &= v_{xx},\ x \in (0,\pi),\ t \in (0,T),\\
v(x,0) &= f(x),\\
v(0,t) &= v(\pi,t) = 0.
\end{aligned} \tag{1.30}
$$

Given the function $y(x) = v(x,T)$, determine the initial condition $f(x)$ in (1.30).

Define the operator $F : L_2(0,\pi) \to L_2(0,\pi)$ as $F(f) = v(x,T)$. It is known from the standard PDEs course that

$$
F(f) = v(x,T) = \int_0^\pi G(x,\xi,T) f(\xi)\,\mathrm{d}\xi, \tag{1.31}
$$

$$
G(x,\xi,t) = \sum_{n=1}^{\infty} \mathrm{e}^{-n^2 t} \sin nx \sin n\xi,
$$

where G is the Green's function for the problem (1.30). In other words, we have obtained the integral equation (1.31) of the first kind. Hence, Theorem 1.2 implies that the operator F^{-1} cannot be continuous.

Following the fundamental concept of Tikhonov, let $y^* \in L_2(0,\pi)$ be the "ideal" noiseless function y, which corresponds to the function f^* in (1.30). Let the function $y_\delta \in L_2(0,\pi)$ be such that $\|y_\delta - y^*\|_{L_2(0,\pi)} \le \delta$. Define the regularization parameter $\alpha := 1/N$ and the regularization operator $R_\alpha(y)$ as

$$
R_\alpha(y_\delta)(x) = \sum_{n=1}^{N} y_n \mathrm{e}^{n^2(T-t)} \sin nx, \tag{1.32}
$$

$$
y_n = \sqrt{\frac{2}{\pi}} \int_0^\pi y_\delta(x) \sin nx\,\mathrm{d}x.
$$

Let $f^* \in C^1[0,\pi]$ and $f^*(0) = f^*(\pi) = 0$. The integration by parts leads to

$$
f_n^* = \sqrt{\frac{2}{\pi}} \int_0^\pi f^*(x) \sin nx\,\mathrm{d}x = \frac{1}{n}\sqrt{\frac{2}{\pi}} \int_0^\pi \left(f^*(x)\right)' \cos nx\,\mathrm{d}x.
$$

Hence,

$$
\left(f_n^*\right)^2 \le \frac{\left\|\left(f^*(x)\right)'\right\|^2}{n^2}.
$$

Hence,

$$
\sum_{n=N+1}^{\infty} \left(f_n^*\right)^2 \le \frac{C\left\|\left(f^*(x)\right)'\right\|^2_{L_2(0,\pi)}}{N}, \tag{1.33}
$$

where $C > 0$ is a constant independent on the function f^*. Consider now the function $R_\alpha(y) - f^*$:

$$R_\alpha(y_\delta) - f^* = \sqrt{\frac{2}{\pi}} \sum_{n=1}^{N} \left(y_n - y_n^*\right) e^{n^2 T} \sin nx - \sqrt{\frac{2}{\pi}} \sum_{n=N+1}^{\infty} f_n^* \sin nx.$$

Since functions $\left\{(2/\pi)^{1/2} \sin nx\right\}_{n=1}^{\infty}$ form an orthonormal basis in $L_2(0,\pi)$, then

$$\|R_\alpha(y) - f^*\|^2_{L_2(0,\pi)} \leq e^{2N^2 T} \sum_{n=1}^{N} \left(y_n - y_n^*\right)^2 + \sum_{n=N+1}^{\infty} \left(f_n^*\right)^2.$$

This implies that

$$\|R_\alpha(y) - f^*\|^2_{L_2(0,\pi)} \leq e^{2N^2 T} \delta^2 + \sum_{n=N+1}^{\infty} \left(f_n^*\right)^2. \tag{1.34}$$

The second term in the right-hand side of (1.34) is independent on the level of error δ. However, it depends on the exact solution as well as on the regularization parameter $\alpha = 1/N$. So, the idea of obtaining the error estimate here is to balance these two terms via equalizing them. To do this, we need to impose an a priori assumption first about the maximum of a certain norm of the exact solution f^*. Hence, we assume that $\left\|(f^*)'\right\|^2_{L_2(0,\pi)} \leq M^2$, where M is a priori given positive constant. This means, in particular, that the resulting estimate of the accuracy of the regularized solution will hold uniformly for all functions f^* satisfying this condition. This is a typical scenario in the theory of ill-posed problems and it goes along well with Theorem 1.3.

Using (1.33), we obtain from (1.34)

$$\|R_\alpha(y_\delta) - f^*\|^2_{L_2(0,\pi)} \leq e^{2N^2 T} \delta^2 + \frac{CM^2}{N}. \tag{1.35}$$

The right-hand side of (1.35) contains two terms, which we need to balance by equalizing them:

$$e^{2N^2 T} \delta^2 = \frac{CM^2}{N}.$$

Since $e^{2N^2 T} N \left(CM^2\right)^{-1} < e^{3N^2 T}$ for sufficiently large N, we set

$$e^{3N^2 T} = \frac{1}{\delta^2}.$$

Hence, the regularization parameter is

$$\alpha(\delta) := \frac{1}{N(\delta)} := \left\{ \left[\ln\left(\delta^{-2/3T}\right) \right]^{1/2} \right\}^{-1}.$$

Here, $\{a\}$ denotes the least integer for a number $a > 0$. Thus, (1.35) implies that

$$\|R_\alpha(y_\delta) - f^*\|^2_{L_2(0,\pi)} \leq \delta^{2/3} + \frac{CM^2}{\left[\ln\left(\delta^{-2/3T}\right) \right]^{1/2}}.$$

It is clear that the right-hand side of this inequality tends to zero as $\delta \to 0$. Hence, $R_{\alpha(\delta)}$ is indeed a regularization operator for the above inverse problem.

In simpler terms, the number N of terms of the Fourier series (1.32) rather than $1/N$ is the regularization parameter here. It is also well known from the literature that the number of iterations in an iterative algorithm can serve as a regularization parameter. Since in this chapter we want to outline only main principles of the theory of ill-posed problems rather than working with advanced topics of this theory, we now derive from the above a simple example illustrating that the iteration number can indeed be used as a regularization parameter; see [65, 93, 124, 153] for more advanced examples. Indeed, in principle, we can construct the regularized solution (1.32) iteratively via

$$\begin{aligned} f_1 &= y_1 e^{n^2(T-t)} \sin x, \ f_2 = f_1 + y_2 e^{2^2(T-t)} \sin 2x, ..., \\ f_N &= f_{N-1} + y_N e^{N^2(T-t)} \sin Nx. \end{aligned} \tag{1.36}$$

It is clear from (1.36) that the number of iterations $N = N(\delta)$ can be considered as a regularization parameter here.

1.7 The Tikhonov Regularization Functional

Tikhonov has constructed a general regularization functional which works for a broad class of ill-posed problems [153, 154]. That functional carries his name in the literature. In the current section, we construct this functional and study its properties. We point out that the first stage of the two-stage numerical procedure of this book does not use this functional. The Tikhonov functional has proven to be a very powerful tool for solving ill-posed problems.

1.7.1 The Tikhonov Functional

Let B_1 and B_2 be two Banach spaces. Let Q be another space, $Q \subset B_1$ as a set, and $\overline{Q} = B_1$, where the closure is understood in the norm of the space B_1. In addition, we assume that Q is compactly embedded in B_1. It follows from Theorems 1.1.3.1 and 1.1.3.2 that Q and B_1 are:

(a) $B_1 = L_2(\Omega), Q = H^k(\Omega), \forall k \geq 1$, where $\Omega \subset \mathbb{R}^n$ is a bounded domain.
(b) $B_1 = C^m\left(\overline{\Omega}\right), Q = C^{m+k}\left(\overline{\Omega}\right), \forall m \geq 0, \forall k \geq 1$, where m and k are integers.
(c) $B_1 = C^m\left(\overline{\Omega}\right), Q = H^k(\Omega), k > [n/2] + m$, assuming that $\partial\Omega \in C^k$.

Let $G \subset B_1$ be the closure of an open set. Consider a continuous one-to-one operator $F : G \to B_2$. The continuity here is in terms of the pair of spaces B_1, B_2, rather that in terms of the pair Q, B_2. We are again interested in solving the equation

$$F(x) = y, x \in G. \tag{1.37}$$

Just as above, we assume that the right-hand side of this equation is given with an error of the level δ. Let y^* be the ideal noiseless right-hand side corresponding to the ideal exact solution x^* :

$$F\left(x^*\right) = y^*, \quad \|y - y^*\|_{B_2} < \delta. \tag{1.38}$$

To find an approximate solution of (1.37), we minimize the Tikhonov regularization functional $J_\alpha(x)$:

$$J_\alpha(x) = \frac{1}{2}\|F(x) - y\|^2_{B_2} + \frac{\alpha}{2}\|x - x_0\|^2_Q, \tag{1.39}$$

$$J_\alpha : G \to \mathbb{R}, \quad x_0 \in G,$$

where $\alpha = \alpha(\delta) > 0$ is a small regularization parameter and the point $x_0 \in Q$. In general, the choice of the point x_0 depends on the problem at hands. Usually, x_0 is a good first approximation for the exact solution x^*. Because of this, x_0 is sometimes called the *first guess* or the *first approximation*. The dependence $\alpha = \alpha(\delta)$ will be specified later. The term $\alpha\|x - x_0\|^2_Q$ is called the *Tikhonov regularization term* or simply the *regularization term*. Consider a sequence $\{\delta_k\}_{k=1}^\infty$ such that $\delta_k > 0, \lim_{k\to\infty}\delta_k = 0$. We want to construct sequences $\{\alpha(\delta_k)\}, \left\{x_{\alpha(\delta_k)}\right\}$ such that

$$\lim_{k\to\infty}\left\|x_{\alpha(\delta_k)} - x^*\right\|_{B_1} = 0.$$

Hence, if such a sequence will be constructed, then we will approximate the exact solution x^* in a stable way, and this would correspond well with the second condition of the fundamental concept of Tikhonov.

Using (1.38) and (1.39), we obtain

$$J_\alpha\left(x^*\right) \leq \frac{\delta^2}{2} + \frac{\alpha}{2}\left\|x^* - x_0\right\|_Q^2 \leq \frac{\delta^2}{2} + \frac{\alpha}{2}\left\|x^* - x_0\right\|_Q^2. \tag{1.40}$$

Let

$$m_{\alpha(\delta_k)} = \inf_G J_{\alpha(\delta_k)}(x).$$

By (1.40),

$$m_{\alpha(\delta_k)} \leq \frac{\delta_k^2}{2} + \frac{\alpha(\delta_k)}{2}\left\|x^* - x_0\right\|_Q^2.$$

Hence, there exists a point $x_{\alpha(\delta_k)} \in G$ such that

$$m_{\alpha(\delta_k)} \leq J_{\alpha(\delta_k)}\left(x_{\alpha(\delta_k)}\right) \leq \frac{\delta_k^2}{2} + \frac{\alpha(\delta_k)}{2}\left\|x^* - x_0\right\|_Q^2. \tag{1.41}$$

Hence, by (1.39) and (1.41),

$$\left\|x_{\alpha(\delta_k)} - x_0\right\|_Q^2 \leq \frac{\delta_k^2}{\alpha(\delta_k)} + \left\|x^* - x_0\right\|_Q^2. \tag{1.42}$$

Suppose that

$$\lim_{k\to\infty} \alpha(\delta_k) = 0 \text{ and } \lim_{k\to\infty} \frac{\delta_k^2}{\alpha(\delta_k)} = 0. \tag{1.43}$$

Then (1.42) implies that the sequence $\left\{x_{\alpha(\delta_k)}\right\} \subset G \subseteq Q$ is bounded in the norm of the space Q. Since Q is compactly embedded in B_1, then there exists a subsequence of the sequence $\left\{x_{\alpha(\delta_k)}\right\}$ which converges in the norm of the space B_1. For brevity and without any loss of generality, we assume that the sequence $\left\{x_{\alpha(\delta_k)}\right\}$ itself converges to a point $\overline{x} \in B_1$:

$$\lim_{k\to\infty} \left\|x_{\alpha(\delta_k)} - \overline{x}\right\|_{B_1} = 0.$$

Then (1.41) and (1.43) imply that $\lim_{k\to\infty} J_{\alpha(\delta_k)}\left(x_{\alpha(\delta_k)}\right) = 0$. On the other hand,

$$\begin{aligned}\lim_{k\to\infty} J_{\alpha(\delta_k)}\left(x_{\alpha(\delta_k)}\right) &= \frac{1}{2}\lim_{k\to\infty}\left[\left\|F(x_k) - y_{\delta_k}\right\|_{B_2}^2 + \alpha(\delta_k)\left\|x_{\alpha(\delta_k)} - x_0\right\|_Q^2\right] \\ &= \frac{1}{2}\left\|F(\overline{x}) - y^*\right\|_{B_2}^2.\end{aligned}$$

Hence, $\left\|F(\overline{x}) - y^*\right\|_{B_2} = 0$, which means that $F(\overline{x}) = y^*$. Since the operator F is one-to-one, then $\overline{x} = x^*$. Thus, we have constructed the sequence of regularization parameters $\{\alpha(\delta_k)\}_{k=1}^\infty$ and the sequence $\left\{x_{\alpha(\delta_k)}\right\}_{k=1}^\infty$ such that

$\lim_{k\to\infty}\left\|x_{\alpha(\delta_k)}-x^*\right\|_{B_1}=0$. To ensure (1.43), one can choose, for example, $\alpha(\delta_k)=C\delta_k^{\mu}$, $\mu\in(0,2)$. It is reasonable to call $\left\{x_{\alpha(\delta_k)}\right\}_{k=1}^{\infty}$ *regularizing sequence*.

Note that although both points $x_{\alpha(\delta_k)}$ and x^* belong to the space Q, convergence is proven in a weaker norm of the space B_1, which is typical for ill-posed problems. We point out that the original idea of Theorem 1.3 about compact sets plays a very important role in the above construction. The sequence $\left\{x_{\alpha(\delta_k)}\right\}_{k=1}^{\infty}$ is called *minimizing sequence*. There are two inconveniences in the above construction. First, it is unclear how to find the minimizing sequence computationally. Second, the problem of multiple local minima and ravines of the functional (1.39) presents a significant complicating factor in the goal of the construction of such a sequence.

1.7.2 Regularized Solution

The construction of Sect. 1.7.1 does not guarantee that the functional $J_\alpha(x)$ indeed achieves it minimal value. Suppose now that the functional $J_\alpha(x)$ does achieve its minimal value, $J_\alpha(x_\alpha)=\min_G J_\alpha(x)$, $\alpha=\alpha(\delta)$. Then $x_{\alpha(\delta)}$ is called a *regularized solution* of (1.37) for this specific value $\alpha=\alpha(\delta)$ of the regularization parameter. Let $\delta_0>0$ be a sufficiently small number. Suppose that for each $\delta\in(0,\delta_0)$, there exists an $x_{\alpha(\delta)}$ such that $J_{\alpha(\delta)}\left(x_{\alpha(\delta)}\right)=\min_G J_{\alpha(\delta)}(x)$. Even though one might have several points $x_{\alpha(\delta)}$, we select a single one of them for each $\alpha=\alpha(\delta)$. Indeed, it follows from the construction of Sect. 1.7.1 that all points $x_{\alpha(\delta)}$ are close to the exact solution x^*, as long as δ is sufficiently small. It makes sense now to relax a little bit the definition of Sect. 1.6 of the regularization operator. Namely, instead of the existence of a function $\alpha(\delta)$, we now require the existence of a sequence $\{\delta_k\}_{k=1}^{\infty}\subset(0,1)$ such that

$$\lim_{k\to\infty}\delta_k=0 \text{ and } \lim_{k\to\infty}\left\|R_{\alpha(\delta_k)}\left(y_{\delta_k}\right)-x^*\right\|_{B_1}=0.$$

For each $\delta\in(0,\delta_0)$ and for each y_δ such that $\|y_\delta-y^*\|_{B_2}\leq\delta$, we define the operator $R_{\alpha(\delta)}(y)=x_{\alpha(\delta)}$, where $x_{\alpha(\delta)}$ is a regularized solution. Then it follows from the construction of Sect. 1.7.1 that $R_{\alpha(\delta)}(y)$ is a regularization operator. Hence, the parameter $\alpha(\delta)$ in (1.39) is a regularization parameter for the problem (1.37).

Consider now the case when the space B_1 is a finite dimensional space. Since all norms in finite dimensional spaces are equivalent, we can set $Q=B_1=\mathbb{R}^n$. We denote the standard euclidean norm in $\mathbb{R}^n$ as $\|\cdot\|$. Hence, we assume now that $G\subset\mathbb{R}^n$ is the closure of an open bounded domain. Hence, G is a compact set. Let $x^*\in G$ and $\alpha=\alpha(\delta)$. We have

$$J_{\alpha(\delta)}(x)=\frac{1}{2}\|F(x)-y\|_{B_2}^2+\frac{\alpha(\delta)}{2}\|x-x_0\|^2,$$

$$J_{\alpha(\delta)}:G\to\mathbb{R},\ x_0\in G.$$

By the Weierstrass' theorem, the functional $J_{\alpha(\delta)}(x)$ achieves its minimal value on the set G. Let $x_{\alpha(\delta)}$ be a minimizer of the functional $J_{\alpha(\delta)}(x)$ on G (there might be several minimizers). Then

$$J_{\alpha(\delta)}\left(x_{\alpha(\delta)}\right) \leq J_{\alpha(\delta)}\left(x^*\right) = \frac{1}{2}\left\|F(x^*) - y\right\|_{B_2}^2 + \frac{\alpha}{2}\left\|x^* - x_0\right\|^2$$
$$\leq \frac{\delta^2}{2} + \frac{\alpha(\delta)}{2}\left\|x^* - x_0\right\|^2.$$

Hence,

$$\left\|x_{\alpha(\delta)} - x_0\right\| \leq \sqrt{\frac{\delta^2}{\alpha} + \left\|x^* - x_0\right\|^2} \leq \frac{\delta}{\sqrt{\alpha}} + \left\|x^* - x_0\right\|. \tag{1.44}$$

Since $\left\|x_{\alpha(\delta)} - x_0\right\| \geq \left\|x_{\alpha(\delta)} - x^*\right\| - \left\|x^* - x_0\right\|$, then we obtain from (1.44)

$$\left\|x_{\alpha(\delta)} - x^*\right\| \leq \frac{\delta}{\sqrt{\alpha}} + 2\left\|x^* - x_0\right\|. \tag{1.45}$$

An important conclusion from (1.45) is that for a given pair $(\delta, \alpha(\delta))$, the accuracy of the regularized solution is determined by the accuracy of the first guess x_0. This becomes even more clear when we recall that by (1.43), we should have $\lim_{\delta\to 0}\left(\delta/\sqrt{\alpha}\right) = 0$. This once again points toward the importance of the first central question of this book.

1.8 The Accuracy of the Regularized Solution for a Single Value of α

It was proven in Sect. 1.7.1 that the regularizing sequence $\left\{x_{\alpha(\delta_k)}\right\}_{k=1}^{\infty}$ converges to the exact solution x^* provided that $\lim_{k\to\infty}\delta_k = 0$. However, $\left\{x_{\alpha(\delta_k)}\right\}_{k=1}^{\infty}$ is only a subsequence of a certain sequence, which is inconvenient for computations. In addition, in practical computations, one always works only with a single value of the noise level δ and with a single value of the regularization parameter $\alpha(\delta)$. In these computations, people naturally work with finite dimensional spaces, in which the existence of a regularized solution is guaranteed; see Sect. 1.7.2. Naturally, one would want the regularized solution to be more accurate than the first guess for a single pair $(\delta, \alpha(\delta))$. It has been often observed in numerical studies of many researchers that even though parameters δ and $\alpha(\delta)$ are fixed, the regularized solution $x_{\alpha(\delta)}$ is indeed closer to the exact solution x^* than the first approximation x_0. The first analytical proof of this phenomenon was presented in the work [111]. Basically, Theorem 2 of [111] states that the regularized solution is indeed closer to the exact one than the first approximation in the case when uniqueness theorem

holds for the original ill-posed problem. In this section, we present the main idea of [111]. An application of this idea to specific CIPs can be found in [111].

We assume that conditions of Sect. 1.7.1 which were imposed there on spaces and the operator F hold. Consider again the equation

$$F(x) = y,\ x \in G. \tag{1.46}$$

Just as above, we assume that the right-hand side of this equation is given with an error of the level δ. Let y^* be the ideal noiseless data corresponding to the ideal solution x^*:

$$F\left(x^*\right) = y^*, \quad \|y - y^*\|_{B_2} \leq \delta. \tag{1.47}$$

To find an approximate solution of (1.46), we minimize the Tikhonov regularization functional $J_\alpha(x)$:

$$J_\alpha(x) = \frac{1}{2}\|F(x) - y\|_{B_2}^2 + \frac{\alpha}{2}\|x - x_0\|_Q^2, \tag{1.48}$$

$$J_\alpha : G \to \mathbb{R}, x_0 \in G.$$

Since it is unlikely that one can get a better accuracy of the solution than δ, then it is usually acceptable that all other parameters involved in the regularization process are much larger than δ. For example, let the number $\mu \in (0,1)$. Since $\lim_{\delta \to 0}\left(\delta^{2\mu}/\delta^2\right) = \infty$, then there exists a sufficiently small number $\delta_0(\mu) \in (0,1)$ such that $\delta^{2\mu} > \delta^2, \forall \delta \in (0, \delta_0(\mu))$. Hence, we choose below in this section

$$\alpha(\delta) = \delta^{2\mu}, \mu \in (0,1). \tag{1.49}$$

We introduce the dependence (1.49) for the sake of definiteness only. In fact, other dependencies $\alpha(\delta)$ are also possible. Let $m_{\alpha(\delta)} = \inf_G J_{\alpha(\delta)}(x)$. Then

$$m_{\alpha(\delta)} \leq J_{\alpha(\delta)}\left(x^*\right). \tag{1.50}$$

Let $\dim B_1 = \infty$. As it was noticed in the beginning of Sect. 1.7.2, we cannot prove the existence of a minimizer of the functional J_α in this case. Hence, we work now with the minimizing sequence. It follows from (1.48) and (1.50) that there exists a sequence $\{x_n\}_{n=1}^\infty \subset G$ such that

$$m_{\alpha(\delta)} \leq J_{\alpha(\delta)}(x_n) \leq \frac{\delta^2}{2} + \frac{\alpha}{2}\|x^* - x_0\|_Q^2 \text{ and } \lim_{n\to\infty} J_{\alpha(\delta)}(x_n) = m(\delta). \tag{1.51}$$

By (1.42) and (1.51),

$$\|x_n\|_Q \leq \left(\frac{\delta^2}{\alpha} + \|x^* - x_0\|_Q^2\right)^{1/2} + \|x_0\|_Q. \tag{1.52}$$

Hence, it follows from (1.49) and (1.52) that $\{x_n\}_{n=1}^{\infty} \subset K(\delta, x_0)$, where $K(\delta, x_0) \subset Q$ is a precompact set in B_1 defined as

$$K(\delta, x_0) = \left\{ x \in Q : \|x\|_Q \leq \sqrt{\delta^{2(1-\mu)} + \|x^* - x_0\|_Q^2} + \|x_0\|_Q \right\}. \tag{1.53}$$

Note that the sequence $\{x_n\}_{n=1}^{\infty}$ depends on δ. Let $\overline{K}(\delta, x_0)$ be the closure of the set $K(\delta, x_0)$ in the norm of the space B_1. Hence, $\overline{K}(\delta, x_0)$ is a closed compact set in B_1.

Theorem 1.8 ([111]). *Let B_1 and B_2 be two Banach spaces. Let Q be another Banach space and $Q \subset B_1$ as a set. Assume that $\overline{Q} = B_1$ and Q is compactly embedded in B_1. Let $G \subseteq Q$ be a convex set and $F : G \to B_2$ be a one-to-one operator, continuous in terms of norms $\|\cdot\|_{B_1}, \|\cdot\|_{B_2}$. Consider the problem of solution of (1.46). Let y^* be the ideal noiseless right-hand side of (1.46) and x^* be the corresponding exact solution of (1.46), $F(x^*) = y^*$. Let $\|y - y^*\|_{B_2} \leq \delta$. Consider the Tikhonov functional (1.48), assume that (1.49) holds and that $x_0 \neq x^*$. Let $\{x_n\}_{n=1}^{\infty} \subset K(\delta, x_0) \subseteq \overline{K}(\delta, x_0)$ be a minimizing sequence of the functional (1.48) satisfying (1.52). Let $\xi \in (0,1)$ be an arbitrary number. Then there exists a sufficiently small number $\delta_0 = \delta_0(\xi) \in (0,1)$ such that for all $\delta \in (0, \delta_0)$, the following inequality holds:*

$$\|x_n - x^*\|_{B_1} \leq \xi \|x_0 - x^*\|_Q, \forall n. \tag{1.54}$$

In particular, if $\dim B_1 < \infty$, then all norms in B_1 are equivalent. In this case, we set $Q = B_1$. Then a regularized solution $x_{\alpha(\delta)}$ exists (Sect. 1.7.2) and (1.54) becomes

$$\left\|x_{\alpha(\delta)} - x^*\right\|_{B_1} \leq \xi \|x_0 - x^*\|_{B_1}. \tag{1.55}$$

In the case of noiseless data with $\delta = 0$, the assertion of this theorem remains true if one replaces above $\delta \in (0, \delta_0)$ with $\alpha \in (0, \alpha_0)$, where $\alpha_0 = \alpha_0(\xi) \in (0,1)$ is sufficiently small.

Proof. Note that if $x_0 = x^*$, then the exact solution is found, and all $x_n = x^*$. So this is not an interesting case to consider. By (1.47), (1.48), and (1.50),

$$\|F(x_n) - y\|_{B_2} \leq \sqrt{\delta^2 + \alpha \|x_0 - x^*\|_Q^2} = \sqrt{\delta^2 + \delta^{2\mu} \|x_0 - x^*\|_Q^2}.$$

Hence,

$$\begin{aligned} \left\|F(x_n) - F\left(x^*\right)\right\|_{B_2} &= \left\|(F(x_n) - y) + \left(y - F\left(x^*\right)\right)\right\|_{B_2} \\ &= \left\|(F(x_n) - y) + \left(y - y^*\right)\right\|_{B_2} \\ &\leq \|F(x_n) - y\|_{B_2} + \|y - y^*\|_{B_2} \\ &\leq \sqrt{\delta^2 + \delta^{2\mu} \|x^* - x_0\|_1^2} + \delta. \end{aligned} \tag{1.56}$$

By Theorem 1.3, there exists the modulus of the continuity $\omega_F(z)$ of the operator

$$F^{-1} : F\left(\overline{K}(\delta, x_0)\right) \to \overline{K}(\delta, x_0).$$

By (1.56),

$$\|x_n - x^*\|_{B_1} \leq \omega_F\left(\sqrt{\delta^2 + \delta^{2\mu}\|x_0 - x^*\|_Q^2} + \delta\right). \tag{1.57}$$

Consider an arbitrary $\xi \in (0,1)$. Then one can choose the number $\delta_0 = \delta_0(\xi)$ so small that

$$\omega_F\left(\sqrt{\delta^2 + \delta^{2\mu}\|x^* - x_0\|_Q^2} + \delta\right) \leq \xi\|x_0 - x^*\|_Q, \forall \delta \in (0, \delta_0). \tag{1.58}$$

The estimate (1.54) follows from (1.57) and (1.58). The proof for the case $\delta = 0$ is almost identical with the above. □

Thus, a simple conclusion from Theorem 1.8 is that if a uniqueness theorem holds for an ill-posed problem and the level of the error δ is sufficiently small, then the minimization of the Tikhonov functional leads to a refinement of the first guess x_0 even for a single value of the regularization parameter. This explains why the second stage of the two-stage numerical procedure of this book refines the solution obtained on the first stage.

In estimates (1.54) and (1.55) the number ξ is not specified. We now want to specify the dependence ξ from δ. To do this, we need to impose an additional assumption on the function $\omega(z)$. In fact, this assumption requires the proof of the Lipschitz stability of the problem (1.46) on the compact set $\overline{K}(\delta, x_0)$. However, in order to simplify the presentation, we do not prove the Lipschitz stability of CIPs in this book. We refer to, for example, works [14, 32, 33, 62, 79–81, 104, 161], where the Lipschitz stability was established for some CIPs via the method of Carleman estimates; see Sect. 1.10 for this method.

Corollary 1.8. *Assume that conditions of Theorem 1.8 are satisfied. Let $\omega_F(z)$ be the modulus of the continuity of the operator $F^{-1} : F\left(\overline{K}(\delta, x_0)\right) \to \overline{K}(\delta, x_0)$. Let the function $\omega_F(z)$ be such that $\omega_F(z) \leq Cz, \forall z \geq 0$ with a positive constant C* independent on *z. Then there exists a sufficiently small number $\delta_0 > 0$ such that for all $\delta \in (0, \delta_0)$ (1.54) becomes*

$$\|x_n - x^*\|_{B_1} \leq 3C\delta^{\mu}\|x_0 - x^*\|_Q,$$

and (1.55) becomes

$$\|x_n - x^*\|_{B_1} \leq 3C\delta^{\mu}\|x_0 - x^*\|_{B_1}.$$

In the case of the noiseless data with $\delta = 0$, one should replace δ^{μ} with α in these estimates.

Proof. It was assumed in Theorem 1.8 that $\|x^* - x_0\|_Q \neq 0$. Since, $\delta < \delta^\mu \|x^* - x_0\|_Q$ for sufficiently small δ, then for $\delta \in (0, \delta_0)$,

$$\sqrt{\delta^2 + \delta^{2\mu} \|x^* - x_0\|_Q^2} + \delta \leq \delta + \delta^\mu \|x^* - x_0\|_Q + \delta < 3\delta^\mu \|x^* - x_0\|.$$

Hence,

$$\omega_F \left(\sqrt{\delta^2 + \delta^{2\mu} \|x^* - x_0\|_Q^2} + \delta \right) \leq 3C\delta^\mu \|x^* - x_0\|, \delta \in \left(0, \overline{\delta}\right).$$

The rest of the proof follows from (1.57). □

1.9 Global Convergence in Terms of Definition 1.1.2.4

The goal of this section is to show that the two-stage numerical procedure of this book converges globally to the exact solution in the classical sense in terms of Definition 1.1.2.4. In other words, it converges globally within the frameworks of the pair of approximate mathematical models (M_1, M_2). Since we discuss in this section the two-stage numerical procedure (rather than the first stage only), we rely here on assumption 1.1.2. First, we need to prove that if the locally convergent numerical method of the second stage is based on the minimization of the Tikhonov functional, then it does not face the problem of local minima and ravines in a small neighborhood of the exact solution.

Consider a nonlinear ill-posed problem. Suppose that a numerical method for this problem is approximately globally convergent in terms of Definition 1.1.2.1. Then this method ends up with a good approximation $x_0 := x_{\text{glob}}$ for the element $x^* \in B$. The element x^* represents the unique exact solution of this problem within the framework of the approximate mathematical model M_1. To refine x_{glob}, we apply a locally convergent method satisfying conditions of Definition 1.1.2.3. Consider now the approximate mathematical model M_2 associated with the numerical method of this definition. Let the corresponding k-dimensional Banach space be $B_k \subseteq B, \dim B_k = k < \infty$. Let $x_{\text{glob}}, x^* \in B_k$. We want to refine the solution x_{glob}, which is obtained on the first stage, via the minimization of the Tikhonov functional in which the starting point of iterations would be $x_0 := x_{\text{glob}}$. We anticipate that this refinement would provide a better approximation for the exact solution x^*.

Almost any minimization procedure of a least squares functional is based on a version of the gradient method, which is a locally convergent one. The gradient method stops at a point where a certain norm of the gradient is close to zero. Hence, if this Tikhonov functional has local minima in any neighborhood of x^*, then any version of the gradient method can stop at any of those minima. However, it is unclear which of these minima should be selected as a regularized solution. On the other hand, a strongly convex functional does not have local minima. Furthermore, it

is well known that if a functional is strongly convex on an open set and if it achieves its minimal value on this set, then the point of this minimum is unique, and the gradient method converges to it; see, for example, [128, 137].

Suppose that the Tikhonov functional is strongly convex in a certain small neighborhood of the point $x^* \in B_k$ (i.e., locally strongly convex). In addition, let both the regularized solution and x_{glob} belong to the interior of this neighborhood. Then local minima do not occur on the refinement stage, provided that x_{glob} is the starting point of iterations for this stage. Theorem 3.1 of [29] claims the local strong convexity of this functional in a small neighborhood of a regularized solution. In Theorem 1.9.1.2, we extend that result of [29] to the case of a small neighborhood of the exact solution x^*. In addition, we use here Theorem 1.8, which was not used in [29]. Based on Theorem 1.9.1.2, we conclude in Sect. 1.9.2 that the two-stage numerical procedure of this book converges globally in the classical sense in terms of Definition 1.1.2.4.

The local strong convexity of the Tikhonov functional was also proved in earlier publications [139, 140]. These works require the continuity of the second Fréchet derivative of the original operator F. Unlike this, we require the Lipschitz continuity of the first Fréchet derivative, which is easier to verify for CIPs.

1.9.1 The Local Strong Convexity

First, we remind the notion of the Fréchet derivative [113].

Definition 1.9.1 ([113]). Let B_1 and B_2 be two Banach spaces and $\mathcal{L}(B_1, B_2)$ be the space of bounded linear operators mapping B_1 into B_2. Let $G \subseteq B_1$ be a convex set containing interior points and $A : G \to B_2$ be an operator. Let $x \in G$ be an interior point of the set G. Let $x \in G$ be an interior point of G. Assume that

$$A(x+h) = A(x) + \left(A'(x), h\right) + \varepsilon(x,h), \forall h : x + h \in G,$$

where the operator $A'(x) \in \mathcal{L}(B_1, B_2)$ and $(A'(x), h)$ means that $A'(x)$ acts on h. Assume that

$$\lim_{\|h\|_{B_1} \to 0} \frac{\|\varepsilon(x,h)\|_{B_2}}{\|h\|_{B_1}} = 0.$$

Then the bounded linear operator $A'(x) : B_1 \to B_2$ is called the Fréchet derivative of the operator A at the point x.

Assume that the Fréchet derivative of the operator A exists for all interior points $x \in G$, and it is continuous in terms of the norm of the space $\mathcal{L}(B_1, B_2)$. Let interior points $x, z \in G$. Since G is convex, then the entire segment of the straight line connecting these two points also belongs to G. The following formula is valid:

$$A(x) - A(z) = \int_0^1 \left(A'(z + \theta(x - z)), x - z\right) d\theta. \tag{1.59}$$

Let B be a Banach space, $G \subseteq B$ be a convex set, and $J : G \to \mathbb{R}$ be a functional. The functional J is called *strongly convex* on the set G if there exists a constant $\kappa > 0$ such that for any two interior points $x, z \in G$ and for any number $\lambda \in [0,1]$, the following inequality holds [128]:

$$\kappa \frac{\lambda(1-\lambda)}{2} \|x-z\|_B^2 + J(\lambda x + (1-\lambda) z) \leq \lambda J(x) + (1-\lambda) J(z).$$

The following theorem is well known:

Theorem 1.9.1.1 ([128]). *Let H be a Hilbert space, $G \subseteq H$ be a convex set containing interior points, and $J : G \to \mathbb{R}$ be a functional. Suppose that this functional has the Fréchet derivative $J'(x) \in \mathcal{L}(H, \mathbb{R})$ for any interior point $x \in G$. Then the strong convexity of J on the set G is equivalent with the following condition:*

$$\left(J'(x) - J'(z), x - z\right) \geq 2\rho \|x-z\|^2, \forall x, z \in G, \tag{1.60}$$

where $\rho > 0$ is the strong convexity constant.

Consider now the case when $B_1 = H_1$ and $B_2 = H_2$ are two Hilbert spaces. In order not to work with a stronger norm of the regularization term in the Tikhonov functional, we assume that $\dim H_1 < \infty$ since all norms in a finite dimensional Banach space are equivalent. Denote norms in H_1 and H_2 as $\|\cdot\|$ and $\|\cdot\|_2$, respectively. The norm in the space of bounded linear operators $\mathcal{L}(H_1, H_2)$ we also denote in this section as $\|\cdot\|$ for brevity. It will always be clear from the context of this section whether the sign $\|\cdot\|$ is related to an element of H_1 or to an element of $\mathcal{L}(H_1, H_2)$. Let $G \subseteq H_1$ be a bounded closed convex set and $\widetilde{F} : G \to H_2$ be a continuous operator. Similarly with (1.46), consider the problem of the solution of the equation $\widetilde{F}(x) = y, x \in G$. We again assume that the element y (which we call "the data") is given with an error, $\|y - y^*\|_2 \leq \delta$, where y^* is the exact right-hand side of this equation, which corresponds to its exact solution $x^* \in G$, $\widetilde{F}(x^*) = y^*$. It is convenient to replace in this section the operator $\widetilde{F}$ with $F : G \to H_2$ defined as $F(x) = \widetilde{F}(x) - y$. Hence, we consider the equation

$$F(x) = 0, x \in G, \tag{1.61}$$

where

$$\left\|F\left(x^*\right)\right\|_2 \leq \delta. \tag{1.62}$$

Let the point $x_0 \in G$. Consider the Tikhonov functional corresponding to (1.61):

$$J_\alpha(x) = \frac{1}{2}\|F(x)\|_2^2 + \frac{\alpha}{2}\|x - x_0\|^2. \tag{1.63}$$

For any $\beta > 0$ and for any $x \in H_1$, denote $V_\beta(x) = \{z \in H_1 : \|x - z\| < \beta\}$.

Theorem 1.9.1.2. *Let H_1 and H_2 be two Hilbert spaces,* $\dim H_1 < \infty, G \subset H_1$ *be a closed bounded convex set containing interior points, and $F : G \to H_2$ be a continuous one-to-one operator. Let $x^* \in G$ be the exact solution of (1.61) with the exact data and $\delta \in (0,1)$ be the error in the data . Let (1.62) be satisfied and $V_1(x^*) \subset G$. Assume that for every $x \in V_1(x^*)$, the operator F has the Fréchet derivative $F'(x) \in \mathcal{L}(H_1, H_2)$. Suppose that this derivative is uniformly bounded and Lipschitz continuous in $V_1(x^*)$, i.e.,*

$$\|F'(x)\| \leq N_1, \ \forall x \in V_1(x^*), \tag{1.64}$$

$$\|F'(x) - F'(z)\| \leq N_2 \|x - z\|, \ \forall x, z \in V_1(x^*), \tag{1.65}$$

where $N_1, N_2 = const. > 0$. Let

$$\alpha = \alpha(\delta) = \delta^{2\mu}, \quad \forall \delta \in (0,1), \tag{1.66}$$

$$\mu = const. \in \left(0, \frac{1}{4}\right). \tag{1.67}$$

Then there exists a sufficiently small number $\delta_0 = \delta_0(N_1, N_2, \mu) \in (0,1)$ such that for all $\delta \in (0, \delta_0)$, the functional $J_{\alpha(\delta)}(x)$ is strongly convex in the neighborhood $V_{\alpha(\delta)}(x^*)$ of the exact solution x^* with the strong convexity constant $\alpha/4$. Next, let in (1.63) the first guess x_0 for the exact solution x^* be so accurate that

$$\|x_0 - x^*\| < \frac{\delta^{3\mu}}{3}. \tag{1.68}$$

Then there exists the unique regularized solution $x_{\alpha(\delta)}$ of (1.61) and $x_{\alpha(\delta)} \in V_{\delta^{3\mu}/3}(x^*)$. In addition, the gradient method of the minimization of the functional $J_{\alpha(\delta)}(x)$, which starts at x_0, converges to $x_{\alpha(\delta)}$. Furthermore, let $\xi \in (0,1)$ be an arbitrary number. Then there exists a number $\delta_1 = \delta_1(N_1, N_2, \mu, \xi) \in (0, \delta_0)$ such that

$$\left\|x_{\alpha(\delta)} - x^*\right\| \leq \xi \|x_0 - x^*\|, \ \forall \delta \in (0, \delta_1). \tag{1.69}$$

In other words, the regularized solution $x_{\alpha(\delta)}$ provides a better accuracy than the first guess x_0.

Remark 1.9.1. Consider now the noiseless case with $\delta = 0$. Then one should replace in this theorem $\delta_0 = \delta_0(N_1, N_2, \mu) \in (0,1)$ with $\alpha_0 = \alpha_0(N_1, N_2) \in (0,1)$ to be sufficiently small and require that $\alpha \in (0, \alpha_0)$.

Proof of Theorem 1.9.1.2. For any point $x \in V_1(x^*)$, let $F'^*(x)$ be the linear operator, which is adjoint to the operator $F'(x)$. By (1.63), the Fréchet derivative of the functional $J_\alpha(x)$ acts on the element $u \in H_1$ as

$$\left(J'_\alpha(x), u\right) = \left(F'^*(x) F(x) + \alpha(x - x_0), u\right), \ \forall x \in G, \forall u \in H_1.$$

Consider two arbitrary points $x, z \in V_{\delta^{3\mu}}(x^*)$. We have

$$\begin{aligned}\left(J'_\alpha(x) - J'_\alpha(z), x - z\right) &= \alpha\|x - z\|^2 + \left(F'^*(x)F(x) - F'^*(z)F(z), x - z\right)\\ &= \alpha\|x - z\|^2 + \left(F'^*(x)F(x) - F'^*(x)F(z), x - z\right)\\ &\quad + \left(F'^*(x)F(z) - F'^*(z)F(z), x - z\right).\end{aligned}$$

Denote

$$\begin{aligned}A_1 &= \left(F'^*(x)F(x) - F'^*(x)F(z), x - z\right),\\ A_2 &= \left(F'^*(x)F(z) - F'^*(z)F(z), x - z\right).\end{aligned}$$

Then

$$\left(J'_\alpha(x) - J'_\alpha(z), x - z\right) = \alpha\|x - z\|^2 + A_1 + A_2. \tag{1.70}$$

Estimate A_1, A_2 from the below. Since

$$A_1 = A_1 - \left(F'^*(x)F'(x)(x - z), x - z\right) + \left(F'^*(x)F'(x)(x - z), x - z\right),$$

then by (1.59),

$$\begin{aligned}A_1 &= \left(F'^*(x)\left(\int_0^1 \left(F'(z + \theta(x - z)) - F'(x), x - z\mathrm{d}\theta\right)\right), x - z\right)\\ &\quad + \left(F'^*(x)F'(x)(x - z), x - z\right).\end{aligned} \tag{1.71}$$

Since $\|A\| = \|A^*\|, \forall A \in \mathcal{L}(H_1, H_2)$, then using (1.64) and (1.65), we obtain

$$\begin{aligned}&\left|\left(F'^*(x)\left(\int_0^1 \left(F'(z + \theta(x - z)) - F'(x), x - z\mathrm{d}\theta\right)\right), x - z\right)\right|\\ &\quad\le \left\|F'(x)\right\| \int_0^1 \left\|F'(z + \theta(x - z)) - F'(x), x - z\right\|_2 \mathrm{d}\theta \cdot \|x - z\|\\ &\quad\le \frac{1}{2}N_1N_2\|x - z\|^3.\end{aligned}$$

Next,

$$\begin{aligned}\left(F'^*(x)F'(x)(x - z), x - z\right) &= \left(F'(x)(x - z), F'(x)(x - z)\right)_2\\ &= \left\|F'(x)(x - y)\right\|_2^2 \ge 0,\end{aligned}$$

where $(,)_2$ is the scalar product in H_2. Hence, using (1.71), we obtain

$$A_1 \geq -\frac{1}{2} N_1 N_2 \|x-z\|^3 . \tag{1.72}$$

Now we estimate A_2 :

$$|A_2| \leq \|F(z)\|_2 \left\|F'(x) - F'(z)\right\| \|x-z\| \leq N_2 \|x-z\|^2 \|F(z)\|_2 .$$

By (1.59) and (1.64),

$$\|F(z)\|_2 \leq \left\|F(z) - F\left(x^*\right)\right\|_2 + \left\|F\left(x^*\right)\right\|_2 \leq N_1 \|z-x^*\| + \left\|F\left(x^*\right)\right\|_2 .$$

Hence, using (1.62), we obtain

$$|A_2| \leq N_2 \|x-z\|^2 \left(N_1 \|z-x^*\| + \left\|F\left(x^*\right)\right\|_2\right) \leq N_2 \|x-z\|^2 \left(N_1 \delta^{3\mu} + \delta\right).$$

Thus,

$$A_2 \geq -N_2 \|x-z\|^2 \left(N_1 \delta^{3\mu} + \delta\right). \tag{1.73}$$

By (1.66) and (1.67), we can choose $\delta_0 = \delta_0(N_1, N_2, \mu) \in (0,1)$ and $\tau = \tau(N_1, N_2) \in (0,1)$ so small that

$$\left(N_1 \delta^{3\mu} + \delta\right) \leq 2 N_1 \delta^{3\mu}. \tag{1.74}$$

Combining (1.73) and (1.74) with (1.66)–(1.70) and (1.72) and recalling that $x, z \in V_{\delta^{3\mu}}(x^*)$, we obtain

$$\begin{aligned}
\left(J'_\alpha(x) - J'_\alpha(z), x-z\right) &\geq \|x-z\|^2 \left[\alpha - \frac{N_1 N_2}{2} \|x-z\| - 2 N_1 N_2 \delta^{3\mu}\right] \\
&\geq \|x-z\|^2 \left[\delta^{2\mu} - \frac{5}{2} N_1 N_2 \delta^{3\mu}\right] \\
&\geq \frac{\delta^{2\mu}}{2} \|x-z\|^2 = \frac{\alpha}{2} \|x-z\|^2 .
\end{aligned}$$

Combing this with Theorem 1.9.1.1, we obtain the assertion about the strong convexity.

Since G is a closed bounded set in the finite dimensional space H_1, then there exists a minimizer $x_{\alpha(\delta)} \in G$ of the functional $J_{\alpha(\delta)}$ in (1.63). Combining (1.45) with (1.66), (1.67), and (1.68) and decreasing, if necessary, δ_0, we obtain for $\delta \in (0, \delta_0)$

$$\left\|x_{\alpha(\delta)} - x^*\right\| \leq \frac{\delta}{\sqrt{\alpha}} + 2\left\|x^* - x_0\right\| < \delta^{1-\mu} + \frac{2}{3}\delta^{3\mu}$$
$$= \frac{2}{3}\delta^{3\mu}\left(1 + \frac{3}{2}\delta^{1-4\mu}\right) < \frac{2}{3}\delta^{3\mu} \cdot \frac{3}{2} = \delta^{3\mu}.$$

Thus,

$$\left\|x_{\alpha(\delta)} - x^*\right\| < \delta^{3\mu}.$$

The latter implies that $x_{\alpha(\delta)} \in V_{\delta^{3\mu}}(x^*)$. Since the functional J_α is strongly convex on the set $V_{\delta^{2\mu}}(x^*)$, the set $V_{\delta^{3\mu}}(x^*) \subset V_{\delta^{2\mu}}(x^*)$ for sufficiently small δ and the minimizer $x_{\alpha(\delta)} \in V_{\delta^{3\mu}}(x^*)$, then this minimizer is unique. Furthermore, since by (1.68) the point $x_0 \in V_{\delta^{3\mu}}(x^*)$, then it is well known that the gradient method with its starting point at x_0 converges to the minimizer $x_{\alpha(\delta)}$; see, for example, [137].

Let $\xi \in (0,1)$ be an arbitrary number. By Theorem 1.8 we can choose

$$\delta_1 = \delta_1(N_1, N_2, \mu, \xi) \in (0, \delta_0),$$

so small that

$$\left\|x_{\alpha(\delta)} - x^*\right\| \leq \xi \left\|x_0 - x^*\right\|, \forall \delta \in (0, \delta_1),$$

which proves (1.69). Hence, (1.68) implies that $x_{\alpha(\delta)} \in V_{\delta^{3\mu}/3}(x^*)$. □

1.9.2 The Global Convergence

One of main points of this book is the two-stage numerical procedure for certain CIPs, which addresses both central questions posed in the beginning of Sect. 1.1. This procedure was developed in [25–29, 115, 116, 160]. In this section, we briefly present some arguments showing that this procedure converges globally to the exact solution in terms of Definition 1.1.2.4. Corresponding theorems and numerical confirmations are presented in Chaps. 2–6. Consider one of CIPs of this book.

- On the first stage, a numerical method with the approximate global convergence property (Definition 1.1.2.1) ends up with a function $c_{\text{glob}}(x)$. Let $c^*(x) \in B$ be the exact solution of this CIP. Then corresponding approximate global convergence theorems of either Chap. 2 or Chap. 6 guarantee that the function c_{glob} provides a sufficiently good approximation for c^*.
- On the second stage, we use an approximate mathematical model M_2 to minimize the Tikhonov functional (1.63) associated with our CIP. In the case of the adaptive finite element method (FEM) this model basically means the assumption that the solution belongs to a finite dimensional space generated by all linear combinations of standard piecewise linear finite elements (see details in Chap. 4). This space is equipped with the norm $\|\cdot\|_{L_2(\Omega)}$. In the case when the Tikhonov functional is minimized via the finite difference method (FDM) (Chap. 6), this

model means a finite number of grid points in the finite difference scheme and a finite dimensional space associated with it; see, for example, [146] for this space. In any of these two cases, we have the finite dimensional Hilbert space H_1. We assume that $H_1 \subset B$ as a set, $\|\cdot\|_{H_1} \leq \|\cdot\|_B$ and $c_{\text{glob}} \in H_1$. Also, $c^* \in H_1$ (assumption 1.1.2). Following Definition 1.1.2.4 we assume that in (1.2) $x_n := c_n$ and $\varepsilon \in (0, \rho]$. Here, ρ is the number of Definition 1.1.2.3, and functions c_n are obtained in our iterative process of the numerical method of the first stage. Let $\delta \in (0, \delta_0)$ be the level of the error in the data. Let the number $\rho \in \left(0, \delta^{3\mu}/3\right)$, where the numbers δ_0, μ were defined in Theorem 1.9.1.2 Then (1.2) implies that

$$\left\|c_{\text{glob}} - c^*\right\|_{H_1} < \frac{\delta^{3mu}}{3},$$

which is exactly (1.68) with $x_0 := c_{\text{glob}}, x^* := c^*$. Theorem 1.9.1.2 implies that the regularized solution $c_{\alpha(\delta)}$ exists, and it is unique. Furthermore, (1.69) of Theorem 1.9.1.2 ensures that

$$\left\|c_{\alpha(\delta)} - c^*\right\|_{H_1} < \left\|c_{\text{glob}} - c^*\right\|_{H_1} < \frac{\delta^{3\mu}}{3}.$$

Next, again by Theorem 1.9.1.2, the gradient method of the minimization of the Tikhonov functional with its starting point c_{glob} converges to $c_{\alpha(\delta)}$. Thus, in the limiting case of $\delta \to 0$, we arrive at the exact solution c^*.

- Therefore the two-stage numerical procedure of this book converges globally in the classical sense within frameworks of the pair of approximate mathematical models (M_1, M_2), as described in Definition 1.1.2.4.
- In addition, extensive numerical and experimental studies of follow-up chapters demonstrate that conditions of the informal Definition 1.1.2.2 are also in place.

1.10 Uniqueness Theorems for Some Coefficient Inverse Problems

1.10.1 Introduction

This section is devoted to a short survey of currently known uniqueness theorems for CIPs with the data resulting from a single measurement. As it is clear from the construction of Sect. 1.7.1 as well as from Theorems 1.3, 1.8, and 1.9.1.2, the question of the uniqueness is a very important one for, for example, a justification of the validity of numerical methods for ill-posed problems. Before 1981, only the so-called "local" uniqueness theorems were known for multidimensional CIPs with single measurement data. The word "local" in this case means that it was assumed in these theorems that either the unknown coefficient is sufficiently small, or it is piecewise analytic with respect to at least one variable, or that this coefficient can

be represented in a special form, or that the CIP is linearized near the constant background [124, 143]. The absence of "global" uniqueness results for these CIPs was one of main stumbling blocks of the entire theory of inverse problems at that time. The term "global" means here that the main assumption about the unknown coefficient should be that it belongs to one of main functional spaces, for example, C^k, H^k. In addition, one might probably impose some mild additional assumptions, for example, positivity. But one should not impose abovementioned "local" assumptions.

For the first time, the question about global uniqueness theorems was addressed positively and for a broad class of CIPs with single measurement data in the works of A.L. Bukhgeim and M.V. Klibanov in 1981. First, these results were announced in their joint paper [43]. The first complete proofs were published in two separate papers [44, 95] in the same issue of proceedings. This technique is now called the "Bukhgeim-Klibanov method." Currently, this method is the only one enabling for proofs of global uniqueness results for multidimensional CIPs with single measurement data. Note that the idea of the "elimination" of the unknown coefficient from the governing PDE via the differentiation, which is used in our approximately globally convergent numerical method (Chaps. 2 and 6), was originated by the Bukhgeim-Klibanov method.

The Bukhgeim-Klibanov method is based on the idea of applications of the so-called Carleman estimates to proofs of uniqueness results for CIPs. These estimates were first introduced in the famous paper of the Swedish mathematician Torsten Carleman in 1939 [50]. Roughly speaking, as soon as a Carleman estimate is valid for the operator of a PDE, then the Bukhgeim-Klibanov method leads to a certain uniqueness theorem for a corresponding CIP for this CIP. On the other hand, since Carleman estimates are known for three main types of partial differential operators of the second order (hyperbolic, parabolic, and elliptic), then this method is applicable to a wide class of CIPs. Since the publication of works [43, 44, 95] in 1981, many researchers have discussed this method in their publications. Because uniqueness is not the main topic of this book, we refer only to some samples of those publications in [14, 31–33, 45, 62, 79–81, 83, 84, 96–99, 102–104, 136]. We refer to [161] for a survey with a far more detailed list of references.

Although the Bukhgeim-Klibanov method is a very general one, there is a certain problem associated with it. This problem was viewed as a shortcoming at the time of the inception of this method. Specifically, it is required that at least one initial condition not to be zero in the entire domain of interest Ω. At the same time, the main interest in applications in, for example, the hyperbolic case, is when one of initial conditions is identically zero and another one is either the δ-function or that the wave field is initialized by the plane wave. The uniqueness question in the latter case remains a long-standing and well-known unsolved problem; see [58] for some progress in this direction.

On the other hand, the recent computational experience of the authors indicates that the above is only a mild restriction from the applied standpoint. Indeed, suppose that initial conditions for a hyperbolic equation are

$$u(x,0) = 0, u_t(x,0) = \delta(x - x_0) \tag{1.75}$$

where $x, x_0 \in \mathbb{R}^n$ and the source position $\{x_0\}$ is fixed. Then one can consider an approximation for the δ-function in the sense of distributions as

$$u^\varepsilon(x,0) = 0, u_t^\varepsilon(x,0) = \frac{1}{\left(\sqrt{\pi}\varepsilon\right)^n} \exp\left(-\frac{|x-x_0|^2}{\varepsilon^2}\right) \tag{1.76}$$

for a sufficiently small number $\varepsilon > 0$. Suppose that the domain Ω is located far from the source $\{x_0\}$, which is common in applications. Then the solution of the forward problem with initial conditions (1.76) differs negligibly from the case (1.75) for $x \in \Omega$. If a numerical method of solving this CIP is stable, as it is the case of algorithms of this book, then this negligible difference in the boundary data at $\partial\Omega$ will practically not affect computational results. On the other hand, in the case (1.76), uniqueness is restored. Therefore, the Bukhgeim-Klibanov method addresses properly the applied aspect of the uniqueness question for CIPs with single measurement data.

The single work where the problem of the zero initial condition was partially addressed is [112]. In this paper, the case of a single incident plane wave was considered. Derivatives with respect to variables, which are orthogonal to the direction of the propagation of this wave, are expressed via finite differences. Results of this work are presented in Sect. 1.11.

In Sect. 1.10, we prove uniqueness theorems for some CIPs for hyperbolic, parabolic, and elliptic PDEs using the Bukhgeim-Klibanov method. These theorems were published in somewhat different formulations in [43, 95–97, 99, 102]. For the sake of completeness, we also derive a Carleman estimate for the corresponding hyperbolic operator. Since this is an introductory chapter, we do not include here proofs of Carleman estimates for parabolic and elliptic operators and refer to Chap. 4 of [124] instead. In addition, the Carleman estimate for the Laplace operator is derived in Chap. 6 of this book. The only reason why we assume everywhere in Sect. 1.10 that the domain Ω is $\Omega = \{|x| < R\} \subset \mathbb{R}^n$, $R = \text{const.} > 0$ is our desire to simplify the presentation. Similar arguments can be considered for an arbitrary convex domain with a smooth boundary.

1.10.2 Carleman Estimate for a Hyperbolic Operator

Let $\Omega = \{|x| < R\} \subset \mathbb{R}^n$ and $T = \text{const.} > 0$. Denote

$$Q_T^\pm = \Omega \times (-T, T), S_T^\pm = \partial\Omega \times (-T, T), Q_T = \Omega \times (0, T), S_T = \partial\Omega \times (0, T).$$

Let $x_0 \in \Omega, \eta \in (0,1)$. Consider the function $\psi(x,t)$:

$$\psi(x,t) = |x-x_0|^2 - \eta t^2. \tag{1.77}$$

We now introduce the Carleman weight function (CWF) by

$$W(x,t) = \exp[\lambda\psi(x,t)], \tag{1.78}$$

where $\lambda > 1$ is a large parameter which we will specify later. The level surfaces of the function $W(x,t)$ are hyperboloids $H_d = \left\{|x-x_0|^2 - \eta t^2 = d = \text{const}\right\}$. For $d \in \left(0, R^2\right)$, consider the domain G_d:

$$G_d = \left\{(x,t) : x \in \Omega, |x-x_0|^2 - \eta t^2 > d\right\} \subset Q_T^{\pm}. \tag{1.79}$$

Hence, $G_d \neq \varnothing$ and $\nabla_x \psi(x,t) \neq 0$ in $\overline{G}_d$. Define the hyperbolic operator L_0 as

$$L_0 u = c(x) u_{tt} - \Delta u. \tag{1.80}$$

The Carleman estimate for the operator L_0 is established in Theorem 1.10.2. As to the proof of this theorem, it should be kept in mind that proofs of Carleman estimates are always space consuming; see, for example, Chap. 4 of [124]. For brevity, we assume in Theorem 1.10.2 that the dimension of the space $\mathbb{R}^n$ is $n \geq 2$. An analog of this theorem for the case $n = 1$ can be proven similarly. This theorem was proven in [124] for the case $c \equiv 1$ and in [84, 102] for the case when the function c satisfies conditions (1.81) and (1.82). As it is clear from Theorem 1.10.2, the Carleman estimate for a partial differential operator depends only on its principal part.

Theorem 1.10.2. *Let $\Omega = \{|x| < R\} \subset \mathbb{R}^n, n \geq 2, x_0 \in \Omega$, and L_0 be the hyperbolic operator defined in (1.80). Suppose that in (1.80), the coefficient satisfies the following conditions:*

$$c \in C^1\left(\overline{\Omega}\right), c(x) \in [1, \overline{c}], \text{where } \overline{c} = const. \geq 1, \tag{1.81}$$

$$(x - x_0, \nabla c) \geq 0, \ \forall x \in \overline{\Omega}, \tag{1.82}$$

where $(\cdot,\cdot)$ denotes the dot product in $\mathbb{R}^n$. Let

$$P = P(x_0, \Omega) = \max_{x \in \overline{\Omega}} |x - x_0|. \tag{1.83}$$

Then there exist a sufficiently small number $\eta_0 = \eta_0(\overline{c}, P, \|\nabla c\|_{C(\overline{\Omega})}) \in (0,1]$ such that for any $\eta \in (0, \eta_0]$, one can choose a sufficiently large number $\lambda_0 = \lambda_0(\Omega, \eta, c, x_0) > 1$ and number $C = (\Omega, \eta, c, x_0) > 0$, such that for all $u \in C^2\left(\overline{G}_d\right)$ and for all $\lambda \geq \lambda_0$, the following pointwise Carleman estimate holds

$$(L_0 u)^2 W^2 \geq C\lambda\left(|\nabla u|^2 + u_t^2 + \lambda^2 u^2\right) W^2 + \nabla \cdot U + V_t, \text{ in } G_d, \tag{1.84}$$

where the CWF $W(x,t)$ is defined by (1.78) and components of the vector function (U,V) satisfy the following estimates:

$$|U| \leq C\lambda^3 \left(|\nabla u|^2 + u_t^2 + u^2\right) W^2, \tag{1.85}$$

$$|V| \leq C\lambda^3 \left[|t| \left(u_t^2 + |\nabla u|^2 + u^2\right) + (|\nabla u| + |u|)\,|u_t|\right] W^2. \tag{1.86}$$

In particular, (1.86) implies that if either $u(x,0) = 0$ or $u_t(x,0) = 0$, then

$$V(x,0) = 0. \tag{1.87}$$

Proof. In this proof, C denotes different positive constants depending on the same parameters as indicated in the conditions of this theorem. Also, in this proof, $O(1/\lambda)$ denotes different $C^1\left(\overline{Q}_T^{\pm}\right)$ functions such that

$$\left|O\left(\frac{1}{\lambda}\right)\right| \leq \frac{C}{\lambda}, \forall \lambda > 1, \tag{1.88}$$

and the same is true for the first derivatives of these functions. We use (1.88) in many parts of this proof below. Denote $v = u \cdot W$ and express the operator $L_0(u)$ in terms of the function v. Below $f_i := \partial_{x_i} f$. We have

$$\begin{aligned}
u &= v \cdot \exp\left[\lambda\left(\eta t^2 - |x - x_0|^2\right)\right],\\
u_t &= (v_t + 2\lambda\eta t \cdot v)\exp\left[\lambda\left(\eta t^2 - |x - x_0|^2\right)\right],\\
u_{tt} &= \left(v_{tt} + 4\lambda\eta t \cdot v_t + 4\lambda^2\left(\eta^2 t^2 + O\left(\frac{1}{\lambda}\right)\right)v\right) W^{-1},\\
u_i &= \left[v_i - 2\lambda\left(x_i - x_{0i}\right)v\right]\exp\left[\lambda\left(\eta t^2 - |x - x_0|^2\right)\right],\\
u_{ii} &= \left[v_{ii} - 4\lambda\left(x_i - x_{0i}\right)v_i + 4\lambda^2\left(|x - x_0|^2 + O\left(\frac{1}{\lambda}\right)\right)v\right] W^{-1}.
\end{aligned}$$

Hence,

$$\begin{aligned}
\left(L_0 u\right)^2 W^2 &= \left(c(x)\,u_{tt} - \Delta u\right)^2 W^2\\
&= \left\{\left[c(x)\,v_{tt} - \Delta v - 4\lambda^2\left(|x - x_0|^2 - c\eta^2 t^2 + O\left(\frac{1}{\lambda}\right)\right)v\right]\right.\\
&\qquad \left. + 4\lambda c\eta t v_t + 4\lambda\sum_{i=1}^{n}\left(x_i - x_{0i}\right)v_i\right\}^2.
\end{aligned}$$

Denote

$$z_1 = cv_{tt} - \Delta v - 4\lambda^2 \left(|x - x_0|^2 - c\eta^2 t^2 + O\left(\frac{1}{\lambda}\right)\right) v,$$
$$z_2 = 4\lambda c\eta t \cdot v_t,$$
$$z_3 = 4\lambda \sum_{i=1}^{n} (x_i - x_{0i})\, v_i.$$

Then $(L_0 u)^2 W^2 = (z_1 + z_2 + z_3)^2$. Hence,

$$(L_0 u)^2 W^2 \geq z_1^2 + 2z_1 z_2 + 2z_1 z_3. \tag{1.89}$$

We estimate separately each term in the inequality (1.89) from the below in five steps.

Step 1. Estimate the term $2z_1 z_2$. We have

$$\begin{aligned}
2z_1 z_2 &= 8\lambda c\eta t \cdot v_t \left[cv_{tt} - \Delta v - 4\lambda^2 \left(|x - x_0|^2 - c\eta^2 t^2 + O\left(\frac{1}{\lambda}\right)\right) v \right] \\
&= \left[4\lambda c^2 \eta t \cdot v_t^2 \right]_t - 4\lambda c^2 \eta v_t^2 \\
&\quad + \sum_{i=1}^{n} (-8\lambda c\eta t \cdot v_t v_i)_i + \sum_{i=1}^{n} 8\lambda c\eta t \cdot v_{it} v_i \\
&\quad + 8\lambda \eta t \cdot v_t \sum_{i=1}^{n} c_i v_i + \left[-16\lambda^3 c\eta \left(t\,|x - x_0|^2 - c\eta^2 t^3 + tO\left(\frac{1}{\lambda}\right)\right) v^2 \right]_t \\
&\quad + 16\lambda^3 c\eta \left(|x - x_0|^2 - 3c\eta^2 t^2 + O\left(\frac{1}{\lambda}\right)\right) v^2 \\
&= -4\lambda c^2 \eta v_t^2 + \left(4\lambda c^2 \eta t \cdot v_t^2 + \sum_{i=1}^{n} 4\lambda c\eta t v_i^2 \right)_t - 4\lambda c\eta\, |\nabla v|^2 \\
&\quad + 8\lambda \eta t \cdot v_t \sum_{i=1}^{n} c_i v_i + 16\lambda^3 c\eta \left[|x - x_0|^2 - 3c\eta^2 t^2 + O\left(\frac{1}{\lambda}\right)\right] v^2 \\
&\quad + \nabla \cdot U_1 + \left[4\lambda c^2 \eta t v_t^2 - 16\lambda^3 c\eta \left(t\,|x - x_0|^2 - c\eta^2 t^2 + tO\left(\frac{1}{\lambda}\right)\right) v^2 \right]_t
\end{aligned}$$

Thus, we have obtained that

$$2z_1z_2 = -4\lambda c\eta\left(cv_t^2 + |\nabla v|^2\right) + 8\lambda\eta t\cdot v_t\sum_{i=1}^{n} c_i v_i$$
$$+16\lambda^3 c\eta\left[|x-x_0|^2 - 3c\eta^2t^2 + O\left(\frac{1}{\lambda}\right)\right]v^2 + \nabla\cdot U_1 + (V_1)_t\,, \quad (1.90)$$

where the vector function (U_1, V_1) satisfies the following estimates:

$$|U_1| \le C\lambda^3\left(|\nabla u|^2 + u_t^2 + u^2\right)W^2, \quad (1.91)$$

$$|V_1| \le C\lambda^3|t|\left(u_t^2 + |\nabla u|^2 + u^2\right)W^2. \quad (1.92)$$

To include the function u in the estimate for $|U_1|, |V_1|$, we have replaced v with $u = v\cdot W^{-1}$.

Step 2. We now estimate the term $2z_1z_3$. We have

$$2z_1z_3 = 8\lambda\sum_{i=1}^{n}(x_i - x_{0i})v_i\left[cv_{tt} - \Delta v - 4\lambda^2\left(|x-x_0|^2 - c\eta^2t^2 + O\left(\frac{1}{\lambda}\right)\right)v\right]$$
$$= \left(\sum_{i=1}^{n} 8c\lambda(x_i - x_{0i})v_iv_t\right)_t - \sum_{i=1}^{n} 8\lambda(x_i - x_{0i})cv_{it}v_t$$
$$-\sum_{j=1}^{n}\sum_{i=1}^{n} 8\lambda(x_i - x_{0i})v_iv_{jj}$$
$$+\sum_{i=1}^{n}\left[-16\lambda^3(x_i - x_{0i})\left(|x-x_0|^2 - c\eta^2t^2 + O\left(\frac{1}{\lambda}\right)\right)v^2\right]_i$$
$$+16\lambda^3\left[(n+2)|x-x_0|^2 - nc\eta^2t^2 + O\left(\frac{1}{\lambda}\right)\right]v^2$$
$$= \sum_{i=1}^{n}\left(-4\lambda(x_i - x_{0i})cv_t^2\right)_i + 4\lambda\left[nc + (x-x_0,\nabla c)\right]v_t^2$$
$$+\sum_{j=1}^{n}\left[\sum_{i=1}^{n}\left(-8\lambda(x_i - x_{0i})v_iv_j\right)\right]_j + 8\lambda|\nabla v|^2$$
$$+\sum_{j=1}^{n}\sum_{i=1}^{n} 8\lambda(x_i - x_{0_i})v_{ij}v_j$$

$$
\begin{aligned}
&+16\lambda^3\left[(n+2)\left|x-x_0\right|^2-nc\eta^2t^2+O\left(\frac{1}{\lambda}\right)\right]v^2\\
&+\left(8c\lambda v_t\sum_{i=1}^{n}\left(x_i-x_{0i}\right)v_i\right)_t\\
&=4\lambda\left[nc+\left(x-x_0,\nabla c\right)\right]v_t^2+8\lambda\left|\nabla v\right|^2\\
&+\sum_{i=1}^{n}\left[\sum_{j=1}^{n}4\lambda\left(x_i-x_{0i}\right)v_j^2\right]_i-4\lambda\left|\nabla v\right|^2\\
&+16\lambda^3\left[(n+2)\left|x-x_0\right|^2-c\eta^2t^2+O\left(\frac{1}{\lambda}\right)\right]v^2+\nabla\cdot U_2+\left(V_2\right)_t.
\end{aligned}
$$

Since by (1.82), $\left(x-x_0,\nabla c\right)\geq 0$, then we obtain

$$
\begin{aligned}
2z_1z_3\geq\ &4\lambda nc v_t^2+4\lambda\left|\nabla v\right|^2\\
&+16\lambda^3\left[(n+2)\left|x-x_0\right|^2-nc\eta^2t^2+O\left(\frac{1}{\lambda}\right)\right]v^2\\
&+\nabla\cdot U_2+V_{2t}, \qquad (1.93)
\end{aligned}
$$

$$
\left|U_2\right|\leq C\lambda^3\left(\left|\nabla u\right|^2+u_t^2+u^2\right)W^2, \qquad (1.94)
$$

$$
\left|V_2\right|\leq C\lambda^3\left[\left|t\right|\left(\left|\nabla u\right|^2+\left|u\right|^2\right)+\left(\left|\nabla u\right|+\left|u\right|\right)\left|u_t\right|\right]W^2. \qquad (1.95)
$$

Step 3. In this step, we estimate the term $2z_1z_2+2z_1z_3$. It follows from (1.82) that $\left|x-x_0\right|\leq P, \forall x\in\Omega$. On the other hand, since $\left|x-x_0\right|^2-\eta t^2>d>0$ in G_d, then $\eta\left|t\right|\leq P\sqrt{\eta}$ in G_d. This estimate as well as the Cauchy-Schwarz inequality imply that

$$
\begin{aligned}
8\lambda\eta t\cdot v_t\sum_{i=1}^{n}c_iv_i&=-8\lambda\eta t\cdot v_t\left(\nabla c,\nabla v\right)\geq-8\lambda\eta\left|t\right|\cdot\left|v_t\right|\cdot\left|\nabla v\right|\cdot\left\|\nabla c\right\|_{C\left(\overline{\Omega}\right)}\\
&\geq-4\lambda\sqrt{\eta}P\left\|\nabla c\right\|_{C\left(\overline{\Omega}\right)}\cdot\left(v_t^2+\left|\nabla v\right|^2\right). \qquad (1.96)
\end{aligned}
$$

Since by (1.81), $\overline{c}\geq 1$, then (1.90) and (1.96) imply that

$$
\begin{aligned}
2z_1z_2\geq\ &-4\lambda\left(\overline{c}^2\eta+\sqrt{\eta}P\left\|\nabla c\right\|_{C\left(\overline{\Omega}\right)}\right)\left(v_t^2+\left|\nabla v\right|^2\right)\\
&+16\lambda^3\eta\left[\left|x-x_0\right|^2-3c_1\eta^2t^2+O\left(\frac{1}{\lambda}\right)\right]v^2+\nabla\cdot U_1+\left(V_1\right)_t. \qquad (1.97)
\end{aligned}
$$

Let $U_3 = U_1 + U_2, V_3 = V_1 + V_2$. Hence, (1.93)–(1.97) imply that

$$
\begin{aligned}
2z_1z_2 + 2z_1z_3 \geq\ & 4\lambda\left[nc - \left(\overline{c}^2\eta + \sqrt{\eta}P\left\|\nabla c\right\|_{C(\overline{\Omega})}\right)\right]v_t^2 \\
& + 4\lambda\left(1 - \left(\overline{c}^2\eta + \sqrt{\eta}P\left\|\nabla c\right\|_{C(\overline{\Omega})}\right)\right)|\nabla v|^2 \\
& + 16\lambda^3\left[(n+2+\eta)|x-x_0|^2 - (n+3\eta)\,\overline{c}\eta^2t^2 + O\left(\frac{1}{\lambda}\right)\right]v^2 \\
& + \nabla\cdot U_3 + V_{3t}, \qquad (1.98)
\end{aligned}
$$

$$
|U_3| \leq C\lambda^3\left(|\nabla u|^2 + u_t^2 + u^2\right)W^2, \qquad (1.99)
$$

$$
|V_3| \leq C\lambda^3\left[|t|\left(u_t^2 + |\nabla u|^2 + u^2\right) + \left(|\nabla u| + |u|\right)|u_t|\right]W^2. \qquad (1.100)
$$

Step 4. We now estimate the term z_1^2 from the below. We are doing this only in order to prove Corollary 1.10.2, since multipliers at $v_t^2, |\nabla v|^2, v^2$ in (1.98) are positive anyway for sufficiently small η. Let $b > 0$ be a number, which we will choose later. We have

$$
\begin{aligned}
z_1^2 &= \left[cv_{tt} - \Delta v - 4\lambda^2\left(|x-x_0|^2 - c\eta^2t^2 + O\left(\frac{1}{\lambda}\right)\right)v + \lambda bv\right]^2 \\
&= (2\lambda cbvv_t)_t - 2\lambda cbv_t^2 + \sum_{i=1}^{n}(-2\lambda bvv_i)_i \\
&\quad + 2\lambda b|\nabla v|^2 - 8\lambda^3 b\left[|x-x_0|^2 - c\eta^2t^2 + O\left(\frac{1}{\lambda}\right)\right]v^2.
\end{aligned}
$$

Since by (1.81), $c \geq 1$, then we obtain

$$
\begin{aligned}
z_1^2 \geq\ & 2\lambda b|\nabla v|^2 - 2\lambda cbv_t^2 \\
& - 8\lambda^3 b\left[|x-x_0|^2 - \eta^2t^2 + O\left(\frac{1}{\lambda}\right)\right]v^2 + \nabla\cdot U_4 + V_{4t}, \qquad (1.101)
\end{aligned}
$$

$$
|U_4| \leq C\lambda^3\left(|\nabla u|^2 + u_t^2 + u^2\right)W^2, \qquad (1.102)
$$

$$
|V_4| \leq C\lambda^3\left(|t|\,u^2 + |u_t|\cdot|u|\right)W^2. \qquad (1.103)
$$

Step 5. Finally, we estimate the term $z_1^2 + 2z_1z_2 + 2z_1z_3$, which is the right-hand side of (1.89). Summing up (1.98) and (1.101) and taking into account (1.99), (1.100), (1.102), and (1.103), we obtain

$$z_1^2 + 2z_1z_2 + 2z_1z_3 \geq 4\lambda\left[\left(n - \frac{b}{2}\right)c - \left(\overline{c}^2\eta + \sqrt{\eta}P\left\|\nabla c\right\|_{C(\overline{\Omega})}\right)\right]v_t^2$$
$$+4\lambda\left(1 + \frac{b}{2} - \left(\overline{c}^2\eta + \sqrt{\eta}P\left\|\nabla c\right\|_{C(\overline{\Omega})}\right)\right)|\nabla v|^2$$
$$+16\lambda^3\left[\left(n + 2 + \eta - \frac{b}{2}\right)|x - x_0|^2\right.$$
$$\left.-\left(n\overline{c} + 3\eta\overline{c} - \frac{b}{2}\right)\eta^2t^2 + O\left(\frac{1}{\lambda}\right)\right]v^2$$
$$+\nabla \cdot U_5 + V_{5t}, \tag{1.104}$$

$$|U_5| \leq C\lambda^3\left(|\nabla u|^2 + u_t^2 + u^2\right)W^2, \tag{1.105}$$

$$|V_5| \leq C\lambda^3\left[|t|\left(u_t^2 + |\nabla u|^2 + u^2\right) + (|\nabla u| + |u|)\,|u_t|\right]W^2. \tag{1.106}$$

Choose now $b = 1$ and choose $\eta_0 = \eta_0\left(\overline{c}, P, \left\|\nabla c\right\|_{C(\overline{\Omega})}\right) \in (0,1)$ so small that

$$\frac{3}{2} - \left(\overline{c}^2\eta + \sqrt{\eta}P\left\|\nabla c\right\|_{C(\overline{\Omega})}\right) \geq 1, \forall \eta \in (0, \eta_0], \tag{1.107}$$

$$\left(n\overline{c} + 3\eta\overline{c} - \frac{1}{2}\right)\eta \leq n + \frac{3}{2} + \eta, \forall \eta \in (0, \eta_0]. \tag{1.108}$$

Since $n \geq 2$ and $c \geq 1$, then (1.104) becomes

$$z_1^2 + 2z_1z_2 + 2z_1z_3 \geq 2\lambda\left(v_t^2 + |\nabla v|^2\right)$$
$$+16\lambda^3\left(|x - x_0|^2 - \eta t^2 + O\left(\frac{1}{\lambda}\right)\right)v^2 + \nabla \cdot U_5 + V_{5t}. \tag{1.109}$$

Since $|x - x_0|^2 - \eta t^2 > d > 0$ in G_d, then replacing in (1.109) v with $u = vW^{-1}$ and using (1.88), (1.105), and (1.106) as well as the fact that λ is sufficiently large, we obtain (1.84)–(1.86). □

Corollary 1.10.2. *Assume now that in (1.80), the operator $L_0u = u_{tt} - \Delta u$ and $n \geq 2$. Then, condition (1.82) holds automatically, and in Theorem 1.10.2,one can choose $\eta_0 = 1$.*

Proof. We now can set in (1.81) $\overline{c} := 1$. Since in the above proof $b = 1$, then we have in (1.104) for $n \geq 2$

$$\left(n-\frac{b}{2}\right)c-\left(\overline{c}^2\eta+\sqrt{\eta}P\left\|\nabla c\right\|_{C(\overline{\Omega})}\right)=n-\left(\eta+\frac{1}{2}\right)\geq\frac{1}{2},$$

$$\left(1+\frac{b}{2}-\left(\overline{c}^2\eta+\sqrt{\eta}P\left\|\nabla c\right\|_{C(\overline{\Omega})}\right)\right)=\frac{3}{2}-\eta\geq\frac{1}{2},$$

$$\begin{aligned}&\left(n+2+\eta-\frac{b}{2}\right)|x-x_0|^2-\left(n\overline{c}+3\eta\overline{c}-\frac{b}{2}\right)\eta^2t^2\\&=\left(n+\frac{3}{2}+\eta\right)|x-x_0|^2-\left(n-\frac{1}{2}+3\eta\right)\eta^2t^2\\&\geq|x-x_0|^2-\eta t^2>d.\end{aligned}$$

Therefore, (1.109) is satisfied for all $\eta\in(0,1)$. □

1.10.3 Estimating an Integral

Lemma 1.10.3 is very important for the Bukhgeim-Klibanov method.

Lemma 1.10.3. *Let the function $\varphi\in C^1[0,a]$ and $\varphi'(t)\leq-b$ in $[0,a]$, where $b=const>0$. For a function $g\in L_2(-a,a)$, consider the integral*

$$I(g,\lambda)=\int_{-a}^{a}\left(\int_0^t g(\tau)\,\mathrm{d}\tau\right)^2\exp\left[2\lambda\varphi\left(t^2\right)\right]\mathrm{d}t.$$

Then,

$$I(g,\lambda)\leq\frac{1}{4\lambda b}\int_{-a}^{a}g^2(t)\exp\left[2\lambda\varphi\left(t^2\right)\right]\mathrm{d}t.$$

Proof. We have for $t>0$

$$\begin{aligned}t\exp\left[2\lambda\varphi\left(t^2\right)\right]&=t\frac{4\lambda\varphi'\left(t^2\right)}{4\lambda\varphi'\left(t^2\right)}\exp\left[2\lambda\varphi\left(t^2\right)\right]\\&=\frac{1}{4\lambda\varphi'\left(t^2\right)}\frac{\mathrm{d}}{\mathrm{d}t}\left\{\exp\left[2\lambda\varphi\left(t^2\right)\right]\right\}\\&=-\frac{1}{4\lambda\varphi'\left(t^2\right)}\frac{\mathrm{d}}{\mathrm{d}t}\left\{-\exp\left[2\lambda\varphi\left(t^2\right)\right]\right\}\\&\leq\frac{1}{4\lambda b}\frac{\mathrm{d}}{\mathrm{d}t}\left\{-\exp\left[2\lambda\varphi\left(t^2\right)\right]\right\}.\end{aligned}$$

Hence,

$$\int_0^a \left(\int_0^t g(\tau)\,\mathrm{d}\tau\right)^2 \exp\left(2\lambda\varphi\left(t^2\right)\right)\mathrm{d}t \le \int_0^a \exp\left(2\lambda\varphi\left(t^2\right)\right) t\left(\int_0^t g^2(\tau)\,\mathrm{d}\tau\right)\mathrm{d}t$$

$$\le \frac{1}{4\lambda b}\int_0^a \frac{\mathrm{d}}{\mathrm{d}t}\left[-\exp\left(2\lambda\varphi\left(t^2\right)\right)\right]\left(\int_0^t g^2(\tau)\,\mathrm{d}\tau\right)\mathrm{d}t$$

$$= -\frac{1}{4\lambda b}\exp\left(2\lambda\varphi\left(a^2\right)\right)\int_0^a g^2(\tau)\,\mathrm{d}\tau + \frac{1}{4\lambda b}\int_0^a g^2(\tau)\exp\left(2\lambda\varphi\left(t^2\right)\right)\mathrm{d}t$$

$$\le \frac{1}{4\lambda b}\int_0^a g^2(\tau)\exp\left(2\lambda\varphi\left(t^2\right)\right)\mathrm{d}t.$$

Thus, we have obtained that

$$\int_0^a \exp\left(2\lambda\varphi\left(t^2\right)\right)\left(\int_0^t g(\tau)\,\mathrm{d}\tau\right)^2\mathrm{d}t \le \frac{1}{4\lambda b}\int_0^a g^2(\tau)\exp\left(2\lambda\varphi\left(t^2\right)\right)\mathrm{d}t.$$

Similarly,

$$\int_{-a}^0 \exp\left(2\lambda\varphi\left(t^2\right)\right)\left(\int_0^t g(\tau)\,\mathrm{d}\tau\right)^2\mathrm{d}t \le \frac{1}{4\lambda b}\int_{-a}^0 g^2(\tau)\exp\left(2\lambda\varphi\left(t^2\right)\right)\mathrm{d}t.$$

□

1.10.4 *Cauchy Problem with the Lateral Data for a Hyperbolic Inequality with Volterra-Like Integrals*

Recall that we assume in Sect. 1.10 that $\Omega = \{|x| < R\} \subset \mathbb{R}^n$. Let P be the number defined in (1.83) and $d = \text{const.} \in \left(0, P^2\right)$. Let G_d be the domain defined in (1.79). Define its subdomain G_d^+ as

$$G_d^+ = \left\{(x,t) : |x - x_0|^2 - \eta t^2 > d, t > 0, x \in \Omega\right\}. \tag{1.110}$$

Hence, $G_d^+ = G_d \cap \{t > 0\}$. Let

$$T > \sqrt{\frac{P^2 - d}{\eta}}. \tag{1.111}$$

Using (1.79) and (1.110), we obtain

$$G_d^+ \subset Q_T, \quad G_d^+ = G_d \cap \{t > 0\}, \tag{1.112}$$

$$\overline{G}_d^+ \cap \{t = T\} = \varnothing, \quad \overline{G}_d \cap \{t = \pm T\} = \varnothing. \tag{1.113}$$

Let $A_1 > 0$ and $A_2 \geq 0$ be two constants. Assume that the function $u \in C^2\left(\overline{Q}_T\right)$ satisfies the following hyperbolic inequality with Volterra-like integrals:

$$|c(x) u_{tt} - \Delta u| \leq A_1 \Big(|\nabla u| + |u_t| + |u| \Big)(x,t)$$

$$+A_2 \int_0^t \left(|\nabla u| + |u_t| + |u|\right)(x,\tau)\, d\tau, \text{ in } G_d^+. \tag{1.114}$$

Also, let this function u has zero Cauchy data at the lateral side $S_T \cap \overline{G}_d^+$ of the domain G_d^+ :

$$u\,|_{S_T \cap \overline{G}_d^+} = \frac{\partial u}{\partial n}\,|_{S_T \cap \overline{G}_d^+} = 0. \tag{1.115}$$

In addition, we assume that

$$\text{either } u(x,0) = 0 \text{ or } u_t(x,0) = 0 \text{ for } x \in \overline{G}_d^+ \cap \{t = 0\}. \tag{1.116}$$

The goal of this section is to prove that conditions (1.114)–(1.116) imply that $u(x,t) \equiv 0$ in G_d^+. In particular, if $A_2 = 0$, then integrals are not present in (1.114). Hence, in this case, the corresponding hyperbolic equation

$$c(x) u_{tt} = \Delta u + \sum_{j=1}^{n+1} b_j(x,t) u_j + a(x,t) u \text{ in } G_d^+,$$

where $u_{n+1} := u_t$ with coefficients $b_j, c \in C\left(\overline{G}_d^+\right)$ can be reduced to the inequality (1.114). Hence, Theorem 1.10.4 implies uniqueness for this equation with the Cauchy data (1.115) and one of initial conditions (1.116). The reason why we introduce Volterra integrals in (1.114) is that they appear in the proof of Theorem 1.10.5.1 Furthermore, assume that (1.111) holds. This implies (1.112) and (1.113). Consider now inequality (1.114) with the Cauchy data (1.115) in the domain G_d (thus allowing $t < 0$). Then an obvious analog of Theorem 1.10.4 is also valid, and the proof is almost identical. In the case $A_2 = 0$, such an analog was published in [124].

Theorem 1.10.4. *Let $\Omega = \{|x| < R\} \subset \mathbb{R}^n, n \geq 2$, and $x_0 \in \Omega$. Assume that $d \in \left(0, P^2\right)$ and the inequality (1.111) holds with the constant $\eta := \eta_0 = \eta_0\left(\overline{c}, P, \|\nabla c\|_{C(\overline{\Omega})}\right) \in (0,1]$ of Theorem 1.10.2. Suppose that the function $u \in$*

$C^2\left(\overline{G}_d^+\right)$ satisfies conditions (1.114)–(1.116) and that the coefficient $c(x)$ satisfies conditions (1.81), (1.82). Then

$$u(x,t) = 0 \text{ in } G_d^+. \tag{1.117}$$

In particular, if in (1.110) $x_0 = 0$ and $d = 0$, then

$$u(x,t) = 0 \text{ in } Q_T. \tag{1.118}$$

In addition, if $c(x) \equiv 1$ and in (1.110) $x_0 = 0$ and $d = 0$, then it is sufficient for (1.118) to replace (1.111) with

$$T > R, \eta = 1. \tag{1.119}$$

Proof. We note first that the boundary of the domain G_d^+ consists of three parts:

$$\begin{aligned}
\partial G_d^+ &= \cup_{i=1}^3 \partial_i G_d^+, \\
\partial_1 G_d^+ &= \left\{|x-x_0|^2 - \eta_0 t^2 = d, t > 0, |x| < R\right\} \subset Q_T, \\
\partial_2 G_d^+ &= \left\{|x-x_0|^2 - \eta_0 t^2 > d, t > 0, |x| = R\right\} \subset S_T, \\
\partial_3 G_d^+ &= \left\{|x-x_0|^2 > d, t = 0, |x| < R\right\}.
\end{aligned} \tag{1.120}$$

Hence, the hypersurface $\partial_1 G_d^+$ is a level surface of the CWF W. Let the function $g \in L_2\left(G_d^+\right)$. Then (1.77), (1.78), and (1.120) imply that

$$\begin{aligned}
\int\limits_{G_d^+} \left(\int\limits_0^t g(x,\tau)\,\mathrm{d}\tau\right)^2 W^2 \mathrm{d}x\mathrm{d}t &= \int\limits_{\partial_3 G_d^+} \exp\left(2\lambda\left|x-x_0\right|^2\right) \\
&\quad \times \left[\int\limits_0^{t(x)} \left(\int\limits_0^t g(x,\tau)\,\mathrm{d}\tau\right)^2 \mathrm{e}^{-2\lambda\eta t^2}\mathrm{d}t\right]\mathrm{d}x, \\
t(x) &= \frac{\sqrt{|x-x_0|^2 - d}}{\sqrt{\eta}}.
\end{aligned}$$

Hence, applying Lemma 1.10.3 to the inner integral

$$\int\limits_0^{t(x)} \left(\int\limits_0^t g(x,\tau)\,\mathrm{d}\tau\right)^2 \mathrm{e}^{-2\lambda\eta t^2}\mathrm{d}t,$$

we obtain

$$\int\limits_{G_d^+}\left(\int\limits_0^t g\left(x,\tau\right)\mathrm{d}\tau\right)^2 W^2\mathrm{d}x\mathrm{d}t \leq \frac{1}{4\eta\lambda}\int\limits_{G_d^+} g^2W^2\mathrm{d}x\mathrm{d}t, \quad \forall g\in L_2\left(G_d^+\right). \tag{1.121}$$

Multiply both sides of the inequality (1.114) by the function $W\left(x,t\right)$ with sufficiently large parameter $\lambda > 1$. Then, square both sides, integrate over the domain G_d^+, and use (1.121). We obtain with a constant $A = A\left(A_1, A_2, \eta\right) > 0$

$$\int\limits_{G_d^+}\left(cu_{tt}-\Delta u\right)^2 W^2\mathrm{d}x\mathrm{d}t \leq A\int\limits_{G_d^+}\left(\left|\nabla u\right|^2+u_t^2+u^2\right)W^2\mathrm{d}x\mathrm{d}t. \tag{1.122}$$

We now can apply Theorem 1.10.2 to estimate the left-hand side of (1.122) from the below. Integrating the inequality (1.84) over the domain G_d^+ using (1.85)–(1.87), (1.115), (1.116), and (1.120) and applying the Gauss' formula, we obtain for sufficiently large $\lambda \geq \lambda_0 > 1$

$$\int\limits_{G_d^+}\left(cu_{tt}-\Delta u\right)^2 W^2\mathrm{d}x\mathrm{d}t \geq C\lambda\int\limits_{G_d^+}\left(\left|\nabla u\right|^2+u_t^2+\lambda^2u^2\right)W^2\mathrm{d}x\mathrm{d}t$$

$$-C\lambda^3\mathrm{e}^{2\lambda d}\int\limits_{\partial_1 G_d^+}\left(\left|\nabla u\right|^2+u_t^2+\lambda^2u^2\right)W^2\mathrm{d}S.$$

Comparing this with (1.122), we obtain

$$C\lambda\int\limits_{G_d^+}\left(\left|\nabla u\right|^2+u_t^2+\lambda^2u^2\right)W^2\mathrm{d}x\mathrm{d}t - C\lambda^3\mathrm{e}^{2\lambda d}\int\limits_{\partial_1 G_d^+}\left(\left|\nabla u\right|^2+u_t^2+\lambda^2u^2\right)W^2\mathrm{d}S$$

$$\leq A\int\limits_{G_d^+}\left(\left|\nabla u\right|^2+u_t^2+u^2\right)W^2\mathrm{d}x\mathrm{d}t.$$

Hence, choosing a sufficient large $\lambda_1 > \lambda_0$, we obtain for $\lambda \geq \lambda_1$ with a new constant $C > 0$

$$\lambda\int\limits_{G_d^+}\left(\left|\nabla u\right|^2+u_t^2+\lambda^2u^2\right)W^2\mathrm{d}x\mathrm{d}t \leq C\lambda^3\mathrm{e}^{2\lambda d}\int\limits_{\partial_1 G_d^+}\left(\left|\nabla u\right|^2+u_t^2+\lambda^2u^2\right)\mathrm{d}S. \tag{1.123}$$

Consider a sufficiently small number $\varepsilon > 0$ such that $d+\varepsilon < P^2$. Then by (1.112), $G_{d+\varepsilon}^+ \subset Q_T$. Obviously, $G_d^+ \subset G_{d+\varepsilon}^+$. Hence, replacing in the left-hand side of the

inequality (1.123) G_d^+ with $G_{d+\varepsilon}^+$, we strengthen this inequality. Also, $W^2(x,t) \geq \mathrm{e}^{2\lambda(d+\varepsilon)}$ in $G_{d+\varepsilon}^+$. Hence, we obtain from (1.123)

$$\mathrm{e}^{2\lambda(d+\varepsilon)} \int\limits_{G_{d+\varepsilon}^+} u^2 \mathrm{d}x\mathrm{d}t \leq C\mathrm{e}^{2\lambda d} \int\limits_{\partial_1 G_d^+} \left(|\nabla u|^2 + u_t^2 + \lambda^2 u^2\right) \mathrm{d}S.$$

Dividing this inequality by $\mathrm{e}^{2\lambda(d+\varepsilon)}$, we obtain

$$\int\limits_{G_{d+\varepsilon}^+} u^2 \mathrm{d}x\mathrm{d}t \leq C\mathrm{e}^{-2\lambda\varepsilon} \int\limits_{\partial_1 G_d^+} \left(|\nabla u|^2 + u_t^2 + \lambda^2 u^2\right) \mathrm{d}S. \tag{1.124}$$

Setting in (1.124) $\lambda \to \infty$, we obtain $u = 0$ in $G_{d+\varepsilon}^+$. Since $\varepsilon > 0$ is an arbitrary sufficiently small number, then (1.117) is true.

Consider now the case when in (1.110) $x_0 = 0$ and $d = 0$. Then $P = R$ and by (1.111),

$$T > \frac{R}{\sqrt{\eta_0}}. \tag{1.125}$$

Consider a sufficiently small number $\varepsilon \in \left(0, R^2\right)$. Then by (1.112), $G_\varepsilon^+ \subset Q_T$ and by (1.125),

$$T > \frac{\sqrt{R^2 - \varepsilon}}{\sqrt{\eta_0}}.$$

Hence, (1.117) implies that $u = 0$ in G_ε^+. Hence, $u = 0$ in G_0^+. Next, since $x_0 = 0$, then it follows from (1.122) that $\overline{G}_0^+ \cap \{t = 0\} = \{|x| < R\} = \Omega$. Hence,

$$u(x,0) = u_t(x,0) = 0, x \in \Omega. \tag{1.126}$$

Next, denote $cu_{tt} - \Delta u := f$. Hence, by (1.114),

$$2u_t(cu_{tt} - \Delta u) = 2u_t f \leq u_t^2 + f^2$$
$$\leq u_t^2 + \overline{A}\left[|\nabla u|^2 + u_t^2 + u^2 + \int\limits_0^t \left(|\nabla u|^2 + u_t^2 + u^2\right)(x,\tau)\,\mathrm{d}\tau\right],$$

with a certain positive constant $\overline{A}$. Hence, we now can work with $2u_t(cu_{tt} - \Delta u)$ as it is done in the standard energy estimate for a hyperbolic PDE [119]. In doing so, we can use one of zero boundary conditions (1.115) at S_T and zero initial conditions (1.126). This way, we obtain $u = 0$ in Q_T, which proves (1.118). The case $c \equiv 1$, including (1.119), follows from Corollary 1.10.2 and (1.118). □

The proof of the following corollary can be obtained via a slight modification of the proof of Theorem 1.10.4.

Corollary 1.10.4. *Assume that in Theorem 1.10.4 the domain G_d^+ is replaced with the domain G_d, the integral in (1.114) is replaced with*

$$\left| \int_0^t \left(|\nabla u| + |u_t| + |u| \right)(x,\tau)\, d\tau \right|,$$

and that the rest of conditions of Theorem 1.10.4, except of (1.116), is in place. Then conclusions (1.117)–(1.119) of Theorem 1.10.4 still hold with the replacement of the pair $\left(G_d^+, Q_T\right)$ with the pair $\left(G_d, Q_T^{\pm}\right)$.

1.10.5 Coefficient Inverse Problem for a Hyperbolic Equation

The Hyperbolic Coefficient Inverse Problem. Let the function $u \in C^2\left(\overline{Q}_T\right)$ satisfies the following conditions:

$$c(x)\, u_{tt} = \Delta u + \sum_{|\alpha| \le 1} a_\alpha(x)\, D_x^\alpha u, \text{ in } Q_T, \tag{1.127}$$

$$u(x,0) = f_0(x), \quad u_t(x,0) = f_1(x), \tag{1.128}$$

$$u|_{S_T} = p(x,t), \quad \frac{\partial u}{\partial n}|_{S_T} = q(x,t), \tag{1.129}$$

where functions $a_\alpha, c \in C\left(\overline{Q}_T\right)$, and $c \ge 1$. Determine one of coefficients of (1.127).

The CIP (1.127)–(1.129) is the problem with the single measurement data because only a single pair (f_0, f_1) of initial conditions is used.

Theorem 1.10.5.1. *Let the coefficient $c(x)$ in (1.127) satisfies conditions (1.81) and (1.82). In addition, let coefficients $a_\alpha \in C\left(\overline{\Omega}\right)$. Let the domain $\Omega = \{|x| < R\} \subset \mathbb{R}^n, n \ge 2$. Consider two cases:*

Case 1. The coefficient $c(x)$ is unknown, and all other coefficients $a_\alpha(x)$ are known. In this case, we assume that

$$\Delta f_0(x) + \sum_{|\alpha| \le 1} a_\alpha(x)\, D_x^\alpha f_0(x) \ne 0 \text{ for } x \in \overline{\Omega}. \tag{1.130}$$

Then for a sufficiently large $T > 0$, there exists at most one pair of functions (u, c) satisfying (1.127)–(1.129) and such that $u \in C^4\left(\overline{Q}_T\right)$.

Case 2. The coefficient $a_{\alpha_0}(x)$ is unknown, and the rest of coefficients is known. In this case, we assume that

$$D_x^{\alpha_0} f_0(x) \neq 0 \text{ for } x \in \overline{\Omega}.$$

Then for a sufficiently large $T > 0$, there exists at most one pair of functions (u, a_{α_0}) satisfying (1.127)–(1.129) and such that $u \in C^{3+|\alpha_0|}\left(\overline{Q}_T\right)$.

If in (1.128) $f_0(x) \equiv 0$, then conditions of these two cases should be imposed on the function $f_1(x)$, the required smoothness of the function u should be increased by one and the above statements about uniqueness would still hold.

Proof. First, we note that if $f_0(x) \equiv 0$, then one should consider in this proof u_t instead of u, and the rest of the proof is the same as the one below. We prove this theorem only for Case 1, since Case 2 is similar. Assume that there exist two solutions (u_1, c_1) and (u_2, c_2). Denote $\widetilde{u} = u_1 - u_2, \widetilde{c} = c_1 - c_2$. Since

$$c_1 u_{1tt} - c_2 u_{2tt} = c_1 u_{1tt} - c_1 u_{2tt} + (c_1 - c_2) u_{2tt} = c_1 \widetilde{u}_{tt} + \widetilde{c} u_{2tt},$$

then (1.127)–(1.129) lead to

$$L\widetilde{u} = c_1(x)\widetilde{u}_{tt} - \Delta\widetilde{u} - \sum_{j=1}^{n} a_\alpha(x) D_x^\alpha \widetilde{u} = -\widetilde{c}(x) H(x,t), \text{ in } Q_T, \tag{1.131}$$

$$\widetilde{u}(x,0) = 0, \widetilde{u}_t(x,0) = 0, \tag{1.132}$$

$$\widetilde{u}|_{S_T} = \frac{\partial \widetilde{u}}{\partial n}|_{S_T} = 0, \tag{1.133}$$

$$H(x,t) := u_{2tt}(x,t). \tag{1.134}$$

Setting in (1.127) $c := c_2, u := u_2, t := 0$ and using (1.128), (1.130), and (1.134), we obtain

$$H(x,0) = c_2^{-1}(x)\left(\Delta f_0(x) + \sum_{|\alpha|\leq 1} a_\alpha(x) D_x^\alpha f_0(x)\right) \neq 0 \text{ for } x \in \overline{\Omega}.$$

Hence, there exists a sufficiently small positive number ε, such that

$$H(x,t) \neq 0 \text{ in } \overline{Q}_\varepsilon = \overline{\Omega} \times [0,\varepsilon]. \tag{1.135}$$

Now, we eliminate the unknown coefficient $\widetilde{c}(x)$ from (1.131). We have

$$-\widetilde{c}(x) = \frac{L\widetilde{u}}{H(x,t)} \text{ in } \overline{Q}_\varepsilon.$$

Hence,

$$\frac{\partial}{\partial t}\left[-\widetilde{c}\left(x\right)\right]=\frac{\partial}{\partial t}\left[\frac{L\widetilde{u}}{H\left(x,t\right)}\right]=0 \text{ in } \overline{Q}_{\varepsilon}.$$

Or

$$L\widetilde{u}_{t}=\frac{H_{t}}{H}\left(L\widetilde{u}\right) \text{ in } \overline{Q}_{\varepsilon}. \tag{1.136}$$

Denote

$$h\left(x,t\right)=\frac{H_{t}}{H}\left(x,t\right). \tag{1.137}$$

Since $u\in C^{4}\left(\overline{Q}_{T}\right)$, then (1.134), (1.135), and (1.137) imply that

$$h\in C^{2}\left(\overline{Q}_{\varepsilon}\right). \tag{1.138}$$

Introduce a new function $v\left(x,t\right)$:

$$v\left(x,t\right)=\widetilde{u}_{t}\left(x,t\right)-h\widetilde{u}\left(x,t\right) \tag{1.139}$$

Considering (1.139) as an ordinary differential equation with respect to $\widetilde{u}\left(x,t\right)$ and using (1.132) as well as (1.137), we obtain

$$\widetilde{u}\left(x,t\right)=\int_{0}^{t}K\left(x,t,\tau\right)v\left(x,\tau\right)\mathrm{d}\tau, \tag{1.140}$$

$$K\left(x,t,\tau\right)=\frac{H\left(x,t\right)}{H\left(x,\tau\right)}\in C^{2}\left(\overline{\Omega}\times\left[0,\varepsilon\right]\times\left[0,\varepsilon\right]\right), \tag{1.141}$$

$$v\left(x,0\right)=0. \tag{1.142}$$

Using (1.139)–(1.141), we obtain the following formulas in $\overline{Q}_{\varepsilon}$:

$$\begin{aligned}c_{1}\left(\widetilde{u}_{t}\right)_{tt}-hc_{1}\widetilde{u}_{tt}&=c_{1}\left(\widetilde{u}_{t}-h\widetilde{u}\right)_{tt}+2c_{1}h_{t}\widetilde{u}_{t}+c_{1}h_{tt}\widetilde{u}\\&=c_{1}v_{tt}+2c_{1}h_{t}v+2c_{1}h_{t}\int_{0}^{t}K_{t}\left(x,t,\tau\right)v\left(x,\tau\right)\mathrm{d}\tau\\&\quad+c_{1}h_{tt}\int_{0}^{t}K\left(x,t,\tau\right)v\left(x,\tau\right)\mathrm{d}\tau,\end{aligned}$$

$$\Delta\widetilde{u}_t - h\Delta\widetilde{u} = \Delta\left(\widetilde{u}_t - h\widetilde{u}\right) + 2\nabla h\nabla\widetilde{u} + \Delta h\widetilde{u}$$
$$= \Delta v + 2\nabla h\nabla\left(\int_0^t K(x,t,\tau)\, v(x,\tau)\, d\tau\right)$$
$$+\Delta h\int_0^t K(x,t,\tau)\, v(x,\tau)\, d\tau.$$

By (1.136),

$$L\widetilde{u}_t - hL\widetilde{u} = 0 \text{ in } Q_\varepsilon. \tag{1.143}$$

Hence, substituting the recent formulas in (1.143) and using boundary conditions (1.133) and the initial condition (1.142), we obtain the following inequality:

$$|c_1(x)\, v_{tt} - \Delta v| \le M\left[|\nabla v|(x,t) + |v|(x,t) + \int_0^t (|\nabla v| + |v|)(x,\tau)\, d\tau\right] \text{ in } \overline{Q}_\varepsilon,$$
$$v|_{S_\varepsilon} = \frac{\partial v}{\partial n}|_{S_\varepsilon} = 0, \tag{1.144}$$
$$v(x,0) = 0,$$

where $M > 0$ is a constant independent on v, x, t.

Let $\eta_0 = \eta_0\left(\overline{c}, R, \|\nabla c\|_{C(\overline{\Omega})}\right) \in (0,1]$ be the number considered in Theorems 1.10.2 and 1.10.4. Consider now the domain $G^+_{\eta_0\varepsilon^2}$ defined as

$$G^+_{\eta_0\varepsilon^2} = \left\{(x,t) : |x|^2 - \eta_0 t^2 > R^2 - \eta_0\varepsilon^2, t > 0, |x| < R\right\}.$$

Then, $G^+_{\eta_0\varepsilon^2} \subset \overline{Q}_\varepsilon$. Hence, we can apply now Theorem 1.10.4 to conditions (1.144). Thus, we obtain $v(x,t) = 0$ in $G^+_{\eta_0\varepsilon^2}$. Hence, by (1.140) $\widetilde{u}(x,t) = 0$ in $G^+_{\eta_0\varepsilon^2}$. Therefore, setting $t = 0$ in (1.131) and using (1.135), we obtain

$$\widetilde{c}(x) = 0 \text{ for } x \in \left\{|x| \in \left(\sqrt{R^2 - \eta_0\varepsilon^2}, R\right)\right\}. \tag{1.145}$$

Substitute this in (1.131) and use (1.132) and (1.133). We obtain

$$L\widetilde{u} = c_1(x)\widetilde{u}_{tt} - \Delta\widetilde{u} - \sum_{j=1}^n a_\alpha(x)\, D_x^\alpha\widetilde{u} = 0, \tag{1.146}$$

$$\text{for } (x,t) \in \left\{|x| \in \left(\sqrt{R^2-\eta_0\varepsilon^2}, R\right)\right\} \times (0,T), \tag{1.147}$$

$$\widetilde{u}(x,0) = 0, \widetilde{u}_t(x,0) = 0, \tag{1.148}$$

$$\widetilde{u}|_{S_T} = \frac{\partial \widetilde{u}}{\partial n}|_{S_T} = 0. \tag{1.149}$$

Consider an arbitrary number $t_0 \in (0, T-\varepsilon)$. And consider the domain $G_{\eta_0\varepsilon^2}(t_0)$:

$$G_{\eta_0\varepsilon^2}(t_0) = \left\{(x,t) : |x|^2 - \eta_0 (t-t_0)^2 > R^2 - \eta_0\varepsilon^2, t > 0, |x| < R\right\}.$$

Hence, in this domain $t \in (t_0-\varepsilon, t_0+\varepsilon) \cap \{t > 0\}$. Since $t_0 \in (0, T-\varepsilon)$, then $t \in (0,T)$ in this domain. Hence,

$$G_{\eta_0\varepsilon^2}(t_0) \subset \left\{|x| \in \left(\sqrt{R^2-\eta_0\varepsilon^2}, R\right)\right\} \times (0,T).$$

Hence, we can apply Corollary 1.10.4 to the domain $G_{\eta_0\varepsilon^2}(t_0)$ and conditions (1.146)–(1.149). Therefore, $\widetilde{u}(x,t) = 0$ for $(x,t) \in G_{\eta_0\varepsilon^2}(t_0)$. Since t_0 is an arbitrary number of the interval $(0, T-\varepsilon)$, then, varying this number, we obtain that

$$\widetilde{u}(x,t) = 0 \text{ for } (x,t) \in \left\{|x| \in \left(\sqrt{R^2-\eta_0\varepsilon^2}, R\right)\right\} \times (0, T-\varepsilon).$$

Therefore, we now can replace in (1.131)–(1.134) sets Q_T, S_T with sets

$$Q_T^\varepsilon = \left\{|x| < \sqrt{R^2-\eta_0\varepsilon^2}\right\} \times (0, T-\varepsilon),$$

$$S_T^\varepsilon = \left\{|x| = \sqrt{R^2-\eta_0\varepsilon^2}\right\} \times (0, T-\varepsilon),$$

and repeat the above proof. Hence, we obtain instead of (1.145) that

$$\widetilde{c}(x) = 0 \text{ for } x \in \left\{|x| \in \left(\sqrt{R^2-2\eta_0\varepsilon^2}, R\right)\right\}.$$

Since $\varepsilon > 0$ is sufficiently small, we can always choose ε such that $R^2 = k\eta_0\varepsilon^2$ where $k = k(R,\varepsilon) \geq 1$ is an integer. Suppose that

$$T > k\varepsilon = \frac{R}{\sqrt{\eta_0}\varepsilon}.$$

Hence, we can repeat this process k times until the entire domain $\Omega = \{|x| < R\}$ would be exhausted. Thus, we obtain after k steps that $\widetilde{c}(x) = 0$ in Ω. Thus, the right-hand side of (1.131) is identical zero. This, (1.131)–(1.133) and the standard energy estimate imply that $\widetilde{u}(x,t) = 0$ in Q_T. □

A slightly inconvenient point of Theorem 1.10.5.1 is that the observation time T is assumed to be sufficiently large. Our experience of working with experimental data (Chaps. 5 and 6) indicates that this is not a severe restriction in applications. Indeed, usually the outcoming signal can be measured for quite a long time. Still, it is possible to restrict the value of T to the same one as in Theorem 1.10.4 via imposing the condition $f_1(x) \equiv 0$. This was observed in [80, 81]. The proof of Theorem 1.10.5.2 partially repeats arguments of [80, 81].

Theorem 1.10.5.2. *Assume that all conditions of Theorem 1.10.5.1 are satisfied. In addition, assume that in (1.128) the function* $f_1(x) \equiv 0$. *Then Theorem 1.10.5.1 remains valid if*

$$T > \frac{R}{\sqrt{\eta_0}}. \tag{1.150}$$

In particular, if $c(x) \equiv 1$, *then it is sufficient to have* $T > R$.

Proof. Similarly with the proof of Theorem 1.10.5.1, we consider now only for Case 1. We keep notations of Theorem 1.10.5.1Consider the function $w(x,t) = \widetilde{u}_{tt}(x,t)$. Then (1.131)–(1.134) imply that

$$c_1(x) w_{tt} - \Delta w - \sum_{j=1}^{n} a_\alpha(x) D_x^\alpha w = -\widetilde{c}(x) \partial_t^4 u_2, \text{ in } Q_T, \tag{1.151}$$

$$w_t(x,0) = 0, \tag{1.152}$$

$$w|_{S_T} = \frac{\partial w}{\partial n}|_{S_T} = 0, \tag{1.153}$$

$$w(x,0) = -\widetilde{c}(x) p(x), \tag{1.154}$$

$$p(x) = c_1^{-1}(x) \left(\Delta f_0(x) + \sum_{|\alpha| \le 1} a_\alpha(x) D_x^\alpha f_0(x) \right) \neq 0 \text{ for } x \in \overline{\Omega}. \tag{1.155}$$

Hence, it follows from (1.154) and (1.155) that

$$-\widetilde{c}(x) = \frac{w(x,0)}{p(x)} = \frac{1}{p(x)} \left[w(x,t) - \int_0^t w_t(x,\tau)\, d\tau \right].$$

Substituting this formula in (1.151), using Theorem 1.10.4, (1.150), (1.152), and (1.153) and proceeding similarly with the proof of Theorem 1.10.4, we obtain that $\widetilde{c}(x) = 0$ in Ω and $w(x,t) = \widetilde{u}(x,t) = 0$ in Q_T. □

1.10.6 The First Coefficient Inverse Problem for a Parabolic Equation

Consider the Cauchy problem for the following parabolic equation:

$$c(x)\, u_t = \Delta u + \sum_{|\alpha| \le 1} a_\alpha(x)\, D_x^\alpha u, \text{ in } D_T^{n+1} = \mathbb{R}^n \times (0,T), \tag{1.156}$$

$$u(x,0) = f_0(x), \tag{1.157}$$

$$c, a_\alpha \in C^\beta(\mathbb{R}^n),\ c(x) \ge 1,\ f_0 \in C^{2+\beta}(\mathbb{R}^n),\ \beta \in (0,1). \tag{1.158}$$

So (1.156) and (1.157) is the forward problem. Given conditions (1.158), this problem has unique solution $u \in C^{2+\beta,1+\beta/2}\left(\overline{D}_T^{n+1}\right)$ [120]. Just as in Sect. 1.10.5, assume that $\Omega = \{|x| < R\} \subset \mathbb{R}^n, n \ge 2$. Let $\Gamma \subseteq \partial\Omega$ be a part of the boundary of the domain Ω, $T = \text{const.} > 0$ and $\Gamma_T = \Gamma \times (0,T)$.

The First Parabolic Coefficient Inverse Problem. Suppose that one of coefficients in (1.156) is unknown inside the domain Ω and is known outside of it. Also, assume that all other coefficients in (1.156) are known, and conditions (1.157), (1.158) are satisfied. Determine that unknown coefficient inside Ω, assuming that the following functions $p(x,t)$ and $q(x,t)$ are known,

$$u|_{\Gamma_T} = p(x,t), \quad \frac{\partial u}{\partial n}|_{\Gamma_T} = q(x,t). \tag{1.159}$$

It is yet unclear how to prove a uniqueness theorem for this CIP "straightforwardly." The reason is that one cannot extend properly the solution of the problem (1.156) and (1.157) in $\{t < 0\}$. Thus, the idea here is to consider an associated CIP for a hyperbolic PDE using a connection between these two CIPs via an analog of the Laplace transform. Next, Theorem 1.10.5.1will provide the desired uniqueness result.

That associated hyperbolic Cauchy problem is

$$v_{tt} = \frac{1}{c(x)} \left(\Delta v + \sum_{|\alpha| \le 1} a_\alpha(x)\, D_x^\alpha v \right) \text{ in } D_\infty^{n+1} = \mathbb{R}^n \times (0,\infty), \tag{1.160}$$

$$v|_{t=0} = 0,\ v_t|_{t=0} = f_0(x). \tag{1.161}$$

In addition to (1.158), we assume that the coefficients $c(x), a_\alpha(x)$ and the initial condition $f_0(x)$ are so smooth that the solution v of the problem (1.160) and (1.161) is such that (a) $v \in C^4(\overline{D}_\infty^{n+1})$ if the function $c(x)$ is unknown and (b) $v \in C^{3+|\alpha|}(\overline{D}_\infty^{n+1})$ if the function $c(x)$ is known and any of functions $a_\alpha(x)$ is unknown.

Consider an interesting Laplace-like transform which was proposed, for the first time, by K.G. Reznickaya in 1973 [142] and was widely used since then [102, 123, 124]. Namely, one can easily verify the following connection between solutions u and v of parabolic and hyperbolic Cauchy problems (1.156), (1.157) and (1.160), (1.161)

$$u(x,t) = \frac{1}{2t\sqrt{\pi t}} \int_0^\infty \exp\left[-\frac{\tau^2}{4t}\right] \tau v(x,\tau)\, d\tau. \tag{1.162}$$

Since the transformation (1.162) is one-to-one (as an analog of the Laplace transform), the following two functions $\overline{p}(x,t)$ and $\overline{q}(x,t)$ can be uniquely determined from functions (1.159):

$$v|_{\Gamma_\infty} = \overline{p}(x,t), \quad \frac{\partial v}{\partial n}|_{\Gamma_\infty} = \overline{q}(x,t). \tag{1.163}$$

Therefore, the first parabolic CIP is reduced to the hyperbolic CIP (1.160), (1.161) and (1.163). At the same time, the inversion of the transformation (1.162) is a severely ill-posed procedure. Hence, this inversion cannot be used for computations.

We are almost ready now to apply Theorem 1.10.5.1 The only thing left to do is to replace Γ_∞ in (1.163) with S_∞. To do this, we observe that, using (1.159) and the fact that the unknown coefficient is given outside of the domain Ω, one can uniquely determine the function $u(x,t)$ for $(x,t) \in (\mathbb{R}^n \setminus \Omega) \times (0,T)$. This is because of the well known uniqueness result for the Cauchy problem for the parabolic equation with the Cauchy data given at a part of the lateral boundary [124]. Therefore, we can uniquely determine functions $u, \partial_n u$ at S_T. This means in turn that we can replace in (1.163) Γ_∞ with S_∞. Hence, Theorem 1.10.5.1 leads to Theorem 1.10.6.

Theorem 1.10.6. *Assume that conditions (1.158) hold. Also, assume that coefficients $c(x), a_\alpha(x)$ and the initial condition $f_0(x)$ are so smooth that the solution v of the problem (1.160) and (1.161) is such that:*

(a) $v \in C^4(\overline{D}_\infty^{n+1})$ *if the function $c(x)$ is unknown and*

(b) $v \in C^{3+|\alpha|}(\overline{D}_\infty^{n+1})$ *if any of functions $a_\alpha(x)$ is unknown. Let $\Omega = \{|x| < R\} \subset \mathbb{R}^n, n \geq 2$. Suppose that conditions of either of Cases 1 or 2 of Theorem 1.10.5.1 hold. Also, assume that coefficients of (1.160) and the initial condition (1.157) are so smooth that the smoothness of the solution $v(x,t)$ of the hyperbolic Cauchy problem (1.160) and (1.161) required in Theorem 1.10.5.1 is guaranteed. Then, conclusions of 1.10.5.1 are true with respect to the CIP (1.156)–(1.159).*

1.10.7 The Second Coefficient Inverse Problem for a Parabolic Equation

Theorem 1.10.6 has two inconvenient points. First, one needs to reduce the parabolic CIP to the hyperbolic CIP via inverting the transform (1.162). Second, one needs to use a special form of the elliptic operator in (1.156). The coefficient $c(x)$ in the principal part of this operator must satisfy conditions (1.81) and (1.82). Although these conditions are satisfied for the case $c(x) \equiv 1$, still the question remains whether it is possible to prove uniqueness of a CIP for the case of a general parabolic operator of the second order. It is shown in this section that the latter is possible, provided that one can guarantee the existence of the solution of the parabolic PDE for both positive and negative values of t. This condition is always used in studies of CIPs for parabolic PDEs via the Bukhgeim-Klibanov method; see for example, [33, 62, 79, 161].

Let $\Omega \subset \mathbb{R}^n$ be either finite or infinite domain with the piecewise smooth boundary $\partial\Omega$, $\Gamma \subset \partial\Phi$ be a part of this boundary, and $T = \text{const} > 0$. Denote

$$Q_T^{\pm} = G \times (-T, T), \Gamma_T^{\pm} = \Gamma \times (-T, T).$$

Let L be the following elliptic operator in $P_T^{\pm}$:

$$Lu = \sum_{|\alpha| \le 2} a_\alpha(x,t) D_x^\alpha u, (x,t) \in P_T^{\pm}, \tag{1.164}$$

$$a_\alpha \in C^1\left(\overline{Q}_T^{\pm}\right), \tag{1.165}$$

$$\mu_1 |\xi|^2 \le \sum_{|\alpha|=2} a_\alpha(x,t) \xi^\alpha \le \mu_2 |\xi|^2; \quad \mu_1, \mu_2 = \text{const.} > 0, \tag{1.166}$$

$$\forall \xi \in \mathbb{R}^n, \forall (x,t) \in \overline{Q}_T^{\pm}. \tag{1.167}$$

The Second Parabolic Coefficient Inverse Problem. Assume that one of coefficients a_{α_0} of the operator L is independent of t, $a_{\alpha_0} := a_{\alpha_0}(x)$ and is unknown in Ω, whereas all other coefficients of L are known in $Q_T^{\pm}$. Let the function $u \in C^{4,2}\left(\overline{Q}_T^{\pm}\right)$ satisfy the parabolic equation

$$u_t = Lu + F(x,t), \text{ in } Q_T^{\pm}. \tag{1.168}$$

Determine the coefficient $a_{\alpha_0}(x)$ for $x \in \Omega$ assuming that the function $F(x,t)$ is known in $Q_T^{\pm}$ and that the following functions $f_0(x), p(x,t)$, and $q(x,t)$ are known as well:

$$u(x,0) = f_0(x), x \in \Omega, \tag{1.169}$$

$$u|_{\Gamma_T^{\pm}} = p(x,t), \frac{\partial u}{\partial n}|_{\Gamma_T^{\pm}} = q(x,t). \tag{1.170}$$

Prior to the formulation of the uniqueness theorem for this problem, we present the Carleman estimate for the principal part L_p of the parabolic operator L in (1.164):

$$L_p u = u_t - \sum_{|\alpha|=2} a_\alpha(x,t) D_x^\alpha u.$$

We assume for brevity only that

$$\Omega \subset \{x_1 > 0\} \text{ and } \Gamma = \{x \in \mathbb{R}^n : x_1 = 0, |\overline{x}| \le A\}, A = \text{const.} > 0, \tag{1.171}$$

where $\overline{x} = (x_2, ..., x_n)$. Let $\xi \in (0,1)$. Consider the function

$$\psi(x,t) = x_1 + \frac{|\overline{x}|^2}{A^2} + \frac{t^2}{T^2} + \xi. \tag{1.172}$$

Let $\gamma \in (\xi, 1)$. Consider the domain H_γ :

$$H_\gamma = \{(x,t) : x_1 > 0, \psi(x,t) < \gamma\}. \tag{1.173}$$

Let $\lambda, \nu > 1$ be two large parameters which we will choose later. In the domain H_γ we consider the following function φ, which is the CWF for the operator L_p :

$$\varphi(x,t) = \exp[\lambda \psi^{-\nu}(x,t)].$$

Lemma 1.10.7 was proven in [124] for the case when terms with $1/\lambda$ were not involved in (1.174). However, these terms can still be incorporated if using ideas of the proof of the second fundamental inequality for elliptic operators of Ladyzhenskaya [119].

Lemma 1.10.7. *Let functions $a_\alpha(x,t), |\alpha| = 2$ satisfy conditions (1.165)–(1.167) and:*

$$\max_{|\alpha|=2} \|\|\nabla_{x,t} a_\alpha\|\|_{C\left(\overline{Q}_T^{\pm}\right)} \le B = \text{const.}$$

Then, there exist sufficiently large numbers $\lambda_0 = \lambda_0(\xi, \gamma, \mu_1, \mu_2, B) > 1$, $\nu_0 = \nu_0(\xi, \gamma, \mu_1, \mu_2, B) > 1$ such that for $\nu := \nu_0$, for all $\lambda \ge \lambda_0$, and for all functions $u \in C^{2,1}(\overline{Q}_T^{\pm})$, the following pointwise Carleman estimate holds for the operator L_p:

$$\left(L_p u\right)^2 \varphi^2 \ge \frac{C}{\lambda}\left(u_t^2 + \sum_{|\alpha|=2}\left(D_x^\alpha u\right)^2\right)\varphi^2 + C\lambda|\nabla u|^2\varphi^2 + C\lambda^3|\nabla u|^2\varphi^2$$
$$+\nabla \cdot U + V_t, \quad (x,t) \in H_\gamma, \tag{1.174}$$

where the vector function (U, V) *satisfies the following estimate:*

$$|(U,V)| \leq C\lambda^3 \left[\sum_{|\alpha|\leq 2} \left(D_x^\alpha u\right)^2 + u_t^2 \right] \varphi^2.$$

Here, the constant $C = C(\beta, \gamma, \mu_1, \mu_2, B) > 0$ *is independent on* λ, u.

Theorem 1.10.7. *Assume that (1.171) holds, the unknown coefficient* $a_{\alpha_0}(x)$ *is independent on* t, *and that* $D_x^{\alpha_0} f_0(x) \neq 0$ *in* $\overline{\Omega}$. *Then there exists at most one solution* $(a_{\alpha_0}, u) \in C^1\left(\overline{\Omega}\right) \times C^{4,2}\left(\overline{P}_T^{\pm}\right)$ *of the inverse problem (1.164)–(1.170).*

Proof. Let $B_1 = \|u\|_{C^{4,2}\left(\overline{Q}_T^{\pm}\right)}$. Let $\theta \in (0,1)$ be a parameter which we will choose later. We change variables now only because coefficients in the principal part L_{p} of the operator $\partial_t - L$ depend on t. If they would be independent on t, we would not need this change of variables. Change variables in (1.168) as $(t', x') = \left(\theta t, \sqrt{\theta} x\right)$ and keep the same notations for new functions, new domains, and new variables for brevity. In new variables we have

$$\max_{\overline{P}_T^{\pm}} |\partial_t a_\alpha(x,t)| \leq \theta B, \ \max_{\overline{P}_T^{\pm}} |\nabla_x a_\alpha(x,t)| \leq \sqrt{\theta} B, |\alpha| = 2, \tag{1.175}$$

$$\max_{\overline{P}_T^{\pm}} |\partial_t a_\alpha(x,t)| \leq \theta B', |\alpha| \leq 1, \tag{1.176}$$

where the number B is defined in Lemma 1.10.7 and B' is another positive constant independent on θ. In particular, (1.175) means that the constant $C > 0$ in Lemma 1.10.7 remains the same after this change of variables. Conditions (1.168)–(1.170) become

$$u_t = \sum_{|\alpha|=2} a_\alpha(x,t) D_x^\alpha u + \sum_{|\alpha|\leq 1} \left(\sqrt{\theta}\right)^{|\alpha|-2} a_\alpha(x,t) D_x^\alpha u + \theta F(x,t), \tag{1.177}$$

$$u(x,0) = f_0(x), \tag{1.178}$$

$$u|_{\Gamma_T^{\pm}} = p(x,t), \quad \partial_{x_1} u|_{\Gamma_T^{\pm}} = -\sqrt{\theta} q(x,t). \tag{1.179}$$

Assume that there exist two pairs of functions satisfying conditions of this theorem:

$$\left(a_{\alpha_0}^{(1)}, u_1\right), \left(a_{\alpha_0}^{(2)}, u_2\right), b(x) = a_{\alpha_0}^{(1)}(x) - a_{\alpha_0}^{(2)}(x), \widetilde{u} = u_1 - u_2.$$

Then, similarly with the proof of Theorem 1.10.5.1, we obtain from (1.177)–(1.179)

$$\widetilde{u}_t - \sum_{|\alpha|=2,\alpha\neq\alpha_0} a_\alpha(x,t)\, D_x^\alpha \widetilde{u} - \sum_{|\alpha|\leq 1} \left(\sqrt{\theta}\right)^{|\alpha|-2} a_\alpha(x,t)\, D_x^\alpha u$$
$$- \left(\sqrt{\theta}\right)^{|\alpha_0|-2} a_{\alpha_0}^{(1)}(x)\, D_x^{\alpha_0}\widetilde{u} = -\left(\sqrt{\theta}\right)^{|\alpha_0|-2} b(x)\, D_x^{\alpha_0} u_2, \tag{1.180}$$

$$\widetilde{u}(x,0) = 0, \tag{1.181}$$

$$\widetilde{u}|_{\Gamma_T^\pm} = 0, \quad \partial_{x_1}\widetilde{u}|_{\Gamma_T^\pm} = 0. \tag{1.182}$$

Since (1.171) holds, we can assume without loss of generality that $H_\gamma \subset P_T^\pm$. Next, since $D_x^{\alpha_0} f_0(x) \neq 0$ in $\overline{\Omega}$, we can assume without loss of generality that there exists a constant $d > 0$ such that in old variables $D_x^{\alpha_0} f_0(x) \geq 2d > 0$. Hence, in new variables $|D_x^{\alpha_0} f_0(x)| \geq 2\theta^{\alpha_0/2} d$. Therefore, we can choose in (1.172) and (1.173) $\gamma - \xi > 0$ so small that in new variables

$$D_x^{\alpha_0} u_2(x,t) \geq \theta^{\alpha_0/2} d \text{ in } \overline{H}_\gamma. \tag{1.183}$$

In addition,

$$\left|D^{\alpha+\alpha_0} u_2(x,t)\right| \leq d_1 \text{ in } \overline{H}_\gamma,\ \forall \alpha \in \{|\alpha| \leq 2\}, \tag{1.184}$$

where the constant $d_1 > 0$ is independent on θ, as long as $\theta \in (0,1)$.

Let

$$L_1\widetilde{u} = \sum_{|\alpha|=2,\alpha\neq\alpha_0} a_\alpha(x,t)\, D_x^\alpha \widetilde{u} + \sum_{|\alpha|\leq 1,\alpha\neq\alpha_0} \left(\sqrt{\theta}\right)^{|\alpha|-2} a_\alpha(x,t)\, D_x^\alpha \widetilde{u}$$
$$+ \left(\sqrt{\theta}\right)^{|\alpha_0|-2} a_{\alpha_0}^{(1)}(x)\, D_x^{\alpha_0}\widetilde{u}.$$

Using (1.180), we obtain

$$-\left(\sqrt{\theta}\right)^{|\alpha_0|-2} b(x) = \frac{\widetilde{u}_t - L_1\widetilde{u}}{D_x^{\alpha_0} u_2} \text{ in } H_\gamma.$$

Differentiating this equality with respect to t, we obtain

$$\left(\widetilde{u}_t - L_1\widetilde{u}\right)_t - g(x,t)\left(\widetilde{u}_t - L_1\widetilde{u}\right) = 0 \text{ in } H_\gamma, \tag{1.185}$$

$$g(x,t) = \partial_t \ln\left(D_x^{\alpha_0} u_2\right). \tag{1.186}$$

We have

$$(L_1\widetilde{u})_t = \sum_{|\alpha|=2,\alpha\neq\alpha_0} a_\alpha(x,t)\, D_x^\alpha \widetilde{u}_t + \sum_{|\alpha|\leq 1,\alpha\neq\alpha_0} \left(\sqrt{\theta}\right)^{|\alpha|-2} a_\alpha(x,t)\, D_x^\alpha \widetilde{u}_t$$
$$+ \left(\sqrt{\theta}\right)^{|\alpha_0|-2} a_{\alpha_0}^{(1)}(x)\, D_x^{\alpha_0}\widetilde{u}_t + \sum_{|\alpha|=2,\alpha\neq\alpha_0} \partial_t\left(a_\alpha(x,t)\right) D_x^\alpha \widetilde{u}$$
$$+ \sum_{|\alpha|\leq 1,\alpha\neq\alpha_0} \left(\sqrt{\theta}\right)^{|\alpha|-2} \partial_t\left(a_\alpha(x,t)\right) D_x^\alpha \widetilde{u}.$$

Hence, (1.185) implies that

$$\left(\widetilde{u}_{tt} - g\widetilde{u}_t\right) - \sum_{|\alpha|=2,\alpha\neq\alpha_0} a_\alpha(x,t)\left(D_x^\alpha\widetilde{u}_t - gD_x^\alpha\widetilde{u}\right)$$
$$- \sum_{|\alpha|\leq 1,\alpha\neq\alpha_0} \left(\sqrt{\theta}\right)^{|\alpha|-2} a_\alpha(x,t)\left(D_x^\alpha\widetilde{u}_t - gD_x^\alpha\widetilde{u}\right)$$
$$- \left(\sqrt{\theta}\right)^{|\alpha_0|-2} a_{\alpha_0}^{(1)}(x)\left(D_x^{\alpha_0}\widetilde{u}_t - gD_x^{\alpha_0}\widetilde{u}\right)$$
$$- \sum_{|\alpha|=2,\alpha\neq\alpha_0} \partial_t\left(a_\alpha(x,t)\right) D_x^\alpha\widetilde{u}$$
$$- \sum_{|\alpha|\leq 1,\alpha\neq\alpha_0} \left(\sqrt{\theta}\right)^{|\alpha|-2} \partial_t\left(a_\alpha(x,t)\right) D_x^\alpha\widetilde{u} = 0, \text{ in } H_\gamma. \tag{1.187}$$

Now, use the formula $gD_x^\alpha\widetilde{u} = D_x^\alpha(g\widetilde{u}) + lot$, where lot is a linear combination of derivatives of the function $\widetilde{u}$ whose order is less than $|\alpha|$. Then

$$D_x^\alpha\widetilde{u}_t - gD_x^\alpha\widetilde{u} = D_x^\alpha\left(\widetilde{u}_t - g\widetilde{u}\right) + lot,\ \widetilde{u}_{tt} - g\widetilde{u}_t = D_t\left(\widetilde{u}_t - g\widetilde{u}\right) + g_t\widetilde{u}. \tag{1.188}$$

Denote $v = \widetilde{u}_t - p\widetilde{u}$. Then, (1.181) and (1.186) imply that

$$\widetilde{u}(x,t) = \int_0^t K(x,t,\tau)\, v(x,\tau)\, d\tau, \text{ in } H_\gamma, \tag{1.189}$$
$$K(x,t,\tau) = \frac{D_x^{\alpha_0} u_2(x,t)}{D_x^{\alpha_0} u_2(x,\tau)}. \tag{1.190}$$

It follows from (1.183), (1.184), and (1.190) that

$$\left|D_x^\alpha K(x,t,\tau)\right| \leq M, |\alpha| \leq 2 \text{ for } (x,t), (x,\tau) \in H_\gamma. \tag{1.191}$$

Here and below in this proof, M denotes different positive constants independent on the function v and the parameter $\theta \in (0,1)$.

Hence, using (1.175), (1.176), and (1.187)–(1.191), we obtain

$$\left|L_{\mathrm{p}}v\right| = \left|v_t - \sum_{|\alpha|=2} a_\alpha(x,t)\, D_x^\alpha v\right| \le M\theta \sum_{|\alpha|=2} \left|\int_0^t |D_x^\alpha v|(x,\tau)\,\mathrm{d}\tau\right|$$

$$+\frac{M}{\theta^2}\sum_{|\alpha|\le 1}|D_x^\alpha v| + \frac{M}{\theta^2}\sum_{|\alpha|\le 1}\left|\int_0^t |D_x^\alpha v|(x,\tau)\,\mathrm{d}\tau\right|, \text{ in } H_\gamma, \tag{1.192}$$

$$v|_{\Gamma_T^{\pm}\cap\overline{H}_\gamma} = 0, \quad \partial_{x_1} v|_{\Gamma_T^{\pm}\cap\overline{H}_\gamma} = 0. \tag{1.193}$$

Now, we are ready to apply the Carleman estimate of Lemma 1.10.7, assuming that parameters $\nu := \nu_0, \lambda_0$ are the same as ones in this lemma and that $\lambda \ge \lambda_0$. Multiply both sides of the inequality (1.192) by the function $\varphi(x,t)$, then square it and integrate over the domain H_γ. We obtain

$$\int_{H_\gamma} \left(L_{\mathrm{p}}v\right)^2 \varphi^2 \mathrm{d}x\mathrm{d}t \le M\theta^2 \sum_{|\alpha|=2}\int_{H_\gamma}\left(\int_0^t |D_x^\alpha v|(x,\tau)\,\mathrm{d}\tau\right)^2 \varphi^2\mathrm{d}x\mathrm{d}t$$

$$+\frac{M}{\theta^4}\int_{H_\gamma}\left(\int_0^t (|\nabla v| + |v|)(x,\tau)\,\mathrm{d}\tau\right)^2 \varphi^2\mathrm{d}x\mathrm{d}t$$

$$+\frac{M}{\theta^4}\int_{H_\gamma}\left(|\nabla v|^2 + v^2\right)\varphi^2\mathrm{d}x\mathrm{d}t. \tag{1.194}$$

Using Lemma 1.10.3, we obtain from (1.194)

$$\int_{H_\gamma}(L_0 v)^2\varphi^2\mathrm{d}x\mathrm{d}t \le \frac{M\theta^2}{\lambda}\sum_{|\alpha|=2}\int_{H_\gamma}\left(D_x^\alpha v\right)^2\varphi^2\mathrm{d}x\mathrm{d}t + \frac{M}{\theta^4}\int_{H_\gamma}\left(|\nabla v|^2 + v^2\right)\varphi^2\mathrm{d}x\mathrm{d}t. \tag{1.195}$$

On the other hand, using (1.174) and (1.193), we obtain

$$\int_{H_\gamma}\left(L_{\mathrm{p}}v\right)^2\varphi^2\mathrm{d}x\mathrm{d}t \ge \frac{C}{\lambda}\sum_{|\alpha|=2}\int_{H_\gamma}\left(D_x^\alpha v\right)^2\varphi^2\mathrm{d}x\mathrm{d}t + C\int_{H_\gamma}\left(\lambda|\nabla v|^2 + \lambda^3 v^2\right)\varphi^2\mathrm{d}x\mathrm{d}t$$

$$-C\lambda^3\int_{\partial_1 H_\gamma}\sum_{|\alpha|\le 2}\left(D_x^\alpha v\right)^2\varphi^2\mathrm{d}x\mathrm{d}t, \tag{1.196}$$

where $\partial_1 H_\gamma = \{(x,t) : \psi(x,t) = \gamma, x_1 > 0\}$. Hence,

$$\varphi^2 = \exp\left(2\lambda\gamma^{-\nu}\right) \text{ on } \partial_1 H_\gamma. \tag{1.197}$$

Choose $\theta \in (0,1)$ so small that $M\theta^2 \leq C/2$. Then comparing (1.195) with (1.196) and taking into account (1.197), we obtain for sufficiently large $\lambda \geq \lambda_1(\theta) > 1$

$$\frac{1}{\lambda}\sum_{|\alpha|=2}\int\limits_{H_\gamma}\left(D_x^\alpha v\right)^2\varphi^2 \mathrm{d}x\mathrm{d}t + \int\limits_{H_\gamma}\left(\lambda\left|\nabla v\right|^2 + \lambda^3 v^2\right)\varphi^2 \mathrm{d}x\mathrm{d}t$$

$$\leq M\lambda^3 \exp\left(2\lambda\gamma^{-\nu}\right)\int\limits_{\partial_1 H_\gamma}\sum_{|\alpha|\leq 2}\left(D_x^\alpha v\right)^2\varphi^2 \mathrm{d}S. \tag{1.198}$$

Let $\varepsilon \in (0, \gamma - \xi)$ be an arbitrary number. Then $H_{\gamma-\varepsilon} \subset H_\gamma$ and $\varphi^2(x,t) \geq \exp\left[2\lambda(\gamma-\varepsilon)^{-\nu}\right]$ in $H_{\gamma-\varepsilon}$. Hence, (1.198) implies that

$$\int\limits_{H_{\gamma-\varepsilon}} v^2 \mathrm{d}x\mathrm{d}t \leq M\exp\left\{-2\lambda\left[(\gamma-\varepsilon)^{-\nu} - \gamma^{-\nu}\right]\right\}\int\limits_{\partial_1 H_\gamma}\sum_{|\alpha|\leq 2}\left(D_x^\alpha v\right)^2\varphi^2 \mathrm{d}S.$$

Setting here $\lambda \to \infty$, we obtain that the right-hand side of this inequality tends to zero, which implies that $v(x,t) = 0$ in $H_{\gamma-\varepsilon}$. Since $\varepsilon \in (0, \gamma-\xi)$ is an arbitrary number, then $v(x,t) = 0$ in H_γ. Hence, (1.189) implies that $\widetilde{u}(x,t) = 0$ in H_γ. Next, (1.180) and (1.183) imply that $b(x) = 0$ in $H_\gamma \cap \{t = 0\}$. Hence, $a_{\alpha_0}^{(1)}(x) = a_{\alpha_0}^{(2)}(x)$ in $H_\gamma \cap \{t = 0\}$. Therefore, applying the same method to the homogeneous equation (1.180) with boundary conditions (1.182) and changing, if necessary, variables as $(t'', x'') = (t - t_0, x)$ with appropriate numbers $t_0 \in (-T, T)$, we obtain that

$$\widetilde{u}(x,t) = 0 \text{ for } (x,t) \in \left\{x_1 + \frac{|\overline{x}|^2}{A^2} < \gamma - \xi\right\} \times (-T, T). \tag{1.199}$$

It is clear that changing x variables by rotations of the coordinate system as well as by shifting the location of the origin and proceeding similarly with the above, we can cover the entire time cylinder $Q_T^{\pm}$ by domains, which are similar with the one in (1.199). Thus, $a_{\alpha_0}^{(1)}(x) = a_{\alpha_0}^{(2)}(x)$ in G and $u_1(x,t) = u_2(x,t)$ in $Q_T^{\pm}$. □

1.10.8 The Third Coefficient Inverse Problem for a Parabolic Equation

Let L be the elliptic operator in $\mathbb{R}^n$, whose coefficients depend only on x:

$$Lu = \sum_{|\alpha|\leq 2} a_\alpha(x) D_x^\alpha u, \tag{1.200}$$

$$a_\alpha \in C^{2+\beta}(\mathbb{R}^n), \beta \in (0,1) \tag{1.201}$$

We assume that

$$\mu_1 |\xi|^2 \leq \sum_{|\alpha|=2} a_\alpha (x) \xi^\alpha \leq \mu_2 |\xi|^2, \forall x, \xi \in \mathbb{R}^n. \tag{1.202}$$

Consider the following Cauchy problem

$$u_t = Lu \text{ in } D_T^{n+1}, \quad u \in C^{4+\beta, 2+\beta/2}\left(\overline{D}_T^{n+1}\right), \tag{1.203}$$

$$u|_{t=0} = f(x) \in C^{4+\beta}(\mathbb{R}^n) \tag{1.204}$$

It is well known that the problem (1.203) and (1.204) has unique solution [120].

The Third Parabolic Coefficient Inverse Problem. Let $T_0 \in (0, T)$ and $\Omega \subset \mathbb{R}^n$ be a bounded domain. Suppose that the coefficient $a_{\alpha_0}(x)$ of the operator L is known inside Ω and is unknown outside of Ω. Assume that the initial condition $f(x)$ is also unknown. Determine both the coefficient $a_{\alpha_0}(x)$ for $x \in \mathbb{R}^n \setminus \Omega$ and the initial condition $f(x)$ for $x \in \mathbb{R}^n$, assuming that the following function $F(x)$ is known:

$$F(x) = u(x, T_0), x \in \mathbb{R}^n. \tag{1.205}$$

Theorem 1.10.8. *Assume that conditions (1.200)–(1.202) hold, all coefficients of the operator L belong to $C^\infty(\Omega)$, and*

$$D^{\alpha_0} F(x) \neq 0, \text{ in } \mathbb{R}^n \setminus \Omega.$$

Then, there exists at most one pair of functions $(a_{\alpha_0}(x), u(x,t))$ satisfying conditions (1.203)–(1.205).

Proof. Consider the solution of the following hyperbolic Cauchy problem:

$$v_{tt} = Lv \text{ in } D_\infty^{n+1},$$

$$v(x, 0) = 0, v_t(x, 0) = f(x).$$

Then the Laplace-like transform (1.162) connects functions u and v. Hence, for any $x \in \mathbb{R}^n$ the function $u(x,t)$ is analytic with respect to the variable $t > 0$ as a function of a real variable. We now show that the function $u(x,t)$ can be uniquely determined for $(x,t) \in \Omega \times (0,T)$. Since all coefficients $a_\alpha \in C^\infty(\Omega)$, then the solution u of the Cauchy problem (1.203) and (1.204) is $u \in C^\infty(\Omega \times (0,T))$ [69]. Hence, using (1.203) and (1.205), we obtain

$$D_t^{k+1} u(x, T_0) = L^k [F(x)], x \in \Omega, k = 0, 1, \ldots$$

Thus, one can uniquely determine all t derivatives of the function $u(x,t)$ at $t = T_0$ for all $x \in \Omega$. Hence, the analyticity of the function $u(x,t)$ with respect to

t implies that this function can be uniquely determined for $(x,t) \in \Omega \times (0,T)$. Hence, Theorem 1.10.7 implies that the coefficient $a_{\alpha_0}(x)$ is uniquely determined in the domain $\mathbb{R}^n \setminus \Omega$. To establish that the initial condition $f(x)$ is also uniquely determined, we refer to the well-known theorem about the uniqueness of the solution of the parabolic equation with reversed time [69, 124]. □

1.10.9 A Coefficient Inverse Problem for an Elliptic Equation

We now consider an elliptic analog of the second parabolic CIP. Let $\Omega \subset \mathbb{R}^n$ be either finite or infinite convex domain with the piecewise smooth boundary $\partial\Omega$ and let $\Gamma \subset \partial\Omega$ be a part of this boundary. Let $T = \text{const} > 0$. Denote again

$$Q_T^{\pm} = \Omega \times (-T,T), \Gamma_T^{\pm} = \Gamma \times (-T,T).$$

Let L be an elliptic operator in $Q_T^{\pm}$:

$$Lu = \sum_{|\alpha| \le 2} a_\alpha(x,t) D_x^\alpha u, (x,t) \in Q_T^{\pm}, \tag{1.206}$$

$$a_\alpha \in C^1\left(\overline{Q_T^{\pm}}\right), \tag{1.207}$$

$$\mu_1 |\xi|^2 \le \sum_{|\alpha|=2} a_\alpha(x,t) \xi^\alpha \le \mu_2 |\xi|^2; \quad \mu_1, \mu_2 = \text{const.} > 0 \tag{1.208}$$

$$\forall \xi \in \mathbb{R}^n, \forall (x,t) \in \overline{Q_T^{\pm}}. \tag{1.209}$$

Coefficient Inverse Problem for an Elliptic Equation. Let the function $u \in C^2\left(\overline{Q_T^{\pm}}\right)$ satisfies the following conditions:

$$u_{tt} + Lu = F(x,t) \text{ in } Q_T^{\pm}, \tag{1.210}$$

$$u(x,0) = f_0(x) \text{ in } \Omega, \tag{1.211}$$

$$u|_{\Gamma_T^{\pm}} = p(x,t), \quad \frac{\partial u}{\partial n}|_{\Gamma_T^{\pm}} = q(x,t). \tag{1.212}$$

Assume that the coefficient $a_{\alpha_0}(x)$ of the operator L is independent of t and is unknown in Ω and all other coefficients are known in $Q_T^{\pm}$. Determine the coefficient $a_{\alpha_0}(x)$ from conditions (1.206)–(1.212).

Theorem 1.10.9. *Assume that $D_x^{\alpha_0} f_0(x) \neq 0$ in $\overline{\Omega}$. Then, there exists at most one pair of functions $(a_{\alpha_0}(x), u(x,t))$ such that conditions (1.206)–(1.212) hold and, in addition, the function $u \in C^3\left(\overline{Q_T^{\pm}}\right)$.*

Proof. Lemma 1.10.7 remains valid if the parabolic operator L_p in (1.174) is replaced with the elliptic operator [124]:

$$u_{tt} + \sum_{|\alpha|=2} a_\alpha (x,t) D_x^\alpha u.$$

Therefore, the proof is completely similar with the proof of Theorem 1.10.7. □

1.11 Uniqueness for the Case of an Incident Plane Wave in Partial Finite Differences

We present in this section the result of the paper [112]. Unlike all uniqueness theorems of Sect. 1.10, we assume now that initial conditions equal zero in the entire domain of interest. At the same time, we assume that the underlying hyperbolic PDE is written in the form of finite differences with respect to those variables which are orthogonal to the direction of propagation of the incident plane wave. Derivatives with respect to other variables are understood in the conventional form. In addition, we assume that grid step sizes in finite differences are bounded from the below. In fact, this assumption is quite often used in computations of CIPs.

Both classical forward problems for PDEs and ill-posed problems are routinely solved numerically by the FDM, see; for example, [114–116, 146] as well as Sects. 6.8 and 6.9. Therefore, it is important to prove uniqueness theorems for CIPs for the case when they are written in finite differences. However, there is a fundamental difference between classical forward problems and nonclassical ill-posed problems. Indeed, since classical forward problems are well-posed, then it makes sense to investigate convergence of the FDM when the spatial step grid step size h_{sp} tends to zero; see, for example, [146] for such results.

However, in the case of ill-posed problems, there is no point sometimes to investigate the convergence of FDM-based numerical methods when the spatial step size h_{sp} tends to zero. This is because in the ill-posed case, h_{sp} should usually be limited from the below by an a priori chosen constant, $h_{sp} \geq \overline{h} = \text{const.} > 0$. The constant $\overline{h}$ is usually chosen in numerical experiments. The reason of this limitation is that h_{sp} serves as an implicit regularization parameter in the *discrete* case of the FDM. Because of this, h_{sp} cannot be significantly decreased. The same observation takes place in numerical studies of Chap. 6; see Sect. 6.8.1 as well as [114, 116].

For the sake of brevity, we consider here only the 3D case. Theorems 1.11.1.1 and 1.11.1.2 below have almost identical formulations and proofs for the n-D case with $n \geq 2$. Below, $\mathbf{x} = (x, y, z) \in \mathbb{R}^3$. Let the function $a \in C^2\left(\mathbb{R}^3\right)$ and is bounded in $\mathbb{R}^3$ together with its derivatives. Consider the Cauchy problem

$$u_{tt} = \Delta u + a(\mathbf{x}) u, (\mathbf{x}, t) \in \mathbb{R}^3 \times (0, T), \tag{1.213}$$

$$u(\mathbf{x}, 0) = 0, u_t(\mathbf{x}, 0) = \delta(z). \tag{1.214}$$

Conditions (1.213) and (1.214) mean that the wave field u is initialized by the plane wave at the plane $\{z = 0\}$. This plane wave propagates along the z-axis. Let $A_x, A_y, T = \text{const.} > 0$. Define the strip G as

$$G = \left\{\mathbf{x} : x \in (0, A_x), y \in \left(0, A_y\right)\right\}, \ G_T = G \times (0, T),$$
$$S_T = \left\{z = 0, x \in (0, A_x), y \in \left(0, A_y\right)\right\} \times (0, T).$$

Coefficient Inverse Problem 1.11. *Assume that the function $a(\mathbf{x})$ is unknown in G. Determine the coefficient $a(\mathbf{x})$ for $x \in G$, assuming that the following two functions $r(x,t), s(x,t)$ are given*:

$$u\mid_{S_T} = r(\mathbf{x}, t), \ u_z\mid_{S_T} = s(\mathbf{x}, t). \tag{1.215}$$

The question of the uniqueness of this CIP is a well-known long-standing open problem. Note that (1.215) is the backscattering data. The main challenge is the single measurement, not the backscattering. For the first time, this question was addressed in [34]. However, infinitely many measurements were considered in these references. The second class of uniqueness results for the case of single measurement data with zero initial conditions are ones when the unknown coefficient is represented as a finite sum of a Fourier-like series:

$$a(x, y, z) = \sum_{k=1}^{N} b_k(x, y) a_k(z), N < \infty, \tag{1.216}$$

where functions a_k, b_k are unknown. The main restriction here is $N < \infty$. This kind of results follows from a special method of the integral geometry, which was developed in [124]; see Sect. 6.3 of [124].

In this section, we prove uniqueness theorem for a closely related inverse problem. Specifically, we assume that derivatives with respect to (x, y) are written via finite differences with the grid step sizes (h_1, h_2). Numbers h_1, h_2 do not tend to zero. However, derivatives with respect to z, t are written in the usual form. The uniqueness Theorem 1.11.1.2 uses these assumptions. Since finite differences are often used in computations, then Theorem 1.11.1.2 seems to be more attractive for computations than the assumption (1.216).

First, we prove in Lemma 1.11.3 a new Carleman estimate, which is significantly different from conventional Carleman estimates of Sect. 1.10. The main new element here is that a certain integral over the characteristic curve contains only nonnegative terms with large parameters involved. Usually, the positivity of surface integrals is not the case of Carleman estimates. This new Carleman estimate enables us to apply a new idea, compared with the method of Sect. 1.10. That new idea is generated by the second line of (1.244) in combination with (1.254). Indeed, in all previous publications about the Bukhgeim-Klibanov method, t-integrals of the Volterra type were used; see Sect. 1.10. Unlike this, we do not use those integrals in the proof of Theorem 1.11.1.2.

Discrete Carleman estimates are attracting an interest of researchers [37,38,105]. However, they were not yet used for proofs of uniqueness of discrete CIPs. A discrete Carleman estimate is not used here.

1.11.1 Results

Consider partitions of intervals $x \in (0, A_x)$, $y \in \left(0, A_y\right)$ in small subintervals with step sizes h_1 and h_2, respectively:

$$0 = x_0 < x_1 < ... < x_{N_1} = A_x,\ 0 = y_0 < y_1 < ... < y_{N_2} = A_y, \quad (1.217)$$

$$x_i - x_{i-1} = h_1,\ y_j - y_{j-1} = h_2,\ h := (h_1, h_2),\ h_0 = \min(h_1, h_2);\ N_1, N_2 > 2. \quad (1.218)$$

Hence, we have obtained the grid

$$G_h = \{(x, y) : x = ih_1, y = jh_2\}_{(i,j)=(0,0)}^{(N_1,N_2)}.$$

Consider a vector function $f^h(z,t)$ defined on this grid:

$$f^h(z,t) = \left\{f_{i,j}(z,t)\right\}_{(i,j)=(0,0)}^{(N_1,N_2)}.$$

For two vector functions $f^h(z,t)$, $g^h(z,t)$, define

$$g^h(z,t)\, f^h(z,t) := \left\{k_{i,j}(z,t)\right\}_{(i,j)=(0,0)}^{(N_1,N_2)},\ k_{i,j}(z,t) = g_{i,j}(z,t) \cdot f_{i,j}(z,t). \quad (1.219)$$

Denote

$$\left(f^h(z,t)\right)^2 := \sum_{(i,j)=(0,0)}^{(N_1,N_2)} f_{i,j}^2(z,t).$$

We define finite difference second derivatives $\partial_{x,h}^2 f^h(z,t)$ and $\partial_{y,h}^2 f^h(z,t)$ with respect to x and y, respectively, in the usual way as

$$\partial_{x,h}^2 f^h(z,t) = \left\{\partial_{x,h}^2 f_{i,j}(z,t)\right\}_{(i,j)=(0,0)}^{(N_1,N_2)},$$

$$\partial_{y,h}^2 f^h(z,t) = \left\{\partial_{y,h}^2 f_{i,j}(z,t)\right\}_{(i,j)=(0,0)}^{(N_1,N_2)},$$

$$\partial^2_{x,h} f_{i,j}(z,t) := \frac{1}{h_1^2} \begin{cases} f_{i-1,j}(z,t) - 2f_{i,j}(z,t) + f_{i+1,j}(z,t), & \text{if } i \neq 0, i \neq N_1, \\ f_{i,j}(z,t) - 2f_{i+1,j}(z,t) + f_{i+2,j}(z,t), & \text{if } i = 0, \\ f_{i,j}(z,t) - 2f_{i-1,j}(z,t) + f_{i-2,j}(z,t), & \text{if } i = N_1, \end{cases}$$

and similarly for $\partial^2_{y,h} f^h(z,t)$. Hence, if a function $g(x,y,z,t)$ has continuous derivatives up to the fourth order with respect to x, then $\partial^2_{x,h} g_{i,j}(z,t)$ approximates $g_{xx}(x,y,z,t)$ at the point $(x,y) = (ih_1, jh_2)$ with the accuracy $O\left(h_1^2\right), h_1 \to 0$ in the case when $ih_1 \neq 0, A_x$. And it approximates with the accuracy $O(h_1), h_1 \to 0$ in the case when $ih_1 = 0, A_x$. This is similar for the y derivative. Next, we define the finite difference Laplace operator as

$$\begin{aligned} \Delta_h f_{i,j}(z,t) &:= \partial_z^2 f_{i,j}(z,t) + \Delta_{h,x,y} f_{i,j}(z,t), \\ \Delta_{h,x,y} f_{i,j}(z,t) &:= \partial^2_{x,h} f_{i,j}(z,t) + \partial^2_{y,h} f_{i,j}(z,t), \\ \Delta_h f^h(z,t) &:= \left\{\Delta_h f_{i,j}(z,t)\right\}_{(i,j)=(0,0)}^{(N_1,N_2)} \\ &:= \left(\partial_z^2 f_{i,j}(z,t)\right)_{(i,j)=(0,0)}^{(N_1,N_2)} + \left\{\Delta_{h,x,y} f_{i,j}(z,t)\right\}_{(i,j)=(0,0)}^{(N_1,N_2)} \\ &:= \partial_z^2 f^h(z,t) + \Delta_{h,x,y} f^h(z,t). \end{aligned}$$

Define

$$a^h(z) := \left\{a_{i,j}(z)\right\}_{(i,j)=(0,0)}^{(N_1,N_2)}.$$

Rewrite the problem (1.213), (1.214) in the finite difference form as

$$u^h_{tt} = \Delta^h u^h + a^h(z) u^h, \ (z,t) \in \mathbb{R} \times (0,T), \tag{1.220}$$

$$u^h(z,0) = 0, u^h_t(z,0) = \delta(z), \tag{1.221}$$

where the product $a^h(z) u^h$ is understood as in (1.219).

Coefficient Inverse Problem 1.11.1.1. Let the vector function $u^h(z,t)$ be the solution of the problem (1.220) and (1.221). Determine the vector function $a^h(z)$ assuming that the following two vector functions $r^h(t), s^h(t)$,

$$r^h(t) = \left\{r_{i,j}(t)\right\}_{(i,j)=(0,0)}^{(N_1,N_2)}, \ s^h(t) = \left\{s_{i,j}(t)\right\}_{(i,j)=(0,0)}^{(N_1,N_2)}, \tag{1.222}$$

are given:

$$u^h(0,t) = r^h(t), \ u^h_z(0,t) = s^h(t), \ t \in (0,T). \tag{1.223}$$

Theorem 1.11.1.1. *Let the vector function $a^h(z) \in C^1(\mathbb{R})$ and is bounded in $\mathbb{R}$. Then, there exists unique solution of the forward problem (1.220) and (1.221) of the form*

$$u^h(z,t) = \left\{u_{i,j}(z,t)\right\}_{(i,j)=(0,0)}^{(N_1,N_2)},$$

where

$$u_{i,j}(z,t) = \frac{1}{2}H(t-|z|) + \overline{u}_{i,j}(z,t), (i,j) \in [0,N_1] \times [0,N_2]. \tag{1.224}$$

In (1.223), $H(z)$ is the Heaviside function,

$$H(z) = \begin{cases} 1 \text{ if } & z \geq 0, \\ 0 \text{ if } & z < 0 \end{cases}$$

and the function $\overline{u}_{i,j}$ is such that

$$\overline{u}_{i,j} \in C^3(t \geq |z|), \overline{u}_{i,j}(z,t) = 0 \text{ for } t \in (0,|z|]. \tag{1.225}$$

Theorem 1.11.1.2. *Let $R > 0$ be an arbitrary number and $T > 2R$. Assume that there exist two pairs of vector functions $\left(u_1^h(z,t), a_1^h(z)\right)$, $\left(u_2^h(z,t), a_2^h(z)\right)$ such that $a_1^h, a_2^h \in C^1(\mathbb{R})$ and vector functions u_1^h and $u_2^h$are solutions of the problem (1.220) and (1.221) of the form (1.224) and (1.225) with $a^h := a_1^h$ and $a^h := a_2^h$, respectively. In addition, assume that both vector functions u_1^h, u_2^h satisfy the same conditions (1.223). Then $a_1^h(z) = a_2^h(z)$ for $|z| < R$ and*

$$u_1^h(z,t) = u_2^h(z,t) \text{ for } (z,t) \in \{|z| < R, t \in (0, T-|z|)\}. \tag{1.226}$$

1.11.2 Proof of Theorem 1.11.1.1

Denoting temporarily $f_{i,j}(z,t) = \Delta_{h,x,y}u_{i,j} + a_{i,j}u_{i,j}$, rewrite (1.220) and (1.221) as

$$\partial_t^2 u_{i,j} = \partial_z^2 u_{i,j} + f_{i,j}(z,t), \ (i,j) \in [0,N_1] \times [0,N_2], \tag{1.227}$$

$$u_{i,j}(z,0) = 0, \ \partial_t u_{i,j}(z,0) = \delta(z). \tag{1.228}$$

Using D'Alembert formula, we derive from (1.227) and (1.228) that

$$u_{i,j}(z,t) = \frac{1}{2}H(t-|z|) + \frac{1}{2}\int_0^t d\tau \int_{\tau-t+z}^{t-\tau+z} \left(\Delta_{h,x,y}u_{i,j} + a_{i,j}u_{i,j}\right)(\xi,\tau)\, d\xi, \tag{1.229}$$

for $(i,j) \in [0,N_1] \times [0,N_2]$. In (1.229), the integration is carried out over the triangle $\Delta(z,t)$ in the (ξ,τ)-plane, where the triangle $\Delta(z,t)$ has vertices at $(\xi_1,\tau_1) = (z-t,0), (\xi_2,\tau_2) = (z,t)$, and $(\xi_3,\tau_3) = (z+t,0)$. If we consider the set of equations (1.229) considered for $(i,j) \in [0,N_1] \times [0,N_2]$, then we obtain

a linear system of coupled Volterra-like integral equations. Hence, this system can be solved iteratively:

$$u_{i,j}^{(n)}(z,t) = \frac{1}{2}H(t-|z|) + \frac{1}{2}\int_0^t d\tau \int_{\tau-t+z}^{t-\tau+z} \left(\Delta_{h,x,y} u_{i,j}^{(n-1)} + a_{i,j} u_{i,j}^{(n-1)}\right)(\xi,\tau)\, d\xi,$$

for $(i,j) \in [0,N_1] \times [0,N_2]$. Let

$$\max_{i,j} \sup_R \left|a_{i,j}(z)\right| \le M, M = \text{const.} > 0.$$

The standard technique for Volterra equations leads to the following estimate:

$$\left|u_{i,j}^{(n)}(z,t)\right| \le \sum_{n=0}^{\infty} \frac{(Ct)^n}{n!}, z \in \mathbb{R}, t > 0, \ \forall (i,j) \in [0,N_1] \times [0,N_2], \tag{1.230}$$

where the constant $C = C(h,M)$. Hence, there exists a solution of the integral equation (1.229) such that this solution is continuous for $t \in [0,|z|]$ and for $t \ge |z|$.

Next, let in (1.229) $t < |z|$. Then the triangle $\Delta(z,t)$ is located below $\{\tau = |\xi|\}$ and above $\{\tau = 0\}$. Hence, we obtain from (1.229)

$$u_{i,j}(z,t) = \frac{1}{2}\int_0^t d\tau \int_{\tau-t+z}^{t-\tau+z} \left(\Delta_{h,x,y} u_{i,j} + a_{i,j} u_{i,j}\right)(\xi,\tau)\, d\xi,$$
$$\text{for } t < |z|, \ (i,j) \in [0,N_1] \times [0,N_2]. \tag{1.231}$$

Iterating (1.231), we obtain similarly with (1.230) that

$$\left|u_{i,j}(z,t)\right| \le \frac{(Ct)^n}{n!}, n = 1,2,...; \ (i,j) \in [0,N_1] \times [0,N_2].$$

Hence, $u_{i,j}(z,t) = 0$ for $t < |z|$. The same way uniqueness of the problem (1.229) can be proven.

Let

$$\overline{u}_{i,j}(z,t) = u_{i,j}(z,t) - \frac{1}{2}H(t-|z|).$$

Since $\Delta_{h,x,y}[H(t-|z|)] = 0$ and $\overline{u}_{i,j}(z,t) = 0$ for $t < |z|$, then the integration in (1.229) is actually carried out over the following domain:

$$\{(\xi,\tau) : |\xi| < \tau < t - |z-\xi|\} = \left\{(\xi,\tau) : \xi \in \left(\frac{z-t}{2}, \frac{z+t}{2}\right), \right.$$
$$\left. \tau \in (|\xi|, t-|z-\xi|)\right\}.$$

Hence, (1.229) leads to the following equation for $\overline{u}_{i,j}(z,t)$:

$$\overline{u}_{i,j}(z,t) = \frac{1}{2}\int\limits_{\frac{z-t}{2}}^{\frac{z+t}{2}} d\xi \int\limits_{|\xi|}^{t-|z-\xi|} \left(\Delta_{h,x,y}\overline{u}_{i,j} + a_{i,j}\overline{u}_{i,j}\right)(\xi,\tau)\, d\tau$$

$$+\frac{1}{2}\int\limits_{\frac{z-t}{2}}^{\frac{z+t}{2}} a_{i,j}(\xi)\,(t-|z-\xi|-|\xi|)\, d\xi,\ t > |z|,\ \ (i,j) \in [0,N_1]$$

$$\times [0,N_2].$$

Differentiating these equations, we obtain that

$$\overline{u}_{i,j}(z,t) \in C^3(t \geq |z|), \forall (i,j) \in [0,N_1] \times [0,N_2]$$

Thus, the solution $\left\{u_{i,j}(z,t)\right\}_{(i,j)=(0,0)}^{(N_1,N_2)}$ of the system of equations (1.229) satisfies conditions (1.227), (1.228), (1.224), and (1.225).

It follows from Theorem 1.11.1.1 that we can consider functions $u_{i,j}(z,t)$ only above the characteristic line $\{t = |z|\}$ in the (z,t) plane. Hence, consider new functions $w_{i,j}(z,t) = u_{i,j}(z,t+z), z > 0$. The domain $\{t > z, z > 0\}$ becomes now $\{t > 0, z > 0\}$. Using (1.220), (1.222)–(1.224), and (1.225), we obtain

$$\partial_z^2 w_{i,j} - 2\partial_z\partial_t w_{i,j} = -\Delta_{h,x,y} w_{i,j} + a_{i,j}(z)\, w_{i,j}, (z,t) \in \{z, t > 0\}, \quad (1.232)$$

$$w_{i,j}(z,0) = \tfrac{1}{2}, \quad (1.233)$$

$$w_{i,j}(0,t) = r_{i,j}(t),\ \partial_z w_{i,j}(0,t) = s_{i,j}(t),\ t \in (0,T), \quad (1.234)$$

$$w_{i,j} \in C^3(z, t \geq 0), \quad (1.235)$$

$$(i,j) \in [0,N_1] \times [0,N_2]. \quad (1.236)$$

1.11.3 The Carleman Estimate

Consider parameters α, β, ν where

$$\alpha \in \left(0, \frac{1}{2}\right), \beta, \nu > 0.$$

Also, let $\lambda > 1$ be a sufficiently large parameter. We will choose λ later. Consider functions $\psi(z,t)$ and $\varphi(z,t)$ defined as

$$\psi(z,t) = z + \alpha t + 1,\ \varphi(z,t) = \exp\left(\lambda \psi^{-\nu}\right). \quad (1.237)$$

Define the domain $D_{\beta,\alpha}$ as

$$D_{\beta,\alpha} = \{(z,t) : z,t > 0, \psi(z,t) < 1+\beta\}. \tag{1.238}$$

The boundary of this domain is

$$\partial D_{\beta,\alpha} = \cup_{i=1}^{3} \partial_i D_{\beta,\alpha}, \tag{1.239}$$

$$\partial_1 D_{\beta,\alpha} = \{t = 0, z \in (0,\beta)\}, \tag{1.240}$$

$$\partial_2 D_{\beta,\alpha} = \left\{z = 0, 0 < t < \frac{\beta}{\alpha}\right\}, \tag{1.241}$$

$$\partial_3 D_{\beta,\alpha} = \{z,t > 0, \psi(z,t) = 1+\beta\}, \tag{1.242}$$

$$\varphi(z,t) \mid_{\partial_3 D_{\beta,\alpha}} = \exp\left[\lambda(1+\beta)^{-\nu}\right] = \min_{\overline{D}_{\beta,\alpha}} \varphi(z,t). \tag{1.243}$$

It follows from (1.234) that when applying the Carleman estimate of Lemma 1.11.3 in the proof of Theorem 1.11.1.2, we will have Dirichlet and Neumann data at $\partial_2 D_{\beta,\alpha}$. At $\partial_3 D_{\beta,\alpha}$ the function $\varphi(z,t)$ attains its minimal value, which is one of the key points of any Carleman estimate. However, we will not have any data at $\partial_1 D_{\beta,\alpha}$ when applying Lemma 1.11.3. Note that $\partial_1 D_{\beta,\alpha}$ is not a level curve of the function $\varphi(z,t)$. Still, we prove that the integral over $\partial_1 D_{\beta,\alpha}$, which occurs in the Carleman estimate due to the Gauss' formula, contains only nonnegative terms with the large parameters λ, λ^3; see the second line of (1.244). The latter is the main new feature of Lemma 1.11.3.

Lemma 1.11.3 (Carleman estimate). *Let $\alpha \in (0,1/2)$ and $\beta, \nu > 0$. Then, there exist constants $\lambda_0 = \lambda_0(\alpha,\beta,\nu) > 1, C = C(\alpha,\beta,\nu) > 0$ such that the following Carleman estimate is valid:*

$$\begin{aligned}
&\int\limits_{D_{\beta,\alpha}} (u_{zz} - 2u_{zt})^2 \varphi^2 \mathrm{d}z\mathrm{d}t \geq C\lambda \int\limits_{D_{\beta,\alpha}} \left(u_z^2 + u_t^2 + \lambda^2 u^2\right) \varphi^2 \mathrm{d}z\mathrm{d}t \\
&+C\lambda \int\limits_{\partial_1 D_{\beta,\alpha}} \left(u_z^2 + \lambda^2 u^2\right)(z,0)\varphi^2(z,0)\,\mathrm{d}z \\
&-C\lambda^3 \exp\left[2\lambda(\beta+1)^{-\nu}\right] \int\limits_{\partial_3 D_{\beta,\alpha}} \left(u_z^2 + u_t^2 + u^2\right) \mathrm{d}S,
\end{aligned} \tag{1.244}$$

$$\forall u \in \left\{u : u \in C^2\left(\overline{D}_{\beta,\alpha}\right), u \mid_{\partial_2 D_{\beta,\alpha}} = \partial_z u \mid_{\partial_2 D_{\beta,\alpha}} = 0\right\}, \ \forall \lambda \geq \lambda_0. \tag{1.245}$$

Proof. In this proof, $C = C(\alpha,\beta,\nu) > 0$ denotes different positive constants. Consider a new function $v = u\varphi$ and express $u_{zz} - 2u_{zt}$ via v. By (1.237),

$$
\begin{aligned}
u &= v\exp\left(-\lambda\psi^{-\nu}\right),\\
u_z &= \left(v_z+\lambda\nu\psi^{-\nu-1}v\right)\exp\left(-\lambda\psi^{-\nu}\right),\\
u_{zz} &= \left[v_{zz}+2\lambda\nu\psi^{-\nu-1}v_z+\lambda^2\nu^2\psi^{-2\nu-2}\left(1-\frac{(\nu+1)}{\lambda\nu}\psi^{\nu}\right)v\right]\exp\left(-\lambda\psi^{-\nu}\right),\\
u_{zt} &= \left[v_{zt}+\alpha\lambda\nu\psi^{-\nu-1}v_z+\lambda\nu\psi^{-\nu-1}v_t+\alpha\lambda^2\nu^2\psi^{-2\nu-2}\left(1-\frac{(\nu+1)}{\lambda\nu}\psi^{\nu}\right)v\right]\\
&\quad\times\exp\left(-\lambda\psi^{-\nu}\right),\\
u_{zz}-2u_{zt} &= \left[v_{zz}-2v_{zt}+(1-2\alpha)\lambda^2\nu^2\psi^{-2\nu-2}\left(1-\frac{(\nu+1)}{\lambda\nu}\psi^{\nu}\right)v\right]\\
&\quad\times\exp\left(-\lambda\psi^{-\nu}\right)+\left[2(1-\alpha)\lambda\nu\psi^{-\nu-1}v_z-2\lambda\nu\psi^{-\nu-1}v_t\right]\exp\left(-\lambda\psi^{-\nu}\right).
\end{aligned}
$$

Denote

$$
\begin{aligned}
y_1 &= \left[v_{zz}-2v_{zt}+(1-2\alpha)\lambda^2\nu^2\psi^{-2\nu-2}\left(1-\tfrac{(\nu+1)}{\lambda\nu}\psi^{\nu}\right)v\right],\\
y_2 &= 2(1-\alpha)\lambda\nu\psi^{-\nu-1}v_z,\\
y_3 &= 2\lambda\nu\psi^{-\nu-1}v_t.
\end{aligned}
$$

Hence,

$$
\left(u_{zz}-2u_{zt}\right)^2\varphi^2\geq 2y_1y_2-2y_1y_3. \tag{1.246}
$$

We have

$$
\begin{aligned}
2y_1y_2 &= 4(1-\alpha)\lambda\nu\psi^{-\nu-1}v_z\left[v_{zz}-2v_{zt}+(1-2\alpha)\lambda^2\nu^2\psi^{-2\nu-2}\right.\\
&\qquad\left.\times\left(1-\frac{(\nu+1)}{\lambda\nu}\psi^{\nu}\right)v\right]\\
&= \partial_z\left(2(1-\alpha)\lambda\nu\psi^{-\nu-1}v_z^2\right)+2(1-\alpha)\lambda\nu(\nu+1)\psi^{-\nu-2}v_z^2\\
&\quad+\partial_t\left(-4(1-\alpha)\lambda\nu\psi^{-\nu-1}v_z^2\right)-4\alpha(1-\alpha)\lambda\nu(\nu+1)\psi^{-\nu-2}v_z^2\\
&\quad+\partial_z\left[2(1-\alpha)(1-2\alpha)\lambda^3\nu^3\psi^{-3\nu-3}\left(1-\frac{(\nu+1)}{\lambda\nu}\psi^{\nu}\right)v^2\right]\\
&\quad+6(1-\alpha)(1-2\alpha)\lambda^3\nu^3(\nu+1)\psi^{-3\nu-4}\left(1-\frac{(2\nu+3)}{3\lambda\nu}\psi^{\nu}\right)v^2.
\end{aligned}
$$

Thus,

$$
\begin{aligned}
2y_1y_2 &= 2(1-\alpha)(1-2\alpha)\lambda\nu(\nu+1)\psi^{-\nu-2}v_z^2\\
&\quad+6(1-\alpha)(1-2\alpha)\lambda^3\nu^3(\nu+1)\psi^{-3\nu-4}\left(1-\frac{(2\nu+3)}{3\lambda\nu}\psi^{\nu}\right)v^2
\end{aligned}
$$

$$
\begin{aligned}
&+\partial_t\left(-4\left(1-\alpha\right)\lambda\nu\psi^{-\nu-1}v_z^2\right)\\
&+\partial_z\Bigg[2\left(1-\alpha\right)\lambda\nu\psi^{-\nu-1}v_z^2+2\left(1-\alpha\right)\left(1-2\alpha\right)\lambda^3\nu^3\psi^{-3\nu-3}\\
&\qquad\times\left(1-\frac{\left(\nu+1\right)}{\lambda\nu}\psi^{\nu}\right)v^2\Bigg].
\end{aligned}
\tag{1.247}
$$

Next, we estimate $-2y_1y_3$:

$$
\begin{aligned}
-2y_1y_3 &= -4\lambda\nu\psi^{-\nu-1}v_t\left[v_{zz}-2v_{zt}+\left(1-2\alpha\right)\lambda^2\nu^2\psi^{-2\nu-2}\left(1-\frac{\left(\nu+1\right)}{\lambda\nu}\psi^{\nu}\right)v\right]\\
&= \partial_z\left(-4\lambda\nu\psi^{-\nu-1}v_tv_z\right)+4\lambda\nu\psi^{-\nu-1}v_{zt}v_z-4\lambda\nu\left(\nu+1\right)\psi^{-\nu-2}v_tv_z\\
&\quad+\partial_z\left(4\lambda\nu\psi^{-\nu-1}v_t^2\right)+4\lambda\nu\left(\nu+1\right)\psi^{-\nu-2}v_t^2\\
&\quad+\partial_t\left[-2\left(1-2\alpha\right)\lambda^3\nu^3\psi^{-3\nu-3}\left(1-\frac{\left(\nu+1\right)}{\lambda\nu}\psi^{\nu}\right)v^2\right]\\
&\quad-6\alpha\left(1-2\alpha\right)\lambda^3\nu^3\left(\nu+1\right)\psi^{-3\nu-4}\left(1-\frac{\left(2\nu+3\right)}{3\lambda\nu}\psi^{\nu}\right)v^2.
\end{aligned}
$$

Next,

$$
4\lambda\nu\psi^{-\nu-1}v_{zt}v_z=\partial_t\left(2\lambda\nu\psi^{-\nu-1}v_z^2\right)+2\alpha\lambda\nu\left(\nu+1\right)\psi^{-\nu-2}v_z^2.
$$

Hence,

$$
\begin{aligned}
-2y_3y_1 &= 2\lambda\nu\left(\nu+1\right)\psi^{-\nu-2}\left(\alpha v_z^2-2v_tv_z+2v_t^2\right)\\
&\quad-6\alpha\left(1-2\alpha\right)\lambda^3\nu^3\left(\nu+1\right)\psi^{-3\nu-4}\left(1-\frac{\left(2\nu+3\right)}{3\lambda\nu}\psi^{\nu}\right)v^2\\
&\quad+\partial_t\left[2\lambda\nu\psi^{-\nu-1}v_z^2-2\left(1-2\alpha\right)\lambda^3\nu^3\psi^{-3\nu-3}\left(1-\frac{\left(\nu+1\right)}{\lambda\nu}\psi^{\nu}\right)v^2\right]\\
&\quad+\partial_z\left[-4\lambda\nu\psi^{-\nu-1}v_tv_z+4\lambda\nu\psi^{-\nu-1}v_t^2\right].
\end{aligned}
\tag{1.248}
$$

Summing up (1.247) and (1.248) and taking into account (1.246), we obtain

$$
\begin{aligned}
\left(u_{zz}-2u_{zt}\right)^2\varphi^2 &\geq 2y_2y_1-2y_3y_1\\
&= 2\lambda\nu\left(\nu+1\right)\psi^{-\nu-2}\left[\left(1-2\alpha+3\alpha^2\right)v_z^2-2v_tv_z+2v_t^2\right]\\
&\quad+6\left(1-2\alpha\right)^2\lambda^3\nu^3\left(\nu+1\right)\psi^{-3\nu-4}\left(1-\frac{\left(2\nu+3\right)}{3\lambda\nu}\psi^{\nu}\right)v^2\\
&\quad+\partial_t\Bigg[-2\left(1-2\alpha\right)\lambda\nu\psi^{-\nu-1}v_z^2-2\left(1-2\alpha\right)\lambda^3\nu^3\psi^{-3\nu-3}
\end{aligned}
$$

$$\times \left(1-\frac{(\nu+1)}{\lambda\nu}\psi^{\nu}\right)v^2\Big]$$
$$+\partial_z\Big[2(1-\alpha)\lambda\nu\psi^{-\nu-1}v_z^2+2(1-\alpha)(1-2\alpha)\lambda^3\nu^3\psi^{-3\nu-3}$$
$$\times \left(1-\frac{(\nu+1)}{\lambda\nu}\psi^{\nu}\right)v^2\Big]$$
$$+\partial_z\left[-4\lambda\nu\psi^{-\nu-1}v_t v_z+4\lambda\nu\psi^{-\nu-1}v_t^2\right]. \tag{1.249}$$

For any $\alpha\in(0,1/2)$, there exists a constant $C_1=C_1(\alpha)>0$ such that

$$\left(1-2\alpha+3\alpha^2\right)a^2-2ab+2b^2\geq C_1\left(a^2+b^2\right),\ \forall a,b\in\mathbb{R}.$$

Hence, integrating (1.249) over D_β and using (1.239)–(1.243), and (1.245) as well as the Gauss's formula, we obtain

$$\int\limits_{D_{\beta,\alpha}}(u_{zz}-2u_{zt})^2\varphi^2\mathrm{d}z\mathrm{d}t\geq 2\lambda\nu(\nu+1)C_1\int\limits_{D_{\beta,\alpha}}\left(v_z^2+v_t^2\right)\psi^{-\nu-2}\mathrm{d}z\mathrm{d}t$$
$$+6(1-2\alpha)^2\lambda^3\nu^3(\nu+1)\int\limits_{D_{\beta,\alpha}}\psi^{-3\nu-4}\left(1-\frac{(2\nu+3)}{3\lambda\nu}\psi^{\nu}\right)v^2\mathrm{d}z\mathrm{d}t$$
$$+\int\limits_{\partial_1 D_{\beta,\alpha}}\Big[2(1-2\alpha)\lambda\nu\psi^{-\nu-1}v_z^2+2(1-2\alpha)\lambda^3\nu^3\psi^{-3\nu-3}$$
$$\times\left(1-\frac{(\nu+1)}{\lambda\nu}\psi^{\nu}\right)v^2\Big]\mathrm{d}z$$
$$+\int\limits_{\partial_3 D_{\beta,\alpha}}\Big[-2(1-2\alpha)\lambda\nu\psi^{-\nu-1}v_z^2-2(1-2\alpha)\lambda^3\nu^3\psi^{-3\nu-3}$$
$$\times\left(1-\frac{(\nu+1)}{\lambda\nu}\psi^{\nu}\right)v^2\Big]\cos(n,t)\,\mathrm{d}S$$
$$+\int\limits_{\partial_3 D_{\beta,\alpha}}\Big[2(1-\alpha)\lambda\nu\psi^{-\nu-1}v_z^2+2(1-\alpha)(1-2\alpha)\lambda^3\nu^3\psi^{-3\nu-3}$$
$$\times\left(1-\frac{(\nu+1)}{\lambda\nu}\psi^{\nu}\right)v^2\Big]\cos(n,z)\,\mathrm{d}S$$
$$+\int\limits_{\partial_3 D_{\beta,\alpha}}\left[-4\lambda\nu\psi^{-\nu-1}v_t v_z+4\lambda\nu\psi^{-\nu-1}v_t^2\right]\cos(n,z)\,\mathrm{d}S. \tag{1.250}$$

Here, $\cos(n,t)$ is the cosine of the angle between the unit outward normal vector n at $\partial_3 D_\beta$ and the positive direction of t axis and similarly $\cos(n,z)$. Since the number $\nu > 0$ is fixed, we can incorporate it in the constant C. Change variables back in (1.250) replacing v with $u = v\varphi$. Then we obtain (1.244) for sufficiently large $\lambda \geq \lambda_0(\nu,\beta)$. □

1.11.4 Proof of Theorem 1.11.1.2

We consider in this proof only the case $z \in \{z > 0\}$ since the case $z \in \{z < 0\}$ is similar. Assume that there exist two pairs of vector functions:

$$\left(u^{1,h}(z,t), a^{1,h}(z)\right) \text{ and } \left(u^{2,h}(z,t), a^{2,h}(z)\right)$$

satisfying conditions of this theorem. Then for $z,t > 0$ there exist two pairs of functions:

$$\left(w^{1,h}(z,t), a^{1,h}(z)\right) \text{ and } \left(w^{2,h}(z,t), a^{2,h}(z)\right),$$

where

$$w^{1,h}(z,t) = u^{1,h}(z,t+z) \text{ and } w^{2,h}(z,t) = u^{2,h}(z,t+z).$$

Denote

$$\widetilde{w}^h(z,t) = w^{1,h}(z,t) - w^{2,h}(z,t) = \left\{\widetilde{w}_{i,j}(z,t)\right\}_{(i,j)=(0,0)}^{(N_1,N_2)},$$

$$\widetilde{a}^h(z) = a^{1,h}(z) - a^{2,h}(z) = \left\{\widetilde{a}_{i,j}(z)\right\}_{(i,j)=(0,0)}^{(N_1,N_2)}.$$

Then, (1.232)–(1.236) imply that

$$\widetilde{w}^h_{zz} - 2\widetilde{w}^h_{zt} = -\Delta_{h,x,y}\widetilde{w}^h + a^{1,h}(z)\widetilde{w}^h + \widetilde{a}^h(z)w^{2,h}(z,t), \quad (z,t) \in \{t > 0, z > 0\}, \tag{1.251}$$

$$\widetilde{w}^h(z,0) = 0, \tag{1.252}$$

$$\widetilde{w}^h(0,t) = 0, \ \partial_z\widetilde{w}^h(0,t) = 0, \ t \in (0,T),$$
$$+\widetilde{w}^h \in C^3(\mathbb{R} \times [0,T]). \tag{1.253}$$

Hence, setting $t = 0$ in (1.251) and using (1.252), we obtain

$$\widetilde{a}^h(z) = -4\partial_z\partial_t\widetilde{w}^h(z,0). \tag{1.254}$$

Let

$$\widetilde{v}^h(z,t) = \partial_t\widetilde{w}^h(z,t), \ v^{2,h}(z,t) = \partial_t w^{2,h}(z,t). \tag{1.255}$$

Differentiating (1.251) with respect to t and using (1.253) and (1.254), we obtain for $(z,t) \in \{t > 0, z > 0\}$

$$\widetilde{v}^h_{zz} - 2\widetilde{v}^h_{zt} = -\Delta_{h,x,y}\widetilde{v}^h + a^{1,h}(z)\widetilde{v}^h - 4\partial_z\widetilde{v}^h(z,0)\, v^{2,h}(z,t), \tag{1.256}$$

$$\widetilde{v}^h(0,t) = 0,\ \partial_z\widetilde{v}^h(0,t) = 0,\ t \in (0,T). \tag{1.257}$$

Since $T > 2R$, then $(0, R/T) \subset (0, 1/2)$. In (1.237), choose an arbitrary $\alpha \in (R/T, 1/2)$ and an arbitrary $\nu > 0$. Next, set in (1.238) $\beta := R$. Consider (1.256) for the function $\widetilde{v}_{i,j}$ for an arbitrary pair $(i,j) \in [0,N_1] \times [0,N_2]$. Square both sides of the latter equation, multiply by the function $\varphi^2(z,t)$, and integrate over $D_{R,\alpha}$. We obtain with a constant

$$M = M\left(h_0, \left\|a^{1,h}\right\|_{C[0,R]}, \left\|v^{2,h}\right\|_{C\left(\overline{D}_R\right)}\right) > 0,$$

depending on listed parameters

$$\int\limits_{D_{R,\alpha}} \left(\partial_z^2\widetilde{v}_{i,j} - 2\partial_z\partial_t\widetilde{v}_{i,j}\right)^2 \varphi^2 \mathrm{d}z\mathrm{d}t$$

$$\leq M \int\limits_{D_{R,\alpha}} \left[\widetilde{v}^h(z,t)\right]^2 \varphi^2 dzdt + M \int\limits_{D_{R,\alpha}} \left[\widetilde{v}_{i,j}(z,0)\right]^2 \varphi^2 \mathrm{d}z\mathrm{d}t. \tag{1.258}$$

Since the function $\varphi^2(z,t)$ is decreasing with respect to t, we obtain from (1.241) and (1.258)

$$\int\limits_{D_{R,\alpha}} \left(\partial_z^2\widetilde{v}_{i,j} - 2\partial_z\partial_t\widetilde{v}_{i,j}\right)^2 \varphi^2 \mathrm{d}z\mathrm{d}t$$

$$\leq M \int\limits_{D_{R,\alpha}} \left[\widetilde{v}^h(z,t)\right]^2 \varphi^2 \mathrm{d}z\mathrm{d}t + M_1 \int\limits_{\partial_1 D_{R,\alpha}} \left[\widetilde{v}_{i,j}(z,0)\right]^2 \varphi^2(z,0)\,\mathrm{d}z, \tag{1.259}$$

where the constant $M_1 = M_1(M,R,\alpha) > 0$.

Applying Lemma 1.11.3 to the left-hand side of (1.259) and using (1.257), we obtain

$$C\lambda \int\limits_{D_{R,\alpha}} \left[\left(\partial_z\widetilde{v}_{i,j}\right)^2 + \left(\partial_t\widetilde{v}_{i,j}\right)^2 + \lambda^2\left(\widetilde{v}_{i,j}\right)^2\right]\varphi^2 \mathrm{d}z\mathrm{d}t$$

$$+C\lambda \int\limits_{\partial_1 D_{R,\alpha}} \left[\left(\partial_z\widetilde{v}_{i,j}\right)^2 + \lambda^2\left(\widetilde{v}_{i,j}\right)^2\right](z,0)\,\varphi^2(z,0)\,\mathrm{d}z$$

$$-C\lambda^3 \exp\left(2\lambda (R+1)^{-\nu}\right) \int\limits_{\partial_3 D_{R,\alpha}} \left[\left(\partial_z \widetilde{v}_{i,j}\right)^2 + \left(\partial_t \widetilde{v}_{i,j}\right)^2 + \left(\widetilde{v}_{i,j}\right)^2\right] dS$$

$$\leq M \int\limits_{D_{R,\alpha}} \left[\widetilde{v}^h(z,t)\right]^2 \varphi^2 dz dt + M_1 \int\limits_{\partial_1 D_{R,\alpha}} \left[\widetilde{v}_{i,j}(z,0)\right]^2 \varphi^2(z,0)\, dz. \tag{1.260}$$

Choose a sufficiently large number $\lambda_0 > 1$ such that

$$\max(M, M_1) < \frac{C\lambda_0^3}{2}. \tag{1.261}$$

Then with a new constant $C > 0$, we obtain from the estimate (1.260)

$$C\lambda \int\limits_{D_{R,\alpha}} \left[\left(\partial_z \widetilde{v}_{i,j}\right)^2 + \left(\partial_t \widetilde{v}_{i,j}\right)^2 + \lambda^2 \left(\widetilde{v}_{i,j}\right)^2\right] \varphi^2 dz dt$$

$$+C\lambda^3 \int\limits_{\partial_1 D_{R,\alpha}} \left(\widetilde{v}_{i,j}\right)^2 (z,0)\, \varphi^2(z,0)\, dz$$

$$-C\lambda^3 \exp\left[2\lambda (R+1)^{-\nu}\right] \int\limits_{\partial_3 D_{R,\alpha}} \left[\left(\partial_z \widetilde{v}_{i,j}\right)^2 + \left(\partial_t \widetilde{v}_{i,j}\right)^2 + \left(\widetilde{v}_{i,j}\right)^2\right] dS$$

$$\leq M \int\limits_{D_{R,\alpha}} \left[\widetilde{v}^h(z,t)\right]^2 \varphi^2 dz dt. \tag{1.262}$$

Summing up estimates (1.262) with respect to $(i,j) \in [0,N_1] \times [0,N_2]$ and using (1.261), we obtain a stronger estimate:

$$\int\limits_{D_{R,\alpha}} \left(\widetilde{v}^h\right)^2 \varphi^2 dz dt \leq C \exp\left[2\lambda (R+1)^{-\nu}\right] \int\limits_{\partial_3 D_{R,\alpha}} \left[\left(\widetilde{v}_z^h\right)^2 + \left(\widetilde{v}_t^h\right)^2 + \left(\widetilde{v}^h\right)^2\right] dS. \tag{1.263}$$

Let $\varepsilon \in (0,R)$ be an arbitrary number. By (1.237) and (1.238),

$$\varphi^2(z,t) > \exp\left[2\lambda (R+1-\varepsilon)^{-\nu}\right] \text{ in } D_{R-\varepsilon},\ D_{R-\varepsilon} \subset D_R.$$

Hence, making the estimate (1.263) stronger, we obtain

$$\exp\left[2\lambda (R+1-\varepsilon)^{-\nu}\right] \int\limits_{D_{R-\varepsilon,\alpha}} \left(\widetilde{v}^h\right)^2 dz dt \leq C \exp\left[2\lambda (R+1)^{-\nu}\right]$$

$$\times \int\limits_{\partial_3 D_{R,\alpha}} \left[\left(\widetilde{v}_z^h\right)^2 + \left(\widetilde{v}_t^h\right)^2 + \left(\widetilde{v}^h\right)^2\right] dS$$

or

$$\int\limits_{D_{R-\varepsilon,\alpha}} \left(\widetilde{v}^h\right)^2 \mathrm{d}z\mathrm{d}t \le C \exp\left\{-2\lambda\left[(R+1-\varepsilon)^{-\nu} - (R+1)^{-\nu}\right]\right\}$$
$$\times \int\limits_{\partial_3 D_{R,\alpha}} \left[\left(\widetilde{v}_z^h\right)^2 + \left(\widetilde{v}_t^h\right)^2 + \left(\widetilde{v}^h\right)^2\right] \mathrm{d}S.$$

Setting here $\lambda \to \infty$, we obtain

$$\int\limits_{D_{R-\varepsilon,\alpha}} \left(\widetilde{v}^h\right)^2 \mathrm{d}z\mathrm{d}t = 0. \tag{1.264}$$

Since $\varepsilon \in (0, R)$ is an arbitrary number, then (1.264) implies that

$$\widetilde{v}^h(z,t) = 0 \text{ in } D_{R,\alpha}.$$

Since by (1.254),

$$\widetilde{a}^h(z) = -4\partial_z\partial_t \widetilde{w}^h(z,0) = -4\partial_z \widetilde{v}^h(z,0),$$

then $\widetilde{a}^h(z) = 0$ for $z \in (0, R)$. Thus, the function $a^h(z)$ is uniquely determined for $z \in \{|z| < R\}$.

Equations (1.220) represent a coupled system of 1D wave-like equations. Conditions (1.221) and (1.223) are Cauchy data for this system at $\{t = 0\}$ and $\{z = 0, t \in (0, T)\}$, respectively. Because of the 1D case, the time variable can be treated as the spatial variable and vice versa. Hence, treating for a moment z as the time variable and t as the spatial variable and recalling that the vector function $a^h(z)$ is known for $z \in \{|z| < R\}$, one can apply the standard energy estimate to (1.220), (1.221), and (1.223) for $\{z \in (0, R)\}$. It follows from this estimate that the vector function $u^h(z,t)$ is uniquely determined in the domain

$$(z,t) \in \{z \in (0,R), t \in (0, T-z)\}.$$

Similarly, the function $u^h(z,t)$ is uniquely determined in the domain

$$(z,t) \in \{z \in (-R,0), t \in (0, T+z)\}.$$

Thus, (1.226) is established. □

Chapter 2
Approximately Globally Convergent Numerical Method

In this chapter, we present our approximately globally convergent numerical method for a multidimensional CIP for a hyperbolic PDE. This method also works for a similar CIP for a parabolic PDE. The numerical method of the current chapter addresses the first central question of this book (Sect. 1.1). The first publication about this method was [24] with follow-up works [25–29, 109, 114–117, 160]. We remind that only multidimensional CIPs with single measurement data are considered in this book. Recall that the term "single measurement" means that the boundary data are generated either by a single position of the point source or by a single direction of the initializing plane wave (Sect. 1.1.2). It will become clear from the material below that when approximately solving certain nonlinear integral differential equations with Volterra-like integrals, we use an analog of the well-known predictor-corrector approach.

We describe this numerical method and prove its approximate global convergence property. The development of approximately globally convergent numerical methods for multidimensional CIPs has started from the so-called *convexification* algorithm [100–102, 157–160], which we consider as the approximately globally convergent numerical method of the first generation. First, the convexification comes up with a nonlinear integral differential equation, which is the same as (2.20) in Sect. 2.3. The *key point* is that this equation does not contain the unknown coefficient, which is similar with one of the ideas of the Bukhgeim-Klibanov method; see Sects. 1.10 and 1.11. A numerical method for the solution of this equation represents the main difficulty of both the convexification and the approach of this book. To solve that equation, the convexification uses a layer stripping procedure with respect to a spatial variable z and the projection method with respect to the rest of spatial variables. In this case, both Dirichlet and Neumann boundary conditions at a part of a plane orthogonal to the z-axis are used. Also, z dependent CWFs are involved in the convexification. Because of this, the convexification can use boundary conditions only at one part of the boundary, i.e., at a side of a rectangular prism, which is orthogonal to z.

L. Beilina and M.V. Klibanov, *Approximate Global Convergence and Adaptivity for Coefficient Inverse Problems*, DOI 10.1007/978-1-4419-7805-9_2,

The numerical method of this chapter is the approximately globally convergent numerical method of the second generation. Its radical difference with the convexification is in the solution of the abovementioned nonlinear integral differential equation. Unlike the convexification, the current method is not using neither the projection with respect to some spatial variables nor the layer stripping with respect to a spatial variable. In Chaps. 2–5, the current method uses the Dirichlet boundary condition at the entire boundary $\partial\Omega$ of a finite domain of interest Ω. The target coefficient is unknown in Ω and has a known constant value outside of Ω.

We use the layer stripping procedure with respect to the parameter $s > 0$, where s is the parameter of the Laplace transform of a hyperbolic PDE, for which the CIP is considered. We call *s pseudo frequency*. Since the differential operator with respect to s is not involved in the corresponding PDE, unlike the differential operator with respect to z in the convexification, then this procedure is more stable than the convexification. On each thin s layer, the Dirichlet boundary value problem for a nonlinear elliptic PDE of the second order is solved via the FEM. Dirichlet boundary conditions for these elliptic PDEs are originally generated by the data for the inverse problem. Also, s dependent CWFs are present in our numerical scheme. This presence is important, because it enables one to weaken the influence of the nonlinear term in each of those elliptic PDEs, thus solving a linear problem on each iteration.

Starting from the remarkable work of Carleman [50], weight functions carrying his name have been widely used for proofs of uniqueness and conditional stability results for ill-posed Cauchy problems for PDEs [102, 124], as well as for multidimensional CIPs with the single measurement data (see Sects. 1.10 and 1.11 above for the latter). In this capacity, CWFs were dependent on spatial variables since they have provided weighted estimates for differential operators. However, one of new points of our method is that CWFs are used for integral Volterra-like operators, they are involved in the numerical scheme, and depend on the pseudo frequency s, rather than on a spatial variable.

An important element of our technique is the procedure of working with the so-called *tail functions*. The tail function complements a certain truncated integral with respect to s. We refer to earlier works [73, 155] for similar treatments of tails for some other numerical methods for CIPs.

Theorems 2.8.2 and 2.9.4 ensure the approximate global convergence property of our technique within frameworks of two approximate mathematical models. It follows from these theorems that the accuracy of the solution mainly depends from the accuracy of the reconstruction of the tail functions. On the other hand, it follows from the second approximate mathematical model (Sect. 2.9.2) that the reconstruction of the first tail function can be done via solving the Dirichlet boundary value problem for the Laplace equation. Thus, if the noise in the boundary data is small, then the solution of the latter problem is accurate. The accuracy of the reconstruction of the rest of tail functions depends on the accuracy of the first tail. This indicates that it is because of the successful choice of our approximate mathematical models, a small noise in the boundary data is the main input for a good accuracy of our algorithm. In the theory of ill-posed problems, the small noise condition is a natural requirement.

A substantially different layer stripping procedure with respect to the frequency (rather than pseudo frequency) was previously developed in [55], where a convergence theorem was not proved (see Remark 1.1 in [55]). The paper [55] works with the Fourier transform of the hyperbolic equation $c(x) u_{tt} = \Delta u$ with the unknown coefficient $c(x)$. The iterative process of [55] starts from a low frequency value. Unlike this, we start from a high value of the pseudo frequency.

2.1 Statements of Forward and Inverse Problems

Everywhere in this book, the forward problem is the Cauchy problem for either a hyperbolic or a parabolic PDE. The case of a boundary value problem in a finite domain is not considered here only because an analogue of the asymptotic behavior (2.14) is not proved in this case, since (2.14) is actually derived from Theorem 4.1 of [144] as well as from [145]. That theorem establishes a certain asymptotic behavior of the fundamental solution of a hyperbolic equation near the characteristic cone. In our numerical experiments, we verify the asymptotic behavior (2.14) computationally; see Sect. 3.1.2. We also note that the existence of the fundamental solution of the hyperbolic equation (2.1) is currently proven only for the case when the coefficient $c \in C^k\left(\mathbb{R}^3\right)$ with $k \geq 2$ and the geodesic lines are regular [144, 145]. These justify the assumption (2.4) below.

Consider the Cauchy problem for the hyperbolic equation:

$$c(x) u_{tt} = \Delta u \text{ in } \mathbb{R}^3 \times (0, \infty), \tag{2.1}$$

$$u(x, 0) = 0, \ u_t(x, 0) = \delta(x - x_0). \tag{2.2}$$

Equation (2.1) governs a wide range of applications, including, for example, propagation of acoustic and EM waves. In the acoustical case, $1/\sqrt{c(x)}$ is the sound speed. In the 2D case of EM waves propagation in a non-magnetic medium, the dimensionless coefficient is $c(x) = \varepsilon_r(x)$, where $\varepsilon_r(x)$ is the spatially distributed dielectric constant of the medium, see, for example, [57], where (2.1) was derived from the Maxwell equations in the 2D case. Unlike the 2D case, (2.1) cannot be derived from the Maxwell equations in the 3D case if $c(x) = \varepsilon_r(x) \neq$ const. Nevertheless, this equation was successfully used to work with experimental data in [28, 109] in 3D; see Chap. 5.

Let $\Omega \subset \mathbb{R}^3$ be a convex bounded domain with the boundary $\partial\Omega \in C^3$. Let $d =$ const. > 1. We assume that the coefficient $c(x)$ of (2.1) is such that

$$c(x) \in [1, d], \ \ c(x) = 1 \text{ for } x \in \mathbb{R}^3 \setminus \Omega, \tag{2.3}$$

$$c \in C^3\left(\mathbb{R}^3\right). \tag{2.4}$$

In accordance with the second condition of the fundamental concept of Tikhonov (Sect. 1.4), we a priori assume knowledge of the constant d, which amounts to the

knowledge of the correctness set. However, we do *not* assume that the number $d-1$ is small, i.e., we do not impose smallness assumptions on the unknown coefficient $c(x)$.

Coefficient Inverse Problem 2.1. *Suppose that the coefficient $c(x)$ satisfies (2.3) and (2.4). Assume that the function $c(x)$ is unknown in the domain Ω. Determine the function $c(x)$ for $x \in \Omega$, assuming that the following function $g(x,t)$ is known for a single source position $x_0 \notin \overline{\Omega}$:*

$$u(x,t) = g(x,t), \forall (x,t) \in \partial\Omega \times (0,\infty). \tag{2.5}$$

The reason why we assume here that the source $x_0 \notin \overline{\Omega}$ is that we do not want to deal with singularities near the source location. In applications, the assumption $c(x) = 1$ for $x \in \mathbb{R}^3 \setminus \Omega$ means that the target coefficient $c(x)$ has a known constant value outside of the medium of interest Ω. Another argument here is that one should bound the coefficient $c(x)$ from the below by a positive number to ensure that the operator in (2.1) is a hyperbolic one on all iterations of our method. The function $g(x,t)$ models time-dependent measurements of the wave field at the boundary of the domain of interest. Practical measurements are calculated at a number of detectors, of course. In this case, the function $g(x,t)$ can be obtained via one of standard interpolation procedures.

Remarks 2.1. 1. As it was stated in Sect. 1.10.1, uniqueness theorem for this inverse problem is a long-standing and well-known open question because of the $\delta(x-x_0)$ function in the initial condition (2.2), although see (1.76). Thus, we assume everywhere below that uniqueness theorem is valid for this problem, as well as for all other CIPs considered in this book. It is an opinion of the authors that because of applications, it is worthy to study numerical methods for CIPs of this book, assuming that the uniqueness holds.

2. Our computational experience shows that the assumption of the infinite time interval in (2.5) is not a restrictive one. In the case of a finite time interval, on which measurements are performed, one should assume that this interval is large enough. Thus, the t-integral of the Laplace transform over this interval is approximately the same as the one over $(0,\infty)$. Our work with experimental data in Chaps. 5 and 6 verifies this point.

2.2 Parabolic Equation with Application in Medical Optics

In this section, we formulate both forward and inverse problems for a parabolic equation which governs applications particularly in medical optical imaging. The optical medical imaging consists of two stages. On the first stage, a device collects the light scattering data at the boundary of a human tissue (e.g., at the surface of a

brain or a female breast); see, for example, [150]. On the second stage, a mathematical algorithm for a CIP for a diffusion PDE is applied to approximately calculate the spatially distributed absorption coefficient inside that tissue. The map of this coefficient produces the desired image. We are interested in the second stage. Because of the necessity to solve a CIP, this stage represents a major mathematical challenge.

It was shown experimentally that the diffusion coefficient of light changes slowly in human tissues [76]. Hence, we can assume that it is a known constant and consider the following parabolic equation governing light propagation in human tissues [8]:

$$U_t = D\Delta U - a(x)U \text{ in } \mathbb{R}^3 \times (0,\infty),$$
$$U(x,0) = \delta(x - x_0). \tag{2.6}$$

Here, $\{x = x_0\}$ is the location of the light source, $U(x,t)$ is the light amplitude, $a(x) = \mu_a(x) \geq \text{const.} > 0$ is the absorption coefficient, and $D = D_0 = \text{const.} > 0$ is the diffusion coefficient $D = 1/3\mu_s'$, where μ_s' is the reduced scattering coefficient. We assume below that the diffusion coefficient D_0 is known.

Let $\Omega \subset \mathbb{R}^3$ be a convex bounded domain with the boundary $\partial\Omega \in C^3$. Let $a_0, a_1 = \text{const.} > 0$, $a_0 < a_1$. We assume that the absorption coefficient $a(x)$ of (2.6) is such that

$$a(x) \in [a_0, a_1], \quad a(x) = a_0 \text{ for } x \in \mathbb{R}^3 \setminus \Omega, \tag{2.7}$$
$$a(x) \in C^\alpha\left(\mathbb{R}^3\right), \alpha \in (0,1). \tag{2.8}$$

Let

$$U_0(x,t) = \frac{1}{\left(2\sqrt{\pi t}\right)^3} \exp\left(-\frac{|x - x_0|^2}{4t}\right)$$

be the solution of the problem (2.6) for $a \equiv 0$. It follows from (2.7) and (2.8) that there exists unique solution U of the forward problem (2.6) such that the function $(U - U_0) \in C^{2+\alpha,1+\alpha/2}\left(\mathbb{R}^3 \times [0,T]\right), \forall T > 0$ [120].

It was established experimentally [76, 156] that cancerous tumors absorb light more than the surrounding tissue. The tumor/background absorption contrast is between 2:1 and 3:1 [76]. Realistic value of optical coefficients of light propagation in human tissues are [156] $\mu_a \in [0.004, 0.016]\,\text{mm}^{-1}$, $\mu_s' \in [0.6, 1.2]\,\text{mm}^{-1}$, where μ_a and μ_s' are absorption and reduced scattering coefficients, respectively. The absorption coefficient characterizes blood oxygenation. Since malignant tumors are less oxygenated than healthy tissues, a hope of researchers is to detect these tumors on early stages using optical methods. Thus, our goal is to determine the absorption coefficient in (2.6). We now pose the following inverse problem for (2.6).

Coefficient Inverse Problem 2.2. Let $\Omega \subset R^3$ be a convex bounded domain with the piecewise smooth boundary $\partial\Omega$. Suppose that the coefficient $a(x)$ satisfies conditions (2.7) and (2.8) and is unknown in Ω. Suppose also that the diffusion coefficient $D = D_0 = \text{const.} > 0$ is known. Determine the coefficient $a(x)$ for

$x \in \Omega$, assuming that the following function $\varphi(x,t)$ is known for a fixed source position some position $x_0 \notin \overline{\Omega}$:

$$U(x,t) = \widetilde{g}(x,t), \forall (x,t) \in \partial\Omega \times (0,\infty). \tag{2.9}$$

2.3 The Transformation Procedure for the Hyperbolic Case

In this section, we reduce inverse problem 2.1 to the Dirichlet boundary value problem for a nonlinear integral differential equation. Consider the Laplace transform of the functions u in the hyperbolic equation (2.1):

$$w(x,s) = \int_0^\infty u(x,t)\mathrm{e}^{-st}\mathrm{d}t, \text{ for } s > \underline{s} = \text{const.} > 0, \tag{2.10}$$

where $\underline{s}$ is a certain number. It is sufficient to choose $\underline{s}$ such that the integral (2.10) would converge together with corresponding (x,t) derivatives. So, we can assume that the number $\underline{s}$ is sufficiently large. We call the parameter s *pseudo frequency*. Recall that $x_0 \notin \overline{\Omega}$. It follows from (2.1), (2.2), and (2.10) that the function w is the solution of the following problem:

$$\Delta w - s^2 c(x) w = -\delta(x - x_0), \ x \in \mathbb{R}^3, \tag{2.11}$$

$$\lim_{|x|\to\infty} w(x,s) = 0. \tag{2.12}$$

We prove (2.12) in Theorem 2.7.1 Likewise, we specify properties of the function $w(x,s)$ in Theorem 2.7.2 In particular, it follows from Theorems 2.7.1 and 2.7.2 that $w(x,s) \in C^3\left(\mathbb{R}^3 \setminus \{|x - x_0| < \varepsilon\}\right), \forall \varepsilon > 0$. To justify the asymptotic behavior of the function $w(x,s)$ at $s \to \infty$, we need Lemma 2.3.

Lemma 2.3([102]). *Assume that conditions (2.3) and (2.4) are satisfied. Let the function $w(x,s) \in C^3\left(\mathbb{R}^3 \setminus \{|x - x_0| < \varepsilon\}\right), \forall \varepsilon > 0$ be the solution of the problem (2.11) and (2.12). Assume that geodesic lines, generated by the eikonal equation corresponding to the function $c(x)$ are regular, i.e., any two points in $\mathbb{R}^3$ can be connected by a single geodesic line. Let $l(x,x_0)$ be the length of the geodesic line connecting points x and x_0. Then the following asymptotic behavior of the function w and its derivatives takes place for $|\beta| \leq 3, k = 0,1, x \neq x_0$:*

$$D_x^\beta D_s^k w(x,s) = D_x^\beta D_s^k \left\{ \frac{\exp[-sl(x,x_0)]}{f(x,x_0)} \left[1 + O\left(\frac{1}{s}\right)\right]\right\}, s \to \infty, \tag{2.13}$$

where $f(x,x_0)$ is a certain function and $f(x,x_0) \neq 0$ for $x \neq x_0$. This behavior is uniform for $x \in \overline{\Omega}$.

The C^2-smoothness required by Lemma 2.1 is also because of Theorem 4.1 of [144], which implies the asymptotic behavior (2.13). Note that Theorem 4.1 of [144] actually requires a higher smoothness of coefficients. This is because it is concerned with many terms of the asymptotic behavior of the fundamental solution of the hyperbolic equation near the characteristic cone. However, since (2.13) is dealing only with the first term of this behavior, then it follows from the proof of that theorem that the C^2-smoothness is sufficient; also see [145] for the smoothness.

Remark 2.3.1. Actually, it follows from Theorem 4.1 of [144] that the asymptotic behavior (2.13) is valid for the Laplace transform for a general hyperbolic equation of the second order, as long as the condition of the regularity of geodesic lines is in place. This condition cannot be effectively verified, unless the coefficient $c(x)$ is close to a constant. The authors are unaware about any meaningful analytical results for multidimensional hyperbolic CIPs without either this or somewhat close condition imposed. For example, it was shown in [144] that condition (1.82) is close to the condition of the regularity of geodesic lines. On the other hand, conditions of this lemma are only sufficient, but not necessary ones for the asymptotic behavior (2.13). Therefore, we assume everywhere in this book that the asymptotic behavior (2.13) holds. We verify (2.13) computationally in some of our numerical studies; see Sect. 3.1.2 below.

We now work only with the function $w(x,s)$. It will be shown in Theorems 2.7.1 and 2.7.2 that $w(x,s) > 0$. Hence, we can consider functions $v(x,s)$ and $H(x,s)$ defined as

$$v(x,s) = \frac{\ln w(x,s)}{s^2}.$$

Assuming that the asymptotic behavior (2.13) holds (Remark 2.3.1), we obtain the following asymptotic behavior of the function v:

$$\left\| D_x^\beta D_s^k v(x,s) \right\|_{C^3(\overline{\Omega})} = O\left(\frac{1}{s^{k+1}}\right),\ s \to \infty, k = 0,1. \tag{2.14}$$

Substituting $w = e^v$ in (2.11), keeping in mind that the source $x_0 \notin \overline{\Omega}$ and then dividing the resulting equation for v by s^2, we obtain

$$\Delta v + s^2 (\nabla v)^2 = c(x), x \in \Omega. \tag{2.15}$$

Denote

$$q(x,s) = \partial_s v(x,s). \tag{2.16}$$

By (2.14) and (2.16),

$$v(x,s) = -\int_s^\infty q(x,\tau)\, d\tau.$$

We rewrite this integral as

$$v(x,s) = -\int_s^{\overline{s}} q(x,\tau)\,d\tau + V(x,\overline{s}), \tag{2.17}$$

where the truncation pseudo frequency $\overline{s} > \underline{s}$ is a large number. It is important that in (2.17), $V(x,\overline{s})$ is not an arbitrary function, but rather

$$V(x,\overline{s}) = v(x,\overline{s}) = \frac{\ln w(x,\overline{s})}{\overline{s}^2}, \tag{2.18}$$

where $w(x,\overline{s})$ is the Laplace transform (2.10) of the solution of the forward problem (2.1) and (2.2) at $s := \overline{s}$, or, which is equivalent, the solution of the elliptic forward problem (2.10), (2.10) at $s := \overline{s}$. The number $\overline{s}$ should be chosen in numerical experiments. We call $V(x,\overline{s})$ the "tail," and this function is unknown. By (2.14) and (2.18),

$$\|V(x,\overline{s})\|_{C^3(\overline{\Omega})} = O\left(\frac{1}{\overline{s}}\right), \quad \|\partial_{\overline{s}} V(x,\overline{s})\|_{C^3(\overline{\Omega})} = O\left(\frac{1}{\overline{s}^2}\right). \tag{2.19}$$

In other words, the tail is small for large values of $\overline{s}$. In principle, therefore, one can set $V(x,\overline{s}) := 0$. However, our numerical experience shows that it would be better to update somehow the tail function in an iterative procedure. We call the updating procedure "iterations with respect to tails" and describe it in Sect. 2.7.

Remark 2.3.2. The integral in (2.17) is sort of truncated at a large value $\overline{s}$ of the pseudo frequency, which is similar with a routine truncation of high frequencies in science and engineering. We use words "sort of" because instead of just setting the tail function to zero, as it would be the case of a "straight" truncation, we iteratively update it in our algorithm. Hence, $\overline{s}$ is one of the regularization parameters of our numerical method. In the computational practice, this parameter is chosen in numerical experiments.

Thus, differentiating (2.15) with respect to s and using (2.16) and (2.17), we obtain the following integral nonlinear differential equation:

$$\Delta q - 2s^2 \nabla q \int_s^{\overline{s}} \nabla q(x,\tau)\,d\tau + 2s\left[\int_s^{\overline{s}} \nabla q(x,\tau)\,d\tau\right]^2$$

$$+2s^2 \nabla q \nabla V - 4s \nabla V \int_s^{\overline{s}} \nabla q(x,\tau)\,d\tau + 2s(\nabla V)^2 = 0, x \in \Omega. \tag{2.20}$$

In addition, (2.5) and (2.16) imply that the following Dirichlet boundary condition is given for the function q:

$$q(x,s) = \psi(x,s), \ \forall (x,s) \in \partial\Omega \times [\underline{s}, \overline{s}], \tag{2.21}$$

where:

$$\psi(x,s) = \frac{\partial_s \ln \varphi}{s^2} - \frac{2 \ln \varphi}{s^3},$$

and $\varphi(x,s)$ is the Laplace transform (2.10) of the function $g(x,t)$ in (2.5).

Suppose for a moment that functions q and V are approximated in Ω together with their derivatives $D_x^\alpha q$, $D_x^\alpha V$, $|\alpha| \leq 2$. Then the corresponding approximation for the target coefficient can be found via (2.15) as

$$c(x) = \Delta v + \underline{s}^2 (\nabla v)^2, x \in \Omega, \tag{2.22}$$

where the function H is approximated via (2.17). Although any value of the pseudo frequency $s \in [\underline{s}, \overline{s}]$ can be used in (2.22), we found in our numerical experiments that the best value is $s := \underline{s}$.

If integrals would be absent in (2.20) and the tail function would be known, then (2.20) and (2.21) would be the classical Dirichlet boundary value problem for the Laplace equation. However, the presence of integrals implies the nonlinearity and represents the main difficulty here. Another obvious difficulty is that (2.20) has two unknown functions q and V. The reason why we can handle this difficulty is that we treat functions q and V differently: while we iteratively approximate the function q being sort of "restricted" only to (2.20), we find updates for V using solutions of forward problems (2.1) and (2.2), the Laplace transform (2.10), and the formula (2.18). In those forward problems, we use approximations for the unknown coefficient c obtained from (2.22). The algorithm of approximating both functions q and V is described in Sect. 2.6.

2.4 The Transformation Procedure for the Parabolic Case

The goal of this section is to show that the coefficient inverse problem 2.2 for the parabolic equation (2.6) can be solved numerically along the same lines as the coefficient inverse problem 2.1 for the hyperbolic equation (2.1). However, we do not study further the parabolic case in this book. In the case of parabolic equation (2.6), consider the Laplace transform of the solution of the parabolic Cauchy problem (2.6)

$$W(x,s) = \int_0^\infty U(x,t) \exp\left(-s^2 t\right) dt, \ s \geq \underline{s} = \text{const.} > 0. \tag{2.23}$$

For simplicity, let $D_0 = 1$. It follows from (2.6) and (2.23) that the function W is the solution of the following problem:

$$\Delta W - s^2 W - a(x) W = -\delta(x - x_0), \forall s \geq \underline{s} = \text{const.} > 0,$$
$$\lim_{|x| \to \infty} W(x, s) = 0. \tag{2.24}$$

The second condition (2.24) is valid for sufficiently large $\underline{s}$ and can be proved by the method, which is similar with the one of Sect. 2.5**.** Theorem 11 of Chap. 2 of [69] ensures that the fundamental solution of a general parabolic equation is positive for $t > 0$. This means that $U(x, t) > 0$ for $t > 0$.Hence, $W(x, s) > 0$. Hence, we can consider the function $\overline{P} = \ln W$. Since $x_0 \notin \overline{\Omega}$, we obtain from (2.24)

$$\Delta \overline{P} + \left|\nabla \overline{P}\right|^2 - s^2 = a(x), x \in \Omega. \tag{2.25}$$

Consider now the following hyperbolic Cauchy problem:

$$u_{tt} = \Delta u - a(x) u \text{ in } \mathbb{R}^3 \times (0, \infty),$$
$$u(x, 0) = 0, u_t(x, 0) = \delta(x - x_0).$$

Applying to the function u the Laplace transform (2.10), we obtain (2.24). Hence,

$$W(x, s) = \int_0^\infty u(x, t) \exp(-st)\, dt, \ s \geq \underline{s} = \text{const.} > 0.$$

Geodesic lines are straight lines in this case. Therefore, the asymptotic behavior (2.13) holds (the first sentence of Remark 2.3.1),

$$D_x^\beta D_s^k W(x, s) = D_x^\beta D_s^k \left\{ \frac{\exp[-s|x - x_0|]}{4\pi |x - x_0|} \left[1 + O\left(\frac{1}{s}\right)\right]\right\}, s \to \infty,$$

where $|\beta| \leq 2, k = 0, 1$. Consider the function P:

$$P(x, s) = \overline{P}(x, s) - \ln\left(\frac{\exp[-s|x - x_0|]}{4\pi |x - x_0|}\right) := \overline{P}(x, s) - P_0(x, s).$$

Then the following asymptotic behavior is valid:

$$D_x^\beta D_s^k P(x, s) = O\left(\frac{1}{s^{k+1}}\right), \ s \to \infty, \ |\beta| \leq 2, \ k = 0, 1, \ x \in \overline{\Omega}. \tag{2.26}$$

Next, similarly with (2.16), we "eliminate" the unknown coefficient $a(x)$ from equation for the function P via the differentiation with respect to s. Denote

$$Q(x, s) = \partial_s P(x, s). \tag{2.27}$$

By (2.26) and (2.27),

$$P(x,s) = -\int_s^{\infty} Q(x,\tau)\,d\tau.$$

We represent this integral as

$$P(x,s) = -\int_s^{\bar{s}} Q(x,\tau)\,d\tau + V(x,\bar{s}), \tag{2.28}$$

where $\bar{s} > \underline{s}$ is a large number. Again, we call the function $\tilde{V}(x,\bar{s})$ in (2.28) as "the tail function" and it is defined as

$$V(x,\bar{s}) = P(x,\bar{s}) = \ln W(x,\bar{s}) - \ln\left(\frac{\exp\left[-\bar{s}\,|x-x_0|\right]}{4\pi\,|x-x_0|}\right). \tag{2.29}$$

Similarly with the hyperbolic case, differentiating equation for P with respect to s and using (2.27)–(2.29), we obtain the following integral nonlinear differential equation for the function Q:

$$\Delta Q - 2\frac{(s+1)}{|x-x_0|}(\nabla Q, x-x_0) - 2\nabla Q\int_s^{\bar{s}} \nabla Q(x,\tau)\,d\tau + 2\nabla Q\nabla V$$

$$+\frac{2}{|x-x_0|}\left(\int_s^{\bar{s}} \nabla Q(x,\tau)\,d\tau, x-x_0\right) - \frac{2}{|x-x_0|}(\nabla V, x-x_0) = 0. \tag{2.30}$$

Here, $(\cdot,\cdot)$ denotes the scalar product in $\mathbb{R}^3$. The boundary condition for the function Q is

$$Q\,|_{\Omega} = \bar{\psi}(x,s), (x,s) \in \partial\Omega \times [\underline{s},\bar{s}], \tag{2.31}$$

where the function $\bar{\psi}$ is defined as

$$\bar{\psi}(x,s) = \partial_s \ln \bar{\varphi}(x,s) + |x-x_0|,$$

where $\bar{\varphi}(x,s)$ is the Laplace transform of the function $\widetilde{g}(x,t)$ in (2.9).

Assume that we can approximate both functions Q and V in Ω together with their derivatives $D_x^{\alpha}Q, D_x^{\alpha}V, |\alpha| \leq 2$. Then the corresponding approximation for the absorption coefficient $a(x)$ can be found via (2.25) as

$$a(x) = \Delta(P + P_0) + |\nabla(P + P_0)|^2 - \underline{s}^2,\ x \in \Omega,$$

where the function P is approximated via (2.28). As it was mentioned above, the main difficulty of our method consists in the numerical solution of the nonlinear integral differential equation (2.30) with the boundary condition (2.31).

2.5 The Layer Stripping with Respect to the Pseudo Frequency s

In this section, we introduce the layer stripping procedure with respect to the pseudo-frequency for the solution of the integral-differential equation (2.20). Almost the same procedure can be applied for the solution of (2.30), although it is not presented here.

We approximate the function $q(x,s)$ in (2.20) as a piecewise constant function with respect to the pseudo frequency s. That is, we assume that there exists a partition

$$\underline{s} = s_N < s_{N-1} < ... < s_1 < s_0 = \overline{s}, s_{i-1} - s_i = h$$

of the interval $[\underline{s}, \overline{s}]$ with a sufficiently small grid step size h such that $q(x,s) = q_n(x)$ for $s \in (s_n, s_{n-1}]$. We set

$$q_0 \equiv 0. \tag{2.32}$$

Hence,

$$\int_s^{\overline{s}} \nabla q(x,\tau) \mathrm{d}\tau = (s_{n-1} - s)\nabla q_n(x) + h\sum_{j=0}^{n-1} \nabla q_j(x), s \in (s_n, s_{n-1}). \tag{2.33}$$

We approximate the boundary condition (2.21) as a piecewise constant function:

$$q_n(x) = \overline{\psi}_n(x), x \in \partial\Omega, \tag{2.34}$$

$$\overline{\psi}_n(x) = \frac{1}{h}\int_{s_n}^{s_{n-1}} \psi(x,s)\,\mathrm{d}s. \tag{2.35}$$

For each subinterval $(s_n, s_{n-1}], n \geq 1$, we assume that functions $q_j(x)$, $j = 1, ..., n-1$ for all previous subintervals are known. We obtain from (2.20) the following approximate equation for the function $q_n(x)$:

$$\begin{aligned}
\widetilde{L}_n(q_n) :=& \Delta q_n - 2\left(s^2 - 2s(s_{n-1} - s)\right)\left(h\sum_{j=1}^{n-1}\nabla q_j\right)\nabla q_n \\
&+2\left(s^2 - 2s(s_{n-1} - s)\right)\nabla q_n \nabla V \\
=& \ 2(s_{n-1} - s)\left[s^2 - s(s_{n-1} - s)\right](\nabla q_n)^2 - 2sh^2\left(\sum_{j=1}^{n-1}\nabla q_j\right)^2 \\
&+4s\nabla V\left(h\sum_{j=1}^{n-1}\nabla q_j\right) - 2s|\nabla V|^2, s \in (s_{n-1}, s_n].
\end{aligned} \tag{2.36}$$

Equation (2.36) is nonlinear, and it depends on the parameter s, whereas the function $q_n(x)$ is independent on s. This discrepancy is due to the approximation of the function $q(x,s)$ by a piecewise constant function. Although it seems that (2.36) is over-determined because the function $q_n(x)$ is not changing with the change of s, variations of s dependent coefficients of (2.36) are small over $s \in [s_n, s_{n-1})$ because this interval is small. This discrepancy is actually helpful for our method since it enables us to "mitigate" the influence of the nonlinear term $(\nabla q_n)^2$ in (2.36) via introducing the s dependent CWF.

In addition, we add the term $-\varepsilon q_n$ to the left-hand side of (2.36), where $\varepsilon > 0$ is a small parameter. We are doing so because, by the maximum principle, if a function $p(x,s)$ is the classical solution of the Dirichlet boundary value problem

$$\widetilde{L}_n(p) - \varepsilon p = f(x,s) \text{ in } \Omega, \; p|_{\partial\Omega} = p_b(x,s),$$

then [118] (Chap. 3, Sect. 1)

$$\max_{\overline{\Omega}} |p| \leq \max\left[\max_{\partial\Omega} |p_b|, \varepsilon^{-1} \max_{\overline{\Omega}} |f|\right], \forall s \in (s_{n-1}, s_n]. \tag{2.37}$$

On the other hand, if $\varepsilon = 0$, then an analogue of the estimate (2.37) would be worse because of the involvement of some other constants. Therefore, it is anticipated that the introduction of the term $-\varepsilon q_n$ should provide a better stability of our process, and we indeed observe this in our computations.

After adding the term $-\varepsilon q_n$ to the left-hand side of (2.36), multiply this equation by the CWF of the form:

$$C_{n,\lambda}(s) = \exp[\lambda(s - s_{n-1})], \; s \in (s_n, s_{n-1}], \tag{2.38}$$

and integrate with respect to s over (s_n, s_{n-1}). In (2.38) $\lambda >> 1$ is a parameter, which should be chosen in numerical experiments. Theorem 2.8.2 provides a recipe for this choice. Taking into account (2.34), we obtain

$$\begin{aligned} L_n(q_n) &:= \Delta q_n - A_{1,n}\left(h\sum_{j=0}^{n-1}\nabla q_j\right)\nabla q_n + A_{1n}\nabla q_n \nabla V - \varepsilon q_n \\ &= 2\frac{I_{1,n}}{I_0}(\nabla q_n)^2 - A_{2,n}h^2\left(\sum_{j=0}^{n-1}\nabla q_j(x)\right)^2 \\ &\quad + 2A_{2,n}\nabla V\left(h\sum_{j=0}^{n-1}\nabla q_j\right) - A_{2,n}(\nabla V)^2, n = 1, ..., N, \\ q_n|_{x\in\partial\Omega} &= \overline{\psi}_n(x). \end{aligned} \tag{2.39}$$

In (2.39),

$$I_0 := I_0(\lambda, h) = \int\limits_{s_n}^{s_{n-1}} \mathcal{C}_{n,\lambda}(s)\,\mathrm{d}s = \frac{1 - \mathrm{e}^{-\lambda h}}{\lambda},$$

$$I_{1,n} := I_{1,n}(\lambda, h) = \int\limits_{s_n}^{s_{n-1}} (s_{n-1} - s)\left[s^2 - s(s_{n-1} - s)\right]\mathcal{C}_{n,\lambda}(s)\,\mathrm{d}s,$$

$$A_{1,n} := A_{1,n}(\lambda, h) = \frac{2}{I_0}\int\limits_{s_n}^{s_{n-1}} \left(s^2 - 2s(s_{n-1} - s)\right)\mathcal{C}_{n,\lambda}(s)\,\mathrm{d}s,$$

$$A_{2,n} := A_{2,n}(\lambda, h) = \frac{2}{I_0}\int\limits_{s_n}^{s_{n-1}} s\mathcal{C}_{n,\lambda}(s)\,\mathrm{d}s.$$

Thus, we have obtained the Dirichlet boundary value problem (2.39) for a nonlinear elliptic PDE with the unknown function $q_n(x)$. In (2.39), the tail function V is also unknown. An important observation is that

$$\frac{|I_{1,n}(\lambda, h)|}{I_0(\lambda, h)} \leq \frac{4\bar{s}^2}{\lambda}, \text{ for } \lambda h \geq 1. \tag{2.40}$$

Therefore, by taking $\lambda >> 1$, we mitigate the influence of the nonlinear term with $(\nabla q_n)^2$ in (2.39). This enables us to solve each elliptic Dirichlet boundary value problem (2.34) and (2.39) iteratively at each n via solving a linear problem on each step.

Remarks 2.5. 1. It is clear from (2.40) that the nonlinear term $(\nabla q_n)^2$ in (2.39) can be ignored for large values of λ. This is done in Sect. 2.6. However, ignoring this term does not mean linearization of the original problem. Indeed, the nonlinearity actually surfaces in iterations with respect to n, because of the involvement of terms $\nabla q_j \nabla q_n, \left(\nabla q_j\right)^2, \nabla q_j \nabla q_i; i, j \in [1, n-1]$ in (2.39). In addition, the tail function V, which we will calculate iteratively, depends nonlinearly on q_j, q_n.

2. In principle, one can avoid using the CWF via decreasing the step size h, which would also result in a small influence of the term $(\nabla q_n)^2$ in (2.39). However, this would lead to an unnecessary increase of the number of equations N in (2.39). Hence, one would need to solve too many Dirichlet boundary problems (2.39), which is time-consuming. Thus, the introduction of the s dependent CWF (2.38) in the numerical scheme makes this scheme more flexible.

2.6 The Approximately Globally Convergent Algorithm

The above considerations lead to the algorithm described in this section. This is an algorithm with the approximate global convergence property for coefficient inverse problem 2.1. This property is established in Theorems 2.8.2 and 2.9.4 for two different approximate mathematical models (Definition 1.1.2.1). We present in this section two versions of the algorithm. The first version, which is described in Sect. 2.6.1, is verified computationally in our above cited works. However, a simplified version of the algorithm of Sect. 2.6.2 is not yet verified computationally.

Everywhere below,

$$|f|_{k+\alpha} = \|f\|_{C^{k+\alpha}(\overline{\Omega})}, \ \forall f \in C^{k+\alpha}\left(\overline{\Omega}\right).$$

Our algorithm reconstructs iterative approximations $c_{n,i}(x) \in C^{\alpha}\left(\overline{\Omega}\right)$ of the function $c(x)$ only inside the domain Ω. To update tails, we should solve the forward problem (2.1) and (2.2). Hence, we should extend each function $c_{n,i}(x)$ outside of the domain Ω in such a way that the resulting function $\widehat{c}_{n,i} \in C^{\alpha}\left(\mathbb{R}^3\right)$, $\widehat{c}_{n,i} \geq 1$ in Ω and $\widehat{c}_{n,i} = 1$ outside of Ω. So, we first describe a rather standard procedure of such an extension. Choose a smaller subdomain $\Omega' \subset \Omega$. Choose a function $\chi(x)$ such that

$$\chi \in C^1\left(\mathbb{R}^3\right), \ \chi(x) = \begin{cases} 1 \text{ in } \Omega', \\ \in [0,1] \text{ in } \Omega \setminus \Omega', \\ 0 \text{ outside of } \Omega. \end{cases}$$

The existence of such functions $\chi(x)$ is well known from the real analysis course. Define the target extension of the function $c_{n,i}$ as

$$\widehat{c}_{n,i}(x) := (1 - \chi(x)) + \chi(x) c_{n,i}(x), \forall x \in \mathbb{R}^3.$$

Hence, $\widehat{c}_{n,i}(x) = 1$ outside of the domain Ω and $\widehat{c}_{n,i} \in C^{\alpha}\left(\mathbb{R}^3\right)$. Furthermore, since $c_{n,i}(x) \in [1, d+1]$ in Ω, then $\widehat{c}_{n,i}(x) \in [1, d+1]$ in Ω. Indeed,

$$\begin{aligned} \widehat{c}_{n,i}(x) - 1 &= \chi(x)\left(c_{n,i}(x) - 1\right) \geq 0, \ x \in \Omega, \\ \widehat{c}_{n,i}(x) - (d+1) &= 1 - \chi(x) + \chi(x) c_{n,i}(x) - \chi(x)(d+1) - (1 - \chi(x)) \\ (d+1) &= -(1 - \chi(x)) d + \chi(x)\left(c_{n,i}(x) - d - 1\right) \leq 0, \ x \in \Omega. \end{aligned}$$

In accordance with (2.17), (2.22), and (2.33), denote

$$v_{n,i}(x) = -hq_{n,i}(x) - h\sum_{j=0}^{n-1} q_j(x) + V_{n,i}(x), x \in \Omega, \tag{2.41}$$

$$c_{n,i}(x) = \left[\Delta v_{n,i} + s_n^2 (\nabla v_{n,i})^2\right](x), \ x \in \Omega, \tag{2.42}$$

where functions $q_j, q_{n,i}, V_{n,i}$ are defined in this section below. Here, $V_{n,i}(x)$ is a certain approximation for the tail function and m_n is the number of iterations with respect to tails for a given $n \geq 1$, where $k = 1, ..., m_n$. Recall that by (2.32) $q_0 \equiv 0$. Hence, we set

$$q_{1,1}^0 := 0, V_{1,1}(x) := V_{1,1}^0(x), \tag{2.43}$$

$$q_{n,1}^0 := q_{n-1}, V_{n,1} := V_{n-1,m_{n-1}}, \text{for } n \geq 2, \tag{2.44}$$

where $V_{1,1}^0(x)$ is a certain starting value for the tail function.

In our iterative algorithm below, iterations with respect to k in $q_{n,1}^k$ are conducted in order to take into account the nonlinear term $(\nabla q_n)^2$in (2.39). As a limiting case, we construct the function $q_{n,1}$ for each n. Next, we iterate with respect to the tail and construct functions $q_{n,i}, i = 2, ..., m_n$. However, we do not iterate with respect to the nonlinear term for functions $q_{n,i}$ with $i \geq 2$.

Remarks 2.6. We now need to comment on the choice of the function $V_{1,1}^0(x)$.

1. By (2.14) and (2.18), this function should be small for large $\bar{s}$. In our numerical studies, we work with the incident plane wave rather with the point source in (2.2). The reason is that it is more convenient to computationally implement the case of the plane wave. On the other hand, we have chosen the case of the point source in (2.2) because Lemma 2.3 is actually derived from Theorem 4.1 of [144]. And this theorem was proven for the case of the point source.
2. In the first work [24], we took $V_{1,1}^0(x) \equiv 0$, and this is the case of numerical studies in Chap. 3. In follow-up publications, we have taken $V_{1,1}^0(x) = V_{\text{uniform}}(x)$, where

$$V_{\text{uniform}}(x) = \frac{\ln(w_{\text{uniform}}(x, \bar{s}))}{\bar{s}^2}.$$

   Here, $w_{\text{uniform}}(x, \bar{s})$ is the solution of the problem (2.11) and (2.12) for $c(x) \equiv 1, s := \bar{s}$ in the case of the incident plane wave. The latter is the case of numerical studies in Chaps. 4–6. In other words, $V_{\text{uniform}}(x)$ corresponds to the solution of the problem (2.11) and (2.12) for the case of the uniform medium which surrounds our domain of interest Ω; see (2.3). Recall that we do not assume any knowledge of the function $c(x)$ inside the domain Ω. We have discovered in our computational experiments that both these choices provide about the same solutions. However, the second one leads to a faster numerical convergence.
3. The second approximate mathematical model leads to another choice for the initial tail function $V_{1,1}(x)$; see Sect. 2.9.2. We have tested numerically this choice as well. Our computations have shown that although this choice provides a little bit better accuracy than the above two, the difference is still insignificant.

2.6.1 The First Version of the Algorithm

Step $n_1, n \geq 1$. Suppose that functions

$$q_1, ..., q_{n-1}, q_{n,1}^0 := q_{n-1} \in C^{2+\alpha}(\overline{\Omega}), c_{n-1} \in C^{\alpha}(\overline{\Omega})$$

and the tail function $V_{n,1}(x, \overline{s}) \in C^{2+\alpha}(\overline{\Omega})$ are constructed; see (2.43) and (2.44). We now construct the function $q_{n,1}$. To do this, we solve iteratively the following Dirichlet boundary value problems:

$$\Delta q_{n,1}^k - A_{1,n}\left(h\sum_{j=0}^{n-1}\nabla q_j\right)\cdot\nabla q_{n,1}^k - \varepsilon q_{n,1}^k + A_{1,n}\nabla q_{n,1}^k\cdot\nabla V_{n,1}$$

$$= 2\frac{I_{1n}}{I_0}\left(\nabla q_{n,1}^{k-1}\right)^2 - A_{2,n}h^2\left(\sum_{j=0}^{n-1}\nabla q_j\right)^2 + 2A_{2,n}\nabla V_{n,1}\cdot\left(h\sum_{j=0}^{n-1}\nabla q_j\right)$$

$$-A_{2n}\left(\nabla V_{n,1}\right)^2,\ x \in \Omega, \tag{2.45}$$

$$q_{n,1}^k(x) = \overline{\psi}_n(x), x \in \partial\Omega, \tag{2.46}$$

where $k = 1, 2, ...,$ functions $\overline{\psi}_n(x)$ are defined in (2.34) and (2.35) and functions $q_{n,1}^k \in C^{2+\alpha}\left(\overline{\Omega}\right)$. We call these "iterations with respect to the nonlinear term."It can be proven that this process converges; see Theorem 2.8.2 So, we set

$$q_{n,1} = \lim_{k\to\infty} q_{n,1}^k \text{ in the } C^{2+\alpha}\left(\overline{\Omega}\right) \text{ norm.} \tag{2.47}$$

Our numerical convergence criterion for the sequence $\left\{q_{n,1}^k\right\}_{k=1}^{\infty}$ is described in Chap. 3. Next, we reconstruct an approximation $c_{n,1}(x), x \in \overline{\Omega}$ for the unknown function $c(x)$ using the resulting function $q_{n,1}(x)$ and formulas (2.41) and (2.42) at $i = 1$. Hence, $c_{n,1} \in C^{\alpha}\left(\overline{\Omega}\right)$. Construct the function $\widehat{c}_{n,1}(x) \in C^{\alpha}\left(\mathbb{R}^3\right)$. Next, solve the forward problem (2.1) and (2.2) with $c(x) := \widehat{c}_{n,1}(x)$. We obtain the function $u_{n,1}(x, t)$. Calculate the Laplace transform (2.10) of this function and obtain the function $w_{n,1}(x, \overline{s})$ this way. Next, following (2.18), we set for $x \in \Omega$

$$V_{n,2}(x, \overline{s}) = \frac{\ln w_{n,1}(x, \overline{s})}{\overline{s}^2} \in C^{2+\alpha}\left(\overline{\Omega}\right). \tag{2.48}$$

Step n_i, $i \geq 2, n \geq 1$. We now iterate with respect to the tails. Suppose that functions $q_{n,i-1}, V_{n,i}(x, \overline{s}) \in C^{2+\alpha}\left(\overline{\Omega}\right)$ are constructed. Then we solve the following Dirichlet boundary value problem:

$$\Delta q_{n,i} - A_{1n}\left(h\sum_{j=0}^{n-1}\nabla q_j\right)\cdot\nabla q_{n,i} - \varepsilon q_{n,i} + A_{1n}\nabla q_{n,i}\cdot\nabla V_{n,i}$$

$$= 2\frac{I_{1n}}{I_0}\left(\nabla q_{n,i-1}\right)^2 - A_{2n}h^2\left(\sum_{j=0}^{n-1}\nabla q_j\right)^2 + 2A_{2n}\nabla V_{n,i}\cdot\left(h\sum_{j=0}^{n-1}\nabla q_j\right)$$
$$-A_{2n}\left(\nabla V_{n,i}\right)^2,\ x\in\Omega, \tag{2.49}$$

$$q_{n,i}(x) = \overline{\psi}_n(x), x\in\partial\Omega. \tag{2.50}$$

Having the function $q_{n,i}$, we reconstruct the next approximation $c_{n,i}\in C^{\alpha}(\overline{\Omega})$ for the target coefficient using (2.41) and (2.42). Next, we construct the function $\widehat{c}_{n,i}\in C^{\alpha}(\mathbb{R}^3)$. Next, we solve the forward problem (2.1) and (2.2) with $c(x) := \widehat{c}_{n,i}(x)$, calculate the Laplace transform (2.10), and update the tail as in (2.48), where $(w_{n,1}, V_{n,2})$ is replaced with $(w_{n,i}, V_{n,i+1})$. Alternatively to the solution of the problem (2.1) and (2.2), one can also solve the problem (2.11) and (2.12) at $s := \overline{s}$; see Theorem 2.7.2 for the justification. We iterate with respect to i until convergence occurs at the step $i := m_n$. Then we set

$$q_n := q_{n,m_n}\in C^{2+\alpha}\left(\overline{\Omega}\right), c_n := c_{n,m_n}\in C^{\alpha}\left(\overline{\Omega}\right), \tag{2.51}$$

$$V_{n+1,1}(x,\overline{s}) = \frac{1}{\overline{s}^2}\ln w_{n,m_n}(x,\overline{s})\in C^{2+\alpha}\left(\overline{\Omega}\right). \tag{2.52}$$

While convergence of the sequence $\left\{q_{n,1}^k\right\}_{k=1}^{\infty}$, which is generated by iterations with respect to the nonlinear term (see Step n_1) can be proven (Theorem 2.8.2), convergence of the sequence $\{q_{n,i}\}$ (with respect to i) cannot be proven. Hence, we have established a stopping rule for the latter sequence numerically; see details in Chap. 3. So, if the stopping rule is not yet reached, then we proceed with Step $(n+1)$. Alternatively we stop.

The stopping rule is chosen in numerical experiments; see Chap. 3. In addition, Theorem 2.8.2 claims that a subsequence of the sequence $\{c_{n,i}\}_{i=1}^{\infty}$ converges in the $L_2(\Omega)$-norm. We use the discrete $L_2(\Omega)$ norm in our computations for the stopping rule. This norm is the most convenient one for the computational analysis. Therefore, the stopping rule of Chap. 3 is indeed a reasonable one.

2.6.2 A Simplified Version of the Algorithm

We now briefly present a simplified version of the algorithm, which is not yet computationally verified. The idea is generated by the standard way of solving Volterra integral equations. First, we present the latter idea in brief. Consider a Volterra-like integral equation

$$y(t) = \int_0^t f(t,\tau,y(\tau))\,d\tau + g(t), t > 0, \tag{2.53}$$

where $f, \partial_y f, g$ are continuous functions of their variables. Equation (2.53) can be solved iteratively as

$$y_n(t) = \int_0^t f(t, \tau, y_{n-1}(\tau))\, d\tau + g(t), \ n \geq 1, \ y_0(t) = g(t). \tag{2.54}$$

It is proved in the standard ordinary differential equations course that this process converges as long as $t \in (0, \varepsilon)$, where $\varepsilon > 0$ is a sufficiently small number. Furthermore, solution of (2.53) is unique for all $t > 0$, as long as $f, \partial_y f$ are continuous functions of their variables for appropriate values of τ, t, y. At the same time, existence of the solution of (2.53) as well as convergence of the iterative process (2.54) can be proved only for small values $t \in (0, \varepsilon)$.

Equation (2.20) can be written in the form, which is similar with (2.53):

$$\Delta q = 2s^2 \nabla q \int_s^{\overline{s}} \nabla q(x, \tau)\, d\tau - 2s \left[\int_s^{\overline{s}} \nabla q(x, \tau)\, d\tau \right]^2$$
$$- 2s^2 \nabla q \nabla V + 4s \nabla V \int_s^{\overline{s}} \nabla q(x, \tau)\, d\tau - 2s (\nabla V)^2 = 0, \quad x \in \Omega, s \in [\underline{s}, \overline{s}]. \tag{2.55}$$

The boundary condition (2.21) is

$$q(x, s) = \psi(x, s), \ \forall (x, s) \in \partial\Omega \times [\underline{s}, \overline{s}]. \tag{2.56}$$

Hence, the idea is to solve the problem (2.55) and (2.56) for each appropriate tail function V iteratively via the process, which is similar with (2.54). Next, the tail should be updated, and the process should be repeated.

We use (2.32) and (2.33). Similarly with (2.43), we set

$$q_0 := 0, V_0(x) := V_0^0(x) \in C^{2+\alpha}\left(\overline{\Omega}\right),$$

where $V_0^0(x)$ is the first guess for the tail; see Remarks 2.6.

Step n_0, $n \geq 1$. Assume that functions $q_j^0 \in C^{2+\alpha}\left(\overline{\Omega}\right), j \in [0, n-1]$ are constructed. To find the function q_n^0, solve the following Dirichlet boundary value problem:

$$\Delta q_n^0 - A_{1n} \left(h \sum_{j=0}^{n-1} \nabla q_j^0 \right) \nabla q_n^0 - \varepsilon q_n^0 + A_{1n} \nabla q_n^0 \cdot \nabla V_0$$
$$= -A_{2n} h^2 \left(\sum_{j=0}^{n-1} \nabla q_j \right)^2 + 2A_{2n} \nabla V_0 \left(h \sum_{j=0}^{n-1} \nabla q_j \right) - A_{2n} (\nabla V_0)^2, \ x \in \Omega, \tag{2.57}$$

$$q_n^0(x) = \overline{\psi}_n(x), x \in \partial\Omega. \tag{2.58}$$

Continue until $n = N$. Next, reconstruct an approximation $c_1(x), x \in \Omega$ for the unknown function $c(x)$ using the resulting vector function $q^0(x) = \left(q_0^0, q_1^0, ..., q_N^0\right)$ and obvious analogs of formulas (2.41) and (2.42). Next, construct the function $\widehat{c}_1(x) \in C^\alpha\left(\mathbb{R}^3\right)$ and solve the problem (2.11) and (2.12) with the coefficient $\widehat{c}_1(x)$ at $s = \overline{s}$. We obtain the function $w(x, \overline{s}; \widehat{c}_1)$. Next, construct the function $V_1(x)$ as

$$V_1(x) = \frac{1}{\overline{s}^2} \ln w(x, \overline{s}; \widehat{c}_1) \in C^{2+\alpha}\left(\overline{\Omega}\right). \tag{2.59}$$

Set $q_0^1 := 0$.

Step $n_k, n \geq 1, k \geq 1$. Assume that functions $V_k, q_j^k \in C^{2+\alpha}\left(\overline{\Omega}\right), j \in [0, n-1]$ are constructed and $q_0^k = 0$. To construct the function q_n^k, solve the following analog of the Dirichlet boundary value problem (2.57) and (2.58):

$$\Delta q_n^k - A_{1n}\left(h\sum_{j=0}^{n-1}\nabla q_j^k\right)\nabla q_n^k - \varepsilon q_n^0 + A_{1n}\nabla q_n^k \nabla V_k$$

$$= -A_{2n}h^2\left(\sum_{j=0}^{n-1}\nabla q_j^k\right)^2 + 2A_{2n}\nabla V_k\left(h\sum_{j=0}^{n-1}\nabla q_j^k\right) - A_{2n}(\nabla V_k)^2, \ x \in \Omega,$$

$$q_n^k(x) = \overline{\psi}_n(x), x \in \partial\Omega.$$

Continue until $n = N$. Next, reconstruct an approximation $c_k(x), x \in \Omega$ for the unknown function $c(x)$ using the resulting vector function $q^k(x) = \left(q_0^k, q_1^k, ..., q_N^k\right)$ and obvious analogs of formulas (2.41), (2.42). Next, construct the function $\widehat{c}_k(x) \in C^\alpha\left(\mathbb{R}^3\right)$ and solve the problem (2.11) and (2.12) with the coefficient $\widehat{c}_k(x)$ at $s = \overline{s}$. A "good" solution of this problem exists and is unique; see Theorem 2.7.2 We obtain the function $w(x, \overline{s}; \widehat{c}_k)$. Next, construct the function $V_{k+1}(x)$ similarly with (2.59):

$$V_{k+1}(x) = \frac{1}{\overline{s}^2} \ln w(x, \overline{s}; \widehat{c}_k) \in C^{2+\alpha}\left(\overline{\Omega}\right).$$

Continue above iterations with respect to k until a convergence criterion is met. That convergence criterion should be established computationally.

2.7 Some Properties of the Laplace Transform of the Solution of the Cauchy Problem (2.1) and (2.2)

We need the material of this section for our analysis of the approximate global convergence property of the algorithm of Sect. 2.6.1. Indeed, we have not proven the limit (2.12) in Sect. 2.3. This is done in Sect. 2.7.1. In Sect. 2.7.2, we establish some additional properties of the solution of the problem (2.11) and (2.12).

2.7.1 The Study of the Limit (2.12)

Theorem 2.7.1. *Let $x_0 \notin \overline{\Omega}$, the function $c(x)$ satisfies conditions (2.3) and also $c \in C^{k+\alpha}\left(\mathbb{R}^3\right)$, where $k \geq 0$ is an integer and the number $\alpha \in (0,1)$. Assume that there exist constants*

$$M_1 = M_1(c) > 0, M_2 = M_2(x,c) > 0, \underline{s}_1 = \underline{s}_1(c) > 1,$$

such that for $k = 0,1,2$ and $|\gamma| \leq 2$,

$$\left|D_t^k u(x,t)\right|, \left|D_x^\gamma u(x,t)\right| \leq M_1(c)\, e^{\underline{s}_1 t},\ t > M_2(x,c), \forall x \in \mathbb{R}^3, \tag{2.60}$$

where $u(x,t)$ is the solution of the problem (2.1) and (2.2). Then there exists a constant $\underline{s}_2 = \underline{s}_2(c) \geq \underline{s}_1(c) > 1$ such that for all $s > \underline{s}_2$, the function $w(x,s)$, which is the Laplace transform (2.10) of the function $u(x,t)$, satisfies the following conditions:

$$\Delta w - s^2 c(x) w = -\delta(x - x_0),\ \forall s > \underline{s}_2, \tag{2.61}$$

$$\lim_{|x|\to\infty} w(x,s) = 0,\ \forall s > \underline{s}_2, \tag{2.62}$$

$$w(x,s) > 0 \text{ for } x \neq x_0, \tag{2.63}$$

$$w(x,s) = \frac{\exp(-s|x - x_0|)}{4\pi|x - x_0|} + \overline{w}(x,s) := w_1(x,s) + \overline{w}(x,s),\ \forall s > \underline{s}_2(c), \tag{2.64}$$

$$\overline{w}(x,s) \in C^{k+2+\alpha}\left(\mathbb{R}^3\right),\ \forall s > \underline{s}_2. \tag{2.65}$$

Proof. The limit (2.12) can be proven as follows. First, apply to (2.1) and (2.2) the integral transformation (1.162), which is an analog of the Laplace transform:

$$v(x,t) = \frac{1}{2\sqrt{\pi}t^{3/2}} \int_0^\infty u(x,\tau)\, \tau \exp\left(-\frac{\tau^2}{4t}\right) d\tau := \mathcal{L}_1 u. \tag{2.66}$$

Let $f(t), t \in [0,\infty)$ be a piecewise continuous function such that the function $|f(t)| e^{-\underline{s}_1 t}$ is bounded for $t \in [0,\infty)$. Two other types of the Laplace transform

which we use are

$$\mathcal{L}_2 f = \int_0^\infty f(t)\, e^{-s^2 t} dt, s > \underline{s}_1 > 1, \tag{2.67}$$

$$\mathcal{L} f = \int_0^\infty f(t)\, e^{-st} dt, s > \underline{s}_1 > 1. \tag{2.68}$$

One can easily verify that

$$(\mathcal{L} f)(s) = (\mathcal{L}_2 (\mathcal{L}_1 f))(s), \forall s > \underline{s}_1 > 1. \tag{2.69}$$

It follows from (2.66) that [102, 123, 124]

$$c(x) v_t = \Delta v, \tag{2.70}$$

$$v(x, 0) = \delta(x - x_0). \tag{2.71}$$

Hence, it follows from (2.1), (2.2), (2.60), and (2.67)–(2.71) that the function $w = \mathcal{L}u$ satisfies (2.61). We now need to establish (2.62)–(2.65). First, (2.63) follows from $w = \mathcal{L}_2 v$. Indeed, Theorem 11 of Chap. 2 of the book [69] claims that the fundamental solution of a general parabolic equation is positive for $t > 0$.

Detailed estimates of the fundamental solution of a general parabolic equation with variable coefficients can be found in Sects. 11–13 of Chap. 4 of the book [120]. In particular, it follows from the formula (13.1) of that chapter of [120] that the following estimate is valid for (x, t)-derivatives $D_t^r D_x^n v$ of the function v:

$$|D_t^r D_x^n v| \le v_{r,k} := C_1 \frac{\exp\left(-C_2 \frac{|x-x_0|^2}{t}\right)}{t^p} \exp(C_3 t);\ p = \frac{3 + 2r + n}{2}, \tag{2.72}$$

where $2r + n \le 2$ and C_1, C_2, C_3 are certain positive constants depending only on the upper estimate of the norm $\|c\|_{C^\alpha(\mathbb{R}^3)}$. Let $w_{r,n}(x, s) = \mathcal{L}_2\left(D_t^r D_x^n v\right)$. Using estimate (2.72) as well as formula (29) in Sect. 4.5 in the table of the Laplace transform of the book [13], we obtain

$$|w_{r,n}(x, s)| \le 2C_1 \left(\frac{C_2 |x - x_0|}{\sqrt{s^2 - C_3}}\right)^{(1-p)/2} K_{p-1}\left(2\sqrt{C_2 (s^2 - C_3)} \cdot |x - x_0|\right), \tag{2.73}$$

where $s \ge \underline{s} > \sqrt{C_3}$ and K_{p-1} is the McDonald function. Note that $K_{p-1} = K_{1-p}$ [1]. Since for $y \in \mathbb{R}$, the function $K_{p-1}(y) \in C^\infty(y \ge \varrho), \forall \varrho > 0$, then it follows from (2.73) that the function $w \in C^2(\{|x - x_0| \ge \vartheta\}), \forall \vartheta > 0$, for $s > \sqrt{C_3}$. Furthermore, since the function $K_{p-1}(y)$ decays exponentially when $y \to \infty, y \in$

$\mathbb{R}$, then we obtain from (2.73) that

$$\lim_{|x|\to\infty} D_x^n w(x,s) = 0 \text{ for } n = 0,1,2 \text{ and } s > \sqrt{C_3}, \tag{2.74}$$

from which (2.62) follows.

Consider now the fundamental solution v_0 of the heat equation:

$$v_{0t} = \Delta v_0, \text{ in } \mathbb{R}^3,$$
$$v_0(x,0) = \delta(x - x_0).$$

Hence,

$$v_0(x,t) = \frac{1}{\left(2\sqrt{\pi t}\right)^3} \exp\left(-\frac{|x-x_0|^2}{4t}\right). \tag{2.75}$$

Let $v_1 = v - v_0$. Then (2.70) and (2.71) imply that

$$c(x) v_{1t} = \Delta v_1 - (c(x) - 1) v_{0t}, \tag{2.76}$$

$$v_1(x,0) = 0. \tag{2.77}$$

Since the source $x_0 \notin \overline{\Omega}$, the function $c \in C^{k+\alpha}\left(\mathbb{R}^3\right)$, and by (2.3) $c(x) - 1 = 0$ outside of Ω, then it follows from (2.75) that

$$(c(x) - 1) v_{0t} \in C^{k+\alpha}\left(\mathbb{R}^3 \times [0,T]\right), \forall T > 0.$$

Consider the function $w^{(1)} := \mathcal{L}_2 v_1$ for $s \geq \underline{s} > \sqrt{C_3}$. Estimates for the solution of the Cauchy problem for a general parabolic equation with variable coefficients are obtained in Sect. 14 of Chap. 4 of [120] for the case when the right-hand side of this equation belongs to $C^{\alpha}\left(\mathbb{R}^3 \times [0,T]\right), \forall T > 0$. So, these estimates as well as (2.73), (2.75), (2.76), and (2.77) imply that $w^{(1)} \in C^2\left(\mathbb{R}^3\right)$.

Consider the function $\mathcal{L}_2 v_0$. Formula (28) of Sect. 4.5 of [13] implies that

$$\mathcal{L}_2 v_0 = \frac{\exp(-s|x-x_0|)}{4\pi|x-x_0|} = w_1(x,s). \tag{2.78}$$

Next, by (2.62) and (2.76)–(2.78) the function $\overline{w} = w - w_0$ satisfies the following conditions:

$$\Delta \overline{w} - s^2 c(x) \overline{w} = s^2 (c(x) - 1) w_1, \ s \geq \underline{s} > \sqrt{C_3}, \tag{2.79}$$

$$\lim_{|x|\to\infty} \overline{w}(x,s) = 0. \tag{2.80}$$

Now, since the function $(c(x) - 1) w_1 \in C^{k+\alpha}\left(\mathbb{R}^3\right)$, then Theorem 6.17 of [72] ensures that $\overline{w} \in C^{k+2+\alpha}\left(\mathbb{R}^3\right)$.

We now show that the solution $\overline{w} \in C^2\left(\mathbb{R}^3\right)$ of the problem (2.79) and (2.80) is unique. Suppose that there exists another function $\widetilde{w} \in C^2\left(\mathbb{R}^3\right)$ satisfying conditions (2.79) and (2.80). Let $w_2 = \overline{w} - \widetilde{w}$. Then

$$\Delta w_2 - s^2 c(x) w_2 = 0, \ s > \sqrt{C_3},$$
$$\lim_{|x| \to \infty} w_2(x, s) = 0.$$

Fix a pseudo frequency s, $s > \sqrt{C_3}$. Let $\varepsilon \in (0,1)$ be an arbitrary number. Choose a sufficiently large number $R(\varepsilon) > 0$ such that $|w_2(x,s)| < \varepsilon$ for $x \in \{|x| = R(\varepsilon)\}$. Then by the maximum principle (see Sect. 1 in Chap. 3 of [118])

$$\max_{|x| \le R(\varepsilon)} |w_2(x,s)| \le \max_{|x| = R(\varepsilon)} |w_2(x,s)| < \varepsilon.$$

Since $\kappa \in (0,1)$ is an arbitrary number, then $w_2(x,s) \equiv 0$. Hence, $\overline{w}(x,s) \equiv \widetilde{w}(x,s)$. Furthermore, since the above function $w^{(1)} \in C^2\left(\mathbb{R}^3\right)$ is $w^{(1)} := \mathcal{L}_2 v_1$ for $s \ge \underline{s} > \sqrt{C_3}$, then by (2.76), (2.77), and (2.74) imply that the function $w^{(1)}$ satisfies conditions (2.79) and (2.80). Hence, $w^{(1)} = \overline{w}$. Thus, conditions (2.61)–(2.65) are established. □

2.7.2 *Some Additional Properties of the Solution of the Problem (2.11) and (2.12)*

An inconvenient point of Theorem 2.7.1 is that it works only for $s > \underline{s}_2(c)$. The next natural question is whether its analog would be valid for values of s, which are independent on the function $c(x)$. In addition, the question about lower and upper bounds for the function w is important for our convergence analysis in Sect. 2.9. Thus, we need to prove Theorem 2.7.2 It should be noticed that this theorem does not follow from classical results of the theory of elliptic PDEs, since there results are known only for bounded domains. Unlike this, Theorem 2.7.2 is concerned with the elliptic problem (2.11) and (2.12) in the entire space $\mathbb{R}^3$.

First, we copy condition (2.3) for the convenience of the reader:

$$c(x) \in [1, d], \ \ c(x) = 1 \text{ for } x \in \mathbb{R}^3 \setminus \Omega. \tag{2.81}$$

Theorem 2.7.2. *Let $x_0 \notin \overline{\Omega}$ and the function $c(x)$ satisfies condition (2.81) as well as the following smoothness condition:*

$$c \in C^{k+\alpha}\left(\mathbb{R}^3\right), \ k \ge 0, \ \alpha \in (0,1). \tag{2.82}$$

Denote

$$w_1(x,s)=\frac{\exp(-s|x-x_0|)}{4\pi|x-x_0|}\ \textit{and}\ w_d(x,s)=\frac{\exp\left(-s\sqrt{d}|x-x_0|\right)}{4\pi|x-x_0|}, \tag{2.83}$$

the solutions of the problem (2.11) and (2.12) for $c(x)\equiv 1$ *and* $c(x)\equiv d$, *respectively. Then for any* $s>0$, *there exists unique solution of the problem (2.11) and (2.12) of the form*

$$w(x,s)=w_1(x,s)+\overline{w}(x,s),\ \textit{where}\ \overline{w}\in C^{k+2+\alpha}\left(\mathbb{R}^3\right). \tag{2.84}$$

Furthermore,

$$w_d(x,s)<w(x,s)\le w_1(x,s),\ \forall x\neq x_0. \tag{2.85}$$

Proof. Consider the following parabolic Cauchy problem for $(x,t)\in\mathbb{R}^3\times(0,\infty)$:

$$c(x)v_t=\Delta v,\ v(x,0)=\delta(x-x_0). \tag{2.86}$$

Let the function $v_0(x,t)$ in (2.75) be the solution of the problem (2.86) with $c\equiv 1$. Also, consider the function $\overline{v}(x,t)$:

$$\overline{v}(x,t)=\int_0^t(v-v_0)(x,\tau)\,d\tau. \tag{2.87}$$

Denote $b(x)=c(x)-1$. By (2.81) and (2.82),

$$b(x)=0\ \text{for}\ x\in\mathbb{R}^3\setminus\Omega,\ b\in C^{k+\alpha}\left(\mathbb{R}^3\right). \tag{2.88}$$

We obtain from (2.86) and (2.87)

$$\Delta\overline{v}-c(x)\overline{v}_t=b(x)v_0,\ \overline{v}(x,0)=0,\ \ (x,t)\in\mathbb{R}^3\times(0,\infty). \tag{2.89}$$

Since $x_0\notin\overline{\Omega}$, then it follows from (2.75) and (2.88) that the right hand of (2.89) does not have a singularity in $\mathbb{R}^3\times[0,\infty)$. Let $T,R>0$ be two arbitrary numbers and $B_R(T)=\{|x|<R\}\times(0,T)$. By (2.81) and (2.22), $b(x)v_0(x,t)\ge 0$ for $(x,t)\in\mathbb{R}^3\times(0,\infty)$. Hence, applying to (2.89), the maximum principle of Theorem 1 of Chap. 2 of [69], we obtain $\max_{\overline{B}_R(T)}\overline{v}(x,t)\le 0$. Since $R,T>0$ are arbitrary numbers, then

$$\overline{v}(x,t)\le 0\ \text{in}\ \mathbb{R}^3\times[0,\infty). \tag{2.90}$$

On the other hand, Theorem 11 of Chap. 2 of [69] ensures that the fundamental solution of the parabolic equation is positive for $t > 0$. Hence, (2.87) and (2.90) imply that

$$0 < \int_0^t v(x,\tau)\,d\tau \leq \int_0^t v_0(x,\tau)\,d\tau \text{ and } v(x,t) > 0 \text{ for } t > 0. \tag{2.91}$$

Next, we apply to the function v the operator $\mathcal{L}_2$ of the Laplace transform (2.67):

$$\mathcal{L}_2 v = \int_0^\infty v(x,t)e^{-s^2 t}dt. \tag{2.92}$$

By one of the well-known properties of the Laplace transform,

$$\mathcal{L}_2\left(\int_0^t f(\tau)\,d\tau\right) = \frac{1}{s^2}\mathcal{L}_2 f \tag{2.93}$$

for any appropriate function f. By (2.75), the integral

$$\mathcal{L}_2 v_0 = \int_0^\infty v_0(x,t)e^{-s^2 t}dt$$

converges for all $s > 0$. Formula (28) of Sect. 4.5 of Tables [13] gives $\mathcal{L}_2 v_0 = w_1, \forall s > 0$. Hence, (2.91)–(2.93), and Fubini theorem lead to

$$\mathcal{L}_2\left(\int_0^t v(x,\tau)\,d\tau\right) = \frac{1}{s^2}\mathcal{L}_2 v \leq \frac{1}{s^2}\mathcal{L}_2(v_0) = \frac{1}{s^2}w_1(x,s),\ \forall s > 0. \tag{2.94}$$

Hence, the integral (2.92) converges absolutely. Next, by (2.89), for any $A > 0$,

$$\Delta\int_0^A \bar{v}(x,t)\,e^{-s^2 t}dt = \int_0^A \Delta\bar{v}(x,t)\,e^{-s^2 t}dt = \int_0^A [c\bar{v}_t + (c-1)v_0]\,e^{-s^2 t}dt.$$

Setting here $A \to \infty$ and using that by (2.87) $c\bar{v}_t + (c-1)v_0 = cv - v_0$, we obtain

$$\lim_{A\to\infty}\Delta\int_0^A \bar{v}(x,t)\,e^{-s^2 t}dt = \lim_{A\to\infty}\int_0^A \Delta\bar{v}(x,t)\,e^{-s^2 t}dt = c\mathcal{L}_2 v - \mathcal{L}_2 v_0. \tag{2.95}$$

Hence, it follows from (2.95) that $\Delta\mathcal{L}_2(\overline{v})$ and $\mathcal{L}_2(\Delta\overline{v})$ exist and $\Delta\mathcal{L}_2(\overline{v}) = \mathcal{L}_2(\Delta\overline{v})$. Furthermore, by (2.87) and (2.93)–(2.95):

$$\Delta\mathcal{L}_2(\overline{v}) = s^{-2}\Delta(\mathcal{L}_2 v - \mathcal{L}_2 v_0) = c\mathcal{L}_2 v - \mathcal{L}_2 v_0.$$

Hence, denoting $w := \mathcal{L}_2(v)$ and using $\mathcal{L}_2 v_0 = w_1$ as well as $\Delta w_1 - s^2 w_1 = -\delta(x - x_0)$, we obtain that the function w satisfies (2.11):

$$\Delta w - s^2 c(x) w = -\delta(x - x_0), \ x \in \mathbb{R}^3. \tag{2.96}$$

We now prove (2.12). Since $c\overline{v}_t = \overline{v}_t + b\overline{v}_t$, then using (2.87) and (2.89), we obtain

$$\overline{v}_t - \Delta\overline{v} = -b(x) v, \ \overline{v}(x, 0) = 0. \tag{2.97}$$

Since by (2.88) $b(x) = 0$ near x_0 and $b \in C^{k+\alpha}\left(\mathbb{R}^3\right)$, then at least

$$bv \in C^{\alpha,\alpha/2}\left(\mathbb{R}^3 \times [0, T]\right). \tag{2.98}$$

Hence, it follows from formula (13.2) of Chap. 4 of [120] that

$$\overline{v} \in C^{2+\alpha,1+\alpha/2}\left(\mathbb{R}^3 \times [0, T]\right), \forall T > 0. \tag{2.99}$$

Consider (2.97) as the Cauchy problem for the heat equation with the right hand $(-b(x) v)$. It follows from (2.88), (2.98) and (2.99), and results of Sect. 1 of Chap. 4 of [120] that the solution of the problem (2.97) can be written in the following form:

$$\overline{v}(x, t) = -\int_0^t \int_\Omega v_0(x - \xi, t - \tau) b(\xi) v(\xi, \tau) \, d\xi d\tau. \tag{2.100}$$

By (2.87), (2.92), and (2.94), $\mathcal{L}_2\overline{v} = s^{-2}(\mathcal{L}_2 v - w_1) = s^{-2}(w - w_1)$. Hence, applying the Laplace transform $\mathcal{L}_2$ to both sides of (2.100) and using the convolution theorem, we obtain

$$w(x, s) = w_1(x, s) - s^2 \int_\Omega w_1(x - \xi, s) b(\xi) w(\xi, s) \, d\xi. \tag{2.101}$$

By (2.83) and (2.101), functions $w(x, s)$, $w_1(x, s)$ and $(w - w_1)(x, s)$ satisfy condition (2.12):

$$\lim_{|x|\to\infty} w(x, s) = \lim_{|x|\to\infty} w_1(x, s) = \lim_{|x|\to\infty} (w - w_1)(x, s) = 0. \tag{2.102}$$

We now establish (2.84). Let $\Omega_1 \subset \mathbb{R}^3$ be a bounded domain such that

$$\Omega \subset \Omega_1,\ \partial\Omega \cap \partial\Omega_1 = \varnothing,\ \partial\Omega_1 \in C^3,\ x_0 \notin \overline{\Omega}_1.$$

It follows from (2.101) that the function $w(x,s) \in C^1\left(\overline{\Omega}_1\right)$. Hence, by (2.88), the function $b(x)\, w(x,s) \in C^\alpha\left(\overline{\Omega}_1\right)$. Hence, Lemma 2.9.1.4 (Sect. 2.9.1) and (2.101) imply that the function $(w - w_0)(x,s) \in C^{2+\alpha}\left(\mathbb{R}^3\right)$. Finally, the abovementioned Theorem 6.17 of [72] combined with (2.96) ensures that (2.84) is true for any $k \geq 0$.

Thus, we have proven the existence of the solution of the problem (2.11) and (2.12) in the form (2.84). The proof of the uniqueness is the same as in the last part of the proof of Theorem 2.7.1 (after (2.80)).

Finally, we prove (2.85). We have established above in this proof that $w = \mathcal{L}_2(v)$ and $v \geq 0, b \geq 0$. Hence, the right inequality (2.85) follows from (2.101). Consider the function $\widetilde{w}(x,s) = w(x,s) - w_d(x,s)$. Then (2.96), (2.102), and (2.83) imply that

$$\Delta\widetilde{w} - s^2 c\widetilde{w} = s^2 (c(x) - d)\, w_d, \quad \lim_{|x|\to\infty} \widetilde{w}(x,s) = 0. \tag{2.103}$$

By (2.83) and (2.84),

$$\frac{\widetilde{w}(x,s)}{w_d(x,s)} = \exp\left[s\left(\sqrt{d} - 1\right)|x - x_0|\right][1 + O(|x - x_0|)] > 0, x \to x_0, x \neq x_0.$$

Hence, there exists a sufficiently small number $\varepsilon > 0$ such that

$$\widetilde{w}(x,s) > 0 \text{ for } x \in \{|x - x_0| \leq \varepsilon, x \neq x_0\}. \tag{2.104}$$

For $R > 0$, consider the domain $B_{R,\varepsilon} = \{|x| < R, |x - x_0| > \varepsilon\}$. Assuming that $B_{R,\varepsilon} \neq \varnothing$, which is true for sufficiently large R, we obtain $\widetilde{w} \in C^{2+\alpha}\left(\overline{B}_{R,\varepsilon}\right)$ and $s^2(c(x) - d)\, w_d \leq 0$ in $B_{R,\varepsilon}$. Hence, applying the maximum principle to (2.103), we obtain

$$\min_{\overline{B}_{R,\varepsilon}} \widetilde{w} \geq \min_{\partial B_{R,\varepsilon}} \widetilde{w}.$$

Setting $R \to \infty$ and using the second condition (2.103) as well as (2.104), we obtain

$$\min_{|x-x_0|\geq\varepsilon} \widetilde{w} \geq \min_{|x-x_0|=\varepsilon} \widetilde{w} > 0.$$

Thus, $w(x,s) > w_d(x,s)$ for $x \neq x_0$. □

2.8 The First Approximate Global Convergence Theorem

In this section, we present the first version of the proof of the approximate global convergence property of the algorithm of Sect. 2.6.1 for coefficient inverse problem 2.1. In other words, we show that this algorithm addresses the first central

question of this book; see Sect. 1.1. Following the fundamental concept of Tikhonov (Sect. 1.4), we should assume first that there exists an "ideal" exact solution of an ill-posed problem with the exact data. Next, one should assume the presence of an error of the level σ in the data and construct the solution for each such σ. So constructed solution is called a "regularized solution", if it tends to the exact solution as $\sigma \to 0$.

2.8.1 Exact Solution

Following the fundamental concept of Tikhonov (Sect. 1.4), we introduce first the definition of the exact solution of coefficient inverse problem 2.1. We assume that there exists a coefficient $c^*(x)$ satisfying conditions (2.3) and (2.4), and this function is the exact solution of this CIP with the "ideal" exact data in $g^*(x,t)$ in (2.5). Recall that by Remark 2.1, we always assume that the uniqueness theorem is in place for each inverse problem considered in Chaps. 2–6. The Laplace transform (2.10) of the function $g^*(x,t)$ leads to the exact function $\varphi^*(x,s) = w^*(x,s)$, $\forall (x,s) \in \partial\Omega \times [\underline{s}, \overline{s}]$.

Denote

$$v^*(x,s) = \frac{\ln[w^*(x,s)]}{s^2},\ q^*(x,s) = \frac{\partial v^*(x,s)}{\partial s},\ V^*(x,\overline{s}) = v^*(x,\overline{s}).$$

Recall that (2.20) for the exact function $q^*(x,s)$ is

$$\Delta q^* - 2s^2 \nabla q^* \int_s^{\overline{s}} \nabla q^*(x,\tau)\,d\tau + 2s\left[\int_s^{\overline{s}} \nabla q^*(x,\tau)\,d\tau\right]^2$$
$$+ 2s^2 \nabla q^* \nabla V^* - 4s \nabla V^* \int_s^{\overline{s}} \nabla q^*(x,\tau)\,d\tau + 2s\left(\nabla V^*\right)^2 = 0,$$
$$x \in \Omega, s \in [\underline{s}, \overline{s}]. \tag{2.105}$$

In addition, by (2.21) and (2.15),

$$q^*(x,s) = \psi^*(x,s),\ \forall (x,s) \in \partial\Omega \times [\underline{s}, \overline{s}]. \tag{2.106}$$

$$c^*(x) = \left[\Delta v^* + s^2 |\nabla v^*|^2\right](x,s),\ (x,s) \in \Omega \times [\underline{s}, \overline{s}]. \tag{2.107}$$

In (2.106),

$$\psi^*(x,s) = \frac{1}{\varphi^* s^2} \cdot \frac{\partial \varphi^*}{\partial s} - \frac{2\ln \varphi^*}{s^3}.$$

The formula (2.107) is used to reconstruct the exact solution c^* from the function v^*.

Definition 2.8.1. We call the function $q^*(x,s)$ the *exact solution* of the problem (2.20) and (2.21), or, equivalently, of the problem (2.105) and (2.106), with the *exact boundary* condition $\psi^*(x,s)$.

Hence,

$$q^*(x,s) \in C^{3+\alpha}\left(\overline{\Omega}\right) \times C^1[\underline{s},\overline{s}]. \tag{2.108}$$

We now follow (2.33)–(2.36), (2.38), and (2.39). First, we approximate functions $q^*(x,s)$ and $\psi^*(x,s)$ via piecewise constant functions with respect to $s \in [\underline{s},\overline{s}]$. For $n \in [1,N]$, let

$$q_n^*(x) = \frac{1}{h}\int\limits_{s_n}^{s_{n-1}} q^*(x,s)\,ds,\ \overline{\psi}_n^*(x) = \frac{1}{h}\int\limits_{s_n}^{s_{n-1}} \psi^*(x,s)\,ds,\ q_0^*(x) \equiv 0. \tag{2.109}$$

Hence,

$$\begin{aligned} q^*(x,s) &= q_n^*(x) + Q_n(x,s),\ \psi^*(x,s) \\ &= \overline{\psi}_n^*(x) + \Psi_n(x,s), n \in [1,N], \quad s \in [s_n, s_{n-1}], \end{aligned}$$

where by (2.108), functions Q_n, Ψ_n are such that

$$|Q_n(x,s)|_{2+\alpha} \le C^*h,\ |\Psi_n(x,s)|_{2+\alpha} \le C^*h, \text{ for } s \in [s_n, s_{n-1}]. \tag{2.110}$$

Here, the constant $C^* = C^*(\|q^*\|_{C^{2+\alpha}(\overline{\Omega})\times C^1[\underline{s},\overline{s}]}) > 0$ depends only on the $C^{2+\alpha}\left(\overline{\Omega}\right) \times C^1[\underline{s},\overline{s}]$ norm of the function $q^*(x,s)$. Hence, we can assume that

$$\max_{1\le n\le N} |q_n^*|_{2+\alpha} \le C^*. \tag{2.111}$$

Without any loss of generality, we assume that

$$C^* \ge 1. \tag{2.112}$$

By the fundamental concept of Tikhonov (Sect. 1.4), we assume that the constant C^* is known a priori. By (2.14), it is reasonable to assume that C^* is independent on $\overline{s}$, although we do not use this assumption. By (2.109),

$$q_n^*(x) = \overline{\psi}_n^*(x),\ x \in \partial\Omega. \tag{2.113}$$

Hence, we obtain from (2.105) the following analogue of (2.39):

$$\Delta q_n^* - A_{1,n}\left(h\sum_{j=0}^{n-1}\nabla q_j^*\right)\nabla q_n^* + A_{1,n}\nabla q_n^*\nabla V^*$$

$$= 2\frac{I_{1,n}}{I_0}\left(\nabla q_n^*\right)^2 - A_{2,n}h^2\left(\sum_{i=1}^{n-1}\nabla q_i^*\right)^2$$

$$+2A_{2,n}\nabla V^*\left(h\sum_{j=0}^{n-1}\nabla q_j^*\right) - A_{2,n}\left|\nabla V^*\right|^2 + F_n\left(x,h,\lambda\right), \tag{2.114}$$

where the function $F_n\left(x,h,\lambda\right) \in C^\alpha\left(\overline{\Omega}\right)$ and

$$\max_{\lambda h\geq 1}\left|F_n\left(x,h,\lambda\right)\right|_\alpha \leq C^* h,\ \lambda h \geq 1. \tag{2.115}$$

Let

$$v_n^*\left(x\right) = -hq_n^*\left(x\right) - h\sum_{j=0}^{n-1} q_j^*\left(x\right) + V^*\left(x\right),\ x\in\Omega,\ n\in[1,N]. \tag{2.116}$$

Then (2.107), (2.108), and (2.115) imply that

$$c^*\left(x\right) = \left[\Delta v_n^* + s_n^2\left|\nabla v_n^*\right|^2\right]\left(x\right) + \overline{F}_n\left(x\right), \tag{2.117}$$

where $\left|\overline{F}_n\right|_\alpha \leq C^* h$. To simplify the presentation, we replace the latter inequality with

$$\left|\overline{F}_n\right|_\alpha \leq h. \tag{2.118}$$

This is not a severe restriction since a similar convergence analysis can be conducted for the case $\left|\overline{F}_n\right|_\alpha \leq C^* h$, although it would take more space.

We also assume that the function $g(x,t)$ in (2.5) is given with an error. This naturally produces an error in the function $\psi\left(x,s\right)$ in (2.21). An additional error is introduced due to the averaging in (2.35) and (2.109). Hence, we assume that in (2.34) functions $\overline{\psi}_n\left(x\right) \in C^{2+\alpha}\left(\partial\Omega\right)$ and

$$\left\|\overline{\psi}_n^*\left(x\right) - \overline{\psi}_n\left(x\right)\right\|_{C^{2+\alpha}(\partial\Omega)} \leq C^*\left(\sigma + h\right), \tag{2.119}$$

where $\sigma > 0$ is a small parameter characterizing the level of the error in the data $\psi\left(x,s\right)$. The parameter h can also be considered as a part of the error in the data.

2.8.2 The First Approximate Global Convergence Theorem

First, we reformulate the Schauder theorem in a simplified form, which is sufficient for our case; see Chap. 3, Sect. 1 in [118] for this theorem. Assuming that

$$\overline{s} > 1,\ \lambda h \geq 1, \tag{2.120}$$

and using (2.38) as well as formulas for numbers $A_{1,n}, A_{2,n}$, we obtain [24]

$$\max_{1\leq n\leq N} \{|A_{1,n}| + |A_{2,n}|\} \leq 8\overline{s}^2. \tag{2.121}$$

Introduce the positive constant $M^* = M^*(C^* : \overline{s})$,

$$M^* = 16C^*\overline{s}^2 = 2C^* \max\left(8\overline{s}^2, \max_{1\leq n\leq N} \{|A_{1,n}| + |A_{2,n}|\}\right) > 16. \tag{2.122}$$

The inequality $M^* > 16$ follows from (2.112) and (2.120). Consider the Dirichlet boundary value problem:

$$\Delta u + \sum_{j=1}^{3} b_j(x) u_{x_j} - b_0(x)u = f(x), x \in \Omega,$$
$$u|_{\partial\Omega} = g(x) \in C^{2+\alpha}(\partial\Omega). \tag{2.123}$$

Assume that the following conditions are satisfied:

$$b_j, b_0, f \in C^{\alpha}\left(\overline{\Omega}\right), b_0(x) \geq 0;\ \max_{j\in[0,n]} \left(\left|b_j\right|_{\alpha}\right) \leq 1. \tag{2.124}$$

This upper bound is chosen to simplify the presentation since this is sufficient for our goal. By the Schauder theorem, there exists unique solution $u \in C^{2+\alpha}\left(\overline{\Omega}\right)$ of the boundary value problem (2.123). Furthermore, with a constant $K = K(\Omega) > 1$, depending only on the domain Ω, the following estimate holds:

$$|u|_{2+\alpha} \leq K\left[\|g\|_{C^{2+\alpha}(\partial\Omega)} + |f|_{\alpha}\right]. \tag{2.125}$$

We point out that the constant K depends only on the domain Ω as long as estimate (2.124) for coefficients is in place. In general, however, K depends on both the domain Ω and the upper estimate of the $C^{\alpha}\left(\overline{\Omega}\right)$-norm of coefficients. Note that the definition of the $C^{\alpha}\left(\overline{\Omega}\right)$-norm implies that

$$|f_1 f_2|_{\alpha} \leq |f_1|_{\alpha} |f_2|_{\alpha},\ \forall f_1, f_2 \in C^{\alpha}\left(\overline{\Omega}\right). \tag{2.126}$$

Theorem 2.8.2. *Let $\Omega \subset \mathbb{R}^3$ be a bounded domain with the boundary $\partial\Omega \in C^3$. Consider the algorithm of Sect. 2.6.1, where $\overline{s} = \text{const.} > 1$. Assume that all functions $c_{n,i}$ reconstructed in this algorithm are such that*

$$c_{n,i}(x) \geq 1,\ x \in \Omega. \tag{2.127}$$

Let the exact coefficient $c^*(x)$ *satisfies conditions (2.3) and (2.4), i.e.,*

$$c^*(x) \in [1,d], \quad c^*(x) = 1 \text{ for } x \in \mathbb{R}^3 \setminus \Omega,$$

$$c^* \in C^3\left(\mathbb{R}^3\right),$$

where the number $d > 1$ *is given. Let* $C^* \geq 1$ *be the constant defined in (2.111) and (2.112). Let in (2.34) boundary functions* $\overline{\psi}_n \in C^{2+\alpha}(\partial\Omega)$. *Assume that (2.115), (2.119), and (2.120) hold. For any function* $c(x) \in C^\alpha\left(\mathbb{R}^3\right)$ *such that* $c(x) \in [1, d+1]$ *in* Ω *and* $c(x) = 1$ *in* $\mathbb{R}^3 \setminus \Omega$, *consider the solution* $w_c(x,\overline{s})$ *of the problem (2.11) and (2.12),*

$$\Delta w_c - \overline{s}^2 c(x) w_c = -\delta(x - x_0), \ x \in \mathbb{R}^3, \tag{2.128}$$

$$\lim_{|x|\to\infty} w_c(x,\overline{s}) = 0, \tag{2.129}$$

satisfying condition (2.84) with $k = 0$. *Consider the corresponding tail functions,*

$$V^*(x) = \frac{\ln w^*(x,\overline{s})}{\overline{s}^2} \in C^{2+\alpha}\left(\overline{\Omega}\right), \ V_c(x) = \frac{\ln w_c(x,\overline{s})}{\overline{s}^2} \in C^{2+\alpha}\left(\overline{\Omega}\right), \tag{2.130}$$

where $w^*(x,\overline{s})$ *is the solution of the problem (2.128) and (2.129) of the form (2.84) with* $k = 3$ *for* $c(x) := c^*(x)$. *Suppose that the number* $\overline{s}$ *is so large that the following estimates hold*

$$|V^*|_{2+\alpha} \leq \xi, \ |V_c|_{2+\alpha} \leq \xi, \tag{2.131}$$

for all such functions c, *where* $\xi \in (0,1)$ *is a sufficiently small number. Let* $V_{1,1}(x,\overline{s}) \in C^{2+\alpha}\left(\overline{\Omega}\right)$ *be the initial tail function and let*

$$|V_{1,1}|_{2+\alpha} \leq \xi. \tag{2.132}$$

Denote

$$\eta := 2(h + \sigma + \xi + \varepsilon). \tag{2.133}$$

Let $K = K(\Omega) > 1$ *be the constant of the Schauder theorem in (2.84) and* $\overline{N} \leq N$ *be the total number of functions* q_n *calculated by the algorithm of Sect. 2.6.1. Suppose that the number* $\overline{N} = \overline{N}(h)$ *is connected with the step size* h *via* $\overline{N}(h)\, h = \beta$, *where the constant* $\beta > 0$ *is independent on* h. *Let* β *be so small that*

$$\beta \leq \frac{1}{24KM^*} = \frac{1}{384K\overline{s}^2}, \tag{2.134}$$

where the number M^* was defined in (2.122). In addition, let the number η in (2.133) and the parameter λ of the CWF in (2.38) satisfy the following estimates:

$$\eta \leq \eta_0\left(K, C^*, \overline{s}\right) = \frac{1}{16KM^*} = \frac{1}{256KC^*\overline{s}^2}, \tag{2.135}$$

$$\lambda \geq \lambda_0\left(C^*, K, \overline{s}, \eta\right) = \max\left(\left(C^*\right)^2, 96KC^*\overline{s}^2, \frac{1}{\eta^2}\right). \tag{2.136}$$

Then for each $n \in \left[1, \overline{N}\right]$, the sequence $\left\{q_{n,1}^k\right\}_{k=1}^{\infty}$ converges in $C^{2+\alpha}\left(\overline{\Omega}\right)$. Furthermore, functions

$$c_{n,i} \in C^{\alpha}\left(\overline{\Omega}\right), \widehat{c}_{n,k} \in C^{\alpha}\left(\mathbb{R}^3\right),$$

$$c_{n,i}(x), \widehat{c}_{n,i}(x) \in [1, d+1] \text{ in } \Omega.$$

In addition, the following estimates hold :

$$|q_n - q_n^*|_{2+\alpha} \leq 2KM^*\left(\frac{1}{\sqrt{\lambda}} + 3\eta\right), \ n \in \left[1, \overline{N}\right], \tag{2.137}$$

$$|q_n|_{2+\alpha} \leq 2C^*, \ n \in \left[1, \overline{N}\right], \tag{2.138}$$

$$|c_n - c^*|_{\alpha} \leq \frac{1}{2 \cdot 9^{n-1}}\eta + \frac{23}{8}\eta, \ n \in \left[2, \overline{N}\right]. \tag{2.139}$$

Denote

$$\varepsilon = \left(\frac{1}{18} + \frac{23}{8}\right)\eta = \frac{211}{72}\eta.$$

By (2.135), $\varepsilon \in (0, 0.012)$. Therefore, estimate (2.139) implies the approximate global convergence property of the algorithm of Sect. 2.6.1 of the level ε within the framework of the first approximate mathematical model of Sect. 2.8.4 (below).

It is worthy to make some comments prior to the proof of this theorem. We formulate these comments as the following remarks:

Remarks 2.8.2. 1. The existence and uniqueness of the solution of the problem (2.128) and (2.129) is guaranteed by Theorem 2.7.2 This theorem also guarantees that $w_c(x, \overline{s}) > 0$ for $x \neq x_0$, which justifies the consideration of $\ln w_c(x, \overline{s})$ in (2.130). We impose condition (2.127) because of Theorem 2.7.2

2. We have observed in our computations that the inequality (2.127) holds indeed for computed functions $c_{n,i}(x)$; see Sect. 3.1.2. In fact, if we would need to estimate norms $\|c_n - c^*\|_{L_2(\Omega)}$ instead of Hölder norms above, then we would ensure (2.127) via replacing (2.42) with

$$c_{n,i}(x) = \min\left\{1, \left[\Delta v_{n,i} + s_n^2\left(\nabla v_{n,i}\right)^2\right](x)\right\}, \ x \in \Omega. \tag{2.140}$$

Clearly, this function belongs to $C^{\alpha}\left(\overline{\Omega}\right)$ if the function $\left[\Delta v_{n,i}+s_n^2\left(\nabla v_{n,i}\right)^2\right]\in C^{\alpha}\left(\overline{\Omega}\right)$. An analog of (2.140) is used in Sect. 6.4.3, since the follow up Theorem 6.7 estimates the reconstruction accuracy in the L_2-norm.

3. In fact, it is established in the proof of this theorem that $|c_n-c^*|_{\alpha}\leq 8\eta/3$, which is stronger than estimate (2.139). Nevertheless, estimate (2.139) is interesting in its own right because it shows the dependence from the iteration number n. Indeed, it follows from (2.139) that initially, the reconstruction accuracy improves with iterations. However, for larger values of n, one should expect a stabilization of functions c_n, since $\eta/\left(2\cdot 9^{n-1}\right)\approx 0$ for large n. This is exactly what we observe in our computations.
4. The number $\beta=\overline{N}\left(h\right)h$ is the length of the s interval, which is covered by the algorithm of Sect. 2.6.1. The smallness condition (2.134) imposed on β seems to be inevitable since (2.39) are actually generated by (2.20), which contains Volterra integrals in nonlinear terms.

Proof of Theorem 2.8.2. We obtain from (2.112), (2.135), and (2.136) that

$$\frac{C^*}{2\sqrt{\lambda}}\leq 1,\quad \frac{1}{\sqrt{\lambda}}+3\eta\leq\frac{C^*}{2KM^*},\quad \frac{KM^*}{\lambda}\leq\frac{1}{3},\quad \frac{1}{\sqrt{\lambda}}\leq\eta. \tag{2.141}$$

Denote

$$\widetilde{q}_{n,1}^{k}=q_{n,1}^{k}-q_n^*,\ \widetilde{q}_{n,i}=q_{n,i}-q_n^*,$$
$$\widetilde{V}_{n,i}=V_{n,i}-V^*,\ \widetilde{c}_{n,i}=c_{n,i}-c^*,\widetilde{\psi}_n=\overline{\psi}_n-\overline{\psi}_n^*,$$
$$\widetilde{v}_{n,i}\left(x\right)=v_{n,i}\left(x\right)-v^*\left(x,s_n\right),\ \widetilde{v}_n\left(x\right)=v_n\left(x\right)-v^*\left(x,s_n\right),$$

where $H^*\left(x,s\right)$ is the function $H_n\left(x\right)$ in (2.41) in the case when functions q_j and V_n are replaced with q_j^* and V^*, respectively. Recall that by (2.40),

$$\frac{\left|I_{1,n}\left(\lambda,h\right)\right|}{I_0\left(\lambda,h\right)}\leq\frac{4\overline{s}^2}{\lambda},\ \text{for}\ \lambda h\geq 1. \tag{2.142}$$

The proof of Theorem 2.8.2 basically consists in estimating norms $|\widetilde{q}_{n,1}^{k}|_{2+\alpha}$, $|\widetilde{q}_{n,i}|_{2+\alpha}$ from the above. First, we estimate norms $|\widetilde{q}_{1,k}^{1}|_{2+\alpha}$. By (2.132) and (2.133),

$$\left|\widetilde{V}_{1,1}\right|_{2+\alpha}\leq 2\xi\leq\eta. \tag{2.143}$$

Substituting $n=1$ in (2.114), subtracting it from (2.45), and subtracting (2.113) from (2.46), we obtain

$$\Delta\widetilde{q}_{1,1}^{k}-\varepsilon\widetilde{q}_{1,1}^{k}+A_{1,1}\nabla V_{1,1}\nabla\widetilde{q}_{1,1}^{k}=2\frac{I_{1,1}}{I_0}\nabla\widetilde{q}_{1,1}^{k-1}\left(\nabla q_{1,1}^{k-1}+\nabla q_1^*\right)$$
$$-A_{1,1}\nabla\widetilde{V}_{1,1}\nabla q_1^*-A_{2,1}\nabla\widetilde{V}_{1,1}\left(\nabla V_{1,1}+\nabla V^*\right)+\varepsilon q_1^*-F_1, \tag{2.144}$$

$$\widetilde{q}_{1,1}^{1}(x) = \widetilde{\psi}_1(x), x \in \partial\Omega. \tag{2.145}$$

By (2.133) and (2.135), $\varepsilon \leq \eta/2 < 1$. Also, since $K, C^* > 1$, then by (2.122), (2.132), (2.133), and (2.135),

$$|A_{1,1}\nabla V_{1,1}| \leq 4\bar{s}^2\eta \leq \frac{1}{64KC^*} \leq \frac{1}{64K} < 1. \tag{2.146}$$

Hence, combining the Schauder theorem (2.125) with (2.115)–(2.122), (2.131), (2.135), and (2.143)–(2.146), we obtain

$$\left|\widetilde{q}_{1,1}^{k}\right|_{2+\alpha} \leq \frac{KM^*}{2C^*\lambda}\left|\widetilde{q}_{1,1}^{k-1}\right|_{1+\alpha}\left|q_{1,1}^{k-1} + q_1^*\right|_{1+\alpha} + 3KM^*\eta. \tag{2.147}$$

First, let $k = 1$. Since by (2.43) and (2.44), $q_{1,1}^{0} = 0$, then $\widetilde{q}_{1,1}^{0} = -q_1^*$. By (2.111) $\left|\nabla q_1^*\right|_{\alpha}^{2} \leq (C^*)^2$. Hence, (2.147) implies that

$$\left|\widetilde{q}_{1,1}^{1}\right|_{2+\alpha} \leq KM^*\left[\frac{C^*}{2\lambda} + 3\eta\right].$$

Hence, using the first inequality (2.141), we obtain

$$\left|\widetilde{q}_{1,1}^{1}\right|_{2+\alpha} \leq KM^*\left(\frac{1}{\sqrt{\lambda}} + 3\eta\right) \leq 2KM^*\left(\frac{1}{\sqrt{\lambda}} + 3\eta\right).$$

Hence, the second inequality (2.141) and (2.111) imply that

$$\left|q_{1,1}^{1}\right|_{2+\alpha} \leq \left|\widetilde{q}_{1,1}^{1}\right|_{2+\alpha} + |q^*|_{2+\alpha} \leq 2C^*. \tag{2.148}$$

Assume now that

$$\left|\widetilde{q}_{1,1}^{k-1}\right|_{2+\alpha} \leq 2KM^*\left(\frac{1}{\sqrt{\lambda}} + 3\eta\right), k \geq 2. \tag{2.149}$$

Then similarly with (2.148), we obtain

$$\left|q_{1,1}^{k-1}\right|_{2+\alpha} \leq 2C^*. \tag{2.150}$$

We obtain from (2.147), (2.149), and (2.150)

$$\left|\widetilde{q}_{1,1}^{k}\right|_{2+\alpha} \leq \frac{3(KM^*)^2}{\lambda}\left(\frac{1}{\sqrt{\lambda}} + 3\eta\right) + 3KM^*\eta.$$

Hence, the third inequality (2.141) leads to

$$\left|\widetilde{q}_{1,1}^{k}\right|_{2+\alpha} \leq 2KM^{*}\left(\frac{1}{\sqrt{\lambda}}+3\eta\right), k \geq 1. \tag{2.151}$$

Hence, we obtain similarly with (2.148) that

$$\left|q_{1,1}^{k}\right|_{2+\alpha} \leq 2C^{*}, k \geq 1. \tag{2.152}$$

Estimates (2.151) and (2.152) enable us to prove convergence of functions $q_{1,1}^{k}$ for $k \to \infty$. Let $m, r > 2$ be two positive integers. Denote $a_{m,r} = q_{1,1}^{m} - q_{1,1}^{r}$. Then, $a_{m,r} = \widetilde{q}_{1,1}^{m} - \widetilde{q}_{1,1}^{r}$. First, set in (2.144) $k := m$ and then set $k := r$. Next, subtract two resulting equations and use the following:

$$\begin{aligned}
&\nabla\widetilde{q}_{1,1}^{m-1}\left(\nabla q_{1,1}^{m-1}+\nabla q_{1}^{*}\right)-\nabla\widetilde{q}_{1,1}^{r-1}\left(\nabla q_{1,1}^{r-1}+\nabla q_{1}^{*}\right)\\
&\quad=\nabla\widetilde{q}_{1,1}^{m-1}\left(\nabla q_{1,1}^{m-1}+\nabla q_{1}^{*}\right)-\nabla\widetilde{q}_{1,1}^{r-1}\left(\nabla q_{1,1}^{m-1}+\nabla q_{1}^{*}\right)\\
&\qquad+\nabla\widetilde{q}_{1,1}^{r-1}\left(\nabla q_{1,1}^{m-1}+\nabla q_{1}^{*}\right)-\nabla\widetilde{q}_{1,1}^{r-1}\left(\nabla q_{1,1}^{r-1}+\nabla q_{1}^{*}\right)\\
&\quad=\nabla a_{m-1,r-1}\left(\nabla q_{1,1}^{m-1}+\nabla q_{1}^{*}\right)+\nabla\widetilde{q}_{1,1}^{r-1}\cdot\nabla a_{m-1,r-1}\\
&\quad=\nabla a_{m-1,r-1}\left(\nabla q_{1,1}^{m-1}+\nabla\widetilde{q}_{1,1}^{r-1}+\nabla q_{1}^{*}\right).
\end{aligned}$$

We obtain

$$\Delta a_{m,r}-\varepsilon a_{m,r}+A_{1,1}\nabla V_{1,1}\nabla a_{mr}=2\frac{I_{1,1}}{I_{0}}\nabla a_{m-1,r-1}\cdot\left(\nabla q_{1,1}^{m-1}+\nabla\widetilde{q}_{1,1}^{r-1}+\nabla q_{1}^{*}\right),$$

$$a_{m,r}\,|_{\partial\Omega}=0.$$

Hence, by the Schauder theorem (2.125), second and third inequalities (2.141), (2.151), (2.152), and (2.142),

$$|a_{m,r}|_{2+\alpha} \leq \frac{2KM^{*}}{\lambda}|a_{m-1,r-1}|_{2+\alpha} \leq \frac{2}{3}|a_{m-1,r-1}|_{2+\alpha}. \tag{2.153}$$

It follows from (2.153) that the sequence $\left\{q_{1,1}^{k}\right\}_{k=1}^{\infty}$ satisfies the Cauchy convergence criterion. Convergence of other sequences $\left\{q_{n,1}^{k}\right\}_{k=1}^{\infty}$ can be proven similarly. Thus, these proofs are omitted below.

Since functions $\widetilde{q}_{1,1}$ and $q_{1,1}$ are estimated via (2.151) and (2.152), we now can estimate the norm $\left|\widetilde{c}_{1,1}\right|_{\alpha}$. First, we note that by (2.41), (2.42), and (2.116)–(2.118),

$$\left|\widetilde{c}_{1,1}\right|_{\alpha} \leq \left(\left|\widetilde{v}_{1,1}\right|_{2+\alpha}+\frac{\eta}{2}\right)\left[1+\overline{s}^{2}\left(|v_{1,1}|_{2+\alpha}+|v_{1}^{*}|_{2+\alpha}\right)\right].$$

As to the truncation in (2.42), it does not affect this estimate because $c^* \geq 1$. By (2.41), (2.116), (2.131)–(2.134) and the fourth inequality (2.141),

$$|\widetilde{c}_{1,1}|_{2+\alpha} + \frac{\eta}{2} \leq 8KM^*\beta\eta + \frac{3}{2}\eta \leq \frac{1}{3}\eta + \frac{3}{2}\eta = \frac{11}{6}\eta.$$

Next, (2.41), (2.116), (2.132), (2.134), (2.135), and (2.152) lead to

$$1 + \overline{s}^2\left(|v_{1,1}|_{2+\alpha} + |v_1^*|_{2+\alpha}\right) \leq 1 + 3\overline{s}^2C^*\beta + \overline{s}^2\eta \leq 1 + \frac{M^*}{5}\beta + \frac{1}{256}$$
$$\leq 1 + \frac{1}{120} + \frac{1}{256} < \frac{16}{11}.$$

Thus, the last three inequalities combined with (2.135) imply that

$$|\widetilde{c}_{1,1}|_{\alpha} \leq \frac{8}{3}\eta < \frac{1}{2}. \tag{2.154}$$

Since the function c^* satisfies conditions (2.42), then it follows from (2.154) and (2.127) that functions $c_{1,1}, \widehat{c}_{1,1} \in [1, d + 1/2]$. This, along with one of conditions of Theorem 2.8.2, ensures that $|V_{1,2}|_{2+\alpha} \leq \xi$. Hence, similarly with the above, one can prove that estimates (2.151), (2.152), and (2.154) are valid for functions $\widetilde{q}_{1,2}, q_{1,2}$ and $\widetilde{c}_{1,2}$, respectively. To do this, one should use (2.45) and (2.46) at $n = 1$, $i = 2$. Repeating this process m_1 times, we obtain the same estimates for functions $\widetilde{q}_1, q_1, \widetilde{c}_1$. In addition, we also obtain that functions $c_1, \widehat{c}_1 \in [1, d + 1/2]$. Hence, one of conditions of this theorem implies that $|V_{2,1}|_{2+\alpha} \leq \xi$.

Let now $n \geq 2$. Assume that

$$\left|\widetilde{q}_j\right|_{2+\alpha} \leq 2KM^*\left(\frac{1}{\sqrt{\lambda}} + 3\eta\right), \ j \in [1, n-1], \tag{2.155}$$

$$\left|q_j\right|_{2+\alpha} \leq 2C^*, \ j \in [1, n-1], \tag{2.156}$$

$$\left|\widetilde{c}_j\right|_{\alpha} \leq \frac{8}{3}\eta < \frac{1}{2}, \ j \in [1, n-1], \tag{2.157}$$

$$c_j, \widehat{c}_j \in [1, d+1], \ \widehat{c}_j(x) = 1 \text{ in } \mathbb{R}^3 \setminus \Omega, \ c_j, \widehat{c}_j \in C^{\alpha}\left(\mathbb{R}^3\right), \ j \in [1, n-1]. \tag{2.158}$$

We now obtain these estimates at $j = n$. It follows from (2.131), (2.133), and (2.158) that

$$|V_{n,1}|_{2+\alpha} \leq \xi \leq \frac{\eta}{2}, \ \left|\widetilde{V}_{n,1}\right| \leq 2\xi \leq \eta. \tag{2.159}$$

For brevity, consider only functions $q_{n,i}$ with $i \geq 1$, since convergence of the sequence $\left\{q_{n,1}^k\right\}_{k=1}^{\infty}$ can be proved very similarly with the above case of $\left\{q_{1,1}^k\right\}_{k=1}^{\infty}$. Also, for brevity set,

$$q_{n,0} := q_{n-1}. \tag{2.160}$$

Recall that by (2.47), $\lim_{k\to\infty} q_{n,1}^k = q_{n,1}$ in the norm of the space $C^{2+\alpha}\left(\overline{\Omega}\right)$.

Subtracting (2.114) from (2.45) and (2.113) from (2.46), we obtain for $i \geq 1$

$$\begin{aligned}
&\Delta\widetilde{q}_{n,i} - A_{1,n}\left(h\sum_{j=0}^{n-1}\nabla q_j\,(x)\right)\nabla\widetilde{q}_{n,i} + A_{1,n}\nabla V_{n,i}\cdot\nabla\widetilde{q}_{n,i} - \varepsilon\widetilde{q}_{n,i}\\
&\quad = 2\frac{I_{1,n}}{I_0}\left[\nabla\widetilde{q}_{n,i-1}\left(\nabla q_{n,i-1} + \nabla q_n^*\right)\right]\\
&\qquad + \left(A_{1,n}\nabla q_n^* - A_{2,n}h\sum_{j=0}^{n-1}\left(\nabla q_j + \nabla q_j^*\right) + 2A_{2,n}\nabla V_{n,i}\right)\left(h\sum_{j=0}^{n-1}\nabla\widetilde{q}_j\right)\\
&\qquad + \left[2A_{2,n}h\sum_{j=0}^{n-1}\nabla q_j^* - A_{1,n}\nabla q_n^* - A_{2,n}\left(\nabla V_{n,i} + \nabla V^*\right)\right]\nabla\widetilde{V}_{n,i} + \varepsilon q_n^* - F_n,
\end{aligned} \tag{2.161}$$

$$\widetilde{q}_{n,i}\mid_{\partial\Omega} = \widetilde{\psi}_n(x). \tag{2.162}$$

We estimate the sum of 2nd, 3rd, 4th, and 5th terms in the right-hand side of (2.161). As to the second term, using (2.111), (2.122), (2.135), (2.156), and (2.159), we obtain

$$\begin{aligned}
&\left|A_{1,n}\nabla q_n^* - A_{2,n}h\sum_{j=1}^{n-1}\left(\nabla q_j + \nabla q_j^*\right) + 2A_{2,n}\nabla V_{n,1}\right|_\alpha\\
&\quad \leq \frac{M^*}{2} + \frac{3M^*\beta}{2} + \frac{M^*}{2} = M^*\left(1 + \frac{3}{2}\beta\right).
\end{aligned}$$

On the other hand, by (2.155),

$$h\sum_{j=0}^{n-1}\left|\nabla\widetilde{q}_j\right|_\alpha \leq 2KM^*\beta\left(\frac{1}{\sqrt{\lambda}} + 3\eta\right). \tag{2.163}$$

Hence, (2.131), (2.133), and (2.163) imply that

$$\begin{aligned}
&\left|A_{1,n}\nabla q_n^* - A_{2,n}h\sum_{j=0}^{n-1}\left(\nabla q_j + \nabla q_j^*\right) + 2A_{2,n}\nabla V_{n,1}\right|_\alpha \cdot \left|h\sum_{j=1}^{n-1}\nabla\widetilde{q}_j\,(x)\right|_\alpha\\
&\quad \leq 2K\left(M^*\right)^2\beta\left(1 + \frac{3}{2}\beta\right)\left(\frac{1}{\sqrt{\lambda}} + 3\eta\right).
\end{aligned} \tag{2.164}$$

Estimate now the sum of 3rd, 4th, and 5th terms in the right-hand side of (2.161). We obtain similarly with the above:

$$\left|\left(2A_{2,n}h\sum_{j=0}^{n-1}\nabla q_j^* - A_{1,n}\nabla q_n^* - A_{2,n}\left(\nabla V_{n,1}+\nabla V^*\right)\right)\nabla\widetilde{V}_{n,1} + \varepsilon q_n^* - F_1\right|_\alpha$$
$$\leq 2M^*\left(1+\frac{\beta}{2}\right)\eta. \tag{2.165}$$

Combining (2.165) with (2.163), we obtain the following estimate the sum of 3rd, 4th, and 5th terms in the right-hand side of (2.161):

$$\left|\left(A_{1,n}\nabla q_n^* - A_{2,n}h\sum_{j=0}^{n-1}\left(\nabla q_j+\nabla q_j^*\right) + 2A_{2,n}\nabla V_{n,1}\right)\left(h\sum_{j=0}^{n-1}\nabla\widetilde{q}_j\right)\right|_\alpha$$
$$+\left|\left(2A_{2,n}h\sum_{j=0}^{n-1}\nabla q_j^* - A_{1,n}\nabla q_n^* - A_{2,n}\left(\nabla V_{n,1}+\nabla V^*\right)\right)\nabla\widetilde{V}_{n,1} + \varepsilon q_n^* - F_1\right|_\alpha$$
$$\leq 2K\left(M^*\right)^2\beta\left(1+\frac{3}{2}\beta\right)\left(\frac{1}{\sqrt{\lambda}}+3\eta\right) + 2M^*\left(1+\frac{\beta}{2}\right)\eta. \tag{2.166}$$

Since $K, M^* > 1$, then (2.134) and the 4th inequality (2.141) imply that

$$2K\left(M^*\right)^2\beta\left(1+\frac{3}{2}\beta\right)\left(\frac{1}{\sqrt{\lambda}}+3\eta\right) \leq 8K\left(M^*\right)^2\beta\left(1+\frac{3}{2}\beta\right)\eta \leq \frac{1}{2}M^*\eta. \tag{2.167}$$

By (2.134),

$$2M^*\left(1+\frac{\beta}{2}\right)\eta \leq \frac{5}{2}M^*\eta. \tag{2.168}$$

Hence, we obtain from (2.166)–(2.168) that

$$\left|\left(A_{1,n}\nabla q_n^* - A_{2,n}h\sum_{j=0}^{n-1}\left(\nabla q_j+\nabla q_j^*\right) + 2A_{2,n}\nabla V_{n,1}\right)\left(h\sum_{j=0}^{n-1}\nabla\widetilde{q}_j\right)\right|_\alpha$$
$$+\left|\left(2A_{2,n}h\sum_{j=0}^{n-1}\nabla q_j^* - A_{1,n}\nabla q_n^* - A_{2,n}\left(\nabla V_{n,1}+\nabla V^*\right)\right)\nabla\widetilde{V}_{n,1} + \varepsilon q_n^* - F_1\right|_\alpha$$
$$\leq \frac{1}{2}M^*\eta + \frac{5}{2}M^*\eta = 3M^*\eta. \tag{2.169}$$

It follows from (2.134), (2.137), and (2.156) that $C^\alpha\left(\overline{\Omega}\right)$ norms of coefficients at $\nabla\widetilde{q}_{n,i}, \widetilde{q}_{n,i}$ in the left-hand side of (2.161) do not exceed 1. Hence, we can apply the estimate (2.125) of the Schauder theorem to the Dirichlet boundary value problem (2.161) and (2.162). Using that estimate and (2.142), we obtain

$$|\widetilde{q}_{n,i}|_{2+\alpha} \leq \frac{KM^*}{2C^*\lambda} |\nabla\widetilde{q}_{n,i-1}|_\alpha |\nabla q_{n,i-1} + \nabla q_n^*|_\alpha + 3KM^*\eta.$$

First, consider the case $i = 1$. By (2.160) $q_{n,0} = q_{n-1}$. Since estimates (2.155) and (2.156) hold true for functions $\widetilde{q}_{n-1}, q_{n-1}$, then (2.111), (2.136), (2.155), and (2.156) imply that

$$|\widetilde{q}_{n,1}|_{2+\alpha} \leq \frac{3KM^*}{\lambda} KM^* \left(\frac{1}{\sqrt{\lambda}} + 3\eta\right) + 3KM^*\eta \leq 2KM^* \left(\frac{1}{\sqrt{\lambda}} + 3\eta\right), \tag{2.170}$$

which establishes (2.155) for the function $\widetilde{q}_{n,1}$. Hence, similarly with (2.148), we obtain $|q_{n,1}|_{2+\alpha} \leq 2C^*$, which proves (2.156) for $q_{n,1}$. Using (2.41), (2.42), (2.116)–(2.118), (2.155), (2.156), (2.170), and the fourth inequality (2.141), we obtain similarly with (2.154) that

$$|\widetilde{c}_{n,1}|_\alpha \leq \frac{8}{3}\eta < \frac{1}{2},$$

which establishes (2.157) for $\widetilde{c}_{n,1}$. We obtain from (2.127) and (2.157) that functions

$$c_{n,1}, \widehat{c}_{n,1} \in [1, d+1],\ \widehat{c}_n(x) = 1 \text{ in } \mathbb{R}^3 \setminus \Omega,\ c_{n,1}, \widehat{c}_{n,1} \in C^\alpha\left(\mathbb{R}^3\right).$$

This establishes (2.158) for functions $c_{n,1}, \widehat{c}_{n,1}(x)$. The latter, (2.48), and one of conditions of this theorem guarantee that $|V_{n,2}|_{2+\alpha} \leq \xi$. Recalling that $q_n = q_{n,m_n}$ and applying the mathematical induction principle, we obtain that estimates (2.155)–(2.159) are valid for $j = n$.

Having estimates (2.155)–(2.158) for $j = 1, ..., n$, we now obtain estimate (2.139). Denote

$$p_n := \sum_{j=0}^{n} \left|\widetilde{q}_j\right|_{2+\alpha}, g_n = hp_n, n \in \left[1, \overline{N}\right].$$

It follows from the above proof that

$$\left| \left(A_{1,n}\nabla q_n^* - A_{2,n}h\sum_{j=0}^{n-1}\left(\nabla q_j + \nabla q_j^*\right) + 2A_{2,n}\nabla V_{n,1}\right) \left(h\sum_{j=0}^{n-1}\nabla\widetilde{q}_j\right)\right|_\alpha$$
$$\leq M^*\left(1 + \frac{3}{2}\beta\right)hp_{n-1} \leq 2M^*hp_{n-1}.$$

Hence, it follows from (2.165) and (2.168) that the sum of all terms in the right-hand side of (2.161), excluding the first one, can be estimated from the above via $2M^*hp_{n-1} + 5/2 \cdot M^*\eta$. First, consider the case when in (2.161) $\widetilde{q}_{n,i}$ is replaced with $\widetilde{q}^k_{n,1}$ and $\widetilde{q}_{n,i-1}$ is replaced with $\widetilde{q}^{k-1}_{n,1}$, respectively. Since the sequence $\{q^k_{n,1}\}_{k=1}^{\infty}$ converges, we can replace in (2.161) the vector $(\widetilde{q}^k_{n,1}, q^{k-1}_{n,1})$ with the vector $(\widetilde{q}_{n,1}, q_{n,1})$. Hence, applying to the boundary value problem (2.161) and (2.162), the estimate (2.125) of the Schauder theorem as well as (2.135)–(2.137), and the fourth inequality (2.141), we obtain

$$|\widetilde{q}_{n,1}|_{2+\alpha} \le \frac{|\widetilde{q}_{n,1}|_{2+\alpha}}{4} + 2KM^*hp_{n-1} + \frac{5}{2}KM^*\eta$$

or

$$|\widetilde{q}_{n,1}|_{2+\alpha} \le \frac{8}{3}KM^*hp_{n-1} + \frac{10}{3}KM^*\eta. \tag{2.171}$$

Similarly, we obtain for $\widetilde{q}_{n,i}, i \in [2, m_n]$

$$\begin{aligned}
|\widetilde{q}_{n,i}|_{2+\alpha} &\le \frac{KM^*}{2C^*\lambda}|\widetilde{q}_{n,i-1}|_{2+\alpha}|\nabla q_{n,i-1} + \nabla q^*_n| + 2KM^*hp_{n-1} + \frac{5}{2}KM^*\eta \\
&\le \frac{3KM^*}{\lambda}|\widetilde{q}_{n,i-1}|_{2+\alpha} + 2KM^*hp_{n-1} + \frac{5}{2}KM^*\eta \\
&\le \frac{24\,(KM^*)^2}{\lambda}\eta + 2KM^*hp_{n-1} + \frac{5}{2}KM^*\eta \le 2KM^*hp_{n-1} \\
&\quad + \frac{11}{4}KM^*\eta.
\end{aligned} \tag{2.172}$$

Thus, it follows from (2.171) and (2.172) that

$$|\widetilde{q}_{n,i}|_{2+\alpha} \le 2KM^*hp_{n-1} + \frac{10}{3}KM^*\eta,\ i \in [1, m_n].$$

Hence, recalling that $\widetilde{q}_n = \widetilde{q}_{n,m_n}$, we obtain

$$|\widetilde{q}_n|_{2+\alpha} \le \frac{8}{3}KM^*hp_{n-1} + \frac{10}{3}KM^*\eta. \tag{2.173}$$

Substituting in (2.173) $\widetilde{q}_{n-k}$ for $\widetilde{q}_n$, we obtain the following sequence of estimates:

$$|\widetilde{q}_{n-k}|_{2+\alpha} \le \frac{8}{3}KM^*hp_{n-k-1} + \frac{10}{3}KM^*\eta,\ 0 \le k \le n-2. \tag{2.174}$$

Summing up all estimates (2.174) for functions $\widetilde{q}_{n-k}$ with $0 \le k \le n-2$, we obtain

$$p_n - |\widetilde{q}_1|_{2+\alpha} \le \frac{8}{3}KM^*h\sum_{i=1}^{n-1}p_i + \frac{10}{3}KM^*n\eta.$$

Since $|p_i|_{2+\alpha} \leq |p_{i+1}|_{2+\alpha}$ and $h\overline{N} = \beta$, then

$$|p_n|_{2+\alpha} \leq \frac{8}{3} KM^* \beta\, p_{n-1} + \frac{10}{3} KM^* \overline{N} \eta + |\widetilde{q}_1|_{2+\alpha}.$$

Hence, multiplying by h and using (2.155) and the fourth inequality (2.141), we obtain

$$g_n \leq \frac{8}{3} KM^* \beta g_{n-1} + \frac{10}{3} KM^* \beta \eta + 4KM^* \eta^2.$$

Hence, (2.134) and (2.135) imply that

$$g_n \leq \frac{1}{9} g_{n-1} + \frac{7}{18}\eta,\ n \in \left[2, \overline{N}\right].$$

Iterating this inequality and using the formula for the sum of the geometrical progression, we obtain

$$g_n \leq \frac{1}{9^{n-1}} g_1 + \frac{7}{16}\eta,\ n \in \left[2, \overline{N}\right].$$

Since $g_1 = h\,|\widetilde{q}_1|_{2+\alpha} \leq |\widetilde{q}_1|_{2+\alpha}\,\eta/2$, then (2.135), (2.155), and the fourth inequality (2.141) imply that

$$g_n \leq \frac{\eta}{4 \cdot 9^{n-1}} + \frac{7}{16}\eta,\ n \in \left[2, \overline{N}\right]. \tag{2.175}$$

We now prove (2.139). Repeating the above arguments, which were presented for $|\widetilde{c}_{1,1}|_\alpha$, we obtain

$$|\widetilde{c}_n|_\alpha \leq |\widetilde{v}_n|_{2+\alpha} \left[1 + \overline{s}^2 \left(|v_n|_{2+\alpha} + |v_n^*|_{2+\alpha}\right)\right] \leq 2\,|\widetilde{v}_n|_{2+\alpha}. \tag{2.176}$$

Also, by (2.41) and (2.131), $|\widetilde{v}_n|_{2+\alpha} \leq g_n + \eta$. Hence, it follows from (2.176) that $|\widetilde{c}_n|_\alpha \leq 2\,(g_n + \eta)$. Combining this with (2.175), we obtain

$$|\widetilde{c}_n|_\alpha \leq \frac{1}{2 \cdot 9^{n-1}}\eta + \frac{23}{8}\eta,\ n \in \left[2, \overline{N}\right],$$

which is (2.139). □

2.8.3 *Informal Discussion of Theorem 2.8.2*

In this section, we informally discuss the meaning of the parameter ξ. In Sect. 2.8.4, we formalize this discussion via the introduction of the first approximate mathematical model; see Definition 1.1.2.1 in Sect. 1.1.2 for this notion. Theorem 2.8.2, which

fits this model, was our first result about the approximate global convergence [24]. The second approximate mathematical model of Sect. 2.9.2 imposes less restrictive conditions than the first one. That model is free from the discrepancy mentioned below in the current section.

By (2.14), (2.18), (2.131), and (2.132) the parameter ξ is small as long as the truncated pseudo frequency $\overline{s}$ is large. This implies, of course that the parameter η is also small since other numbers in (2.133) are those occurred either in the approximation procedure or the noise level. And the latter parameters traditionally assumed to be small in the numerical analysis. There is nothing unusual in the smallness assumption imposed on ξ. Indeed, since by (2.19), (2.131), and (2.132)

$$\xi = O\left(\frac{1}{\overline{s}}\right), \ \overline{s} \to \infty, \tag{2.177}$$

then that smallness assumption is similar with the truncation of high frequencies. And the latter is routinely done in engineering. Nevertheless, Theorem 2.8.2 has a discrepancy related to the parameter ξ. Indeed, by (2.135) we should have

$$\eta \leq \frac{1}{256KC^*\overline{s}^2}. \tag{2.178}$$

Conditions (2.177) and (2.178) are incompatible. In addition, since by (2.122) $M^* = O\left(\overline{s}^2\right)$ as $\overline{s} \to \infty$, then there is no guarantee that the right-hand side of (2.137) is indeed small.

We explain the discrepancy between (2.177) and (2.178) the same way as we have explained Definition 1.1.2.1 of the approximate global convergence property. The problem of construction of globally convergent numerical methods for our CIP is obviously an extremely challenging one because of three factors combined: nonlinearity, ill-posedness, and single measurement data. Hence, we need to come up with a certain compromise. One version of such a compromise is outlined in the previous paragraph. In simple terms, not everything can be covered by the theory, while numerical results are fortunately more optimistic than theoretical ones. Analogously, see the fifth Remark 1.1.2.1 about the well-known discrepancy between the Huygens-Fresnel theory of optics and the Maxwell equations.

Likewise, if we would prove convergence of our method as $\overline{s} \to \infty$, then we would also prove uniqueness of the above formulated inverse problems, which is a long-standing and not yet addressed question; see Remark 2.1

2.8.4 The First Approximate Mathematical Model

We now introduce the first approximate mathematical model which ensures that, within the framework of this model, Theorem 2.8.2 claims the approximate global convergence property of the algorithm of Sect. 2.6.1. We follow Definition 1.1.2.1 in Sect. 1.1.2.

Let $\Omega \subset \mathbb{R}^3$ be a convex bounded domain with the boundary $\partial\Omega \in C^3$. Let the exact coefficient $c^*(x)$ satisfies conditions (2.3) and (2.4):

$$c^*(x) \in [1, d], \quad c^*(x) = 1 \text{ for } x \in \mathbb{R}^3 \setminus \Omega,$$

$$c^* \in C^3\left(\mathbb{R}^3\right), |c^*|_\alpha \leq \overline{d},$$

where the numbers $d, \overline{d} > 1$ are given. Let the cut-off pseudo frequency $\overline{s} = \text{const.} > 1$. For any function $c(x)$ such that

$$c \in [1, d+1] \text{ in } \Omega, \; c(x) = 1 \text{ for } x \in \mathbb{R}^3 \setminus \Omega, \tag{2.179}$$

$$c(x) \in C^\alpha\left(\mathbb{R}^3\right), |c|_\alpha \leq \overline{d}, \tag{2.180}$$

consider the solution $w_c(x, \overline{s})$ of the problem:

$$\Delta w_c - \overline{s}^2 c(x) w_c = -\delta(x - x_0), \; x \in \mathbb{R}^3,$$

$$\lim_{|x| \to \infty} w_c(x, \overline{s}) = 0.$$

We seek solution of this problem in the class represented as

$$w_c(x, s) = w_1(x, s) + \overline{w}_c(x, s),$$

where

$$w_1(x, s) = \frac{\exp(-s|x - x_0|)}{4\pi |x - x_0|}, \; \overline{w}_c \in C^{2+\alpha}\left(\mathbb{R}^3\right).$$

Consider the corresponding tail function $V_c(x)$:

$$V_c(x) = \frac{\ln w_c(x, \overline{s})}{\overline{s}^2} \in C^{2+\alpha}\left(\overline{\Omega}\right).$$

Suppose that the following inequality holds for all functions c satisfying (2.179) and (2.180):

$$|\nabla V_c|_{1+\alpha} \leq \xi, \tag{2.181}$$

where $\xi \in (0, 1)$ is a sufficiently small number. It follows from Theorem 2.9.1.2 that norms $|\nabla V_c|_{1+\alpha}$ are indeed uniformly bounded for all functions $c(x)$ satisfying conditions (2.179) and (2.180).

The First Approximate Mathematical Model for the Algorithm of Sect. 2.6.1 consists of the following two assumptions.

Assumptions:

1. We assume that the number ξ in (2.181) is a free parameter, which can be made infinitely small independently on the parameter $\overline{s}$.
2. We assume that the tail function $V^*(x)$ is unique.

Actually, the first assumption was realized numerically in our works with experimental data [28,109]; also see Sect. 5.7. Indeed, it is stated in Sect. 7.2 of [109] that we have used derivatives of tails $\partial_{\overline{s}} V_c(x,\overline{s})$ instead of tails $V_c(x,\overline{s})$ themselves. Assuming that conditions of Lemma 2.3 hold, it follows from this lemma and (2.19) that

$$|\partial_{\overline{s}} V_c(x,\overline{s})|_{2+\alpha} << |V_c(x,\overline{s})|_{2+\alpha}, \ \overline{s} \to \infty. \tag{2.182}$$

Hence, it is reasonable to assume that in the formulation of Theorem 2.8.2, tails V^* and V_c are replaced with $\partial_{\overline{s}} V^*$ and $\partial_{\overline{s}} V_c$, respectively. Theorem 2.8.2 is still valid in this case with an insignificant change of its proof.

The second above assumption is imposed to make sure that the solution of (2.105) with the boundary condition (2.106) and the smoothness condition (2.108) is unique. Recall that its existence is assumed a priori by the fundamental concept of Tikhonov (Sects. 1.4 and 2.8.1). Uniqueness can be proven similarly with the proof of Lemma 2.9.2.

Remarks 2.8.4.

1. As it is stated in Theorem 2.8.2, (2.139) implies the approximate global convergence property of the algorithm of Sect. 2.6.1 within the framework of the first approximate mathematical model.
2. The only way to justify assumption 1 is via numerical studies. Numerical experiments of Chaps. 3 and 4 demonstrate that this model is reasonable since computational results confirm the validity of Theorem 2.8.2. The same is true for the second approximate mathematical model of Sect. 2.9.2. It is an opinion of the authors that results of testing of experimental data in [109] and [28] completely justify both approximate mathematical models; see the informal Definition 1.1.2.2 of the approximate global convergence property. Indeed, in [109], very accurate images of both locations and refractive indices of dielectric abnormalities were obtained for the most challenging case of *blind* experimental data when answers were unknown in advance. The follow-up refinement stage of nonblind testing in [28] led to very accurate images of all three components: locations, shapes, and refractive indices of those dielectric abnormalities. These results are presented in Chap. 5.

2.9 The Second Approximate Global Convergence Theorem

In this section, we present the second version of the proof of the approximate global convergence property of the algorithm of Sect. 2.6.1. Unlike Sect. 2.8, we estimate tail functions first. Next, we present the second approximate mathematical model. This model sounds more convenient than the first one because it basically amounts to the truncation of all terms of the asymptotic series for the tail function $V(x,\overline{s})$ at $\overline{s} \to \infty$, except of the first one. Finally, based on this model as

well as on estimates for tail functions, we prove the second approximate global convergence Theorem 2.9.4 This theorem claims that the algorithm of Sect. 2.6.1 has the approximate global convergence property within the framework of the second approximate mathematical model; see Definition 1.1.2.1 in Sect. 1.1.2 for this property.

For reader's convenience, we remind here some facts from previous sections of this chapter. Let $\Omega \subset \mathbb{R}^3$ be a convex bounded domain with the boundary $\partial\Omega \in C^3$. Let $c^*(x)$ be the exact solution of Inverse Problem 2.1. Just as above, we assume that the exact coefficient $c^*(x)$ satisfies the following conditions:

$$c^*(x) \in [1,d], \quad c^*(x) = 1 \text{ for } x \in \mathbb{R}^3 \setminus \Omega, \tag{2.183}$$

$$c^* \in C^3\left(\mathbb{R}^3\right), |c^*|_\alpha \leq \overline{d}, \tag{2.184}$$

where the numbers $d, \overline{d} > 1$ are given. In addition, we consider functions $c(x)$ satisfying conditions (2.179) and (2.180):

$$c \in [1, d+1] \text{ in } \Omega, \ c(x) = 1 \text{ for } x \in \mathbb{R}^3 \setminus \Omega, \tag{2.185}$$

$$c(x) \in C^\alpha\left(\mathbb{R}^3\right), |c|_\alpha \leq \overline{d}. \tag{2.186}$$

For each such function c and for each $s > 0$, we consider the solution $w_c(x,s)$ of the following problem

$$\Delta w_c - \overline{s}^2 c(x) w_c = -\delta(x - x_0), \ x \in \mathbb{R}^3, \tag{2.187}$$

$$\lim_{|x| \to \infty} w_c(x, \overline{s}) = 0, \tag{2.188}$$

such that

$$w_c(x,s) = w_1(x,s) + \overline{w}_c(x,s), \text{ where } \overline{w}_c \in C^{2+\alpha}\left(\mathbb{R}^3\right), \tag{2.189}$$

$$w_1(x,s) = \frac{\exp(-s|x - x_0|)}{4\pi|x - x_0|}. \tag{2.190}$$

The existence and uniqueness of the solution w_c of the problem (2.187)–(2.190) is guaranteed by Theorem 2.7.2. Let the function $w_{d+1}(x,s)$ be the solution of the problem (2.187) and (2.188) for the case $c(x) \equiv d+1$:

$$w_{d+1}(x,s) = \frac{\exp\left(-s\sqrt{d+1}|x - x_0|\right)}{4\pi|x - x_0|}. \tag{2.191}$$

By Theorem 2.7.2,

$$w_{d+1}(x,s) < w_c(x,s) \leq w_1(x,s), \forall s > 0, \tag{2.192}$$

for all functions $c(x)$ satisfying conditions (2.179) and (2.180). Also, we define tail functions as

$$V^*(x) := V^*(x,\overline{s}) = \frac{\ln w^*(x,\overline{s})}{\overline{s}^2}, \tag{2.193}$$

$$V_c(x) := V_c(x,\overline{s}) = \frac{\ln w_c(x,\overline{s})}{\overline{s}^2}, \tag{2.194}$$

where $w^*(x,\overline{s})$ is the solution of the problem (2.187)–(2.190) with the function $c(x) := c^*(x)$ satisfying conditions (2.183) and (2.184).

2.9.1 Estimates of the Tail Function

In Theorem 2.9.1.1 of this section, we estimate tails in non-Hölder norms. We will need these estimates in Chap. 6. And in Theorem 2.9.1.2, we estimate tails in Hölder norms. We will use Theorem 2.9.1.2 in Sect. 2.9.4.

Theorem 2.9.1.1. *Let $\Omega \subset \mathbb{R}^3$ be a bounded domain. Let the source $x_0 \notin \overline{\Omega}$. Let the function $c^*(x)$ satisfying (2.183) and (2.184) be the exact solution of Inverse Problem 2.1 and the parameter $\overline{s} > 1$ and $V^*(x)$ be the exact tail function as in (2.193). For each function $c(x)$ satisfying condition (2.185) and (2.186), let $w(x,\overline{s}) := w_c(x,\overline{s})$ be the solution of the problems (2.187)–(2.190) (Theorem 2.7.2) and $V_c(x)$ be the corresponding tail function as defined in (2.194). Then there exists a constant $B = B(\Omega,\overline{s},d,x_0) > 2$ depending only on listed parameters such that for all functions $c(x)$ satisfying (2.185) and (2.186) the following inequalities hold:*

$$\|\nabla V_c\|_{C(\overline{\Omega})}, \|\nabla V^*\|_{C(\overline{\Omega})} \leq B, \tag{2.195}$$

$$\|\nabla V_c - \nabla V^*\|_{L_2(\Omega)} + \|\Delta V_c - \Delta V^*\|_{L_2(\Omega)} \leq B\|c - c^*\|_{L_2(\Omega)}. \tag{2.196}$$

Proof. In this proof, $B = B(\Omega,\overline{s},d,x_0) > 1$ denotes different constants depending on listed parameters. Temporary denote in this proof only $\mathbf{x} = (x,y,z)$. For brevity, we estimate only $\|V_x\|_{C(\overline{\Omega})}$. Estimates of two other first derivatives are similar. By (2.192)–(2.194)

$$|\partial_x V_c| = \left|\frac{w_x}{w}(\mathbf{x},\overline{s})\right| \leq B|w_x(\mathbf{x},\overline{s})|, \quad |\partial_x V^*| = \left|\frac{w_x^*}{w^*}(\mathbf{x},\overline{s})\right| \leq B|w_x^*(\mathbf{x},\overline{s})|. \tag{2.197}$$

Theorem 2.7.2, (2.190), and (2.101) imply that for $\boldsymbol{\xi} = (\xi_1,\xi_2,\xi_3)$, $\mathbf{x} \in \Omega$, $b(\mathbf{x}) = c(\mathbf{x}) - 1$,

$$w_x(\mathbf{x},\overline{s}) = w_{1x}(\mathbf{x},\overline{s}) + \frac{s^2}{4\pi}\int\limits_{\Omega}\left[\left(s\frac{x-\xi_1}{|\mathbf{x}-\boldsymbol{\xi}|^2}+\frac{x-\xi_1}{|\mathbf{x}-\boldsymbol{\xi}|^3}\right)\right.$$
$$\left.\times\exp\left(-\overline{s}\,|\mathbf{x}-\boldsymbol{\xi}|\right)b(\boldsymbol{\xi})\,w(\boldsymbol{\xi},\overline{s})\right]\mathrm{d}\xi. \tag{2.198}$$

Since $x_0 \notin \overline{\Omega}$, then functions w_0, w_{0x} do not have a singularity for $\mathbf{x} \in \overline{\Omega}$. Hence, (2.192) and (2.198) imply that

$$|w_x(\mathbf{x},\overline{s})| \leq B + B\int\limits_{\Omega}\left(\frac{1}{|\mathbf{x}-\boldsymbol{\xi}|}+\frac{1}{|\mathbf{x}-\boldsymbol{\xi}|^2}\right)\exp\left(-\overline{s}\,|\mathbf{x}-\boldsymbol{\xi}|\right)\mathrm{d}\boldsymbol{\xi} \leq B,\ \mathbf{x}\in\Omega. \tag{2.199}$$

Hence, (2.196) follows from (2.197) and (2.199). Denote $\widetilde{w} := w - w^*$. Then (2.193) and (2.194) imply that

$$\partial_x V_c - \partial_x V^* = \left(\frac{\widetilde{w}_x}{w} - \frac{w_x^*}{ww^*}\widetilde{w}\right)(\mathbf{x},\overline{s}),\ \mathbf{x}\in\Omega.$$

Hence, by (2.192) and (2.199),

$$\|\nabla V_c - \nabla V^*\|_{L_2(\Omega)} \leq B\left(\|\nabla\widetilde{w}\|_{L_2(\Omega)} + \|\widetilde{w}\|_{L_2(\Omega)}\right)$$
$$\leq B\left(\|\nabla\widetilde{w}\|_{L_2(\mathbb{R}^3)} + \|\widetilde{w}\|_{L_2(\mathbb{R}^3)}\right). \tag{2.200}$$

Let $\widetilde{c}(\mathbf{x}) = c(\mathbf{x}) - c^*(\mathbf{x})$. Since

$$c(\mathbf{x})\,w(\mathbf{x},\overline{s}) - c^*(\mathbf{x})\,w^*(\mathbf{x},\overline{s}) = c(\mathbf{x})\,\widetilde{w}(\mathbf{x},\overline{s}) + \widetilde{c}(\mathbf{x})\,w^*(\mathbf{x},\overline{s}),$$

we obtain from (2.187)

$$\Delta\widetilde{w}(\mathbf{x},\overline{s}) - \overline{s}^2 c(\mathbf{x})\,\widetilde{w}(\mathbf{x},\overline{s}) = \overline{s}^2\widetilde{c}(\mathbf{x})\,w^*(\mathbf{x},\overline{s}),\ \mathbf{x}\in\mathbb{R}^3. \tag{2.201}$$

Since $\widetilde{c}(\mathbf{x}) = 0$ outside of Ω and $\mathbf{x}_0 \notin \overline{\Omega}$, then $\overline{s}^2\widetilde{c}(\mathbf{x})\,w^*(\mathbf{x},\overline{s}) = 0$ near x_0. In particular, $\overline{s}^2\widetilde{c}(\mathbf{x})\,w^*(\mathbf{x},\overline{s}) = 0$ for $\mathbf{x}\in\mathbb{R}^3\setminus\Omega$. Let the number $R > 0$ be so large that $\Omega \subset B_R = \{|\mathbf{x}| < R\}$. Multiply both sides of (2.201) by $(-\widetilde{w})$ and integrate over B_R. We obtain

$$\int\limits_{B_R}\left(|\nabla\widetilde{w}(\mathbf{x},\overline{s})|^2 + \overline{s}^2 c(\mathbf{x})\,\widetilde{w}^2(\mathbf{x},\overline{s})\right)\mathrm{d}\mathbf{x} - \int\limits_{\partial B_R}\left(\widetilde{w}\frac{\partial\widetilde{w}}{\partial n}\right)(\mathbf{x},\overline{s})\,\mathrm{d}S$$
$$= -\overline{s}^2\int\limits_{\Omega}\widetilde{c}(\mathbf{x})\left[w^*\widetilde{w}\right](\mathbf{x},\overline{s})\,\mathrm{d}\mathbf{x}. \tag{2.202}$$

It follows from (2.101) and (2.198) that $\nabla\widetilde{w}(\mathbf{x},\overline{s}),\widetilde{w}(\mathbf{x},\overline{s}) \in L_2\left(\mathbb{R}^3\right)$ and the second term in the left-hand side of (2.202) tends to zero as $R \to \infty$. Hence, setting in (2.202) $R \to \infty$, we obtain

$$\int\limits_{\mathbb{R}^3}\left(|\nabla\widetilde{w}(\mathbf{x},\overline{s})|^2+\overline{s}^2c(\mathbf{x})\widetilde{w}^2(\mathbf{x},\overline{s})\right)d\mathbf{x}=-\overline{s}^2\int\limits_{\Omega}\widetilde{c}(\mathbf{x})\left(w^*\widetilde{w}\right)(\mathbf{x},\overline{s})\,d\mathbf{x}.$$

Since $c \geq 1$, then $\overline{s}^2c(\mathbf{x})\widetilde{w}^2(\mathbf{x},\overline{s}) \geq \overline{s}^2\widetilde{w}^2(\mathbf{x},\overline{s})$. Hence, using (2.192) and the Cauchy-Schwarz inequality, we obtain

$$\|\widetilde{w}(\mathbf{x},\overline{s})\|_{H^1\left(\mathbb{R}^3\right)} \leq B\|\widetilde{c}\|_{L_2(\Omega)}. \tag{2.203}$$

Next,

$$\Delta V_c-\Delta V^*=\left[\frac{\Delta\widetilde{w}}{w}-\frac{\nabla(w+w^*)}{w^2}\nabla\widetilde{w}-\left(\frac{\Delta w^*}{ww^*}-\frac{(\nabla w^*)^2(w+w^*)}{(ww^*)^2}\right)\widetilde{w}\right](\mathbf{x},\overline{s}). \tag{2.204}$$

Since $\Delta w^*(\mathbf{x},\overline{s})=\overline{s}^2c^*(\mathbf{x})w^*(\mathbf{x},\overline{s})$ for $\mathbf{x}\in\overline{\Omega}$, then (2.192), (2.199), and (2.204) imply that

$$|\Delta V_c-\Delta V^*| \leq B\left(|\Delta\widetilde{w}|+|\nabla\widetilde{w}|+|\widetilde{w}|\right), \mathbf{x}\in\overline{\Omega}. \tag{2.205}$$

By (2.201),

$$\|\Delta\widetilde{w}\|_{L_2\left(\mathbb{R}^3\right)} \leq B\left(\|\widetilde{w}\|_{L_2\left(\mathbb{R}^3\right)}+\|\widetilde{c}\|_{L_2(\Omega)}\right).$$

Hence, (2.200), (2.203), and (2.205) imply (2.196). □

We now want to prove an analog of Theorem 2.9.1.1 for the Hölder norms. Let $c^*(x)$ be the exact solution of Inverse Problem 2.1. In applications, the domain of interest Ω can often be increased if necessary. In terms of Inverse Problem 2.1, this means that one can have measured data $g(x,t)$ in (2.5) at the boundary of a domain which is a little bit larger than the original domain of interest. Hence, let $\Omega' \subset \Omega$ be a subdomain of the domain Ω and $\partial\Omega' \cap \partial\Omega = \varnothing$. We replace condition (2.183) by a little bit different one:

$$c^*(x) \in [1,d], \quad c^*(x)=1 \text{ for } x \in \mathbb{R}^3 \setminus \Omega'. \tag{2.206}$$

Recall that in Sect. 2.6 we have introduced the following cut-off function $\chi(x)$:

$$\chi \in C^3\left(\mathbb{R}^3\right), \ \chi(x)=\begin{cases}1 \text{ in } \Omega',\\ \text{between 0 and 1 in } \Omega\setminus\Omega',\\ 0 \text{ outside of } \Omega.\end{cases} \tag{2.207}$$

Consider the set of functions $P\left(d,\overline{d}\right)$ defined as

$$P\left(d,\overline{d}\right)=\left\{c\in C^{\alpha}\left(\overline{\Omega}\right):|c|_{\alpha}\leq\overline{d}+1,c\in[1,d+1]\right\}. \tag{2.208}$$

Hence, (2.184) and (2.206) imply that

$$c^{*}\in P\left(d,\overline{d}\right). \tag{2.209}$$

For each function $c\in P\left(d,\overline{d}\right)$, consider the function $\widehat{c}\,(x)$:

$$\widehat{c}\,(x)=(1-\chi(x))+\chi(x)\,c(x), \tag{2.210}$$

where the function $\chi(x)$ is defined in (2.207). Then (Sect. 6.1),

$$\widehat{c}\in C^{\alpha}\left(\mathbb{R}^{3}\right),\ \widehat{c}\in[1,d+1]\ \text{in}\ \Omega,\ \widehat{c}\,(x)=1\ \text{for}\ x\in\mathbb{R}^{3}\backslash\Omega. \tag{2.211}$$

Next, consider the solution $w_{\widehat{c}}(x,\overline{s})$ of the problem (2.187)–(2.190) with $c(x):=\widehat{c}\,(x)$. The existence and uniqueness of this solution is guaranteed by Theorem 2.7.2 Hence, by (2.192),

$$w_{d+1}(x,\overline{s})<w_{\widehat{c}}(x,\overline{s})\leq w_{1}(x,\overline{s}),\ \forall x\neq x_{0},\ \forall c\in P\left(d,\overline{d}\right). \tag{2.212}$$

Lemma 2.9.1.1. *Let functions $c,c^{*}\in P\left(d,\overline{d}\right)$ (see (2.209) for c^{*}). Consider the function $\widehat{c}\,(x)$ defined in (2.210). Then*

$$|\widehat{c}-c^{*}|_{\alpha}\leq|\chi|_{\alpha}\,|c-c^{*}|_{\alpha}.$$

Proof. By (2.210),

$$\widehat{c}\,(x)-c^{*}(x)=\chi(x)\left(c(x)-c^{*}(x)\right)+(1-\chi(x))\left(1-c^{*}(x)\right).$$

Since $1-c^{*}(x)=0$ for $x\in\Omega\backslash\Omega'$ and $1-\chi(x)=0$ in Ω', then $(1-\chi(x))(1-c^{*}(x))\equiv 0$. Hence, $\widehat{c}\,(x)-c^{*}(x)=\chi(x)(c(x)-c^{*}(x))$, which implies the assertion of this lemma. □

Note that there exists a constant $C=C(\Omega,\alpha)>0$ depending only on the domain Ω and the parameter $\alpha\in(0,1)$ such that

$$|f|_{\alpha}\leq C\,\|f\|_{C^{1}\left(\overline{\Omega}\right)},\ \forall f\in C^{1}\left(\overline{\Omega}\right). \tag{2.213}$$

Lemma 2.9.1.2. *Let the source $x_{0}\notin\overline{\Omega}$. Let the function $c\in P\left(d,\overline{d}\right)$. Consider the function $\widehat{c}(x)$ defined in (2.210). Let $w_{\widehat{c}}(x,\overline{s})$ be the solution of the*

problem (2.187)–(2.190) with $c(x) := \widehat{c}(x)$. *Then* $w_{\widehat{c}}(x,\overline{s}) \in C^{2+\alpha}\left(\overline{\Omega}\right)$. *Also, there exists a constant* $Y = Y\left(\Omega,\overline{s},d,\overline{d},\chi,x_0\right) > 0$ *depending on listed parameters such that*

$$\left|w_{\widehat{c}}(x,\overline{s})\right|_{\alpha} \leq Y,\ \forall c \in P\left(d,\overline{d}\right).$$

Proof. Below in this proof, $Y = Y\left(\Omega,\overline{s},d,\overline{d},\chi,x_0\right) > 0$ denotes different constants depending on listed parameters. Denote $b(x) = \widehat{c}(x) - 1$. Recall that by (2.101),

$$w_{\widehat{c}}(x,\overline{s}) = w_1(x,\overline{s}) - \overline{s}^2 \int\limits_{\Omega} w_1(x-\xi,\overline{s})\, b(\xi)\, w_{\widehat{c}}(\xi,\overline{s})\, d\xi. \tag{2.214}$$

Since $x_0 \notin \overline{\Omega}$, then by (2.189), $w_{\widehat{c}}(x,\overline{s}) \in C^{2+\alpha}\left(\overline{\Omega}\right)$. Next, (2.211), (2.212), and (2.214) imply

$$\left|w_{\widehat{c}}(x,\overline{s})\right| \leq Y + Y\left\|b\right\|_{C\left(\overline{\Omega}\right)} \int\limits_{\Omega} w_1(x-\xi,\overline{s})\, d\xi \leq Y,\ x \in \Omega.$$

In addition, by (2.211) and (2.199), $\left|\nabla w_{\widehat{c}}(x,\overline{s})\right| \leq Y$, $x \in \Omega$. Hence, $\left\|w_{\widehat{c}}(x,\overline{s})\right\|_{C^1\left(\overline{\Omega}\right)} \leq Y$. The rest of the proof follows from (2.213). □

Consider a bounded domain $\Omega_1 \subset \mathbb{R}^3$ such that

$$\Omega \subset \Omega_1,\ \partial\Omega \cap \partial\Omega_1 = \varnothing,\ \partial\Omega_1 \in C^3,\ x_0 \notin \overline{\Omega}_1. \tag{2.215}$$

Lemma 2.9.1.3. *Let* $\Omega, \Omega_1 \subset \mathbb{R}^3$ *be two bounded domains satisfying conditions (2.215). Let the function* $c \in P\left(d,\overline{d}\right)$. *Consider the function* $\widehat{c}(x)$ *defined in (2.210). Let* $w_{\widehat{c}}(x,\overline{s})$ *be the solution of the problem (2.187)–(2.190) with* $c(x) := \widehat{c}(x)$. *Then the function* $w_{\widehat{c}}(x,\overline{s}) \in C^3(\partial\Omega_1)$. *Furthermore, there exists a constant* $B = B\left(\Omega,\Omega_1,\overline{s},d,\overline{d},\chi,x_0\right) > 2$ *depending only on listed parameters such that*

$$\left\|w_{\widehat{c}}(x,\overline{s})\right\|_{C^3(\partial\Omega_1)} \leq B,\ \forall c \in P\left(d,\overline{d}\right). \tag{2.216}$$

Let two functions $c_1, c_2 \in P\left(d,\overline{d}\right)$. *Denote* $\widetilde{w}(x) = w_{\widehat{c}_1}(x,\overline{s}) - w_{\widehat{c}_2}(x,\overline{s})$. *Then*

$$\left\|\widetilde{w}\right\|_{C^3(\partial\Omega_1)} \leq B\left|c_1 - c_2\right|_{\alpha},\ \forall c_1, c_2 \in P\left(d,\overline{d}\right).$$

Proof. In this proof, B denotes different positive constant depending on above parameters. The integrand of the formula (2.214) does not have a singularity for $x \in \Omega_1 \setminus \overline{\Omega}$. Hence, it follows from (2.214) that $w_{\widehat{c}}(x,\overline{s}) \in C^3(\partial\Omega_1)$. Next, (2.216) follows from (2.192) and (2.214).

Denote $\widetilde{c}(x) = c_1(x) - c_2(x)$. By (2.210) $\widehat{c}_1(x) - \widehat{c}_2(x) = \chi(x)\widetilde{c}(x)$. First, substitute in (2.214) $\left(b_1, w_{\widehat{c}_1}\right) = \left(\widehat{c}_1 - 1, w_{\widehat{c}_1}\right)$. Next, substitute $\left(b_2, w_{c_2}\right) = \left(\widehat{c}_2 - 1, w_{\widehat{c}_2}\right)$ and subtract the second equation from the first one. We obtain

$$\widetilde{w}(x) = -\overline{s}^2 \int\limits_{\Omega} w_1(x-\xi,\overline{s})\,\chi(\xi)\widetilde{c}(\xi)\,w_{\widehat{c}_1}(\xi,\overline{s})\,d\xi$$

$$-\overline{s}^2 \int\limits_{\Omega} w_1(x-\xi,\overline{s})\,b_2(\xi)\,\widetilde{w}(\xi)\,d\xi.$$

Let

$$I_1(x) = -\overline{s}^2 \int\limits_{\Omega} w_1(x-\xi,\overline{s})\,\chi(\xi)\widetilde{c}(\xi)\,w_{\widehat{c}_1}(\xi,\overline{s})\,d\xi,$$

$$I_2(x) = -\overline{s}^2 \int\limits_{\Omega} w_1(x-\xi,\overline{s})\,b_2(\xi)\,\widetilde{w}(\xi)\,d\xi.$$

Using the same arguments as ones in the proof of Lemma 2.9.1.2 as well the assertion of this lemma, we obtain

$$\|I_1\|_{C^3(\partial\Omega_1)} \leq B\,\|\widetilde{c}\|_{L_2(\Omega)} \leq B\,|\widetilde{c}|_\alpha.$$

Next, by (2.203),

$$\|\widetilde{w}\|_{L_2(\Omega)} \leq B\,\|\widetilde{c}\|_{L_2(\Omega)} \leq B\,|\widetilde{c}|_\alpha.$$

The latter estimate implies that $\|I_2\|_{C^3(\partial\Omega_1)} \leq B\,|\widetilde{c}|_\alpha$. □

We need Lemma 2.9.1.4 since we have referred to this lemma in the course of the proof of Theorem 2.7.2**.**

Lemma 2.9.1.4. *Let $\Omega, \Omega_1 \subset \mathbb{R}^3$ be two convex bounded domains satisfying conditions (2.215) and let $\partial\Omega \in C^3$. Let the function $f \in C^\alpha\left(\overline{\Omega}_1\right)$ and $f(x) = 0$ outside of the domain Ω. For a number $s > 0$ consider the function $u(x)$:*

$$u(x) = \int\limits_{\Omega_1} w_1(x-\xi,s)\,f(\xi)\,d\xi = \int\limits_{\Omega_1} \frac{\exp(-s|x-\xi|)}{4\pi|x-\xi|} f(\xi)\,d\xi. \tag{2.217}$$

Then,

$$u \in C^{2+\alpha}\left(\mathbb{R}^3\right), \quad \lim_{|x|\to\infty} u(x) = 0, \tag{2.218}$$

$$|u|_{2+\alpha} \leq C\,|f|_{\alpha}\,, \tag{2.219}$$

$$\Delta u - s^2 u = -f \quad in\ \mathbb{R}^3, \tag{2.220}$$

where the constant $C > 0$ is independent on the function f.

Proof. In this proof, $C > 0$ denotes different constants independent on the function f. Since the function $w_1(x-\xi, s)$ does not have a singularity for $x \in \partial\Omega_1, \xi \in \overline{\Omega}$, then by (2.217), $u \in C^3(\partial\Omega_1)$ and

$$\|u\|_{C^{2+\alpha}(\partial\Omega_1)} \leq C\,|f|_{\alpha}\,. \tag{2.221}$$

First, consider the case when the function $f \in C^1\left(\overline{\Omega}_1\right)$. We have

$$\Delta w_1(x-\xi) - s^2 w_1(x-\xi) = -\delta(x-\xi)\,.$$

Hence, using the same method as the one used in the standard PDE course for the Poisson equation,

$$\Delta v = -g(x)\,, g \in C^1\left(\mathbb{R}^3\right),\ g(x) = 0 \text{ for } x \in \mathbb{R}^3 \setminus \Omega,$$

$$\lim_{|x|\to\infty} v(x) = 0,$$

one can prove that the function $u \in C^2\left(\overline{\Omega}_1\right)$ and satisfies (2.220). Hence, by the Schauder theorem and (2.221), $u \in C^{2+\alpha}\left(\overline{\Omega}_1\right)$ and

$$\|u\|_{C^{2+\alpha}\left(\overline{\Omega}_1\right)} \leq C\,\|u\|_{C^{2+\alpha}(\partial\Omega_1)} \leq C\,|f|_{\alpha}\,, \forall f \in C^1\left(\overline{\Omega}_1\right),$$
$$f(x) = 0 \text{ for } x \in \mathbb{R}^3 \setminus \Omega. \tag{2.222}$$

Consider now a function f such that $f \in C^{\alpha}\left(\overline{\Omega}_1\right)$ and $f(x) = 0$ for $x \in \Omega_1 \setminus \Omega$. Consider a sequence of functions $\{f_n(x)\}_{n=1}^{\infty} \subset C^1\left(\overline{\Omega}_1\right)$ such that $f_n(x) = 0$ for $x \in \Omega_1 \setminus \Omega$ and:

$$\lim_{n\to\infty} |f_n - f|_{\alpha} = 0.$$

Let $\{u_n(x)\}_{n=1}^{\infty}$ be the corresponding sequence of functions defined via (2.217), where f is replaced with f_n. Then $u_n \in C^{2+\alpha}\left(\overline{\Omega}_1\right)$ and estimate (2.222) is valid for each n with the replacement of the vector (u, f) with the vector (u_n, f_n) is valid. Hence, $\{u_n(x)\}_{n=1}^{\infty}$ is the Cauchy sequence in the space $C^{2+\alpha}\left(\overline{\Omega}_1\right)$. Hence, this is a convergent sequence. On the other hand, (2.217) implies that

$$\lim_{n\to\infty} \|u_n - u\|_{C^1\left(\overline{\Omega}_1\right)} = 0.$$

Hence, it is the function u which is the limit of the sequence $\{u_n(x)\}_{n=1}^{\infty}$ in the space $C^{2+\alpha}\left(\overline{\Omega}_1\right)$. Hence, (2.218) and (2.220) are valid. Also, it follows from the above that in (2.222), "$\forall f \in C^1\left(\overline{\Omega}_1\right)$" can be replaced with "$\forall f \in C^{\alpha}\left(\overline{\Omega}_1\right)$". The latter implies (2.219). □

Theorem 2.9.1.2 provides estimates of tails in Hölder norms.

Theorem 2.9.1.2. *Let $\Omega, \Omega', \Omega_1 \subset \mathbb{R}^3$ be bounded domain with the boundaries $\partial\Omega, \partial\Omega_1 \in C^3$. Let condition (2.215) be satisfied and also let $\Omega' \subset \Omega, \partial\Omega' \cap \partial\Omega = \varnothing$. Let the function $c^*(x)$ satisfying conditions (2.206) and (2.209) be the exact solution of Inverse Problem 2.1, where constants $d, \overline{d} > 1$ are given. Let the parameter $\overline{s} > 1$ and $V^*(x)$ be the exact tail function as in (2.193). For each function ,$c \in P\left(d, \overline{d}\right)$ construct the function $\widehat{c}(x)$ by the formula (2.210), where the function $\chi(x)$ is defined in (2.207). Let $w_{\widehat{c}}(x, \overline{s})$ be the solution of the problems (2.187)–(2.190) with $c(x) := \widehat{c}(x)$ (Theorem 2.7.2). Let $V(x)$ be the corresponding tail function as defined in (2.194), where $c(x) := \widehat{c}(x)$. Then, there exists a constant $B = B\left(\Omega, \Omega_1, \overline{s}, d, \overline{d}, \chi, x_0\right) > 2$ depending only on listed parameters such that for all functions $c \in P(d, d^*)$ the following inequalities hold:*

$$|\nabla V^*|_{1+\alpha} \leq B, \tag{2.223}$$

$$|\nabla V_c|_{1+\alpha} \leq B, \tag{2.224}$$

$$|\nabla V_c - \nabla V^*|_{1+\alpha} \leq B\,|c - c^*|_{\alpha}. \tag{2.225}$$

Proof. In this proof, $B = B\left(\Omega, \Omega_1, \overline{s}, d, \overline{d}, \chi, x_0\right) > 2$ denotes different constants depending on listed parameters. It follows from (2.197), (2.204), and (2.212) that in order to prove (2.223), (2.224), and (2.225), it is sufficient to prove that

$$|w^*|_{2+\alpha}, \left|w_{\widehat{c}}\right|_{2+\alpha} \leq B, \tag{2.226}$$

$$\left|w_{\widehat{c}} - w^*\right|_{2+\alpha} \leq B\,|c - c^*|_{\alpha}. \tag{2.227}$$

For $x \in \partial\Omega_1$, denote $f_{\widehat{c}}(x) = w_{\widehat{c}}(x, \overline{s})\,|_{\partial\Omega_1}$. By (2.187) and (2.188), we have the following Dirichlet boundary value problem in the domain Ω_1:

$$\Delta w_{\widehat{c}} - \overline{s}^2 \widehat{c}(x)\, w_{\widehat{c}} = 0, x \in \Omega_1, \tag{2.228}$$

$$w_{\widehat{c}}(x, \overline{s})\,|_{\partial\Omega_1} = f_{\widehat{c}}(x). \tag{2.229}$$

By Lemma 2.9.1.3,

$$f_{\widehat{c}} \in C^3(\partial\Omega_1), \quad \left\| f_{\widehat{c}} \right\|_{C^3(\partial\Omega_1)} \leq B. \tag{2.230}$$

In addition, by (2.189),

$$w_{\widehat{c}}(x,\overline{s}) = w_1(x,\overline{s}) + \overline{w}_{\widehat{c}}(x,\overline{s}), \text{ where } \overline{w}_{\widehat{c}} \in C^{2+\alpha}\left(\mathbb{R}^3\right).$$

Since $x_0 \notin \overline{\Omega}_1$, then it follows from (2.190) that $w_1(x,\overline{s}) \in C^\infty\left(\overline{\Omega}_1\right)$. Hence, $w_{\widehat{c}}(x,\overline{s}) \in C^{2+\alpha}\left(\overline{\Omega}_1\right)$. Hence, Schauder theorem, (2.228)–(2.230) imply that

$$\left|w_{\widehat{c}}\right|_{2+\alpha} \leq \left\|w_{\widehat{c}}\right\|_{C^{2+\alpha}\left(\overline{\Omega}_1\right)} \leq B \left\| f_{\widehat{c}} \right\|_{C^{2+\alpha}(\partial\Omega_1)} \leq B \left\| f_{\widehat{c}} \right\|_{C^3(\partial\Omega_1)} \leq B,$$

which establishes (2.226) for the function $w_{\widehat{c}}(x,\overline{s})$. The proof for case of the function $w^*(x,\overline{s})$ is almost identical.

We now prove (2.227). Denote

$$\widetilde{w}(x) = w^*(x,\overline{s}) - w_{\widehat{c}}(x,\overline{s}), \ \widetilde{c}(x) = \widehat{c}(x) - c^*(x).$$

By Lemma 2.9.1.1,

$$|\widetilde{c}|_\alpha \leq |\chi|_\alpha |c - c^*|_\alpha. \tag{2.231}$$

Rewriting (2.228) for the function w^* and subtracting the resulting equation from (2.228), we obtain

$$\Delta\widetilde{w} - \overline{s}^2 c^*(x)\widetilde{w} = -\overline{s}^2\widetilde{c}(x) w_{\widehat{c}}(x,\overline{s}) \text{ in } \Omega_1, \tag{2.232}$$

$$\widetilde{w}|_{\partial\Omega_1} = f^*(x) - f_{\widehat{c}}(x), \tag{2.233}$$

where $f^*(x) = w^*|_{\partial\Omega_1}$. Using Lemma 2.9.1.3 and (2.231), we obtain

$$\left\| f^* - f_{\widehat{c}} \right\|_{C^3(\partial\Omega_1)} \leq B |c - c^*|_\alpha. \tag{2.234}$$

Next, since $\widetilde{c}(x) = 0$ outside of the domain Ω, then, using the second inequality (2.226) as well as (2.231), we obtain

$$\left\| \overline{s}^2\widetilde{c}(x) w_{\widehat{c}}(x,\overline{s}) \right\|_{C^\alpha\left(\overline{\Omega}_1\right)} = \left\| \overline{s}^2\widetilde{c}(x) w_{\widehat{c}}(x,\overline{s}) \right\|_{C^\alpha(\Omega)} \leq B |c - c^*|_\alpha. \tag{2.235}$$

Hence, applying the Schauder theorem to the Dirichlet boundary value problem (2.232), (2.233) and using (2.234) and (2.235), we obtain

$$|\widetilde{w}|_{2+\alpha} \leq \|\widetilde{w}\|_{C^{2+\alpha}\left(\overline{\Omega}_1\right)} \leq B |c - c^*|_\alpha. \qquad \square$$

2.9.2 The Second Approximate Mathematical Model

Assuming that the asymptotic behavior (2.13) holds, assumption below basically means that we take into account only the first term of the asymptotic behavior of each of functions $V^*(x,\overline{s}), q^*(x,\overline{s})$ at $\overline{s}\to\infty$ and ignore the rest:

$$V^*(x,\overline{s}) = \frac{p^*(x)}{\overline{s}} + O\left(\frac{1}{\overline{s}^2}\right) \approx \frac{p^*(x)}{\overline{s}},\ \overline{s}\to\infty,$$

$$q^*(x,\overline{s}) = -\frac{p^*(x)}{\overline{s}^2} + O\left(\frac{1}{\overline{s}^3}\right) \approx -\frac{p^*(x)}{\overline{s}^2},\ \overline{s}\to\infty.$$

Such assumptions are quite common in science. As an example, we refer to the geometrical optics assumption. Still, our technique is not just geometrical optics since we take into account not only the information at $s := \overline{s}$ but also the lower values of $s \in [\underline{s},\overline{s}]$. In addition, we update tails in the "corrector" procedure, via solving the problems (2.187)–(2.190), which is not the geometrical optics. Just as above, we assume that $\Omega \subset \mathbb{R}^3$ is a convex bounded domain with the boundary $\partial\Omega \in C^3$ and the source $x_0 \notin \overline{\Omega}$.

Recall that (2.105) for the exact function $q^*(x,s)$ is

$$\begin{aligned}\Delta q^* \ &-2s^2\nabla q^*\int_s^{\overline{s}}\nabla q^*(x,\tau)\,d\tau + 2s\left[\int_s^{\overline{s}}\nabla q^*(x,\tau)\,d\tau\right]^2\\ &+2s^2\nabla q^*\nabla V^* - 4s\nabla V^*\int_s^{\overline{s}}\nabla q^*(x,\tau)\,d\tau + 2s\left(\nabla V^*\right)^2 = 0,\\ x\ &\in\Omega, s\in[\underline{s},\overline{s}]. \end{aligned} \tag{2.236}$$

In addition, by (2.106) and (2.108),

$$q^*(x,s) = \psi^*(x,s),\ \forall (x,s)\in\partial\Omega\times[\underline{s},\overline{s}], \tag{2.237}$$

$$q^*(x,s)\in C^{3+\alpha}\left(\overline{\Omega}\right)\times C^1[\underline{s},\overline{s}]. \tag{2.238}$$

The second approximate mathematical model for the algorithm of Sect. 2.6.1 consists of the following:

Assumption. There exists a function $p^*(x)\in C^{2+\alpha}\left(\overline{\Omega}\right)$ such that the exact tail function $V^*(x)$ has the form:

$$V^*(x,s) := \frac{p^*(x)}{s},\ \forall s\ge\overline{s}. \tag{2.239}$$

And also (see (2.193)),

$$\frac{p^*(x)}{\overline{s}} = \frac{\ln w^*(x,\overline{s})}{\overline{s}^2}. \tag{2.240}$$

Since $q^*(x,s) = \partial_s V^*(x,s)$ for $s \geq \overline{s}$, we derive from (2.239) that

$$q^*(x,\overline{s}) = -\frac{p^*(x)}{\overline{s}^2}. \tag{2.241}$$

Set in (2.236), $s = \overline{s}$. Then, using (2.237), (2.239), and (2.241), we obtain the following *approximate* Dirichlet boundary value problem for the function $p^*(x)$:

$$\Delta p^* = 0 \text{ in } \Omega,\ p^* \in C^{2+\alpha}\left(\overline{\Omega}\right), \tag{2.242}$$

$$p^*|_{\partial\Omega} = -\overline{s}^2 \psi^*(x,\overline{s}). \tag{2.243}$$

The approximate (2.242) is valid only within the framework of the above assumption. Although (2.242) is linear, formulas (2.107) and (2.117) of the reconstruction of the target coefficient c^* are nonlinear.

Recall that by (2.21),

$$q(x,s) = \psi(x,s),\ \forall (x,s) \in \partial\Omega \times [\underline{s},\overline{s}].$$

Assume that

$$\psi(x,\overline{s}) \in C^{2+\alpha}\left(\overline{\Omega}\right). \tag{2.244}$$

Consider the solution $p(x)$ of the following boundary value problem:

$$\Delta p = 0 \text{ in } \Omega,\ p \in C^{2+\alpha}\left(\overline{\Omega}\right), \tag{2.245}$$

$$p|_{\partial\Omega} = -\overline{s}^2 \psi(x,\overline{s}). \tag{2.246}$$

By the Schauder theorem, there exists unique solution p of the problem (2.245) and (2.246). Furthermore, it follows from (2.242)–(2.246) that

$$|p - p^*|_{2+\alpha} \leq K\overline{s}^2 \|\psi(x,\overline{s}) - \psi^*(x,\overline{s})\|_{C^{2+\alpha}(\partial\Omega)}, \tag{2.247}$$

where $K = K(\Omega) > 1$ is the constant defined in formula (2.125) of Sect. 2.8.2**.** As the first guess for the tail function in the formula (2.43) of Sect. 2.6, we take

$$V_{1,1}(x) := \frac{p(x)}{\overline{s}}. \tag{2.248}$$

Remarks 2.9.2. 1. Let $p(x)$ be the solution of the problem (2.245), (2.246). Substituting (2.248) in (2.41), (2.42) at $n = i = 1$ and setting temporary $q_{1,1} := 0$, one obtains a good approximation for the exact coefficient $c^*(x)$.

Furthermore, Theorem 2.9.4 guarantees that all functions $c_{n,k}$ are good approximations for c^*, as long as the total number of iterations is not too large. Since we find the function $p(x)$ only using the boundary data, then this means that our approximate mathematical model is indeed a good one. Hence, we can stop iterations on any function $c_{n,k}$ for those indices (n,k), which are "allowed" by Theorem 2.9.4. Next, one can use the adaptivity procedure to refine the solution. However, if not using the adaptivity for refinement, then, quite naturally, one needs to find an optimal iteration number to stop. These considerations correspond well with Definitions 1.1.2.1, 1.1.2.2, and they are confirmed numerically in Chaps. 3–6.

2. Because of the approximate nature of our mathematical model, equation (2.242) does not match the asymptotic behavior (2.13). Indeed, actually one should have $|\nabla p^*(x)|^2 = c(x)$. The same can be stated about the Third Approximate Mathematical Model of Chap. 6. Nevertheless, it has been consistently demonstrated that our numerical method works well for both computationally simulated and experimental data, see Chaps. 3–6. Based on our numerical experience, we believe that this is because of two factors: (1) The truncation of the asymptotic series with respect to $1/\overline{s}$ at $\overline{s} \to \infty$ is reasonable, and (2) The procedure of updating tails via solutions of forward problems.

We now establish uniqueness within the framework of our approximate mathematical model.

Lemma 2.9.2. *Let assumption of this section holds. Then for $(x,s) \in \Omega \times [\underline{s}, \overline{s}]$, there exists at most one function $q^*(x,s)$ satisfying conditions (2.236)–(2.238). In addition, let (2.107) be true, i.e.,*

$$c^*(x) = \left[\Delta v^* + s^2 |\nabla v^*|^2\right](x,s), (x,s) \in \Omega \times [\underline{s}, \overline{s}], \tag{2.249}$$

where

$$v^*(x,s) = -\int_s^{\overline{s}} q^*(x,\tau)\, d\tau + V^*(x,\overline{s}), \tag{2.250}$$

with the tail function $V^*(x,s)$ satisfying conditions (2.239) and (2.240). Then there exists at most one function $c^*(x)$.

Proof. It follows from (2.242) and (2.243) that there exists unique function $p^*(x)$ satisfying these conditions. Hence, (2.239) implies uniqueness of the function $V^*(x,\overline{s})$. Below in this proof, $V^* := V^*(x,\overline{s})$. Assume that there exist two functions q_1^* and q_2^*. Let $\widetilde{q} = q_1^* - q_2^*$. Use the formulas

$$a_1 b_1 - a_2 b_2 = \widetilde{a} b_1 + a_2 \widetilde{b}, \ \forall a_1, b_1, a_2, b_2 \in \mathbb{R},$$

$$\widetilde{a} = a_1 - a_2, \ \widetilde{b} = b_1 - b_2.$$

Hence, (2.236) and (2.237) lead to

$$\Delta\widetilde{q} - 2s^2\left(\int\limits_s^{\overline{s}} \nabla q_1^*(x,\tau)\,d\tau\right)\nabla\widetilde{q} + 2s^2\nabla V^*\nabla\widetilde{q}$$

$$= -2s\left[\int\limits_s^{\overline{s}} \nabla\left(q_1^* + q_2^*\right)(x,\tau)\,d\tau\right]\int\limits_s^{\overline{s}} \nabla\widetilde{q}(x,\tau)\,d\tau + 4s\nabla V^*\int\limits_s^{\overline{s}} \nabla\widetilde{q}(x,\tau)\,d\tau,$$

$$(x,s) \in \Omega \times [\underline{s},\overline{s}], \quad \widetilde{q}(x,s)\mid_{\partial\Omega} = 0. \tag{2.251}$$

Let

$$M_1 = 2\overline{s}^2 \max_{(x,s)\in\overline{\Omega}\times[\underline{s},\overline{s}]}\left\{\int\limits_s^{\overline{s}} \left[|\nabla q_1^*| + |\nabla q_2^*|\right](x,\tau)\,d\tau\right\},$$

$$M_2 = \max\left(2\overline{s}^2, 4\overline{s}\right)\|V^*\|_{C^1(\overline{\Omega})},$$

$$M_3 = \max\left(M_1, M_2\right),$$

$$M = \max_{s\in[\underline{s},\overline{s}]} \|\widetilde{q}(x,s)\|_{C^2(\overline{\Omega})}.$$

For each fixed value of the parameter $s \in [\underline{s},\overline{s}]$, we consider (2.251) as the Dirichlet boundary value problem for the linear elliptic equation with the same right-hand side as one in (2.251). Then, Schauder theorem and implies that there exists a constant $K_1 = K_1(\Omega, M_3) > 0$ such that

$$\max_{s\in[\underline{s},\overline{s}]} \|\widetilde{q}(x,s)\|_{C^2(\overline{\Omega})} = M \le K_1(\overline{s} - s), \ \forall s \in [\underline{s},\overline{s}].$$

Substituting this in (2.251), we obtain

$$\max_{s\in[\underline{s},\overline{s}]} \|\widetilde{q}(x,s)\|_{C^2(\overline{\Omega})} = M \le K_1^2\int\limits_s^{\overline{s}} (\overline{s} - \tau)\,d\tau = K_1^2\frac{(\overline{s} - s)^2}{2}.$$

Substituting this again in (2.251), we obtain

$$\max_{s\in[\underline{s},\overline{s}]} \|\widetilde{q}(x,s)\|_{C^2(\overline{\Omega})} = M \le \frac{1}{2}K_1^2\int\limits_s^{\overline{s}} (\overline{s} - \tau)^2\,d\tau = K_1^3\frac{(\overline{s} - s)^2}{3!}.$$

Continuing this process, we obtain

$$\max_{s\in[\underline{s},\bar{s}]} \|\widetilde{q}(x,s)\|_{C^2(\overline{\Omega})} = M \leq K_1^n \frac{(\bar{s}-s)^n}{n!}.$$

Setting here, $n \to \infty$ leads to $M = 0$. Hence, (2.249) and (2.250) imply that the function $c^*(x)$ is also unique. □

2.9.3 Preliminaries

The goal of this and next sections is to prove the theorem about the approximate global convergence property within the framework of the second approximate mathematical model of Sect. 2.9.2. We assume that in (2.39) and (2.256),

$$2\frac{I_{1,n}}{I_0}(\nabla q_n)^2 := 0. \tag{2.252}$$

Therefore, we set

$$2\frac{I_{1,n}}{I_0}(\nabla q_{n,k})^2 := 0. \tag{2.253}$$

The Assumption (2.252) can be justified by (2.40) via choosing the parameter $\lambda >> 1$, which we do in our computations. We point out that an analog of Theorem 2.9.4 can be proven similarly even without (2.252). We are not doing so here only because we want to simplify the presentation. Assumptions (2.252) and (2.253) do not mean a linearization of the original problem, since the nonlinearity surfaces in terms $\nabla q_j \nabla q_{n,i}$ in (2.49). Also, tails $V_{n,i}$ in (2.49) depend nonlinearly on functions q_j, $j \in [0, n-1]$.

Assume that in (2.34), functions $\overline{\psi}_n \in C^{2+\alpha}(\partial\Omega)$. Then by (2.119),

$$\left\|\overline{\psi}_n(x) - \overline{\psi}_n^*(x)\right\|_{C^{2+\alpha}(\partial\Omega)} \leq C^*(h+\sigma). \tag{2.254}$$

Recall that by (2.114)–(2.118) we have for $x \in \Omega$

$$\Delta q_n^* - A_{1,n}\left(h\sum_{j=0}^{n-1}\nabla q_j^*\right)\nabla q_n^* + A_{1,n}\nabla q_n^*\nabla V^* = 2\frac{I_{1,n}}{I_0}\left(\nabla q_n^*\right)^2$$
$$- A_{2,n}h^2\left(\sum_{i=1}^{n-1}\nabla q_i^*\right)^2 + 2A_{2,n}\nabla V^*\left(h\sum_{j=0}^{n-1}\nabla q_j^*\right) - A_{2,n}|\nabla V^*|^2 + F_n(x,h,\lambda), \tag{2.255}$$

$$F_n(x,h,\lambda) \in C^\alpha\left(\overline{\Omega}\right),\ \max_{\lambda h \geq 1} |F_n(x,h,\lambda)|_\alpha \leq C^* h, \tag{2.256}$$

$$v_n^*(x) = -hq_n^*(x) - h\sum_{j=0}^{n-1} q_j^*(x) + V^*(x),\ x \in \Omega,\ n \in [1,N], \tag{2.257}$$

$$c^*(x) = \left[\Delta v_n^* + s_n^2 |\nabla v_n^*|^2\right](x) + \overline{F}_n(x),\ n \in [1,N], \tag{2.258}$$

$$\left|\overline{F}_n\right|_\alpha \leq C^* h. \tag{2.259}$$

By (2.254), Eq. (2.49) and the boundary condition (2.50) become:

$$\Delta q_{n,k} - A_{1n}\left(h\sum_{j=0}^{n-1}\nabla q_j\right)\nabla q_{n,k} - \varkappa q_{n,k} + A_{1n}\nabla V_{n,k}\nabla q_{n,k}$$

$$= -A_{2n}h^2\left(\sum_{j=0}^{n-1}\nabla q_j\right)^2 + 2A_{2n}\nabla V_{n,k}\left(h\sum_{j=0}^{n-1}\nabla q_j\right) - A_{2n}(\nabla V_{n,k})^2,\ x \in \Omega, \tag{2.260}$$

$$q_{n,k}(x) = \overline{\psi}_n(x), x \in \partial\Omega, \tag{2.261}$$

where $\varkappa \in (0,1)$ is a small parameter of ones choice. Recall that by (2.41) and (2.42), $q_0(x) \equiv q_0^*(x) \equiv 0$,

$$v_{n,k}(x) = -hq_{n,k}(x) - h\sum_{j=0}^{n-1} q_j(x) + V_{n,k}(x),\ x \in \Omega,\ n \in [1,N], \tag{2.262}$$

$$c_{n,k}(x) = \left[\Delta v_{n,k} + s_n^2(\nabla v_{n,k})^2\right](x),\ x \in \Omega,\ n \in [1,N]. \tag{2.263}$$

We now reformulate the estimate of the Schauder theorem of Sect. 2.8.2 since we impose now upper estimates on the coefficients of the elliptic equation, which are different from ones imposed in Sect. 2.8.2. Just as in Sect. 2.8.2, consider the Dirichlet boundary value problem

$$\Delta u + \sum_{j=1}^{3} b_j(x)u_{x_j} - b_0(x)u = f(x), x \in \Omega, u|_{\partial\Omega} = g(x) \in C^{2+\alpha}(\partial\Omega). \tag{2.264}$$

Assume that the following conditions are satisfied,

$$b_j, b_0, f \in C^\alpha\left(\overline{\Omega}\right),\ b_0(x) \geq 0,\ \max_{j\in[0,n]}\left(\left|b_j\right|_\alpha\right) \leq Q, \tag{2.265}$$

where $Q > 0$ is a certain constant. Then by the Schauder theorem (see Chap. 3, Sect. 1 in [118]), there exists unique solution $u \in C^{2+\alpha}\left(\overline{\Omega}\right)$ of the boundary value problem (2.264). Furthermore, there exists a constant $\overline{K} = \overline{K}(\Omega, Q) > 2$, depending only on the domain Ω and the constant Q such that the following estimate holds:

$$|u|_{2+\alpha} \leq \overline{K}\left[\|g\|_{C^{2+\alpha}(\partial\Omega)} + |f|_{\alpha}\right]. \tag{2.266}$$

2.9.4 The Second Approximate Global Convergence Theorem

Let N be the total number of functions q_n computed in the algorithm of Sect. 2.6.1. In principle, $\widetilde{N} \in (1, N]$. However, to avoid new notations, we denote for brevity $\widetilde{N} := N$. Keeping this in mind, we assume in Theorem 2.9.4 that the total number N of functions q_n of the algorithm of 2.6.1 is independent on the grid step size h in the s-direction. In addition, the number m_n of functions $\{q_{n,k}\}_{k=1}^{m_n}$ is bounded from the above:

$$\max_{n\in[1,N]} m_n = m. \tag{2.267}$$

Condition (2.280) of Theorem 2.9.4 provides a linkage between the level of the error η in the data and the total "allowable" number of iterations Nm, i.e., the allowable number of functions $\{c_{n,k}\}_{(n,k)=(1,1)}^{(N,m)}$. This is going along well with the theory of ill-posed problems. Indeed, it is well known that the maximal number of iterations and the error in the data are often connected with each other. So that the maximal number of iterations is a regularization parameter in this case, see pp. 156 and 157 of [65] as well as Sect. 1.6. Hence, Theorem 2.9.4 provides another example of such a connection, in addition to those of [65] and Sect. 1.6.

Theorem 2.9.4. *Consider the algorithm of Sect. 2.6.1. As in Theorem 2.9.1.2, let $\Omega, \Omega_1 \subset \mathbb{R}^3$ be two convex bounded domain with the boundaries $\partial\Omega, \partial\Omega_1 \in C^3$ and let condition (2.215) hold. Let the maximal pseudo frequency $\overline{s} = \text{const.} > 1$:*

- *Let assumptions of Sect. 2.9.2 be valid, the number N of functions $\{q_n\}_{n=1}^{N}$ be independent on the grid step size h of the partition of the s interval, and (2.267) holds.*
- *In addition, assume that all functions $c_{n,k}(x)$ in (2.263) are such that*

$$c_{n,k}(x) \geq 1, x \in \Omega. \tag{2.268}$$

- *Let in (2.34) and (2.35) functions $\overline{\psi}_n \in C^{2+\alpha}(\partial\Omega)$.*
- *Let the function $c^*(x)$ satisfying conditions (2.206) and (2.209) be the exact solution of Inverse Problem 2.1, where constants $d, \overline{d} > 1$ are given, where $\Omega' \subset \Omega$ is a subdomain of the domain Ω, $\partial\Omega' \cap \partial\Omega = \varnothing$, and let $\chi(x)$ be the cut-off function defined in (2.207).*

- *Assume that conditions (2.120), (2.244), (2.252)–(2.254), (2.259), and (2.267) hold, where the constant $C^* \geq 1$ is defined in (2.112).*
- *Let the first tail function $V_{1,1}(x)$ be constructed via (2.245), (2.246), and (2.248).*
- *Let h be the grid step size in the layer-stripping procedure with respect to s, σ be level of the error in the data, and $\varkappa \in (0,1)$ be a small parameter in (2.260). Denote*

$$\eta = 2(h + \sigma + \varkappa). \tag{2.269}$$

- *Choose the parameter λ of the CWF (2.38) so large that*

$$\lambda \geq \frac{8(\overline{s}C^*)^2}{\eta}. \tag{2.270}$$

- *Let $B = B\left(\Omega, \Omega_1, \overline{s}, d, \overline{d}, \chi, x_0\right) > 2$ be the constant of Theorem 2.9.1.2*

Then there exists a constant $B_1 = B_1\left(\Omega, \Omega_1, \overline{s}, d, \overline{d}, C^*, \chi, x_0\right) \geq B > 2$ such that if $\overline{K} = \overline{K}\left(\overline{s}^2 B_1\right) > 2$ is the constant in (2.266) and the parameter η is so small that

$$\eta \in (0, \eta_0), \ \eta_0 = \frac{1}{\overline{K} N B_1^{3Nm}}, \tag{2.271}$$

then functions

$$c_{n,k} \in C^\alpha\left(\overline{\Omega}\right), \widehat{c}_{n,k} \in C^\alpha\left(\mathbb{R}^3\right), \ (n,k) \in [1,N] \times [1,m], \tag{2.272}$$

$$c_{n,k}(x), \widehat{c}_{n,k}(x) \in [1, d+1] \text{ in } \Omega, \ (n,k) \in [1,N] \times [1,m]. \tag{2.273}$$

In particular, all functions $c_{n,k} \in P\left(d, \overline{d}\right)$, where the set of functions $P\left(d, \overline{d}\right)$ is defined in (2.208). In addition, the following estimates hold for $(n,k) \in [1,N] \times [1,m]$:

$$|\nabla V_{n,k}|_{1+\alpha}, |\Delta V_{n,k}|_\alpha \leq B_1, \tag{2.274}$$

$$|\nabla V_{n,k} - \nabla V^*|_{1+\alpha} \leq B_1^{3[k-1+(n-1)m]+1} \cdot \eta, \tag{2.275}$$

$$|\Delta V_{n,k} - \Delta V^*|_\alpha \leq B_1^{3[k-1+(n-1)m]+1} \cdot \eta, \tag{2.276}$$

$$|q_{n,k} - q_n^*|_{2+\alpha} \leq \overline{K} B_1^{3[k+(n-1)m]} \cdot \eta, \tag{2.277}$$

$$|q_{n,k}|_{2+\alpha} \leq 2C^*, \ n \in [1,N], \tag{2.278}$$

$$|c_{n,k} - c^*|_\alpha \leq B_1^{3[k+(n-1)m]} \cdot \eta. \tag{2.279}$$

Denote

$$\omega = \frac{\ln\left(\overline{K}N\right)}{3Nm\ln B_1 + \ln\left(\overline{K}N\right)} \in (0,1). \tag{2.280}$$

Then (2.279) becomes

$$|c_{n,k} - c^*|_\alpha \leq \eta^\omega := \varepsilon, \tag{2.281}$$

where the number $\varepsilon \in (0,1)$. *Hence, the algorithm of Sect. 2.6.1 possesses the approximate globally convergent property of the level* ε *in the framework of the second approximate mathematical model of Sect. 2.9.2.*

Remarks 2.9.4. 1. Since $\omega \in (0,1)$, then (2.281) is a Hölder-like estimate. We impose condition (2.268) to ensure that the right inequality (2.192) holds for all functions $c_{n,k}$. Indeed, we use the latter inequality quite extensively in Sect. 2.9.4. We have observed computationally that (2.268) holds; see Sect. 3.1.2.

2. The fact that the constant B_1 depends not only on the domain Ω but also on the domain Ω_1 as well does not affect the approximate global convergence property. It follows from (2.281) and (2.280) that as long as total iteration number Nm is not too large, conditions of the approximate global convergence of Definition 1.1.2.1 are satisfied. Hence, one can take any function $c_{n,k}(x)$ as $c_{\text{glob}}(x)$. The question of an optimal choice of the pair (n,k) should be decided in numerical experiments.

3. Theorem 2.9.4 implies that $P\left(d,\overline{d}\right)$ is our correctness set for the second approximate mathematical model, see Definitions 1.4.2 and 1.4.2 for the correctness set.

4. It is hard to establish a priori the upper limit for the number N in practical computations. This is the reason why we have consistently observed in our numerical tests that certain numbers indicating convergence grow steeply for $n \geq \overline{N}$ with a number $\overline{N} < N$, while they stabilize a few iterations before $\overline{N}$, i.e., at $n = \widetilde{N} < \overline{N}$. This phenomenon means that the process should be stopped at $n = \widetilde{N}$. The third Remark 1.1.2.1 is relevant here.

Proof of Theorem 2.9.4. The estimate (2.281) follows from (2.271) and (2.280). Thus, we focus below on the proof of estimates (2.272)–(2.279). Denote

$$\widetilde{V}_{n,k} = V_{n,k} - V^*,\ \widetilde{q}_{n,k} = q_{n,k} - q_n^*,$$
$$\widetilde{v}_{n,k} = v_{n,k} - v_{n,k}^*,\ \widetilde{c}_{n,k} = c_{n,k} - c^*,\ \widetilde{\psi}_n = \psi_n - \psi_n^*.$$

Estimates (2.274)–(2.276) for functions $V_{1,1}, \widetilde{V}_{1,1}$ follow from (2.111), (2.239)–(2.241) and (2.244)–(2.247).

Assume for a moment that the estimate (2.279) is valid. Then the function $c_{n,k} \in P(d,d^*)$. Indeed, by (2.209), (2.271), and (2.279),

$$|c_{n,k}|_\alpha = |c_{n,k} - c^* + c^*|_\alpha \leq |c_{n,k} - c^*|_\alpha + |c^*|_\alpha$$
$$\leq B_1^{3[k+(n-1)m]}\eta + \overline{d} < \overline{d} + 1.$$

Similarly, $c_{n,k} \leq d+1$. These two estimates combined with (2.208) and (2.268) imply that $c_{n,k} \in P\left(d,\overline{d}\right)$. Next, since the function $c_{n,k} \in P\left(d,\overline{d}\right)$, then Theorem 2.9.1.2 implies (2.274). Also, since the function $c_{n,k} \in [1,d+1]$, then the function $\widehat{c}_{n,k} \in [1,d+1]$ as well; see Sect. 2.6. Thus, if (2.279) is valid, then (2.273) is valid as well.

We now prove (2.275)–(2.279) for $(n,k) = (1,1)$. Set in (2.255) and (2.260) $(n,k) = (1,1)$. Subtracting (2.255) from (2.260), we obtain

$$\Delta\widetilde{q}_{1,1} + A_{1,1}\nabla V_{1,1}\nabla\widetilde{q}_{1,1} - \varkappa\widetilde{q}_{1,1} = -A_{1,1}\nabla\widetilde{V}_{1,1}\nabla q_1^*$$
$$-A_{2,1}\nabla\widetilde{V}_{1,1}\left(\nabla V_{1,1} + \nabla V^*\right) + \varkappa q_1^* - \widehat{F}_1, \tag{2.282}$$

$$\widetilde{q}_{1,1}(x) = \widetilde{\psi}_1(x), x \in \partial\Omega, \tag{2.283}$$

$$\widehat{F}_n = F_n - \frac{2I_{1,n}}{I_0}\left(\nabla q_n^*\right)^2, \ n \in [1,N]. \tag{2.284}$$

Recall that by (2.111) and (2.112),

$$\max_{n\in[1,N]} |q_n^*|_{2+\alpha} \leq C^*, \ C^* \geq 1. \tag{2.285}$$

Hence, (2.142), (2.256), (2.269), (2.270), (2.284), and (2.285) imply that

$$\left|\widehat{F}_n\right|_\alpha \leq C^*\eta. \tag{2.286}$$

Estimate now the right-hand side of (2.282). Using (2.121), (2.223), (2.224), (2.269), (2.286) as well as (2.274) and (2.275) at $(n,k) = (1,1)$, we obtain

$$\left|A_{1,1}\nabla\widetilde{V}_{1,1}\nabla q_1^* + A_{2,1}\nabla\widetilde{V}_{1,1}\left(\nabla V_{1,1} + \nabla V^*\right) + \varkappa q_1^* - \widehat{F}_1\right|_\alpha$$
$$\leq 8\overline{s}^2 BC^*\eta + 16\overline{s}^2 B^2\eta + 2C^*\eta = 8\overline{s}^2 B\left(2B + C^* + \frac{C^*}{4\overline{s}^2}\right)\eta.$$

We choose the constant $B_1 = B_1\left(\Omega,\Omega_1,\overline{s},d,\overline{d},C^*,\chi,x_0\right) \geq B > 2$ such that

$$C^* + 2B + \frac{C^*}{4\overline{s}^2} \leq 2B\left(1 + \frac{C^*}{B}\right) \leq 3B_1. \tag{2.287}$$

By (2.287),

$$C^* < \frac{B_1}{2}. \tag{2.288}$$

Hence, it follows from (2.287) that

$$\left| A_{1,1}\nabla\widetilde{V}_{1,1}\nabla q_1^* + A_{2,1}\nabla\widetilde{V}_{1,1}\left(\nabla V_{1,1} + \nabla V^*\right) + \varkappa q_1^* - \widehat{F}_1 \right|_\alpha \leq 24\overline{s}^2 B_1^2\eta. \tag{2.289}$$

Next, consider coefficients in the left-hand side of (2.282). We have

$$|A_{1,1}\nabla V_{1,1}| \leq 8\overline{s}^2 B_1,\ \varkappa \in (0,1)\,.$$

Hence, conditions (2.265) are satisfied. Hence, it follows from (2.266) and (2.289) that the solution of the Dirichlet boundary value problem (2.282), (2.283) can be estimated as

$$|\widetilde{q}_{1,1}|_{2+\alpha} \leq 24\overline{s}^2\overline{K}B_1^2\eta + \overline{K}\left\|\widetilde{\psi}_1\right\|_{C^{2+\alpha}(\partial\Omega)}.$$

Using (2.254) and (2.269), we obtain from this inequality and (2.288)

$$|\widetilde{q}_{1,1}|_{2+\alpha} \leq \overline{K}B^2\left(24\overline{s}^2 + \frac{C^*}{2B_1^2}\right)\eta \leq \overline{K}B_1^2\left(24\overline{s}^2 + \frac{1}{8}\right)\eta \leq 25\overline{s}^2\overline{K}B_1^2\eta.$$

In addition to (2.287), we can assume without any loss of generality that

$$40\overline{s}^2 \leq B_1. \tag{2.290}$$

Hence,

$$|\widetilde{q}_{1,1}|_{2+\alpha} \leq \overline{K}B_1^3\eta. \tag{2.291}$$

Estimate (2.291) establishes (2.277) for the function $\widetilde{q}_{1,1}$. Next, using (2.271), (2.285), and (2.291), we obtain

$$|q_{1,1}|_{2+\alpha} \leq |\widetilde{q}_{1,1}|_{2+\alpha} + |q_1^*|_{2+\alpha} \leq \overline{K}B_1^3\eta + C^* \leq 2C^*. \tag{2.292}$$

This establishes (2.278) for $|q_{1,1}|_{2+\alpha}$.

Now, we estimate the norm $|\widetilde{c}_{1,1}|_\alpha$. Subtracting (2.258) from (2.263) for $(n,k) = (1,1)$, we obtain

$$\widetilde{c}_{1,1} = \Delta\widetilde{v}_{1,1} + s_n^2\nabla\widetilde{v}_{1,1}\left(\nabla v_{1,1} + \nabla v_1^*\right) - \overline{F}_1. \tag{2.293}$$

Since by (2.257) and (2.262), the function $\widetilde{v}_{1,1} \in C^{2+\alpha}\left(\overline{\Omega}\right)$, then it follows from (2.293) that the function $\widetilde{c}_{1,1} \in C^\alpha\left(\overline{\Omega}\right)$. Since $c^* \in C^\alpha\left(\overline{\Omega}\right)$ as well, then also $c_{1,1} \in C^\alpha\left(\overline{\Omega}\right)$, which establishes (2.272) for $(n,k) = (1,1)$. Hence, taking into account the estimate (2.259) for the function $\overline{F}_1$, we obtain from (2.293)

$$|\widetilde{c}_{1,1}|_\alpha \leq \max\left(|\Delta\widetilde{v}_{1,1}|_\alpha, |\nabla\widetilde{v}_{1,1}|_\alpha\right)\left[1 + \overline{s}^2\left(|\nabla v_{1,1}|_\alpha + |\nabla v_1^*|_\alpha\right)\right] + \frac{C^*}{2}\eta. \tag{2.294}$$

By (2.257) and (2.262),

$$\widetilde{v}_{1,1} = -h\widetilde{q}_{1,1} + \widetilde{V}_{1,1}.$$

Hence, it follows from (2.269), (2.271), (2.287), (2.291) as well as from (2.275) and (2.276) at $(n,k) = (1,1)$ that

$$|\Delta\widetilde{v}_{1,1}|_\alpha, |\nabla\widetilde{v}_{1,1}|_\alpha \leq \frac{1}{2}\overline{K}B_1^3\eta^2 + B_1\eta \leq 2B_1\eta. \tag{2.295}$$

Next, using (2.223), (2.257), (2.262), (2.269) and (2.274) at $(n,k) = (1,1)$ and (2.292), we obtain

$$1 + \bar{s}^2\left(|\nabla v_{1,1}|_\alpha + |\nabla v_1^*|_\alpha\right) \leq 1 + \bar{s}^2\left(2C^*\eta + 2B_1\right) \leq 4\bar{s}^2B_1. \tag{2.296}$$

Hence, comparing this with (2.288), (2.290), (2.294), and (2.295), we obtain

$$|\widetilde{c}_{1,1}|_\alpha \leq 9\bar{s}^2B_1^2\eta \leq B_1^3\eta. \tag{2.297}$$

This establishes (2.279) for $(n,k) = (1,1)$. Hence, using Theorem 2.9.1.2 and (2.297), we obtain estimates (2.274)–(2.276) for the tail function at $(n,k) = (1,2)$:

$$|\nabla V_{1,2}|_{1+\alpha}, |\Delta V_{1,2}|_\alpha \leq B_1,$$

$$|\nabla V_{1,2} - \nabla V^*|_{1+\alpha} \leq B_1^4\eta, \ |\Delta V_{1,2} - \Delta V^*|_\alpha \leq B_1^4\eta.$$

Recall that by the algorithm of Sect. 2.6.1,

$$q_n := q_{n,m_n}, c_n := c_{n,m_n},$$

$$V_{n+1,1}(x,\bar{s}) = \frac{1}{\bar{s}^2}\ln w_{n,m_n}(x,\bar{s}).$$

Also, recall that by (2.267) $m_n \in [1,m]$. Having functions q_n and $V_{n+1,1}(x,\bar{s})$, we calculate next the function $q_{n+1,1}$. Also, recall that $q_0 = q_0^* = 0$. Thus, for the convenience of the mathematical induction, we temporary set $q_{n,0} := q_{n-1}$ for $n \geq 1$ and also $c_0 := c^*$, $V_{0,0} := V_{1,1}$. Hence, (2.272)–(2.279) are valid for $(n,k) = (0,0)$. In addition, since we have established (2.272)–(2.279) for $(n,k) = (1,1)$, we can assume now that we have proved (2.272)–(2.279) for $(n',k') \in [0,n] \times [0,k-1]$, where $k \geq 2$. We now want to prove (2.272)–(2.279) for $(n',k') = (n,k)$.

Subtracting (2.255) from (2.260), we obtain

$$\Delta\widetilde{q}_{n,k} - A_{1,n}\left(h\sum_{j=0}^{n-1}\nabla q_j\,(x)\right)\nabla\widetilde{q}_{n,k} + A_{1,n}\nabla V_{n,k}\cdot\nabla\widetilde{q}_{n,k} - \varkappa\widetilde{q}_{n,k}$$
$$= \left(A_{1,n}\nabla q_n^* - A_{2,n}h\sum_{j=0}^{n-1}\left(\nabla q_j + \nabla q_j^*\right) + 2A_{2,n}\nabla V_{n,k}\right)\left(h\sum_{j=0}^{n-1}\nabla\widetilde{q}_j\right)$$
$$+\left[2A_{2,n}h\sum_{j=0}^{n-1}\nabla q_j^* - A_{1,n}\nabla q_n^* - A_{2,n}\left(\nabla V_{n,k} + \nabla V^*\right)\right]\nabla\widetilde{V}_{n,k} + \varkappa q_n^* - \widehat{F}_n, \tag{2.298}$$

$$\widetilde{q}_{n,i}\mid_{\partial\Omega} = \widetilde{\psi}_n(x). \tag{2.299}$$

The function $\widehat{F}_n$ is defined in (2.284), and the estimate (2.286) is valid. First, we estimate the difference of tails $\widetilde{V}_{n,k}$. Since estimates (2.272)–(2.279) are valid for $(n',k') \in [0,n]\times[0,k-1]$, then by Theorem 2.9.1.2,

$$|\nabla V_{n,k}|_{1+\alpha}, |\Delta V_{n,k}|_\alpha \le B_1,$$
$$\left|\nabla\widetilde{V}_{n,k}\right|_{1+\alpha} \le B\left|\widetilde{c}_{n,k-1}\right|_\alpha \le B_1 B_1^{3[k-1+(n-1)m]}\cdot\eta = B_1^{3[k-1+(n-1)m]+1}\cdot\eta,$$
$$\left|\Delta\widetilde{V}_{n,k}\right|_\alpha \le B^{3[k+(n-1)m]+1}\cdot\eta.$$

The last three estimates establish (2.274)–(2.276) for $(n',k') = (n,k)$.

We now need to estimate the right-hand side of (2.298) using (2.121) as well as above established estimates. We have

$$\left|A_{1,n}\nabla q_n^* - A_{2,n}h\sum_{j=0}^{n-1}\left(\nabla q_j + \nabla q_j^*\right) + 2A_{2,n}\nabla V_{n,k}\right|_\alpha$$
$$\le 8\overline{s}^2\left(C^* + 3C^*Nh + 2B_1\right) \le 8\overline{s}^2\left(C^* + 1 + 2B_1\right).$$

Since $B_1 > 2$, then this inequality and (2.288) imply that

$$\left|A_{1,n}\nabla q_n^* - A_{2,n}h\sum_{j=0}^{n-1}\left(\nabla q_j + \nabla q_j^*\right) + 2A_{2,n}\nabla V_{n,k}\right|_\alpha \le 25\overline{s}^2 B_1. \tag{2.300}$$

Next, since estimates (2.277) are valid for functions $\widetilde{q}_j = q_j - q_j^*$, $j \in [0, n-1]$, then using (2.271), we obtain

$$\left| h \sum_{j=0}^{n-1} \nabla \widetilde{q}_j \right|_\alpha \leq \frac{1}{2} \overline{K} B_1^{3Nm} N \eta^2 \leq \frac{\eta}{2}.$$

Hence, using (2.300), we obtain the following estimate for the first term in the right-hand side of (2.298):

$$\left| A_{1,n} \nabla q_n^* - A_{2,n} h \sum_{j=0}^{n-1} \left(\nabla q_j + \nabla q_j^* \right) + 2 A_{2,n} \nabla V_{n,k} \right|_\alpha \left| h \sum_{j=0}^{n-1} \nabla \widetilde{q}_j \right|_\alpha \leq 14 \overline{s}^2 B_1 \eta. \tag{2.301}$$

Next, using (2.121), (2.223), (2.271), and (2.274), we obtain

$$\left| 2 A_{2,n} h \sum_{j=0}^{n-1} \nabla q_j^* - A_{1,n} \nabla q_n^* - A_{2,n} \left(\nabla V_{n,k} + \nabla V^* \right) \right|_\alpha$$

$$\leq 4 \overline{s}^2 C^* N \eta + 8 \overline{s}^2 C^* + 16 \overline{s}^2 B_1 \leq \frac{1}{4} \overline{s}^2 C^* + 4 \overline{s}^2 B_1 + 16 \overline{s}^2 B_1 \leq 21 \overline{s}^2 B_1.$$

Hence,

$$\left| 2 A_{2,n} h \sum_{j=0}^{n-1} \nabla q_j^* - A_{1,n} \nabla q_n^* - A_{2,n} \left(\nabla V_{n,k} + \nabla V^* \right) \right|_\alpha \left| \nabla \widetilde{V}_{n,k} \right|_\alpha + \left| \varkappa q_n^* - \widehat{F}_n \right|_\alpha$$

$$\leq 21 \overline{s}^2 B_1 B_1^{3[k-1+(n-1)m]+1} \cdot \eta + \frac{3}{2} C^* \eta \leq 21 \overline{s}^2 B_1 B_1^{3[k-1+(n-1)m]+1} \eta + B_1 \eta.$$

Combining this with (2.301), we obtain

$$\begin{aligned} |rhs|_\alpha &\leq 21 \overline{s}^2 B_1 B_1^{3[k-1+(n-1)m]+1} \cdot \eta + 15 \overline{s}^2 B_1 \eta \\ &= 21 \overline{s}^2 B_1 B_1^{3[k-1+(n-1)m]+1} \left(1 + \frac{15}{22 B_1} \right) \eta \\ &\leq 21 \overline{s}^2 B_1 B_1^{3[k-1+(n-1)m]+1} \left(1 + \frac{1}{2} \right) \eta \\ &= 32 \overline{s}^2 B_1 B_1^{3[k-1+(n-1)m]+1} \cdot \eta, \end{aligned}$$

where rhs is the right-hand side of (2.298). Thus,

$$|rhs|_\alpha \leq 32 \overline{s}^2 B_1 B_1^{3[k-1+(n-1)m]+1} \cdot \eta. \tag{2.302}$$

We now estimate coefficients in the left-hand side of (2.298) using (2.271), (2.288), as well as (2.278) for functions q_j with $j \in [0, n-1]$. The first resulting estimate is

$$\left| A_{1,n} \left(h \sum_{j=0}^{n-1} \nabla q_j(x) \right) \right|_\alpha \leq 12\overline{s}^2 C^* N \eta \leq \frac{6\overline{s}^2}{\overline{K} B_1^{3Nm-1}} \leq \frac{3}{4}\overline{s}^2. \tag{2.303}$$

Next, by (2.121) and (2.274),

$$|A_{1,n} \nabla V_{n,k}|_\alpha \leq 8\overline{s}^2 B_1. \tag{2.304}$$

Hence, it follows from (2.303) and (2.304) that condition (2.265) is satisfied for (2.298). Hence, (2.254), (2.266), (2.288), (2.299), and (2.302) imply that

$$\begin{aligned} |\widetilde{q}_{n,k}|_{2+\alpha} &\leq \overline{K} \left[32\overline{s}^2 B_1 B_1^{3[k-1+(n-1)m]+1} + \frac{C^*}{2} \right] \eta \\ &\leq \overline{K} \cdot 40\overline{s}^2 B B^{3[k-1+(n-1)m]+1} \cdot \eta. \end{aligned}$$

Since by (2.290), $40\overline{s}^2 \leq B$, then the last estimate implies that

$$|\widetilde{q}_{n,k}|_{2+\alpha} \leq \overline{K} B^{3[k+(n-1)m]} \cdot \eta,$$

which proves (2.277). The inequality (2.278) can be derived from (2.277) similarly with the derivation of (2.292).

Estimate now the norm $|\widetilde{c}_{n,k}|_\alpha$. Using (2.288), we obtain similarly with (2.294)

$$|\widetilde{c}_{n,k}|_\alpha \leq \max\left(|\Delta \widetilde{v}_{n,k}|_\alpha, |\nabla \widetilde{v}_{n,k}|_\alpha \right) \left[1 + \overline{s}^2 \left(|\nabla v_{n,k}|_\alpha + |\nabla v_n^*|_\alpha \right) \right] + \frac{B_1}{4}\eta. \tag{2.305}$$

We have

$$\widetilde{v}_{n,k}(x) = -h\widetilde{q}_{n,k}(x) - h \sum_{j=0}^{n-1} \widetilde{q}_j(x) + \widetilde{V}_{n,k}(x), \ x \in \Omega.$$

Hence, by (2.271), (2.275), and (2.277)

$$\begin{aligned} |\Delta \widetilde{v}_{n,k}|_\alpha, |\nabla \widetilde{v}_{n,k}|_\alpha &\leq \frac{1}{2}\overline{K} N B_1^{3[k+(n-1)m]} \eta^2 + B_1^{3[k-1+(n-1)m]+1} \eta \\ &\leq \frac{5}{4} B_1^{3[k-1+(n-1)m]+1} \cdot \eta. \end{aligned} \tag{2.306}$$

Next, using expressions (2.257) and (2.262) for functions $v_{n,k}$ and v_n^*, we obtain

$$1+\overline{s}^2\left(|\nabla v_{n,k}|_\alpha+|\nabla v_n^*|_\alpha\right)\leq 1+\frac{3}{2}\overline{s}^2C^*N\eta+2\overline{s}^2B_1\leq 3\overline{s}^2B_1.$$

Combining this with (2.305) and (2.306) and taking into account (2.290), we obtain

$$\begin{aligned}\left|\widetilde{c}_{n,k}\right|_\alpha &\leq 4\overline{s}^2B_1B_1^{3[k-1+(n-1)m]+1}\cdot\eta+\frac{B_1}{4}\eta\leq 5\overline{s}^2B_1B_1^{3[k-1+(n-1)m]+1}\cdot\eta\\ &\leq B_1^2B_1^{3[k-1+(n-1)m]+1}\cdot\eta=B_1^{3[k+(n-1)m]}\cdot\eta.\end{aligned}$$

Thus, $\left|\widetilde{c}_{n,k}\right|_\alpha\leq B^{3[k+(n-1)m]}\eta$. This establishes (2.279). □

2.10 Summary

One can see from Theorem 2.9.4 that the accuracy of the reconstruction strongly depends from the accuracy of the reconstruction of the tail functions. On the other hand, it follows from the second approximate mathematical model that the first tail function $V_{1,1}(x)$ is proportional to the solution of the Dirichlet boundary value problem for the Laplace equation; see (2.245) and (2.246) in Sect. 2.9.2. Therefore, it follows from estimate (2.247) that as long as the noise in the boundary data is small, the function $V_{1,1}(x)$ is reconstructed accurately. On the other hand, the accuracy of the reconstruction of other tail functions $V_{n,k}(x)$ depends on the accuracy of the reconstruction of the function $V_{1,1}(x)$. This explains why the approximately globally convergent algorithm of Sect. 2.9.4 works well numerically; see Chaps. 3–5 for computational studies. The "small noise" assumption is a natural one which is used in almost all numerical methods.

Thus, all what our approximately globally convergent numerical method requires is that the noise in the boundary data should be small. Under this assumption, we have a rigorous guarantee, within the framework of the second approximate mathematical model, that our resulting solution will be located in a small neighborhood of the exact solution. The size of this neighborhood is completely defined by the "noise" parameter η in (2.269), as it is conventionally done in standard convergence theorems. It is important that no a priori knowledge of any point in a small neighborhood of the exact solution is required. Therefore, the approximately globally convergent numerical method of this chapter indeed addresses the first central question of this book (Sect. 1.1).

Now, about the constants in convergence estimates of Theorems 2.8.2 and 2.9.4. They are probably large. However, this is not a discouraging factor. Indeed, it is well known that constants in almost all convergence estimates of numerical analysis are largely over-estimated for both well-posed and ill-posed problems. Consider, for example, standard energy estimates for classical initial boundary value

problems for hyperbolic and parabolic PDEs with variable coefficients and non-self-adjoint elliptic operators [119, 120]. The final step of these estimates usually consists in the application of the Gronwall's theorem. It is well known that this theorem implies that constants in those estimates are bounded from the above by $C_1 := \exp(CT)$, where T is the final time and $C > 0$ is a constant depending on coefficients of the corresponding PDE as well as on the spatial domain. Thus, the number C_1 is expected to be sufficiently large. On the other hand, it is well known that convergence estimates for both finite difference and FEMs are based on those energy estimates.

Chapter 3
Numerical Implementation of the Approximately Globally Convergent Method

In this chapter, we describe our computational implementation of the approximately globally convergent numerical method of Chap. 2. We use the algorithm of Sect. 2.6.1. Theorems 2.8.2 and 2.9.4 ensure the approximate global convergence of this algorithm within either of above two approximate mathematical models. Thus, we verify in this chapter the second condition of the informal Definition 1.1.2.2 of the approximate global convergence property. Computations of Chaps. 3–5 and Sect. 6.8.5 for simulation of the forward problem in 2D and 3D were performed using the software package WavES, see www.waves24.com.

In each 2D numerical test of this chapter, we choose the first approximation for the tail function $V_{1,1}(x,\bar{s}) \equiv 0$. Thus, no a priori information about the solution of our CIP is included in this choice. In 3D tests of Sect. 3.2 as well as in Chaps. 4–6 we use another alternative of the choice of the initial tail function. More precisely, we take the same function $V_{1,1}(x,\bar{s})$ as one for the homogeneous domain with the coefficient $c \equiv 1$. This choice is a natural one since it reflects ones knowledge of the value of the unknown coefficient $c(x)$ outside of the domain of interest; see (2.3).

The choice $V_{1,1}(x,\bar{s}) \equiv 0$ corresponds well with the first approximate mathematical model of Sect. 2.8.4, since it requires all tails to be bounded from the above by a small number $\xi > 0$. Suppose now that the nonlinear term with $\left(\nabla q_{n,1}^{k-1}\right)^2$ in the right-hand side of (2.45) is ignored, as it is done in the second approximate mathematical model of Sect. 2.9.2. Indeed, our numerical experience shows that the nonlinear term $\left(\nabla q_{n,1}^{k-1}\right)^2$ does not provide an essential impact to computational results. Then (2.260) and (2.261) imply that the choice $V_{1,1}(x,\bar{s}) \equiv 0$ means that in order to find the function $q_{1,1}$, one should solve the following Dirichlet boundary value problem:

$$\Delta q_{1,1} - \varkappa q_{1,1} = 0,\ x \in \Omega,$$
$$q_{1,1}\,|_{\partial\Omega} = \overline{\psi}_1(x).$$

This equation differs from the Laplace equation (2.245) for the function p only by the term $-\varkappa q_{1,1}$, where $\varkappa \in (0,1)$ is sufficiently small. Also, the boundary

L. Beilina and M.V. Klibanov, *Approximate Global Convergence and Adaptivity for Coefficient Inverse Problems*, DOI 10.1007/978-1-4419-7805-9_3,

condition (2.246) is $p\mid_{\partial\Omega}=-\overline{s}^2\overline{\psi}_1(x)$. This means that the choice of the initial tail function $V_{1,1}(x,\bar{s})\equiv 0$ is basically equivalent to the choice (2.248) as $V_{1,1}(x,\bar{s})=p(x)/\overline{s}$ of the second approximate mathematical model.

Two key steps of the algorithm of Sect. 2.6.1 are:

1. Iterative solutions of the boundary value problems (2.39), which is equivalent to the layer-stripping procedure.
2. Updating tail functions $V_{n,i}(x)$ via solving the Cauchy problem (2.1) and (2.2) on each iterative step and using formula (2.52) then.

Instead of solving the problem (2.1) and (2.2), one can solve the problem (2.11) and (2.12) at $s=\overline{s}$. Note that while functions $q_{n,i}$ are approximated via inner iterations "inside" the domain Ω, tail functions $V_{n,i}(x)$ are updated via outer iterations via solving either the problem (2.1) and (2.2) or the problem (2.11) and (2.12) in the entire space. Thus, the information that (2.1) is valid in the entire space rather than in the domain Ω only is "embedded" in functions $V_{n,i}(x)$. In other words, the problem (2.1) and (2.2) plays the role of the second equation for functions q, V.

Following a statement in the beginning of Chap. 1 in numerical studies of both this and follow-up chapters, we focus on imaging of small sharp inclusions embedded in an otherwise slowly changing background medium. However, we are not interested to image slowly changing backgrounds. This is because such inclusions represent the main interest in many applications, for example, imaging of explosives and medical imaging. Indeed, it is well known from tables of dielectric constants that those constants in explosives are usually much higher than in regular materials; see tables [151]. A discussion about applications of (2.1) to solutions of CIPs of propagations of EM waves is presented in Sect. 2.1 as well as Chaps. 5 and 6. In this case, the coefficient of interest $c(x)=\varepsilon_r(x)$ is the spatially distributed dielectric constant.

We present in this chapter several numerical experiments which demonstrate robustness of our method and provide good quality images with up to 15% multiplicative random noise in the data. It is worthy to mention that the numerical method of Chap. 2 does not require any a priori knowledge of the unknown coefficient $c(x)$ inside the domain of interest Ω. In particular, it does not require a knowledge of the background medium inside Ω.

3.1 Numerical Study in 2D

In this section, we test numerical method of Chap. 2 in the 2D case. Specifically, we test the algorithm of Sect. 2.6.1.

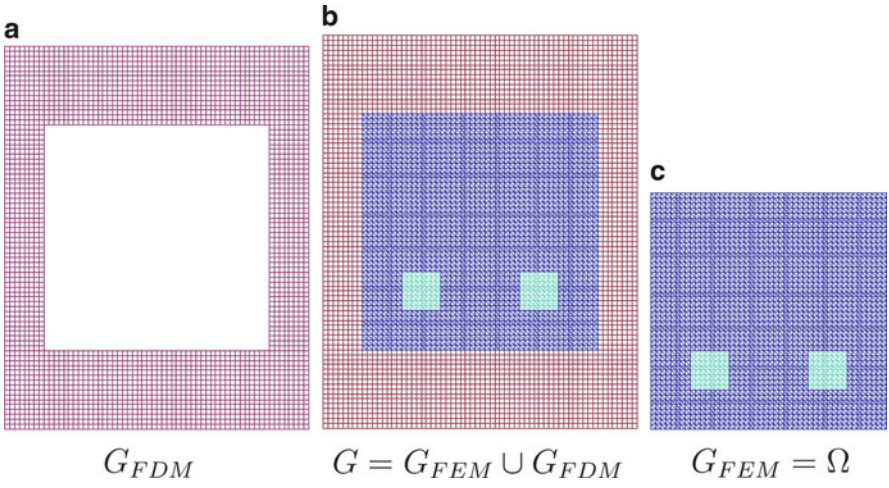

Fig. 3.1 The hybrid mesh (**b**) is a combination of a structured mesh (**a**), where FDM is applied, and a mesh (**c**), where we use FEM, with a thin overlapping of structured elements. The solution of the inverse problem is computed in the square Ω and $c(x) = 1$ for $x \in G \setminus \Omega$. Source: L. Beilina and M.V. Klibanov, A globally convergent numerical method for a coefficient inverse problem, *SIAM J. Sci. Comp.*, 31, 478–509, 2008. © 2008 Society for Industrial and Applied Mathematics. Reprinted with permission

3.1.1 The Forward Problem

In the numerical tests of this chapter, we use only the computationally simulated data. That is, the data are generated by computing the forward problem (3.2) with the given function $c(x)$. To solve the forward problem, we use the hybrid FEM/FDM method described in [30]. The computational domain in all our tests is $= G = G_{\text{FEM}} \cup G_{\text{FDM}}$. In the 2D case, $G = [-4, 4] \times [-5, 5]$. The domain G is split into a finite element subdomain $G_{\text{FEM}} := \Omega = [-3, 3] \times [-3, 3]$ and a surrounding subdomain G_{FDM} with a structured mesh; see Fig. 3.1. The space mesh in Ω consists of triangles, and it consists of squares in G_{FDM}, with the mesh size $\tilde{h} = 0.125$ in the overlapping regions. At the top and bottom boundaries of G, we use first-order absorbing boundary conditions [66] which are exact in this particular case. At the lateral boundaries, the zero Neumann boundary condition is used. Since the initializing plane wave propagates downward, then the zero Neumann boundary condition allows us to model an infinite space domain in the lateral direction.

The forward problem is computed in the rectangle $G \subset \mathbb{R}^2$ (Fig. 3.1). The coefficient $c(x)$ is unknown only in the square $\Omega \subset G$, and

$$c(x) = 1 \text{ in } G \setminus \Omega; \tag{3.1}$$

see the original statement of Inverse Problem 2.1. The trace $g(x,t)$ of the solution of the forward problem is recorded at the boundary $\partial\Omega$; see (2.5). This trace generates the Dirichlet boundary data $\psi(x,s)$ in (2.21) (after the Laplace transform). Next, the coefficient $c(x)$ is "forgotten,"and our goal is to reconstruct this coefficient for $x \in \Omega$ from the data $\psi(x,s)$. The boundary of the rectangle G is $\partial G = \partial G_1 \cup \partial G_2 \cup \partial G_3$. Here, ∂G_1 and ∂G_2 are respectively top and bottom sides of the largest rectangle of Fig. 3.1, and ∂G_3 is the union of left and right sides of this rectangle. The forward problem for data generation is

$$\begin{aligned} c(x)u_{tt} - \Delta u &= 0, \quad \text{in } G \times (0,T), \\ u(x,0) &= 0,\ u_t(x,0) = 0, \text{ in } G, \\ \partial_n u\big|_{\partial G_1} &= f(t), \text{ on } \partial G_1 \times (0,t_1], \\ \partial_n u\big|_{\partial G_1} &= \partial_t u, \text{ on } \partial G_1 \times (t_1,T), \\ \partial_n u\big|_{\partial G_2} &= \partial_t u, \text{ on } \partial G_2 \times (0,T), \\ \partial_n u\big|_{\partial G_3} &= 0, \text{ on } \partial G_3 \times (0,T), \end{aligned} \tag{3.2}$$

where T is the final time. Since it is impossible to calculate an integral over the infinite interval $(0,\infty)$, it is natural that when calculating the Laplace transform (2.10) of the boundary data, we integrate for $t \in (0,T)$, thus calculating an approximation of this transform. On the other hand, since the kernel e^{-st} of this transform decays rapidly with $t \to \infty$, then this is a good approximation. Our work with the experimental data in Chaps. 5 and 6 confirms this, since experimental data were measured on a finite time interval.

We use in our tests the plane wave instead of the point source; see Sect. 3.1.2. The plane wave f in (3.3) is initialized at the top boundary ∂G_1 of the computational domain G during the time period $t \in (0,t_1]$, propagates downward into G, and is absorbed at the bottom boundary ∂G_2 for all times $t \in (0,T)$. In addition, it is also absorbed at the top boundary ∂G_1 for times $t \in (t_1,T)$. Here,

$$f(t) = \begin{cases} \frac{1}{10}(\sin(\overline{s}t - \pi/2) + 1) \text{ for } t \in (0,t_1],\ t_1 = \frac{2\pi}{\overline{s}}, \\ 0 \text{ for } t \in (t_1,T),\ T = 17.8t_1. \end{cases}$$

In order to produce updates for tails, we have solved on each iterative step the forward problem (3.2). Next, we have calculated the Laplace transform (2.10) to obtain the function $w_{n,i}(x,\overline{s})$; see Sect. 2.6.1.

We have found that the s-interval $[\underline{s},\overline{s}] = [6.7, 7.45]$ is the optimal one for the above domains G, Ω. Thus, we have used this interval in our computations.

3.1.2 Main Discrepancies Between the Theory and the Numerical Implementation

It is well known that quite often, some discrepancies take place between the theory of a numerical method and its computational implementation. In this section, we summarize main discrepancies between the above theory and our numerical implementation.

The *first main discrepancy* is that in order to generate the data for the inverse problem, we solve the forward problem (3.2) in the finite domain G with the plane wave instead of the Cauchy problem (2.1) and (2.2) with the point source. Indeed, because of the singularity associated with the point source, it is easier to implement computationally the case of the plane wave compared with the case of the point source. In addition, if a point source is located far from the medium of interest, then this medium "percepts" it as a plane wave. On the other hand, our theory needs the point source in the problem (2.1) and (2.2) rather than the plane wave only for the formulation of Lemma 2.3 about the asymptotic behavior as well as for establishing (2.12). In turn, this lemma is derived from Theorem 4.1 of the book [144], which is about the structure of the fundamental solution of the hyperbolic equation.

The *second main discrepancy* is that conditions of Lemma 2.3 are hard to verify computationally when reconstructing the unknown coefficient via an iterative procedure. Therefore, in all our numerical Tests 1–3 of Sect. 3.1.3, we have verified numerically the asymptotic behavior (2.13) of this lemma. To do this, we have considered functions $g_1(s)$ and $g_2(s)$, for $s \in [6.5, 7.5] \supset [\underline{s}, \overline{s}] = [6.7, 7.45]$, where

$$g_1(s) = \frac{1}{s} \left\| \nabla \ln w(x,s) \right\|_{L_2(\Omega)}, \; g_2(s) = s^2 \left\| \nabla q(x,s) \right\|_{L_2(\Omega)}.$$

Graphs of functions $g_1(s)$ and $g_2(s)$ (not presented here) have shown that these functions are very close to constants for $s \in [6.5, 7.5]$, which corresponds well with (2.13).

We now describe the *third main discrepancy*. Instead of using the extension procedure described in the beginning of Sect. 2.6, we simply set $c_{n,i}(x) := 1$ in $G \setminus \Omega$. In addition, since by (2.3) we need a priori lower bound $c(x) \geq 1$, we enforce that the coefficient $c(x)$ belongs to the set of admissible coefficient $C_{\text{adm}} = \{c(x) \geq 0.5\}$ as follows: If $c_{n,i}(x_0) < 0.5$ for a certain point $x_0 \in \Omega$, then we set $c_{n,i}(x_0) := 1$. The reason why we use the value 1 in this setting is that the set of functions $P(d, d^*)$ is our correctness set in the second approximate mathematical model; see Definitions 1.4.2 and 1.4.3 for the correctness set and the third Remark 2.9.4 for $P(d, d^*)$. The set $P(d, d^*)$ was defined in (2.208). Therefore, this setting as well as the fact that we allow the function $c(x)$ to attain values between 0.5 and 1 does not mean that we assume the knowledge of the background value of the function $c(x)$. Still, we have observed in our numerical tests that all resulting functions $c_{n,i}(x) \geq 1$ for all $x \in \overline{\Omega}$, i.e., "allowed" values

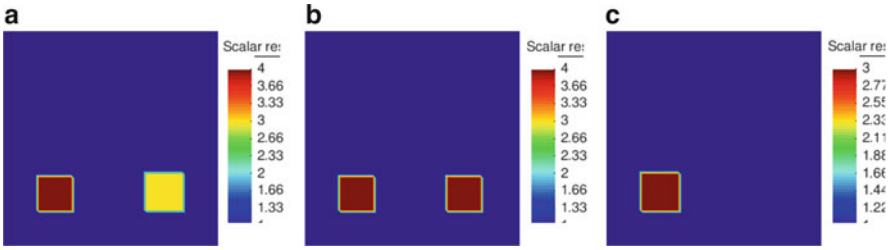

Fig. 3.2 Three different coefficients $c(x), x \in \Omega$, to be imaged in our numerical tests. In all cases $c(x) = 1$ everywhere, except of small squares. In (**a**), $c(x) = 4$ and $c(x) = 3$ in the *left and right small squares*, respectively. In (**b**), $c(x) = 4$ in both *small squares*. In (**c**), $c(x) = 3$ in the *small square*. Source: L. Beilina and M.V. Klibanov, A globally convergent numerical method for a coefficient inverse problem, *SIAM J. Sci. Comp.*, 31, 478-509, 2008. © 2008 Society for Industrial and Applied Mathematics. Reprinted with permission

between 0.5 and 1 are not actually attained in iterations. In particular, the latter means that conditions (2.127) and (2.268) of Theorems 2.8.2 and 2.9.4 are satisfied in our computations.

The *fourth main discrepancy* is that our square Ω does not have a smooth boundary, as it is required by the Schauder theorem. Furthermore, the Dirichlet boundary value problems (2.49) and (2.50) for functions $q_{n,i}$ in the square Ω were solved by the FEM. The FEM cannot guarantee that resulting functions $q_{n,i} \in C^{2+\alpha}\left(\overline{\Omega}\right)$, as it is required by Theorems 2.8.2 and 2.9.4 Nevertheless, analogues of these theorems can be proved for the discrete case when the FEM analogues of equations for functions $q_{n,i}$ are used, and also, the domain Ω with $\partial\Omega \in C^3$ is replaced respectively with either a rectangular prism in $\mathbb{R}^3$ or a rectangle in $\mathbb{R}^2$, as in our numerical examples.

The *fifth main discrepancy* is that we use discrete $L_2(\Omega)$ norms in (3.8) and (3.9) for our stopping rule. This is because all norms in discrete spaces of finite elements are equivalent as well as because the discrete $L_2(\Omega)$ norm is computationally easier to work with than the $C^{\alpha}\left(\overline{\Omega}\right)$ norm.

3.1.3 Results of the Reconstruction

In this section, we present results of our reconstructions. We have performed numerical experiments to reconstruct the medium, which is homogeneous with $c(x) = 1$ except of either two small squares or a single square; see Fig. 3.2. However, we have not assumed a priori knowledge neither of the structure of this medium nor of the background constant $c(x) = 1$ outside of those squares.

In all our numerical experiments, we have chosen $s \in [\underline{s}, \overline{s}] = [6.7, 7.45]$ and the step size with respect to the pseudo frequency $h = 0.05$. Hence, $N = 15$ in our case. We have chosen two sequences of regularization parameters $\lambda := \lambda_n$

and $\varepsilon = \varepsilon_n$ for $n = 1, \dots, \overline{N}$. Both formulations and proofs of Theorems 2.8.2 and 2.9.4 remain almost unchanged for this case. The reason of choosing different values of λ_n and ε_n is that values of gradients $|\nabla q_1|$ and $|\nabla q_2|$ are very small. Hence, in order not to eliminate totally the influence of the nonlinear term $(\nabla q_{n,i-1})^2, n = 1, 2$ in (2.49), the values of λ_1 and λ_2 should not be too large. Starting from $n = 3$, values of the nonlinear term start to grow. Hence, we balance them by choosing a larger value of λ_n for $n = 3, 4, 5$. For $n > 5$, values of the nonlinear term become even lager. Thus, we balance them via increasing the value of λ_n again. Considerations for choosing different values of ε_n are similar. In Tests 1–4, the values of the parameters λ_n and ε_n were:

$$\begin{aligned} &\lambda_n = 20, n = 1, 2; \lambda_n = 200, n = 3, 4, 5; \lambda_n = 2000, n \geq 6; \\ &\varepsilon_n = 0, n = 1, 2; \varepsilon_n = 0.001, n = 3, 4, 5; \varepsilon_n = 0.01, n = 6, 7, \\ &\varepsilon_n = 0.1, n \geq 8. \end{aligned} \tag{3.3}$$

Once the function $q_{n,i}$ is calculated, we update the function $c := c_{n,i}$ using formulas (2.41) and (2.42). To find second derivatives in (2.42), we use the standard finite difference approximations of both the Laplacian and the gradient on a structured Cartesian mesh. More precisely, in two dimensions, we use the following approximation to calculate the function $c(x)$ at the point (i, j):

$$\begin{aligned} c^{i,j} = &\frac{v_{i+1,j} - 2v_{i,j} + v_{i-1,j}}{dx^2} + \frac{v_{i,j+1} - 2v_{i,j} + v_{i,j-1}}{dy^2} \\ &+ \underline{s}^2 \left(\left(\frac{v_{i+1,j} - v_{i,j}}{dx} \right)^2 + \left(\frac{v_{i,j+1} - v_{i,j}}{dy} \right)^2 \right), \end{aligned} \tag{3.4}$$

where dx and dy are grid step sizes of the finite difference mesh in the directions x and y, respectively. An additional important procedure is averaging. For each inner grid point (x_i, y_j), we average the value $c^{i,j}$ over neighboring points. The averaging helps to smooth out solutions. The resulting value at (x_i, y_j) is $\overline{c}^{i,j}$:

$$\overline{c}^{i,j} = \frac{c^{i-1,j} + c^{i,j} + c^{i+1,j} + c^{i,j-1} + c^{i,j+1}}{5}. \tag{3.5}$$

Once the number $\overline{c}^{i,j}$ is obtained, in any neighboring point, the number $\overline{c}^{i,j}$ is used in (3.5) instead of $c^{i,j}$.

The final computed function is $c(x) := c_{\overline{N}}(x)$. Recall that the number of iterations is a part of the vectorial regularization parameter in our case. The number m_n of iterations with respect to tails was

$$m_n = 4 \text{ for } n \leq n_0, \; m_n = 7 \text{ for } n = n_0 + 1, \dots, \overline{N}, \tag{3.6}$$

where numbers n_0 and $\overline{N}$ are chosen on the basis of an *objective* stopping rule described below. Hence, while the pairs $\left(n_0, \overline{N}\right)$ differ in our tests, the rule of their choice (i.e., the stopping rule) remains the same. As it is always the case in ill-posed problems, the choice of proper regularization parameters as well as of a proper stopping rule was time-consuming. However, once the stopping rule and regularization parameters $\lambda_n, \varepsilon_n, m_n, \overline{s}$ are chosen for one test example, they remain the same for all our numerical experiments described in Tests 1–4 below. Hence, results were not "conveniently adjusted" for each specific test in order to obtain the best possible image for that test.

In all our tests, we have introduced the multiplicative random noise in the boundary data by adding relative error to computed data u_{obs} using the following expression:

$$u_\sigma\left(x_i, y_i, t_j\right) = u_{\text{obs}}\left(x_i, y_i, t_j\right)\left[1 + \alpha_j (u_{\max} - u_{\min})\sigma\right]. \tag{3.7}$$

The function u_σ was used for the inversion. Here, $u_{\text{obs}}\left(x_i, y_i, t_j\right) = u\left(x_i, y_i, t_j\right)$, $(x_i, y_i) \in \partial\Omega$ is a mesh point at the boundary $\partial\Omega, t_j \in (0, T)$ is the mesh point in time, α_j is a random number in the interval $[-1; 1]$, $u_{\max}$ and $u_{\min}$ are maximal and minimal values of the computed data u_{obs}, respectively, and σ is the noise level. Next, we apply the Laplace transform (2.10) to the boundary data, which helps to do both: "smooth out" and decrease the noise due to the integration. Because of that, we have successfully used the following formula for the s-derivative of the boundary data $\varphi(x, s)$ to obtain the function $\psi(x, s_n)$ in (2.21):

$$\frac{\partial\varphi(x, s_n)}{\partial s} \approx \frac{\varphi(x, s_{n-1}) - \varphi(x, s_n)}{h}, \; h = 0.05.$$

Test 1. We reconstruct of the structure given on Fig. 3.2a. In this figure:

$$c = \begin{cases} 4 \text{ in the left small square of Fig. 3.2a,} \\ 3 \text{ in the right small square of Fig. 3.2a,} \\ 1 \text{ everywhere else.} \end{cases}$$

We use $\sigma = 10\%$ in (3.7).

Figure 3.3 displays isosurfaces of functions $c_{n,i}, n = 1, 8, 12$. Figure 3.4 presents one-dimensional cross-sections of computed images of functions $c_{n,k}$ along the vertical line passing through the center of the left small square. Comparison of images of functions $c_{n,i}$ for different values n and i shows that the inclusion/background contrasts grow with the grow of both n and i. In particular, these contrasts are very low for $n = i = 1$, since they do not exceed 1.006/1. The final computed image is $c_{12,7}(x) := c_{12}(x) = c_{\text{comp}}(x)$. The right Fig. 3.4 depicts those 1D cross-sections of computed functions $c_{12,i}$ being superimposed with the correct one.

Figure 3.5 displays one-dimensional cross-sections of the image of the functions $c_{n,k}$ along the vertical line passing through the center of the right small square. These

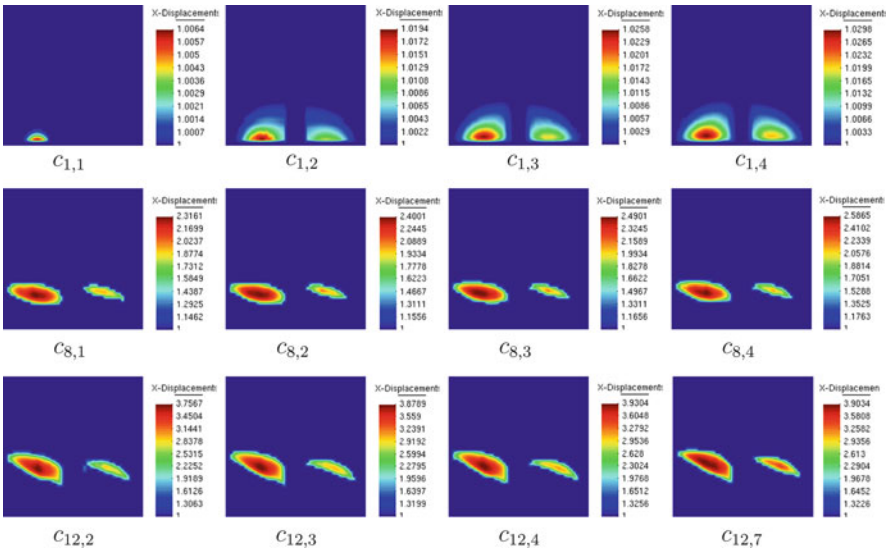

Fig. 3.3 Test 1: Spatial distribution of some functions $c_{n,i}(x)$ obtained after computing functions $q_{n,i}(x)$. Here, $n = 1, 8, 12$. The final computed image corresponds to $c_{12,7}(x) := c_{\text{comp}}(x)$. Compare with Fig. 3.2a, where the real image is displayed. Maximal values $c_{\text{comp}}(x) = 4$ and $c_{\text{comp}}(x) = 3.2$ in the left and right imaged inclusions, respectively. Correct values are 4 and 3, respectively. Also, $c_{\text{comp}}(x) = 1$ outside of imaged inclusions, which is the correct value. Source: L. Beilina and M.V. Klibanov, A globally convergent numerical method for a coefficient inverse problem, *SIAM J. Sci. Comp.*, 31, 478–509, 2008. © 2008 Society for Industrial and Applied Mathematics. Reprinted with permission

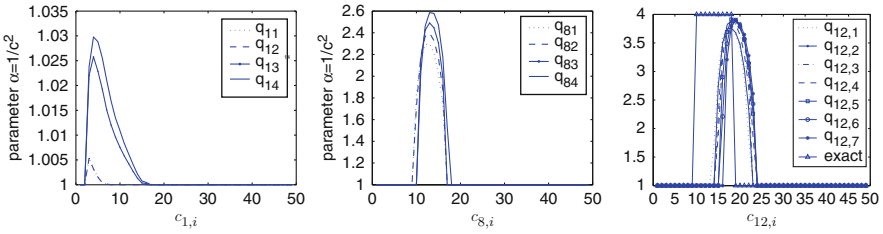

Fig. 3.4 Test 1: One-dimensional cross-sections of computed images $c_{n,i}(x)$ of the *left small square* along the vertical line passing through the *center* of this *square*. The function $c_{n,i}(x)$ is obtained after computing the function $q_{n,i}(x)$. Here, $n = 1, 8, 12$. On the *right figure*, computed 1D cross-sections functions $c_{12,i}(x)$ are superimposed with the correct one. The final computed image corresponds to $c_{12,7}(x) := c_{\text{comp}}(x)$. Source: L. Beilina and M.V. Klibanov, A globally convergent numerical method for a coefficient inverse problem, *SIAM J. Sci. Comp.*, 31, 478–509, 2008. © 2008 Society for Industrial and Applied Mathematics. Reprinted with permission

cross-sections are superimposed with the correct one. One can see from Fig. 3.4 that the 4 : 1 contrast in the left square is imaged accurately. As to the right square, we got the 3.5 : 1 contrast. The function $c(x) = 1$ outside of these squares is also imaged accurately. Locations of imaged inclusions are somewhat shifted upward.

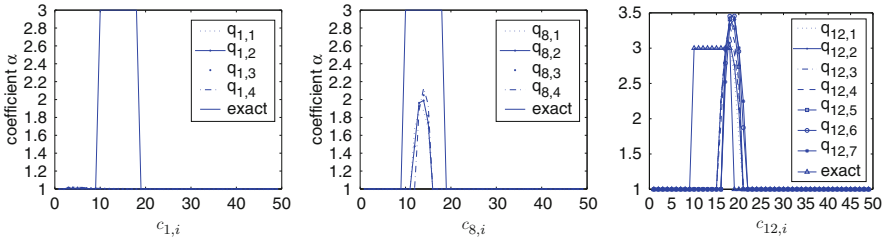

Fig. 3.5 Test 1: One-dimensional cross-sections of computed images $c_{n,i}(x)$ of the *right small square* along the vertical line passing through the *center* of this *square*. These cross-sections are superimposed with the correct one. Here, $n = 1, 8, 12$. The final computed image corresponds to $c_{12,7}(x) := c_{\text{comp}}(x)$. Source: L. Beilina and M.V. Klibanov, A globally convergent numerical method for a coefficient inverse problem, *SIAM J. Sci. Comp.*, 31, 478–509, 2008. © 2008 Society for Industrial and Applied Mathematics. Reprinted with permission

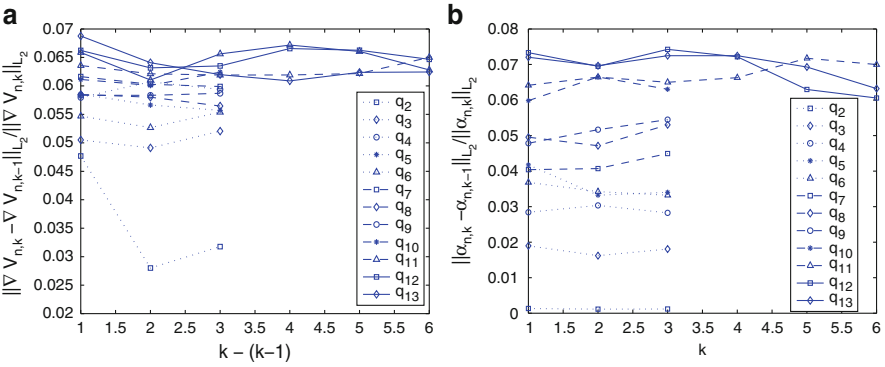

Fig. 3.6 Test 1: Computed discrete relative L_2-norms: (**a**) of the $\frac{||\nabla V_{n,i} - \nabla V_{n,i-1}||}{||\nabla V_{n,i}||}$ and (**b**) of the $\frac{||c_{n,i} - c_{n,i-1}||}{||c_{n,i}||}$. Source: L. Beilina and M.V. Klibanov, A globally convergent numerical method for a coefficient inverse problem, *SIAM J. Sci. Comp.*, 31, 478–509, 2008. © 2008 Society for Industrial and Applied Mathematics. Reprinted with permission

We now explain our *objective stopping criterion*. Figure 3.6a displays computed discrete relative L_2-norms of gradients of tails

$$\frac{||\nabla V_{n,i} - \nabla V_{n,i-1}||}{||\nabla V_{n,i}||}, \tag{3.8}$$

and Fig. 3.6b displays relative L_2-norms of the target coefficient

$$\frac{||c_{n,i} - c_{n,i-1}||}{||c_{n,i}||}. \tag{3.9}$$

We use these norms as the stopping rule for computations in our iterative algorithm. We stop our iterations for computing the new function q_n when both relative norms

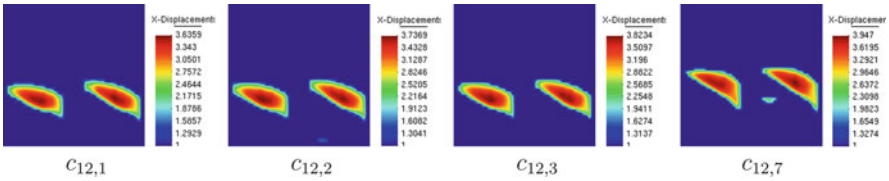

Fig. 3.7 Test 2: Spatial distribution of functions $c_{12,i}$. The final image is $c_{12,7}(x) := c_{\text{comp}}(x)$. Compare with Fig. 3.2b where the real image is displayed. Maximal values of $c_{\text{comp}}(x) = 4$ in both imaged inclusions, which is the correct value. Also, $c_{\text{comp}}(x) = 1$ outside of imaged inclusions, which is the correct value. Source: L. Beilina and M.V. Klibanov, A globally convergent numerical method for a coefficient inverse problem, *SIAM J. Sci. Comp.*, 31, 478–509, 2008. © 2008 Society for Industrial and Applied Mathematics. Reprinted with permission

(3.8) and (3.9) are stabilized. Here is how we do this. First, we observe on Fig. 3.6a that relative L_2-norms (3.8) of the computed gradients of tails grow until $n = 10$. For $n \geq 10$, norms (3.8) change slowly. Thus, we conclude that at $n = 9$, tails are stabilized. However, norms (3.9) still grow for $n > n_0 = 9$; see Fig. 3.6b. We repeat our iterative procedure for $n = 10, 11, 12, 13$. And for $n \geq 10$, we also increase the number of iterations with respect to tails: we now take seven iterations instead of four; see (3.6). We observe that at $n = 12$, both relative norms (3.8) and (3.9) are stabilized. Thus, we set $\overline{N} = 12$ and take $c_{12,7}(x)$ as our final reconstructed image. On Fig. 3.6, we also present results for $n = 13$ which confirms that norms (3.8) and (3.9) are stabilized.

Remark 3.1.3. At the same time, we have observed that for $n = 14, 15$, norms (3.9) abruptly grow, which was reflected in an abrupt move of positions of imaged inclusions upward (not shown). This confirms that our choice of $\overline{N}$ was correct one. A similar behavior was observed in Tests 2 and 3; see the fourth Remark 2.9.4 for explanations. In addition, the same type of behavior was observed on Figs. 5.8 and 5.9 for experimental data; see Chap. 5. We use exactly the same stopping criterion in Tests 2, 3 and 4.

Test 2. We now test our numerical method on the reconstruction of the structure given on Fig. 3.2b. We introduce $\sigma = 5\%$ of the multiplicative random noise in the boundary data u_{obs} in (3.7). We take $c = 4$ for both small squares of Fig. 3.2b and $c = 1$ outside of these squares. Hence, the inclusion/background contrast is $4 : 1$. Figure 3.7 presents isosurfaces of resulting images of functions $c_{12,i}$.

Using the above stopping rule, we have observed that $n_0 = 9$ and $\overline{N} = 12$. The behavior of norms (3.8) and (3.9) (not shown) was similar with the one of Fig. 3.6. The last image on Fig. 3.7 represents the final computed image $c_{12,7}(x) := c_{12}(x) = c_{\text{comp}}(x)$ of the target coefficient. Figure 3.8 displays the one-dimensional cross-sections of the images of the functions $c_{n,k}$ along the vertical line passing through the center of the left small square. These cross-sections are superimposed

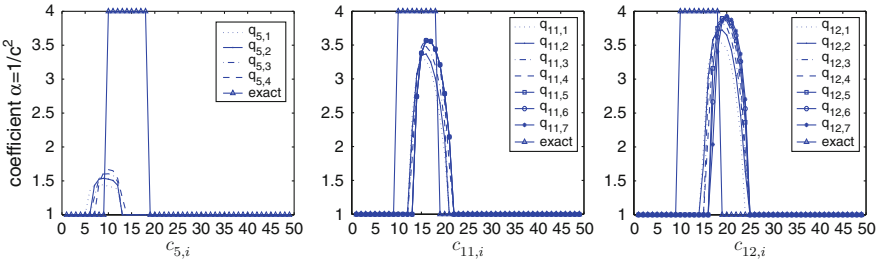

Fig. 3.8 Test 2: One-dimensional cross-sections of computed images $c_{n,i}(x)$ of the *left small square* along the vertical line passing through the *center* of this *square*. These cross-sections are superimposed with the correct one. The function $c_{n,i}(x)$ is obtained after computing the function $q_{n,i}(x)$. Here, $n = 5, 11, 12$. The final computed image corresponds to $c_{12,7}(x) := c_{\text{comp}}(x)$. Source: L. Beilina and M.V. Klibanov, A globally convergent numerical method for a coefficient inverse problem, *SIAM J. Sci. Comp.*, 31, 478–509, 2008. © 2008 Society for Industrial and Applied Mathematics. Reprinted with permission

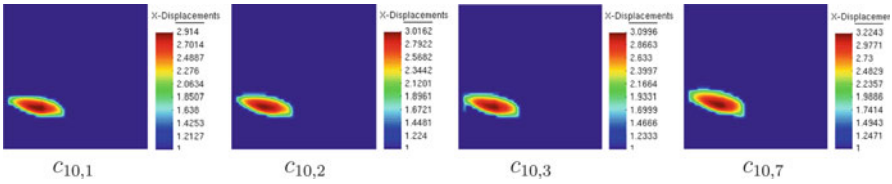

Fig. 3.9 Test 3: The case of the 5% multiplicative random noise in the data. Spatial distribution of functions $c_{10,i}$. The final image is $c_{10,7}(x) := c_{\text{comp}}(x)$. Compare with Fig. 3.2c where the real image is displayed. The maximal values of $c_{\text{comp}}(x) = 3.2$ in the imaged inclusion. The correct value is 3. Also, $c_{\text{comp}}(x) = 1$ outside of the imaged inclusion, which is the correct value. Source: L. Beilina and M.V. Klibanov, A globally convergent numerical method for a coefficient inverse problem, *SIAM J. Sci. Comp.*, 31, 478–509, 2008. © 2008 Society for Industrial and Applied Mathematics. Reprinted with permission

with the correct one. One can see that the value of the function $c_{12,7}(x) := c_{\text{comp}}(x)$ both inside and outside of both inclusions is imaged correctly, although the locations of inclusions are somewhat shifted to the top.

Test 3. We now consider a single small square of Fig. 3.2c with $c = 3$ in it, leaving all other parameters the same as above. We perform computations with two values $\sigma = 5\%$ and $\sigma = 15\%$ of the multiplicative random noise in the boundary data u_{obs} in (3.7).

Figure 3.9 displays isosurfaces of functions $c_{10,i}$ for the case of 5% noise in the boundary data. Figure 3.10 presents one-dimensional cross-sections of images of functions $c_{n,k}$ for $n = 9, 10, 11$ along the vertical line passing through the center of this small square. The imaged function $c(x)$ is superimposed with the correct one. We observe that we obtain the $3.2 : 1$ contrast of the reconstructed function $c(x) := c_{10,7}(x)$, which is quite accurate, since the correct contrast is $3 : 1$.

Figure 3.11 shows computed relative L_2-norms (3.8) and (3.9) with the noise level $\sigma = 5\%$ in data. Using Fig. 3.11, we analyze results of the reconstruction.

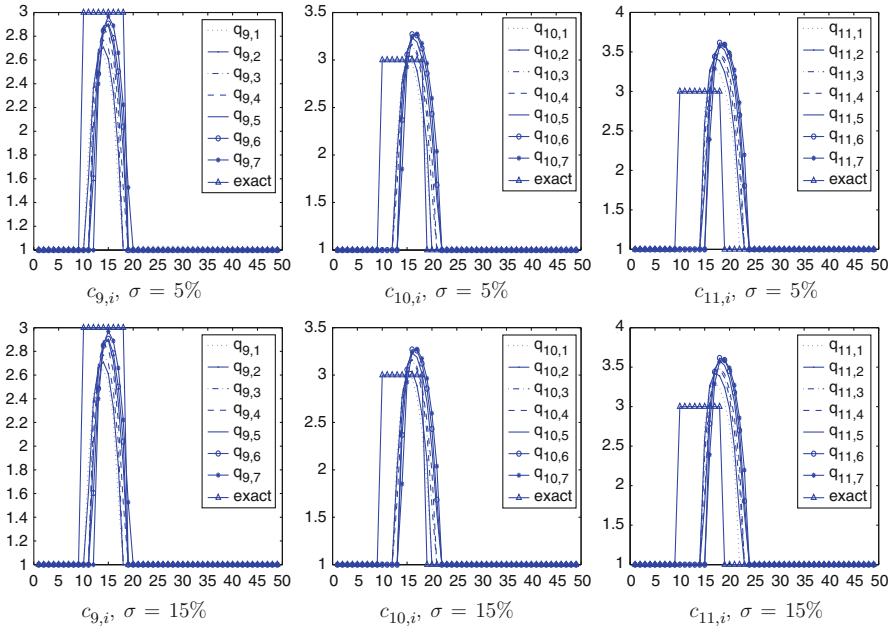

Fig. 3.10 Test 3: One-dimensional cross-sections of computed images $c_{n,i}(x)$through the *middle* of the *small square*. These cross-sections are superimposed with the correct one. Source: L. Beilina and M.V. Klibanov, A globally convergent numerical method for a coefficient inverse problem, *SIAM J. Sci. Comp.*, 31, 478–509, 2008. © 2008 Society for Industrial and Applied Mathematics. Reprinted with permission

On Fig. 3.11a we observe that relative L_2-norms (3.8) of the computed gradients of tails grow until computing the function q_7. After that, tails change slowly, which means that $n_0 = 7$ in (3.6). However, norms (3.9) are not yet stabilized. Hence, we now want to stabilize norms (3.9). We repeat our iterative procedure for $n = 8, 9, 10, 11$ and with seven iterations with respect to tails for these values of n instead of previous four; see (3.6). On Fig. 3.11b we observe that at $n = 9$, both norms (3.8) and (3.9) are stabilized, and at $n = 10, 11$, these norms almost do not change, although the norm for $q_{11,7}$ starts to grow. Thus, following the fourth Remark 2.9.4, we conclude, that we have achieved the solution of our problem at $c_{10}(x) := c_{10,7}(x) = c_{\text{comp}}(x)$ with $\overline{N} = 10$. We have observed a similar behavior of our solution with the relative noise level $\sigma = 15\%$ (not shown).

Test 4. The goal of this test is to confirm that the error in the reconstructed images is mainly determined by the error in the tail function. From the analytical standpoint, this is clear from both approximate mathematical models presented in Sects. 2.8.4 and 2.9.2. Still, it would be good to confirm this numerically. We consider the same parameters, as ones in previous tests, except that we take the exact initial tail $V_{1,1}(x, \overline{s}) = V^*(x, \overline{s})$ and the noise level $\sigma = 5\%$. We use the same iterative algorithm as in previous tests. We stop our iterative algorithm after computing the

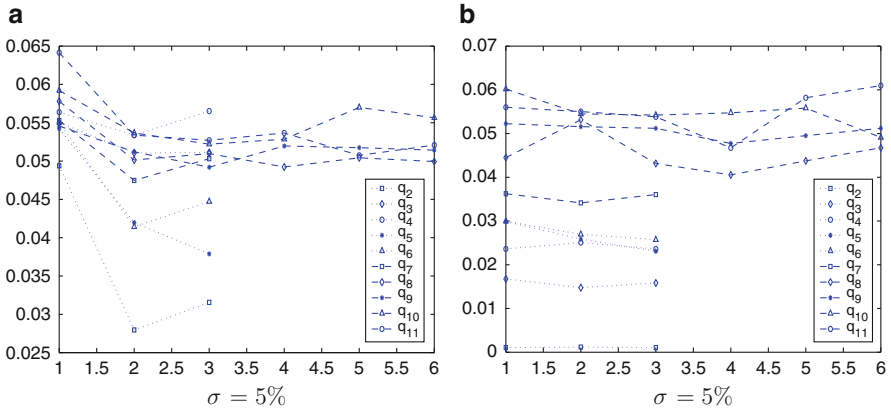

Fig. 3.11 Test 3: Computed discrete relative L_2-norms. (**a**) $\frac{||\nabla V_{n,i} - \nabla V_{n,i-1}||}{||\nabla V_{n,i}||}$, (**b**) $\frac{||c_{n,i} - c_{n,i-1}||}{||c_{n,i}||}$. Source: L. Beilina and M.V. Klibanov, A globally convergent numerical method for a coefficient inverse problem, *SIAM J. Sci. Comp.*, 31, 478–509, 2008. © 2008 Society for Industrial and Applied Mathematics. Reprinted with permission

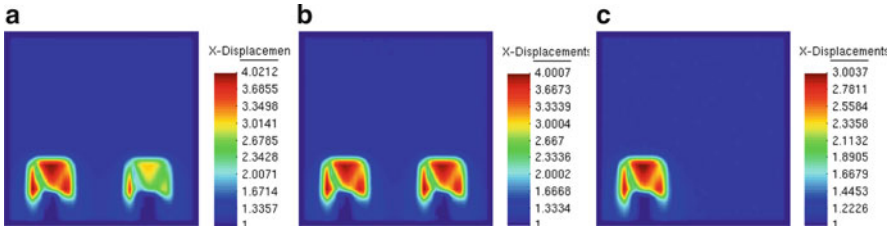

Fig. 3.12 Test 4: The spatial distribution of the function $c_{1,1}(x)$ with the exact tail using the finite difference formula (3.4). (**a**), (**b**) and (**c**) correspond to (**a**), (**b**) and (**c**) of Fig. 3.2, respectively. Source: L. Beilina and M.V. Klibanov, A globally convergent numerical method for a coefficient inverse problem, *SIAM J. Sci. Comp.*, 31, 478–509, 2008. © 2008 Society for Industrial and Applied Mathematics. Reprinted with permission

function $q_{1,1}$, since we have observed computationally that relative L_2-norms (3.8) and (3.9) equal zero for $n = k = 1$.

We present reconstruction results using two different methods for computing of the function $c_{1,1}(x)$. On Fig. 3.12, the function $c_{1,1}(x)$ is approximated using finite difference discretization formula (3.4). However, on Fig. 3.13, we have computed $c_{1,1}(x)$ using the variational formulation of (2.11). On Figures 3.12a and 3.13a $c = 4$ in the left small square and $c = 3$ in the right small square (as in Test 1). On Figs. 3.12b and 3.13b $c = 4$ in both small squares (as in Test 2), and $c = 3$ in the one small square on Figs. 3.12c and 3.13c (as in Test 3).

One can observe that reconstructions are almost ideal ones. Indeed, even shapes of inclusions resemble well the correct ones. Reconstructions are not completely ideal ones on Fig. 3.12 because of inevitable computational and approximation

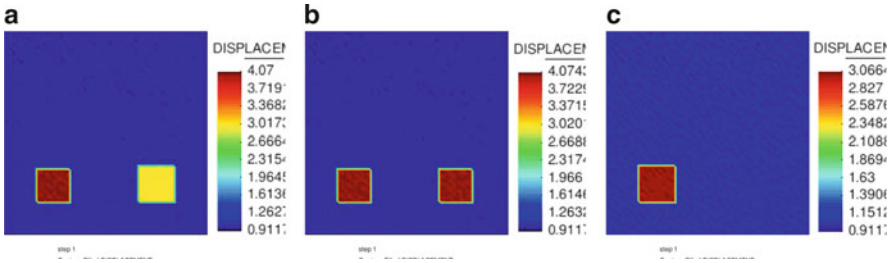

Fig. 3.13 Test 4: The spatial distribution of the function $c_{1,1}(x)$ with the exact tail using the variational formulation; see (3.10)–(3.13). (**a**), (**b**) and (**c**) correspond to (**a**), (**b**) and (**c**) of Fig. 3.2, respectively. Comparison with Fig. 3.12 shows that the variational formulation (3.14) provides a better accuracy than the finite difference formula (3.4)

errors in (3.4), as well as the 5% noise in the data. At the same time, the reconstruction on Fig. 3.13 is more accurate than the one of Fig. 3.12.

We now explain how do we reconstruct the function $c(x)$ in Test 4, using the variational formulation of (2.11). This formulation is similar with the one of [9,110, 135,147,149,150]. Once the pair of functions $(V_{n,i}, q_{n,i})$ is calculated, we calculate the function $v_{n,i}(x)$ by (2.41):

$$v_{n,i}(x) = -hq_{n,i}(x) - h\sum_{j=0}^{n-1} q_j(x) + V_{n,i}(x), \ x \in \Omega. \tag{3.10}$$

Next, we recall that we should have

$$v_{n,i}(x) = \frac{\ln w_{c_{n,i}}(x, s_n)}{s_n^2}, \tag{3.11}$$

where the function $w_{c_{n,i}}(x, s_n)$ is the solution of the following analog of the problem (2.11) and (2.12):

$$\Delta w_{c_{n,i}} - s_n^2 c_{n,i}(x) w_{c_{n,i}} = 0 \text{ in } \Omega, \tag{3.12}$$

$$\partial_n w_{c_{n,i}} |_{\partial\Omega} = f_{n,i}(x), \tag{3.13}$$

where:

$$f_{n,i}(x) = \partial_n \exp\left[s_n^2 v_{n,i}(x)\right] \text{ for } x \in \partial\Omega.$$

Hence, using (3.10), we calculate the function $w_{c_{n,i}}(x) = \exp\left[s_n^2 v_{n,i}(x)\right]$.

To find $c_{n,i}$ from (3.12), we will formulate the FEM for the problem (3.12) and (3.13). First, we introduce the finite element trial space V_h, defined by

$$V_h := \{u \in H^1(\Omega) : u|_K \in P_1(K), \forall K \in K_h\},$$

where $P_1(K)$ denotes the set of linear functions on the element K of the finite element mesh K_h. Hence, the finite element space V_h consists of continuous piecewise linear functions in space. To approximate functions $c_{n,i}$, we introduce space of piecewise constants C_h defined by

$$C_h := \{u \in L_2(\Omega) : u|_K \in P_0(K), \forall K \in K_h\},$$

where $P_0(K)$ is the piecewise constant function defined in the vertices of the element K of the mesh K_h; see also assumption about functions $c_{n,i}$ in Sect. 4.2.

Now, the finite element formulation for (3.12) and (3.13) reads, find $c_{n,i} \in C_h, w_{c_{n,i}} \in V_h$ such that $\forall v \in V_h$

$$(c_{n,i} w_{c_{n,i}}, v) = -\frac{1}{s_n^2}(\nabla w_{c_{n,i}}, \nabla v) + \frac{1}{s_n^2}(f_{n,i}, v)_{\partial\Omega}, \tag{3.14}$$

where:

$$(\alpha, \beta) = \int_\Omega \alpha\beta \, dx$$

is L_2 inner product.

Next, we expand $w_{c_{n,i}}$ in terms of the standard continuous piecewise linear functions $\{\varphi_k\}_{k=1}^N$ in space as

$$w_{c_{n,i}} = \sum_{k=1}^N w_{c_{n,i}k}\varphi_k(x),$$

where $w_{c_{n,i}k}$ denote the nodal values of the already computed functions $v_{n,i}$ with the nodal values $v_{n,ik}$,

$$w_{c_{n,i}k} = \exp\left[s_n^2 v_{n,ik}(x)\right] \forall x \in \Omega,$$

substitute this expansion in the variational formulation (3.14) with $v(x) = \varphi_j(x)$, and obtain the following system of discrete equations:

$$\sum_{k,j=1}^N c_{n,ik}(w_{c_{n,i}k}\varphi_k, \varphi_j) = -\frac{1}{s_n^2}\sum_{k,j=1}^N w_{c_{n,i}k}(\nabla\varphi_k, \nabla\varphi_j) + \frac{1}{s_n^2}\sum_{j=1}^N (f_{n,i}, \varphi_j)_{\partial\Omega}, \tag{3.15}$$

which can be rewritten for all elements $K \in \Omega$ as

$$\sum_{K\in\Omega}\sum_{k,j=1}^N c_{n,ik}(w_{c_{n,ik}}\varphi_k \circ F_K, \varphi_j \circ F_K)_K = -\frac{1}{s_n^2}\sum_{K\in\Omega}\sum_{k,j=1}^N w_{c_{n,ik}}(\nabla\varphi_k \circ F_K, \nabla\varphi_j \circ F_K)_K$$
$$+ \frac{1}{s_n^2}\sum_{K\in\Omega}\sum_{j=1}^N (f_{n,i}, \varphi_j \circ F_K)_{\partial\Omega(K)}.$$

In the formula above F_K defines the mapping such that $F_K(\hat{K}) = K$ where $\hat{\varphi}$ defines the basis function on the reference element $\hat{K}$. For computations of entries in the above system we define

$$\begin{aligned} \varphi \circ F_K &= \hat{\varphi}, \\ \nabla\varphi \circ F_K &= DF_K^{*-1}\hat{\nabla}\hat{\varphi}. \end{aligned} \tag{3.16}$$

Here, $\nabla = (\partial/\partial_x, \partial/\partial_y, \partial/\partial_z)^T$, $\hat{\nabla} = (\partial/\partial_{\hat{x}}, \partial/\partial_{\hat{y}}, \partial/\partial_{\hat{z}})^T$ and DF_K^{*-1} is the inverse of the transposed Jacobian matrix of F_K, see details in [61].

The system (3.15), can be rewritten in the matrix form for the unknown $c_{n,i}$ and known $w_{c_{n,i}}$ as

$$Mc_{n,i} = -\frac{1}{s_n^2}Gw_{c_{n,i}} + \frac{1}{s_n^2}F. \tag{3.17}$$

Here, M is the block mass matrice in space, G is the stiffness matrix corresponding to the gradient term and F is the load vector. At the element level, the matrix entries in (3.17) are explicitly given by

$$M_{k,j}^K = (w_{c_{n,i}k}\,\varphi_k \circ F_K, \varphi_j \circ F_K)_K, \tag{3.18}$$

$$G_{k,j}^K = (\nabla\varphi_k \circ F_K, \nabla\varphi_j \circ F_K)_K, \tag{3.19}$$

$$F_{j,m}^K = (f_{n,i}, \varphi_j \circ F_K)_{\partial\Omega(K)}, \tag{3.20}$$

where $\partial\Omega(K)$ is the boundary of the element K and $\partial\Omega(K) \in \partial\Omega$.

To obtain an explicit scheme for the computation of the coefficients $c_{n,i}$, we approximate M by the lumped mass matrix M^{L} in space, i.e., the diagonal approximation obtained by taking the row sum of M [78, 89], and get the following equation:

$$c_{n,i} = -\frac{1}{s_n^2}(M^{\mathrm{L}})^{-1}Gw_{c_{n,i}} + \frac{1}{s_n^2}(M^{\mathrm{L}})^{-1}F. \tag{3.21}$$

Test 5. While our method does not require a good a priori guess about the solution, the main point of this test is to show that a reconstruction algorithm, which is based on the minimization of a least squares objective functional, might lead to a poor reconstruction, if a good first guess about the solution is unavailable. We use the reconstruction algorithm described in [21], where the inverse problem is formulated as an optimal control problem of the minimization of a least squares objective functional. The latter is solved by the quasi-Newton method, which is known to be a good method for this purpose. This method minimizes the Lagrangian; see details in Chap. 4. We generate the data for the inverse problem using the same computational mesh as well as the same parameters as the ones of Test 2. We start the minimization the quasi-Newton method with different values of the first guess for the parameter $c_{\text{guess}}(x) \equiv$ const. at all points of the computational domain Ω. Figure 3.14 displays the images of the computed function $c_{\text{comp}}(x)$ for the following initial guesses: on (a), $c_{\text{guess}}(x) \equiv 1$; on (b), $c_{\text{guess}}(x) \equiv 1.5$; and on (c), $c_{\text{guess}}(x) \equiv 2$. We observe

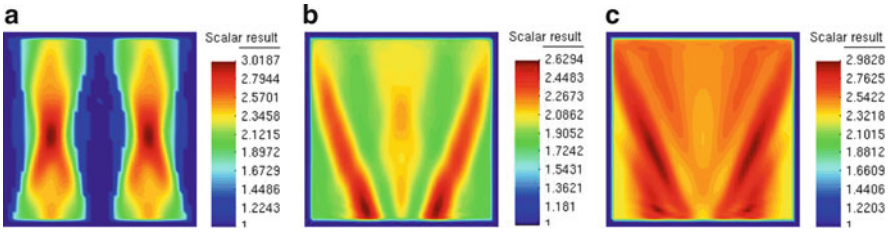

Fig. 3.14 Test 5: Spatial distributions of functions $c_{\text{comp}}(x)$ for different initial guesses $c_{\text{guess}}(x) \equiv$ const. These images were obtained via the minimization of a least squares residual functional by the quasi-Newton method. The correct image is displayed on Fig. 3.2b. (**a**) $c_{\text{guess}}(x) \equiv 1$. (**b**) $c_{\text{guess}}(x) \equiv 1.5$. (**c**) $c_{\text{guess}}(x) \equiv 2$. Compare with the last image of Fig. 3.7 (Test 2), which was obtained for the same data by the approximately globally convergent numerical method. Source: L. Beilina and M.V. Klibanov, A globally convergent numerical method for a coefficient inverse problem, *SIAM J. Sci. Comp.*, 31, 478–509, 2008. © 2008 Society for Industrial and Applied Mathematics. Reprinted with permission

that images deteriorate from (a) to (c) with the deterioration of the first guess. Even the closest first guess $c_{\text{guess}}(x) \equiv 1$ provides an image whose quality is significantly worse than the quality of the last image on Fig. 3.7. We conjecture that local minima are achieved in all these three cases.

3.2 Numerical Study in 3D

3.2.1 Computations of the Forward Problem

We work with the computationally simulated data. To solve the forward problem, we again use the hybrid FEM/FDM method described in [30]. The computational domain in all our tests is the rectangular prism:

$$G = [-4, 4] \times [-5, 5] \times [-2.4, 2].$$

We represent G as $G = G_{\text{FEM}} \cup G_{\text{FDM}}$, where the finite element subdomain is

$$G_{\text{FEM}} := \Omega = [-3, 3] \times [-3, 3] \times [-2, 1.4],$$

and the surrounding subdomain G_{FDM} is the one where the finite differences are used with a structured mesh; see Fig. 3.15. The space mesh in the domain $\Omega = G_{\text{FEM}}$ consists of tetrahedra. The space mesh in G_{FDM} consists of cubes with the mesh size $\tilde{h} = 0.2$ in the overlapping regions. The inclusion which we intend to reconstruct is a small cube inside Ω. This cube is $[1, 2] \times [-2, -1] \times [-1, 0]$. Thus, the length of the side of this cube equals 1. We remind that our algorithm does not use any knowledge of the background values of the unknown coefficient inside the domain of interest Ω.

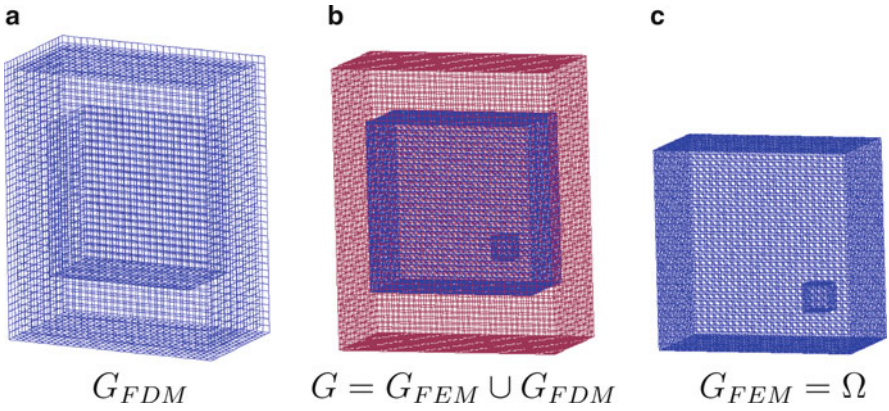

Fig. 3.15 The hybrid mesh (**b**) is a combinations of a structured mesh (**a**), where the FDM is applied and a mesh (**c**), where we use the FEM, with a thin overlapping of structured elements. The solution of the inverse problem is computed in the rectangular prism Ω and $c(x) = 1$ for $x \in G \setminus \Omega$

The forward problem is computed in the domain $G \subset \mathbb{R}^3$ (Fig. 3.15). The coefficient $c(x)$ is unknown in the domain $\Omega \subset G$ and

$$c(x) = 1 \text{ in } G \setminus \Omega;$$

see (2.3). The trace $g(x,t)$ of the solution of the forward problem is recorded at the boundary $\partial\Omega$; see (2.5). Next, the coefficient $c(x)$ is "forgotten," and our goal is to reconstruct this coefficient for $x \in \Omega$ from the data $\varphi(x,s)$. The function $\varphi(x,s)$ is the Laplace transform (2.10) of the function $g(x,t)$ in (2.5). The boundary of the domain G is $\partial G = \partial G_1 \cup \partial G_2 \cup \partial G_3$. Here, ∂G_1 and ∂G_2 are respectively top and bottom sides of the largest domain of Fig. 3.15, and ∂G_3 is the union of vertical (i.e., lateral) sides of this domain. The forward problem in this test is as in (3.2) (Fig. 3.16). The time dependence of the incident plane wave $f(t)$ is

$$f(t) = \begin{cases} \sin(\bar{s}t), \text{ if } 0 \le t \le t_1 := \dfrac{2\pi}{\bar{s}}, \\ 0, \text{ if } t \in (t_1, T), \ T = 12. \end{cases}$$

Thus, the plane wave is initialized at the top boundary ∂G_1 and propagates into G for $t \in (0, t_1]$. First-order absorbing boundary conditions are used on $\partial G_1 \times (t_1, T]$ and $\partial G_2 \times (0, T]$, and the zero Neumann boundary condition is used on the lateral boundary ∂G_3. Since we use explicit scheme to compute hybrid FEM/FDM solution of the wave equation, the time step τ is chosen correspondingly to CFL (Courant-Friedrichs-Lewy) condition [61]

$$\tau \le \frac{h}{\sqrt{3}c_{\max}} \tag{3.22}$$

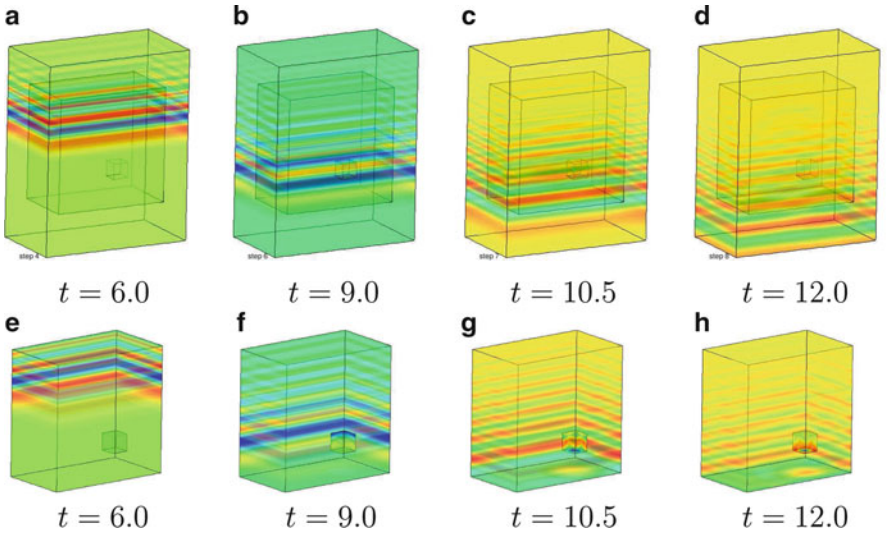

Fig. 3.16 Test 1: Isosurfaces of the simulated exact solution to the forward problem (3.2) at different times with a plane wave initialized at the top boundary. In (**a**)–(**d**) are presented isosurfaces of the hybrid FEM/FDM solution, and in (**e**)–(**h**) are corresponding isosurfaces only for FEM solution

with

$$c_{\max} = \max_{\bar{\Omega}} \frac{1}{\sqrt{c(x)}}$$

in the case of (3.2) and is $\tau = 0.03$ in our particular case. This time step corresponds to 400 iterations in time for the time interval $[0, 12]$.

3.2.2 Result of the Reconstruction

We have performed a numerical experiment to reconstruct the medium, which is homogeneous with $c(x) = 1$ except of one small cube, where $c(x) = 4$; see Fig. 3.15c. In our test, we have introduced the multiplicative random noise of the level $\sigma = 5\%$ in the boundary data; see (3.7). We have not assumed any a priori knowledge of neither the structure of this medium nor of the background constant $c(x) = 1$ outside of this small cube. Because of this, the starting value for the tail $V_{1,1}(x, \overline{s})$ was computed via solving the forward problem (3.2) for $c \equiv 1$, which reflects our knowledge of this coefficient only outside of the domain of interest Ω; see (2.3). Let $w_{c\equiv 1}(x, \overline{s})$ be the corresponding function $w(x, s)$ at $s = \overline{s}$. Then, we took

$$V_{1,1}(x, \overline{s}) = \frac{\ln w_{c\equiv 1}(x, \overline{s})}{\overline{s}^2}.$$

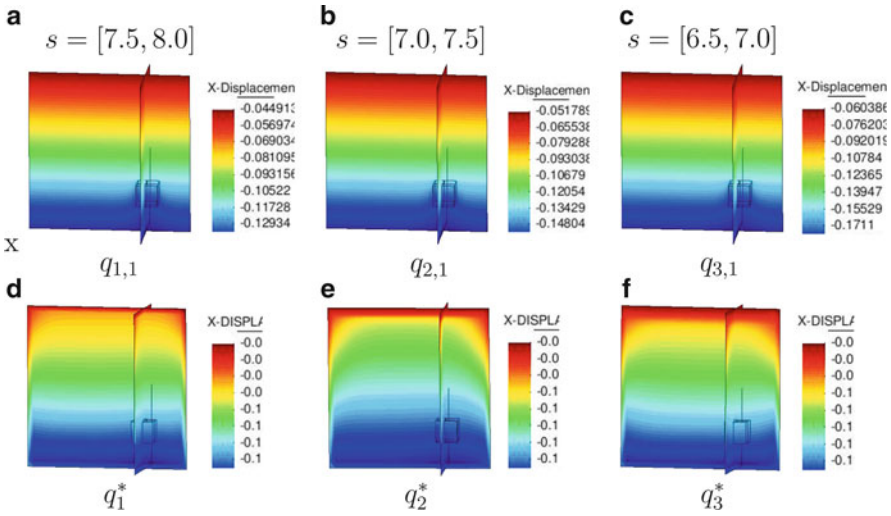

Fig. 3.17 Slices of computed $q_{n,1}$ and exact function q_n^* for $n = 1, 2, 3$. Here, the pseudo frequency interval is $[\underline{s}, \overline{s}] = [4, 8]$, and the step size in pseudo frequency is $h = 0.5$

We have found that the s-interval $s \in [\underline{s}, \overline{s}] = [4, 8]$ is the optimal one for these domains G, Ω. Thus, we have used this interval in our numerical test. We have chosen the step size with respect to the pseudo frequency $h = 0.5$ (Fig. 3.17). Hence, $N = 8$ in our case. Values of parameters λ and ε were

$$\lambda = 20,\ n \in [1, \overline{N}];$$
$$\varepsilon_1 = 0.01;\ \varepsilon_n = 0.003, 1 < n \leq 5;\ \varepsilon_n = 0, n \in [6, \overline{N}].$$

The resulting computed function was $c(x) := c_{\overline{N}}(x)$.

We now choose a new stopping rule. When calculating iterations with respect to the nonlinear term (Sect. 2.6.1), we consider discrete numbers F_n^k:

$$F_n^k = \frac{||q_{n,1}^k|_{\partial\Omega} - \overline{\psi}_n||_{L_2(\partial\Omega)}}{||\overline{\psi}_n||_{L_2(\partial\Omega)}}, \tag{3.23}$$

where L_2-norms are understood in the discrete sense. For each n, we stop our iterations with respect to the nonlinear terms when, i.e., with respect to k, if

$$\begin{aligned} &\text{either } F_n^k \geq F_n^{k-1} \\ &\text{or } |F_n^k - F_n^{k-1}| \quad \leq \theta, \end{aligned} \tag{3.24}$$

where $\theta = 0.001$ is a small tolerance number of our choice. Next, we iterate with respect to the tails. Similarly with (3.23), let

Table 3.1 $F_{n,i}, n = 1, \ldots, 10$. Computations was performed with the noise level $\sigma = 5\%$ and with the regularization parameter $\gamma = 0.01$

It.nr.	$i = 1$	$i = 2$	$i = 3$	$i = 4$	$i = 5$	$i = 6$
1	0.202592	0.202984				
2	0.208818	0.191831	0.19212			
3	0.187327	0.175833	0.176045			
4	0.152134	0.203397	0.204205			
5	0.17487	0.202605	0.202889	0.203076	0.203103	0.202986
6	0.206424	0.202276	0.202091	0.201566	0.201046	0.200468
7	0.203256	0.200669	0.198746	0.195911	0.195683	
8	0.191367	0.195898	0.194232			
9	0.188395	0.195584	0.194025			
10	0.187154	0.19684	0.197282			

$$F_{n,i} = \frac{||q_{n,i}|_{\partial\Omega} - \overline{\psi}_n||_{L_2(\partial\Omega)}}{||\overline{\psi}_n||_{L_2(\partial\Omega)}}. \tag{3.25}$$

For each n, we stop iterations with respect to the tails, i.e., with respect to i, if

$$\begin{aligned} &\text{either } F_{n,i} \geq F_{n,i-1} \\ &\text{or } |F_{n,i} - F_{n,i-1}| \leq \theta. \end{aligned} \tag{3.26}$$

In other words, we stop iterations with respect to the tails, when either norms $F_{n,i}$ start to grow or are stabilized. The number i, on which these iterations are stopped, is denoted as $i := m_n$. Once the criterion (3.26) is met, we take the last computed pair (q_{n,m_n}, V_{n,m_n}), set $q_n := q_{n,m_n}$, $V_{n+1,1} := V_{n,m_n}$, and run computations again for q_{n+1}. Hence, the number m_n of iterations with respect to the tails as well as the reconstructed function $c_n(x)$ is chosen automatically "inside" each iteration for q_n, which means that m_n varies with n (Table 3.1).

Therefore, new criteria (3.23)–(3.26) mean a more flexible stopping rule in the globally convergent algorithm compared with Sect. 3.1.3, since in Sect. 3.1.3, numbers m_n where not chosen automatically.

The next important question is about the stopping rule with respect to n. We stop iterations with respect to n at $n = \overline{N}$ when the norms $F_{n,i}$ generally stabilize with respect to n; see the fourth Remark 2.9.4 for explanations.

Table 4.8 shows computed norms $F_{n,i}$. Using this table, we analyze results of the reconstruction. One can see from Table 4.8 that the number m_n of iterations with respect to tails indeed varies with n, since m_n is chosen automatically now using the criterion (3.24). We observe that the norms $F_{n,i}$ decrease until computing the function $q_{4,1}$. Next, they slightly grow and are stabilize for $n = 6$. The computed L_2-norms of the reconstructed functions $c_{n,i}(x)$ (not presented here) are also stabilized for $n = 6$. Thus, we conclude that we can take $c_{6,6}(x)$ as the solution resulting from our approximately globally convergent method, $c_{6,6}(x) := c_{\text{glob}}(x)$.

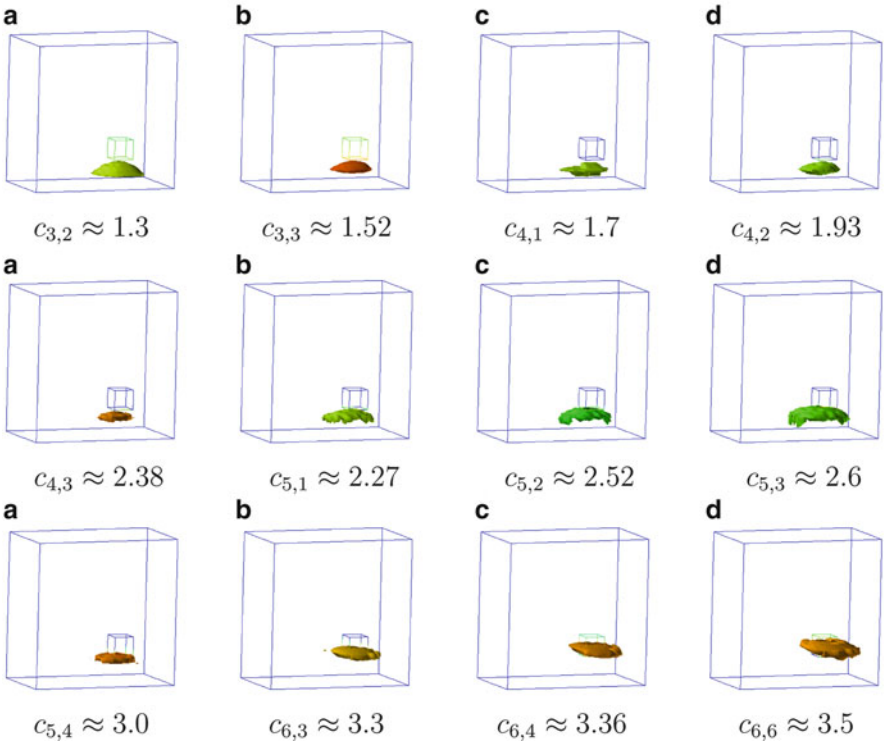

Fig. 3.18 Spatial distribution of functions $c_{n,i}$ after computing $q_{n,i}; n = 1$–5, where n is the number of the computed function q and i is the number of the iteration with respect to the tails. The final image is $c_{6,6}(x) := c_{\text{comp}}(x)$. Compare with Fig. 3.15c where the real image is displayed. The maximal value of $c_{\text{comp}}(x) = 3.5$ in the imaged inclusion. Also, $c_{\text{comp}}(x) = 1$ outside of the imaged inclusion, which is the correct value

One can see from Fig. 3.18 that the location of the small cube is imaged well. It follows from Fig. 3.18d that the imaged contrast in this cube is $3.5 : 1 = \max c_{6,6} : 1$ at $n := \overline{N} = 6$. Thus, we have obtained the 12.5% error (0.3/4) in the imaged contrast with the level of noise in the data $\sigma = 5\%$. The value of the function $c(x) = 1$ outside of this cube is imaged accurately.

3.3 Summary of Numerical Studies

We have tested our algorithm for three different structures of the medium in the 2D case and for one structure in the 3D case. We have successfully imaged both $4 : 1$ and $3 : 1$ inclusion/background contrasts, which are considered high in inverse problems. Our regularization parameters were the truncation pseudo frequency $\overline{s}$,

the sequences $\{\lambda_n\}_{n=1}^{\overline{N}}$, and $\{\varepsilon_n\}_{n=1}^{\overline{N}}$, as well as iteration numbers n_0 and $\overline{N}$. Here, n_0 is the iteration number at which relative norms (3.8) of gradients of tails are stabilized, and $\overline{N} \in (n_0, N)$ is the total number of functions q_n we have computed. The number $\overline{N}$ is such that the relative norms (3.8) of the unknown coefficient are stabilized. We have used $m_1 = \ldots = m_{n_0} = 4, m_{n_0+1} = \ldots = m_{\overline{N}} = 7$ for the number of iterations with respect to tails. Numbers n_0 and $\overline{N}$ were chosen on the basis of an objective stopping rule. On the other hand, for $n \in \left[\overline{N} + 2, N\right]$, norms (3.8) and (3.9) were abruptly growing. This indicates that our choices of the number $\overline{N}$ of iterations as a regularization parameter were correct ones. In the 3D case, we have stopped when norms $F_{n,i}$ in (3.25) have generally stabilized with respect to n; see Table 4.8.

It is important that our numerical experiments have *consistently* demonstrated good reconstruction results for the *same* parameters and the same *objective* stopping rule in all 2D tests. Levels of the random noise were 5% and 15%. These point toward the robustness of our numerical method. The robustness will be more evident from Chaps. 5 and 6 where results for experimental data with a huge noise are presented.

Another important factor, which we have constantly observed in all our computations of this book, is that parameters, once chosen, work well for all other tests of a series of tests considered. This once again points toward the robustness of our approximately globally convergent algorithm. In all experiments, we have stopped iterations with respect to n when the stabilization occurred. This goes along well with the fourth Remark 2.9.4.

An interesting conclusion can be drawn from the comparison of Fig. 3.6a with Fig. 3.6b as well as from the comparison of Fig. 3.11a with Fig. 3.11b. One can observe that the relative errors in final tails are about the same as those in reconstructed coefficients. This provides a numerical confirmation for estimates (2.275), (2.276), (2.279), and (2.281) of the approximate global convergence Theorem 2.9.4 Indeed, comparison of (2.275) and (2.276) with (2.279) and (2.281) shows that one should anticipate that the error in the reconstructed coefficient should be about the same as the error in the tail function. In addition, results of Test 4 of Sect. 3.1.3 indicate that the main input in the reconstruction error is provided by the error in the tail function; see Figs. 3.12 and 3.13.

On the other hand, results of Test 5 of Sect. 3.1.3 indicate the advantage of our approach over traditional locally convergent numerical methods. It is clear from Fig. 3.14 that the image quality in traditional approaches heavily depends on the quality of the first guess about the solution. This is likely because of the local minima problem of least squares residual functionals.

Chapter 4
The Adaptive Finite Element Technique and Its Synthesis with the Approximately Globally Convergent Numerical Method

4.1 Introduction

In Chap. 2, we have described our approximately globally convergent numerical method for a CIP for the hyperbolic PDE $c(x) u_{tt} = \Delta u$. We remind that the notion of the approximate global convergence was introduced in Definition 1.1.2.1. This method addresses the first central question of this book posed in the beginning of the introductory Chap. 1: *Given a CIP, how to obtain a good approximation for the exact solution without an advanced knowledge of a small neighborhood of this solution?* Theorems 2.8.2 and 2.9.4 guarantee that, within the frameworks of the first and the second approximate mathematical models respectively (Sects. 2.8.4 and 2.9.2), this approximation is obtained indeed for our CIP.

At the same time, since certain approximations were made, the room is left for a refinement. In this chapter, we present a numerical method which is, by our experience, an optimal one for the refinement goal. This is the so-called adaptive finite element technique, which we call *adaptivity* below, for brevity. The adaptivity addresses the second central question of this book posed in the beginning of Chap. 1: *Given a good approximation for the solution of our CIP, how to refine it?* The adaptivity is a locally convergent numerical method, which has a special feature of adaptive local refinements of finite element meshes. As a result, a two-stage numerical procedure is developed in this chapter; see Sect. 4.1.1.

4.1.1 The Idea of the Two-Stage Numerical Procedure

An important part of the current chapter is the synthesis of the adaptivity with the approximately globally convergent numerical method of Chap. 2. This synthesis represents a natural two-stage numerical procedure:

Stage 1. On this stage, the approximately globally convergent method of Chap. 2 is applied. As a result, a good first approximation for the exact solution is obtained.

L. Beilina and M.V. Klibanov, *Approximate Global Convergence and Adaptivity for Coefficient Inverse Problems*, DOI 10.1007/978-1-4419-7805-9_4,

Stage 2. The adaptivity technique is applied. The adaptivity takes the solution of the first stage as the starting point for iterations and refines it.

The first stage provides the input for the adaptivity which any locally convergent algorithm needs at most: a guaranteed good first approximation for the exact solution. An important advantage of using the two-stage numerical procedure follows from Theorem 1.8 Indeed, by this theorem, the approximation obtained on the first stage should be inevitably refined on the second stage. However, a subtle point of Theorem 1.8 is that the refinement is achieved only at a minimizer. Indeed, unless a good first approximation for the exact solution is available, it is unclear how to practically find this minimizer—because of the problem of local minima of the Tikhonov functional. On the other hand, as soon as a good approximation is available, Theorem 1.9.1.2 guarantees that this minimizer can be found indeed and also that it refines that approximation. This once again points toward the importance of the first stage.

The adaptivity minimizes the Tikhonov functional on a sequence of locally refined meshes of standard piecewise linear finite elements. Local mesh refinements enable one to maintain a reasonable compromise between not using an exceedingly large number of finite elements and a good accuracy of resulting solutions. This compromise is the main attractive point of the adaptivity.

4.1.2 The Concept of the Adaptivity for CIPs

The adaptivity technique for classical well-posed problems for PDEs is well known; see, for example, [2,67,87,141]. However, the unstable nature of ill-posed problems represents a radically new difficulty for the adaptivity as compared with the well-posed case. First publications on the adaptivity for ill-posed problems were [15,16]. In [16] a CIP, which is similar with the one of this book, was considered. The adaptivity for this as well as for some other CIPs was also considered in [17–23] and references therein. In addition, we refer to publications [12, 68, 74] where the adaptivity technique for various inverse problems was considered. In particular, in [125], the adaptivity was, quite surprisingly, applied to the classical Cauchy problem for the Laplace equation, for the first time. A significant improvement of computational results was observed in [125].

The first publication of the abovementioned two-stage numerical procedure was the one of the authors of this book [25] with follow-up publications [26–29, 111, 160]. Along with the two-stage procedure, some new ideas of a posteriori error analysis for the adaptivity were developed in [26–29]. Unlike previous works [16–23, 68], a posteriori error analysis of [26–29] does not use specific properties of finite elements. As a result, derivations of a posteriori error estimates became more compact and more sounding from the functional analysis standpoint. Another important new element of [26–29] is that these works analyze the original Tikhonov functional rather than the secondary Lagrangian of some previous publications. We also refer to the publication [11] where a new idea of an a posteriori error estimate for an abstract nonlinear operator is presented.

We point out that we consider a posteriori error estimates only as an auxiliary tool. Indeed, usually a posteriori error analysis is about estimating the accuracy of computing an approximate solution. Unlike this, our goal is to use that accuracy estimate as a tool to decide where to refine the mesh in order to improve the accuracy further.

Previously, a posteriori error estimates in the adaptivity for both CIPs, and the so-called "parameter identification" problems were derived for the Lagrangian. However, because of the ill-posedness, there is no guarantee that such an estimate would imply an error estimate for the regularized coefficient. On the other hand, the regularized coefficient is the true quantity of interest. Motivated by these considerations, the authors of [28, 29] have established a posteriori error estimates for the regularized coefficient. This was done on the basis of an analog of the local strong convexity Theorem 1.9.1.2. Furthermore, the work [111] has actually justified the effort of the accuracy improvement of the regularized coefficient rather than the exact coefficient. Indeed, it follows from [111] and from above Theorems 1.8 and 1.9.1.2, respectively, that the regularized coefficient is closer to the exact coefficient than the first guess, provided that uniqueness theorem holds. Therefore, an improvement of the accuracy of the reconstruction of the regularized coefficient (due to the adaptivity) leads to an improvement of the accuracy of the reconstruction of the exact solution.

In addition, in [29], a new framework of functional analysis for the adaptivity technique for ill-posed problems was proposed; also see, for example, [15], for another possible framework. The main result of [29] is a rigorous guarantee that the accuracy of the reconstruction obtained on a finer mesh is indeed better than the one obtained on the coarser mesh (see Theorems 4.9.3 and 4.11.1 below). The latter is the central fact which justifies mesh refinements for ill-posed problems. Prior to [29], image improvements with mesh refinements were observed only numerically rather than analytically. In this chapter, we describe main results of [16–29]. In particular, we obtain a posteriori error estimates of the accuracy of the reconstruction of the regularized coefficient, rather than of the accuracy of the Lagrangian of previous publications [12, 15, 17, 18, 20–23].

In summary, six main new elements of the results of the authors for the adaptivity technique which are presented in publications [26–29] as well as in the current chapter are:

1. The originating Tikhonov functional rather than the secondary Lagrangian is considered.
2. A certain smoothness of solutions of state and adjoint problems for our hyperbolic CIP is established. This smoothness is a necessary ingredient for a rigorous derivation of the Fréchet derivative of the Tikhonov functional.
3. A new framework of functional analysis is proposed.
4. In a posteriori error analysis, we use Theorem 1.9.1.2.
5. Theorem 1.9.1.2 leads to a posteriori error estimates for the regularized coefficient.
6. It is rigorously guaranteed that the accuracy of the regularized solution improves with mesh refinements.

We now briefly outline the main concept of the adaptivity technique for CIPs. It is inefficient to use an exceedingly fine mesh in computations. Thus, the idea of the adaptivity is to obtain a good accuracy of solutions via local mesh refinements, i.e., refinements in certain rather small subdomains of the original domain. In other words, the adaptivity minimizes the Tikhonov functional several times on a *sequence of locally refined meshes*. Therefore, the *main question* of the adaptivity is, *how to find those subdomains where the mesh should be locally refined?* In the case of nonlinear ill-posed problems, such as CIPs are, this question conventionally is addressed via a posteriori error analysis of the regularization functional. More recently, the accuracy of the reconstruction of the regularized coefficient was estimated a posteriori [111], and it is the latter what is done in this chapter. This became possible because of the local strong convexity Theorem 1.9.1.2. Thus, the mesh is refined locally in such subdomains of the original domain Ω, where a posteriori error analysis indicates the largest error in the reconstructed regularized coefficient. Next, the regularization functional is minimized again on that refined mesh. It is important that the a posteriori analysis uses an upper estimate of the solution rather than the solution itself since the solution is unknown. The latter goes along well with Definitions 1.4.2 and 1.4.3, i.e., with the notion of the conditional well-posedness of Sect. 1.4.

In addition to the above two-stage numerical procedure, the adaptivity was applied in [9] "inside" the approximately globally convergent numerical algorithm of Sect. 2.6.1. Thus, the technique of [9] is a one-stage numerical procedure. An advantage of the idea of [9] is that it leads to faster reconstructions than the two-stage numerical procedure.

4.2 Some Assumptions

First, we need to make a few remarks about some assumptions used in this chapter. It is well known that our CIP is a very complex problem with many yet unknown factors. It is natural, therefore, that some simplifications should be in place to develop the adaptivity theory for this CIP. We now list main simplifying assumptions. The first one is about the smoothness of initial conditions. Indeed, the solution of the Cauchy problem (2.1) and (2.2) is not smooth, because of the δ-function in the initial condition. However, if one would replace the $\delta(x - x_0)$ with its approximation in the distribution sense $\delta_\theta(x - x_0)$, then smoothness would be restored. Here, $\theta \in (0, 1)$ is a small number. The function $\delta_\theta(x - x_0)$ is

$$\delta_\theta(x - x_0) = \begin{cases} C_\theta \exp\left(\frac{1}{|x-x_0|^2-\theta^2}\right), & |x - x_0| < \theta, \\ 0, & |x - x_0| > \theta, \end{cases},$$

$$\int\limits_{\mathbb{R}^3} \delta_\theta(x - x_0)\, \mathrm{d}x = 1.$$

Hence, the constant $C_\theta > 0$ is chosen to ensure the value of this integral. Since the source $x_0 \notin \overline{\Omega}$, then for sufficiently small θ

$$\delta_\theta (x - x_0) = 0 \text{ for } x \in \Omega. \tag{4.1}$$

Thus, the problem (2.1) and (2.2) becomes

$$c(x) u_{tt} = \Delta u, \ (x,t) \in \mathbb{R}^3 \times (0,\infty), \tag{4.2}$$

$$u(x,0) = 0, \ u_t(x,0) = \delta_\theta (x - x_0). \tag{4.3}$$

Recall that the condition (2.5) for the coefficient inverse problem 2.1 is

$$u(x,t) = g(x,t), \forall (x,t) \in \partial\Omega \times (0,\infty). \tag{4.4}$$

To simplify the presentation, we intentionally do not go into tiny details formulating minimal smoothness assumptions for state and adjoint initial boundary value problems. Hence, we impose smoothness assumptions in Sects. 4.6 and 4.7 which can probably be relaxed. Also, instead of formulating in these sections stronger results, which follow from these assumptions, we formulate only those results which we need for our goals. We extensively use in this chapter results of Chap. 4 of the book of Ladyzhenskaya [119] about the smoothness of the solution of the initial boundary value problem for the hyperbolic equation with the Dirichlet boundary condition. Thus, we work only with the Dirichlet boundary condition in Sect. 4.6. It seems from Sect. 5 of Chap. 4 of [119] that the Neumann boundary condition can also be used. However, the full proof of this would require a substantial and space consuming effort to work out results for forward hyperbolic problems. Thus, since we are interested in inverse rather than in forward problems, we consider only the Dirichlet boundary condition in Sect. 4.6. On the other hand, since we also need the same smoothness results for the case of the Neumann boundary condition, we simply assume that these results are valid.

Let the number $T > 0$. Denote

$$Q_T = \Omega \times (0,T), \ S_T = \partial\Omega \times (0,T), \ \Omega_t = \{(x,\tau) : x \in \Omega, \tau = t\}, \forall t \in [0,T]. \tag{4.5}$$

For this value of T, we can consider conditions (4.2)–(4.4) as the initial boundary value problem for (4.2) in $\left(\mathbb{R}^3 \setminus \Omega\right) \times (0,T)$. Since by (2.3), $c(x) = 1$ outside of Ω, then this problem can be uniquely solved. Hence, the function $u(x,t)$ is known in $\left(\mathbb{R}^3 \setminus \Omega\right) \times (0,T)$. Hence, the following two functions g and p are known at the lateral side S_T of the cylinder Q_T

$$u|_{S_T} = g(x,t), \ \partial_n u|_{S_T} = p(x,t). \tag{4.6}$$

Let $\omega \in (0,1)$ be a sufficiently small number. Keeping in mind that we work with piecewise linear functions, we introduce the set Y of functions $c(x)$ satisfying the following conditions:

$$Y = \begin{cases} c \in C\left(\overline{\Omega}\right) \cap H^1(\Omega), \partial_{x_i} c \in L_\infty(\Omega), i = 1,2,3, \\ c(x) \in (1-\omega, d+\omega) \text{ for } x \in \overline{\Omega}. \end{cases} \tag{4.7}$$

We introduce now another simple assumption. In all our analytical derivations, we assume that the function $c(x) \in Y$. However, in computations, the function $c(x)$ is piecewise constant defined at the mesh points.

4.3 State and Adjoint Problems

In the adaptivity, we work with a finite dimensional space of standard piecewise linear finite elements. In other words, we assume that the unknown coefficient $c(x)$ in (4.2) belongs to this space. We minimize the following Tikhonov functional on a sequence of locally refined meshes:

$$E_\alpha(c) = \frac{1}{2}\int\limits_{S_T} (u|_{S_T} - g(x,t))^2 z_\zeta(t)\, d\sigma dt + \frac{1}{2}\alpha \int\limits_{\Omega} (c - c_{\text{glob}})^2 \, dx, \tag{4.8}$$

where c_{glob} is the solution obtained on the first stage of our two-stage numerical procedure, i.e., c_{glob} is the solution obtained by the approximately globally convergent method of Sect. 2.6. In (4.8), α is the regularization parameter. Here, the function $z_\zeta(t)$ is introduced to ensure that compatibility conditions are satisfied for the adjoint problem (4.10) at $t = T$. Let $\zeta > 0$ be a sufficiently small number. Then the function $z_\zeta(t) \in C^\infty[0,T]$ is

$$z_\zeta(t) = \begin{cases} 1 \text{ for} \in [0, T-\zeta], \\ 0 \text{ for } t \in \left(T - \frac{\zeta}{2}, T\right], \\ \text{between 0 and 1 for } t \in \left(T-\zeta, T-\frac{\zeta}{2}\right). \end{cases}$$

We use the $L_2(\Omega)$ norm in the second term of the right-hand side of (4.8) because we work in a finite dimensional space of finite elements.

We now introduce the *state* and *adjoint* initial boundary value problems. The state problem is

$$\begin{aligned} c(x) u_{tt} - \Delta u &= 0 \text{ in } Q_T, \\ u(x,0) = u_t(x,0) &= 0, \\ \partial_n u|_{S_T} &= p(x,t). \end{aligned} \tag{4.9}$$

The *adjoint problem* is the one with the reversed time:

$$\begin{aligned} c(x)\lambda_{tt} - \Delta\lambda &= 0 \text{ in } Q_T, \\ \lambda(x,T) &= \lambda_t(x,T) = 0, \\ \partial_n\lambda\,|_{S_T} &= z_\zeta(t)(g-u)(x,t). \end{aligned} \tag{4.10}$$

In (4.9) and (4.10), functions p and g are the ones of (4.6). Hence, to solve the adjoint problem, one should solve the state problem first.

The weak solution of the problem (4.9) is defined as any function $u \in H^1(Q_T)$ with $u(x,0) = 0$ satisfying the following integral identity (see Sect. 5 of Chap. 4 of [119]):

$$\int\limits_{Q_T} (-c(x)u_t v_t + \nabla u \nabla v)\,dxdt - \int\limits_{S_T} pv\,dS_{x,t} = 0,\ \forall v \in H^1(Q_T),\ v(x,T) = 0. \tag{4.11}$$

The weak solution of the adjoint problem (4.10) is the function $\lambda \in H^1(Q_T)$ such that $\lambda(x,T) = 0$ and

$$\int\limits_{Q_T} (-c(x)\lambda_t v_t + \nabla\lambda\nabla v)\,dxdt - \int\limits_{S_T} z_\zeta(g-u)v\,dS_{x,t} = 0, \forall v \in H^1(Q_T), v(x,0) = 0. \tag{4.12}$$

We now formulate an error estimate for interpolants in the format, which is convenient for our derivations below. Let h and be the maximal grid step size of standard piecewise linear finite elements with for $x \in \Omega$. For any function $f \in C(\overline{\Omega}) \cap H^1(\Omega)$, let f^I be its interpolant via those finite elements. Let partial derivatives $f_{x_i} \in L_\infty(\Omega)$. Then

$$\left\| f - f^I \right\|_{C(\overline{\Omega})} \leq K \left\| \nabla f \right\|_{L_\infty(\Omega)} h, \tag{4.13}$$

where the positive constant $K = K(\Omega)$ depends only on the domain Ω. Estimate (4.13) follows from the formula 76.3 in [67].

4.4 The Lagrangian

We start our derivations for the adaptivity from the Lagrangian rather than from the Tikhonov functional. This is because historically it was started from the Lagrangian in [16–22]. The Tikhonov functional is more general, and the Lagrangian is only a secondary one to the Tikhonov functional. Thus, we work with the Tikhonov functional in Sects. 4.7–4.11.

Introduce the following spaces of real valued functions:

$$H_u^1(Q_T) = \left\{f \in H^1(Q_T) : f(x,0) = 0\right\},$$
$$H_\lambda^1(Q_T) = \left\{f \in H^1(Q_T) : f(x,T) = 0\right\},$$
$$U^2 = H^2(Q_T) \times H^2(Q_T) \times C\left(\overline{\Omega}\right),$$
$$U^1 = H_u^1(Q_T) \times H_\lambda^1(Q_T) \times C\left(\overline{\Omega}\right),$$
$$U^0 = L_2(Q_T) \times L_2(Q_T) \times L_2(\Omega).$$

Hence, $U^2 \subset U^1 \subset U^0$ as a sets, and sets U^2, U^1 are dense in U^0. Let h be the maximal grid step size of standard piecewise linear finite elements in space. We introduce finite element subspaces $W_h^u \subset H_u^1(Q_T)$ and $W_h^\lambda \subset H_\lambda^1(Q_T)$ of standard piecewise linear finite elements in space and time. Obviously,

$$u(x,0) = 0, \forall u \in W_h^u,$$
$$\lambda(x,T) = 0, \forall \lambda \in W_h^\lambda.$$

To work with the target coefficient $c(x)$, we also introduce the subspace $V_h \subset L_2(\Omega)$ of standard piecewise linear finite elements. Denote $U_h = W_h^u \times W_h^\lambda \times V_h$. Obviously, $\dim U_h < \infty$, $U_h \subset U^1$ and $U_h \subset U^0$ as a set. So, we consider U_h as a discrete analogue of the space U^1. We introduce the same norm in U_h as the one in U^0, $\|\bullet\|_{U_h} := \|\bullet\|_{U^0}$.

To solve the problem of the minimization of the functional (4.8), we introduce the Lagrangian

$$L(v) = E_\alpha(c) - \int\limits_{Q_T} c(x) u_t \lambda_t \mathrm{d}x\mathrm{d}t + \int\limits_{Q_T} \nabla u \nabla \lambda \mathrm{d}x\mathrm{d}t - \int\limits_{S_T} p\lambda \mathrm{d}\sigma\mathrm{d}t, \tag{4.14}$$

where functions $u \in H_u^1(Q_T)$ and $\lambda \in H_\lambda^1(Q_T)$ are weak solutions of problems (4.9) and (4.10), respectively, and $v = (u, \lambda, c)$. By (4.11) the sum of integral terms in (4.14) equals zero. The reason of considering the Lagrangian instead of $E_\alpha(u,c)$ is that it is easier to find a stationary point of $L(v)$ compared with $E_\alpha(u)$. To minimize the Lagrangian, we need to calculate its Fréchet derivative and set it to zero.

Both functions u and λ depend on the coefficient c. Hence, in order to calculate the Fréchet derivative rigorously, one should assume that variations of functions u and λ depend on variations of the coefficient c and calculate the Fréchet derivative of $\widetilde{L}(c) := L(v(c))$. To do this, one needs, therefore, to consider Fréchet derivatives of functions u and λ with respect to the coefficient c in certain functional spaces. A rigorous derivation of the Fréchet derivative for the Tikhonov functional (4.8) is far from trivial. We need two preparatory Sects. 4.6 and 4.7 to finally derive it rigorously in Sect. 4.8.

Now, we describe a simpler heuristic approach of the derivation of the Fréchet derivative for (4.14). The advantage of the heuristic approach is that it is free from lengthy calculations, while the final result is still the same as the one for the rigorous approach. We assume that in (4.14), functions u, λ, c can be varied independently on each other. However, as soon as the Fréchet derivative is calculated, we assume that solutions u and λ of state (4.9) and adjoint (4.10) problems do depend on the coefficient c.

Thus, we search for a stationary point of the functional $L(v), v \in U^1$ satisfying

$$L'(v)(\overline{v}) = 0, \quad \forall \overline{v} = (\overline{u}, \overline{\lambda}, \overline{c}) \in U^1, \tag{4.15}$$

where $L'(v)(\cdot)$ is the Fréchet derivative of L at the point v under the above assumption of the mutual independence of functions u, λ, c. To find $L'(v)(\overline{v})$, consider $L(v+\overline{v}) - L(v)$, $\forall \overline{v} \in U^1$ and single out the linear, with respect to $\overline{v}$, part of this expression. We obtain from (4.14) and (4.15)

$$\begin{aligned} L'(v)(\overline{v}) = & \int_\Omega \left(\alpha \left(c - c_{\text{glob}}\right) - \int_0^T u_t \lambda_t \, \mathrm{d}t \right) \overline{c} \, \mathrm{d}x \\ & + \left[\int_{Q_T} \left(-c u_t \overline{\lambda}_t + \nabla u \nabla \overline{\lambda} \right) \mathrm{d}x\mathrm{d}t - \int_{S_T} p \overline{\lambda} \, \mathrm{d}\sigma \mathrm{d}t \right] \\ & + \left[\int_{Q_T} \left(-c \lambda_t \overline{u}_t + \nabla \lambda \nabla \overline{u} \right) \mathrm{d}x\mathrm{d}t - \int_{S_T} z_\zeta \left(g - u \mid_{S_T} \right) \overline{u} \, \mathrm{d}\sigma \mathrm{d}t \right] = 0, \\ & \forall \overline{v} = \left(\overline{u}, \overline{\lambda}, \overline{c} \right) \in U^1. \end{aligned} \tag{4.16}$$

Using (4.9)–(4.12), we obtain that second and third lines of (4.16) equal zero. Hence,

$$L'(v)(x) = \alpha \left(c - c_{\text{glob}}\right)(x) - \int_0^T (u_t \lambda_t)(x,t) \, \mathrm{d}t, \quad x \in \Omega. \tag{4.17}$$

Hence, to find the stationary point of the Lagrangian, one should solve the following equation with respect to the function $c(x)$:

$$c(x) = \frac{1}{\alpha} \int_0^T (u_t \lambda_t)(x,t) \, \mathrm{d}t + c_{\text{glob}}(x), x \in \Omega, \tag{4.18}$$

where functions $u \in H_u^1(Q_T)$ and $\lambda \in H_\lambda^1(Q_T)$ are weak solutions of initial boundary value problems (4.9) and (4.10), respectively.

4.5 A Posteriori Error Estimate for the Lagrangian

Let the function $c^*(x)$ satisfying (2.3) and (2.4) be the exact solution of our CIP, $g^*(x,t)$ be the corresponding function (2.5), and $u(c^*)$ be the solution of the Cauchy problem (2.1) and (2.2) with $c := c^*$. Hence, $u^* \mid_{S_T} - g^* = 0$, and the corresponding solution of the adjoint problem (4.10) $\lambda(c^*) = 0$. Denote $v^* = (u(c^*), 0, c^*) \in U^2$. Since the adaptivity is a locally convergent numerical method, we work in this section in a small neighborhood of the exact solution v^*. Hence, since $U^2 \subset U^1$ as a set, we work in this section in the set $V_\delta \subset U^1$,:

$$V_\delta = \left\{ \widehat{v} \in U^1 : \| \widehat{v} - v^* \|_{U^1} < \delta \right\}, \tag{4.19}$$

where $\delta \in (0,1)$ is a sufficiently small number. Let Y be the class of functions defined in (4.7). Suppose that there exists a minimizer $v = (u(c), \lambda(c), c) \in V_\delta$ of the Lagrangian $L(v)$ in (4.14) on the set (4.19). We assume that this minimizer $v = (u(c), \lambda(c), c) \in U^2$. Here, the coefficient $c \in Y$, and functions $u(c) \in H^2(Q_T)$ and $\lambda(c) \in H^2(Q_T)$ are solutions of initial boundary value problems (4.9) and (4.10), respectively. Assume that there exists a minimizer $v_h = (u_h(c_h), \lambda_h(c_h), c_h) \in U_h \cap V_\delta$ of $L(v)$ on the discrete subspace U_h, where the function $c_h \in Y$. Here and below, $u_h(c_h) \in W_h^u$ and $\lambda_h(c_h) \in W_h^\lambda$ are finite element solutions of problems (4.9) and (4.10), respectively, with $c := c_h$ and boundary functions $p, g, u \mid_{S_T}$ in (4.9) and (4.10) are the same as ones for functions $u(c), \lambda(c)$. Hence, the vector function v_h is a solution of the following problem:

$$L'(v_h)(\overline{v}) = 0, \forall \overline{v} \in U_h. \tag{4.20}$$

The equality (4.20) is called *the Galerkin orthogonality principle*; also see, for example, [15, 16], for this principle. Following [16–22], we now present the main steps in the derivation of an a posteriori error estimate for the Lagrangian. We start by writing the equation for the error e in Lagrangian (4.14) as

$$e := L(v) - L(v_h) = \int_0^1 L'(\theta v + (1-\theta) v_h) \, \mathrm{d}\theta = L'(v_h)(v - v_h) + R, \tag{4.21}$$

where the remainder term R has the second order of smallness with respect to δ, and $L'(v_h)$ is the Fréchet derivative of the Lagrangian at the point $v_h = (u_h, \lambda_h, c_h)$. Because the number δ in (4.19) is small, we ignore R in (4.21). Let $v_h^I = (u_h^I, \lambda_h^I, c_h^I) \in U_h$ be the interpolant of $v = (u, \lambda, c)$. We have

$$v - v_h = \left(v_h^I - v_h\right) + \left(v - v_h^I\right). \tag{4.22}$$

Since $(v_h^I - v_h) \in U_h$, then by (4.20),

$$L'(v_h)(v_h^I - v_h) = 0. \tag{4.23}$$

Hence, (4.22) and (4.23) imply that

$$L'(v_h)(v - v_h) = L'(v_h)(v_h^I - v_h) + L'(v_h)(v - v_h^I) = L'(v_h)(v - v_h^I). \quad (4.24)$$

Hence, (4.21) implies that the following approximate error estimate for the Lagrangian holds:

$$e = L(v) - L(v_h) \approx L'(v_h)(v - v_h^I). \quad (4.25)$$

The estimate (4.23) taken alone does not provide anything of a significance. This is because it was derived by the series of steps (4.20)–(4.24) which did not contain any specific information about the Lagrangian L. To make the estimate (4.23) valuable, we need to specify it using the specific form (4.14) of the Lagrangian L. The latter is done below in this section. More precisely, we need to incorporate specifics in the expression $L'(v_h)(v - v_h^I)$.

If state and adjoint problems are solved exactly, then only the first line in the right-hand side of (4.16) should be considered in a posteriori error the analysis of the Fréchet derivative of the Lagrangian. This is because two other lines equal zero by (4.11) and (4.12). However, since we work with $L'(v_h)$ in (4.23) and the vector function $v_h = (u_h(c_h), \lambda_h(c_h), c_h) \in U_h \cap V_\delta$ includes approximate FEM solutions $u_h(c_h), \lambda_h(c_h)$ of state and adjoint problems, then the second and third lines in the right-hand side of (4.16) do not equal zero when functions $u_h(c_h), \lambda_h(c_h), c_h$ are involved in them. Hence, these lines should be taken into account in a posteriori error estimates.

Consider a mesh which is split into triangles/tetrahedral elements K such that $\overline{\Omega} = \cup \overline{K}$. Let h_K be the diameter of the element K. Consider a uniform partition of the time interval $I = [0, T]$ into subintervals $J_k = (t_{k-1}, t_k]$, $0 = t_0 < t_1 < ... < t_N = T$. Let $\tau = t_k - t_{k-1}$ be the grid step size of this partition. In a general case, we allow meshes in space and time with hanging nodes and assume that the local mesh size has bounded variation in such meshes. This means that there exists a constant $\gamma > 0$ such that $\gamma h_{K^+} \le h_{K^-} \le \gamma^{-1} h_{K^+}$ for all neighboring elements K^- and K^+. We define also by h_K the diameter of the finite element K.

Let S be the internal face of the nonempty intersection of the boundaries of two neighboring elements K^+ and K^-. We denote the jump of the derivative of v_h computed from the two elements K^+ and K^- sharing S as

$$[\partial_s v_h] = \partial_s v_h^+ - \partial_s v_h^-. \quad (4.26)$$

The jump of v_h in time computed from the two neighboring time intervals J^+ and J^- is defined similarly:

$$[\partial_t v_h] = \partial_t v_h^+ - \partial_t v_h^-. \quad (4.27)$$

Theorem 4.5 is proved by the technique, which was developed in the earlier publications [16–22]. We derive here an approximate error estimate of the Lagrangian.

In the context of Theorem 4.5, the word "approximate" means not only ignoring the remainder term R in (4.21) but also ignoring residuals of various interpolation estimates appearing in the proof of this theorem. A more advanced approach, which is free from these approximations, was developed in joint publications of the authors of this book [26–29], and it is presented in this chapter below.

Theorem 4.5. *Let Y be the class of functions defined in (4.7). Assume that there exists a minimizer $v = (u(c), \lambda(c), c) \in V_\delta$ of the Lagrangian L in (4.14) on the set (4.19) and $v = (u(c), \lambda(c), c) \in U^2$. Here, the function $c \in Y$ and functions $u(c) \in H^2(Q_T)$ and $\lambda(c) \in H^2(Q_T)$ are solutions of initial boundary value problems (4.9) and (4.10), respectively. Let functions $u(c), \lambda(c) \in C^2(\overline{Q}_T)$. Suppose that there exists a minimizer $v_h = (u_h(c_h), \lambda_h(c_h), c_h) \in U_h \cap V_\delta$ of the Lagrangian L on the discrete subspace U_h, where the function $c_h \in Y$. Then the following approximate estimate of the error $e = L(v) - L(v_h)$ of the Lagrangian holds:*

$$
\begin{aligned}
|e| \le & \int\limits_{S_T} R_{u_1}\sigma_\lambda \,\mathrm{d}\sigma\mathrm{d}t + \int\limits_{Q_T} R_{u_2}\sigma_\lambda \,\mathrm{d}x\mathrm{d}t + \int\limits_{Q_T} R_{u_3}\sigma_\lambda \,\mathrm{d}x\mathrm{d}t \\
& + \int\limits_{Q_T} R_{\lambda_1}\sigma_u \,\mathrm{d}x\mathrm{d}t + \int\limits_{Q_T} R_{\lambda_2}\sigma_u \,\mathrm{d}x\mathrm{d}t + \int\limits_{Q_T} R_{\lambda_3}\sigma_u \,\mathrm{d}x\mathrm{d}t \\
& + \int\limits_{Q_T} R_{c_1}\sigma_c \,\mathrm{d}x\mathrm{d}t + \int\limits_{\Omega} R_{c_2}\sigma_c \,\mathrm{d}x, \qquad (4.28)
\end{aligned}
$$

where the residuals are defined by

$$
\begin{aligned}
& R_{u_1} = |p|, \; R_{u_2} = \max_{S\subset\partial K} h_K^{-1}\left|\left[\partial_s u_h\right]\right|, \\
& R_{u_3} = c_h\tau^{-1}\left|\left[\partial_t u_h\right]\right|, \\
& R_{\lambda_1} = z_\zeta\left|g - u|_{S_T}\right|, R_{\lambda_2} = \max_{S\subset\partial K} h_K^{-1}\left|\left[\partial_s \lambda_h\right]\right|, \\
& R_{\lambda_3} = c_h\tau^{-1}\left|\left[\partial_t \lambda_h\right]\right|, \\
& R_{c_1} = |\partial_t\lambda_h|\cdot|\partial_t u_h|, \; R_{c_2} = |c_h - c_{\mathrm{glob}}|, \qquad (4.29)
\end{aligned}
$$

and the interpolation errors are

$$
\begin{aligned}
& \sigma_\lambda = C\tau\,|[\partial_t\lambda_h]| + Ch_K\,|[\partial_n\lambda_h]|, \\
& \sigma_u = C\tau\,|[\partial_t u_h]| + Ch_K\,|[\partial_n u_h]|, \\
& \sigma_c = C\left|[c_h]\right|. \qquad (4.30)
\end{aligned}
$$

Remark 4.5. In publications [16–22], only the sum of two terms in the last line of (4.28) was used to single out subdomains of the domain Ω where the mesh should be locally refined. The same conclusion is derived from the theory which was developed in joint works of the authors of this book [26–29]; see (4.188) and (4.189).

Proof of Theorem 4.5. In this proof, $C > 0$ denotes different constants independent on h, τ as well as on functions we consider. Using (4.16) and (4.23), we obtain

$$e \approx L'(v_h)(v - v_h^I) = (I_1 + I_2 + I_3), \tag{4.31}$$

where:

$$I_1 = \int\limits_{Q_T} \left[-c_h \partial_t (\lambda - \lambda_h^I) \partial_t u_h + \nabla(\lambda - \lambda_h^I) \nabla u_h \right] \mathrm{d}x\mathrm{d}t - \int\limits_{S_T} p(\lambda - \lambda_h^I)\, \mathrm{d}\sigma\mathrm{d}t, \tag{4.32}$$

$$I_2 = \int\limits_{S_T} z_\zeta (g - u|_{S_T})(u - u_h^I)\, \mathrm{d}\sigma\mathrm{d}t + \int\limits_{Q_T} \left[-c_h \left(\partial_t \lambda_h\right) \partial_t \left(u - u_h^I\right) + \nabla \lambda_h \nabla (u - u_h^I) \right] \mathrm{d}x\mathrm{d}t, \tag{4.33}$$

$$I_3 = -\int\limits_{Q_T} \left(\partial_t \lambda_h\right) \left(\partial_t u_h\right) \left(c - c_h^I\right) \mathrm{d}x\mathrm{d}t + \alpha \int\limits_{\Omega} (c_h - c_{\mathrm{glob}})(c - c_h^I) \mathrm{d}x. \tag{4.34}$$

Integrating by parts in the first and second terms of (4.32), we obtain the following estimate:

$$\begin{aligned} \left|I_1\right| = \Big| & \int_{Q_T} \left(c_h \left(\partial_t^2 u_h\right) (\lambda - \lambda_h^I) - \Delta u_h (\lambda - \lambda_h^I) \right) \mathrm{d}x\mathrm{d}t \\ & - \int_{S_T} p(\lambda - \lambda_h^I)\, \mathrm{d}S\mathrm{d}t + \sum_K \int_0^T \int_{\partial K} \partial_{n_K} u_h (\lambda - \lambda_h^I)\, \mathrm{d}S\mathrm{d}t \\ & - \sum_k \int_\Omega c_h \left[\partial_t u_h\left(t_k\right)\right] (\lambda - \lambda_h^I)(t_k)\, \mathrm{d}x \Big|. \end{aligned} \tag{4.35}$$

Here, terms $\partial_{n_K} u_h$ and $\left[\partial_t u_h\right]$ appear due to the integration by parts and denote, respectively, the derivative of u_h in the outward normal direction n_K at the boundary ∂K of the element K and the jump of the derivative of u_h in time. In the third term of (4.35), we sum over the all boundaries of the element K, and each internal side

$S \in S_h$ occurs twice. Denoting by $\partial_s u_h$, the derivative of a function u_h in one of the normal directions of each side S, we obtain

$$\sum_K \int_{\partial K} \partial_{n_K} u_h (\lambda - \lambda_h^I)\, \mathrm{d}S = \sum_S \int_S \left[\partial_s u_h\right] (\lambda - \lambda_h^I)\, \mathrm{d}s,$$

where $\left[\partial_s u_h\right]$ is the jump of the derivative $\partial_s u_h$ computed from the two elements sharing S defined by (4.26). We distribute each jump equally to the two sharing elements and return to the sum over edges ∂K of the element:

$$\sum_S \int_S \left[\partial_s u_h\right] (\lambda - \lambda_h^I)\, \mathrm{d}S = \sum_K \frac{1}{2} h_K^{-1} \int_{\partial K} \left[\partial_s u_h\right] (\lambda - \lambda_h^I)\, h_K\, \mathrm{d}S.$$

Since $dx \approx h_K dS$, we approximately set $dx = h_K dS$ and replace the integrals over the boundaries ∂K of finite elements by integrals over the finite elements K. Then

$$\left| \sum_K \frac{1}{2} h_K^{-1} \int_{\partial K} \left[\partial_s u_h\right] (\lambda - \lambda_h^I)\, h_K\, \mathrm{d}S \right| \le C \int_\Omega \max_{S \subset \partial K} h_K^{-1} \left|\left[\partial_s u_h\right]\right|_K \cdot \left|\lambda - \lambda_h^I\right| \mathrm{d}x,$$

where $\left[\partial_s u_h\right]\big|_K = \max_{S \subset \partial K} \left[\partial_s u_h\right]\big|_S$.

Similarly we can estimate the fourth term in (4.35):

$$\begin{aligned}
&\left| \sum_k \int_\Omega c_h \left[\partial_t u_h(t_k)\right] (\lambda - \lambda_h^I)(t_k)\, \mathrm{d}x \right| \\
&\quad \le \sum_k \int_\Omega c_h \tau^{-1} \cdot \left|\left[\partial_t u_h(t_k)\right]\right| \cdot \left| (\lambda - \lambda_h^I)(t_k) \right| \, \tau \, \mathrm{d}x \\
&\quad \le C \sum_k \int_{J_k} \int_\Omega c_h \tau^{-1} \cdot \left|\left[\partial_{t_k} u_h\right]\right| \cdot \left|\lambda - \lambda_h^I\right| \mathrm{d}x \mathrm{d}t \\
&\quad = C \int_{Q_T} c_h \tau^{-1} \cdot \left|\left[\partial_t u_h\right]\right| \cdot \left|\lambda - \lambda_h^I\right| \mathrm{d}x \mathrm{d}t,
\end{aligned}$$

where:

$$\left|\left[\partial_{t_k} u_h\right]\right| = \max_{J_k} \left(\left|\left[\partial_t u_h(t_k)\right]\right|, \ \left|\left[\partial_t u_h(t_{k+1})\right]\right| \right), \tag{4.36}$$

and $[\partial u_{ht}]$ is defined as the maximum of the two jumps in time on each time interval J_k appearing in (4.36):

$$[\partial_t u_h] = [\partial_{t_k} u_h] \text{ on } J_k.$$

Substituting both above expressions in the second and third terms in (4.35), we obtain

$$\begin{aligned}\left|I_1\right| \leq & \left| \int_{Q_T} \left(c_h \partial_t^2 u_h - \Delta u_h\right)(\lambda - \lambda_h^I)\, \mathrm{d}x\mathrm{d}t \right| + \left| \int_{S_T} p(\lambda - \lambda_h^I)\, \mathrm{d}\sigma\mathrm{d}t \right| \\ & + C \int_{Q_T} \max_{S \subset \partial K} h_K^{-1} \cdot \left|\left[\partial_s u_h\right]\right| \cdot \left|\lambda - \lambda_h^I\right| \mathrm{d}x\mathrm{d}t \\ & + C \int_{Q_T} c_h \tau^{-1} \cdot \left|\left[\partial_t u_h\right]\right| \cdot \left|\lambda - \lambda_h^I\right| \mathrm{d}x\mathrm{d}t.\end{aligned}$$

Next, we use the standard, elementwise, interpolation estimate for $\lambda - \lambda_h^I$ for every element K and the time interval J_k [67]

$$||\lambda - \lambda_h^I||_{L_2(K \times J_k)} \leq C_i \left(\tau^2 \left\|\lambda_{tt}\right\|_{C\left(\overline{K} \times \overline{J}_k\right)} + h_K^2 \left\|D^2 \lambda\right\|_{C\left(\overline{K} \times \overline{J}_k\right)}\right), \tag{4.37}$$

with an interpolation constant C_i. Here, $D^2\lambda$ denote second order derivative of λ. We obtain

$$\begin{aligned}\left|I_1\right| \leq & C \int_{Q_T} \left|c_h \partial_t^2 u_h - \Delta u_h\right| \cdot \left(\tau^2 \left\|\lambda_{tt}\right\|_{C\left(\overline{K} \times \overline{J}_k\right)} + h_K^2 \left\|D^2 \lambda\right\|_{C\left(\overline{K} \times \overline{J}_k\right)}\right) \mathrm{d}x\mathrm{d}t \\ & + C \int_{S_T} |p| \left(\tau^2 \left\|\lambda_{tt}\right\|_{C\left(\overline{K} \times \overline{J}_k\right)} + h_K^2 \left\|D^2 \lambda\right\|_{C\left(\overline{K} \times \overline{J}_k\right)}\right) \mathrm{d}\sigma\mathrm{d}t \\ & + C \int_{Q_T} \left(\max_{S \subset \partial K} h_K^{-1}\right) |[\partial_s u_h]| \left(\tau^2 \left\|\lambda_{tt}\right\|_{C\left(\overline{K} \times \overline{J}_k\right)} + h_K^2 \left\|D^2 \lambda\right\|_{C\left(\overline{K} \times \overline{J}_k\right)}\right) \mathrm{d}x\mathrm{d}t \\ & + C \int_{Q_T} c_h \tau^{-1} |[\partial_t u_h]| \left(\tau^2 \left\|\lambda_{tt}\right\|_{C\left(\overline{K} \times \overline{J}_k\right)} + h_K^2 \left\|D^2 \lambda\right\|_{C\left(\overline{K} \times \overline{J}_k\right)}\right) \mathrm{d}x\mathrm{d}t.\end{aligned} \tag{4.38}$$

Note that the first integral in (4.38) disappears, since u_h is a continuous piecewise linear function in space and time. We use the following approximation [88]:

$$\begin{aligned}\partial_t^2 \lambda & \approx \frac{\left[\partial_t \lambda_h\right]}{\tau},\ t \in \overline{J}_k, \\ D^2 \lambda & \approx \frac{\left[\partial_n \lambda_h\right]}{h_K}, x \in \overline{K}.\end{aligned} \tag{4.39}$$

Hence,

$$
\begin{aligned}
|I_1| \le\ & C \int\limits_{S_T} |p| \left(\tau^2 \left\| \frac{[\partial_t \lambda_h]}{\tau} \right\|_{C(\overline{K}\times\overline{J}_k)} + h_K^2 \left\| \frac{[\partial_n \lambda_h]}{h_K} \right\|_{C(\overline{K}\times\overline{J}_k)} \right) \mathrm{d}\sigma \mathrm{d}t \\
& + C \int\limits_{Q_T} \max_{S\subset\partial K} h_K^{-1} |[\partial_s u_h]| \left(\tau^2 \left\| \frac{[\partial_t \lambda_h]}{\tau} \right\|_{C(\overline{K}\times\overline{J}_k)} + h_K^2 \left\| \frac{[\partial_n \lambda_h]}{h_K} \right\|_{C(\overline{K}\times\overline{J}_k)} \right) \mathrm{d}x\mathrm{d}t \\
& + C \int\limits_{Q_T} c_h \tau_J^{-1} |[\partial_t u_h]| \left(\tau^2 \left\| \frac{[\partial_t \lambda_h]}{\tau} \right\|_{C(\overline{K}\times\overline{J}_k)} + h_K^2 \left\| \frac{[\partial_n \lambda_h]}{h_K} \right\|_{C(\overline{K}\times\overline{J}_k)} \right) \mathrm{d}x\mathrm{d}t.
\end{aligned}
$$

We estimate I_2 similarly:

$$
\begin{aligned}
|I_2| \le & \int\limits_{Q_T} \left| c_h \partial_t^2 \lambda_h (u - u_h^I) - \Delta \lambda_h (u - u_h^I) \right| \mathrm{d}x\mathrm{d}t + \int_{S_T} z_\zeta \left| (g - u|_{S_T})(u - u_h^I) \right| \mathrm{d}\sigma\mathrm{d}t \\
& + C \int\limits_{Q_T} \max_{S\subset\partial K} h_K^{-1} \cdot \left| \left[\partial_s \lambda_h \right] \right| \cdot \left| u - u_h^I \right| \mathrm{d}x\mathrm{d}t \\
& + C \int\limits_{Q_T} c_h \tau^{-1} \cdot \left| \left[\partial_t \lambda_h \right] \right| \cdot \left| u - u_h^I \right| \mathrm{d}x\mathrm{d}t \\
\le & C \int_0^T \int\limits_{\Omega} \left| c_h \partial_t^2 \lambda_h - \Delta \lambda_h \right| \cdot \left| u - u_h^I \right| \mathrm{d}x\mathrm{d}t \\
& + \int\limits_{S_T} z_\zeta \left| (g - u|_{S_T}) \right| \cdot \left| u - u_h^I \right| \mathrm{d}\sigma\mathrm{d}t \\
& + C \int\limits_{Q_T} \max_{S\subset\partial K} h_K^{-1} \cdot \left| \left[\partial_s \lambda_h \right] \right| \cdot \left| u - u_h^I \right| \mathrm{d}x\mathrm{d}t \\
& + C \int\limits_{Q_T} c_h \tau^{-1} \cdot \left| \left[\partial_t \lambda_h \right] \right| \cdot \left| u - u_h^I \right| \mathrm{d}x\mathrm{d}t.
\end{aligned}
$$

Using (4.37) and (4.39), we estimate the function $\left| u - u_h^I \right|$. Also, we use the fact that λ_h is a piecewise linear function. We obtain

$$
|I_2| \le C \int\limits_{Q_T} \left| c_h \partial_t^2 \lambda_h - \Delta \lambda_h \right| \left(\tau^2 \left\| \frac{[\partial_t u_h]}{\tau} \right\|_{C(\overline{K}\times\overline{J}_k)} + h_K^2 \left\| \frac{[\partial_n u_h]}{h_K} \right\|_{C(\overline{K}\times\overline{J}_k)} \right) \mathrm{d}x\mathrm{d}t
$$

$$
\begin{aligned}
&+\int_{S_T} z_\zeta \,|g-u_{S_T}|\left(\tau^2\left\|\frac{[\partial_t u_h]}{\tau}\right\|_{C(\overline{K}\times\overline{J}_k)}+h_K^2\left\|\frac{[\partial_n u_h]}{h_K}\right\|_{C(\overline{K}\times\overline{J}_k)}\right)\mathrm{d}\sigma\mathrm{d}t\\
&+C\int_{Q_T}\max_{S\subset\partial K} h_K^{-1}\cdot|[\partial_s\lambda_h]|\left(\tau^2\left\|\frac{[\partial_t u_h]}{\tau}\right\|_{C(\overline{K}\times\overline{J}_k)}+h_K^2\left\|\frac{[\partial_n u_h]}{h_K}\right\|_{C(\overline{K}\times\overline{J}_k)}\right)\mathrm{d}x\mathrm{d}t\\
&+C\int_{Q_T} c_h\tau^{-1}\cdot|[\partial_t\lambda_h]|\cdot\left(\tau^2\left\|\frac{[\partial_t u_h]}{\tau}\right\|_{C(\overline{K}\times\overline{J}_k)}+h_K^2\left\|\frac{[\partial_n u_h]}{h_K}\right\|_{C(\overline{K}\times\overline{J}_k)}\right)\mathrm{d}x\mathrm{d}t\\
\le\ &C\int_{S_T} z_\zeta\,|g-u_{S_T}|\cdot\left(\tau^2\left\|\frac{[\partial_t u_h]}{\tau}\right\|_{C(\overline{K}\times\overline{J}_k)}+h_K^2\left\|\frac{[\partial_n u_h]}{h_K}\right\|_{C(\overline{K}\times\overline{J}_k)}\right)\mathrm{d}x\mathrm{d}t\\
&+C\int_{Q_T}\max_{S\subset\partial K} h_K^{-1}\,|[\partial_s\lambda_h]|\left(\tau^2\left\|\frac{[\partial_t u_h]}{\tau}\right\|_{C(\overline{K}\times\overline{J}_k)}+h_K^2\left\|\frac{[\partial_n u_h]}{h_K}\right\|_{C(\overline{K}\times\overline{J}_k)}\right)\mathrm{d}x\mathrm{d}t\\
&+C\int_{Q_T} c_h\tau^{-1}\,|[\partial_t\lambda_h]|\left(\tau^2\left\|\frac{[\partial_t u_h]}{\tau}\right\|_{C(\overline{K}\times\overline{J}_k)}+h_K^2\left\|\frac{[\partial_n u_h]}{h_K}\right\|_{C(\overline{K}\times\overline{J}_k)}\right)\mathrm{d}x\mathrm{d}t
\end{aligned}
$$

To estimate I_3, we use the standard interpolation estimate (4.13) for every element K for the coefficient $c(x)$:

$$\left\|c-c_h^I\right\|_{C(\overline{K})}\le C h_K\left\|\nabla c\right\|_{L_\infty(\overline{K})}$$

Also [88],

$$|\nabla c|\approx\frac{|[c_h]|}{h_K}.$$

We obtain

$$
\begin{aligned}
\left|I_3\right|&\le C\int_{Q_T}|\partial_t\lambda_h|\cdot|\partial_t u_h|\cdot\left\|\nabla c\right\|_{L_\infty(\overline{K})}h_K\,\mathrm{d}x\mathrm{d}t\\
&\quad+C\int_{\Omega}\left|c_h-c_{\mathrm{glob}}\right|\cdot\left\|\nabla c\right\|_{L_\infty(\overline{K})}h_K\,\mathrm{d}x\\
&\le C\int_{Q_T}|\partial_t\lambda_h|\cdot|\partial_t u_h|\cdot|[c_h]|\,\mathrm{d}x\mathrm{d}t\\
&\quad+C\int_{\Omega}|c_h-c_{\mathrm{glob}}|\cdot|[c_h]|\,\mathrm{d}x.
\end{aligned}
$$

Collecting above estimates for I_1, I_2, and I_3, we get a posteriori error estimate (4.28) of the Lagrangian.

4.6 Some Estimates of the Solution an Initial Boundary Value Problem for Hyperbolic Equation (4.9)

In Sect. 4.4, we have heuristically derived formula (4.17) for the Fréchet derivative of the Lagrangian (4.14). It is shown in Sect. 4.8 that the same formula can be derived rigorously for the case of the Tikhonov functional (4.8). However, in order to derive it rigorously, we need to make some preparations in Sects. 4.6 and 4.7. In particular, in this section, we establish certain estimates for the solution of the initial boundary value problem with the Dirichlet boundary condition for the hyperbolic equation (4.9). The initial boundary value problem with the Dirichlet boundary condition for a general hyperbolic equation was studied in Chap. 4 of the book [119]. In particular, Theorems 3.1 and 3.2 of that chapter establish existence and uniqueness of the weak solution of this problem in the space $H^1(Q_T)$. In addition, Theorem 4.1 and Corollary 4.1 of Sect. 4 of Chap. 4 of [119] establish a higher smoothness of the weak solution. It is also important that the proofs of both Theorem 4.1 and Corollary 4.1 provide a tool for the further increase of the smoothness. At the same time, some constants in proofs of these results of [119] are not specified in the form which is convenient for our particular goal. Thus, we specify them in this section. Naturally, we extensively use Theorem 4.1 and Corollary 4.1 of the book [119] in the current section. Still, since we are interested in this book in inverse rather than in forward problems, we do not reformulate these results here.

We refer to (4.5) for notations of domains. Let the function $c \in Y$, where the set Y was defined in (4.7). Denote

$$b(x) = \frac{1}{c(x)}. \tag{4.40}$$

Then

$$b(x) \in \left(\frac{1}{d+\omega}, \frac{1}{1-\omega} \right). \tag{4.41}$$

If

$$c(x) v_{tt} = \Delta v + g(x,t), \tag{4.42}$$

then

$$v_{tt} = \nabla \cdot (b(x) \nabla v) - \nabla b \nabla v + \widetilde{g}(x,t), \ \widetilde{g}(x,t) = b(x) g(x,t). \tag{4.43}$$

Let the function $f(x,t) \in L_2(Q_T)$. Because of (4.40)–(4.43), consider the following initial boundary value problem with the Dirichlet boundary condition:

$$u_{tt} = \nabla \cdot (b(x) \nabla u) - \nabla b \nabla u + f(x,t) \text{ in } Q_T, \tag{4.44}$$

$$u(x,0) = u_t(x,0) = 0, \tag{4.45}$$

$$u|_{S_T} = 0. \tag{4.46}$$

We remind that the function $u \in H^1(Q_T)$ is called the weak solution of the problems (4.44)–(4.46) if it satisfies the initial condition (4.45) as well as the following integral identity:

$$\int\limits_{Q_T} \left(-u_t \eta_t + b(x) \nabla u \nabla \eta\right) \mathrm{d}x\mathrm{d}t + \int\limits_{Q_T} (\nabla b \nabla u) \eta \mathrm{d}x\mathrm{d}t$$
$$= \int\limits_{Q_T} f \eta \mathrm{d}x\mathrm{d}t, \ \forall \eta \in H_0^1(Q_T), \eta(x,T) = 0,$$

where

$$H_0^1(Q_T) = \left\{v \in H^1(Q_T) : v|_{S_T} = 0\right\}.$$

Consider now the case when the function $f(x,t)$ in (4.44) satisfies the following conditions:

$$\partial_t^k f(x,t) \in L_2(Q_T), \ k \in [1,3], \tag{4.47}$$
$$\partial_t^n f(x,0) = 0 \text{ in } \Omega, \ n \in [0,2]. \tag{4.48}$$

Note that (4.47) and (4.48) imply that

$$f, f_t, f_{tt} \in L_2(\Omega_t), \ \forall t \in [0,T], \tag{4.49}$$
$$\|\partial_t^s f(x,t)\|_{L_2(\Omega_t)} \leq T^{(3-s)/2} \left\|\partial_t^3 f\right\|_{L_2(Q_T)}, \ s \in [0,2]. \tag{4.50}$$

To prove (4.49) and (4.50), we note that since

$$f_{tt}(x,t) = \int\limits_0^t \partial_t^3 f(x,\tau) \mathrm{d}\tau, \tag{4.51}$$

then

$$\|f_{tt}(x,t)\|_{L_2(\Omega_t)} = \int\limits_\Omega f_{tt}^2(x,t) \mathrm{d}x \leq T \left\|\partial_t^3 f\right\|_{L_2(Q_T)}. \tag{4.52}$$

Theorem 4.6. *Let $\Omega \subset \mathbb{R}^3$ be a convex bounded domain with the boundary $\partial\Omega \in C^2$. Let the function $c \in Y$, where the set Y was defined in (4.7), and let $b(x)$ be the function defined in (4.40). Let the function $f(x,t)$ in (4.44) satisfies conditions (4.47) and (4.48). Denote*

$$m = \|c\|_{C(\overline{\Omega})}. \tag{4.53}$$

Then, there exists unique weak solution $u \in H^1(Q_T)$ *of the problem (4.44)–(4.46). Furthermore,*

$$u, u_t, u_{tt} \in H^2(Q_T), \tag{4.54}$$

Also,

$$u_t \in H^2(\Omega_t) \cap C\left(\overline{\Omega}_t\right), \ \forall t \in [0,T]. \tag{4.55}$$

Let

$$u^1(t) = \|u_t(x,t)\|_{C\left(\overline{\Omega}_t\right)}.$$

Then, the function $u^1(t) \in L_\infty(0,T)$ *and there exists a constant* $C = C(\Omega, d, \omega) > 0$ *such that*

$$\left\|u^1\right\|_{L_\infty(0,T)} \leq m \exp(CT) \left\|\partial_t^3 f\right\|_{L_2(Q_T)}. \tag{4.56}$$

Proof. In this proof, $C = C(\Omega, d, \omega) > 0$ denotes different constants depending on these parameters. Using (4.40), (4.41), and (4.53), we obtain

$$\|\nabla b\|_{L_\infty(\Omega)} \leq \frac{M}{(1-\omega)^2} \tag{4.57}$$

with a certain constant $M > 0$. Since by (4.47), the function $f_t \in L_2(Q_T)$, then (4.57) and Corollary 4.1 of Sect. 4 of Chap. 4 of the book [119] imply that $u \in H^2(Q_T)$. Consider now the solution u_1 of the following initial boundary value problem:

$$\partial_t^2 u_1 = \nabla \cdot (b(x) \nabla u_1) - \nabla b \nabla u_1 + f_t(x,t) \text{ in } Q_T, \tag{4.58}$$

$$u_1(x,0) = \partial_t u_1(x,0) = 0, \tag{4.59}$$

$$u_1 \mid_{S_T} = 0. \tag{4.60}$$

This problem is obtained from the problem (4.44)–(4.46) via the differentiation of (4.44) with respect to t keeping in mind (4.49). Since by (4.47) and (4.48), the function $f_{tt} \in L_2(Q_T)$, then, using the same arguments again, we obtain that $u_1 \in H^2(Q_T)$.

Consider the function $\overline{u}$:

$$\overline{u}(x,t) = \int_0^t u_1(x,\tau)\, d\tau.$$

Since $u_1 \in H^2(Q_T)$, then obviously, $\overline{u} \in H^2(Q_T)$. We apply to both sides of (4.58) and (4.60) the operator

$$\int_0^t (\cdot)\, d\tau.$$

Using (4.49), we obtain that the function $\overline{u} \in H^2(Q_T)$ satisfies conditions (4.44)–(4.46). Hence, $\overline{u} \equiv u$. Hence, $u_t = u_1 \in H^2(Q_T)$. Similarly, $u_{tt} \in H^2(Q_T)$. Thus, (4.54) is true.

Hence,

$$\int_0^t D_t^2 D_x^\alpha u(x,\tau)\,\mathrm{d}\tau = D_t D_x^\alpha u(x,t) \in L_2(\Omega_t),\ \forall t \in [0,T];\ |\alpha| \le 2.$$

Hence, $u_t \in H^2(\Omega_t)$. Using (4.40) and boundary condition (4.46), we now rewrite (4.58) and as

$$\Delta u_t = g(x,t),\ \text{in } \Omega_t, \tag{4.61}$$

$$u_t\,|_{\partial\Omega_t} = 0, \tag{4.62}$$

$$g(x,t) = c(x)\,\partial_t^3 u(x,t) - c(x)\,f_t(x,t). \tag{4.63}$$

One can consider (4.61) and (4.62) as the Dirichlet boundary value problem for the Poisson equation for the function $u(x,t)$. It is well known that this problem has unique solution in the space $H_0^2(\Omega_t)$:

$$H_0^2(\Omega_t) = \left\{v \in H^2(\Omega_t) : v\,|_{\Omega_t} = 0\right\}.$$

Since by (4.46), the function $u_t \in H_0^2(\Omega_t)$, then this function is exactly that solution. Furthermore, the second fundamental inequality for elliptic operators of O.A. Ladyzhenskaya implies that

$$\sum_{i,j=1}^{3} \left\|v_{x_i x_j}\right\|^2_{L_2(\Omega_t)} \le \|\Delta v\|^2_{L_2(\Omega_t)},\ \forall v \in H_0^2(\Omega_t);$$

see Sect. 6 of Chap. 2 of the book [119]. In addition, the Poincare inequality is

$$\|v\|_{L_2(\Omega_t)} \le C_1 \|\nabla v\|_{L_2(\Omega_t)},\ \forall v \in H_0^1(\Omega_t) = \left\{v \in H^1(\Omega_t) : v\,|_{\Omega_t} = 0\right\},$$

where the constant $C_1 = C_1(\Omega)$ depends only on the domain Ω. Thus, the combination of the two latter inequalities with (4.61)–(4.63), (4.47)–(4.50), and (4.53) implies that

$$\|u_t(x,t)\|_{H^2(\Omega_t)} \le C\left[m\left\|\partial_t^3 u(x,t)\right\|_{L_2(\Omega_t)} + T\left\|\partial_t^3 f\right\|_{L_2(Q_T)}\right]. \tag{4.64}$$

Since by the embedding Theorem 1.1.3.2 $H^2(\Omega_t) \subset C\left(\overline{\Omega_t}\right)$, then (4.64) implies that the function $u_t \in C\left(\overline{\Omega_t}\right)$. Thus, (4.55) is true.

Hence, it follows from (4.64) that with a different constant C,

$$u^1(t) = \|u_t(x,t)\|_{C(\overline{\Omega}_t)} \leq C\left[m\left\|\partial_t^3 u(x,t)\right\|_{L_2(\Omega_t)} + T\left\|\partial_t^3 f\right\|_{L_2(Q_T)}\right]. \quad (4.65)$$

Therefore, we now need to estimate the norm $\left\|\partial_t^3 u(x,t)\right\|_{L_2(\Omega_t)}$ from the above. Denote $w = u_{tt}$. By (4.54), the function $w \in H^2(Q_T)$. It follows from (4.44)–(4.49) that the function w is the solution of the following initial boundary value problem:

$$c(x) w_{tt} - \Delta w = c(x) f_{tt}(x,t) \text{ in } Q_T, \quad (4.66)$$

$$w(x,0) = w_t(x,0) = 0, \quad (4.67)$$

$$w|_{S_T} = 0. \quad (4.68)$$

We now use the standard method of energy estimates. Multiply both sides of (4.66) by $2w_t$ and integrate over the time cylinder $Q_t = \Omega \times (0,t)$ using integration by parts as well (4.68). We obtain

$$\int_{Q_t} \partial_\tau \left[c(x) w_t^2(x,t)\right] \mathrm{d}x\mathrm{d}\tau + \int_{Q_t} \partial_\tau \left(\nabla w(x,\tau)\right)^2 \mathrm{d}x\mathrm{d}\tau = 2\int_{Q_t} c(x) f_{tt} w_t \,\mathrm{d}x\mathrm{d}t. \quad (4.69)$$

Integrating with respect to τ in the integrals in the left-hand side of (4.69) and using (4.67), we obtain

$$\int_{\Omega_t} \left[c(x) w_t^2 + (\nabla w)^2\right](x,t)\,\mathrm{d}x = 2\int_{Q_t} c(x) f_{tt} w_t \mathrm{d}x\mathrm{d}t. \quad (4.70)$$

Since $c(x) \geq 1 - \omega$, then

$$\int_{\Omega_t} \left[c(x) w_t^2 + (\nabla w)^2\right](x,t)\,\mathrm{d}x \geq (1-\omega)\int_{\Omega_t} \left[w_t^2 + (\nabla w)^2\right](x,t)\,\mathrm{d}x. \quad (4.71)$$

Hence, using the Cauchy-Schwarz inequality, we obtain from (4.70) and (4.71)

$$\int_{\Omega_t} \left[w_t^2 + (\nabla w)^2\right](x,t)\,\mathrm{d}x \leq C\int_0^t \left[\int_\Omega \left(w_t^2 + (\nabla w)^2\right)(x,\tau)\,\mathrm{d}x\right]\mathrm{d}\tau$$

$$+C\int_{Q_t} f_{tt}^2 \mathrm{d}x\mathrm{d}\tau. \quad (4.72)$$

Denote

$$I(t) = \int\limits_{\Omega_t} \left[w_t^2 + (\nabla w)^2 \right](x,t)\,\mathrm{d}x,$$

$$G(t) = C \int\limits_{Q_t} f_{tt}^2 \mathrm{d}x\mathrm{d}\tau.$$

Then by (4.72),

$$I(t) \le C \int\limits_0^t I(\tau)\,\mathrm{d}\tau + G(t).$$

Hence, using the well-known Gronwall's inequality (see, e.g., Lemma 1.1 in Sect. 1 of Chap. 3 of the book [119]), we obtain

$$I(t) \le \exp(Ct)\, G(T),\ t \in [0,T].$$

The latter inequality means that

$$\begin{aligned} \|w_t(x,t)\|_{L_2(\Omega_t)} + \|\nabla w(x,t)\|_{L_2(\Omega_t)} &\le \exp(CT)\, \|f_{tt}\|_{L_2(Q_T)} \\ &\le \exp(CT) \left\|\partial_t^3 f\right\|_{L_2(Q_T)}, \end{aligned} \tag{4.73}$$

$t \in [0,T]$. Recall that $w = u_{tt}$. Hence, $w_t = \partial_t^3 u$. Therefore, (4.65) and (4.73) imply (4.56). □

In Sect. 4.7, we will need the following:

Corollary 4.6. *Let in (4.47) $k \in \left[0, \overline{k}\right]$, where $\overline{k} \in [1,4]$. Also, let other conditions of Theorem 4.6 hold true. Then functions*

$$\partial_t^i u \in H^2(Q_T),\ i \in \left[0, \overline{k} - 1\right] \tag{4.74}$$

and the following estimates hold for $(k,i,j) \in \left[0,\overline{k}\right] \times \left[0,\overline{k}-1\right] \times [1,3]$:

$$\left\|\partial_t^k u\right\|_{L_2(Q_T)}, \left\|\partial_t^i u_{x_j}(x,t)\right\|_{L_2(\Omega_t)} \le \exp(CT) \left\|\partial_t^{\overline{k}-1} f\right\|_{L_2(Q_T)},\ t \in [0,T], \tag{4.75}$$

where $C = C(\Omega, d, \omega) > 0$ is the constant of Theorem 4.6

Proof. The assertion (4.74) can be proved similarly with (4.54). To prove (4.75), consider the following initial boundary value problem:

$$v_{tt} = \nabla \cdot (b(x) \nabla v) - \nabla b \nabla v + \partial_t^{\overline{k}-1} f(x,t) \text{ in } Q_T, \tag{4.76}$$

$$v(x,0) = v_t(x,0) = 0, \tag{4.77}$$

$$v|_{S_T} = 0. \tag{4.78}$$

Since the function $\partial_t^{\overline{k}} f \in L_2(Q_T)$, then Corollary 4.1 of Sect. 4 of Chap. 4 of the book [119] implies that the problem (4.76)–(4.78) has unique solution $v \in H^2(Q_T)$. Similarly with the proof of Theorem 4.6, we verify that $v = \partial_t^{\overline{k}-1} u$. We now rewrite (4.76) in the equivalent form:

$$c(x) v_{tt} = \Delta v + c(x) \partial_t^{\overline{k}-1} f(x,t) \text{ in } Q_T. \tag{4.79}$$

Next, applying to the problem (4.77)–(4.79) the standard energy estimate in the same manner as it was done in the proof of Theorem 4.6, we obtain (4.75) for $k = \overline{k}, i = \overline{k} - 1$. The cases $0 \leq k \leq \overline{k} - 1, 0 \leq i \leq \max\left(0, \overline{k} - 2\right)$ can be considered similarly with (4.51) and (4.52). □

4.7 Fréchet Derivatives of Solutions of State and Adjoint Problems

This is the second preparatory section for the rigorous derivation of the Fréchet derivative of the Tikhonov functional. Here, we use Theorem 4.6 to derive Fréchet derivatives of solutions of state and adjoint initial boundary value problems (4.9) and (4.10). However, the inconvenient point of Theorem 4.6 is that it is valid only for the case of the Dirichlet boundary condition in (4.46). On the other hand, we have the Neumann boundary condition in each of the problems (4.9) and (4.10). Nevertheless, the material of Sect. 5 of Chap. 4 of the book [119] indicates that Theorem 4.5 can be extended to the case of the Neumann boundary condition. The actual proof would be quite space consuming, since we would need to prove first analogs of Theorems 3.1, 3.2 and Theorem 4.1 of Chap. 4 of [119]. However, since we focus here on inverse rather than forward problems, this proof is outside of the scope of the current book. Thus, we simply assume that Theorem 4.6 holds for this case. Therefore, when referencing to Theorem 4.6 in this section, we mean an obvious analog of this theorem for the case of the Neumann boundary condition.

Just as in Theorem 4.6, we assume here that $\Omega \subset \mathbb{R}^3$ is a convex bounded domain with $\partial\Omega \in C^2$. We also assume that there exists a function $a(x)$ such that

$$a \in C^2\left(\overline{\Omega}\right), \ a|_{\partial\Omega} = 0, \ \partial_n a|_{\partial\Omega} = 1. \tag{4.80}$$

For example, if $\Omega = \{|x| < R\}$, then one can choose $a(x) = (|x| - R)\chi(|x|)$, where the function χ is such that

$$\chi(z) \in C^{\infty}[0,R],\ \chi(z) = \begin{cases} 1 \text{ for } z \in \left[\frac{R}{2}, R\right], \\ 0 \text{ for } z \in \left[0, \frac{R}{4}\right], \\ \text{between 0 and 1 for } z \in \left[\frac{R}{4}, \frac{R}{2}\right]. \end{cases}$$

Although such functions $a(x)$ might also likely be constructed for more general convex domains, we are not doing this here for brevity.

For the convenience of the reader, we rewrite state and adjoint problems (4.9) and (4.10) in this section as problems (4.81) and (4.82), respectively:

$$\begin{aligned} c(x) u_{tt} - \Delta u &= 0 \text{ in } Q_T, \\ u(x,0) &= u_t(x,0) = 0, \\ \partial_n u\,|_{S_T} &= p(x,t) \end{aligned} \tag{4.81}$$

$$\begin{aligned} c(x) \lambda_{tt} - \Delta \lambda &= 0 \text{ in } Q_T, \\ \lambda(x,T) &= \lambda_t(x,T) = 0, \\ \partial_n \lambda\,|_{S_T} &= z_{\zeta}(t)(g-u)(x,t). \end{aligned} \tag{4.82}$$

The function $z_{\zeta}(t)$ was introduced in Sect. 4.3.

We need to extend boundary functions $p(x,t), z_{\zeta}(t) g(x,t)$ in (4.81) and (4.82) from the boundary S_T inside the domain Q_T. Let $P(x,t)$ and $G(x,t)$ be extensions of $p(x,t)$ and $z_{\zeta}(t) g(x,t)$, respectively. Because of (4.47)–(4.49), we need these extensions to be sufficiently smooth. Also, the function $P(x,t)$ should be equal zero at $\{t = 0\}$ together with some of its t-derivatives. The function $G(x,t)$ should be equal zero together with some of its t-derivatives at $\{t = T\}$. Note that it is quite natural to assume that the function $p(x,t) = 0$ for sufficiently small t. Indeed, since the source $x_0 \notin \overline{\Omega}$, then (4.1) implies that the solution of the problem (4.2) and (4.3) $u(x,t) = 0$ for $(x,t) \in \overline{\Omega} \times [0,\varepsilon]$ for a sufficiently small $\varepsilon > 0$.As to the function $G(x,t)$, it is also natural to assume that $G(x,T) = 0$ together with some of its derivatives, since the function $z_{\zeta}(t) = 0$ near $\{t = T\}$. Thus, we assume that there exist functions P and G such that

$$P \in H^6(Q_T),\ \Phi \in H^5(Q_T), \tag{4.83}$$

$$\partial_n P\,|_{S_T} = p(x,t), \quad \partial_n \Phi\,|_{S_T} = z_{\zeta}(t) g(x,t), \tag{4.84}$$

$$\partial_t^k P(x,0) = \partial_t^k \Phi(x,T) = 0 \text{ in } \Omega,\ k \in [0,4]. \tag{4.85}$$

Theorem 4.7.1. *Let $\Omega \subset \mathbb{R}^3$ be a convex bounded domain with the boundary $\partial\Omega \in C^2$. Suppose that there exists a function $a(x)$ satisfying conditions (4.80). Let the function $c \in Y$, where the set Y was defined in (4.7). Suppose that*

there exist functions $P(x,t)$ *and* $\Phi(x,t)$ *satisfying conditions (4.83)–(4.85). Then each of problems (4.81) and (4.82) has unique weak solution* $u \in H^1(Q_T)$ *and* $\lambda \in H^1(Q_T)$*, respectively. Furthermore, derivatives* $\partial_t^{k_1} u, \partial_t^{k_2} \lambda$ *exist for* $k_1 \in [0,3], k_2 \in [0,2]$ *and*

$$\partial_t^{k_1} u \in H^2(Q_T), \ k_1 \in [0,3], \tag{4.86}$$

$$\partial_t^{k_2} \lambda \in H^2(Q_T), \ k_2 \in [0,2]. \tag{4.87}$$

In addition, there exists a constant $C = C(\Omega, d, \omega, z_\zeta, a) > 0$ *such that the following estimates hold for* $(k,i,j) \in [0,4] \times [0,3] \times [1,3]$ *and* $t \in [0,T]$ *:*

$$\left\| \partial_t^k u \right\|_{L_2(Q_T)}, \left\| \partial_t^i u_{x_j}(x,t) \right\|_{L_2(\Omega_t)} \leq \exp(CT) \|P\|_{H^6(Q_T)}. \tag{4.88}$$

Also, for $(r,s,j) \in [0,3] \times [0,2] \times [1,3]$*,*

$$\|\partial_t^r \lambda\|_{L_2(Q_T)}, \left\| \partial_t^s \lambda_{x_j}(x,t) \right\|_{L_2(\Omega_t)} \leq \exp(CT) \left(\|P\|_{H^6(Q_T)} + \|\Phi\|_{H^5(Q_T)} \right). \tag{4.89}$$

In addition, functions

$$u, u_t \in H^2(\Omega_t) \cap C\left(\overline{\Omega}_t\right), \ \forall t \in [0,T], \tag{4.90}$$

$$\lambda, \lambda_t \in H^2(\Omega_t) \cap C\left(\overline{\Omega}_t\right), \ \forall t \in [0,T] \tag{4.91}$$

and the following estimates hold

$$\|u_t(x,t)\|_{C\left(\overline{\Omega}_t\right)} \leq m \exp(CT) \|P\|_{H^6(Q_T)}, \tag{4.92}$$

$$\|\lambda_t(x,t)\|_{C\left(\overline{\Omega}_t\right)} \leq m \exp(CT) \left(\|P\|_{H^6(Q_T)} + \|\Phi\|_{H^5(Q_T)} \right), \tag{4.93}$$

where the number $m = \|c\|_{C\left(\overline{\Omega}\right)}$ *was defined in (4.53).*

Proof of Theorem 4.7.1. First, we prove assertions of this theorem for the function u. To obtain the zero Neumann boundary condition at S_T, introduce the function $\widetilde{u}(x,t) = u(x,t) - P(x,t)$. Then (4.81) implies that

$$\begin{aligned} c(x) \widetilde{u}_{tt} &= \Delta \widetilde{u} - \left(c(x) \partial_t^2 P - \Delta P \right), \\ \widetilde{u}(x,0) &= \widetilde{u}_t(x,0) = 0, \\ \partial_n \widetilde{u}|_{S_T} &= 0. \end{aligned} \tag{4.94}$$

It follows from (4.83)–(4.85) that conditions of both Theorem 4.6 and Corollary 4.6 are valid for the problem (4.94). Hence, Theorem 4.6 and Corollary 4.6 imply that assertions (4.86), (4.88), (4.90), and (4.92) are valid for the function $\widetilde{u}$. Since $u = \widetilde{u} + P$, then these assertions are also true for the function u.

Consider now the function $\overline{\lambda}(x,t)$:

$$\overline{\lambda}(x,t) = \lambda(x,t) - \left[\Phi(x,t) - z_\zeta(t)\, a(x)\, u(x,t)\right]. \tag{4.95}$$

Substituting this in (4.82) and using (4.81), we obtain

$$c(x)\,\overline{\lambda}_{tt} = \Delta\overline{\lambda} + \overline{f}(x,t), \tag{4.96}$$

$$\overline{\lambda}(x,T) = \overline{\lambda}_t(x,T) = 0, \tag{4.97}$$

$$\partial_n \overline{\lambda}\,|_{S_T} = 0, \tag{4.98}$$

$$\begin{aligned}\overline{f}(x,t) = &-\left(c(x)\,\partial_t^2\Phi - \Delta\Phi\right) + 2c(x)\,a(x)\,z_\zeta' u_t + c(x)\,a(x)\,z_\zeta'' u \\ &-2z_\zeta \nabla a \nabla u - z_\zeta u \Delta a.\end{aligned} \tag{4.99}$$

Hence, (4.83), (4.85), (4.86), (4.88), and (4.99) imply that

$$\partial_t^k \overline{f}(x,t) \in L_2(Q_T),\ k \in [0,3], \tag{4.100}$$

$$\partial_t^n \overline{f}(x,T) = 0,\ n \in [0,2], \tag{4.101}$$

$$\left\|\partial_t^3 \overline{f}\right\|_{L_2(Q_T)} \le C\left(\|P\|_{H^6(Q_T)} + \|\Phi\|_{H^5(Q_T)}\right). \tag{4.102}$$

Conditions (4.100) and (4.101) are the same as conditions (4.47) and (4.48) in Sect. 4.6. This means that conditions of Theorem 4.6 are valid for the problem (4.96)–(4.99). Hence, Theorem 4.6, Corollary 4.6 (for the case $\overline{k} = 3$), and (4.102) imply that there exists unique solution $\overline{\lambda} \in H^2(Q_T)$ of the problem (4.96)–(4.99), the function $\overline{\lambda}$ satisfies (4.87), and assertions (4.89), (4.91), and (4.93) are true for $\overline{\lambda}$. Finally, the above established assertion for the function u as well as (4.95) ensure that the function λ also satisfies (4.87), (4.89), (4.91), and (4.93). □

Introduce the set Z of functions as

$$Z = \left\{f : f \in C\left(\overline{\Omega}\right) \cap H^1(\Omega),\ \partial_{x_i} f \in L_\infty(\Omega),\ i = 1,2,3\right\},$$

where $\partial_{x_i} f$ is the weak derivative of the function f with respect to the variable x_i. Define the norm in Z as

$$\|f\|_Z := \|f\|_{C(\overline{\Omega})} + \sum_{i=1}^{3} \|\partial_{x_i} f\|_{L_\infty(\Omega)}. \tag{4.103}$$

Hence, Z is a Banach space. Then the set $Y \subset Z$, where Y was defined in (4.7). In Theorem 4.7.2, we derive Fréchet derivatives of solutions of both state and adjoint problems with respect to the coefficient $c(x)$.

Theorem 4.7.2. *Let $\Omega \subset \mathbb{R}^3$ be a convex bounded domain with the boundary $\partial\Omega \in C^2$. Suppose that there exists a function $a(x)$ satisfying conditions (4.80). For each function $c \in Y$, consider solutions of state and adjoin initial boundary value problems (4.81) and (4.82). Assume that there exist functions $P(x,t)$ and $\Phi(x,t)$ satisfying conditions (4.83)–(4.85). Consider the set Y as an open set in the space Z. Define operators $A_1 : Y \to H^1(Q_T)$ and $A_2 : Y \to H^1(Q_T)$ as those which map every function $c \in Y$ in the weak solution $u(x,t,c)$ of the problem (4.81) and the weak solution $\lambda(x,t,c)$ of the problem (4.82), respectively, where in (4.82) $u|_{S_T} := u(x,t,c)|_{S_T}$. Then functions $u(x,t,c), \lambda(x,t,c) \in H^2(Q_T)$ and relations (4.86)–(4.93), are valid for these functions. Each of the operators A_1 and A_2 has the Fréchet derivative $A_1'(c)(b), A_2'(c)(b)$:*

$$A_1'(c)(b) = \widetilde{u}(x,t,c,b) \in H^1(Q_T),$$
$$A_2'(c)(b) = \widetilde{\lambda}(x,t,c,b) \in H^1(Q_T),$$

at each point $c \in Y$, where $b(x) \in Z$ is an arbitrary function. Functions $\widetilde{u} \in H^2(Q_T)$ and $\widetilde{\lambda} \in H^2(Q_T)$ are solutions of initial boundary value problems (4.104) and (4.105), respectively, where

$$\begin{aligned} c(x)\widetilde{u}_{tt} &= \Delta\widetilde{u} - b(x)u_{tt}(x,t,c), \text{ in } Q_T, \\ \widetilde{u}(x,0) &= \widetilde{u}_t(x,0) = 0, \\ \partial_n\widetilde{u}|_{S_T} &= 0, \end{aligned} \tag{4.104}$$

$$\begin{aligned} c(x)\widetilde{\lambda}_{tt} &= \Delta\widetilde{\lambda} - b(x)\lambda_{tt}(x,t,c), \text{ in } Q_T, \\ \widetilde{\lambda}(x,T) &= \widetilde{\lambda}_t(x,T) = 0, \\ \partial_n\widetilde{\lambda}|_{S_T} &= -z_\zeta\widetilde{u}|_{S_T} \end{aligned} \tag{4.105}$$

In addition, the following estimates are valid:

$$\|\widetilde{u}\|_{H^1(Q_T)} \leq \exp(CT)\|P\|_{H^6(Q_T)}\|b\|_Z, \tag{4.106}$$

$$\left\|\widetilde{\lambda}\right\|_{H^1(Q_T)} \leq \exp(CT)\left(\|P\|_{H^6(Q_T)} + \|\Phi\|_{H^5(Q_T)}\right)\|b\|_Z, \tag{4.107}$$

where $C = C\left(\Omega, d, \omega, z_\zeta, a\right) > 0$ is the constant of Theorem 4.7.1.

Consider the operator $A_3(c)$ defined in Y:,

$$A_3(c)(x) := \int_0^T (u_t\lambda_t)(x,t,c)\,dt, x \in \Omega, \ \forall c \in Y. \tag{4.108}$$

Then

$$A_3 : Y \to L_\infty(\Omega) \tag{4.109}$$

and

$$\|A_3(c)\|_{L_\infty(\Omega)} \leq m^2 \exp(CT)\left(\|P\|^2_{H^6(Q_T)} + \|\Phi\|^2_{H^5(Q_T)}\right), \tag{4.110}$$

where the number m was defined in (4.53).

Proof. Consider an arbitrary function $c \in Y$. Theorem 4.7.1 implies that relations (4.86)–(4.93) for $u(x,t,c), \lambda(x,t,c) \in H^2(Q_T)$ are valid. Relations (4.109) and (4.110) for the operator $A_3(c)$ in (4.108) follow from (4.90)–(4.93).

By (4.88), the function $\partial_t^4 u \in L_2(Q_T)$. Hence, Theorems 3.1 and 3.2 of Chap. 3 of the book [119] imply that there exists unique weak solution $\widetilde{u} \in H^1(Q_T)$ of the problem (4.104). Furthermore, Corollary 4.1 of Sect. 4 of Chap. 4 of [119] implies that functions $\widetilde{u}, \widetilde{u}_t \in H^2(Q_T)$. In addition, Corollary 4.6 implies that

$$\|\widetilde{u}_{tt}\|_{L_2(Q_T)}, \left\|\partial_t \widetilde{u}_{x_j}\right\|_{L_2(Q_T)} \leq \exp(CT)\|P\|_{H^6(Q_T)}\|b\|_Z. \tag{4.111}$$

The estimate (4.106) follows from (4.111).

Consider now the function $\widetilde{\lambda}$. Let $v = \widetilde{\lambda} + z_\zeta(t)a(x)\widetilde{u}$. Then (4.104) and (4.105) imply that

$$cv_{tt} = \Delta v + \varphi(x,t) - b(x)\lambda_{tt}(x,t,c), \tag{4.112}$$

$$v(x,0) = v_t(x,0) = 0, \tag{4.113}$$

$$\partial_n v|_{S_T} = 0, \tag{4.114}$$

$$\varphi(x,t) = -a(x)b(x)z_\zeta(t)u_{tt} + (ac)(x)\left(z''_\zeta(t)\widetilde{u} + 2z'_\zeta(t)\widetilde{u}_t\right)$$
$$-z_\zeta(\widetilde{u}\Delta a + 2\nabla a \nabla \widetilde{u}). \tag{4.115}$$

Since functions $\widetilde{u}, \widetilde{u}_t \in H^2(Q_T)$. In addition, by Theorem 4.7.1, the function $u_{tt} \in H^2(Q_T)$. Hence, (4.115) and Theorems 3.1 and 3.2 of Sect. 3 of Chap. 3 of the book [119] imply that there exists unique weak solution $v \in H^1(Q_T)$ of the problem (4.112)–(4.114). Furthermore, Corollary 4.1 of Sect. 4 of Chap. 4 of [119] and (4.111) imply that the function $v \in H^2(Q_T)$. In addition, Corollary 4.6, (4.88), (4.89), and (4.111) imply that

$$\|v\|_{H^1(Q_T)} \leq \exp(CT)\|P\|_{H^6(Q_T)}\|b\|_Z.$$

Hence, the function $\widetilde{\lambda} \in H^2(Q_T)$ and (4.107) holds.

We prove now that the function $\widetilde{u}(x,t,c,b) \in H^1(Q_T)$ is indeed the Fréchet derivative of the operator A_1. It follows from (4.7) that there exists a sufficiently small number $\sigma \in (0,1)$ such that $1 - \omega(1-\sigma) \leq c(x) \leq d + \omega(1-\sigma)$ in $\overline{\Omega}$. Let the function $b \in Z$ be such that $\|b\|_{C(\overline{\Omega})} < \sigma\omega$. Hence, $c + b \in Y$. Consider functions u^{c+b}, u^c and u_1 defined by

$$u^{c+b}(x,t) := u(x,t,c+b),$$
$$u^{c}(x,t) := u(x,t,c),$$
$$u_1 := u_1(x,t,c,b) = \left(u^{c+b} - u^{c} - \widetilde{u}\right)(x,t). \tag{4.116}$$

Hence, $u_1 \in H^2(Q_T)$. We now figure out the equation for the function u_1. First, substitute in (4.81) $c := c + b$. Next, substitute $c := c$. Next, subtract the second resulting equation from the first one and then subtract (4.104) from the resulting equation. First, we have

$$(c+b)u_{tt}^{c+b} - cu_{tt}^{c} - c\widetilde{u}_{tt} = (c+b)u_{tt}^{c+b} - (c+b)u_{tt}^{c} - (c+b)\widetilde{u}_{tt}$$
$$+bu_{tt}^{c} + b\widetilde{u}_{tt} = (c+b)u_{1tt} + bu_{tt}^{c} + b\widetilde{u}_{tt}.$$

Hence,

$$(c+b)u_{1tt} = \Delta u_1 - bu_{tt}^{c} + bu_{tt}^{c} - b\widetilde{u}_{tt} = \Delta u_1 - b\widetilde{u}_{tt}.$$

Hence, the function u_1 is the solution of the following initial boundary value problem:

$$(c+b)u_{1tt} = \Delta u_1 - b\widetilde{u}_{tt},$$
$$u_1(x,0) = u_{1t}(x,0) = 0,$$
$$\partial_n u_1 \mid_{S_T} = 0.$$

Hence, using (4.106), we obtain

$$\|u_1\|_{H^1(Q_T)} \leq \exp(CT)\,\|P\|_{H^6(Q_T)}\,\|b\|_Z^2.$$

Hence,

$$\lim_{\|b\|_Z \to 0} \left(\frac{\|u_1\|_{H^1(Q_T)}}{\|b\|_Z} \right) = 0. \tag{4.117}$$

Since the function $\widetilde{u}$ depends linearly on the function b, then (4.116) and (4.117) imply that the function $\widetilde{u}(x,t,c,b) \in H^1(Q_T)$ is indeed the Fréchet derivative of the operator $A_1 : Y \to H^1(Q_T)$ at the point $c \in Y$. The proof for the function $\widetilde{\lambda}(x,t,c,b)$ is similar and is, therefore, omitted. □

4.8 The Fréchet Derivative of the Tikhonov Functional

After two preparatory Sects. 4.6 and 4.7, we are ready now to derive the Fréchet derivative of the Tikhonov functional (4.8). We assume in this section that conditions of Theorem 4.7.2 hold. For functions $c \in Y$, we consider the Tikhonov functional

$E(c)$ (4.8) and the associated Lagrange functional $L(c)$ defined in (4.14). For the convenience of the reader, we copy here both functionals (4.8) and (4.14) as well as the definitions (4.11) and (4.12) of weak solutions of the state and adjoint problems, respectively. So these are formulas (4.118)–(4.121):

$$E_\alpha(c) = \frac{1}{2}\int\limits_{S_T} (u\mid_{S_T} - g(x,t))^2 z_\zeta(t)\,\mathrm{d}\sigma\mathrm{d}t + \frac{1}{2}\alpha\int\limits_{\Omega}(c-c_{\mathrm{glob}})^2\mathrm{d}x, \tag{4.118}$$

$$L(c) = E_\alpha(c) - \int\limits_{Q_T} c(x)u_t\lambda_t\mathrm{d}x\mathrm{d}t + \int\limits_{Q_T}\nabla u\nabla\lambda\mathrm{d}x\mathrm{d}t - \int\limits_{S_T} p\lambda\mathrm{d}\sigma\mathrm{d}t, \quad v=(u,\lambda,c), \tag{4.119}$$

$$\int\limits_{Q_T}(-c(x)u_t v_t + \nabla u\nabla v)\,\mathrm{d}x\mathrm{d}t - \int\limits_{S_T} pv\mathrm{d}S_{x,t} = 0,\ \forall v\in H^1(Q_T),\ v(x,T)=0. \tag{4.120}$$

$$\int\limits_{Q_T}(-c(x)\lambda_t v_t + \nabla\lambda\nabla v)\,\mathrm{d}x\mathrm{d}t - \int\limits_{S_T} z_\zeta(g-u)v\,\mathrm{d}S_{x,t} = 0,$$
$$\forall v\in H^1(Q_T),\ v(x,0)=0. \tag{4.121}$$

In (4.118)–(4.121), $c\in Y$ is an arbitrary function, $u\in H^2(Q_T)$ is the solution of the state problem (4.81), and $\lambda\in H^2(Q_T)$ is the solution of the adjoint problem (4.82). Since by (4.82), $\lambda(x,T)=0$, then the integral term in (4.119) equals zero. Hence, $L(c)=E_\alpha(c)$, implying that

$$L'(c) = E'_\alpha(c), \forall c\in Y, \tag{4.122}$$

where $L'(c)$ and $E'_\alpha(c)$ are Fréchet derivatives of functionals $L(c)$ and $E_\alpha(c)$, respectively. By Definition 1.9.1 of the Fréchet derivative, in order to obtain an explicit expression for $L'(c)=E'_\alpha(c)$, we need to vary in (4.120) the function c via considering $c+b\in Y$ for $b\in Z$ and then to single out the term, which is linear with respect to b. When varying c, we also need to consider respective variations of functions u and λ, since these functions depend on the function c as solutions of state and adjoint problems (4.81) and (4.82). By Theorem 4.7.2, linear, with respect to c, parts of variations of u and λ are functions $\widetilde{u}(x,t,c,b)$, $\widetilde{\lambda}(x,t,c,b)$.

Theorem 4.8. *Assume that conditions of Theorem 4.7.2 hold. Then for every function $c\in Y$, the Fréchet derivative of the Tikhonov functional $E(c)$ in (4.118) is the function $E'(c)(x)$ defined as*

$$E'_\alpha(c)(x) = L'(c)(x) = \alpha\left(c-c_{\mathrm{glob}}\right)(x) - \int\limits_0^T (u_t\lambda_t)(x,t)\,\mathrm{d}t,\ x\in\Omega. \tag{4.123}$$

The functional of the Fréchet derivative acts on an arbitrary function $b \in Z$ as follows:

$$\left(E'_\alpha(c), b\right) = \int\limits_\Omega \left[\alpha\left(c - c_{\text{glob}}\right) - \int\limits_0^T u_t \lambda_t \mathrm{d}t\right](x) \cdot b(x)\,\mathrm{d}x, \ \forall b \in Z, \quad (4.124)$$

where the functional space Z was introduced in Sect. 4.7. Also,

$$E'_\alpha(c)(x) \in L_\infty(\Omega). \quad (4.125)$$

Proof. Considering in (4.119), $L(c+b) - L(c) = E_\alpha(c+b) - E_\alpha(c)$, singling out the term, which is linear with respect to b, and using Theorem 4.7.2 as well as (4.122), we obtain

$$\begin{aligned} L'(c)(b) = E'_\alpha(c)(b) = &\int\limits_\Omega \left[\alpha\left(c - c_{\text{glob}}\right) - \int\limits_0^T u_t \lambda_t \mathrm{d}t\right] b(x)\,\mathrm{d}x \\ &+ \int\limits_{Q_T} \left(-c u_t \widetilde{\lambda}_t + \nabla u \nabla \widetilde{\lambda}\right) \mathrm{d}x\mathrm{d}t - \int\limits_{S_T} p\widetilde{\lambda}\mathrm{d}x\mathrm{d}t \\ &+ \int\limits_{Q_T} \left(-c\lambda_t \widetilde{u}_t + \nabla\lambda\nabla\widetilde{u}\right)\mathrm{d}x\mathrm{d}t - \int\limits_{S_T} \left(g - u\,|_{S_T}\right) z_\zeta(t)\,\widetilde{u}\mathrm{d}\sigma\mathrm{d}t, \\ &\forall c \in Y, \forall b \in Z, \end{aligned} \quad (4.126)$$

where functions $\widetilde{u} \in H^2(Q_T)$ and $\widetilde{\lambda} \in H^2(Q_T)$ are solutions of problems (4.104) and (4.105), respectively. Since $\widetilde{u}(x,0) = \widetilde{\lambda}(x,T) = 0$, then (4.120) and (4.121) imply that second and third lines in (4.126) equal zero, which proves (4.123) and (4.124). The validity of (4.125) follows from (4.108) and (4.109).

Thus, Theorem 4.8 rigorously establishes the same expression for the Fréchet derivative of the Tikhonov functional as the one established heuristically for the Lagrangian in (4.17) (Sect. 4.4). One can see that this rigorous derivation has required a significant preparation described in Sects. 4.6 and 4.7. We also note that the Tikhonov functional is the primary one (Chap. 1). On the other hand, the Lagrangian is a secondary one. Nevertheless, quite often, a simple derivation like the one in Sect. 4.4 is preferable when one wants to skip lengthy discussions. In fact, we use such simplified derivations in Chaps. 5 and 6.

We refer to [77, 91] for different approaches to derivations of the Fréchet derivatives for the Tikhonov functionals for some 1D CIPs. In the earlier work [53], the Fréchet derivative for the Tikhonov functional was derived for a parameter identification problem. Parameter identification problems are different from CIPs.

The author of [53] has kindly informed us that the complete proof of the result of [53] is presented in his Ph.D. thesis (1971).

4.9 Relaxation with Mesh Refinements

The goal of this section is establish the *central property* of the adaptivity technique for ill-posed problems: the relaxation. In other words, we prove that the accuracy of the reconstruction of the regularized solution indeed improves with mesh refinements. This improvement takes place until the regularized solution is indeed achieved. While such improvements were constantly observed computationally in all previous works on the adaptivity, the first analytical confirmation of this phenomenon was done in the paper [29]. The proof of the relaxation property is presented in Sect. 4.9.3. This proof is significantly simplified compared with the one of [29]. Sections 4.9.1 and 4.9.2 are preparatory ones, and ideas of [29] are used in these sections quite essentially. The local strong convexity Theorem 1.9.1.2 plays a significant role in this section. We remind that an analog of this theorem was proved in [29].

First, we introduce one of possible frameworks of functional analysis for the adaptive FEM for ill-posed problems, see, e.g., [15], for another possible framework. Next, we prove the relaxation property of the adaptivity. In other words, we prove that the next mesh refinement indeed provides a more accurate approximation for the regularized coefficient than the previous one. This is done for an abstract nonlinear operator. Since in real computations we work with finite dimensional spaces of standard piecewise linear finite elements, we focus our theory only on these spaces.

To explain intuitively the importance of the relaxation property, consider first an example of the FDM for a "good" boundary value problem. Let h be the grid step size of the FDM, U be the exact solution of that problem, and U_h the FDM solution. Then the standard convergence theorem ensures that [146]

$$\|U - U_h\| \leq C h^p, \ p = \text{const.} > 0, \tag{4.127}$$

where $\|\cdot\|$ is a certain norm in the discrete space which corresponds to finite differences. The inequality (4.127) ensures of course that the accuracy of the FDM solution improves as $h \to 0$. However, (4.127) does not imply a more subtle effect. Specifically, consider now two grid step sizes h_1 and h_2 with $h_2 < h_1$. Then (4.127) does not guarantee that $\|U - U_{h_2}\| \leq \theta \|U - U_{h_1}\|$, where $\theta \in (0, 1)$ is called "the relaxation parameter."

Unlike the above, the relaxation property for the adaptivity guarantees just that. Roughly speaking, let x_n be the minimizer of the Tikhonov functional obtained after n mesh refinements. Let $x_{\alpha(\delta)}$ be the regularized solution, the existence and uniqueness of which is guaranteed by Theorem 1.9.1.2 The relaxation property

means that if $x_n \neq x_\alpha$, then for any number $\eta_n \in (0,1)$, one can choose the maximal grid step size h_{n+1} of the next mesh refinement so small that

$$\left\| x_{n+1} - x_{\alpha(\delta)} \right\| \leq \eta_n \left\| x_n - x_{\alpha(\delta)} \right\|. \tag{4.128}$$

Hence, the improvement of the accuracy with mesh refinements is guaranteed by (4.128).

The next natural question to pose is *what does (4.128) give us in terms of a better approximation of the exact solution* x^*? To address this question, we recall the estimate (1.69) of Theorem 1.9.1.2:

$$\left\| x_{\alpha(\delta)} - x^* \right\| \leq \xi \left\| x_0 - x^* \right\|, \ \forall \delta \in (0, \delta_1), \tag{4.129}$$

where $\xi \in (0,1)$ and $\delta_1 = \delta_1(\xi) \in (0,1)$. It follows from (4.128) and (4.129) that

$$\left\| x_{n+1} - x^* \right\| \leq \xi \left\| x_0 - x^* \right\| + \eta_n \left\| x_n - x_{\alpha(\delta)} \right\|.$$

Therefore, the accuracy of the reconstruction of the exact solution x^* improves with mesh refinements, and when n grows, it approaches its limiting value of $\left\| x_{\alpha(\delta)} - x^* \right\|$ for a given noise level δ. Furthermore, this limiting value is strictly less than the distance between the first guess x_0 and the exact solution x^*. In other words, an improvement of the accuracy of the reconstruction of the regularized solution leads to an improvement of the accuracy of the reconstruction of the exact solution, compared with the first guess.

4.9.1 The Space of Finite Elements

We consider only standard piecewise linear finite elements, which are triangles in 2D and tetrahedra in 3D. Let $\Omega \subset \mathbb{R}^n, n = 2,3$ be a bounded domain. Consider a triangulation T_0 of Ω with a rather coarse mesh. We will have several more triangulations with finer meshes. Let T be one of such triangulations such that

$$\Omega = \cup_{j=1}^{el} K_j, \quad K_j \in T,$$

where el is the number of non-overlapping elements K_j in the mesh T.

Following Sect. 76.3 of [67], we construct the linear space of piecewise linear functions, which are continuous in $\overline{\Omega}$. Let $\{N_j\}_{j=1}^{p(T)}$ be the set of nodal points of those triangles/tetrahedra and $\{e_j\}_{j=1}^{p(T)}$ be the corresponding nodal basis for the finite element space $V_h(T)$ defined as

$$V_h(T) = \left\{ v(x) \in V(T) : v \in C\left(\overline{\Omega}\right), v|_{K_j} \text{ is linear on } K_j \in T \right\},$$

where

$$V(T) = \left\{ v(x) : v(x) \in H^1(\Omega) \right\}. \tag{4.130}$$

Here, $p(T)$ denotes the number of the points in the mesh T. The finite element space $V_h(T) \subset V(T)$, where $V(T)$ is defined by (4.130). Thus, the functions $\{e_j(x,T)\}_{j=1}^{p(T)} \subset C\left(\overline{\Omega}\right)$ are piecewise linear functions. They are called *test* functions.

These functions are linearly independent in Ω and satisfy

$$e_j(N_i,T) = \begin{cases} 1, i = j, \\ 0, i \neq j. \end{cases}$$

Thus, the dimension of the space $V_h(T)$ equals to the number $p(T)$ of test functions $\{e_j(x,T)\}_{j=1}^{p(T)}$,

$$\dim V_h(T) = p(T)$$

and each function $v \in V_h(T)$ can be represented as

$$v(x) = \sum_{j=1}^{p(T)} v_j(N_j) e_j(x,T).$$

Let $h\left(K_j\right)$ be diameter of the triangle/tetrahedra $K_j \subset T$. Then the number h,

$$h = \max_{K_j \subset T} h\left(K_j\right),$$

is called the *maximal grid step size* of the triangulation T. Let ϖ be the radius of the maximal circle/sphere contained in K_j. We impose the shape regularity assumption for all triangles/tetrahedra uniformly for all possible triangulations T we consider. Specifically, we assume that in all triangulations T below,

$$a_1 \leqslant h\left(K_j\right) \leqslant \varpi a_2, \quad a_1, a_2 = \text{const.} > 0, \ \forall K_j \subset T, \ \forall T, \tag{4.131}$$

where numbers a_1, a_2 are independent on the triangulation T. Obviously, the number of all possible triangulations satisfying (4.131) is finite. Thus, we introduce the following finite dimensional linear space H_1:

$$H_1 = \bigcup_T \text{Span}\left(V(T)\right), \ \forall T \text{ satisfying (4.131)}.$$

Hence,

$$\dim H_1 < \infty,$$

$$H_1 \subset \left(C\left(\overline{\Omega}\right) \cap H^1(\Omega)\right), \ \partial_{x_i} f \in L_\infty(\Omega), \ \forall f \in H_1, \tag{4.132}$$

where the inclusion is understood as an inclusion of sets. Hence, functions belonging to H_1 have the same properties as those of functions of the space Z defined in (4.103). We equip H_1 with the same inner product as the one in $L_2(\Omega)$. Let $(,)$ and $\|\cdot\|$ be the inner product and the norm in H_1, respectively:

$$\|f\|_{H_1} := \|f\|_{L_2(\Omega)} := \|f\|, \ \forall f \in H_1.$$

Thus, H_1 became a finite dimensional subspace of the space $L_2(\Omega)$.

We view the space H_1 as an "ideal" space of very fine finite elements, which cannot be reached in practical computations. At the same time, all other spaces of finite elements we work with in the adaptivity procedure are subspaces of H_1.

With reference to the mesh refinement process in the adaptivity, we now explain how do we construct triangulations $\{T_n\}$ as well as corresponding subspaces $\{M_n\}$ of the space H_1 with which we work with. First, we set

$$M_0 := V_h(T_0) \subset H_1.$$

Suppose that the pair (T_n, M_n) is constructed after n mesh refinements in the adaptivity and that the basis functions in the space M_n are $\left\{e_j(x, T_n)\right\}_{j=1}^{p(T_n)}$. We now want to refine the mesh again while keeping (4.131). We define the pair (T_{n+1}, M_{n+1}) as follows. First, following mesh refinement recommendations in the adaptivity (Sect. 4.12), we refine the mesh in the standard manner as it is usually done in triangular/tetrahedron finite elements. When doing so, we keep (4.131). Hence, we obtain a triangulation T_{n+1} and the corresponding test functions $\left\{e_j(x, T_{n+1})\right\}_{j=1}^{p(T_{n+1})}$. It is well known that test functions $\left\{e_j(x, T_n)\right\}_{j=1}^{p(T_n)}$ linearly depend from new test functions $\left\{e_j(x, T_{n+1})\right\}_{j=1}^{p(T_{n+1})}$. Thus, we define the subspace M_{n+1} as

$$M_{n+1} := \text{Span}\left(\left\{e_j(x, T_{n+1})\right\}_{j=1}^{p(T_{n+1})}\right).$$

Therefore, we have obtained a finite set of linear subspaces $\{M_n\}_{n=1}^{\widetilde{N}}$ of the space H_1. Each subspace M_n corresponds to the mesh refinement number n and

$$M_n \subset M_{n+1} \subset H_1, n \in \left[0, \widetilde{N}\right].$$

Let I be the identity operator on H_1. For any subspace $M \subset H_1$, let $P_M : H_1 \to M$ be the orthogonal projection operator onto M_n. Denote for brevity:

$$P_n := P_{M_n}.$$

Let h_n be the maximal grid step size of T_n. By construction, $h_{n+1} \leqslant h_n$. Consider an arbitrary function $f \in H_1$. Let f_n^I be its standard interpolant on triangles/tetrahedra of T_n: see Sect. 76.3 of [67]. By properties of orthogonal projection operators,

$$\|f - P_n f\| \leqslant \left\|f - f_n^I\right\|, \ \forall f \in H_1.$$

Hence, (4.13) and (4.132) imply that

$$\|f - P_n f\| \leqslant K \|\nabla f\|_{L_\infty(\Omega)} h_n, \ \forall f \in H_1, \tag{4.133}$$

where $K = K(\Omega, \varpi, a_1, a_2)$ is a positive constant depending only on the domain Ω and numbers ϖ, a_1, a_2 in (4.131).

4.9.2 Minimizers on Subspaces

Since in the adaptivity procedure we sequentially minimize the Tikhonov functional on subspaces $\{M_k\}_{k=0}^{\widetilde{N}}$, we need to prove first the existence of minimizers on each of these subspaces. We impose the same conditions on the operator F as ones in the local strong convexity Theorem 1.9.1.2. Let H_2 be another Hilbert space and $\|\cdot\|_2$ be the norm in H_2. Just as in Sect. 1.9.1, let $\mathcal{L}(H_1, H_2)$ be the space of bounded linear operators mapping from H_1 into H_2. The norm in $\mathcal{L}(H_1, H_2)$ is also denoted as $\|\cdot\|$ for brevity. It will always be clear from the context of this section whether the sign $\|\cdot\|$ is related to an element of H_1 or to an element of $\mathcal{L}(H_1, H_2)$. Let $G \subseteq H_1$ be the closure of a bounded open set and $\widetilde{F} : G \to H_2$ be a continuous operator. Consider the equation

$$\widetilde{F}(x) = y. \tag{4.134}$$

Assume that the element y in (4.134) is given with an error, $\|y - y^*\|_2 \leq \delta$, where y^* is the exact right-hand side of (4.134), which corresponds to its exact solution $x^* \in G$, $\widetilde{F}(x^*) = y^*$. We assume that x^* is an interior point of the set G. Again, we replace the operator $\widetilde{F}(x)$ with the operator $F(x) = \widetilde{F}(x) - y$. Hence, (4.134) becomes

$$F(x) = 0, \ x \in G, \tag{4.135}$$

where

$$\left\|F\left(x^*\right)\right\|_2 \leq \delta. \tag{4.136}$$

Since $\dim H_1 < \infty$, then all norms are equivalent in this space. In particular, there exists a constant $C = C(H_1, \Omega)$ such that

$$\|\nabla x\|_{L_\infty(\Omega)} \leq C \|x\|, \ \forall x \in H_1.$$

Hence, (4.133) implies that there exists a constant $K_1 = K_1(K, H_1) = CK > 0$ independent on the subspace M_n such that

$$\|x - P_n x\| \leq K_1 \|x\| h_n, \ \forall x \in H_1, \forall n \in \left[0, \widetilde{N}\right]. \tag{4.137}$$

Let the point $x_0 \in G$. We consider x_0 as the first guess for the exact solution x^*. In particular, in the case of the CIP of Sect. 2.1, $x_0 = x_{\text{glob}}$ is obtained on the first stage of our two-stage numerical procedure. The Tikhonov functional for the problem (4.135) and (4.136) is

$$J_\alpha(x) = \frac{1}{2}\|F(x)\|_2^2 + \frac{\alpha}{2}\|x - x_0\|^2. \tag{4.138}$$

Recall one of notations of Sect. 1.9.1: for any $\beta > 0$ and for any $x \in H_1$

$$V_\beta(x) = \{z \in H_1 : \|x - z\| < \beta\}.$$

Denote $Int(G)$ the set of interior points of the set G. In other words, for each point $x \in Int(G)$, there exists a number $\beta(x) > 0$ such that $V_\beta(x) \subset G$.

Theorem 4.9.2 claims the existence and uniqueness of the minimizer of the functional (4.138) on each subspace of the space H_1, as long as the maximal grid step size of finite elements, which are involved in that subspace, is sufficiently small. A similar theorem was proved in [29] by a different method. The smallness of that grid step size depends on the upper estimate of the norm $\|x^*\|$ of the exact solution. By the fundamental concept of Tikhonov (Sect. 1.4), one can assume an a priori knowledge of this estimate.

Theorem 4.9.2. *Let H_1 be the space of finite elements introduced in Sect. 4.9.1 and H_2 be another Hilbert space. Let $G \subset H_1$ be the closure of a bounded open set and $F : G \to H_2$ be a continuous one-to-one operator. Let $x^* \in G$ be the exact solution of (4.135) with the exact data y^*, $\delta \in (0,1)$ be the error in the data, as in (4.136). Suppose that $V_1(x^*) \subset Int(G)$. Assume that for every $x \in V_1(x^*)$, the operator F has the Frechét derivative $F'(x) \in \mathcal{L}(H_1, H_2)$. Suppose that this derivative is uniformly bounded and Lipschitz continuous in $V_1(x^*)$, i.e.,*

$$\left\|F'(x)\right\| \leq N_1, \ \forall x \in V_1\left(x^*\right), \tag{4.139}$$

$$\left\|F'(x) - F'(z)\right\| \leq N_2\|x - z\|, \ \forall x, z \in V_1\left(x^*\right), \tag{4.140}$$

where $N_1, N_2 = \text{const.} \geq 1$. Let

$$\alpha = \alpha(\delta) = \delta^{2\mu}, \quad \forall \delta \in (0,1), \tag{4.141}$$

$$\mu = \text{const.} \in \left(0, \frac{1}{4}\right). \tag{4.142}$$

Let $M \subseteq H_1$ be a subspace of H_1. Then there exists a sufficiently small number $\delta_0 = \delta_0(N_1, N_2, \mu) \in (0,1)$ such that for all $\delta \in (0, \delta_0)$ the functional $J_{\alpha(\delta)}(x)$ is strongly convex on the set $V_{\alpha(\delta)}(x^*) \cap M$ with the strong convexity constant $\alpha/2$. Assume that $\|x^*\| \leq A$ and the number A is known in advance. Suppose that the maximal grid step size $\widetilde{h}$ of finite elements of M is so small that

$$\widetilde{h} \leq \frac{\delta^{4\mu}}{5AN_2K_1}, \tag{4.143}$$

where K_1 is the constant in (4.137). Furthermore, assume that the first guess x_0 for the exact solution x^* in the functional (4.138) is so accurate that

$$\|x_0 - x^*\| < \frac{\delta^{3\mu}}{3}. \tag{4.144}$$

Then there exists unique minimizer $x_M \in G \cap M$ of the functional (4.138) and $x_M \in V_{\delta^{3\mu}}(x^*) \cap M$.

Proof. If $M = H_1$, then both the strong convexity of $J_{\alpha(\delta)}(x)$ on the set $V_{\alpha(\delta)}(x^*)$ and the existence of the minimizer follows from Theorem 1.9.1.2 Hence, below, we work with the case $M \neq H_1$. We now establish the strong convexity of the functional $J_{\alpha(\delta)}$ on the set $V_{\alpha(\delta)}(x^*) \cap M$ with the strong convexity constant $\alpha(\delta)/2$. In terms of Theorem 1.9.1.2 **,** we should work in this case with $P_M J'_{\alpha(\delta)}$ rather than with $J'_{\alpha(\delta)}$. Consider two arbitrary points $x, y \in V_{\alpha(\delta)}(x^*) \cap M$. Then

$$((I - P_M) z, x - y) = 0, \forall z \in H_1.$$

Hence, using Theorem 1.9.1.2, we obtain

$$\begin{aligned}\left(P_M J'_{\alpha(\delta)}(x) - P_M J'_{\alpha(\delta)}(y), x-y\right) &= \left((I-P_M)\left(J'_{\alpha(\delta)}(x) - J'_{\alpha(\delta)}(y)\right), x - y\right) \\ &+ \left(P_M J'_{\alpha(\delta)}(x) - P_M J'_{\alpha(\delta)}(y), x - y\right) \\ &= \left(J'_{\alpha(\delta)}(x) - J'_{\alpha(\delta)}(y), x - y\right) \geq \frac{\alpha}{2}\|x - y\|^2.\end{aligned}$$

We now prove that the point $P_M x^* \in Int(G)$ if the number δ_0 is sufficiently small. Indeed, by (4.137) and (4.143),

$$\|x^* - P_M x^*\| \leq K_1 \|x^*\| \widetilde{h} \leq AK_1\widetilde{h} \leq \frac{\delta^{4\mu}}{5} < 1.$$

Hence, $P_M x^* \in V_1(x^*)$. Since $V_1(x^*) \subset Int(G)$, then $P_M x^* \in Int(G)$.

Since G is a closed bounded set in a finite dimensional space, then there exists a minimizer $x_M \in G$ of the functional (4.138). We have $J_{\alpha(\delta)}(x_M) \leq J_{\alpha(\delta)}(P_M x^*)$. Hence,

$$\begin{aligned}\|x_M - x_0\| &\leq \frac{\|F(P_M x^*)\|_2}{\sqrt{\alpha}} + \|P_M x^* - x_0\| \\ &\leq \frac{\|F(P_M x^*)\|_2}{\sqrt{\alpha}} + \|P_M x^* - x^*\| + \|x^* - x_0\|. \end{aligned} \tag{4.145}$$

Since $\|x_M - x_0\| \geq \|x_M - x^*\| - \|x^* - x_0\|$, then (4.137) and (4.143)–(4.145) imply that

$$\|x_M - x^*\| \leq \frac{\|F(P_M x^*)\|_2}{\sqrt{\alpha}} + \frac{3}{4}\delta^{3\mu}. \tag{4.146}$$

Next, by (4.136) and (4.141),

$$\begin{aligned}\frac{\|F(P_M x^*)\|_2}{\sqrt{\alpha}} &= \frac{\|F(P_M x^*) - F(x^*)\|_2}{\sqrt{\alpha}} + \frac{\|F(x^*)\|_2}{\sqrt{\alpha}} \\ &\leq \frac{\|F(P_M x^*) - F(x^*)\|_2}{\sqrt{\alpha}} + \delta^{1-\mu}.\end{aligned}$$

Thus,

$$\frac{\|F(P_M x^*)\|_2}{\sqrt{\alpha}} \leq \frac{\|F(P_M x^*) - F(x^*)\|_2}{\sqrt{\alpha}} + \delta^{1-\mu}. \tag{4.147}$$

By (1.59) (Sect. 1.9.1),

$$F\left(P_M x^*\right) - F\left(x^*\right) = \int_0^1 \left(F'\left(x^* + \theta\left(P_M x^* - x^*\right)\right), P_M x^* - x^*\right) \mathrm{d}\theta.$$

Hence, using (4.137), (4.139), and (4.143), we obtain

$$\left\|F\left(P_M x^*\right) - F\left(x^*\right)\right\|_2 \leq N_2 \|x^* - P_M x^*\| \leq A K_1 N_2 \widetilde{h} \leq \frac{\delta^{4\mu}}{5}.$$

Hence, by (4.141) and (4.147)

$$\frac{\|F(P_M x^*)\|_2}{\sqrt{\alpha}} \leq \frac{\delta^{3\mu}}{5} + \delta^{1-\mu}.$$

This and (4.146) lead to

$$\|x_M - x^*\| \leq \frac{19}{20}\delta^{3\mu}\left(1 + \frac{20}{19}\delta^{1-4\mu}\right) < \delta^{3\mu}.$$

Thus, any minimizer $x_M \in G \cap M$ of the functional $J_{\alpha(\delta)}$ is such that $x_M \in V_{\delta^{3\mu}}(x^*) \cap M$. Since the functional $J_{\alpha(\delta)}$ is strongly convex on the set $V_{\delta^{3\mu}}(x^*) \cap M$, then the minimizer $x_M \in G \cap M$ of $J_{\alpha(\delta)}$ is unique. □

4.9.3 Relaxation

Theorem 4.9.3 establishes the relaxation property of mesh refinements.

Theorem 4.9.3. *Let $M_n \subset H_1$ be the subspace obtained after n mesh refinements, as described in Sect. 4.9.1. Let h_n be the maximal grid step size of the subspace M_n. Suppose that all conditions of Theorem 4.9.2 hold with the only exception that the subspace M is replaced with the subspace M_n and the inequality (4.143) is replaced with*

$$h_n \leq \frac{\delta^{4\mu}}{5AN_2K_1}. \tag{4.148}$$

Let $x_n \in V_{\delta^{3\mu}}(x^*) \cap M_n$ be the minimizer of the Tikhonov functional (4.138) on the set $G \cap M_n$, the existence of which is guaranteed by Theorem 4.9.2. Assume that the regularized solution $x_{\alpha(\delta)} \neq x_n$, i.e., $x_{\alpha(\delta)} \notin M_n$, meaning that the regularized solution is not yet reached after n mesh refinements. Let $\eta_n \in (0,1)$ be an arbitrary number and $K_1 > 0$ be the constant in (4.137). Then one can choose the maximal grid size $h_{k+1} = h_{k+1}(N_3, \delta, A, K_1) \in (0, h_k]$ of the mesh refinement number $(n+1)$ so small that

$$\left\| x_{n+1} - x_{\alpha(\delta)} \right\| \leq \eta_n \left\| x_n - x_{\alpha(\delta)} \right\|, \tag{4.149}$$

where $x_{n+1} \in V_{\delta^{3\mu}}(x^*) \cap M_{n+1}$ is the minimizer of the Tikhonov functional (4.138) on the set $G \cap M_{n+1}$ and $N_3 = N_3(N_1, N_2) = \text{const.} > 0$ is a constant depending only on constants N_1 and N_2 in (4.139) and (4.140).

Proof. In this proof, we denote for brevity $\alpha(\delta) := \alpha$. Let x_{n+1} be a minimizer of the functional (4.138) on the set $G \cap M_{n+1}$. Since inequality (4.148) is valid for h_{n+1}, then Theorem 4.9.2 implies that the minimizer x_{n+1} is unique and $x_{n+1} \in V_{\delta^{3\mu}}(x^*) \cap M_{n+1}$. Since by Theorem 4.9.2, the functional (4.138) is strongly convex on the set $V_{\delta^{3\mu}}(x^*) \cap M_{k+1}$ with the strong convexity constant $\alpha/2$, then Theorem 1.9.1.1 implies that

$$\frac{\alpha}{2} \left\| x_{n+1} - x_\alpha \right\|^2 \leq \left(J'_\alpha(x_{n+1}) - J'_\alpha(x_\alpha), x_{n+1} - x_\alpha \right). \tag{4.150}$$

Since x_{n+1} is the minimizer on $G \cap M_{n+1}$, then

$$\left(J'_\alpha(x_{n+1}), y \right) = 0, \ \forall y \in M_{n+1}.$$

Next, since x_α is the minimizer on the set $G \subset H_1$, then

$$\left(J'_\alpha(x_\alpha), z \right) = 0, \ \forall z \in H_1.$$

These justify the application of the *Galerkin orthogonality principle*,which is similar with (4.23) in Sect. 4.5 (also see references in that section):

$$\left(J'_\alpha(x_{n+1}) - J'_\alpha(x_\alpha), x_{n+1} - P_{n+1}x_\alpha\right) = 0. \tag{4.151}$$

Next,

$$x_{n+1} - x_\alpha = (x_{n+1} - P_{n+1}x_\alpha) + (P_{n+1}x_\alpha - x_\alpha).$$

Hence, (4.150) and (4.151) imply that

$$\frac{\alpha}{2}\|x_{n+1} - x_\alpha\|^2 \le \left(J'_\alpha(x_{n+1}) - J'_\alpha(x_\alpha), P_{n+1}x_\alpha - x_\alpha\right). \tag{4.152}$$

It was shown in the proof of Theorem 1.9.1.1 that conditions (4.139) and (4.140) imply that

$$\left\|J'_\alpha(x_{n+1}) - J'_\alpha(x_\alpha)\right\| \le N_3\|x_{n+1} - x_\alpha\|, \tag{4.153}$$

with a constant $N_3 = N_3(N_1, N_2) > 0$. Also, by (4.133),

$$\|x_\alpha - P_{n+1}x_\alpha\| \le K_1\|x_\alpha\| h_{n+1}. \tag{4.154}$$

Using the Cauchy-Schwarz inequality as well as (4.153) and (4.154), we obtain from (4.152)

$$\|x_{n+1} - x_\alpha\| \le \frac{2K_1N_3}{\delta^{2\mu}}\|x_\alpha\| h_{n+1}. \tag{4.155}$$

Since by one of conditions of Theorem 4.9.2 we have an a priori known upper estimate

$$\|x^*\| \le A, \tag{4.156}$$

we now estimate the norm $\|x_\alpha\|$ in (4.155) via the number A. Since by Theorem 4.9.2 $x_\alpha \in V_{\delta^{3\mu}/3}(x^*)$, then (4.156) leads to

$$\|x_\alpha\| \le \|x_\alpha - x^*\| + \|x^*\| \le \frac{\delta^{3\mu}}{3} + A.$$

Hence, (4.155) becomes

$$\|x_{n+1} - x_\alpha\| \le \frac{2K_1N_3}{\delta^{2\mu}}\left(\frac{\delta^{3\mu}}{3} + A\right)h_{n+1}. \tag{4.157}$$

Let $\eta_n \in (0,1)$ be an arbitrary number. Since $\|x_n - x_\alpha\| \ne 0$, then we can choose $h_{n+1} = h_{n+1}(N_2, \delta, A, K_1) \in (0, h_k]$ so small that

$$\frac{2K_1N_3}{\delta^{2\mu}}\left(\frac{\delta^{3\mu}}{3} + A\right)h_{n+1} \le \eta_n\|x_n - x_\alpha\|. \tag{4.158}$$

Comparing (4.157) with (4.158), we obtain the target estimate (4.149). □

Remarks 4.9.3. 1. An inconvenient aspect of Theorem 4.9.3 is that is not a constructive one. Indeed, since we do not know the regularized solution x_α, then we cannot effectively estimate the norm $\|x_n - x_\alpha\|$ from the below. This means that it is unclear how to practically choose the number h_{n+1} to ensure (4.149). In our numerical studies, we choose grid step sizes of local mesh refinements on the basis of our computational experience. Nevertheless, the main point of this theorem is that it ensures the image improvement in the case when the grid step size h_{n+1} is properly chosen. In other words, it says that the adaptive mesh refinement process is worthy to work with. The inequality (4.155) can be used for one of mesh refinement recommendations; see Sect. 4.12.

2. Furthermore, Theorem 4.9.3 as well as its specification Theorem 4.11.4 actually helps to decide when to stop mesh refinements; see tests in Sects. 4.15.3 and 4.16.2.

4.10 From the Abstract Scheme to the Coefficient Inverse Problem 2.1

In Sect. 4.9, we have considered an abstract operator F. Now, however, the question is on how to "project" those results on our specific coefficient inverse problem 2.1 formulated in Sect. 2.1. The goal of this section is to address this question. In other words, we reformulate here results of Sect. 4.9 for our specific case. In doing so, we restrict our attention to state and adjoint problems (4.81) and (4.82) of Sect. 4.7 since only solutions of these problems are involved in the Fréchet derivative (4.123) of the Tikhonov functional (4.118) for our CIP.

Let Y be the set of functions defined in (4.7) (Sect. 4.3) and H_1 be the finite dimensional space of finite elements constructed in Sect. 4.9.1. We define the set Y_1 as $Y_1 := Y \cap H_1$. And consider the closure $G := \overline{Y}_1$ in the norm $\|\cdot\|$, which is the norm in H_1. Hence,

$$G = \left\{c(x) \in H_1 : c(x) \in [1-\omega, d+\omega] \text{ for } x \in \overline{\Omega}\right\},$$

where $\omega \in (0,1)$ is a sufficiently small positive number. For every coefficient $c \in G$, consider the weak solution $u := u(x,t,c)$ of the state problem (4.81):

$$\begin{aligned} c(x)\, u_{tt} - \Delta u &= 0 \text{ in } Q_T, \\ u(x,0) &= u_t(x,0) = 0, \\ \partial_n u\,|_{S_T} &= p(x,t). \end{aligned} \tag{4.159}$$

Let $z_\zeta(t)$ be the function introduced in Sect. 4.3. Let the Hilbert space $H_2 := L_2(S_T)$. We define the operator F as

$$F : G \to H_2, \tag{4.160}$$

$$F(c)(x,t) = z_\zeta(t)\left[g(x,t) - u(x,t,c)\right], \ (x,t) \in S_T, \tag{4.161}$$

where the function $u := u(x,t,c)$ is the weak solution of the problem (4.159).

Theorem 4.10. *Let $\Omega \subset \mathbb{R}^3$ be a convex bounded domain with the boundary $\partial\Omega \in C^2$. Suppose that there exists a function $a(x)$ satisfying conditions (4.80). Assume that there exists a function $P(x,t)$ satisfying conditions (4.83)–(4.85) of Sect. 4.7. Then the operator F in (4.160) and (4.161) has the Fréchet derivative $F'(c)(b)$ for every function $c \in Int(G)$, where $b \in H_1$ is an arbitrary function. The expression for the operator $F'(c)(b)$ is*

$$F'(c)(b) = -z_\zeta(t)\widetilde{u}(x,t,c,b)\,|_{S_T}, \tag{4.162}$$

where the function $\widetilde{u}(x,t,c,b) \in H^2(Q_T)$ is the solution of the boundary value problem (4.104) of Sect. 4.7. Let $C = C\left(\Omega, d, \omega, z_\zeta, a\right) > 0$ be the constant of Theorem 4.7.1 Then

$$\left\|F'(c)\right\|_{\mathcal{L}(H_1,H_2)} \leq \exp(CT)\,\|P\|_{H^6(Q_T)}, \ \forall c \in Int(G). \tag{4.163}$$

In addition, the operator $F'(c)$ is Lipschitz continuous:

$$\left\|F'(c_1) - F'(c_2)\right\|_{\mathcal{L}(H_1,H_2)} \leq \exp(CT)\,\|P\|_{H^6(Q_T)}\,\|c_1 - c_2\|, \ \forall c_1, c_2 \in Int(G). \tag{4.164}$$

Proof. The existence of the Fréchet derivative $F'(c)$ of the operator F and the formula (4.162) follow from Theorem 4.7.2 and the trace theorem. Next, by (4.106),

$$\|\widetilde{u}(x,t,c,b)\|_{H^1(Q_T)} \leq \exp(CT)\,\|P\|_{H^6(Q_T)}\,\|b\|, \ \forall b \in H_1.$$

Hence, the trace theorem and (4.162) imply

$$\left\|F'(c)(b)\right\|_{H_2} \leq \exp(CT)\,\|P\|_{H^6(Q_T)}\,\|b\|, \ \forall b \in H_1,$$

which leads to (4.163).

We now prove (4.164). Denote

$$\widetilde{u}^{(1)} = \widetilde{u}(x,t,c_1,b), \ \widetilde{u}^{(2)} = \widetilde{u}(x,t,c_2,b), \ v = \widetilde{u}^{(1)} - \widetilde{u}^{(2)}, \tag{4.165}$$

$$u^{(1)} = u(x,t,c_1), \ u^{(2)} = u(x,t,c_2), \ U = u^{(1)} - u^{(2)}. \tag{4.166}$$

It follows from (4.162) and the trace theorem that it is sufficient to prove that

$$\|v\|_{H^1(Q_T)} \leq \exp(CT)\,\|P\|_{H^6(Q_T)}\,\|c_1 - c_2\| \cdot \|b\|, \ \forall b \in H_1, \forall c_1, c_2 \in Int(G). \tag{4.167}$$

It can be derived from (4.104), (4.159), (4.165), and (4.166) that functions U and v are solutions of the following initial boundary value problems:

$$\begin{aligned} c_1 U_{tt} &= \Delta U - (c_1 - c_2)\, u_{tt}^{(2)}, \text{ in } Q_T, \\ U(x,0) &= U_t(x,0) = 0, \\ \partial_n U\,|_{S_T} &= 0; \end{aligned} \tag{4.168}$$

$$\begin{aligned} c_1 v_{tt} &= \Delta v - (c_1 - c_2)\, \widetilde{u}_{tt}^{(2)} - b(x)\, U_{tt}, \text{ in } Q_T, \\ v(x,0) &= v_t(x,0) = 0, \\ \partial_n v\,|_{S_T} &= 0. \end{aligned} \tag{4.169}$$

It follows from Corollary 4.6 and estimate (4.88) of Theorem 4.7.1 that the following estimate holds for the solution U of the problem (4.168):

$$\|U_{tt}\|_{L(Q_T)} \leq \exp(CT)\, \|P\|_{H^6(Q_T)}\, \|c_1 - c_2\|. \tag{4.170}$$

By Theorem 4.7.2, the function $\widetilde{u} \in H^2(Q_T)$. Hence, by (4.165), the function $v \in H^2(Q_T)$. Next, by (4.111),

$$\|\widetilde{u}_{tt}\|_{L_2(Q_T)} \leq \exp(CT)\, \|P\|_{H^6(Q_T)}\, \|b\|_Z. \tag{4.171}$$

Hence, a combination of (4.170) and (4.171) with the standard energy estimate applied to the initial boundary value problem (4.169) leads to (4.167). □

4.11 A Posteriori Error Estimates for the Regularized Coefficient and the Relaxation Property of Mesh Refinements

Theorem 4.10 implies that the operator F in (4.160) and (4.161) satisfies conditions of Theorem 1.9.1.2 On the other hand, it is this operator which forms the Tikhonov functional (4.118) of Sect. 4.8. Therefore, Theorems 1.9.1.2, 4.9.2, and 4.9.3, which were initially formulated for the Tikhonov functional generated by an abstract operator F, can be reformulated for the specific Tikhonov functional (4.118). The latter is done in this section. Theorems 4.11.1 and 4.11.2 of this section are a posteriori error estimates. In other words, in these theorems, the accuracy of the reconstruction of the regularized coefficient is estimated via the $L_2(\Omega)$-norm of the Fréchet derivative of the Tikhonov functional. The validity of all theorems of this

section follows from Theorem 4.10 as well as from the validity of corresponding theorems proved above for the abstract operator F. In this section, $\|\cdot\|$ denotes the norm in the space of finite elements H_1, which was introduced in Sect. 4.9.1.

For the convenience of the reader, we remind that the Tikhonov functional (4.118) has the form

$$E_\alpha(c) = \frac{1}{2}\int\limits_{S_T} (u\mid_{S_T} - g(x,t))^2 z_\zeta(t)\,\mathrm{d}\sigma\mathrm{d}t + \frac{1}{2}\alpha\int\limits_{\Omega}(c-c_{\mathrm{glob}})^2\mathrm{d}x, \tag{4.172}$$

where $c_{\mathrm{glob}} \in Int(G)$ is the solution of our coefficient inverse problem 2.1 obtained via the approximately globally convergent algorithm of Sect. 2.6.1. In other words, c_{glob} is obtained on the first stage of our two-stage numerical procedure. By our common scheme, we also introduce the error of the level δ in the function $g(x,t)$ in (4.161). So, we assume that

$$g(x,t) = g^*(x,t) + g_\delta(x,t);\ g^*, g_\delta \in L_2(S_T) = H_2, \tag{4.173}$$

where $g^*(x,t)$ is the exact data and the function $g_\delta(x,t)$ represents the error in these data, i.e.,

$$\|g_\delta\|_{L_2(S_T)} \leq \delta. \tag{4.174}$$

As it was stated in Remark 2.1 as well as in Sect. 1.10.1, the question of uniqueness of the coefficient inverse problem 2.1 is not yet addressed. The same is true for the uniqueness of the solution of (4.161). On the other hand, we need uniqueness in the local strong convexity Theorem 1.9.1.2 Therefore, we have no choice but to assume that uniqueness takes place. Thus, we introduce the following:

Assumption 4.11. The operator $F(c)$ defined in (4.160) and (4.161) is one-to-one.

Theorem 4.11.1 is the direct analog of Theorem 1.9.1.2 for the specific case of the Tikhonov functional (4.172). Note that if a function $c \in H_1$ is such that $c \in [1,d]$, then $c \in Int(G)$.

Theorem 4.11.1. *Let $\Omega \subset \mathbb{R}^3$ be a convex bounded domain with the boundary $\partial\Omega \in C^3$. Suppose that there exists a function $a(x)$ satisfying conditions (4.80) and that there exist functions $P(x,t), \Phi(x,t)$ satisfying conditions (4.83)–(4.85) of Sect. 4.7. Suppose that assumption 4.11 as well as conditions (4.173) and (4.174) hold. Let the function $u = u(x,t,c) \in H^2(Q_T)$ in (4.172) be the solution of the state problem (4.159) for the function $c \in G$, where the set $G \subset H_1$ is defined in (4.158). Assume that there exists the exact solution $c^* \in G$ of the equation $F(c^*) = 0$ for the case when the function g in (4.161) is replaced with the function g^* in (4.173). Let $c^*(x) \in [1,d]$. Let in (4.174)*

$$\alpha = \alpha(\delta) = \delta^{2\mu}, \quad \forall \delta \in (0,1),$$

$$\mu = \text{const.} \in \left(0, \frac{1}{4}\right).$$

Furthermore, let in (4.172) the function $c_{\text{glob}} \in G$ *be such that*

$$\left\| c_{\text{glob}} - c^* \right\| < \frac{\delta^{3\mu}}{3}.$$

Then there exists a sufficiently small number $\delta_0 = \delta_0 \left(\Omega, d, \omega, z_\zeta, a, \|P\|_{H^6(Q_T)}, \mu\right) \in (0,1)$ *such that for all* $\delta \in (0, \delta_0)$*, the functional* $E_{\alpha(\delta)}(c)$ *in (4.172) is strongly convex in the neighborhood* $V_{\alpha(\delta)}(c^*)$ *of the function* c^* *with the strong convexity constant* $\alpha/2$*. In other words,*

$$\|c_1 - c_2\|^2 \leq \frac{2}{\delta^{2\mu}} \left(E'_{\alpha(\delta)}(c_1) - E'_{\alpha(\delta)}(c_2), c_1 - c_2 \right), \ \forall c_1, c_2 \in H_1, \tag{4.175}$$

where $(,)$ *is the scalar product in* $L_2(\Omega)$ *and the expression for the Fréchet derivative* $E'_{\alpha(\delta)}$ *is in (4.123). Also, there exists the unique regularized solution* $c_{\alpha(\delta)}$ *of (4.172) and* $c_{\alpha(\delta)} \in V_{\delta^{3\mu}/3}(x^*)$*. In addition, the gradient method of the minimization of the functional* $E_{\alpha(\delta)}(c)$*, which starts at* c_{glob}*, converges to* $c_{\alpha(\delta)}$*. Furthermore, let* $\xi \in (0,1)$ *be an arbitrary number. Then there exists a number* $\delta_1 = \delta_1 \left(\Omega, d, \omega, z_\zeta, a, \|P\|_{H^6(Q_T)}, \mu, \xi\right) \in (0, \delta_0)$ *such that*

$$\left\| c_{\alpha(\delta)} - c^* \right\| \leq \xi \left\| c_{\text{glob}} - c^* \right\|, \ \forall \delta \in (0, \delta_1).$$

In other words, the regularized solution $c_{\alpha(\delta)}$ *provides a better accuracy than the solution obtained on the first stage of our two-stage numerical procedure.*

Theorem 4.11.2 specifies the estimate of the norm $\left\| c_{\alpha(\delta)} - c^* \right\|$ via the norm of the Fréchet derivative of the functional $E_{\alpha(\delta)}(c)$.

Theorem 4.11.2. *Assume that conditions of Theorem 4.11.1 hold. Then, for any function* $c \in V_{\alpha(\delta)}(c^*)$*,*

$$\left\| c - c_{\alpha(\delta)} \right\| \leq \frac{2}{\delta^{2\mu}} \left\| P_{H_1} E'_{\alpha(\delta)}(c) \right\| \leq \frac{2}{\delta^{2\mu}} \left\| E'_{\alpha(\delta)}(c) \right\|_{L_2(\Omega)}, \tag{4.176}$$

where the function $E'_{\alpha(\delta)}(c)(x)$ *is defined in (4.123) and* $P_{H_1} : L_2(\Omega) \to H_1$ *is the orthogonal projection operator of the space* $L_2(\Omega)$ *on its subspace* H_1*.*

Proof. By Theorem 4.8, the Fréchet derivative $E'_{\alpha(\delta)}(c)(x) \in L_\infty(\Omega)$. Hence, $E'_\alpha(c) \in L_2(\Omega)$. Next, since $c_{\alpha(\delta)}$ is the minimizer of the functional $E_{\alpha(\delta)}(c)$ on the set G and $c_{\alpha(\delta)} \in Int(G)$, then

$$P_{H_1} E'_{\alpha(\delta)} \left(c_{\alpha(\delta)} \right) = 0. \tag{4.177}$$

Also, since $c - c_{\alpha(\delta)} \in H_1$, then

$$\left(E'_{\alpha(\delta)}(c) - E'_{\alpha(\delta)}\left(c_{\alpha(\delta)}\right), c - c_{\alpha(\delta)}\right)$$
$$= \left(P_{H_1} E'_{\alpha(\delta)}(c) - P_{H_1} E'_{\alpha(\delta)}\left(c_{\alpha(\delta)}\right), c - c_{\alpha(\delta)}\right).$$

Hence, by (4.175) and (4.177),

$$\left\|c - c_{\alpha(\delta)}\right\|^2 \leq \frac{2}{\delta^{2\mu}}\left(E'_{\alpha(\delta)}(c) - E'_{\alpha(\delta)}\left(c_{\alpha(\delta)}\right), c - c_{\alpha(\delta)}\right)$$
$$= \frac{2}{\delta^{2\mu}}\left(P_{H_1} E'_{\alpha(\delta)}(c) - P_{H_1} E'_{\alpha(\delta)}\left(c_{\alpha(\delta)}\right), c - c_{\alpha(\delta)}\right)$$
$$= \frac{2}{\delta^{2\mu}}\left(P_{H_1} E'_{\alpha(\delta)}(c), c - c_{\alpha(\delta)}\right) \leq \frac{2}{\delta^{2\mu}}\left\|P_{H_1} E'_{\alpha(\delta)}(c)\right\| \cdot \left\|c - c_{\alpha(\delta)}\right\|.$$

Thus,

$$\left\|c - c_{\alpha(\delta)}\right\|^2 \leq \frac{2}{\delta^{2\mu}}\left\|P_{H_1} E'_{\alpha(\delta)}(c)\right\| \cdot \left\|c - c_{\alpha(\delta)}\right\|.$$

Dividing this by $\left\|c - c_{\alpha(\delta)}\right\|$ and noting that

$$\left\|P_{H_1} E'_{\alpha(\delta)}(c)\right\| \leq \left\|E'_{\alpha(\delta)}(c)\right\|_{L_2(\Omega)},$$

we obtain (4.176). □

Theorem 4.11.3. *Assume that conditions of Theorem 4.11.1 hold. Let* $\|c^*\| \leq A$, *where the constant* A *is given. Let* $M_n \subset H_1$ *be the subspace obtained after* n *mesh refinements as described in Sect. 4.9.1. Let* h_n *be the maximal grid step size of the subspace* M_n. *Let* $C = C\left(\Omega, d, \omega, z_\zeta, a\right) > 0$ *be the constant in (4.163) and (4.164) and* $K_1 > 0$ *be the constant in (4.137). There exists a constant* $\overline{N}_2 = \overline{N}_2\left(\exp(CT)\|P\|_{H^6(Q_T)}\right)$ *such that if*

$$h_n \leq \frac{\delta^{4\mu}}{A\overline{N}_2 K_1}, \tag{4.178}$$

then there exists the unique minimizer $c_n \in G \cap M_n$ *of the functional equation (4.172),* $c_n \in V_{\delta^{3\mu}}(x^*) \cap M$ *and*

$$\left\|c_n - c_{\alpha(\delta)}\right\| \leq \frac{2}{\delta^{2\mu}}\left\|E'_{\alpha(\delta)}(c_n)\right\|_{L_2(\Omega)}. \tag{4.179}$$

Theorem 4.11.4. *[(relaxation property of mesh refinements)] Assume that conditions of Theorem 4.11.2 hold. Let* $c_n \in V_{\delta^{3\mu}}(x^*) \cap M_k$ *be the minimizer of the Tikhonov functional (4.172) on the set* $G \cap M_n$*, the existence of which is guaranteed by Theorem 4.11.3. Assume that the regularized solution* $c_{\alpha(\delta)} \neq c_n$*, i.e.,* $c_{\alpha(\delta)} \notin M_n$*. Let* $\eta_n \in (0,1)$ *be an arbitrary number. Then one can choose the maximal grid size* $h_{n+1} = h_{n+1}\left(\overline{N}_2, \delta, A, K_1\right) \in (0, h_n]$ *of the mesh refinement number* $(n+1)$ *so small that*

$$\left\| c_{n+1} - c_{\alpha(\delta)} \right\| \leq \eta_n \left\| c_n - c_{\alpha(\delta)} \right\|.$$

4.12 Mesh Refinement Recommendations

The estimate (4.179) provides one with an idea on where to refine mesh locally in order to improve the accuracy of the reconstruction of the regularized coefficient $c_{\alpha(\delta)}$. Indeed, it follows from (4.179) that, given a subspace of finite elements, the less is the norm of the Fréchet derivative at the point of the minimizer on this subspace, the less is the distance between this minimizer and the regularized coefficient $c_{\alpha(\delta)}$. Given a function $f \in L_2(\Omega) \cap C\left(\overline{\Omega}\right)$, the main impact in the norm $\| f \|_{L_2(\Omega)}$ is provided by neighborhoods of those points $x \in \overline{\Omega}$ where $|f(x)|$ achieves its maximal value. Therefore, the idea of mesh refinements is that neighborhoods of points where the function $\left| P_n E'_{\alpha(\delta)}(c_n)(x) \right|$ achieves its maximal value are indicators of subdomains of the domain Ω where the mesh should be refined. On the other hand, since in practical computations the function $E'_{\alpha(\delta)}(c_n)(x)$ is always expressed as a linear combination of finite elements of the subspace M_n, then one simply does not see the difference between functions $E'_{\alpha(\delta)}(c_n)(x)$ and $P_n E'_{\alpha(\delta)}(c_n)(x)$ in those computations. Therefore, below, we always work only with the function $E'_{\alpha(\delta)}(c_n)(x)$. Since it is convenient to differentiate between subspaces $\{M_n\}$ below, we denote the minimizer on the subspace M_n as $c_n := c_h \in G$.

The first mesh refinement recommendation is derived on the basis of (4.179). Let $c_n := c_h \in G$ be the minimizer of the functional (4.172) obtained after n mesh refinements. The existence and uniqueness of this minimizer is guaranteed by Theorem 4.11.3. Let functions $u := u(x,t,c_h) \in H^2(Q_T)$ and $\lambda := \lambda(x,t,c_h) \in H^2(Q_T)$ be solutions of the following state and adjoint initial boundary value problems:

$$\begin{aligned} c_h(x)\, u_{tt} - \Delta u &= 0 \text{ in } Q_T, \\ u(x,0) &= u_t(x,0) = 0, \\ \partial_n u\,|_{S_T} &= p(x,t); \end{aligned} \tag{4.180}$$

$$\begin{aligned} c_h(x)\, \lambda_{tt} - \Delta \lambda &= 0 \text{ in } Q_T, \\ \lambda(x,T) &= \lambda_t(x,T) = 0, \\ \partial_n \lambda\,|_{S_T} &= z_\zeta(t)(g-u)(x,t). \end{aligned} \tag{4.181}$$

The existence and uniqueness of such solutions are guaranteed by Theorem 4.7.1. Recall that by (4.123),

$$E'_{\alpha(\delta)}(c_h)(x) = \alpha\left(c_h - c_{\text{glob}}\right)(x) - \int_0^T (u_t\lambda_t)(x,t)\,dt,\ x \in \Omega. \tag{4.182}$$

First Mesh Refinement Recommendation. *Refine the mesh in neighborhoods of those grid points $x \in \Omega$ where the function $\left|E'_{\alpha(\delta)}(c_h)(x)\right|$ attains its maximal values. More precisely, refine the mesh in such subdomains of the domain Ω where*

$$\left|E'_{\alpha(\delta)}(c_h)(x)\right| \geq \beta_1 \max_{\overline{\Omega}} \left|E'_{\alpha(\delta)}(c_h)(x)\right|, \tag{4.183}$$

where $\beta_1 \in (0,1)$ is the tolerance number.

To figure out the second mesh refinement recommendation, we take into account estimates (4.92) and (4.93) of Theorem 4.7.1 By these estimates, the function $\left|E'_{\alpha(\delta)}(c_h)(x)\right|$ can be estimated as

$$\left|E'_{\alpha(\delta)}(c_h)(x)\right| \leq \alpha\left(m + \max_{\overline{\Omega}} c_{\text{glob}}\right) + m^2 \exp(CT)\left(\|P\|^2_{H^6(Q_T)} + \|\Phi\|^2_{H^5(Q_T)}\right), \tag{4.184}$$

$$m = \max_{\overline{\Omega}} c_h(x). \tag{4.185}$$

Since functions c_{glob} and c_h are close to each other, it is reasonable to assume that points where these two functions achieve their maximal values are also close to each other. Next, since we have decided to refine the mesh in neighborhoods of those points which deliver maximal values for the function $\left|E'_{\alpha(\delta)}(c_h)(x)\right|$, then (4.184) and (4.185) lead to the following:

Second Mesh Refinement Recommendation. *Refine the mesh in neighborhoods of those grid points $x \in \Omega$ where the function $c_h(x)$ attains its maximal values. More precisely, refine the mesh in such subdomains of the domain Ω where*

$$c_h(x) \geq \beta_2 \max_{\overline{\Omega}} c_h(x), \tag{4.186}$$

where $\beta_2 \in (0,1)$ is the tolerance number.

In fact, these two mesh refinement recommendations do not guarantee of course that the minimizer obtained on the corresponding finer mesh would be indeed more accurate than the one obtained on the coarser mesh. This is because right-hand sides

of formulas (4.183) and (4.186) are indicators only. Nevertheless, we will show now that the second mesh refinement recommendation is close to be a sufficient condition ensuring a better accuracy on the finer mesh. To do this, we recall the formula (4.155). This formula and Theorem 4.11.4 imply that

$$\|c_{n+1} - c_\alpha\| \leq \frac{Q}{\delta^{2\mu}} \|c_\alpha\| h_{n+1} \leq \eta_n \|c_n - c_\alpha\|, \tag{4.187}$$

where $Q > 0$ is a certain constant, $\eta_n \in (0,1)$ and h_{n+1} is the maximal grid step size of the mesh refinement number $n+1$. After n mesh refinements, the function c_α is unknown, unlike the function $c_n := c_h$. Nevertheless, functions c_h and c_α are close to each other, since both of them are located in a small neighborhood of the exact solution. Hence, similarly with the above, it is reasonable to assume that points, where functions c_h and c_α achieve their maximal values, are close to each other. Although the number h_{n+1} in (4.187) is uniform for the entire mesh on the refinement step number $n+1$, it can be made nonuniform. Indeed, let $\widehat{\Omega} \subset \Omega$ be such a subdomain of the domain Ω, which includes neighborhoods of all points where the maximal value of the function c_α is achieved. We want to refine mesh locally only in $\widehat{\Omega}$. We have

$$\|c_\alpha\|^2 = \|c_\alpha\|^2_{L_2(\Omega)} = \|c_\alpha\|^2_{L_2\left(\widehat{\Omega}\right)} + \|c_\alpha\|^2_{L_2\left(\Omega \setminus \widehat{\Omega}\right)}.$$

Hence, one can choose two grid step sizes $h^{(1)}_{n+1} := h_{n+1}$ and $h^{(2)}_{n+1} := h_n$ in (4.187), where $h^{(1)}_{n+1} < h^{(2)}_{n+1}$. The smaller grid step size $h^{(1)}_{n+1}$ would be used in the subdomain $\widehat{\Omega}$, where the mesh would be refined. And the larger grid step size $h^{(2)}_{n+1} = h_n$ from the previous mesh would be used in $\Omega \setminus \widehat{\Omega}$. Numbers $h^{(1)}_{n+1}$ and $h^{(2)}_{n+1}$ can be balanced in such a way that

$$\|c_{n+1} - c_\alpha\| \leq \frac{B}{\delta^{2\mu}} \left(\|c_\alpha\|_{L_2\left(\widehat{\Omega}\right)} h^{(1)}_{n+1} + \|c_\alpha\|_{L_2\left(\Omega \setminus \widehat{\Omega}\right)} h_n \right) \leq \eta_n \|c_n - c_\alpha\|.$$

In other words, the local mesh refinement in the subdomain $\widehat{\Omega}$ still guarantees an improvement of the accuracy of the reconstruction of the regularized coefficient.

We conclude that the use of the second mesh refinement recommendation is close to be a rigorous guarantee of an improvement of the accuracy. Nevertheless, such an improvement should be verified in numerical experiments.

Now, about the choice of tolerance numbers β_1 and β_2 in (4.183) and (4.186). If we would choose $\beta_1, \beta_2 \approx 1$, then we would refine the mesh in too narrow regions. On the other hand, if we would choose $\beta_1, \beta_2 \approx 0$, then we would refine the mesh in almost the entire domain Ω, which is inefficient. Hence, tolerance numbers β_1, β_2 should be chosen numerically.

4.13 The Adaptive Algorithm

4.13.1 The Algorithm In Brief

Numerically, we proceed as follows for both first and second mesh refinement recommendations. By (4.182), we need to approximately solve the following equation on each mesh:

$$E'_\alpha(c)(x) = 0.$$

We start our computations on the same mesh on which the approximately globally convergent algorithm of Sect. 2.6.1 has worked. In our experience, this mesh does not provide an improvement of the image. For each newly refined mesh, we first linearly interpolate the function $c_{\text{glob}}(x)$ on it. Since this function was initially computed as a linear combination of finite elements forming the initial mesh and since these finite elements are piecewise linear functions, then subsequent linear interpolations on finer meshes do not change the function $c_{\text{glob}}(x)$. On each mesh, we iteratively update approximations $c^n_{\alpha h}$ of the function $c_{\alpha h}$. To do so, we use the quasi-Newton method with the classic BFGS update formula with the limited storage [134]. Denote

$$g^n(x) = \alpha(c^n_h - c_{\text{glob}})(x) - \int_0^T (u_{ht}\lambda_{ht})\left(x,t,c^n_h\right)\mathrm{d}t,$$

where functions $u_h\left(x,t,c^n_h\right), \lambda_h\left(x,t,c^n_h\right)$ are FEM solutions of state and adjoint problems (4.180) and (4.181) with $c := c^n_h$. We stop computing c^n_h if either $||g^n||_{L_2(\Omega)} \leq 10^{-5}$ or norms $||g^n||_{L_2(\Omega)}$ are stabilized. Of course, only discrete norms $||g^n||_{L_2(\Omega)}$ are considered here.

For a given mesh, let c_h be the last computed function on which we have stopped. Next, we compute the function $|E'_\alpha(c_h)(x)|$ by formula (4.182), where $u := u_h(x,t,c_h), \lambda := \lambda_h(x,t,c_h)$. Next, we consider all grid points in this mesh where (4.183) is fulfilled. Next, we refine the mesh in neighborhoods of all grid points satisfying (4.183). In those numerical studies when we use both above mesh refinement recommendations, we also consider all grid points where (4.186) is fulfilled and refine mesh in those subdomains where both (4.183) and (4.186) are fulfilled. The stopping criterion for the mesh refinement process is described in this Sect. 4.13.2.

4.13.2 The Algorithm

Step 0. Choose an initial mesh K_h in the domain Ω and a time partition J_0 of the time interval $(0,T)$. Start with the initial approximation $c^0_h := c_{\text{glob}}$ and compute the sequence of functions c^n_h via steps described below.

Step 1. Compute FEM solutions $u_h\left(x,t,c_h^n\right), \lambda_h\left(x,t,c_h^n\right)$ of state and adjoint problems (4.180) and (4.181) on K_h, J_0.

Step 2. Update the coefficient $c := c_h^{n+1}$ on K_h as described in Sect. 4.13.1.

Step 3. Stop updating functions c_h^n if either $||g^n||_{L_2(\Omega)} \leq \theta_1$ or norms $||g^n||_{L_2(\Omega)}$ are stabilized. Otherwise, set $n := n+1$ and go to Step 1. In our computations, we took $\theta_1 = 10^{-5}$.

Step 4. Compute the function $B_h(x)$:

$$B_h(x) = \left|\alpha(c_h - c_{\text{glob}})(x) - \int_0^T (u_{ht}\lambda_{ht})(x,t,c_h)\,\mathrm{d}t\right|. \tag{4.188}$$

Next, refine the mesh in neighborhoods of all points where

$$B_h(x) \geq \beta_1 \max_{\overline{\Omega}} B_h(x). \tag{4.189}$$

In the case when the second mesh refinement recommendation is used in addition to the first one, also refine the mesh in neighborhoods of all points where

$$c_h(x) \geq \beta_2 \max_{\overline{\Omega}} c_h(x). \tag{4.190}$$

Here, tolerance numbers β_1, β_2 are chosen by the user.

Step 5. Construct a new mesh K_h on the basis of mesh refinements of Step 4. Also, construct a new partition J_h of the time interval $(0,T)$. The new time step τ of J_h should be such that the CFL condition would be satisfied. Interpolate the initial approximation c_{glob} from the previous mesh on the new mesh. Next, return to Step 1 and perform all the above steps on the new mesh.

Step 6. Stop mesh refinements when a stopping criterion is satisfied. Stopping criteria are described in follow-up sections of this chapter.

4.14 Numerical Studies of the Adaptivity Technique

In this section, results of two numerical studies of the adaptive algorithm of Sect. 4.13.2 are presented. This is done in the case when that algorithm works without the first stage of our two-stage numerical procedure. We are not using the function $z_\zeta(t)$ here, since we have observed that the solution of the state problem is close to zero for $t \approx T$. We have established computationally that the tolerance numbers $\beta_1 = 0.8$ in (4.189) and $\beta_2 = 0.2$ in (4.190) were the optimal ones for our tests in Sects. 4.14.1 and 4.14.2.

We start our presentation in Sect. 4.14.1 where numerical results of [20] are presented. Next, numerical results of [21] are described in Sect. 4.14.2, where we discuss an application of the adaptivity technique to ultrasound imaging using the scanning acoustic microscope.

In numerical results of both Sects. 4.14.1 and 4.14.2, Theorem 4.5 was used to derive mesh the refinement recommendation, which is similar with the one of (4.189). More precisely, in accordance with (4.28) and (4.29), denote

$$R_{c_1}(x,t) = \left(|\partial_t \lambda_h| \cdot |\partial_t u_h|\right)(x,t), \tag{4.191}$$

$$R_{c_2}(x) = |c_h(x) - c_0(x)|, \tag{4.192}$$

$$R_c(x) = \int_0^T R_{c_1}(x,t)\,dt + R_{c_2}(x). \tag{4.193}$$

Mesh refinement recommendations of Sects. 4.14.1 and 4.14.2 were derived respectively in [20] and [21] on the basis of

$$R_c(x) \geq \beta_1 \max_{\overline{\Omega}_{\text{FEM}}} R_c(x). \tag{4.194}$$

In both Sects. 4.14.1 and 4.14.2, $\beta_1 = 0.8$ was used in (4.194).

In (4.192), $c_0(x) \equiv 1$ is the starting point for iterations in numerical examples of both Sects. 4.14.1 and 4.14.2. It should be pointed out, however, that since the quasi-Newton method is a locally convergent one, the reconstructed function $c(x)$ is very sensitive to the starting values of the parameters in the optimization algorithm; also see Test 5 in Sect. 3.1.3 as well as Sect. 3.3 for a similar conclusion.

4.14.1 Reconstruction of a Single Cube

In the numerical example of this section, the adaptive algorithm of Sect. 4.9.3 is tested for the case of the reconstruction of a single cube from scattered data at the boundary of the domain of interest. Just as in Sect. 3.2.1, the hybrid FEM/FDM method [30] is used to solve the forward problem of data generation. The computational domain is

$$G = [0, 5.0] \times [0, 2.5] \times [0, 2.5].$$

The rectangular prism $G = \Omega_{\text{FEM}} \cup \Omega_{\text{FDM}}$ is split into a finite element domain:

$$\Omega_{\text{FEM}} := \Omega = [0.3, 4.7] \times [0.3, 2.3] \times [0.3, 2.3]$$

with a nonstructured mesh and a surrounding domain Ω_{FDM} with a structured mesh see Fig. 4.1 for the exact scatterer and the domain Ω_{FEM}. The space mesh in Ω_{FEM} consists of tetrahedra and of hexahedra in Ω_{FDM} with the mesh size $h = 0.2$ in overlapping regions.

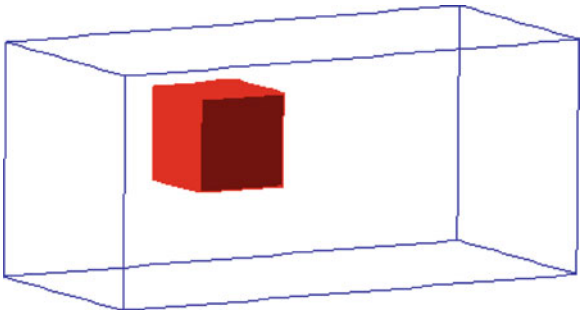

Fig. 4.1 Cubic scatterer to be reconstructed. It is located inside the domain of interest Ω_{FEM}. Source: L. Beilina and C. Johnson, A posteriori error estimation in computational inverse scattering, *Mathematical Models and Methods in Applied Sciences*, 15, 23–37, 2005. © World Scientific Publishing Company. Reprinted with permission

The forward problem is computed in the domain G, and the coefficient $c(x)$ is unknown only in the domain Ω_{FEM} with the known value $c(x) = 1$ in $G \setminus \Omega_{\text{FEM}}$. In the test of this section,

$$c(x) = \begin{cases} 2 \text{ inside the small cube,} \\ 1 \text{ everywhere else.} \end{cases}$$

Location, size, and value of the function $c(x)$ inside that small cube are unknown. However, since a locally convergent method is applied, the knowledge of the background value of the function $c(x) = 1$ outside of that small cube is known. The starting point of iterations for the minimization of the Lagrangian (4.14) is $c_0 \equiv 1$. In other words, in (4.8), c_{glob} is replaced with $c_0 \equiv 1$ (Sect. 4.3).

In this test, the forward problem is

$$\begin{aligned} c(x)\,\partial_t^2 u &= \Delta u + p(t) \sum_{i=1}^{6} f(|x - x_i|), \quad \text{in } G \times (0,T), \\ u(x,0) &= u_t(x,0) = 0 \text{ in } G, \\ \partial_n u\big|_{\partial G} &= -\partial_t u, \text{ on } \partial G \times (0,T), \end{aligned} \tag{4.195}$$

where T is the final time. In (4.195), the function $f(z), z \in \mathbb{R}$ is a Gaussian which approximates the function $\delta(z)$ in the distribution sense. Six sources $\{x_i\}_{i=1}^6$ were used. They were located close to the top boundary of the domain Ω_{FEM} on the same straight line. Therefore, the case of six simultaneously launched spherical waves was modeled. Points $\{x_i\}_{i=1}^6$ were:

$$x_1 = (0.45, 2.2, 1.25),\ x_2 = (1.25, 2.2, 1.25),\ x_3 = (2.05, 2.2, 1.25),$$
$$x_4 = (2.95, 2.2, 1.25),\ x_5 = (3.75, 2.2, 1.25),\ x_6 = (4.55, 2.2, 1.25).$$

The source function $p(t)$ is

$$p(t) = \begin{cases} 10^3 \sin^2 \pi t & \text{if } t \in [0,1], \\ 0 & \text{otherwise.} \end{cases}$$

Coefficient Inverse Problem. Suppose that the following function $g(x,t)$ is given,

$$u|_{S_T} = g(x,t).$$

Given the function $g(x,t)$, determine the function $c(x)$ for $x \in \Omega = \Omega_{\text{FEM}}$, assuming that $c(x) = 1$ for $x \in G \setminus \Omega$ and also $c(x) = 1$ outside of a small inclusion located inside the domain Ω. Both this inclusion and the function $c(x)$ inside it are unknown.

The computed solution of the forward problem (4.195) inside the domain Ω_{FEM} for different times is presented on Fig. 4.2. The test was performed for $T = 3.0$ and with 300 time steps satisfying the CFL condition (4.198).

In Tables 4.1 and 4.2, we show computed norms $||u|_{S_T} - g||_{L_2(S_T)}$ with the regularization parameters $\alpha = 0.0001, 0.001$, respectively. In Fig. 4.3, the spatial distribution of the computed coefficient c_h on different adaptively refined meshes is presented. It can be observed from Tables 4.1 and 4.2 that norms $\|u|_{S_T} - g\|_{L_2(S_T)}$ at the boundary S_T of the domain Ω_{FEM} generally decrease as meshes are refined, and they are stabilized on the fifth refined mesh.

Recall that the relaxation Theorem 4.11.4 ensures an improvement of the accuracy of the reconstruction of the regularized coefficient with mesh refinements as long as that coefficient is not yet reached on a certain mesh. Hence, the stabilization of norms $\|u|_{S_T} - g\|_{L_2(S_T)}$ indicates that the regularized coefficient is likely reached on the fifth refined mesh. Thus, we stop our procedure on the fifth refined mesh. The corresponding image is displayed on Fig. 4.3f. One can see from this figure that all three components of the unknown abnormality are accurately reconstructed: location, shape, and contrast.

4.14.2 Scanning Acoustic Microscope

In this section, we address a CIP which occurs in the modeling of a scanning acoustic microscope [21].

4.14.2.1 Ultrasound Microscopy

In the daily medical practice, ultrasound imaging is a widely accepted imaging technology. The main clinical focus up to now has been on detecting pathological soft tissue changes, for example, malignant tumors. However, it is impossible to

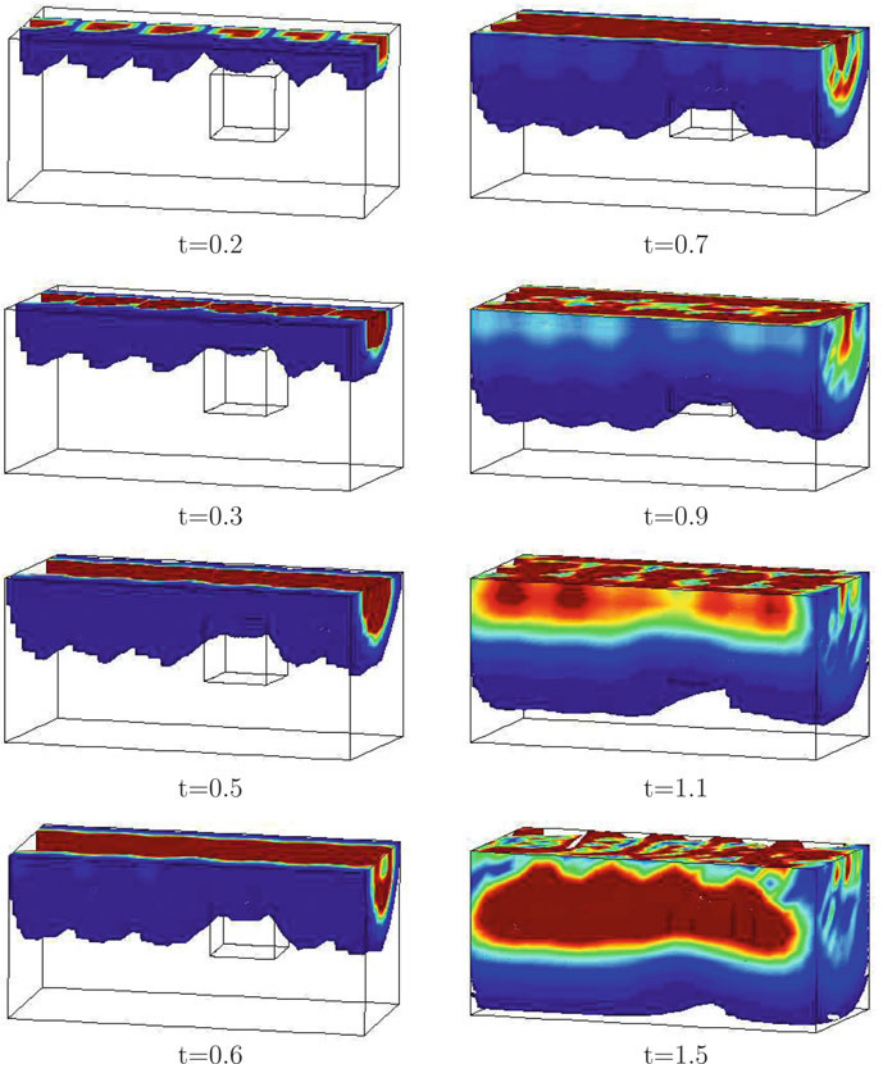

Fig. 4.2 Isosurfaces of the exact solution in Ω_{FEM} for the forward problem (4.195) at different times with six spherical pulses initialized in the domain Ω_{FDM}. Source: L. Beilina and C. Johnson, A posteriori error estimation in computational inverse scattering, *Mathematical Models and Methods in Applied Sciences*, 15, 23–37, 2005. © World Scientific Publishing Company. Reprinted with permission

apply these low-frequency technologies to the hard tissue, for example, bone. On the other hand, the ultrasound microscopy on high frequencies is used for nondestructive material testing; see, for example, [39]. This technology might be also potentially used in medicine to image the microstructure of human cortico-spongious bone as well as the growing patterns of cell cultures [64, 70].

Table 4.1 Computed norms $\|u\|_{S_T} - g\|_{L_2(S_T)}$ at the boundary S_T of the domain Ω_{FEM} with the regularization parameter $\alpha = 0.0001$ on different adaptively refined meshes with five stored corrections of the quasi-Newton method

Opt.it.	2,783 nodes	2,847 nodes	3,183 nodes	3,771 nodes	4,283 nodes	6,613 nodes
1	0.0493302	0.0516122	0.051569	0.0529257	0.0535081	0.0537523
2	0.0405683	0.0423093	0.0419412	0.0428817	0.0433272	0.0439134
3	0.0235056	0.0239327	0.0245081	0.0271383	0.0285571	0.031920
4	0.0191902	0.0192185	0.0187792	0.0205331	0.0221997	0.0239426
5	0.0115005	0.0110448	0.0174202		0.0205711	0.0104240
6			0.0156732		0.0112331	0.0101503
7			0.0121359		0.0102246	

Source: L. Beilina and C. Johnson, A posteriori error estimation in computational inverse scattering, *Mathematical Models and Methods in Applied Sciences*, 15, 23–37, 2005. © World Scientific Publishing Company. Reprinted with permission

Table 4.2 Computed norms $\|u\|_{S_T} - g\|_{L_2(S_T)}$ at the boundary S_T of the domain Ω_{FEM} with the regularization parameter $\alpha = 0.001$ on different adaptively refined meshes with five stored corrections of the quasi-Newton method

Opt.it.	2,783 nodes	2,847 nodes	3,183 nodes	3,771 nodes	4,283 nodes	6,613 nodes
1	0.0493302	0.0516122	0.051569	0.0529257	0.0535081	0.0537523
2	0.0409375	0.0426592	0.0422985	0.0432254	0.043665	0.0439134
3	0.0258043	0.0260785	0.0263276	0.0286128	0.029808	0 0.03192
4	0.0224222	0.0221598	0.0206731	0.0209556	0.0212633	0.0.0239426
5	0.0171107	0.0142682	0.0105603	0.01003	0.0104199	0.010424
6	0.0157419					0.0101503

Source: L. Beilina and C. Johnson, A posteriori error estimation in computational inverse scattering, *Mathematical Models and Methods in Applied Sciences*, 15, 23–37, 2005. © World Scientific Publishing Company. Reprinted with permission

The available modern ultrasound microscope of the KSI company (Kraemer Scientific Instruments Herborn/Germany) is based on the so-called "scanning acoustic microscopy" concept. This microscope uses high-frequency (up to 2 GHz) pulsed and focused raster scanning of the investigated object. An electrical input signal is converted by an acoustic transducer over a modulation network into plane acoustic waves; see Fig. 4.4 for the sketch of the scanning acoustic microscope. These waves are focused by an acoustic-optical lens on the substrate. The reflected signal is send back via the lens to the same transducer and is transformed back then in an electrical output signal.

4.14.2.2 The Adaptivity Method for an Inverse Problem of Scanning Acoustic Microscopy

We model the problem of imaging of biomechanical parameters of the bone as an inverse problem for the scalar acoustic wave equation $c^{-2}(x)\, u_{tt} = \Delta u$ with

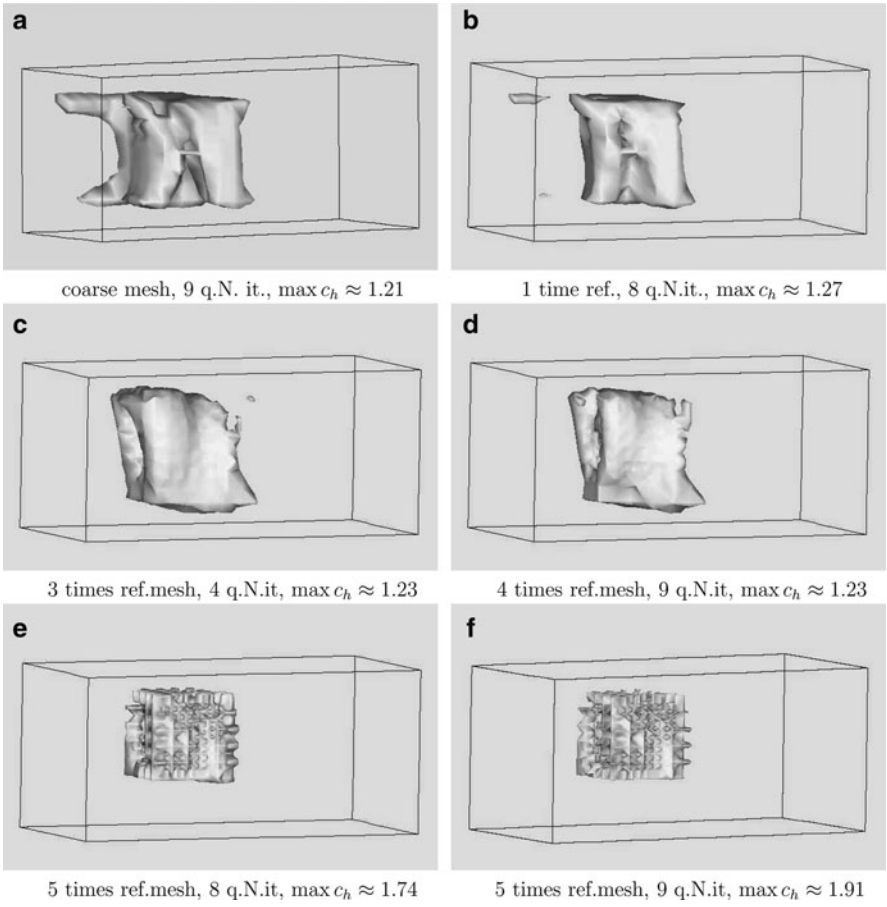

Fig. 4.3 Maximal values of the reconstructed coefficient c with $\alpha = 0.001$ on adaptively refined meshes with different number of quasi-Newton iterations (q.N.it) in the optimization algorithm. Source: L. Beilina and C. Johnson, A posteriori error estimation in computational inverse scattering, *Mathematical Models and Methods in Applied Sciences*, 15, 23–37, 2005. © World Scientific Publishing Company. Reprinted with permission

the (longitudinal) wave speed $c\,(x)$. The backscattering data are considered. Quite often, the surrounding medium is homogeneous, and the material inhomogeneities occupy only a small portion of the body. In other words, a small inclusion should be imaged.

The geometry of the problem (see Fig. 4.5) is taken from a specific microscope (WinSAM 2000, KSI Germany). The computational domain G and the finite element domain $\Omega_{\text{FEM}} \subset G$ are set as

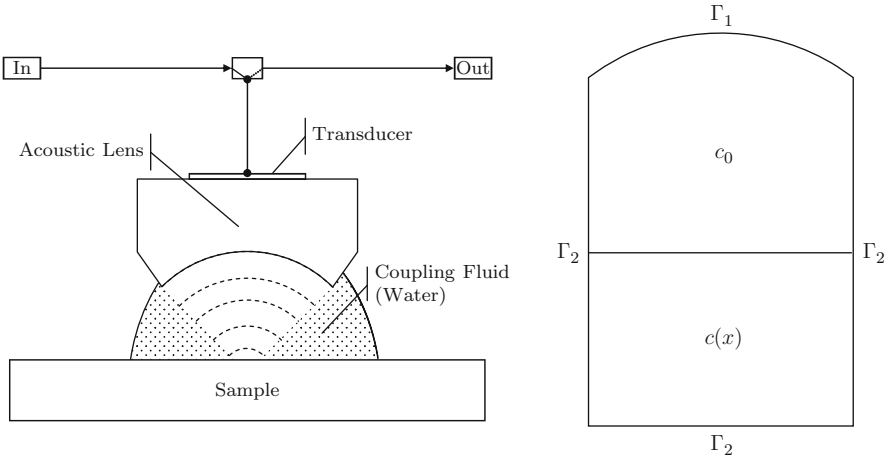

Fig. 4.4 Schematic diagram of the scanning acoustic microscope (*left*) and a 2D cross-section of this microscope by a vertical plane (*right*). Here, $c_0 = 1$ corresponds to the region filled with water and $c(x)$ corresponds to the investigated sample. $\widetilde{\Gamma}_1$ is the cross-section of the spherical surface Γ_1 of a lens. The plane wave is initialized at Γ_1 and propagates into the medium. The time-dependent backreflected wave is recorded at Γ_1. The inverse problem then consists in the recovery of the function $c(x)$ from these backscattering data. Source: L. Beilina and C. Clason, An adaptive hybrid FEM/FDM method for an inverse scattering problem in scanning acoustic microscopy, *SIAM J. Sci. Comp.,* 28, 382–402, 2006. © 2006 Society for Industrial and Applied Mathematics. Reprinted with permission

$$G = [-10.0, 10.0] \times [-14.0, 16.0] \times [-10.0, 10.0],$$
$$\Omega_{\text{FEM}} = [-9.0, 9.0] \times [-10.0, -12.0] \times [-9.0, 9.0].$$

We have an unstructured mesh in and Ω_{FEM} and a structured mesh in the surrounding domain Ω_{FDM}. The space mesh in Ω_{FEM} consists of tetrahedra, and in Ω_{FDM} of hexahedra. The mesh step size h in Ω_{FDM} is $h = 1.0$. To solve the forward problem of data simulation, the hybrid FEM/FDM method with finite elements in Ω_{FEM} and finite differences in Ω_{FDM} is applied. First-order absorbing boundary conditions at the entire boundary ∂G are used [66].

Consider Fig. 4.5. On this figure, the cylinder represents the microscope. Let Ω be the domain occupied by this microscope. Then $\Omega \subset \Omega_{\text{FEM}}$. A 2D cross-section by of this microscope by a vertical plane is displayed on Fig. 4.4 (right). The top of this cylinder is a spherical surface, which we denote as Γ_1. This spherical surface is the surface of a lens. The plane wave with three components $v = (v_1, v_2, v_3)(t)$ is initialized at Γ_1 during the time period $t \in [0, t_1]$ and propagates downward. This plane wave interacts with the substrate. A part of the wave field is reflected back. The backscattering wave field is recorded at Γ_1.

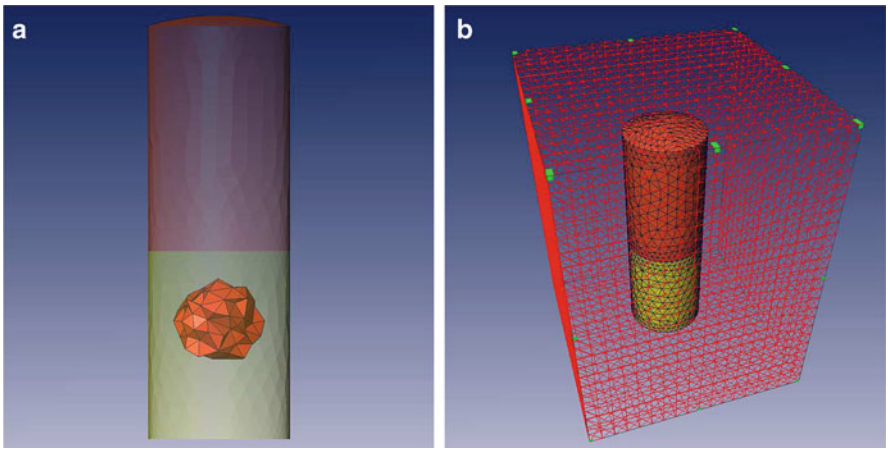

Fig. 4.5 (**a**) The acoustical microscope with the unknown inclusion. Location and shape of this inclusion as well as the coefficient $c(x)$ inside it are unknown. (**b**) The domain Ω_{FEM}. The acoustical microscope is located inside this domain. Surrounding mesh (*outlined*) with overlapping nodes at the boundary. Source: L. Beilina and C. Clason, An adaptive hybrid FEM/FDM method for an inverse scattering problem in scanning acoustic microscopy, *SIAM J. Sci. Comp.*, 28, 382–402, 2006. © 2006 Society for Industrial and Applied Mathematics. Reprinted with permission

Thus, the forward problem in our test is

$$\begin{aligned} c^{-2}(x)\, u_{tt} - \Delta u &= 0, && \text{in } G \times (0,T), T = 40, \\ u(x,0) &= 0, && \text{in } G, \\ u_t(x,0) &= 0, && \text{in } G, \\ \partial_n u(x,t) &= v(t), && \text{on } \Gamma_1 \times (0,t_1], \\ \partial_n u(x,t) &= -\partial_t u(x,t), && \text{on } \partial G \times (0,T), \end{aligned} \tag{4.196}$$

where the forced acoustic field at Γ_1 is $v(t) = (v_1, v_2, v_3)(t)$:

$$v_i(t) = \begin{cases} -((\sin(100t - \pi/2) + 1)/10) \cdot n_i, \ 0 \le t \le t_1 := \frac{2\pi}{100}, \\ 0, t \in (t_1, T), i = 1,2,3. \end{cases} \tag{4.197}$$

Thus, the acoustic wave field initiates at the spherical boundary Γ_1 of the lens in Ω_{FEM} and propagates in the normal direction $n = (n_1, n_2, n_3)$ into Ω. This acoustic field models the excitation pulse generated by the transducer of the microscope. We assume that the coefficient $c(x) = 1$ for $x \in G \setminus \Omega$. The observation points are placed on the surface of the lens Γ_1. Hence, only the backscattering acoustic wave field is measured. Also, $u(x,t) = (u_1, u_2, u_3)(x,t)$ is the vector function Fig. (4.6).

In all computational tests, we choose the time step τ in the forward problem (4.196) on the basis of the CFL stability condition in 3D:

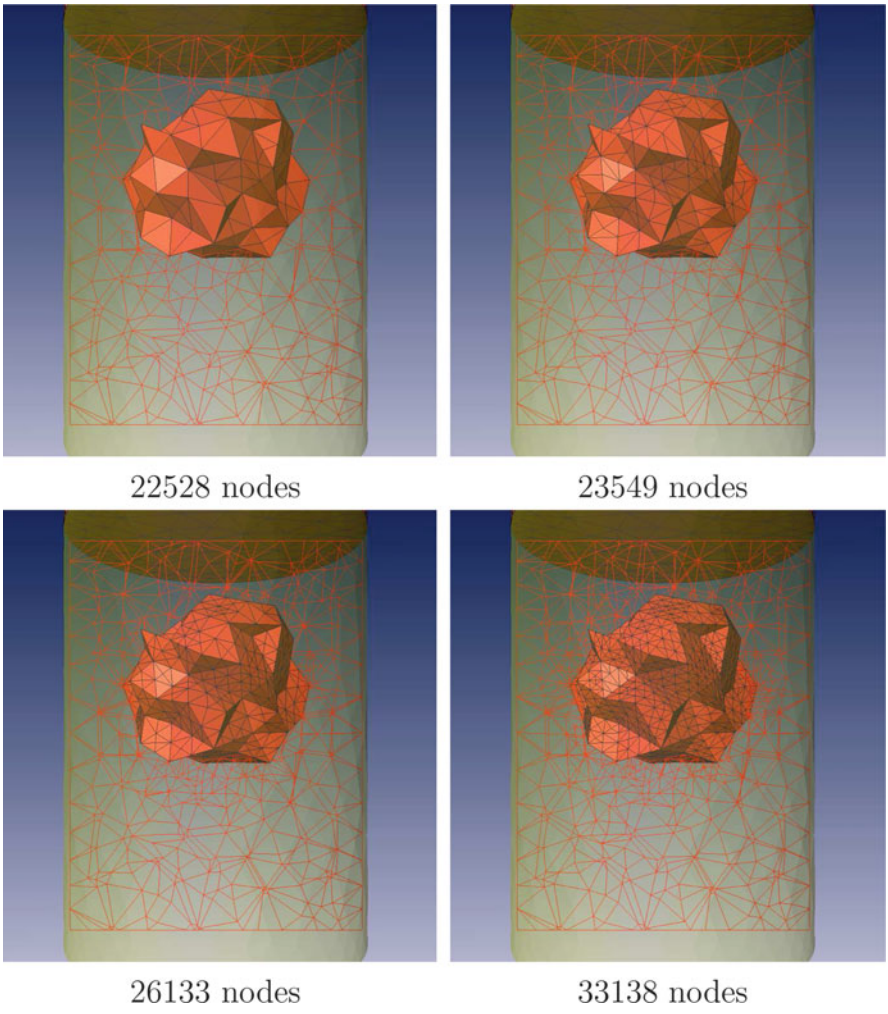

Fig. 4.6 Adaptively refined meshes. Source: L. Beilina and C. Clason, An adaptive hybrid FEM/FDM method for an inverse scattering problem in scanning acoustic microscopy, *SIAM J. Sci. Comp.,* 28, 382–402, 2006. © 2006 Society for Industrial and Applied Mathematics. Reprinted with permission

$$\tau \leq \frac{h}{\sqrt{3}c_{\max}}, \tag{4.198}$$

where h is the minimal local mesh size and $c_{\max}$ is an a priori given upper bound for the coefficient $c(x)$. To generate the data at the observation points, we solve the forward problem in the time interval $t \in [0, 40]$ with the exact value of the parameter $c = 0.5$ inside a spherical inclusion depicted on Fig. 4.5a and $c = 1$ everywhere else in G. Figure 4.6 displays adaptively refined meshes. In Fig. 4.7, we present isosurfaces of the function

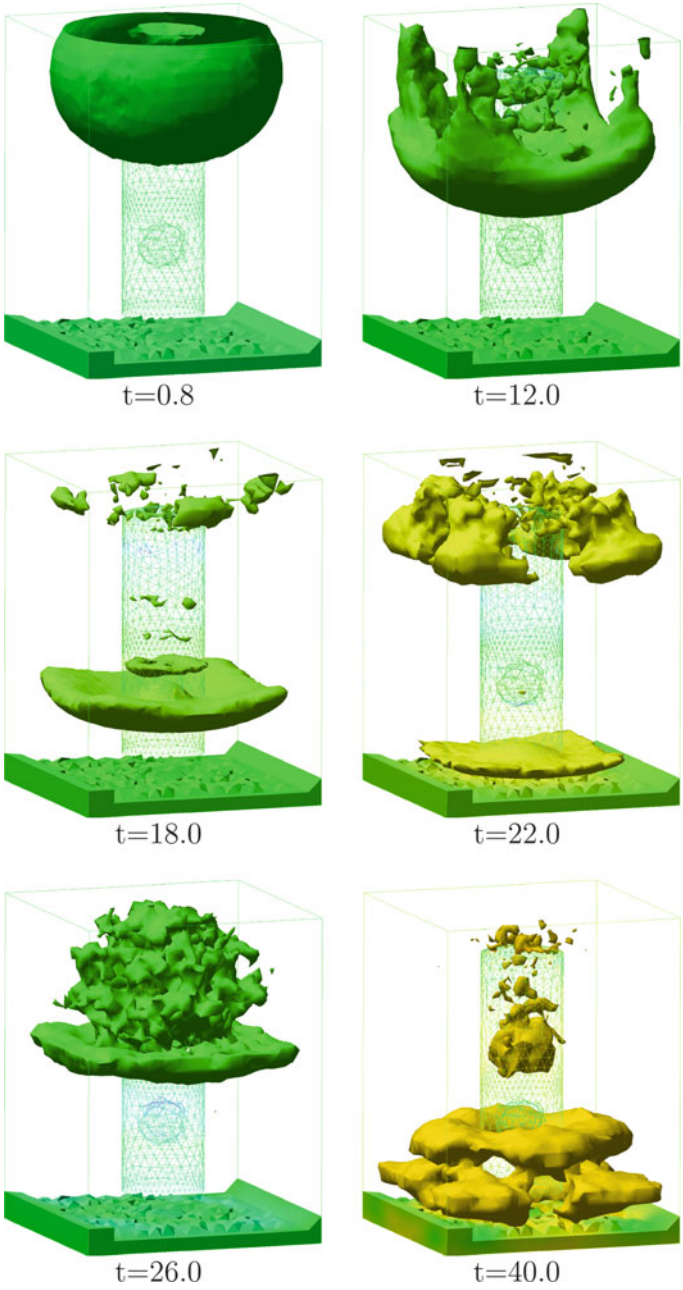

Fig. 4.7 Isosurfaces of the computed function $|u(x,t)| = \sqrt{\left(u_1^2 + u_2^2 + u_3^2\right)}(x,t)$ for different times with the exact $c(x) = 0.5$ inside the spherical inclusion and $c(x) = 1$ everywhere else. Source: L. Beilina and C. Clason, An adaptive hybrid FEM/FDM method for an inverse scattering problem in scanning acoustic microscopy, *SIAM J. Sci. Comp.*, 28, 382–402, 2006. © 2006 Society for Industrial and Applied Mathematics. Reprinted with permission

$$|u(x,t)| = \sqrt{u_1^2 + u_2^2 + u_3^2}(x,t),$$

which corresponds to the solution of the forward problem (4.196) with the exact parameters. The function $|u(x,t)|$ is presented at different times inside the domain Ω_{FEM}. We consider the following

Coefficient Inverse Problem. Let the vector function $u(x,t)$ be the solution of the problem (4.196) and (4.197). Suppose that the following vector function $g(x,t) = (g_1, g_2, g_3)(x,t)$ is known,

$$u|_{\Gamma_1 \times (0,T)} = g(x,t).$$

Determine the coefficient $c(x)$ inside the domain Ω, assuming that $c(x) = 1$ for all $x \in \Omega$ outside of a *small unknown inclusion* located inside Ω as well as for all $x \in G \setminus \Omega$.

Since we need to work with the vector function $v(t)$, we consider the vectorial form of both state and adjoint problems. Let $Q_T = \Omega \times (0,T)$, $S_T = \partial\Omega \times (0,T)$. The state problem for the vector function $u(x,t) = (u_1, u_2, u_3)(x,t)$ is

$$\begin{aligned} c^{-2}(x)\partial_t^2 u &= \Delta u, \text{ in } Q_T, \\ u(x,0) &= u_t(x,0) = 0 \text{ in } \Omega, \\ \partial_n u|_{\Gamma_1} &= v(t), \text{ on } \Gamma_1 \times (0,t_1], \\ \partial_n u|_{\Gamma_1} &= 0, \text{ on } \Gamma_1 \times (t_1,T), \\ \partial_n u|_{\partial\Omega \setminus \Gamma_1} &= 0 \text{ for } t \in (0,T). \end{aligned} \tag{4.199}$$

Denote

$$\widetilde{g}(x,t) = \begin{cases} g(x,t), & (x,t) \in \Gamma_1 \times (0,T), \\ 0, & (x,t) \in (\partial\Omega \setminus \Gamma_1) \times (0,T). \end{cases}$$

The adjoint problem for the vector function $\lambda(x,t) = (\lambda_1, \lambda_2, \lambda_3)(x,t)$ is

$$\begin{aligned} c^{-2}(x)\partial_t^2 \lambda &= \Delta\lambda, \quad \text{in } Q_T, \\ \lambda(x,T) &= \lambda_t(x,T) = 0 \text{ in } \Omega, \\ \partial_n \lambda|_{S_T} &= \widetilde{g} - u. \end{aligned} \tag{4.200}$$

Hence, the Lagrangian (4.14) in Sect. 4.3 should be replaced with its analog:

$$\begin{aligned} L(w) = \frac{1}{2}\int\limits_{S_T} (u - \widetilde{g})^2 \, dS_x dt - \int\limits_{Q_T} c^{-2}(x) u_t \lambda_t dx dt \\ + \int\limits_{Q_T} \nabla u \nabla \lambda dx dt - \int\limits_{S_T} p\lambda dS_x dt + \frac{\alpha}{2}\int\limits_{\Omega} (c(x) - 1)^2, \end{aligned}$$

$$w = (u, \lambda, c),$$

$$p(t) = (p_1, p_2, p_3)(t) = \begin{cases} v(t), \text{ on } \Gamma_1 \times (0, t_1], \\ 0, \text{ on } \Gamma_1 \times (t_1, T), \\ 0, \text{ on } (\partial\Omega \setminus \Gamma_1) \times (0, T), \end{cases}$$

where vector functions $u(x,t) = (u_1, u_2, u_3)(x,t)$ and $\lambda(x,t) = (\lambda_1, \lambda_2, \lambda_3)(x,t)$ are solutions of problems (4.199) and (4.200), respectively. Here,

$$\int\limits_{S_T} (u - \widetilde{g})^2 \, dS_x dt = \sum_{i=1}^{3} \int\limits_{S_T} (u_i - \widetilde{g}_i)^2 \, dS_x dt,$$

$$\int\limits_{Q_T} c^{-2}(x) u_t \lambda_t \, dx dt = \sum_{i=1}^{3} \int\limits_{Q_T} c^{-2}(x) \partial_t u_i \, \partial_t \lambda_i \, x dt,$$

$$\int\limits_{Q_T} \nabla u \nabla \lambda \, dx dt = \sum_{i=1}^{3} \int\limits_{Q_T} \nabla u_i \nabla \lambda_i \, dx dt,$$

$$\int\limits_{S_T} p \lambda \, dS_x dt = \sum_{i=1}^{3} \int\limits_{S_T} p_i \lambda_i \, dS_x dt.$$

Similarly with the formula (4.17) of Sect. 4.4, we obtain

$$L'(w)(x) = \alpha (c-1)(x) - \int\limits_0^T (u_t \lambda_t)(x,t) \, dt, \quad x \in \Omega.$$

Hence, we can now proceed as in Sect. 4.13.2 using (4.194) with $\beta_1 = 0.8$; see beginning of Sect. 4.14. In this section, the regularization parameter $\alpha = 0.1$.

In Table 4.3, computed norms

$$\| u(x,t) \mid_{\Gamma_1} - g(x,t) \|_{L_2(\Gamma_1 \times (0,T))} \tag{4.201}$$

on different adaptively refined meshes at each optimization iteration are shown. The computational tests show that the best results are obtained on a four times adaptively refined mesh, where norms (4.201) are reduced approximately by a factor four between two optimization iterations.

Isosurfaces of the reconstructed coefficient $c(x)$ on different adaptively refined meshes on the final optimization iteration is presented in Fig. 4.8. Maximal values of the reconstructed function $c(x)$ are indicated. We see that although the qualitative reconstruction on the coarse grid is already good enough for the recovery of

Table 4.3 $\|u(x,t)\mid_{\Gamma_1} - g(x,t)\|_{L_2(\Gamma_1\times(0,T))}$ on adaptively refined meshes

Opt.it.	22,205 nodes	22,528 nodes	23,549 nodes	26,133 nodes	33,138 nodes
1	0.0506618	0.059448	0.0698214	0.0761904	0.120892
2	0.050106	0.0594441	0.0612598	0.063955	0.0358431
3	0.0358798	0.0465678	0.028501	0.0618176	
4	0.0244553	0.0413165			
5	0.0219676				

The number of stored corrections in the quasi-Newton method is $m = 5$

Source: L. Beilina and C. Clason, An adaptive hybrid FEM/FDM method for an inverse scattering problem in scanning acoustic microscopy, *SIAM J. Sci. Comp.,* 28, 382–402, 2006. © 2006 Society for Industrial and Applied Mathematics. Reprinted with permission

the shape of the inclusion, the accuracy of the reconstruction of the contrast becomes acceptable only on the fourth refined mesh. Additionally, with successive refinement, the boundary of the reconstructed inclusion becomes sharper (compare the isosurface in Fig. 4.8a,b with those in Fig. 4.8d,e). On the grid with 33,138 nodes (Fig. 4.8f), the calculated maximal value of the coefficient $c(x)$ inside the inclusion as $\max c(x) = 0.51$. This is very accurate, since the true maximal value is $\max c(x) = 0.5$.

4.15 Performance of the Two-Stage Numerical Procedure in 2D

In this section, we present numerical results of our papers [26, 111, 160] for the two-stage numerical procedure in two dimensions.

4.15.1 Computations of the Forward Problem

To simulate the data for the inverse problem, we solve the forward problem via the hybrid FEM/FDM method described in [30], just as in Sect. 3.1.1. The computational domain for the forward problem in our test is $G = [-4.0, 4.0] \times [-5.0, 5.0]$. This domain is split into a finite element domain $G_{\text{FEM}} := \Omega = [-3.0, 3.0] \times [-3.0, 3.0]$ and a surrounding domain G_{FDM} with a structured mesh, $G = G_{\text{FEM}} \cup G_{\text{FDM}}$; see Fig. 4.9. The reason of using the hybrid method is that since it is known that

$$c(x) = 1 \text{ in } G \setminus \Omega, \tag{4.202}$$

then there is no point to have a locally fine mesh in $G \setminus \Omega$. On the other hand, since inhomogeneities are located inside Ω, then it is natural to have a locally fine mesh in Ω, which is provided by finite elements. The space mesh in Ω and in G_{FDM}

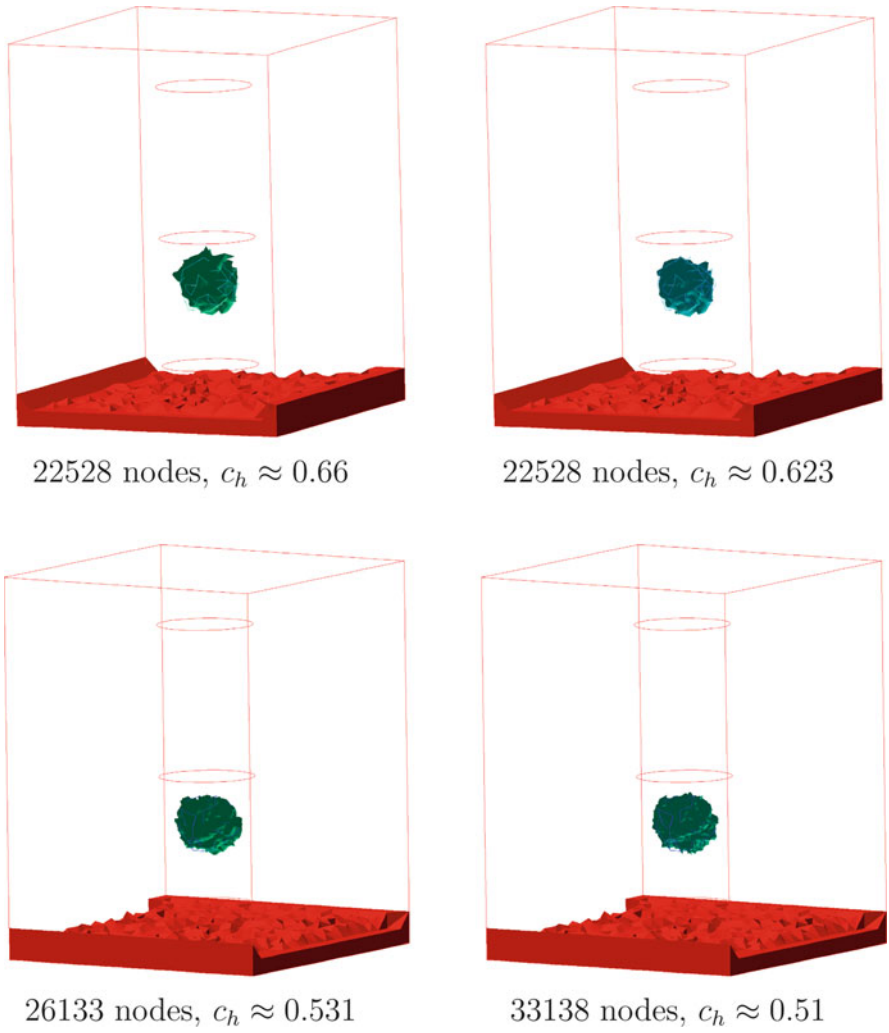

Fig. 4.8 Reconstructed coefficient $c(x)$ on different adaptively refined meshes. Only maximal values of $c_h(x)$ are shown. Source: L. Beilina and C. Clason, An adaptive hybrid FEM/FDM method for an inverse scattering problem in scanning acoustic microscopy, *SIAM J. Sci. Comp.*, 28, 382–402, 2006. © 2006 Society for Industrial and Applied Mathematics. Reprinted with permission

consists of triangles and squares, respectively, with the mesh size $\widetilde{h} = 0.125$ in the overlapping regions. The boundary of the domain G is $\partial G = \partial G_1 \cup \partial G_2 \cup \partial G_3$. Here, ∂G_1 and ∂G_2 are respectively top and bottom sides of the largest domain of Fig. 4.9, and ∂G_3 is the union of left and right sides of this domain.

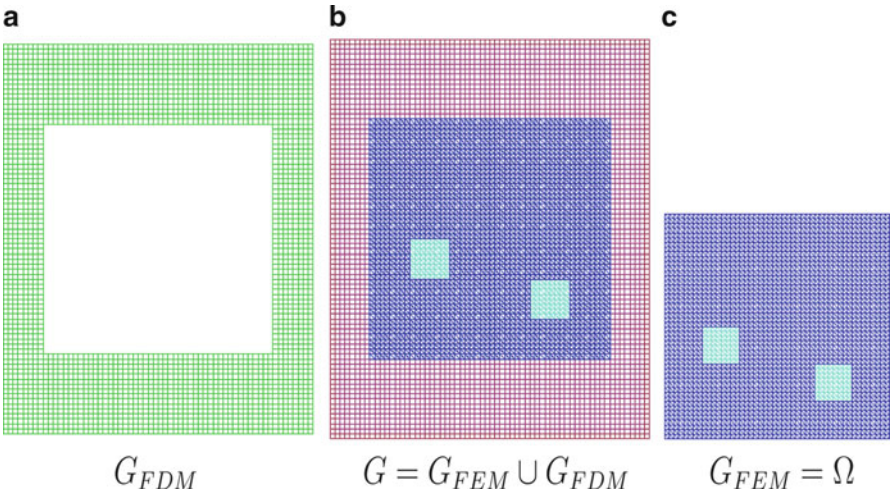

Fig. 4.9 The hybrid mesh (**b**) is a combinations of a structured mesh (**a**), where FDM is applied, and a mesh (**c**), where we use FEM, with a thin overlapping of structured elements. The solution of the inverse problem is computed in the square Ω and $c(x) = 1$ for $x \in G \setminus \Omega$. Source: L. Beilina and M.V. Klibanov, A posteriori error estimates for the adaptivity technique for the Tikhonov functional and global convergence for a coefficient inverse problem, *Inverse Problems*, 26, 045012, doi:10.1088/0266-5611/26/4/045012, 2010. © IOP Publishing. Reprinted with permission

Thus, the forward problem in our test is

$$\begin{aligned} c(x)\, u_{tt} - \Delta u &= 0, \quad \text{in } G \times (0,T), \\ u(x,0) &= 0,\ u_t(x,0) = 0, \ \text{in } G, \\ \partial_n u\big|_{\partial G_1} &= f(t), \ \text{on } \partial G_1 \times (0,t_1], \\ \partial_n u\big|_{\partial G_1} &= -\partial_t u, \ \text{on } \partial G_1 \times (t_1,T), \\ \partial_n u\big|_{\partial G_2} &= -\partial_t u, \ \text{on } \partial G_2 \times (0,T), \\ \partial_n u\big|_{\partial G_3} &= 0, \ \text{on } \partial G_3 \times (0,T), \end{aligned} \tag{4.203}$$

where $f(t)$ is the time dependent amplitude of the incident plane wave,

$$f(t) = \frac{(\sin(\overline{s}t - \pi/2) + 1)}{10},\ 0 \le t \le t_1 := \frac{2\pi}{\overline{s}}, T = 17.8 t_1.$$

Thus, the plane wave is initialized at the top boundary ∂G_1 and propagates into G for $t \in (0, t_1]$. Just as in Sect. 3.1.1, first-order absorbing boundary conditions [66] are used on top $\partial G_1 \times (t_1, T]$ and bottom $\partial G_2 \times (0, T]$ boundaries, and the Neumann boundary condition is used on ∂G_3. The zero Neumann boundary condition at ∂G_3 allows us to model an infinite space domain in the lateral direction. The trace $g(x,t)$

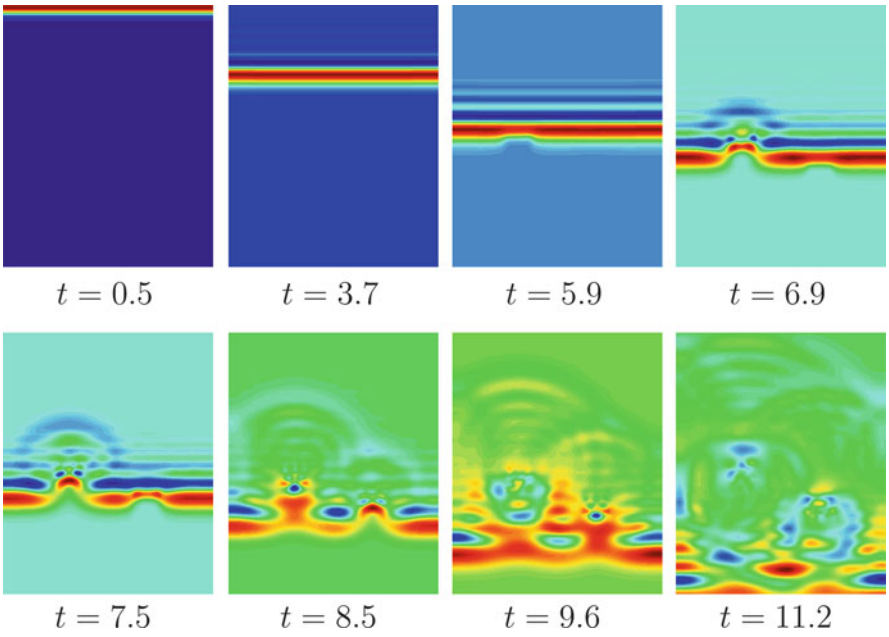

Fig. 4.10 Isosurfaces of the simulated exact solution to the forward problem (4.203) at different times with a plane wave initialized at the top boundary. Source: L. Beilina and M.V. Klibanov, A posteriori error estimates for the adaptivity technique for the Tikhonov functional and global convergence for a coefficient inverse problem, *Inverse Problems*, 26, 045012, doi:10.1088/0266-5611/26/4/045012, 2010. © IOP Publishing. Reprinted with permission

of the solution of the forward problem is recorded at the boundary $\partial\Omega$. Next, the coefficient $c(x)$ is "forgotten,"and our goal is to reconstruct this coefficient for $x \in \Omega$ from the data $g(x,t)$; see (2.5). Figures 4.10 show how the plane wave propagates for the structure given on Fig. 4.9.

4.15.2 The First Stage

In our numerical experiment, we reconstruct the medium, which is homogeneous with $c(x) = 1$ except of two small squares, where $c(x) = 4$; see Fig. 4.9c. However, we have not assumed any a priori knowledge neither of the structure of this medium nor of the background constant $c(x) = 1$ outside of those two small squares. We have only assumed the knowledge of the lower bound $c(x) \geq 1$ and also that $c(x) = 1$ outside of the domain of interest Ω; see (2.3). The assumption $c(x) \geq 1$ was used as follows: If at any point x', the reconstructed value of the coefficient was $c_{n,k}(x') < 1$, then we have assigned a new value at this point by setting $\widetilde{c}_{n,k}(x') := 1$.

Because of (4.202), the starting value for the tail $V_{1,1}(x,\overline{s})$ was computed via solving the forward problem (4.203) for $c \equiv 1$. Let $w_{c\equiv 1}(x,\overline{s})$ be the corresponding function $w(x,s)$ at $s=\overline{s}$. Then, using (2.18), we took

$$V_{1,1}(x,\overline{s}) = \frac{\ln w_{c\equiv 1}(x,\overline{s})}{\overline{s}^2}. \tag{4.204}$$

We have used the same parameters as ones in Sect. 3.1.3. The s-interval was $[\underline{s},\overline{s}] = [6.7, 7.45]$. The step size with respect to the pseudo frequency s was $h = 0.05$. Hence, $N = 15$ in our case. We have chosen two sequences of regularization parameters $\lambda := \lambda_n$ and $\varepsilon := \varepsilon_n$ for $n \in [1, N]$ which were the same ones as in (3.3). Once the function $q_{n,k}$ is calculated, we update the function $c := c_{n,k}$ via backward calculation as in (3.4). The resulting computed function is $c_{\text{glob}}(x)$.

In this test, we have chosen a stopping rule which is similar with the rule (3.23)–(3.26) of Sect. 3.2.2. We have observed that the lower boundary Γ of the square Ω,

$$\Gamma = \{x_2 = -3\} \cap \overline{\Omega}, \tag{4.205}$$

is such a part of the boundary $\partial\Omega$, which is the most sensitive one to the presence of inclusions. Denote $\Gamma_{\widetilde{h}} = \left\{(x_1,x_2) \in \Omega : x_2 = -3 + \widetilde{h}\right\}$. In other words, $\Gamma_{\widetilde{h}}$ is the part of the horizontal straight line, which is inside the square Ω, and the distance between $\Gamma_{\widetilde{h}}$ and the lower boundary $\{x_2 = -3\}$ of Ω is $\widetilde{h} = 0.125$. When calculating iterations with respect to the nonlinear term, we consider norms F_n^k:

$$F_n^k = \frac{||q_{n,1}^k|_{\Gamma_{\widetilde{h}}} - \overline{\psi}_n||_{L_2(-3,3)}}{||\overline{\psi}_n||_{L_2(-3,3)}}.$$

Given the number n, we stop our iterations with respect to the nonlinear term when

$$\begin{gathered} \text{either } F_n^k \geq F_n^{k-1} \\ \text{or } |F_n^k - F_n^{k-1}| \leq \varepsilon, \end{gathered} \tag{4.206}$$

where $\varepsilon = 0.001$ is a small tolerance number of our choice. In other words, we stop iterations, when either norms F_n^k start to grow or stabilize. Next, we iterate with respect to the tails and use the same stopping criterion. Namely, we stop our iterations with respect to tails when

$$\text{either } F_{n,i} \geq F_{n,i-1} \text{ or } |F_{n,i} - F_{n,i-1}| \leq \varepsilon, \tag{4.207}$$

where

$$F_{n,i} = \frac{||q_{n,i}|_{\Gamma_{\widetilde{h}}} - \overline{\psi}_n||_{L_2(-3,3)}}{||\overline{\psi}_n||_{L_2(-3,3)}}.$$

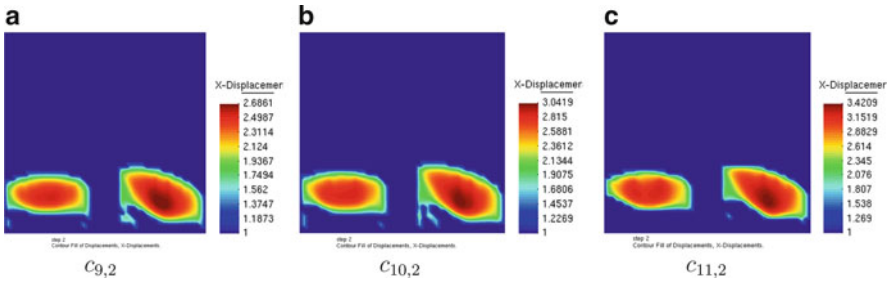

Fig. 4.11 Results of the performance of the globally convergent stage of our two-stage numerical procedure. Spatial distributions of some functions $c_{n,i}$ are shown. The function $c_{11,2}$ is taken as the final result of this stage (see details in the text). The maximal value of $c_{11,2}(x) = 3.8$ within each imaged inclusion. Also, imaged inclusions. Hence, the contrast is imaged with only 5% of error (the correct one is $4 : 1$). However, while the location of the right inclusion is imaged accurately, comparison with Fig. 4.9c shows that the left imaged inclusion is located below its correct position. Hence, it is desirable to move the left imaged square upward. This paves the way for a subsequent application of the adaptivity technique, which takes the function $c_{11,2} := c_{\text{glob}}$ as the starting point for computations. Source: L. Beilina and M.V. Klibanov, A posteriori error estimates for the adaptivity technique for the Tikhonov functional and global convergence for a coefficient inverse problem, *Inverse Problems*, 26, 045012, doi:10.1088/0266-5611/26/4/045012, 2010. © IOP Publishing. Reprinted with permission

Recall that the number i, on which these iterations are stopped, is denoted as $i := m_n$. Once the convergence criterion (4.207) is satisfied, we take the last computed tail V_{n,m_n}, set $V_{n+1,1} := V_{n,m_n}$, and run computations again for q_{n+1}. Hence, the number m_n of iterations with respect to tails is chosen automatically "inside" each iteration for q_n, which means that m_n varies with n.

In our numerical test, we have considered the noisy boundary data g_{noise} introduced as in (3.7) in Sect. 3.1.1:

$$g_\sigma\left(x^i, t^j\right) = g\left(x^i, t^j\right)\left[1 + \alpha_j (g_{\max} - g_{\min})\sigma\right]. \tag{4.208}$$

Here, $g\left(x^i, t^j\right) = u\left(x^i, t^j\right), x^i \in \partial\Omega$ is a mesh point at the boundary $\partial\Omega, t^j \in (0, T)$ is a mesh point in time, α_j is a random number in the interval $[-1, 1]$, $\sigma = 0.05$ is the level of noise and $g_{\max}$ and $g_{\min}$ are respectively maximal and minimal values of the computed boundary data g in (2.5). Hence, the noise level in the boundary data was 5%.

Figure 4.11 displays results of the performance of the approximately globally convergent stage of our two-stage numerical procedure. One can see that the location of the right small square is imaged well. It follows from Fig. 4.11c that the imaged contrast in this square is

$$\max c_{11,2} : 1 = 3.8 : 1,$$

where $n := \overline{N} = 11$ is our final iteration number (see below for this choice of $\overline{N}$). Thus, we have obtained the 5% error (0.2/4) in the imaged contrast, which is the same as the error in the input data. As to the left small square, we got the same

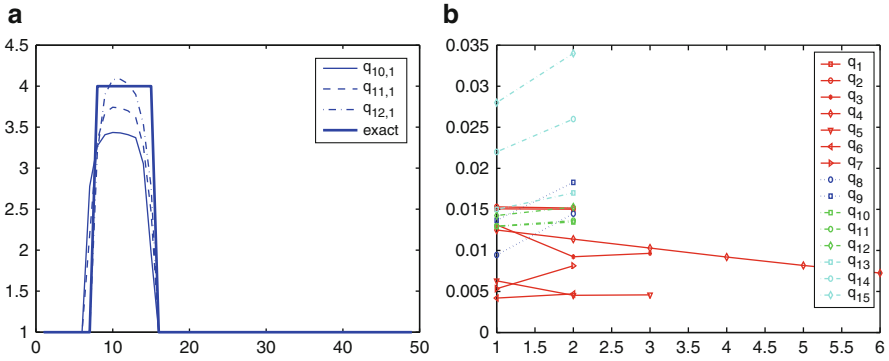

Fig. 4.12 (**a**) The one-dimensional cross-sections of the image of the function $c_{n,k}$ computed for corresponding functions $q_{n,1}$ along the vertical line passing through the middle of the right small square; (**b**) Computed L_2 -norms of the $F_{n,i} = \frac{||q_{n,i}|_{\partial\Omega} - \overline{\psi}_n||_{L_2(-3,3)}}{||\overline{\psi}_n||_{L_2(-3,3)}}$. Source: L. Beilina and M.V. Klibanov, A posteriori error estimates for the adaptivity technique for the Tikhonov functional and global convergence for a coefficient inverse problem, *Inverse Problems*, 26, 045012, doi:10.1088/0266-5611/26/4/045012, 2010. © IOP Publishing. Reprinted with permission

3.8 : 1 contrast in it for $c_{11,2}(x)$. Values of the function $c_{11,2}(x) = 1$ outside of these squares are imaged accurately. However, the location of the left square is shifted downward. Hence, both imaged squares are on about the same horizontal level. Therefore, comparison with Fig. 4.9c reveals that it is desirable to shift the left imaged square upward. This opens the door for the subsequent application of the adaptivity technique.

Figure 4.12b shows computed numbers $F_{n,i}$. Using this figure, we analyze results of our reconstruction. One can see on Fig. 4.12b that the number m_n of iterations with respect to tails indeed varies with n, since m_n is chosen automatically now, using the criterion (4.207). We observe that the norms $F_{n,i}$ generally decrease until computing the function q_7. Next, they slightly grow, decay from $F_{9,2}$ to $F_{10,2}$ and then these norms stabilize on $n = 11, 12$. For $n = 13, 14, 15$, these $F_{n,i}$ grow steeply. Thus, following the fourth Remark 2.9.4, we conclude, that we should stop our iterations when the stabilization occurs first, i.e., at $\overline{N} = 11$. So, we take the function $c_{11,2} := c_{\text{glob}}$ as our final reconstruction result on the globally convergent stage.

4.15.3 The Second Stage

We show in this section that the second stage of our two-stage numerical procedure can refine the image of the first stage, which was presented in the previous section. More precisely, we take the function $c_{\text{glob}} := c_{11,2}$ of Fig. 4.11c as the starting point for the adaptivity algorithm. We demonstrate in this section that the left square on

Fig. 4.11c can be indeed moved upward to its correct location of Fig. 4.9c, while the right figure would still remain in its correct location of Fig. 4.11c. At the same time, the calculated inclusions/background contrasts in both imaged squares as well as the value of the computed function $c_{\text{comp}}(x)$ outside of these squares will remain accurate.

We now solve state and adjoint problems (4.180) and (4.181) in the domain $Q_T^{(1)} = \Omega_1 \times (0,T)$, where

$$\Omega_1 = G \cap \{x_2 > -3\}.$$

Hence, $\Omega \subset \Omega_1$ and the line $\Gamma \subset \partial\Omega$ in (4.205) is a part of the lower boundary of the rectangle Ω_1. We have not used here the function $z_\zeta(t)$ since we have observed that $u(x,t) \approx 0$ for $t \approx T = 15$ in our case. To simplify, computations, we have found the normal derivative $\partial_n u\,|_{\partial\Omega_1 \times (0,T)}$, which we need to solve the state problem, via solving the forward problem (4.203); also see Sect. 4.2 for a more rigorous way to find this normal derivative.

We use the adaptive algorithm of Sect. 4.13.2 with the refinement criterion (4.189). The tolerance number β_1 is chosen via numerical experiments; see Sect. 4.12 for relevant explanations. We take $\beta_1 = 0.1$ on the initial coarse mesh, $\beta_1 = 0.2$ on the one, two, and three times refined meshes, and $\beta_1 = 0.6$ for all follow-up refinements of the initial mesh.

On all refined meshes, we have used a cut-off parameter C_{cut} for the reconstructed coefficient c_h. Thus, we redefine c_h as

$$c_h(x) := \begin{cases} c_h(x), \text{ if } |c_h(x) - c_{\text{glob}}(x)| \geq C_{\text{cut}} \\ c_{\text{glob}}(x), \text{ elsewhere.} \end{cases}$$

We choose $C_{\text{cut}} = 0$ for $m < 3$ and $C_{\text{cut}} = 0.3$ for $m \geq 3$, where m is the number of iterations in the quasi-Newton method on each mesh. Hence, the cut-off parameter ensures that we do not go too far from our good first guess for the solution $c_{\text{glob}}(x)$.

In the adaptive algorithm, we can use box constrains for the reconstructed coefficient. We obtain these constraints using the solution computed on the first stage. Namely, minimal and maximal values of the target coefficient in box constraints are taken using results of the first stage, since approximate global convergence Theorems 2.8.2 and 2.9.4 guarantee that the function c_{glob} obtained on the first stage is a good approximation for the correct solution. Since $c_{\text{glob}}(x) \in [1, 3.8]$, then we enforce that the coefficient $c(x)$ belongs to the following set of admissible parameters $c \in \{c \in C(\overline{\Omega}) | 1 \leq c(x) \leq 4\}$. Hence, this is similar with the correctness set $P\left(d, \overline{d}\right)$ of Theorem 2.9.4; see (2.208) in Sect. 2.9.1 for $P\left(d, \overline{d}\right)$ as well as the third Remark 2.9.4. Thus, in our case, the number $d := 4$ (Table 4.4).

First, the function $c_{\text{glob}}(x)$ was taken on the initial coarse mesh shown on Fig. 4.13a and the quasi-Newton method was applied on this mesh. Comparison of Figs. 4.13d and 4.11c (for $c_{11,2} := c_{\text{glob}}$) shows that the image was not improved, compared with the one obtained on the globally convergent stage. Next,

Table 4.4 Norms $||u\ |_{\Gamma_T} - g||_{L_2(\Gamma_T)}$ on adaptively refined meshes

n	4,608 elements	5,340 elements	6,356 elements	10,058 elements	14,586 elements
1	0.0992683	0.097325	0.0961796	0.0866793	0.0880115
2	0.0988798	0.097322	0.096723	0.0868341	0.0880866
3	0.0959911	0.096723			0.0876543
4		0.096658			

Here, $\Gamma_T = \Gamma \times (0, T)$ and n is the number of updates in the quasi-Newton method. These norms generally decrease as meshes are refined. Then they slightly increase on the fourth refinement. Thus, because of this increase on the fourth mesh refinement, we use relaxation Theorems 4.9.3 and 4.11.4 to decide that our final solution corresponds to the fourth mesh refinement; also see the second Remark 4.9.3

Source: L. Beilina and M.V. Klibanov, A posteriori error estimates for the adaptivity technique for the Tikhonov functional and global convergence for a coefficient inverse problem, *Inverse Problems*, 26, 045012, doi:10.1088/0266-5611/26/4/045012, 2010. © IOP Publishing. Reprinted with permission

the mesh was adaptively refined four times. Adaptively refined meshes are shown on Fig. 4.13b,c,g,h. Table 4.4 presents computed norms of $||u\ |_{\Gamma_T} - g||_{L_2(\Gamma_T)}$, where $\Gamma_T = \Gamma \times (0, T)$ and Γ was defined in (4.205). The first mesh refinement correspond to the second column. We observe that norms at the boundary generally decrease as meshes are refined. Then they slightly increase at the fourth refinement. Thus, because of this increase on the fourth mesh refinement, we use relaxation Theorems 4.9.3 and 4.11.4 to decide that our final solution corresponds to the fourth mesh refinement; also see the second Remark 4.9.3. This solution is displayed on Fig. 4.13j. One can see on Fig. 4.13j that we are able to accurately reconstruct locations of both small squares. At the same time, an accurate inclusion/background contrast obtained on the globally convergent stage is preserved and even improved. This contrast is now $4 : 1 = \max c_f(x) : 1$ instead of 3.8:1 calculated on the first stage, where $c_f(x)$ is the final imaged coefficient. The value of the coefficient $c_f(x) = 1$ outside of small squares is also imaged well.

4.16 Performance of the Two-Stage Numerical Procedure in 3D

In this section, Figs. 4.14a–c, 4.15a,b, 4.16a–f, 4.17a–p, 4.18a–p, 4.19a–l and 4.20a–l as well as Tables 4.5–4.7 were published in *Journal of Inverse and Ill-Posed Problems* [25]. In addition, Figs. 4.14a and 4.17p were published in *IEEE J. Computing in Science and Engineering* [160], © 2010, IEEE. All above listed figures are reprinted with permission.

In this section, we present numerical results of our paper [25]. Numerical studies of [25] were concerned with analyzing the performance of the two-stage numerical procedure in the 3D case. We work here with the computationally simulated data.

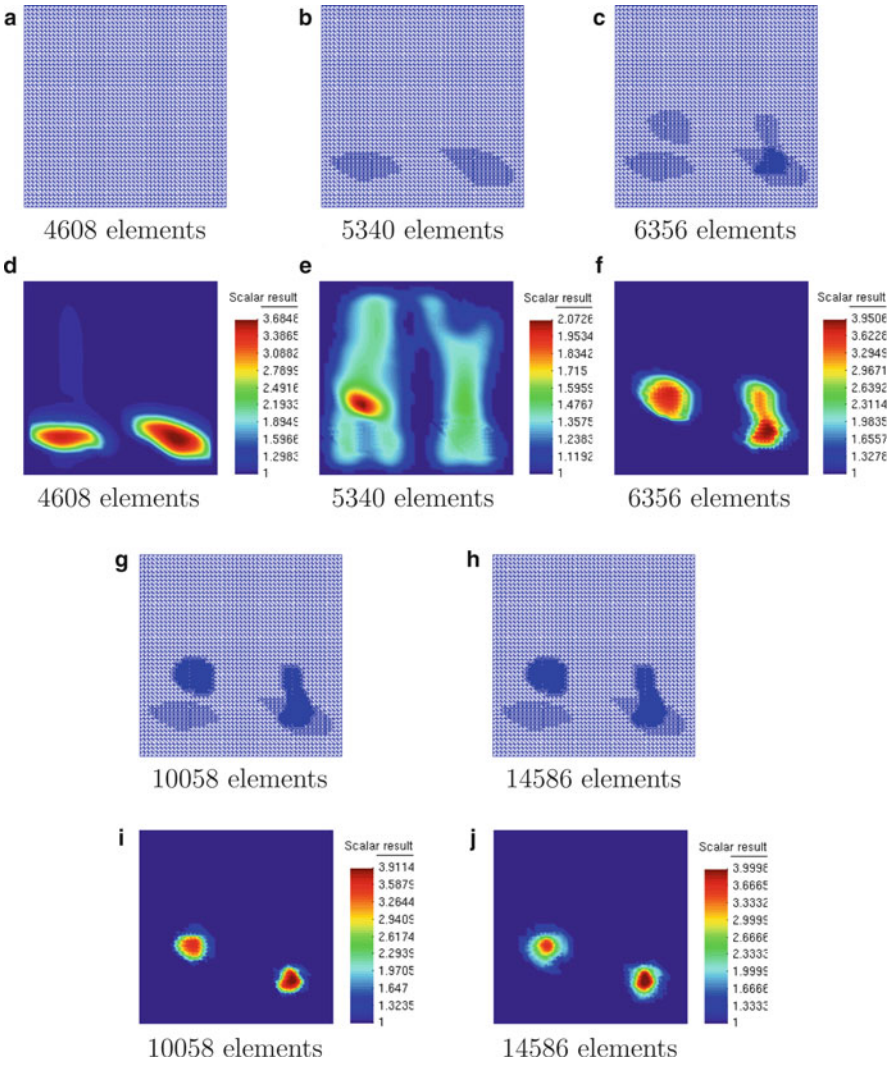

Fig. 4.13 Adaptively refined meshes (**a**)–(**c**), (**g**), (**h**) and corresponding images (**d**)–(**f**), (**i**), (**j**) on the second stage of our two-stage numerical procedure. In a) the same mesh was used as one on the globally convergent stage. Comparison of (**d**) with Fig. 4.25c (for $c_{11,2} = c_{\text{glob}}$) shows that the image was not improved compared with the globally convergent stage when the same mesh was used. However, the image was improved due to further mesh refinements. Figure 4.13j displays the final image obtained after four mesh refinements. Locations of both inclusions as well as 4:1 inclusions/background contrasts in them are imaged accurately; see details in the text and compare with Fig. 4.9c. Source: L. Beilina and M.V. Klibanov, A posteriori error estimates for the adaptivity technique for the Tikhonov functional and global convergence for a coefficient inverse problem, *Inverse Problems*, 26, 045012, doi:10.1088/0266-5611/26/4/045012, 2010.

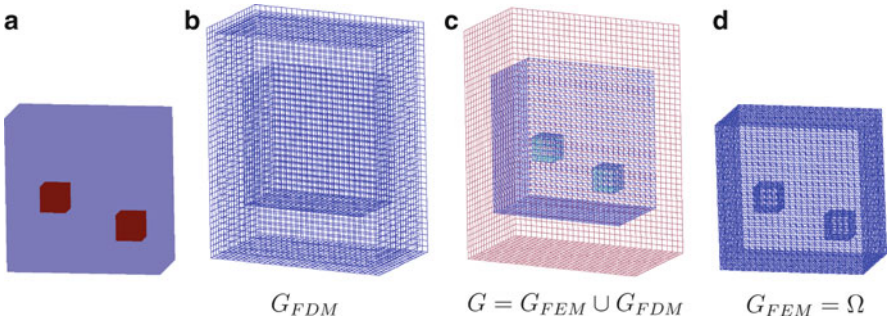

Fig. 4.14 (**a**) The exact geometry with two scatterers. Domain decomposition (**b**)–(**d**): the hybrid mesh (**c**) is a combinations of a structured mesh (**b**), where FDM is applied, and a mesh (**d**), where we use FEM, with a thin overlapping of structured elements. The solution of the inverse problem is computed in the hexahedron Ω and $c(x) = 1$ for $x \in G \setminus \Omega$. Source: L. Beilina and M.V. Klibanov, Synthesis of global convergence and adaptivity for a hyperbolic coefficient inverse problem in 3D, *J. Inverse and Ill-posed Problems,* 18, 85–132, 2010. © de Gruyter 2010. Reprinted with permission

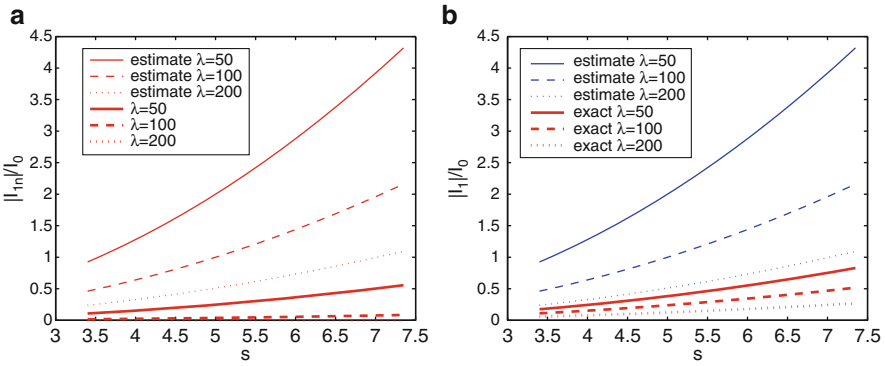

Fig. 4.15 Test 1: On (**a**), we show computed and on (**b**), exact values of $|I_{1,n}|/I_0$ compared with the estimation $|I_{1,n}|/I_0 \leq 4\bar{s}^2/\lambda$ (see (2.40)) for different values of λ. Computations performed on pseudo frequency interval $[3.4, 7.4]$ with $h = 0.05$. Here, x-axis presents pseudo-frequency interval. One can see that (2.40) significantly overestimates the value of $|I_{1,n}|/I_0$. Source: L. Beilina and M.V. Klibanov, Synthesis of global convergence and adaptivity for a hyperbolic coefficient inverse problem in 3D, *J. Inverse and Ill-posed Problems,* 18, 85–132, 2010. © de Gruyter 2010. Reprinted with permission

That is, the data $g(x,t)$ in (2.5) are generated by computing the forward problem (4.210) with the given function $c(x)$. Just as in all tests above, we use the hybrid FEM/FDM method of [30] to solve the forward problem. The computational domain in all our tests $G = G_{\text{FEM}} \cup G_{\text{FDM}}$ is set as

$$G = \{(x_1, x_2, x_3) \in [-4, 4] \times [-2.5, 2] \times [-5, 5]\}.$$

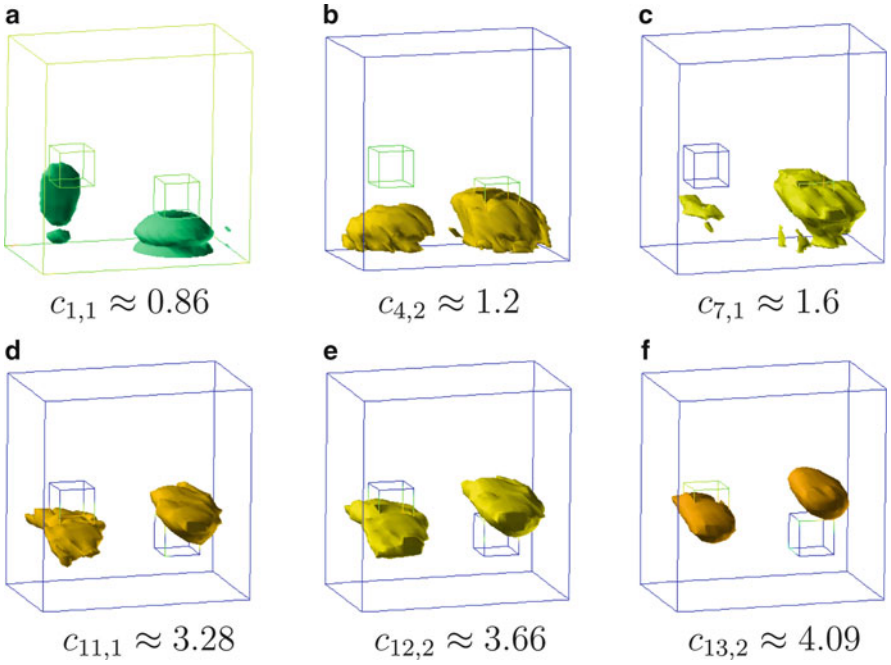

Fig. 4.16 Test 1. The spatial distribution of c_h after computing $q_{n,i}$; $n = 1, 3, 7, 11, 12, 13$ where n is the number of the computed function q. Maximal values of the imaged coefficient are displayed. Its computed value outside of imaged inclusions is 1. Results are presented with numerically approximated integrals I_0, $I_{1,n}$, $A_{1,n}$, $A_{2,n}$, with the noise level $\sigma = 5\%$ and with $\lambda = 200$. Source: L. Beilina and M.V. Klibanov, Synthesis of global convergence and adaptivity for a hyperbolic coefficient inverse problem in 3D, *J. Inverse and Ill-posed Problems,* 18, 85–132, 2010. © de Gruyter 2010. Reprinted with permission

This domain is split into the finite element domain G_{FEM}:

$$G_{\text{FEM}} := \Omega = \{(x_1, x_2, x_3) \in [-3, 3] \times [-2, 1.5] \times [-3, 3]\}$$

and the surrounding domain G_{FDM} with the structured mesh; see Fig. 4.14. The space mesh in Ω consists of tetrahedra, and it consists of cubes in G_{FDM}, with the mesh size $\widetilde{h} = 0.25$ in the overlapping regions. At the top and bottom boundaries of G, we use first-order absorbing boundary conditions [66]. At the lateral boundaries, zero Neumann boundary conditions allow us to assume an infinite space domain in the lateral direction.

The forward problem is computed in the domain $G \subset \mathbb{R}^3$ (Fig. 4.14). The coefficient $c(x)$ is unknown only in the domain $\Omega \subset G$. Following (2.3) and (4.207), we assume the knowledge of this coefficient only outside of the domain Ω:

$$c(x) = 1 \text{ in } G \setminus \Omega. \tag{4.209}$$

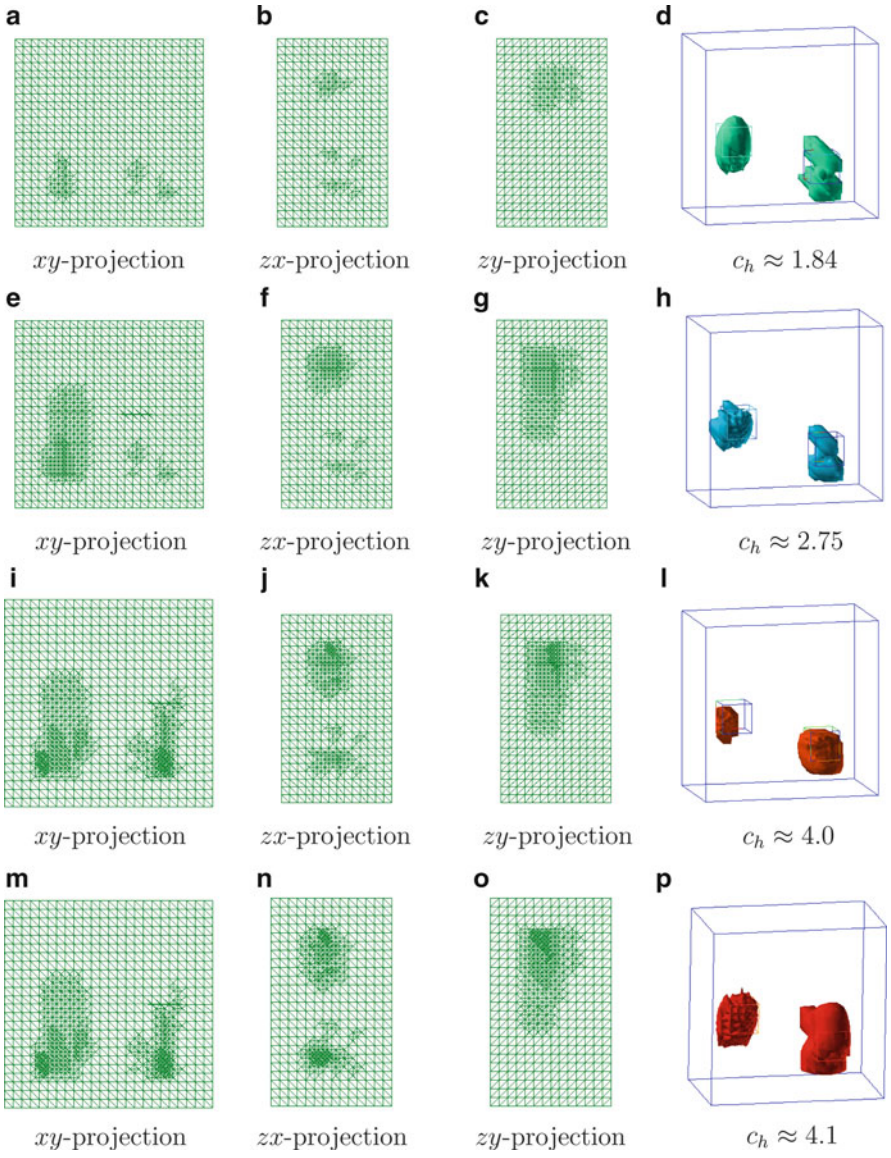

Fig. 4.17 Test 2. The case when the noise level = 0%. First, second, third, and fourth raws correspond to the first, second, third, and fourth mesh refinements, respectively. Maximal values of the computed coefficients on different meshes are displayed. In each case, the computed value of that coefficient outside of imaged inclusions is 1. The final image is displayed on (**l**). Locations of both inclusions as well as the 4 : 1 inclusions/background contrasts are imaged with a good accuracy. See Table 4.6 for the number of mesh points. Source: L. Beilina and M.V. Klibanov, Synthesis of global convergence and adaptivity for a hyperbolic coefficient inverse problem in 3D, *J. Inverse and Ill-posed Problems,* 18, 85–132, 2010. © de Gruyter 2010. Reprinted with permission

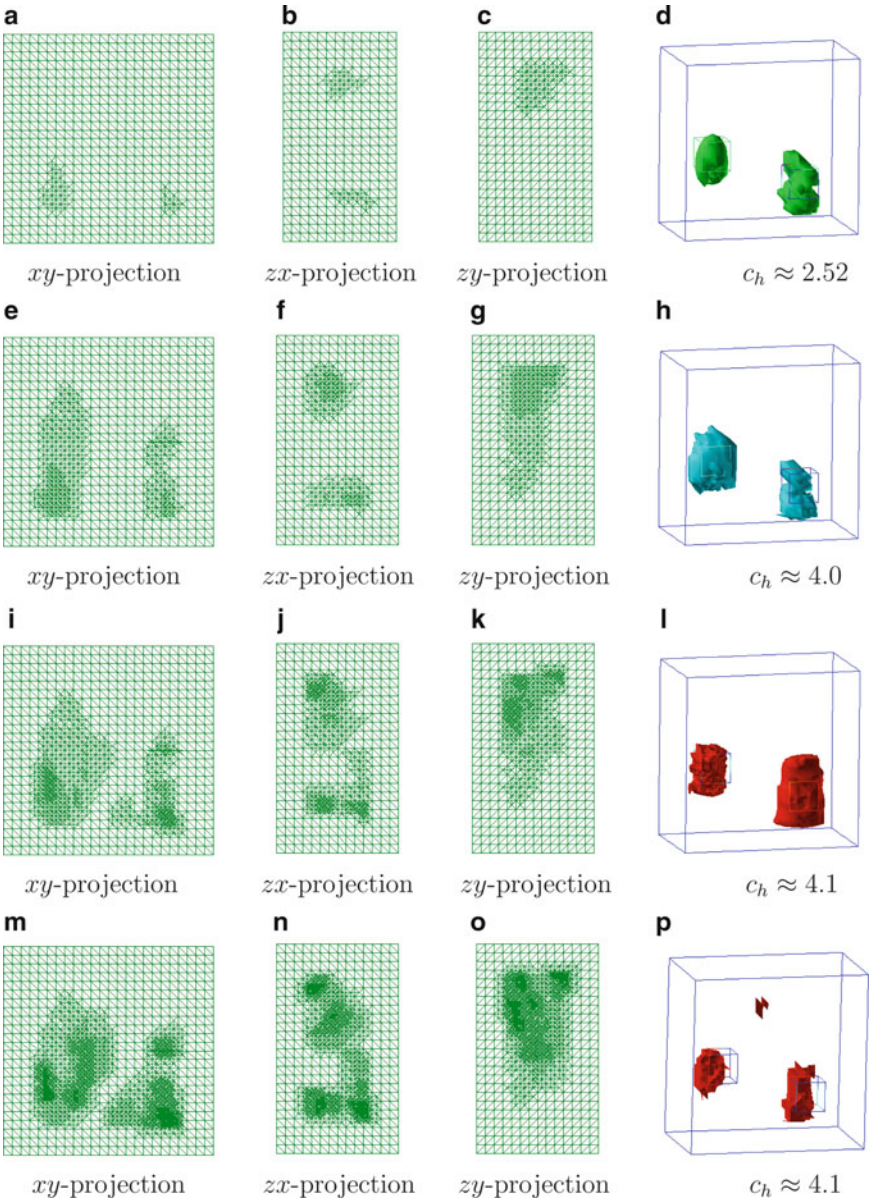

Fig. 4.18 Test 2. The case when the noise level $\sigma = 5\%$. First, second, third, and fourth raws correspond to first, second, third, and fourth mesh refinements respectively. Maximal values of the computed coefficients on different meshes are displayed. In each case, the computed value of that coefficient outside of imaged inclusions is 1. The final image is displayed on (**l**). Locations of both inclusions are imaged with a good accuracy. The correct 4:1 inclusions/background contrasts are imaged as 4.1:1, which is a good accuracy. See Table 4.6 for the number of mesh points. Source: L. Beilina and M.V. Klibanov, Synthesis of global convergence and adaptivity for a hyperbolic coefficient inverse problem in 3D, *J. Inverse and Ill-posed Problems,* 18, 85–132, 2010.

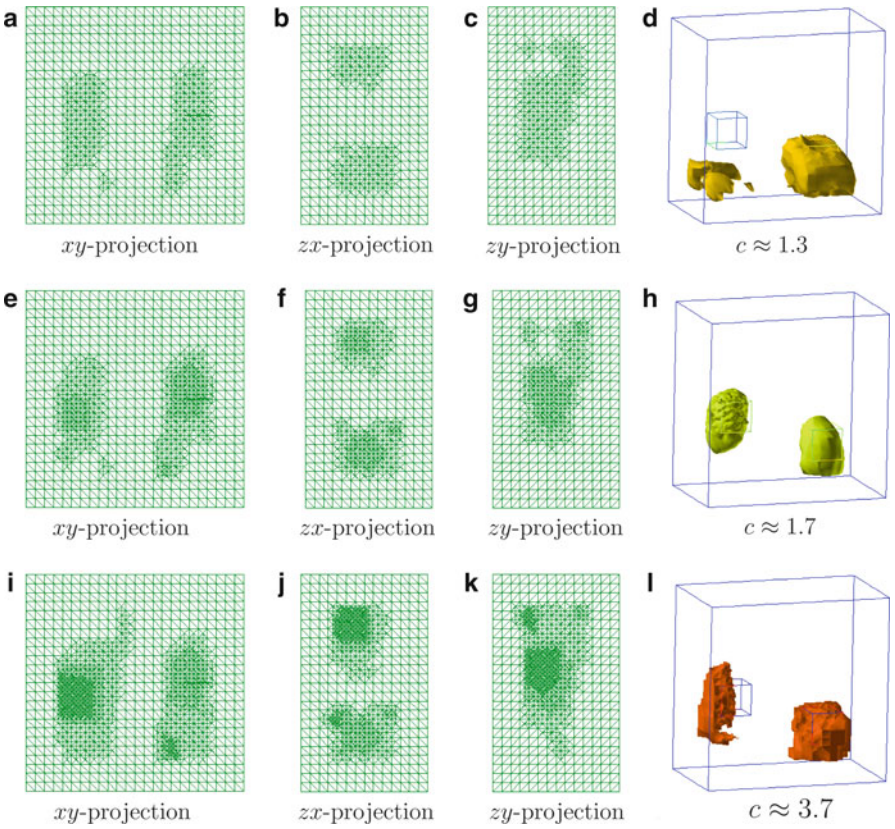

Fig. 4.19 Test 3. The case when the noise level $\sigma = 3\%$. Adaptively refined computational meshes in different projections and corresponding reconstructed coefficients. First, second, and third raws correspond to the first, second, and third refinements, respectively. Maximal values of the computed coefficients on different meshes are displayed. In each case, the computed value of that coefficient outside of imaged inclusions is 1. The final image is displayed on (**l**). Locations of both inclusions are imaged with a good accuracy. The correct 4:1 inclusions/background contrasts are imaged as 3.7 : 1. See Table 4.7 for the number of mesh points. Source: L. Beilina and M.V. Klibanov, Synthesis of global convergence and adaptivity for a hyperbolic coefficient inverse problem in 3D, *J. Inverse and Ill-posed Problems,* 18, 85–132, 2010. © de Gruyter 2010. Reprinted with permission

The trace $g(x,t)$ of the solution of the forward problem is recorded at the boundary $\partial\Omega$. Next, the coefficient $c(x)$ is "forgotten," and our goal is to reconstruct this coefficient for $x \in \Omega$ from the data $g(x,t)$. The boundary of the domain G is $\partial G = \partial G_1 \cup \partial G_2 \cup \partial G_3$. Here, ∂G_1 and ∂G_2 are respectively top and bottom sides of the largest domain of Fig. 4.14, and ∂G_3 is the union of left, right, front, and back sides of this domain. In our tests, the forward problem is

$$c(x)\,\partial_t^2 u - \Delta u = 0, \quad \text{in } G \times (0,T),$$

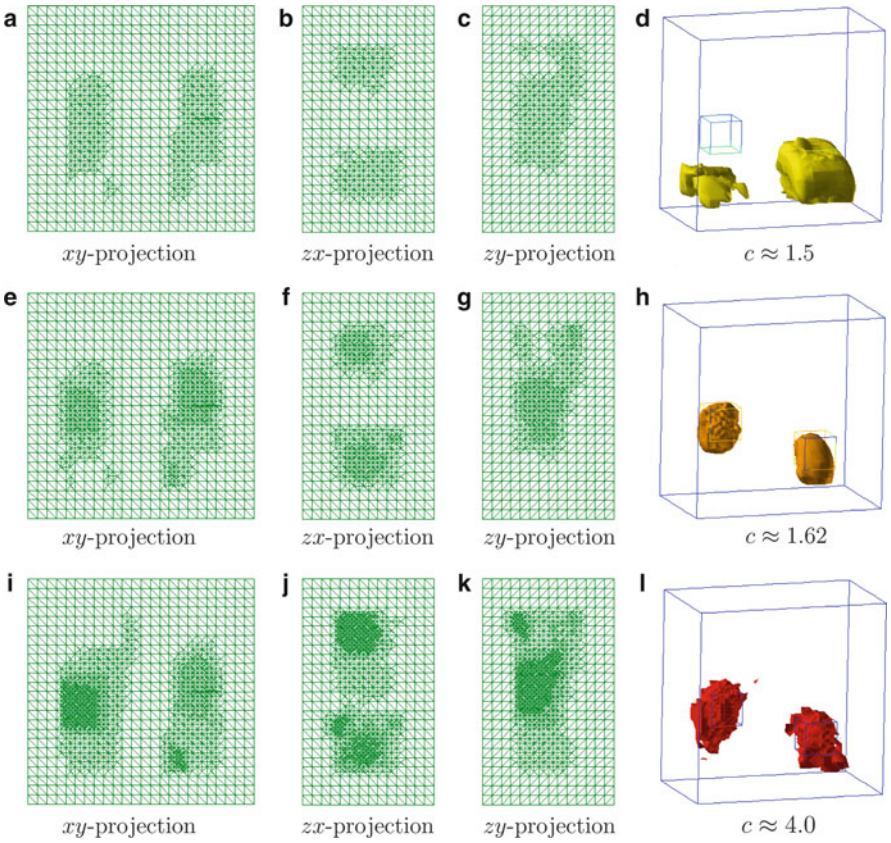

Fig. 4.20 Test 3. The case when the noise level $\sigma = 5\%$. Adaptively refined computational meshes in different projections and corresponding reconstructed coefficients. First, second, and third raws correspond to the first, second, and third refinements, respectively. Maximal values of the computed coefficients on different meshes are displayed. In each case, the computed value of that coefficient outside of imaged inclusions is 1. The final image is displayed on (**l**). Locations of both inclusions are imaged with a good accuracy. The $4:1$ inclusions/background contrasts are also imaged with a good accuracy. See Table 4.7 for the number of mesh points. Source: L. Beilina and M.V. Klibanov, Synthesis of global convergence and adaptivity for a hyperbolic coefficient inverse problem in 3D, *J. Inverse and Ill-posed Problems,* 18, 85–132, 2010. © de Gruyter 2010. Reprinted with permission

$$
\begin{aligned}
&u(x,0) = 0,\ \partial_t u(x,0) = 0,\ \text{in } G,\\
&\partial_n u\big|_{\partial G_1} = f\,(t)\,,\ \text{on } \partial G_1 \times (0,t_1],\\
&\partial_n u\big|_{\partial G_1} = -\partial_t u,\ \text{on } \partial G_1 \times (t_1,T),\\
&\partial_n u\big|_{\partial G_2} = -\partial_t u,\ \text{on } \partial G_2 \times (0,T),\\
&\partial_n u\big|_{\partial G_3} = 0,\ \text{on } \partial G_3 \times (0,T),
\end{aligned}
\tag{4.210}
$$

Table 4.5 Test 1: Computed discrete L_2-norms $F_{n,i} = \frac{||q_{n,i}|_{\widetilde{h}} - \overline{\psi}_n||_{L_2(\Omega_1)}}{||\overline{\psi}_n||_{L_2(\Omega_1)}}$ for $\lambda = 50$ and $\lambda = 200$

It. n $\lambda = 50$	$i = 1$	$i = 2$	$i = 3$	It. n $\lambda = 200$	$i = 1$	$i = 2$	$i = 3$
1	0.0522995	0.0522995		1	0.052307	0.052307	
2	0.0523043	0.0521799		2	0.0523043	0.0521758	
3	0.0535235	0.053353		3	0.0535235	0.053353	
4	0.0516891	0.0556757		4	0.0516891	0.0556757	
5	0.0467661	0.091598		5	0.0467661	0.091598	
6	0.0466467	0.0440336	0.0464053	6	0.0466467	0.0440336	0.0464053
7	0.048653	0.0658041		7	0.048651	0.0658031	
8	0.0631709	0.0893371		8	0.0631753	0.0893179	
9	0.0851995	0.112022		9	0.085511	0.112321	
10	0.0914011	0.106414		10	0.0915352	0.10644	
11	0.0900873	0.104467		11	0.0905234	0.104808	
12	0.111039	0.133793		12	0.111136	0.134055	
13	0.141459	0.167344		13	0.141494	0.166125	
14	0.176421	0.219103		14	0.174968	0.222117	
15	0.238352	0.296523		15	0.240944	0.29716	
16	0.327406	0.463613		16	0.328997	0.464465	
17	0.528386	0.606531		17	0.53069	0.606824	
18	0.630857	0.680105		18	0.630438	0.681458	

Source: L. Beilina and M.V. Klibanov, Synthesis of global convergence and adaptivity for a hyperbolic coefficient inverse problem in 3D, *J. Inverse and Ill-posed Problems,* 18, 85–132, 2010. © de Gruyter 2010. Reprinted with permission

Table 4.6 Test 2. $||u|_{\Gamma_T} - g||_{L_2(\Gamma_T)}$, $\max_{\overline{\Omega}} R_{c_1}$, and $\max_{\overline{\Omega}} R_{c_2}$ on adaptively refined meshes

	$\|\|u\|_{\Gamma_T} - g\|\|_{L_2(\Gamma_T)}$	R_{c_1}	R_{c_2}	q.N.it.	CPU time (s) T	T_{rel}
Mesh $\sigma = 0\%$						
9,375	0.0285508	0.502511	0.0159757	5	23.87	0.0025
9,583	0.0259143	0.358853	0.0440558	5	24.26	0.0025
10,885	0.0301035	0.115057	0.105189	6	27.44	0.0025
11,500	0.028857	0.119722	0.0952689	6	29	0.0025
12,031	0.0342642	0.318698	0.049062	7	30.55	0.0025
Mesh $\sigma = 5\%$					T	
9,375	0.031286	0.501337	0.0160262	4	23.77	0.0025
9,555	0.0417805	0.18959	0.0497364	6	24.16	0.0025
11,248	0.0293965	0.114448	0.0733725	6	28.18	0.0025
13,042	0.0296054	0.126106	0.0723502	6	32.64	0.0025
20,229	0.0398704	0.210689	0.105882	4	50.74	0.0025

Here, q.N.it. denotes the number of iterations in the quasi-Newton method. In this table, coarse mesh consists of 9,375 nodes. CPU time T is given for one q.N.it

Source: L. Beilina and M.V. Klibanov, Synthesis of global convergence and adaptivity for a hyperbolic coefficient inverse problem in 3D, *J. Inverse and Ill-posed Problems,* 18, 85–132, 2010. © de Gruyter 2010. Reprinted with permission

Table 4.7 Test 3: $||u\mid_{\Gamma_T} - g||_{L_2(\Gamma_T)}$ on adaptively refined meshes with different noise level σ in data

Mesh	$\sigma = 3\%$	q.N.it.	CPU time (s)	min CPU time/node (s)
9,375	0.030811	3	26.2	0.0028
10,564	0.029154	3	29.08	0.0028
12,001	0.035018	3	32.91	0.0027
16,598	0.034	8	46.49	0.0028
Mesh	$\sigma = 5\%$	q.N.it.	CPU time (s)	min CPU time/node (s)
9,375	0.0345013	3	26.53	0.0028
10,600	0.0324908	3	29.78	0.0028
12,370	0.03923	2	34.88	0.0028
19,821	0.0277991	8	53.12	0.0027

Here, q.N.it. denotes the number of iterations in the quasi-Newton method. In this table coarse mesh consists of 9,375 nodes. CPU time T is given for one q.N.it

where T is the final time and $f(t)$ is the plane wave defined as

$$f(t) = \frac{(\sin(\overline{s}t - \pi/2) + 1)}{10},\ 0 \le t \le t_1 := \frac{2\pi}{\overline{s}}, T = 8.22t_1.$$

Thus, the plane wave is initialized at the top boundary ∂G_1 and propagates into G for $t \in (0, t_1]$. First-order absorbing boundary conditions [66] are used on $\partial G_1 \times (t_1, T]$ and $\partial G_2 \times (0, T]$, and the Neumann boundary condition is used on the bottom boundary ∂G_3. In our computations, the upper limit of the integral in the Laplace transform (2.10) is T.

4.16.1 The First Stage

We have performed numerical experiments to reconstruct the medium, which is homogeneous with $c(x) = 1$ except of two small cubes, where $c(x) = 4$; see Fig. 4.14a. However, we have not assumed a priori knowledge of the structure of this medium. Because of (4.209), the starting value for the tail $V_{1,1}(x, \overline{s})$ was computed via solving the forward problem (4.210) for $c \equiv 1$. Then, we have used for $V_{1,1}(x, \overline{s})$ the formula (4.204) from Sect. 4.15.2.

We have found that the pseudo frequency interval $s \in [3.3, 4.3]$ was the optimal one for the above domains G, Ω. The step size in the s direction was chosen as $h = 0.05$. Hence, $N = 20$ in our case. We have chosen the same sequence ε_n of regularization parameters as in Sect. 3.1.1. However, we choose here the parameter λ independent on n; see below.

Once the function $q_{n,i}$ is calculated, we update the function $c := c_{n,i}$ via backward calculation as in formula (3.4) in Sect. 3.1.3. The stopping rule for iterations with respect to the nonlinear term as well as with respect to the tails is the same as in Sect. 4.15.2 with the only difference that Γ and $\Gamma_{\widetilde{h}}$ are parts of planes now rather than parts of straight lines:

$$\Gamma = \{x_3 = -3\} \cap \overline{\Omega},\ \Gamma_{\widetilde{h}} = \left\{(x_1, x_2) \in \Omega : x_3 = -3 + \widetilde{h}\right\}, \widetilde{h} = 0.25. \quad (4.211)$$

Hence, Γ is the lower boundary of the domain Ω. We have observed in our numerical tests that the lower boundary of the domain Ω is the most sensitive one to the presence of inclusions. Recall that the incident plane wave falls from the top; see (4.210).

Test 1. We test the approximately globally convergent method for the case of the reconstruction of the structure given on Fig. 4.14a. We take the noise level 5% in (4.208), which means $\sigma = 0.05$. In Table 4.5, we analyze computed relative L_2-norms of the $F_{n,i}$ for different values of the parameter λ in the CWF in (2.38). We observe that significant changes in λ cause only insignificant changes in L_2-norms of the $F_{n,i}$. The results in Table 4.5 are in an agreement with results in Fig. 4.15, where in Fig. 4.15a, we present approximated, and on Fig. 4.15b, exact values of the ratio $|I_{1,n}|/I_0$ compared with the estimate (2.37). Figure 4.15 shows that a significant growth of the value of λ has a very small influence to the value of $|I_{1,n}|/I_0$ on the pseudo frequency interval $[3.3, 4.3]$ which we take in actual computations. Therefore, we can work only with one value of λ for all n.

Figure 4.16 displays isosurfaces of resulting images of functions $c_{n,i}, n = 1, 3, 7, 11, 12, 13$ with numerically approximated integrals $I_0, I_{1,n}, A_{1,n}, A_{2,n}$ by midpoint rule, which corresponds to the computed integrals of the Fig. 4.15a with $\lambda = 200$. Comparison of images of functions $c_{n,i}$ for different values n and i shows that the inclusion/background contrasts grows with the increase of n and i.

One can see from Table 4.5 that the numbers $F_{n,i}$ decrease until computing the function q_7. Next, $F_{7,2} > F_{6,2}$ and numbers $F_{n,i}$ start to grow with the increase of n. They are stabilized for $n = 10, 11$ and then grow steeply for $n = 12, ..., 18$. Thus, we conclude, that convergence of functions c_n occurs at $n = 7$ and we take $c_{7,1} := c_{\text{glob}}$ as our final reconstruction result of the first stage of our two-stage procedure. The function $c_{7,1}$ is depicted on Fig. 4.16c.

We point out, however, that in the above numerical studies of the first stage procedure in Sects. 3.2.2, 3.1.3, and 4.15.2, we have stopped at those values of n for which the stabilization has occurred. Thus, if following the fourth Remark 2.9.4 in this test, then we can also stop at $n = 10$ or $n = 11$. However, we have noticed that the adaptivity stage works better for this specific test when we stop at lower values of n. This is the reason why we took $c_{7,1} := c_{\text{glob}}$. We show in Test 3 (Sect. 4.16.2) that the second stage also works well starting from $c_{4,2}$.

4.16.2 The Second Stage

In Tests 2–4 of this section, we demonstrate the performance of the synthesis of the adaptivity with the approximately globally convergent algorithm. We do not use the function $z_\zeta(t)$ here, since we have observed that $u(x,T) \approx 0$, where $u(x,t)$ is the solution of the state problem. In tests of this section, we use different levels of noise in the boundary data $g = u|_{\partial\Omega}$ for the adaptivity. Although we have introduced the 5% noise in the data in Test 1 for the first stage of our two-stage procedure, we can introduce different levels of noise in (4.208) on the second stage. Still, in all tests of this section, we take the solution of the first stage as the starting point for iterations. Denote $\Gamma_T = \Gamma \times (0,T)$, where Γ was defined in (4.211), and this the lower part of the boundary of our domain of interest Ω. We use the regularization parameter $\alpha = 0.01$ in all tests of this section.

Recall that by (4.194), mesh should be refined locally in those regions were

$$|R_c(x)| \geq \beta_1 \max_{\overline{\Omega}} |R_c(x)|, \tag{4.212}$$

where the number $\beta_1 \in (0,1)$ should be chosen in numerical experiments. We have used $\beta_1 = 0.2$.

Just as in Sect. 4.15.3, we use a cut-off parameter C_{cut} for the reconstructed coefficient c_h on all refined meshes. Specifically,

$$c_h(x) = \begin{cases} c_h(x), \text{ if } |c_h(x) - c_{\text{glob}}(x)| \geq C_{\text{cut}}, \\ c_{\text{glob}}(x), \text{ elsewhere.} \end{cases} \tag{4.213}$$

Let m be the number of mesh refinements. In all tests we choose $C_{\text{cut}} = 0.05$ for $m < 3$ and $C_{\text{cut}} = 0.2$ for $m \geq 3$.

Similarly with Sect. 4.15.3, we use box constrains for the reconstructed coefficient in the adaptivity algorithm. We obtain these constraints using the solution obtained on the first stage of Test 1 To choose the upper bound d for the function c, we observe that Figs. 4.16 implies that for $n \leq 13$, the maximal value of the imaged coefficient did not exceed 4.09, whereas we took $c_{7,1} := c_{\text{glob}}$; see the end of Test 1 for an explanation. On the other hand, approximate global convergence Theorems 2.8.2 and 2.9.4 guarantee that the function c_{glob} is close to the exact solution. Hence, we choose in (2.3) $d = 4.2$. Thus, in Tests 2–4, we enforce that the coefficient $c(x)$ belongs to the set of admissible parameters, $c(x) \in C_M = \{c \in C(\overline{\Omega}) | 1 \leq c(x) \leq 4.2\}$.

Results of computations are presented in Table 4.6. The relative time T_{rel} in this table (CPU time/node) is computed as

$$T_{\text{rel}} = \frac{T}{p}, \tag{4.214}$$

where T is the total CPU time and p is number of nodes in the computational mesh. We note that T_{rel} is approximately the same for all refined meshes which show efficiency of using hybrid FEM/FDM method for solution of the inverse problem. The knowledge of T_{rel} can help to estimate in advance the timing T for the solution of this CIP for any number of mesh points using (4.214).

Test 2. This test consists of two subtests with 0% and 5% noise; see beginning of this section. In both subtests the function $c_{7,1} := c_{\text{glob}}$, which corresponds to Fig. 4.16c, was taken as the starting point on all meshes.

First, we use the coarse mesh and obtain almost the same reconstruction as the one on the first stage, which is similar with the 2D case of Sect. 4.15.3. We repeat the optimization procedure on every new mesh. Already on the first mesh refinement, we have reconstructed shifted location of small cubes; see Figs. 4.17d and 4.18d. Table 4.6 shows computed norms $||u\mid_{\Gamma_T} - g||_{L_2(\Gamma_T)}$ as well as maximal values of residuals R_{c_1} and R_{c_2}. The second row corresponds to the first mesh refinement. We observe that on the fourth mesh refinement, these norms increase by about 20% for $\sigma = 0\%$ and by about 34% for $\sigma = 5\%$.

Hence, relaxation Theorems 4.9.3 and 4.11.4 imply that because of this significant increase of norms $||u\mid_{\Gamma_T} - g||_{L_2(\Gamma_T)}$ on the fourth mesh refinement, our final solution should be taken from the third mesh refinement. Thus, our final images for both levels of noise are presented on Figs. 4.17l and 4.18l.

To compare with Sect. 4.15.3, we note that in that section, these norms $||u\mid_{\Gamma_T} - g||_{L_2(\Gamma_T)}$ have increased on the fourth mesh refinement only by about 1%; see Table 4.8. This is why we took in Sect. 4.15.3 as the final solution the one which was obtained on the four times refined mesh.

Test 3. The goal of this test is to see how the number of iterations n of the approximately globally convergent method of the first stage affects the result of the second stage of our two-stage numerical procedure. Indeed, although in both subtests of Test 2, we have started iterations of the adaptivity from the function $c_{7,1}$, approximate global convergence Theorems 2.8.2 and 2.9.4 guarantee that any function $c_{n,i}$ with $n \in [1,7]$ is close to the correct solution. Hence, in this test, we start iterations of the adaptivity from the function $c_{4,2}$; see Fig. 4.16b for this function.

Just as in Test 2, we again have two sub-tests here, which differ by the level of noise of 3% and 5% in data. First, on the coarse mesh, we obtain almost the same reconstruction as one of the first stage, which is similar with the previous example. On the two times adaptively refined mesh, we have reconstructed shifted location of cubes; see Figs. 4.19h and 4.20h. Table 4.7 shows computed norms of $||u\mid_{\Gamma_T} - g||_{L_2(\Gamma_T)}$. The first mesh refinement corresponds to the second row. The fourth mesh refinement led to a significant increase of this norm in both subtests (not shown in Table 4.7). Thus, using again relaxation Theorems 4.9.3 and 4.11.4, we conclude that we obtain the solution of our CIP on the three times adaptively refined mesh. Our final images for both levels of noise are presented on Figs. 4.19l and 4.20l. Locations of both inclusions are imaged accurately in both cases. In particular,

especially in comparison with the first stage, the resulting computed maximal value $c_h = 3.7$ and $c_h = 4$ for noise levels of 3% and 5%, respectively. Values of $c_h = 1$ outside of imaged inclusions are also accurately calculated.

Thus, although we have replaced in Test 3 the function $c_{7,1}$ of Test 2 with the function $c_{4,2}$ as the starting point for the subsequent adaptivity technique, we have still obtained the same quality images as ones in Test 2 This again verifies computationally convergence estimates of both approximate global convergence Theorems 2.8.2 and 2.9.4.

4.17 Numerical Study of the Adaptive Approximately Globally Convergent Algorithm

In this section, Figs. 4.21a–c, 4.22a–d, 4.23a,b, 4.24a–d, 4.25a–d, 4.26a–d and 4.27a–d as well as Tables 4.8–4.10 were published in Inverse Problems [9]. Reprinted with permission.

In this section, we present the adaptive approximately globally convergent algorithm developed in [9]. The idea of [9] is to use the adaptivity inside the approximately globally convergent algorithm of Sect. 2.6.1. Thus, unlike the above, this is a one-stage numerical procedure. The a posteriori error analysis of [9] is based on the analysis of the sequence of Dirichlet boundary value problems for

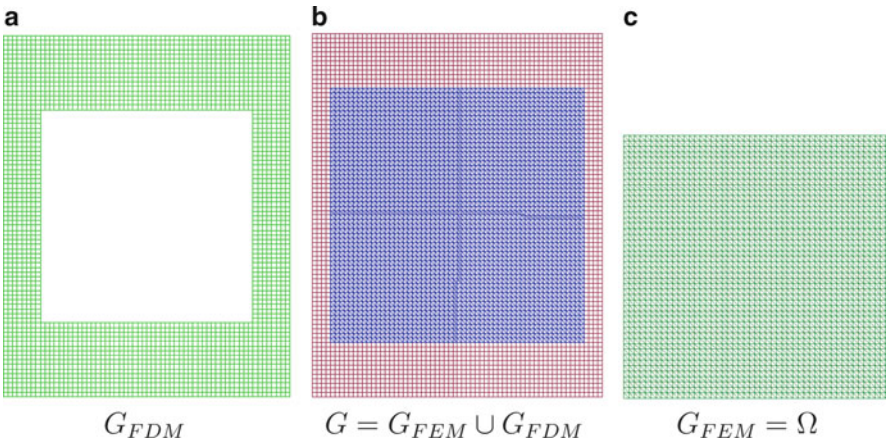

Fig. 4.21 The hybrid mesh (**b**) is a combinations of a structured mesh (**a**), where FDM is applied, and a mesh (**c**), where we use FEM, with a thin overlapping of structured elements. The solution of the inverse problem is computed in the square Ω and $c(x) = 1$ for $x \in G \setminus \Omega$. Source: M. Asadzadeh and L. Beilina, A posteriori error analysis in a globally convergent numerical method for a hyperbolic coefficient inverse problem, *Inverse Problems*, 26, 115007, doi:10.1088/0266-5611/26/11/115007, 2010. © IOP Publishing. Reprinted with permission

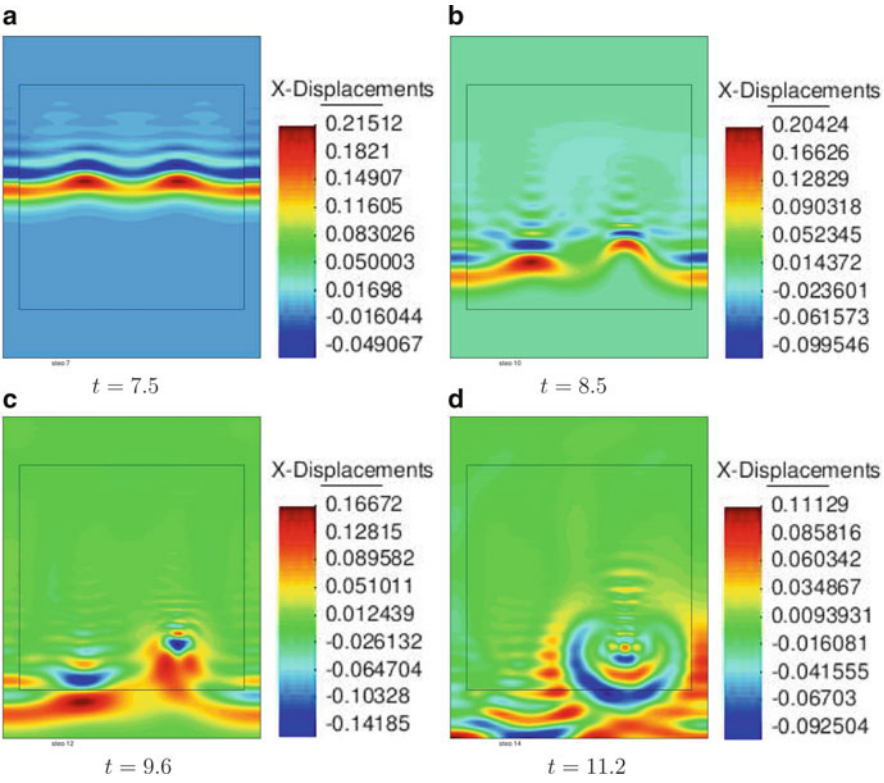

Fig. 4.22 Isosurfaces of the simulated exact solution to the forward problem (4.203) at different times with a plane wave initialized at the top boundary. Source: M. Asadzadeh and L. Beilina, A posteriori error analysis in a globally convergent numerical method for a hyperbolic coefficient inverse problem, *Inverse Problems*, 26, 115007, doi:10.1088/0266-5611/26/11/115007, 2010. © IOP Publishing. Reprinted with permission

elliptic equations (2.49) for functions $q_{n,i}$ with Dirichlet boundary conditions (2.50). We do not discuss this analysis here referring the reader to the publication [9] instead. Rather, we focus here on numerical results of this publication.

That a posteriori error analysis led the authors of [9] to the mesh refinement recommendation which is the direct analog of the second mesh refinement recommendation of Sect. 4.12; see (4.186). Thus, the mesh should be refined in all subdomains, where

$$c_h(x) \geq A \max_{\overline{\Omega}} c_h(x), \tag{4.215}$$

where $c_h(x)$ is the reconstructed coefficient on the current, coarser, mesh. In (4.215), $A \in (0,1)$ is the tolerance number which should be chosen numerically; see Sect. 4.12.

Thus, the procedure works as follows. On the coarse mesh, the algorithm of Sect. 2.6.1 is applied, and the function $c_{\overline{N}} := c_{\text{glob}} := c_h$ is found. Next, the mesh is

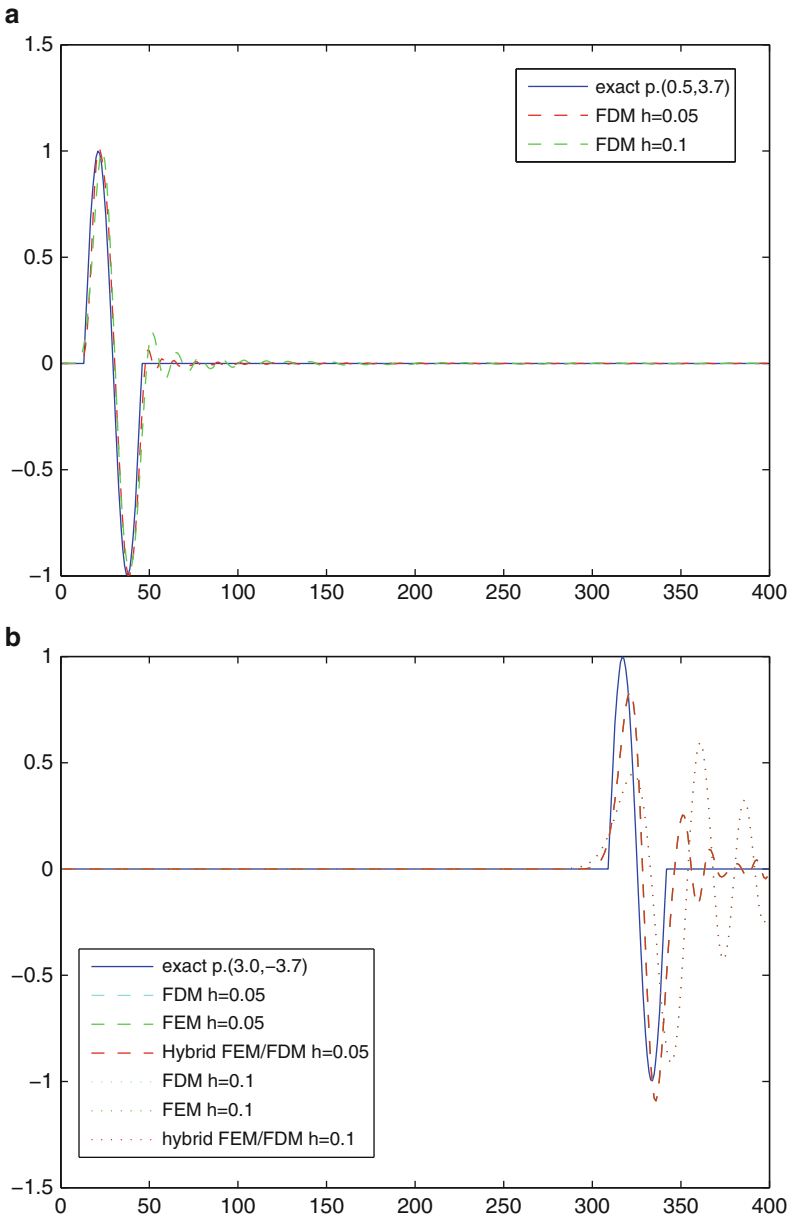

Fig. 4.23 Exact and computed solutions of equation using different methods. (**a**) Comparison of exact solution and computed solutions at the point (0.5, 3.7), which is located at the top of the computational domain G. (**b**) Comparison of exact solution and computed solutions at the point (3.0, −3.7), which is located at the bottom of the computational domain G. Source: M. Asadzadeh and L. Beilina, A posteriori error analysis in a globally convergent numerical method for a hyperbolic coefficient inverse problem, *Inverse Problems*, 26, 115007, doi:10.1088/0266-5611/26/11/115007, 2010. © IOP Publishing. Reprinted with permission

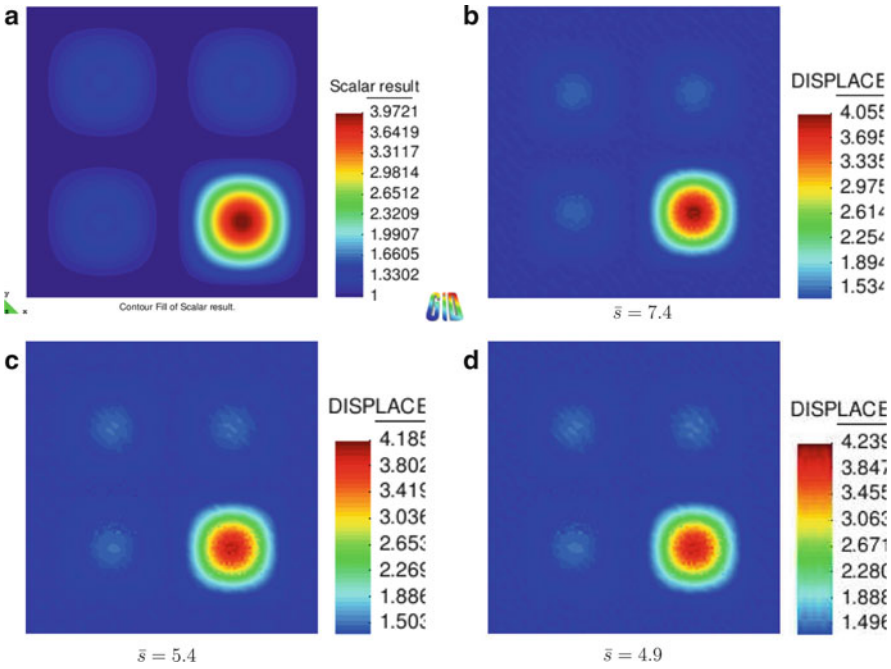

Fig. 4.24 Exact (on (**a**)) and computed (on (**b**)–(**d**)) coefficients $c(x)$ using exact computed values of the tail function $V(x, \bar{s})$. Source: M. Asadzadeh and L. Beilina, A posteriori error analysis in a globally convergent numerical method for a hyperbolic coefficient inverse problem, *Inverse Problems*, 26, 115007, doi:10.1088/0266-5611/26/11/115007, 2010. © IOP Publishing. Reprinted with permission

refined using the criterion (4.215), and the algorithm of Sect. 2.6.1 is applied again using this finer mesh. Next, the mesh is refined again, if necessary, and the process is repeated.

We update functions $c_{n,i}$ using the variational formulation of (2.11); see formulas (3.10)–(3.21) in Sect. 3.1.3. Note that we always set $c_{n,i}(x) = 1$ for $x \in G \setminus \Omega$.

On the refined mesh, the first guess for the tail is computed using the solution of the forward problem (4.219) with so interpolated function $c_{\text{glob}}(x)$. Let $\widetilde{w}(x, s)$ be the Laplace transform of this solution. Then the first guess for tails on the refined mesh is taken as

$$\widetilde{V}_{1,1}(x) = \frac{\ln \widetilde{w}(x, \bar{s})}{\bar{s}^2}.$$

Next, we perform all steps of the algorithm of Sect. 2.6.1 to obtain the function c^1_{n,m_n}.

For each new mesh, we first linearly interpolate the boundary function $\overline{\psi}_n$ and the reconstructed function $c_{\text{glob}}(x)$ obtained on the previous mesh. Then on the new refined mesh for the first guess of the tail, we use the computed solution of the forward problem (4.219) with interpolated function $c_{\text{glob}}(x)$. Let $\widetilde{w}(x, s)$ be the

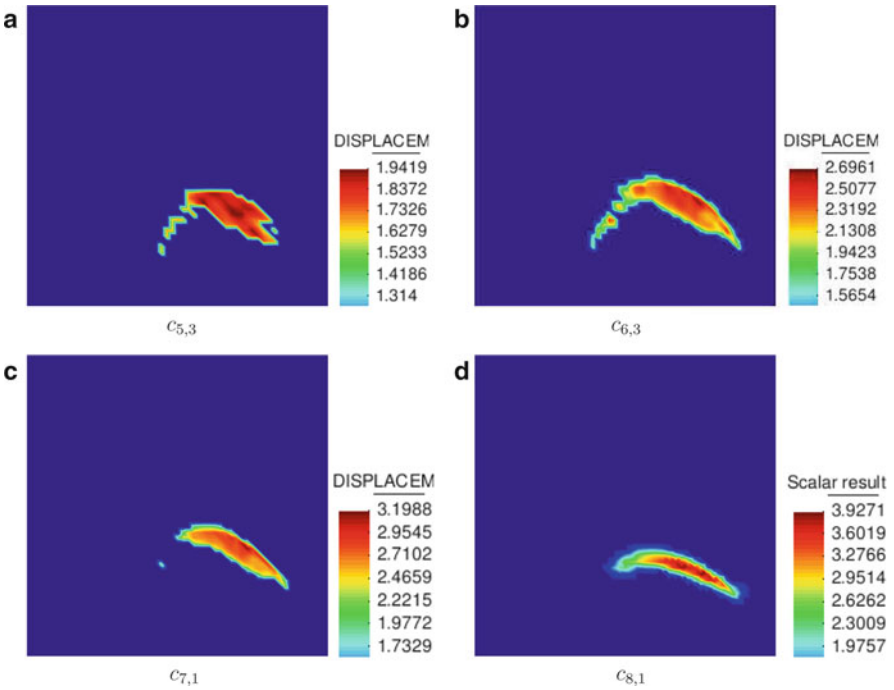

Fig. 4.25 Results of the performance of the globally convergent algorithm. Spatial distributions of some functions $c_{n,i}$. The function $c_{8,1}$ is taken as the final result. The maximal value of $c_{8,1}(x) = 3.8$ within maximal value of function (4.220). Also, $c_{8,1}(x) = 1$ outside of this maximal value. Hence, the $3.8 : 1$ inclusion/background contrast is imaged well (the correct maximal value of function (4.220) is $4 : 1$). However, the form of the imaged function is desirable to be improved. This is why we apply the adaptive globally convergent algorithm, which takes the function $c_{8,1}$ for refinement criterion (4.217). Source: M. Asadzadeh and L. Beilina, A posteriori error analysis in a globally convergent numerical method for a hyperbolic coefficient inverse problem, *Inverse Problems*, 26, 115007, doi:10.1088/0266-5611/26/11/115007, 2010. © IOP Publishing. Reprinted with permission

Laplace transform of the solution of the forward problem (4.219) obtained on a new refined mesh. Then the first guess for tails on the refined mesh is taken as

$$\widetilde{V}_{1,1}(x) = \frac{\ln \widetilde{w}(x, \overline{s})}{\overline{s}^2}.$$

This enables us to solve equations for functions $q^k_{n,1}, q_{n,i}$ on the new refined mesh. Let $c^j_{n,i}$ be the function $c_{n,i}$ computed on the j times refined mesh. In our case, the domain $\Omega = [-3, 3] \times [-3, 3]$ is the same as one in Sects. 3.1.3 and 4.15.1. Hence, to stop iterations with respect to the nonlinear term, i.e., to stop iterating with respect to k in $q^k_{n,1}$, we use the same criterion as the one in Sect. 4.15.2; see (4.206). Next, we

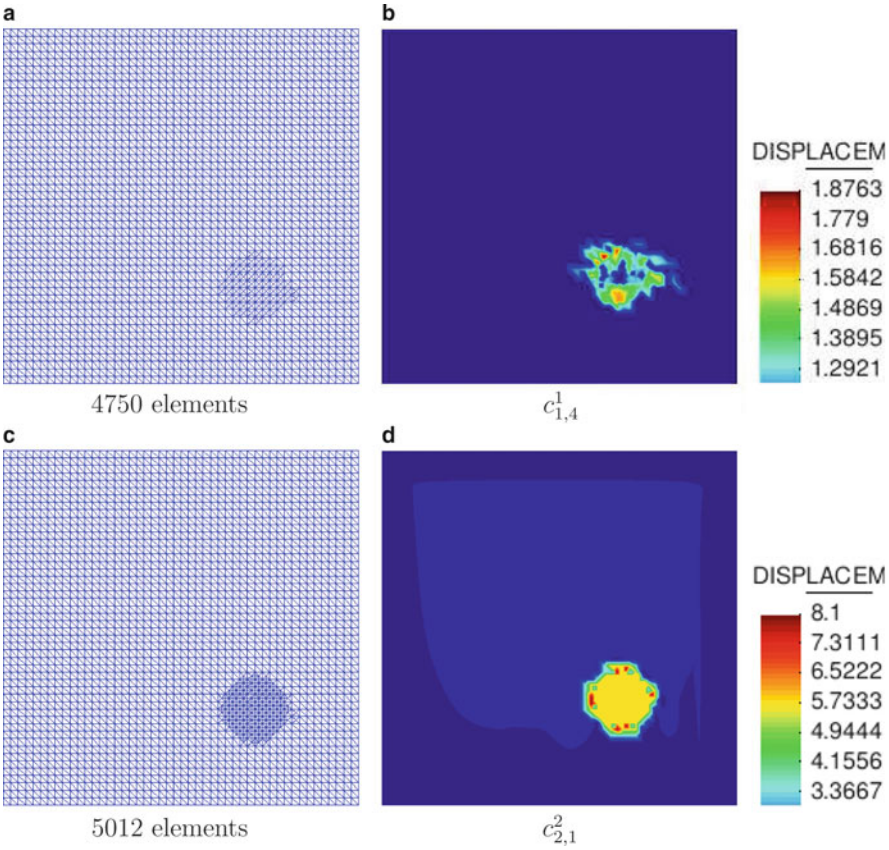

Fig. 4.26 Test 1: Adaptively refined meshes (**a**), (**c**) and corresponding images (**b**)–(**d**) using adaptive globally convergent algorithm. In this test we choose set of admissible parameters for coefficient $c \in P = \{c \in C(\overline{\Omega}) | 1 \leq c(x) \leq 8\}$. Locations of maximum value of the function (4.220) as well as shape and $4:1$ contrasts in them are imaged accurately. Source: M. Asadzadeh and L. Beilina, A posteriori error analysis in a globally convergent numerical method for a hyperbolic coefficient inverse problem, *Inverse Problems*, 26, 115007, doi:10.1088/0266-5611/26/11/115007, 2010. © IOP Publishing. Reprinted with permission

iterate with respect to the tails and use another stopping criterion for computations of functions $c^j_{n,i}$. For each pair (n,i), we stop computing functions $c^j_{n,i}$ when

$$\text{either } N_{n,i} \geq N_{n,i-1} \text{ or } |N_{n,i} - N_{n,i-1}| \leq \varepsilon = 0.001, \tag{4.216}$$

where

$$N_{n,i} = \frac{||c^j_{n,i} - c^j_{n,i-1}||_{L_2(\Omega)}}{||c^j_{n,i-1}||_{L_2(\Omega)}}. \tag{4.217}$$

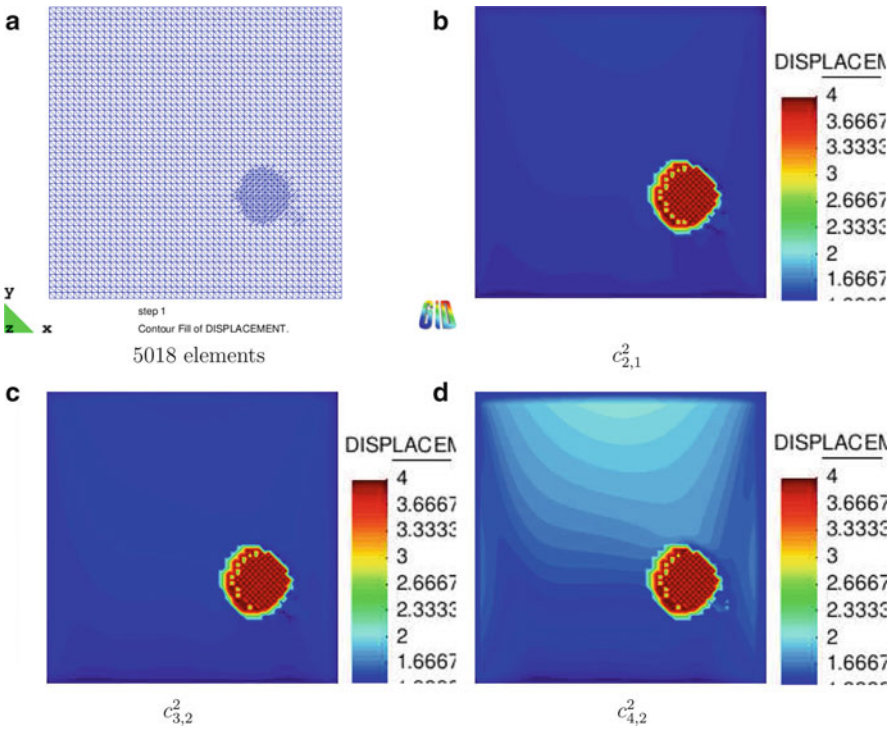

Fig. 4.27 Test 2. Adaptively refined mesh (**a**) and corresponding images (**b**)–(**d**), using adaptive globally convergent algorithm. In this test, we choose set of admissible parameters for coefficient $c \in P = \{c \in C(\overline{\Omega}) | 1 \leq c(x) \leq 5\}$. Locations of maximum value of the function (4.220) as well as shape and $4:1$ contrasts in them are imaged accurately. Source: M. Asadzadeh and L. Beilina, A posteriori error analysis in a globally convergent numerical method for a hyperbolic coefficient inverse problem, *Inverse Problems*, 26, 115007, doi:10.1088/0266-5611/26/11/115007, 2010. © IOP Publishing. Reprinted with permission

To simplify the presentation, we drop the mesh index "j" in notations for numbers $N_{n,i}$. We denote the number i_0 on which these iterations are stopped as $i_0 := m_n$. Also, for the analysis in computed examples, we use numbers N_n denoted as

$$N_n := N_{n,m_n}. \tag{4.218}$$

4.17.1 Computations of the Forward Problem

We work with the computationally simulated data generated by computing the forward problem with the given $c(x)$. To solve the forward problem, we use the hybrid FEM/FDM method mentioned above. The computational domain for the forward problem $G = [-4,4] \times [-5,5]$ here is the same as the one in Sect. 4.15.1. This domain is split into a finite element subdomain $G_{\text{FEM}} := \Omega = [-3,3] \times [-3,3]$

Table 4.8 $F_n^k, n = 1, ..., 10$. Computations was performed with the noise level $\sigma = 5\%$ and with the regularization parameter $\gamma = 0.01$

It.nr.	$i = 1$	$i = 2$	$i = 3$	$i = 4$	$i = 5$	$i = 6$
1	0.202592	0.202984				
2	0.208818	0.191831	0.19212			
3	0.187327	0.175833	0.176045			
4	0.152134	0.203397	0.204205			
5	0.17487	0.202605	0.202889	0.203076	0.203103	0.202986
6	0.206424	0.202276	0.202091	0.201566	0.201046	0.200468
7	0.203256	0.200669	0.198746	0.195911	0.195683	
8	0.191367	0.195898	0.194232			
9	0.188395	0.195584	0.194025			
10	0.187154	0.19684	0.197282			

Source: M. Asadzadeh and L. Beilina, A posteriori error analysis in a globally convergent numerical method for a hyperbolic coefficient inverse problem, *Inverse Problems*, 26, 115007, doi:10.1088/0266-5611/26/11/115007, 2010. © IOP Publishing. Reprinted with permission

Table 4.9 Computational results for the adaptive approximately globally convergent algorithm

Iter., n	c_{n,m_n}	N_n
1	1.26	0.0324175
2	1.33	0.033511
3	1.4	0.0360971
4	1.48	0.0509878
5	1.7	0.11818
6	1.9	0.179527
7	3.2	0.14
8	3.8	0.16
9	3.9	0.16

Source: M. Asadzadeh and L. Beilina, A posteriori error analysis in a globally convergent numerical method for a hyperbolic coefficient inverse problem, *Inverse Problems*, 26, 115007, doi:10.1088/0266-5611/26/11/115007, 2010. © IOP Publishing. Reprinted with permission

Table 4.10 The set of admissible parameters in different tests

Test 1	$c \in P = \{c \in C(\overline{\Omega}) \vert 1 \le c(x) \le 8\}$
Test 2	$c \in P = \{c \in C(\overline{\Omega}) \vert 1 \le c(x) \le 5\}$

and a surrounding region G_{FDM} with a structured mesh, $G = G_{\text{FEM}} \cup G_{\text{FDM}}$; see Fig. 4.21. The spatial mesh in Ω consists of triangles, and it consists of squares in G_{FDM}. In the overlapping regions, the mesh size is $\widetilde{h} = 0.125$. The boundary of the domain G is $\partial G = \partial G_1 \cup \partial G_2 \cup \partial G_3$. Here, ∂G_1 and ∂G_2 are respectively top and bottom sides of the largest domain in Fig. 4.21, and ∂G_3 is the union of left and right sides of this domain. At ∂G_2, we use the first-order absorbing boundary condition for $t \in (0, T)$, and we also use the same condition at ∂G_1 for $t \in [t_1, T)$, where

$t_1 \in (0,T)$ is a certain number. We use the zero Neumann boundary condition at ∂G_3, which models an infinite space in the horizontal direction.

The trace of the solution of the forward problem is recorded at the boundary $\partial\Omega$. Next, the coefficient $c(x)$ is "forgotten," and our goal is to reconstruct this coefficient for $x \in \Omega$ from the data $g(x,t)$; see (2.5). The forward problem here is almost the same as the one in Sect. 4.15.1, except that we now use the Dirichlet boundary condition at ∂G_1 for $t \in (0,t_1)$ instead of the Neumann condition in (4.203) in Sect. 4.15.1. Thus, the forward problem is

$$\begin{aligned} c(x)\,u_{tt} - \Delta u &= 0, \quad \text{in } G \times (0,T), \\ u(x,0) &= 0,\ u_t(x,0) = 0, \text{ in } G, \\ u\big|_{\partial G_1} &= f(t), \text{ on } \partial G_1 \times (0,t_1], \\ \partial_n u\big|_{\partial G_1} &= -\partial_t u, \text{ on } \partial G_1 \times (t_1,T), \\ \partial_n u\big|_{\partial G_2} &= -\partial_t u, \text{ on } \partial G_2 \times (0,T), \\ \partial_n u\big|_{\partial G_3} &= 0, \text{ on } \partial G_3 \times (0,T). \end{aligned} \tag{4.219}$$

Here, $f(t)$ is amplitude of the incident plane wave:

$$f(t) = \frac{(\sin(\bar{s}t - \pi/2) + 1)}{10}, \qquad 0 \le t \le t_1 := \frac{2\pi}{\bar{s}}, \qquad T = 17.8\,t_1.$$

Thus, the plane wave is initialized at the top boundary ∂G_1 and propagates into G for $t \in (0,t_1]$. Figures 4.22 shows how the plane wave propagates for the structure given on Fig. 4.24a.

To perform computations of the forward problem in an optimal way, we need to choose, *optimal*, computational parameters such as the mesh size h and the time step τ. Since we compute the forward problem (4.219) at every iteration in the approximately globally convergent algorithm to compute tails, we want to reduce the computational time of computing the solution of the problem (4.219) without losing an important information from this solution when solving the inverse problem. To do it, we use different meshes in order to select an optimal mesh size h in the computations. Let $\omega > 0$ be a number. We define the plane wave in (4.219) as

$$f(t) = \begin{cases} \sin(\omega t), & \text{if } t \in \left(0, \frac{2\pi}{\omega}\right), \\ 0, & \text{if } t > \frac{2\pi}{\omega}. \end{cases}$$

Consider the case $c \equiv 1$. Let $x := (x,y)$ and $a := 5$. Then the analytical solution of the problem (4.219) with the function $f(t)$ from (4.17.1) is given by the following formula [42]:

$$u(y,t) = \begin{cases} 0, & \text{if } t \in (0, a-y). \\ \sin\omega(t-a+y), & \text{if } t \in \left(a-y, a-y+\frac{2\pi}{\omega}\right). \\ 0, & \text{if } t > a-y+\frac{2\pi}{\omega}. \end{cases}$$

We have compared different computed solutions obtained via FEM, FDM, and hybrid methods with the exact solution (4.17.1). Figure 4.23 displays these comparisons at two different points of the computational domain G for different mesh sizes. We observe that major differences between exact and computed solutions occur at the bottom of the computational domain G. The computed solution on the mesh with the mesh size $h = 0.05$ approximates the exact solution more accurately than the one with $h = 0.1$. We have also tested the solution of our inverse problem on different meshes. It turns out that the mesh size $h = 0.05$ gives similar solution for the inverse problem as the ones on the meshes with mesh sizes $h = 0.1$ and $h = 0.125$. On the other hand, compared with the computations on the mesh with $h = 0.125$, computations on the mesh with the mesh size $h = 0.05$ are much more time-consuming. Therefore, in computations of the forward problem below, we use the mesh with $h = 0.125$.

4.17.2 Reconstruction by the Approximately Globally Convergent Algorithm

In numerical experiments of previous sections, we have simulated the data for the case of a homogeneous medium with sharp inclusions inside. When solving the inverse problem, we have not assumed any knowledge of the background inside the domain of interest. In this numerical experiment, we also do not rely on any knowledge of the background. However, unlike previous cases, we simulate the data for the case when a sharp inclusion (the third line in (4.220)) is embedded in a nonhomogeneous background. We are still interested in the reconstruction of this inclusion only rather than of the background.

Thus, we simulate the data for the case when the unknown function $c(x)$ is

$$c(x) = \begin{cases} 1 + 0.5\sin^2(\frac{\pi}{3}x)\cdot\sin^2(\frac{\pi}{3}y), & -3 \le x < 0, \text{ and } -3 \le y < 3, \\ 1 + 0.5\sin^2(\frac{\pi}{3}x)\cdot\sin^2(\frac{\pi}{3}y), & 0 \le x \le 3, \text{ and } 0 \le y \le 3, \\ 1 + 3\sin^2(\frac{\pi}{3}x)\cdot\sin^2(\frac{\pi}{3}y), & 0 \le x \le 3, \text{ and } -3 \le y \le 0, \end{cases} \tag{4.220}$$

see Fig. 4.24a. Our starting value for the tail function is the same as in (4.204); see Sect. 4.15.2.

Since our domains G, Ω are the same ones as in Sects. 3.1.3 and 4.15.2, the interval $[\underline{s}, \overline{s}] = [6.7, 7.45]$ is also the same as in those sections. We choose the step size with respect to the pseudo frequency $h = 0.05$. Hence, $N = 15$. The regularization parameter λ in the CWF is $\lambda := 20$ and $\varepsilon = 0$ for $n \in [1, N]$. Once the function $q_{n,i}$ is calculated, we update the function $c := c_{n,i}$ by backward calculations using the variational approach; see formulas (3.12), (3.13), (3.15), and (3.21) of Sect. 3.1.3. The resulting computed function is $c_{n,m_n} := c_{\overline{N}}(x)$. The choice of $\overline{N}$ is described below. In our tests, we have considered the noisy boundary data g_σ as in the formula (4.208) of Sect. 4.15.2. We have used the 5% noise level, which means that $\sigma = 0.05$ in (4.208).

Figure 4.25 displays results of the performance of the approximately globally convergent algorithm of Sect. 2.6.1. One can see that both the location of the maximal value of the function (4.220) are imaged very accurately. It follows from Fig. 4.25d that the imaged contrast in this function is $3.8 : 1 = \max c_{8,1} : 1$, $c_{8,1} := c_{\text{glob}}$. However, the values of the slowly changing background function

$$1 + 0.5 \sin^2\left(\frac{\pi}{3}x\right) \cdot \sin^2\left(\frac{\pi}{3}y\right)$$

in (4.220) are not reconstructed. Comparison with Fig. 4.24a reveals that it is desirable to improve the shape of the imaged function. This is done below via applying the adaptivity technique inside the approximately globally convergent algorithm.

Using Table 4.9, we analyze results of our reconstruction; see (4.216)–(4.218) for N_n. Observe that the numbers N_n increase until computing the function q_7. Next, they stabilize for $n = 8, 9$. For $n = 10, ..., 15$ the numbers grow steeply (not shown). Hence, using, just as above, the fourth Remark 2.9.4, we conclude that we should stop our iterations at $\overline{N} = 8$. Thus, we take the function $c_{8,1} := c_{\text{glob}}$ as our final reconstruction result on this stage.

4.17.3 The Adaptive Part

In this section, we apply the adaptivity inside the approximately globally convergent algorithm of Sect. 2.6.1. As it was pointed out in the beginning of Sect. 4.17, the tolerance $A \in (0, 1)$ in (4.215) should be chosen numerically. We take $A = 0.6$ for all meshes. On each new mesh refinement, we refine the mesh at the all points located in the circle with the centre at $\max_{\Omega} c^0_{n,m_n}$ and with the radius $r = A \max_{\Omega} c^0_{n,m_n}$.

In the adaptive algorithm, we use box constrains for the reconstructed coefficient. Since approximate global convergence Theorems 2.8.2 and 2.9.4 guarantee that the above function c_{glob} is a good approximation for the correct solution c^*, and since $c_{\text{glob}}(x) \in [1, 3.8]$, then we use two different upper limits for this function in our tests; see Table 4.10 for the other second set of admissible parameters.

We have carried out two tests described below. In both tests, we start with the function $c_{\text{glob}}(x)$ on the initial coarse mesh. This function is shown on Fig. 4.25d. Using the criterion (4.215), we refine the coarse mesh and interpolate the function $c_{\text{glob}}(x)$. On the refined mesh, the first guess for the tail is computed using the solution of the forward problem (4.219) with so interpolated function $c_{\text{glob}}(x)$. Let $\widetilde{w}(x, s)$ be the Laplace transform of this solution. Then, the first guess for tails on the refined mesh is taken as

$$\widetilde{V}_{1,1}(x) = \frac{\ln \widetilde{w}(x, \overline{s})}{\overline{s}^2}.$$

Table 4.11 Computational results for adaptive approximately globally convergent algorithm

Test 1			Test 2		
Iter., n	c^1_{n,m_n}	N_n	Iter., n	c^1_{n,m_n}	N_n
1	1.6	0.05	1	1.87	0.038
2	1.5	0.04	2	1.43	0.09
3	1.6	0.05	3	1.48	0.13
4	1.6	0.05	4	1.53	0.16
5	1.7	0.16	5	1.59	0.2
6	1.6	0.16			
Iter., n	c^2_{n,m_n}	N_n	Iter., n	c^2_{n,m_n}	N_n
1	1.9	0.08	1	2.45	0.04
2	3.99	0.342	4.0	0.25	
3	3.99	0.33	3	4.0	0.25
4	3.99	0.33	4	4.0	0.25
			Iter., n	c^3_{n,m_n}	N_n
			1	2.25	0.04
			2	3.8	0.16
			3	3.9	0.16
			4	4.0	0.16

Source: M. Asadzadeh and L. Beilina, A posteriori error analysis in a globally convergent numerical method for a hyperbolic coefficient inverse problem, *Inverse Problems*, 26, 115007, doi:10.1088/0266-5611/26/11/115007, 2010. © IOP Publishing. Reprinted with permission

Next, we perform all steps of the algorithm of Sect. 2.6.1 to obtain the function c^1_{n,m_n}. And continue mesh refinements similarly until stopped. We analyze the results of this reconstruction using Table 4.11.

Test 1. We observe in Table 4.11 that numbers N_n in (4.218) are stable first until computing c_4. Next, $N_5 = 3.2N_4$, which is a steep growth. Thus, we conclude, that we should stop the iterations when the stabilization occurs first, i.e., at $\overline{N} = 1$. So, we take the function $c^1_{1,4}$ as our final reconstruction result on the first iteration of adaptive refinement procedure. Comparison of Figs. 4.25d and 4.26b reveals that the image has worsened, since the maximal value of the reconstructed coefficient is $\max c^1_{1,4} = 2$. On the other hand, the correct maximum value is 4.

Next, we refine the mesh locally again using the criterion (4.215) and the same function $c_{\text{glob}}(x)$ of Fig. 4.25d, and perform the algorithm on the new mesh. Using the Table 4.11, we analyze again results of our reconstruction on this twice refined mesh. We observe that $N_2 = 4.25N_1$, which is a steep growth. Next, these numbers stabilize for $n = 2, 3, 4$. For $n = 5, ..., 7$, numbers N_n grow steeply (not shown). Hence, we again conclude, that one should stop iterations when the stabilization occurs first, i.e., at $\overline{N} = 2$. Thus, we take the function $c^2_{2,1}$ as our final reconstruction result on twice adaptively refined mesh.

One can see on Fig. 4.26d that we are able to accurately reconstruct both location and shape of the inclusion with the largest inclusion/background contrast of 4. As to the inclusion/background contrast, at the majority of points of the imaged inclusion $c^2_{2,1} = 4.5$, whereas the correct value is 4. The value of the coefficient $c(x) = 1$ outside of the imaged inclusion is imaged accurately, except of three other "bumps" of Fig. 4.24a.

Therefore, although our "allowable" upper bound 8 for the coefficient c is twice larger than the real maximal value of this coefficient, we still got a quite accurate image after the second mesh refinement.

Test 2. Since approximate global convergence Theorems 2.8.2 and 2.9.4 guarantee that the function c_{glob} is close to the exact solution, we take in Test 2 the maximal value in the set of admissible parameters for the coefficient to be $c = 5$; see Table 4.10, which is close to the maximal value of the function c_{glob}. We observe on Table 4.11 that after one mesh refinement of the mesh, the numbers N_n grow. Hence, we conclude that we should stop our iterations at $\overline{N} = 1$ and take the function $c^1_{1,1}$ as the final reconstruction result on the first adaptively refined mesh. This function is not shown, since the image is not improved compared with the image of c_{glob}.

Next, we refine the mesh locally again. Table 4.11 reveals that, similarly with the above, we should stop at $\overline{N} = 2$. Thus, we take $c^2_{2,1}$ as our final reconstruction result on the twice adaptively refined mesh. We observe on Fig. 4.27b that we are able to very accurately reconstruct location, shape, and the maximal value of 4 of the function (4.220). This result is similar to the results of Test 1, although the contrast here is much closer to the exact one. To demonstrate the stability of the process with respect to the third mesh refinement, we also display on Fig. 4.27 functions $c^2_{3,2}$ and $c^2_{4,2}$. Hence, the reconstruction is more accurate now than in Test 1.

4.18 Summary of Numerical Studies of Chapter 4

In numerical experiments of Sects. 4.15 and 4.16, the two-stage numerical procedure was considered. In this case, the approximately globally convergent numerical algorithm of Sect. 2.6.1 is applied on the first stage. On the second stage, the locally convergent adaptivity technique is applied, in which case the solution c_{glob} of the first stage is taken as the starting point of iterations. In Sect. 4.17, the adaptivity was applied inside the algorithm of Sect. 2.6.1 via refining the mesh in the area near the points where the maximal value of the function c_{glob} is achieved.

Recall that in Sects. 3.1 and 3.2, we have tested the case of either a single inclusion or two inclusions located on the same horizontal level with the incident plane wave propagating in the vertical direction. In this case, we were able to obtain accurate reconstructions using the algorithm of the first stage only. However, in Sects. 4.15 and 4.16, we have tested a more complicated scenario when two inclusions are located on different horizontal levels. It was shown that in this case location of the lower inclusion as well as the contrast in both can be accurately

reconstructed using the first stage only (at least in 2D). However, both imaged inclusions remained on the same horizontal level in the 2D case, and their locations were even less accurate in the 3D case. Next, the subsequent application of the adaptivity technique has led to the correct shift of locations. As a result, both locations and inclusions/background contrasts were accurately imaged. On the other hand, it was pointed out in Sect. 4.1 and confirmed in Test 5 of Sect. 3.1.3 that, as a locally convergent numerical method, the adaptivity is remains sensitive to the starting point of iterations. This is why the start from the solution obtained on the first stage leads to stable results.

Numerical testing of the first stage has consistently demonstrated that results are in a good agreement with approximate global convergence Theorems 2.8.2 and 2.9.4. In particular, because of the fourth Remark 2.9.4, we have chosen in most cases those iteration numbers for stopping criteria which correspond to the stabilization of certain residuals at the boundary. Also, it was demonstrated numerically in Test 3 of Sect. 4.16 that even if the adaptivity starts from the solution obtained on a lower iteration number, the final result is still accurate. This is in a good agreement with Theorems 2.8.2 and 2.9.4

We point out that relaxation Theorems 4.9.3 and 4.11.4 have always helped us to figure out the final mesh refinement number. Indeed, these theorems claim that if the regularized solution is not achieved yet on a certain mesh, then one can improve the accuracy of the reconstruction of this solution via a proper mesh refinement. Hence, as long as one is rather far from the regularized solution, residuals at the boundary are expected to decay with mesh refinements. Therefore, the growth of residuals indicates that one is likely close to the regularized solution, which means that one should stop mesh refinements.

In all tests with the adaptivity in Sects. 4.14–4.16, we have used only the first mesh refinement recommendation (4.189) of Sect. 4.13.2. Since the adaptivity has indeed improved the quality of images, then one can anticipate that the gradient (4.188) of the Tikhonov functional (4.172) (Sect. 4.11) is sensitive to the locations of inclusions. Figure 4.28 shows that this is true. This figure displays the absolute value of the gradient (4.188) of the Tikhonov functional (4.172) for the 2D case configuration considered on Fig. 4.9c of Sect. 4.15. Mesh refinements on Fig. 4.28 are obtained using both mesh refinement recommendations (4.189) and (4.190). Thus, Fig. 4.28 shows that the gradient (4.188) of the Tikhonov functional (4.172) for the CIP 2.1 "senses" locations of inclusions. Furthermore, the gradient becomes more sensitive to those locations when meshes are refined.

We now comment on results of Sect. 4.17, where the mesh was adaptively refined inside the approximately globally convergent algorithm. Comparison of Fig. 4.25d with Fig. 4.26d and Fig. 4.27b–d shows that this kind of mesh refinement can indeed significantly improve the image of the shape of the inclusion. In the case when the "allowable" upper limit for the unknown coefficient is twice larger than the real one (Test 1), one can still obtain quite accurate inclusion/background contrast. At the same time, Theorems 2.8.2 and 2.9.4 guarantee that the image obtained prior to these mesh refinements is accurate already (Fig. 4.25d). Hence, the assumption of

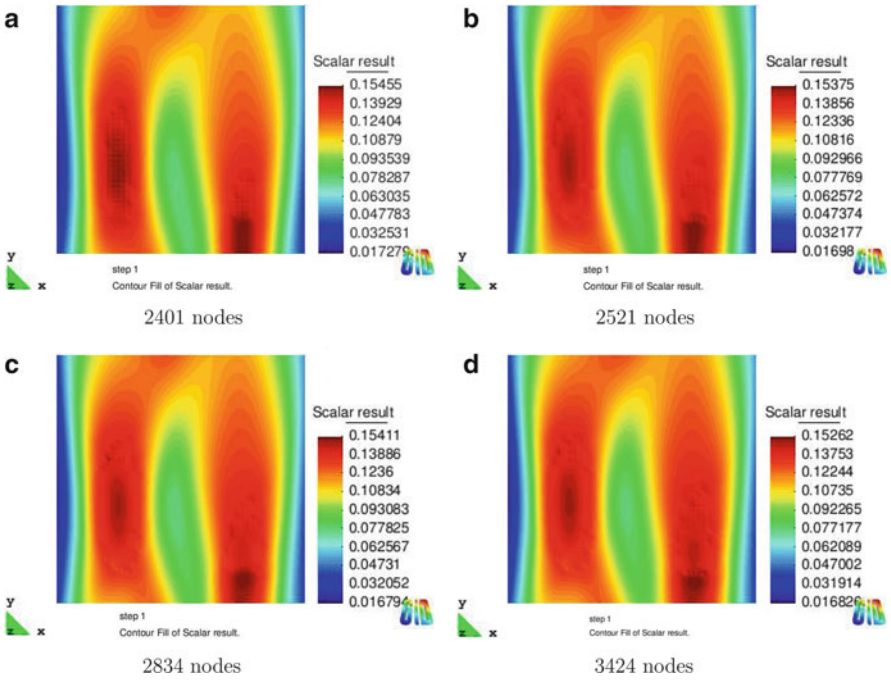

Fig. 4.28 Computed absolute values of the gradient (4.188) of the Tikhonov functional (4.172) for the 2D case configuration considered in Sect. 4.15. Mesh refinements here are obtained using both mesh refinement recommendations (4.189) and (4.190). Therefore, the absolute value of the gradient of the Tikhonov functional for our coefficient inverse problem 2.1 is sensitive to the locations of inclusions. We cannot guarantee, of course, that a similar sensitivity takes place for other CIPs

Test 2 of Sect. 4.17 that the "allowable" upper limit is rather close to the already calculated inclusion/background contrast is a more realistic one. As a result, Test 2 shows a very accurate image of all three components of the inclusion with the largest inclusion/background contrast: location, shape, and value of the unknown coefficient inside that inclusion. Still, we have observed that while the algorithm of Sect. 4.17 can image one inclusion well, it cannot image two shifted inclusions, for example, the case of Fig. 4.9 in Sect. 4.15.

Consider now numbers $d, \overline{d}$ characterizing upper limits of the unknown coefficient $c(x)$; see (2.208) in Sect. 2.9.1. Another point worthy to mention here is that we have used these numbers only in the convergence analysis in Theorem 2.9.4 of the algorithm of Sect. 2.6.1. However, we have not used neither of numbers $d, \overline{d}$ in the numerical implementation of this algorithm. Rather, we have relied only on the knowledge of the lower limit $c(x) \geq 1$. We have used the number d only in Tests 1 and 2 of Sect. 4.17.

Chapter 5
Blind Experimental Data

All tables and figures of this chapter were published in *Inverse Problems* either in [109] or in [28]. All of them are reprinted with permission. In particular, Tables 5.1–5.5 and 5.6 were published in [109]. Tables 5.6 and 5.7 were published in [28]. Figure 5.1 was published in both [109] and [28]. Figures 5.2a–d, 5.3a, b, 5.4a–d, 5.5a–h and 5.6a–f were published in [109]. Figures 5.7a–c, 5.8a–c, 5.9a–f, 5.10, 5.11, 5.12, 5.13, 5.14a–i and 5.15a, b were published in [28].

5.1 Introduction

In this chapter, we demonstrate the performance of the two-stage numerical procedure of Chaps. 2 and 4 for the case of experimental data. Specifically, we present results of publications [28, 109]. Experimental data were collected by Drs. Michael A. Fiddy and John Schenk in a laboratory of The University of North Carolina at Charlotte.

While numerical studies of Chaps. 3 and 4 have confirmed the property number 2 of the informal Definition 1.1.2.1 of the approximate global convergence, results of this chapter confirm the property number 3 of that definition. The first stage of our two-stage numerical procedure was originally applied to the most challenging case of **blind** experimental data [109]. In this chapter, the term "blind" means the following:

1. In each experiment, the coauthors of [109] knew the location of the dielectric inclusion. However, this information was not used in computations, since the approximately globally convergent algorithm of Sect. 2.6.1 does not use such an information.
2. Most importantly, the coauthors of [109], did not know refractive indices of dielectric inclusions. First, the computational results were obtained via the algorithm of Sect. 2.6.1. Next, those refractive indices were measured directly by two independent and well established in physics experimental methods.

L. Beilina and M.V. Klibanov, *Approximate Global Convergence and Adaptivity for Coefficient Inverse Problems*, DOI 10.1007/978-1-4419-7805-9_5,

3. Finally, numerical results were compared with results of those direct measurements.

The comparison of item 3 has revealed that the difference between computed and directly measured refractive indices was only a few percent in six out of six cases. Furthermore, in five out of six cases, this difference was even less than the measurement error of direct measurements; see Tables 5.5 and 5.6 below.

While results of [109] have demonstrated very accurate blind reconstructions results of both locations and refractive indices of dielectric inclusions, their shapes were not imaged well since the latter was outside of the scope of publication [109]. Therefore, the adaptive procedure of the second stage of our two-stage numerical procedure was not applied in [109]. Both stages were applied later to the same experimental data in [28]. The work on [28] was carried out later than one on [109]. Thus, the experimental data were blind only during the work on [109] and were not blind when we have worked on [28]. It was demonstrated in [28] that the two-stage numerical procedure very accurately reconstructs all three components of dielectric inclusions: locations, shapes, and refractive indices.

A simple visual comparison of Fig. 5.3a, b reveals a **huge misfit** between the experimental computationally simulated data. This misfit has caused the main difficulty of the work with experimental data. Indeed, it was unclear what kind of PDE, if any, can describe the highly oscillatory behavior of the measured signal even for the free space case. These oscillations took place regardless on the fact that only one period of the sinusoidal function was used as the shape of the input pulse. Hence, it became clear that standard denoising procedures, for example, Fourier transform, Hilbert transform, spline interpolation, etc., can provide only an insignificant help in our case. As a result, a **radically new** data pre-processing procedure was proposed in [109]. Later, this procedure was complemented by one more step in [28]. This step was necessary for the adaptive stage.

The goal of the data pre-processing is to transform experimental data in such a way which would lead to acceptable boundary conditions for both stages of the two-stage numerical procedure. The idea of data pre-processing is based on the intuition only, and it cannot be justified neither by mathematics nor by physics. The single justification of it is the accuracy of results of reconstructions.

The data processing has likely introduced a large modeling noise. This noise was on the top of the regular measurement noise as well as on the top of the huge misfit between the experimental data and our mathematical model. In addition, we have used only a single hyperbolic PDE (5.1) (the same as (2.1)) for our mathematical model. The Maxwell's system was not used since only a single component of the electric field was measured. Thus, the level of the resulting noise in the boundary data was likely very large and was. Furthermore, the noise level was unknown to the authors of [28, 109]. This is why a very good accuracy of results of [28, 109] is quite surprising. These results are presented in the current chapter.

We remind that our two-stage algorithm does not assume neither any knowledge of the background medium nor any knowledge of the presence/absence of small

"sharp" abnormalities of our interest in the medium. It uses only the knowledge of the target coefficient outside of the medium of interest.

We show in Sect. 5.8.4 that a modified gradient method being applied alone to these experimental data in the "pseudo frequency domain" leads to poor quality results. In other words, a locally convergent algorithm, if taken alone, does not work well for our experimental data. Therefore, the application of the approximately globally convergent method is *crucial* for these data.

5.2 The Mathematical Model

We model the process of electric wave field propagation via a single hyperbolic PDE, which is the same as our main PDE (2.1). We use this mathematical model only for our experimental data. Other kinds of experimental data might require different mathematical models. As the forward problem, we consider the following Cauchy problem:

$$\varepsilon_r(x)u_{tt} = \Delta u, \text{ in } \mathbb{R}^3 \times (0,\infty), \tag{5.1}$$

$$u(x,0) = 0,\ u_t(x,0) = \delta(x - x_0). \tag{5.2}$$

Here, $\varepsilon_r(x)$ is the spatially distributed dielectric constant (relative dielectric permittivity),

$$\varepsilon_r(x) = \frac{\varepsilon(x)}{\varepsilon_0},\ \sqrt{\varepsilon_r(x)} = n(x) = \frac{c_0}{c(x)} \geq 1, \tag{5.3}$$

where ε_0 is the dielectric permittivity of the vacuum (which we assume to be the same as the one in the air), $\varepsilon(x)$ is the dielectric permittivity of the medium of interest, $n(x)$ is the refractive index of the medium of interest, $c(x)$ is the speed of the propagation of the EM field in this medium, and c_0 is the speed of light in the vacuum, which we assume to be the same as one in the air. We point out that it is the refractive index, which is measured in physics. Dielectric constants are not measured. The assumption $n(x) \geq 1$ means that the speed of the EM field propagation in the medium is less or equal than the one in the air, which is reasonable.

Let $\Omega \subset \mathbb{R}^3$ be a convex bounded domain with the boundary $\partial\Omega \in C^3$. We assume that the coefficient $\varepsilon_r(x)$ of equation (5.1) satisfies the same conditions as ones in (2.3), (2.4):

$$\varepsilon_r(x) \in [1,d],\ \varepsilon_r(x) = 1 \text{ for } x \in \mathbb{R}^3 \setminus \Omega, \tag{5.4}$$

$$\varepsilon_r(x) \in C^3\left(\mathbb{R}^3\right). \tag{5.5}$$

The inequality $\varepsilon_r(x) \geq 1$ follows from (5.3). An upper estimate for the constant $d > 1$ is assumed to be known, although we do not assume that the number $d - 1$ is small. The assumption $\varepsilon_r(x) = 1$ for $x \in \mathbb{R}^3 \setminus \Omega$ means that one has air outside of the medium of interest Ω.

Coefficient Inverse Problem 5.2. Suppose that the coefficient $\varepsilon_r(x)$ satisfies (5.4) and (5.5). Assume that the function $\varepsilon_r(x)$is unknown in the domain Ω. Determine the function$\varepsilon_r(x)$ *for* $x \in \Omega$,assuming that the following function $g(x,t)$is known for a single source position $x_0 \notin \overline{\Omega}$:

$$u(x,t) = g(x,t), \forall (x,t) \in \partial\Omega \times (0,\infty). \tag{5.6}$$

The function $g(x,t)$ in (5.6) represents the data for this inverse problem. This function models the data resulting from experimental measurements. Here is a brief outline of the two-step procedure by which we have obtained the function $g(x,t)$:

Step 1. First, we have measured the time resolved signal, for a single source location, as it is schematically depicted on Fig. 5.1. The rectangular prism on this figure is a schematic representation of our domain Ω. We have measured this signal only on the lower side of Ω, i.e., on the transmitted side. Hence, we had a very narrow view angle in these measurements. Although it seem to follow from (5.6) that we should also measure the signal on other five sides of the prism Ω, our computational simulations have demonstrated that these sides are much less sensitive to the presence of dielectric abnormalities than the lower side of this prism. Hence, we have not conducted any measurements on those five sides. Instead, we have prescribed to them such boundary values of the function $u := g$ which were calculated via solving the initial boundary value problem (5.11) for $\varepsilon_r \equiv 1$.

Step 2. As to the lower side of the rectangular prism Ω, we have applied our data pre-processing procedure to the experimental data collected at this side. Thus, the function, which has resulted from this procedure, is our function $g(x,t)$ on the lower side of Ω.

5.3 The Experimental Setup

Below x denotes both a vector $x = (x,y,z) \in \mathbb{R}^3$ and the first component of this vector, where z is the vertical coordinate. It is always clear from the context what is what there. Our source/detectors configuration is schematically depicted on Fig. 5.1. The source has generated an EM wave. Only one component of the vector of the electric field was generated by our source. The same component was measured at the bottom side of the rectangular prism Ω depicted on Fig. 5.1. Actually, the voltage was measured.

The prism Ω was our computational domain. It was filled with Styrofoam. Styrofoam is a material, whose dielectric constant $\varepsilon_r \approx 1$, i.e., it is the same as in the air. The sizes of Ω were $240 \times 140 \times 240$ mm, where "mm" stands for "millimeter."

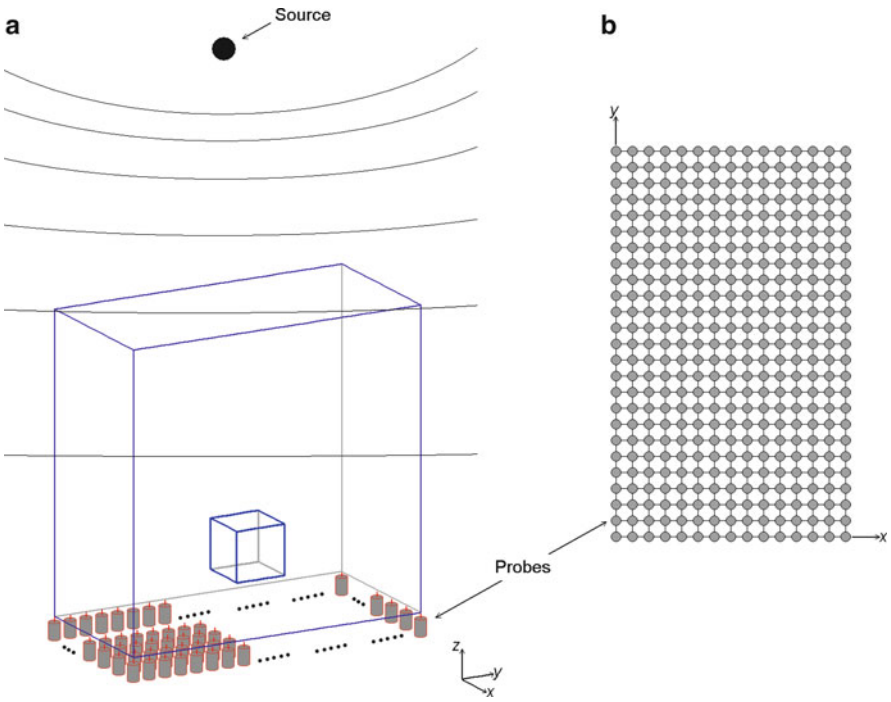

Fig. 5.1 Schematic diagram of the source/detectors configuration. (**a**) The rectangular prism depicts our computational domain Ω. Only a single-source location outside of this prism was used. Tomographic measurements of the scattered time resolved EM wave were conducted on the bottom side of this prism. (**b**) Schematic diagram of locations of detectors on the bottom side of the prism Ω. The distance between neighboring detectors was 10 mm. Source:M. V. Klibanov, M. A. Fiddy, L. Beilina, N. Pantong and J. Schenk, Picosecond scale experimental verification of a globally convergent numerical method for a coefficient inverse problem, *Inverse Problems*, 26, 045003, doi:10.1088/0266-5611/26/4/045003, 2010. © IOP Publishing. Reprinted with permission

Hence, sizes of front and back sides of the prism of Fig. 5.1 are 240×240 mm, and sizes of other four sides are 240×140 mm. The distance between the wave source and the top side of the domain Ω was 130 mm. The initializing pulse was 100 ps duration. Here, "ps" stands for "picosecond," 1 ps $= 10^{-12}$ s. Since the speed of the EM wave propagation in the air is 0.3 mm/ps, then it requires 433 ps $\approx$ 130/03 ps for this wave to travel from the source to the top boundary of Ω. Hence, it follows from (5.7) that the wave did not yet reach the domain Ω during the 100 ps duration of this pulse. The initializing pulse was

$$f(\tau) = \begin{cases} \approx A \sin\left(\frac{\pi}{50}\tau\right), \text{ for } \tau \in (0, 100) \text{ ps}, \\ 0, \text{ for } \tau > 100 \text{ ps}, \end{cases} \tag{5.7}$$

where $A > 0$ is the amplitude and τ is the time in picoseconds. Our data processing procedure does not rely on a knowledge of A.

The time resolved signal was measured on a grid on the bottom side of the prism Ω, as indicated on Fig. 5.1b. The grid step size was 10 mm. The detector was moved mechanically from one location to a neighboring one. For each location of the detector, the electric pulse was sent, and one time resolved component of the scattered electric field was measured for the total period of 12,300 ps $=$ 12.3 ns. Hence, it is reasonable to assume in the mathematical model that only one electric pulse was sent and that the wave field was measured simultaneously at all those detectors.

We had two measurements at each detector location. First, we have measured the reference signal when the dielectric inclusion was not present. Actually, this is the case of free space. Next, we have measured the signal when the inclusion was present. In principle, our technique allows the measurement of the reference signal only at a few locations outside of the medium of interest: for the calibration purposes. The only reason why we have measured the reference signal for each location of the detector was that our current numerical implementation works only with the case when the incident wave field is a plane wave. However, it was impossible to arrange a true plane wave in that experiment. In other words, we actually had a spherical wave. On the other hand, using measurements of the reference signal, our data pre-processing procedure has "transformed" this spherical wave into the plane wave.

Although real sizes of the domain Ω were given above, we have naturally worked with the dimensionless domain. Let x' be the vector of variables with dimensions in millimeters. Then our dimensionless vector was $x = x'/50$ mm. Since the distance between two neighboring detectors was 10 mm, then the dimensionless distance is $\tilde{h} = 10/50$ mm $= 0.2$. Thus, our dimensionless computational domain Ω and the dimensionless distance $\tilde{h}$ between two neighboring detectors were

$$\Omega = \{(x, y, z) \in [-2.4, 2.4] \times [-1.4, 1.4] \times [-2.4, 2.4]\}, \tilde{h} = 0.2, \ t \in (0, 12). \tag{5.8}$$

Let P be the bottom side of the domain Ω in (5.8):

$$P = \{(x, y, z) : (x, y) \in [-2.4, 2.4] \times [-1.4, 1.4], \ z = -2.4\}. \tag{5.9}$$

We now explain how we got the dimensionless time. First, about the zero time. We knew that the signal arrives at the detector approximately at 11,520 ps. Since the distance between the planar surface P in (5.9) and the source was 370 mm, the speed of light in the air is 0.3 mm/ps and (370 mm) / (0.3 mm/ps) $=$ 1,233 ps, then the zero time should be at $11,520\,\text{ps} - 1,233\,\text{ps} \approx 10,300\,\text{ps} := \tau_0$. Hence, we should work with a new time variable $\tau' = \tau - \tau_0$. The refractive index outside of the domain Ω is $n(x) = 1$. Hence, the EM wave should travel the dimensionless distance of $\tilde{h} = 0.2$ between two neighboring detectors in 0.2 dimensionless time units. On the other hand, 0.2 corresponds to the 10 mm distance between two neighboring detectors. Let t denotes the dimensionless time. Then we should choose such a multiplier $\gamma > 0$, which has dimension in picoseconds, that $\gamma t = \tau'$. Hence, we should have

$$0.2\gamma \text{ ps} = \frac{10\,\text{mm}}{0.3\,(\text{mm/ps})},$$

which implies that $\gamma = 166.67\,\text{ps}$. Thus, the dimensionless time t is

$$t = \frac{\tau'}{166.67}.$$

However, the above transformations to dimensionless variables did not affect our governing PDE (5.1) because of the data pre-processing procedure described below in this chapter.

5.4 Data Simulations

Since the computationally simulated data play an important role in our data pre-processing procedure, we outline here the solution of the forward problem for equation (5.1). Since it is practically impossible to solve the PDE (5.1) in the entire space $\mathbb{R}^3$, we have solved it in a larger rectangular prism:

$$G = \{(x, y, z) \in [-3, 3] \times [-2, 2] \times [-5, 5]\}.$$

By (5.8), $\Omega \subset G$. Our initializing plane wave in simulations was $v(t)$:

$$v(t) = \begin{cases} \sin(\omega t), \text{ for } t \in \left(0, \frac{2\pi}{\omega}\right), \\ 0, \text{ for } t > \frac{2\pi}{\omega}, \omega = 7. \end{cases} \tag{5.10}$$

Let ∂G_1 and ∂G_2 be respectively top and bottom sides of G and $\partial G_3 = \partial G \setminus (\partial G_1 \cup \partial G_2)$ be the rest of the boundary of G. We have numerically solved the following initial boundary value problem:

$$\begin{aligned} \varepsilon_r(x)\, u_{tt} &= \Delta u, \quad \text{in } G \times (0, T), T = 12, \\ u(x, 0) &= 0,\ u_t(x, 0) = 0, \text{ in } G, \\ \partial_n u\big|_{\partial G_1} &= v(t), \text{ on } \partial G_1 \times (0, 2\pi/\omega], \\ \partial_n u\big|_{\partial G_1} &= -\partial_t u, \text{ on } \partial G_1 \times (t_1, T), \\ \partial_n u\big|_{\partial G_2} &= -\partial_t u, \text{ on } \partial G_2 \times (0, T), \\ \partial_n u\big|_{\partial G_3} &= 0, \text{ on } \partial G_3 \times (0, T). \end{aligned} \tag{5.11}$$

In the case when the data are simulated for the reference medium, we have in (5.11) $\varepsilon_r(x) \equiv 1$. We denote this solution as $u_1(x, t)$. Thus, in (5.11), the plane wave is initialized at the top boundary ∂G_1 for times $t \in (0, 2\pi/\omega]$ and propagates

into G. First-order absorbing boundary conditions were used on the top boundary for $t \in (2\pi/\omega, T)$ as well as on the bottom boundary ∂G_2 for $t \in (0, T)$. The zero Neumann boundary condition was used on the rest of the boundary of the prism G. The latter boundary condition is used because the "pure" plane wave with $\varepsilon_r(x) \equiv 1$ satisfies this condition. The problem (5.11) was solved by the hybrid FEM/FDM method. In this method, FDM is used outside of the domain Ω, i.e., in $G \setminus \Omega$, and FEM is used inside Ω. The step size in the overlapping region was $\tilde{h} = 0.2$ which is the same as the distance between any two neighboring detectors.

5.5 State and Adjoint Problems for Experimental Data

First, we remind the Tikhonov functional (4.8) of Sect. 4.3. Let $\varepsilon_r^{\text{glob}}(x)$ be the coefficient $\varepsilon_r(x)$ which was reconstructed on the first stage of our two-stage numerical procedure, i.e. when applying the approximately globally convergent algorithm of Sect. 2.6.1. The Tikhonov regularization functional is

$$E_\alpha(\varepsilon_r) = \frac{1}{2}\int\limits_{S_T} (u\mid_{S_T} - g(x,t))^2 z_\xi(t)\,\mathrm{d}S_x\mathrm{d}t + \frac{1}{2}\alpha\int\limits_{\Omega} (\varepsilon_r - \varepsilon_r^{\text{glob}})^2\mathrm{d}x. \tag{5.12}$$

Our goal now is to find a minimizer $\varepsilon_{r,\alpha}$ of this functional, i.e., to find the *regularized solution*. Let Y be the set of functions defined in (4.7) (Sect. 4.3) and H_1 be the finite dimensional space of finite elements constructed in Sect. 4.9.1. We remind that the set Y_1 is defined as $Y_1 := Y \cap H_1$. We assume that $\varepsilon_r^{\text{glob}} \in Y_1$ and assume that conditions of Theorems 4.11.1–4.11.4 hold. In particular, these theorems imply existence and uniqueness of the minimizer $\varepsilon_{r,\alpha} \in Y_1$ in a small neighborhood of the exact solution ε_r^*. Thus, below in this section, we work only in that small neighborhood of ε_r^*.

As to state and adjoint problems, although the theory of Chap. 4 works with solutions of those problems only in the domain $Q_T = \Omega \times (0,T)$, we consider in the current chapter different domains for these problems. Still, we believe that the theory of the adaptivity of Chap. 4 can be extended to this case, although we have not yet done this. At this time, however, this difference of domains represents one of discrepancies between the above theory and its numerical implementation. Indeed, if defining solutions of state and adjoint problems like in (4.9) and (4.10) (Sect. 4.3), then, in the case of our experimental data, it is unclear how to figure out the normal derivative $p(x,t) = \partial_n u\mid_{S_T}$ at the lateral boundary $S_T = \partial\Omega \times (0,T)$ of the time cylinder Q_T.

Hence, consider the rectangular prism $G' = G \cap \{z > -2.4\}$. Let the rectangle $P_{\text{obs}} = \{z = -2.4\} \cap G$ be the bottom side of G'. By (5.9), the rectangle $P \subset P_{\text{obs}}$. Let

$$G_T' = G' \times (0,T),\ S_T' = P_{\text{obs}} \times (0,T),\ S_T'' = \left(\partial G' \setminus P_{\text{obs}}\right) \times (0,T). \tag{5.13}$$

Recall that the lower side P of the rectangular prism Ω is much more sensitive to experimental data than other five sides of this prism (Sect. 5.2). For this reason, we have prescribed the same data to those five sides as the ones for the case of the free space. Hence, let $u(x,t,\varepsilon_r)$ be the solution of the initial boundary value problem (5.11). Also, let $u_1(x,t)$ be the solution of this problem for $\varepsilon_r(x) \equiv 1$. For the same reason as above, we *approximately* assume that

$$u(x,t,\varepsilon_r) = u_1(x,t) \text{ for } (x,t) \in S''_T. \tag{5.14}$$

Thus, we define state and adjoint problems for our case as:

1. The state problem is the initial boundary value problem (5.11).
2. The adjoint problem is

$$\begin{aligned} \varepsilon_r(x)\lambda_{tt} - \Delta\lambda = 0, \quad (x,t) \in G'_T, \\ \lambda(x,T) = \lambda_t(x,T) = 0, \\ \partial_n\lambda\,|_{S'_T} = (g-u)(x,t), \\ \partial_n\lambda\,|_{S''_T} = 0. \end{aligned} \tag{5.15}$$

The last line of (5.15) follows from (5.14). Similarly with Sects. 4.15.3 and 4.16.2, we have dropped the function $z_\zeta(t)$ in the third line of (5.15), since this function is used only for the compatibility conditions at $t = T$, and we have observed that $u(x,T) \approx g(x,T) \approx 0$ for $x \in \partial G'$. Thus, we have not used the function $z_\zeta(t)$ in (5.12) in our computations of this chapter.

However, since measurements give us (after pre-processing) the function $g(x,t)$ only for $x \in P$, it follows from (5.13) and (5.14) that we should somehow extend this function on the set $P_{\text{obs}} \setminus P$. Hence, we actually need to know the function $g(x,t)$ not only for $x \in P$ but also for x belonging to a wider rectangle $P_{\text{obs}}, x \in P_{\text{obs}}$. In general, this extension problem is very similar with the problem of analytic continuation. And the latter problem is very unstable. However, using some features of our specific arrangement, we have found a different way of this extension via the so-called *third stage* of our data immersing procedure, which is described in Sect. 5.6.

Assuming that the function $g(x,t)$ is properly extended from P into a larger rectangle P_{obs}, the Tikhonov functional (5.12) becomes

$$E_\alpha(\varepsilon_r) = \frac{1}{2}\int\limits_{S'_T} (u\,|_{S'_T} - g(x,t))^2 \mathrm{d}S_x \mathrm{d}t + \frac{1}{2}\alpha \int\limits_{\Omega} (\varepsilon_r - \varepsilon_r^{\text{glob}})^2 \mathrm{d}x. \tag{5.16}$$

Now, we reformulate two mesh refinement recommendations (4.189) and (4.190) of Sect. 4.13.2 for our particular case. Let $\varepsilon_{r,h}(x)$ be the minimizer of the Tikhonov functional (5.12) on the current mesh.

First Mesh Refinement Recommendation. *Refine the mesh in such a subdomain of the domain Ω where*

$$\left|E'_\alpha\left(\varepsilon_{r,h}\right)(x)\right| \geq \beta_1 \max_{\overline{\Omega}} \left|E'_\alpha\left(\varepsilon_{r,h}\right)(x)\right|, \tag{5.17}$$

where $\beta_1 \in (0,1)$ is the tolerance number and

$$\left|E'_\alpha\left(\varepsilon_{r,h}\right)(x)\right| = \left|\alpha(\varepsilon_{r,h} - \varepsilon_r^{\text{glob}})(x) - \int_0^T \left(u_{ht}\lambda_{ht}\right)(x,t,\varepsilon_{r,h})\,\mathrm{d}t\right|.$$

Here, functions $u_{ht}(x,t,\varepsilon_{r,h})$ and $\lambda_{ht}(x,t,\varepsilon_{r,h})$ are solutions of state and adjoint problems, respectively, on the current mesh.

The Second Mesh Refinement Recommendation. *Refine the mesh in such a subdomain of the domain Ω where*

$$\varepsilon_{r,h}(x) \geq \beta_2 \max_{\overline{\Omega}} \varepsilon_{r,h}(x), \tag{5.18}$$

where $\beta_2 \in (0,1)$ is the tolerance number.

Recall that tolerance numbers β_1, β_2 are chosen numerically. In our tests below, we use

$$\beta_1 = 0.8, \beta_2 = 0.2, \alpha = 0.001. \tag{5.19}$$

5.6 Data Pre-Processing

The main idea of the data pre-processing procedure is to *immerse* the experimental data in the computationally simulated ones. The data pre-processing procedure provides us with the boundary data at $\partial\Omega$, which we use in our computations. Recall that measurements were not carried out at $\partial\Omega \setminus P$. We have prescribed

$$u(x,t)\mid_{\partial\Omega\setminus P} := u_1(x,t)\mid_{\partial\Omega\setminus P},$$

where $u_1(x,t)$ is the solution of the problem (5.11) with $\varepsilon_r(x) \equiv 1$. So, in this section we describe how we pre-process the data only on the bottom side P of the rectangular prism Ω.

5.6.1 The First Stage of Data Immersing

Samples of unprocessed time resolved experimental data are depicted on Fig. 5.2. We work only with the first burst. Figure 5.2c, d display the curves which are

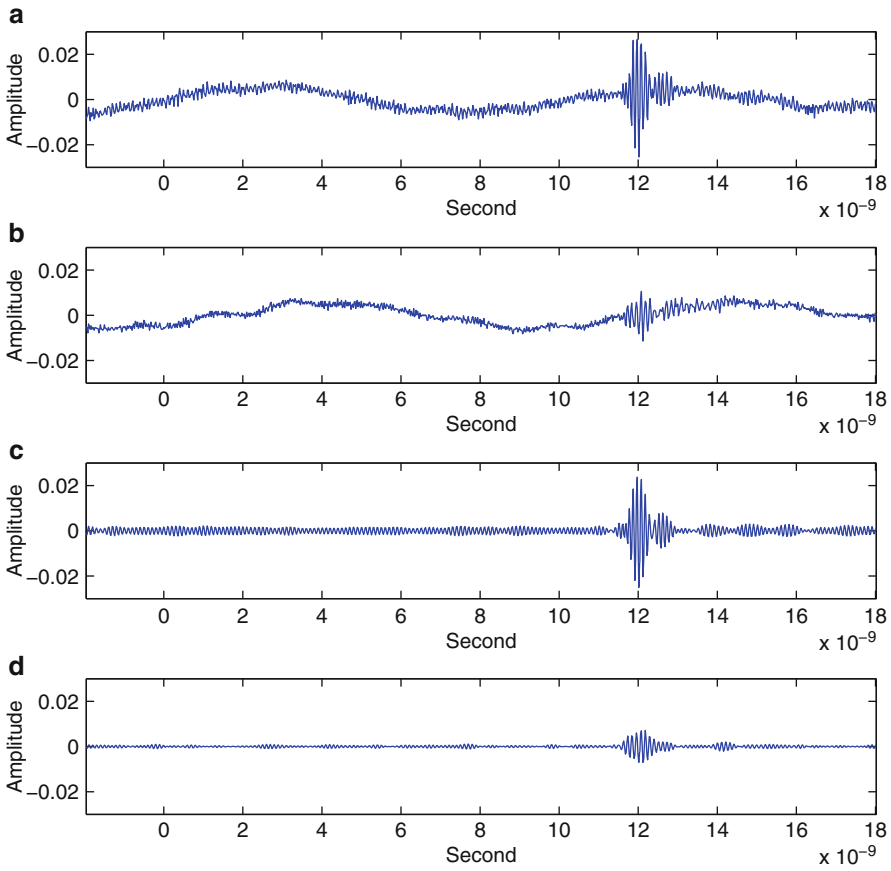

Fig. 5.2 (**a**) A sample of the measured reference time resolved signal (i.e., no inclusion present) at the location $x_m \in P$ of the probe number m. (**b**) The measured signal with inclusion present at the same probe location. The first burst starts when the EM wave arrives at the probe. The signal before this burst reflects a process within the probe itself. (**c**) And (**d**) represent signals (**a**) and (**b**), respectively, after cleaning some noise via applying the fast Fourier transform procedure of MATLAB and truncating too low and too high frequencies. We are interested in the area of the first burst only. One can observe that the amplitude of the signal with the dielectric inclusion present (**d**) is generally less than one of the reference signal. Source: M. V. Klibanov, M. A. Fiddy, L. Beilina, N. Pantong and J. Schenk, Picosecond scale experimental verification of a globally convergent numerical method for a coefficient inverse problem, *Inverse Problems*, 26, 045003, doi:10.1088/0266-5611/26/4/045003, 2010. © IOP Publishing. Reprinted with permission

obtained from curves Fig. 5.2a, b, respectively, after a partial denoising via the Fourier transform. Both Fig. 5.2c, d are for the same detector. Fig. 5.2c is for the case of free space and Fig. 5.2d is for the case when a dielectric inclusion is present. The most troubling feature of Fig. 5.2 is the highly oscillatory behavior of the first burst. Indeed, given that the input data was the sinusoidal function $f(t)$ in (5.7) with

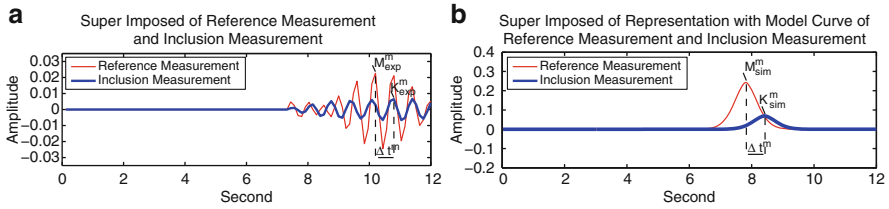

Fig. 5.3 This figure explains the idea of the first stage of data immersing in the time domain. We have intentionally set to zero the small amplitude fluctuations before that first burst. (**a**) Resulting superimposed experimental curves. The *red curve* (*thin*) is for the reference signal and the *blue curve* (*thick*) is for the signal with a dielectric inclusion present, both at the same location $x_m \in P$ of the detector number m. (**b**) The *red curve* (*thin*) displays computationally simulated data $u_1(x_m, t)$. The *blue curve* (*thick*) $u_{\text{incl}}(x_m, t) = u_1(x_m, t - \Delta t^m) K^m_{\text{exp}} / M^m_{\text{exp}}$ represents a sample of the immersed experimental data in the time domain at the same detector location $x_m \in P$. It is only the *blue curve* (*thick*) with which we work further. The *red curve* (*thin*) is displayed for the illustration purpose only. Source: M. V. Klibanov, M. A. Fiddy, L. Beilina, N. Pantong and J. Schenk, Picosecond scale experimental verification of a globally convergent numerical method for a coefficient inverse problem, *Inverse Problems*, 26, 045003, doi:10.1088/0266-5611/26/4/045003, 2010. © IOP Publishing. Reprinted with permission

only one period of the sinusoid, one cannot expect high oscillations of the output signal for, for example, the case of the free space. These oscillations represent the abovementioned huge misfit between experimentally measured and simulated data.

Figure 5.3a displays superimposed Fig. 5.2c, d after their parts prior the first burst was made zero. The thin curve on Fig. 5.3a corresponds to the free space and the thick curve corresponds to the case when the inclusion is present. Let $x_m \in P$ be the detector number m at the bottom side P of the prism Ω; see (5.9) for P. We have decided to "immerse" our experimental data in the computationally simulated data using the following two peaks for each detector x_m:

1. The largest peak in the thin curve with the peak value of $M^m_{\text{exp}} > 0$.
2. The next peak after it on the thick curve with the peak value of $K^m_{\text{exp}} > 0$. This next peak was chosen because the presence of a dielectric inclusion results in a time delay of the EM wave; see (5.3).

Recall that the function $u_1(x, t)$ is the solution of the problem (5.11) with computationally simulated data for $\varepsilon_r \equiv 1$. Obviously,

$$u_1\left(x^{(1)}, t\right) = u_1\left(x^{(2)}, t\right), \ \forall x^{(1)}, x^{(2)} \in P, \ \forall t \in (0, T).$$

The first peak of the function $u_1(x, t), x \in P$ is the largest peak of Fig. 5.3b. Below t is the *dimensionless* time. Let $t := t^{\text{sim}}_{\text{ref}}$ be the time of the first arrival of the computationally simulated plane wave $u_1(x, t)$ at the plane P. In other words, for all $x \in P$, we have $u_1(x, t) = 0$ for $t < t^{\text{sim}}_{\text{ref}}$ and $u_1(x, t) > 0$ for time values $t > t^{\text{sim}}_{\text{ref}}$ that are rather close to $t^{\text{sim}}_{\text{ref}}$; see the reference curve on Fig. 5.3b.

We point out that amplitudes of largest peaks of experimental curves for the reference medium were different for different detectors. This is because we had

in the experiment a spherical incident wave instead of the desired plane wave. Nevertheless, we have "forced" the spherical wave to be a plane wave via applying the first stage of our data immersing procedure.

Let $y = y_m^{\text{ref}}(t)$ be the experimentally measured curve at the detector $\{x_m\}$ for the free space, i.e., this is the thin curve of Fig. 5.3a. Let the above chosen largest peak of this curve is achieved at $\left\{t = t_m^{\text{ref}}\right\}$ and $y_m^{\text{ref}}\left(t_m^{\text{ref}}\right) = M_{\text{exp}}^m > 0$. Let $y = y_m^{\text{incl}}(t)$ be the experimentally measured curve at the detector $\{x_m\}$ for the case when the inclusion is present. We choose such a local maximum of the function $y = y_m^{\text{incl}}(t)$ which is achieved at the first point $\left\{t = t_m^{\text{incl}}\right\}$ which follows after the point $\left\{t = t_m^{\text{ref}}\right\}$; see Fig. 5.3a. Let $y_m^{\text{incl}}\left(t_m^{\text{incl}}\right) = K_{\text{exp}}^m$. Hence, K_{exp}^m is the value of the latter peak; see Fig. 5.3a. We have observed that $K_{\text{exp}}^m \leq M_{\text{exp}}^m$ on all detectors. This is because the presence of dielectrics decreases the amplitude of the EM wave.

Now, we are ready to immerse our experimental data in the computationally simulated data. Let $\Delta t_m = t_m^{\text{incl}} - t_m^{\text{ref}}$ be the time delay between two above chosen peaks; see Fig. 5.3a. We set

$$u_{\text{incl}}(x_m, t) := \begin{cases} \frac{K_{\text{exp}}^m}{M_{\text{exp}}^m} u_1(x_m, t - \Delta t_m), & \text{if } \frac{K_{\text{exp}}^m}{M_{\text{exp}}^m} < \frac{2}{3}, \\ u_1(x_m, t) \text{ and } \Delta t_m := 0, & \text{if } \frac{K_{\text{exp}}^m}{M_{\text{exp}}^m} \geq \frac{2}{3}. \end{cases} \tag{5.20}$$

Thus, (5.20) is our *first immersed data in the time domain* for the detector number m. Figure 5.3b illustrates (5.20). After this data immersing, we use only the curve $u_{\text{incl}}(x_m, t)$ and do not use anymore the curve which corresponds to the reference medium. In other words, on each detector, we use only such curve which corresponds to the thick curve on Fig. 5.3b. We cannot rigorously justify our above decision to work with those peaks only. However, since our results of blind imaging in [109] were very accurate ones, then this justifies our purely intuitive choice.

5.6.2 The Second Stage of Data Immersing

Although the thick curve on Fig. 5.3b is smooth, in fact the noise went into the noise with respect to spatial variables on the rectangle P, and this will be seen in the current section. We have found that the following frequency interval was the optimal one for our computations:

$$s \in [3.5, 7.5]. \tag{5.21}$$

We apply the Laplace transform (2.10) to each function $u_{\text{incl}}(x_m, t)$ for nine values of $s = 3.5, 4, \ldots, 7.5$ from the interval (5.21). Denote $w_{\text{incl}}(x_m, s)$ the Laplace transform of the function $u_{\text{incl}}(x_m, t)$. Let

$$\tilde{w}_{\text{incl}}(x_m, s) = -\frac{\ln w_{\text{incl}}(x_m, s)}{s^2}.$$

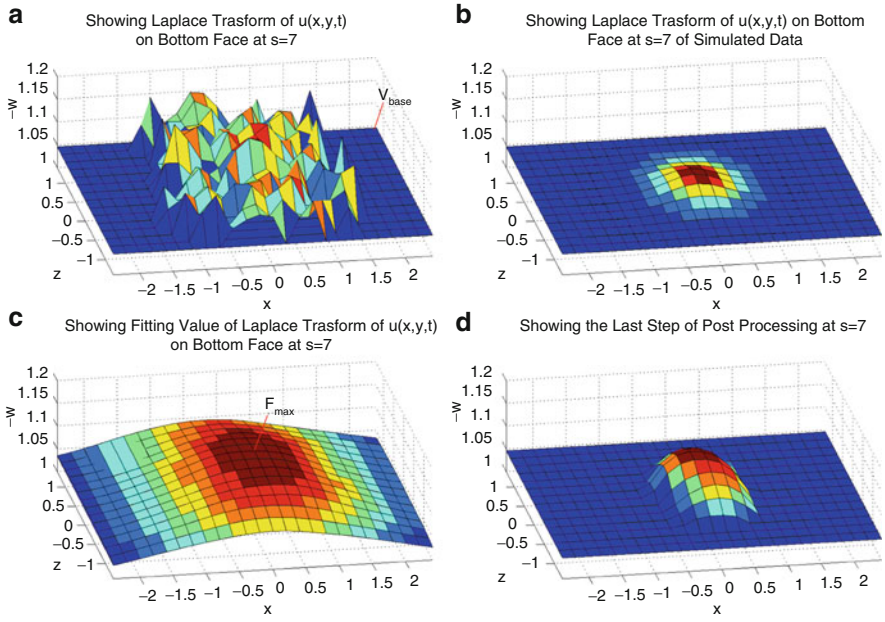

Fig. 5.4 (**a**) The function $\tilde{w}_{\text{incl}}(x,\overline{s})$, $\overline{s}=7.5$. (**b**) The function $-(\ln w_{\text{sim}}(x,\overline{s}))/\overline{s}^2$is depicted, where $w_{\text{sim}}(x,\overline{s})$is the Laplace transform of the function $u_{\text{sim}}(x,t)$for a computationally simulated data. Figure (**b**) is given only for the sake of comparison with Figure (**a**). (**c**) The function $\tilde{w}_{\text{smooth}}(x,\overline{s})$ resulting from fitting of (**a**) by the lowess fitting procedure in the 2D case; see MATLABR 2009a. (**d**) The final function $\tilde{w}_{\text{immers}}(x,\overline{s})$. Values of $\tilde{w}_{\text{immers}}(x,s)$are used to produce the Dirichlet boundary conditions $\tilde{\psi}_n(x)$for PDEs (2.36) of the globally convergent algorithm. Source: M. V. Klibanov, M. A. Fiddy, L. Beilina, N. Pantong and J. Schenk, Picosecond scale experimental verification of a globally convergent numerical method for a coefficient inverse problem, *Inverse Problems*, 26, 045003, doi:10.1088/0266-5611/26/4/045003, 2010. © IOP Publishing. Reprinted with permission

Let $\overline{w}_{\text{incl}}(x,s)$ be the standard linear interpolation of the values $\{\tilde{w}_{\text{incl}}(x_m,s)\}$ over the plane P. We have observed that the function $\overline{w}_{\text{incl}}(x,s)$ is very noisy with respect to $x\in P$. Figure 5.4a displays a sample of the function $\overline{w}_{\text{incl}}(x,\overline{s})$. Hence, the noise went from the time dependence into the spatial dependence.

On the other hand, we have computationally simulated the data with a single inclusion and have obtained the function $w_{\text{sim}}(x,\overline{s})$; see Fig. 5.4b for the function

$$-\frac{\ln w_{\text{sim}}(x,\overline{s})}{s^2}.$$

One can observe that, unlike Fig. 5.4a, b is smooth and has only a single bump. Comparison of Fig. 5.4a, b has motivated us to perform additional procedures with the function $\overline{w}_{\text{incl}}(x,s)$.

Thus, we have applied a smoothing procedure with respect to $(x, y) \in P$ to the function $\overline{w}_{\text{incl}}(x_m, s)$ for each of above nine values of s. Specifically, we have used the *Lowess fitting procedure* in the 2D case, which we took from MATLABR 2009. As a result, we have obtained the function $\overline{w}_{\text{smooth}}(x, s)$. The function $\overline{w}_{\text{smooth}}(x, \overline{s})$ is displayed on Fig. 5.4c. Still, comparison of Fig. 5.4b, c tells one that we should transform Fig. 5.4c in such a way which would end up with a single bump. Let $w_1(x, s)$, $x \in P$ be the Laplace transform of the function $u_1(x, t)$, i.e., for the case of the plane wave propagating in the air. Then we finally set for each of those nine values of s:

$$\overline{w}_{\text{immers}}(x, s) = \begin{cases} \overline{w}_{\text{smooth}}(x, s), & \text{if } \overline{w}_{\text{smooth}}(x, s) \geq 0.985 \max_{\overline{P}} \overline{w}_{\text{smooth}}(x, s), \\ -s^{-2} \ln w_1(x, s), & \text{otherwise.} \end{cases}$$

Figure 5.4d the function $\overline{w}_{\text{immers}}(x, \overline{s})$, which is obtained from the function $\overline{w}_{\text{incl}}(x, s)$ of Fig. 5.4a.

We use the function $\overline{w}_{\text{immers}}(x, s)$ to obtain Dirichlet boundary conditions for elliptic equations for functions q_n of Sect. 2.6.1. Namely, we use finite differences to approximately compute the s-derivative by

$$\psi_n(x) = \frac{\overline{w}_{\text{immers}}(x, s_n - 0.5) - \overline{w}_{\text{immers}}(x, s_n)}{0.5}, \quad x \in P. \tag{5.22}$$

As to the values of the function $\psi_n(x)$ on other five sides of the prism Ω, they were computed by the same finite difference formula using the function resulting from the Laplace transform of the function $u_1(x, t)$.

5.7 Some Details of the Numerical Implementation of the Approximately Globally Convergent Algorithm

We point out that all details of the numerical implementation of the approximately globally convergent algorithm, which are described in this section, were implemented a few months before the experimental data were collected. When working with the experimental data, we have not changed neither our original numerical code for the algorithm of Sect. 2.6.1 nor our parameters listed in this section. In other words, our computations of images from experimental data were **unbiased.**

When solving equations (2.49) for functions $q_{n,i}$ (Sect. 2.6.1) in our computations, we have used in (2.49) $\overline{s}$-derivatives of tails $\partial_{\overline{s}} V_{n,i}(x, \overline{s})$ instead of tails $V_{n,i}(x, \overline{s})$ themselves. These derivatives were calculated via finite differences, similarly with (5.22). We remind that by (2.19) (Sect. 2.3) one should expect that

$$|\partial_{\overline{s}} V_{n,i}(x, \overline{s})|_{2+\alpha} << |V_{n,i}(x, \overline{s})|_{2+\alpha}. \tag{5.23}$$

Hence, the replacement of $V_{n,i}(x,\overline{s})$ with $\partial_{\overline{s}}V_{n,i}(x,\overline{s})$ goes along well with the first approximate mathematical model; see Sect. 2.8.4 for some details. At the same time, when computing functions $\varepsilon_r^{(n,i)}(x)$ via (5.24), we have used the function $V_{n,i}(x,\overline{s})$ itself rather than its derivative $\partial_{\overline{s}}V_{n,i}(x,\overline{s})$.

Suppose that we have computed the function $q_{n,i}(x)$. Then, we find the approximation $\varepsilon_r^n(x)$ for the function $\varepsilon_r(x)$ via backward calculation using (3.4) as

$$\varepsilon_r^{(n,i)}(x) = \begin{cases} f_{n,i}(x) := \Delta v_{n,i} + s_n^2 (\nabla v_{n,i})^2, x \in \Omega, \text{ if } f_{n,i}(x) \geq 1, \\ 1, \text{ if } f_{n,i}(x) < 1, \end{cases} \tag{5.24}$$

$$v_{n,i}(x) = -hq_{n,i}(x) - h\sum_{j=0}^{n-1} q_j(x) + V_{n,i}(x),$$

where $q_0 \equiv 0$ and $V_{n,i}(x)$ is the corresponding approximation for the tail function. We make the cut-off to unity in (5.24) because of (5.4).

The parameter of the CWF was $\lambda = 50$. Likewise, as it is quite often the case in imaging, we have made truncations to unity of those computed functions $\varepsilon_r^{(n,i)}(x)$ which were below a certain threshold. More precisely, for each n, we have chosen a cut-off value $C_{\text{cut}}(n) > 0$ and have assigned a new value $\tilde{\varepsilon}_r^{(n,i)}(x)$ for the function $\varepsilon_r^{(n,i)}(x)$ as

$$\tilde{\varepsilon}_r^{(n,i)}(x) = \begin{cases} \varepsilon_r^{(n,i)}(x), \text{ if } \varepsilon_r^{(n,i)}(x) > 1 + C_{\text{cut}}(n), \\ 1, \text{ if } \varepsilon_r^{(n,i)}(x) \in [1, 1 + C_{\text{cut}}(n)]. \end{cases} \tag{5.25}$$

Note that by (5.24), $\varepsilon_r^{(n,i)}(x) \geq 1$, $\forall x \in \Omega$. The numbers $C_{\text{cut}}(n)$ were chosen as follows:

$$C_{\text{cut}}(1) = 0, C_{\text{cut}}(2) = 0.2, C_{\text{cut}}(3) = C_{\text{cut}}(4) = 0.8, C_{\text{cut}}(5) = 0.6,$$
$$C_{\text{cut}}(6) = C_{\text{cut}}(7) = 0.4, C_{\text{cut}}(8) = 0.8.$$

We now define stopping rules of iterations for functions $q_{n,1}^k$ with respect to the nonlinear term as well as for functions $\{q_{n,i}\}$ with respect to the tails. These rules are almost the same as in Sect. 4.15.2. Consider the planar surface $P_{\tilde{h}}$ which is parallel to the surface P in (5.9). The surface $P_{\tilde{h}}$ is obtained from the surface P via shifting upward by $\tilde{h} = 0.2$:

$$P_{\tilde{h}} = \left\{(x,y,z) : (x,y) \in [-2.4, 2.4] \times [-1.4, -1.4], z = -2.4 + \tilde{h} = -2.2\right\}.$$

Let $\Omega' = \{(x,y) \in [-2.4, 2.4] \times [-1.4, -1.4]\}$ be the orthogonal projection of both surfaces P and $P_{\tilde{h}}$ on the (x,y) plane. Consider norms

$$F_n^k = ||q_{n,1}^k|_{P_{\tilde{h}}} - \overline{\psi}_n||_{L_2(\Omega')}.$$

We stop iterations of functions $q_{n,1}^k$ when either $F_n^{k+1} \geq F_n^k$ or $\left|F_n^k - F_n^{k-1}\right| \leq \varepsilon$, where $\varepsilon = 0.001$ is a small tolerance number of our choice. Next, we iterate with respect to the tails. We similarly introduce norms $F_{n,i} = ||q_{n,i}|_{P_{\tilde{h}}} - \overline{\psi}_n||_{L_2(\Omega')}$ and use the same stopping rule as the one for F_n^k.

We now describe the stopping rule for computing functions $\varepsilon_r^{(n)}(x)$. Let

$$a_n = \frac{\left\|\tilde{\varepsilon}_r^{(n)} - \tilde{\varepsilon}_r^{(n-1)}\right\|_{L_2(\Omega)}}{\left\|\tilde{\varepsilon}_r^{(n-1)}\right\|_{L_2(\Omega)}}, \; b_n = \frac{a_n}{a_{n-1}}.$$

5.7.1 *Stopping Rule for*

$\varepsilon_r^{(n)}$:

$$\text{If} \begin{cases} b_n \in [1.9, 4] \text{ and } n > 3, \text{ then take the final solution } \varepsilon_r^f = \varepsilon_r^{(n)}, \\ b_n > 4 \text{ and } n > 3, \text{ then take the final solution } \varepsilon_r^f = \varepsilon_r^{(n-1)}, \\ \text{alternatively compute } \varepsilon_r^{(n+1)}. \end{cases} \tag{5.26}$$

We have chosen $n > 3$ in (5.26) because we have observed in our work with computationally simulated data that images are becoming more or less close to the correct ones only starting from $n = 4$.

5.8 Reconstruction by the Approximately Globally Convergent Numerical Method

5.8.1 *Dielectric Inclusions and Their Positions*

Our dielectric inclusions to be imaged were two wooden cubes of 40 mm size of the side of the first cube and 60-mm size of the side of the second cube; see Table 5.1.

Let CL be the center line, i.e., the straight line which is orthogonal to the plane P and which passes through the source of EM waves. Then $CL = \{(x, y, z) : x = y = 0\}$. We have placed both those cubes in two positions. In the first position, the center of each cube was on CL. In the second position, the center was shifted off CL by 10 mm in the positive direction of x axis (0.2 in dimensionless units). In addition, we have used the third position for cube number 1. In the third position, the center of this cube was shifted by 60 mm off CL in the positive direction of the x axis (1.2 in dimensionless variables), which was rather far from CL. We have observed on the experimental data that since we had a spherical rather than a plane wave, then the magnitude of the EM field has significantly

Table 5.1 Sizes and coordinates of centers of two wooden cubes used in experiments

Cube number	Original sizes, mm	Dimensionless sizes	Dimensionless coordinates of centers
1	$40 \times 40 \times 40$	$0.8 \times 0.8 \times 0.8$	$(0, 0, -1.2)$
2	$60 \times 60 \times 60$	$1.2 \times 1.2 \times 1.2$	$(0.2, 0, -1.2)$

Source: M.V. Klibanov, M.A. Fiddy, L. Beilina, N. Pantong and J. Schenk, Picosecond scale experimental verification of a globally convergent numerical method for a coefficient inverse problem, *Inverse Problems*, 26, 045003, doi:10.1088/0266-5611/26/4/045003, 2010. © IOP Publishing. Reprinted with permission

Table 5.2 Positions of centers of two wooden cubes to be imaged in six cases. The difference between cases 1.1(1) and 1.1(2) is that they were measured on two different days for the same position of cube 1

Cube number	Case number	Center
1	1.1(1)	$(0, 0, -1.2)$
1	1.1(2)	$(0, 0, -1.2)$
1	1.2	$(0.2, 0, -1.2)$
1	1.3	$(1.2, 0, -1.2)$
2	2.1	$(0, 0, -1.2)$
2	2.2	$(0.2, 0, -1.2)$

Source: M.V. Klibanov, M.A. Fiddy, L. Beilina, N. Pantong and J. Schenk, Picosecond scale experimental verification of a globally convergent numerical method for a coefficient inverse problem, *Inverse Problems*, 26, 045003, doi:10.1088/0266-5611/26/4/045003, 2010. © IOP Publishing. Reprinted with permission

decayed when the point has moved rather far from CL. So the goal of placing cube number 1 in the third position was to see how this decay of the magnitude of the EM field would affect the image quality. Due to some logistical reasons, we have measured the scattering field from cube number 1 in the first position twice: in two consecutive days. Therefore, we have obtained total six (6) pieces of data for the case when either of those two cubes was present. In addition, the data for the reference medium, was measured only once. Table 5.2 lists all six cases.

5.8.2 Tables and Images

We have made computations using the approximately globally convergent algorithm of Sect. 2.6.1. Functions $\psi_n(x)$ in (5.22) were used as boundary conditions. The stopping rules were the same as the one in Sect. 5.7. We point out again that we did not know in advance values refractive indices of above wooden cubes. Therefore, we were **unbiased** when applying stopping rules. Table 5.3 presents numbers a_n and $b_n = a_n/a_{n-1}$ for the case 1.1(1) (see Table 5.2 for labeling of our cases). It is clear from the stopping rule (5.26) why we have stopped in this table at $n = 6$.

Table 5.3 Computational results for the case 1.1(1); see Table 5.2 for labeling of cases and (49) for the stopping rule

Iter., n	$\varepsilon_r^{(n)}$	a_n	b_n	ε_r^f	$n_f = \sqrt{\varepsilon_r^f}$
2	1.28	0.027	0.21		
3	2.53	0.209	7.74		
4	2.9	0.160	0.76		
5	3.76	0.266	1.66		
6	4.66	0.580	2.18	$\varepsilon_r^f = \varepsilon_r^{(6)} = 4.66$	2.16
7	5.6	0.683	1.18		
8	8.1	0.809	1.18		

Source: M.V. Klibanov, M.A. Fiddy, L. Beilina, N. Pantong and J. Schenk, Picosecond scale experimental verification of a globally convergent numerical method for a coefficient inverse problem, *Inverse Problems*, 26, 045003, doi:10.1088/0266-5611/26/4/045003, 2010. © IOP Publishing. Reprinted with permission

Table 5.4 Computational results for five cases; see (5.8.2) for the stopping rule and Table 5.2 for labeling of cases. The rest of iterations for all these five cases was similar with Table 5.3. Comparison of this table with (5.26) makes it clear why either of function $\varepsilon_r^{(n)}$ or $\varepsilon_r^{(n-1)}$ was chosen as the final imaging result ε_r^f

Case	Iter., n	b_n	ε_r^f	$n_f = \sqrt{\varepsilon_r^f}$
1.1(2)	5	2.07	$\varepsilon_r^f := \varepsilon_r^{(5)} = 4$	2
1.2	6	2.40	$\varepsilon_r^f := \varepsilon_r^{(6)} = 4.65$	2.16
1.3	6	3.57	$\varepsilon_r^f := \varepsilon_r^{(6)} = 4.82$	2.19
2.1	6	5.74	$\varepsilon_r^f := \varepsilon_r^{(5)} = 2.98$	1.73
2.2	6	5.36	$\varepsilon_r^f := \varepsilon_r^{(5)} = 3.19$	1.79

Source: M.V. Klibanov, M.A. Fiddy, L. Beilina, N. Pantong and J. Schenk, Picosecond scale experimental verification of a globally convergent numerical method for a coefficient inverse problem, *Inverse Problems*, 26, 045003, doi:10.1088/0266-5611/26/4/045003, 2010. © IOP Publishing. Reprinted with permission

Behavior of numbers a_n and b_n for other cases was similar. Table 5.4 presents only numbers b_n for the final iteration. Again, the stopping rule (5.26) explains the choice of the final image ε_r^f. Figures 5.5 and 5.6 display computed images. Figure 5.5 is for the case 1(1). One can see from Fig. 5.5g, h how the image "explodes" after the stopping criterion (5.26) is reached at $n = 6$; see Table 5.3. Figure 5.6 show that locations of inclusions are imaged with a good accuracy. The latter is true even in the most difficult case 1.3 when the inclusion was located far off the center line CL, which meant a low amplitude of the signal; see Sect. 5.8.1.

Still, shapes of abnormalities are not imaged well on Fig. 5.6. Recall, however, that our goal for the first stage of our two-stage numerical procedure was twofold: (1) to obtain accurate locations of inclusions and (2) to accurately image refractive indexes in them. However, we did not have the goal to accurately image shapes of inclusions on the first stage of our two-stage numerical procedure.

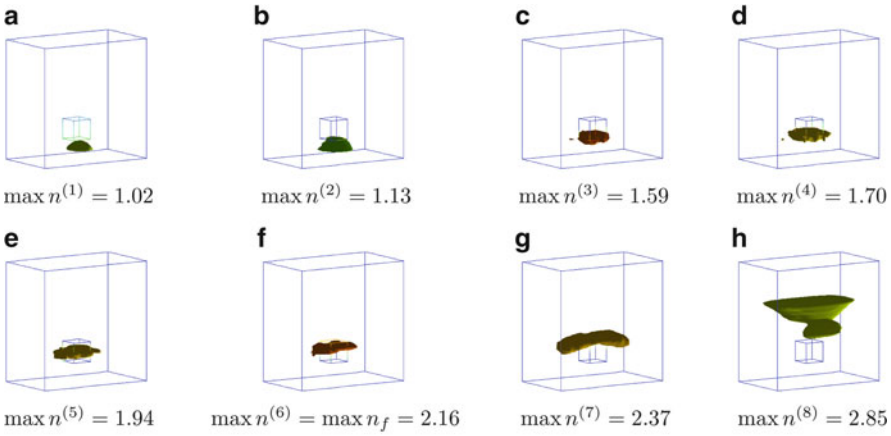

Fig. 5.5 (**a**)–(**h**) represent the dynamics of the sequence of images for the case number 1.1(1). Maximal values of refractive indexes $\max_{\overline{P}} n^{(k)} = \sqrt{\max_{\overline{P}} \varepsilon_r^{(k)}}$ are displayed. Each image represents the level surface $x : n^{(k)}(x) = \max_{\overline{P}} n^{(k)}(x)$. The final image is presented on (**f**). (**h**) shows that the image "explodes" on the second iteration after the stop; see the stopping rule (5.26) and Table 5.3. Source: M. V. Klibanov, M. A. Fiddy, L. Beilina, N. Pantong and J. Schenk, Picosecond scale experimental verification of a globally convergent numerical method for a coefficient inverse problem, *Inverse Problems*, 26, 045003, doi:10.1088/0266-5611/26/4/045003, 2010. © IOP Publishing. Reprinted with permission

5.8.3 Accuracy of the Blind Imaging

We have independently measured refractive indices **after** the above images were obtained. Those measurements were performed by two methods which are well established in Physics: the waveguide method [133] and the oscilloscope method [71]. In the case of the waveguide Method the measurement error was 11% for cube number 1 and 3.5% for cube number 2. In the case of the oscilloscope method the measurement error was 6% for both cubes. Tables 5.5 and 5.6 display both errors: in computations and direct measurements. Only maximal values of computed refractive indices are presented in these tables. One can see that the computational error does not exceed the measurement error in five (5) out of six (6) cases. And it exceeds the measurement error in the sixth case by less than 2%.

Therefore, we conclude that the approximately globally convergent numerical method has produced images of an excellent accuracy for both locations and refractive indices of dielectric abnormalities in blind testing. Furthermore, this result was obtained for the case of a huge misfit between the experimental and computationally simulated data. Therefore, this accuracy fully justifies our data pre-processing procedure.

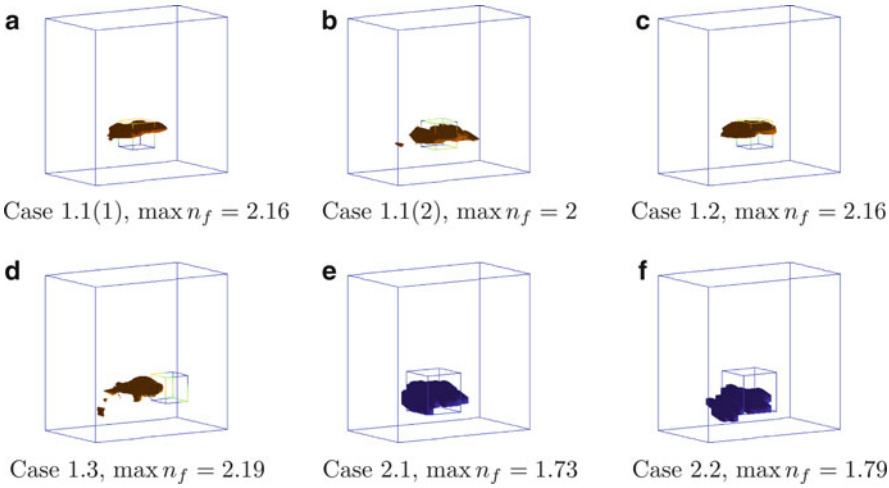

Fig. 5.6 Resulting images. It should be kept in mind that we did not have a goal to image shapes of inclusions accurately. Rather, our goal was only to image their locations and maximal values of refractive indexes $n_f(x) = \sqrt{\varepsilon_r^f}$. On each figure, $n_f(x) = \max n_f$ for all points of the image of the corresponding cube. In addition to the cut-offs (5.25), we have made the last postprocessing cut-off of the imaged function ε_r^f each figure just to make it look better. That cut-off was made around the center of the image. For all cases, the dynamics of the change of images of functions $\varepsilon_r^{(n)}$ with iterations was similar with one on Fig. 5.5a–h. Source: M. V. Klibanov, M. A. Fiddy, L. Beilina, N. Pantong and J. Schenk, Picosecond scale experimental verification of a globally convergent numerical method for a coefficient inverse problem, *Inverse Problems*, 26, 045003, doi:10.1088/0266-5611/26/4/045003, 2010. © IOP Publishing. Reprinted with permission

Table 5.5 Comparison of imaging results of values of refractive indexes for six cases of Table 5.2 with measurements by the waveguide method

Case	Blindly imaged $n := n_f$	Measured n, error (%)	Imaging error (%)
1.1(1)	2.16	2.07, 11	4.3
1.1(2)	2	2.07, 11	3.4
1.2	2.16	2.07, 11	4.3
1.3	2.19	2.07, 11	5.8
2.1	1.73	1.71, 3.5	1.2
2.2	1.79	1.71, 3.5	4.7

Source: M.V. Klibanov, M.A. Fiddy, L. Beilina, N. Pantong and J. Schenk, Picosecond scale experimental verification of a globally convergent numerical method for a coefficient inverse problem, *Inverse Problems*, 26, 045003, doi:10.1088/0266-5611/26/4/045003, 2010. © IOP Publishing. Reprinted with permission

Table 5.6 Comparison of imaging results of values of refractive indexes for six cases of Table 5.2 with measurements by the oscilloscope method

Case	Blindly imaged $n := n_f$	Measured n, error (%)	Imaging error (%)
1.1(1)	2.16	2.17, 6	0.5
1.1(2)	2	2.17, 6	7.8
1.2	2.16	2.17, 6	0.5
1.3	2.19	2.17, 6	1
2.1	1.73	1.78, 6	2.8
2.2	1.79	1.78, 6	0.56

Source: M.V. Klibanov, M.A. Fiddy, L. Beilina, N. Pantong and J. Schenk, Picosecond scale experimental verification of a globally convergent numerical method for a coefficient inverse problem, *Inverse Problems*, 26, 045003, doi:10.1088/0266-5611/26/4/045003, 2010.

5.8.4 *Performance of a Modified Gradient Method*

We have decided to compare performances of the approximately globally convergent numerical method with a modified gradient method for the case of above experimental data. Since the gradient method is outside of our main focus, our discussion is intentionally brief here. First, we need to introduce the Tikhonov functional for the above CIP in the pseudo frequency domain and derive its Fréchet derivative. We call the technique of this section the "modified gradient method" because instead of making usual steps in the gradient method, we find the zero of the Fréchet derivative of the Tikhonov functional via solving an equation with a contractual mapping operator. Our derivation of the Fréchet derivative of the Tikhonov functional is similar with the heuristic derivation in Sect. 4.4.

Let $u(x,t)$ be the solution of the problem (5.1), (5.2) and

$$w(x,s) = \int_0^\infty u(x,t)\, e^{-st} dt. \tag{5.27}$$

Then by Theorem 2.7.2,

$$\Delta w - s^2 \varepsilon_r(x)\, w = -\delta(x - x_0), \tag{5.28}$$

$$\lim_{|x|\to\infty} w(x,s) = 0. \tag{5.29}$$

Let $\tilde{g}(x,s)$ be the Laplace transform (5.27) of the function $g(x,t)$ in (5.6). Then

$$w(x,s)\,|_{\partial\Omega} = \tilde{g}(x,s). \tag{5.30}$$

Since by (5.3), the coefficient $\varepsilon_r(x) = 1$ outside of Ω, then we can uniquely solve the boundary value problem (5.28), (5.29), (5.30) in the domain $\mathbb{R}^3 \setminus \Omega$ for every value of s of our interest. Hence, we can uniquely find the normal derivative

$p(x,s) = \partial_n w(x,s) \mid_{\partial\Omega}$. Hence, we obtain the so-called "state" boundary value problem for the function w inside the domain Ω:

$$\begin{aligned} \Delta w - s^2 \varepsilon_r(x) w &= 0 \text{ in } \Omega, \\ \partial_n w(x,s) \mid_{\partial\Omega} &= p(x,s). \end{aligned} \tag{5.31}$$

In addition, consider the so-called "adjoint" boundary value problem for the function λ:

$$\begin{aligned} \Delta\lambda - s^2 \varepsilon_r(x) \lambda &= 0 \text{ in } \Omega, \\ \partial_n \lambda(x,s) \mid_{\partial\Omega} &= (w \mid_{\partial\Omega} - \tilde{g})(x,s). \end{aligned} \tag{5.32}$$

The idea of the gradient method is to find a zero of the Fréchet derivative of the Tikhonov functional:

$$E(\varepsilon_r) = \frac{1}{2} \int_{s_1}^{s_2} \int_{\partial\Omega} (w \mid_{\partial\Omega} - \tilde{g})^2 \, d\sigma_x ds + \frac{\alpha}{2} \int_{\Omega} \left(\varepsilon_r(x) - \varepsilon_r^{(0)}(x) \right)^2 dx,$$

where (s_1, s_2) is an interval of pseudo frequencies, $w = w(x,s;\varepsilon_r)$ is the solution of the problem (5.31), and $\varepsilon_r^{(0)}$ is a first approximation for the unknown coefficient ε_r: In order to simplify the derivation of the Fréchet derivative of this functional, consider the associated Lagrangian $L(\varepsilon_r)$,

$$L(\varepsilon_r) = E(\varepsilon_r) + \int_{s_1}^{s_2} \int_{\partial\Omega} p\lambda \, d\sigma_x ds - \int_{s_1}^{s_2} \int_{\Omega} \left(\nabla w \nabla \lambda + s^2 \varepsilon_r(x) w\lambda \right) dx ds. \tag{5.33}$$

It follows from the definition of the weak solution of the problem (5.31) that the integral term in (5.33) equals zero. Hence, $L(\varepsilon_r) = E(\varepsilon_r)$ for all admissible function $\varepsilon_r(x)$. To figure out the Fréchet derivative $L'(\varepsilon_r)$, we need to vary in (5.33) the function ε_r via considering the function $\varepsilon_r(x) + b(x)$, where the functions $b(x)$ is an appropriate small perturbation of the function $\varepsilon_r(x)$. But since functions $w = w(x,s;\varepsilon_r)$ and $\lambda = \lambda(x,s;\varepsilon_r)$ depend on ε_r as solutions of boundary value problems (5.31) and (5.32), then we should also consider respective variations of these functions. In other words, we should consider Fréchet derivatives of functions $w(x,s;\varepsilon_r)$, $\lambda(x,s;\varepsilon_r)$ with respect to ε_r. These Fréchet derivatives are actually solutions of such boundary value problems, which are obtained via the linearization of problems (5.31) and (5.32) with respect to b. Finally, the linear, with respect to $b(x)$, part of the difference $L(\varepsilon_r + b) - L(\varepsilon_r)$ is $L'(\varepsilon_r)(b)$. Again, the necessary formalism for the hyperbolic case can be found in Chap. 4, and our elliptic case is similar. So, finally, we obtain

$$E'(\varepsilon_r) = \alpha \left(\varepsilon_r - \varepsilon_r^{(0)} \right)(x) - \int_{s_1}^{s_2} s^2 (w\lambda)(x,s;\varepsilon_r) \, ds.$$

At a point of a minimum of the functional $E(\varepsilon_r)$ one should have $E'(\varepsilon_r) = 0$. Therefore, we should solve the following equation:

$$\varepsilon_r(x) = \frac{1}{\alpha}\int_{s_1}^{s_2} s^2 (w\lambda)(x,s;\varepsilon_r)\,ds + \varepsilon_r^{(0)}(x), x \in \Omega. \tag{5.34}$$

It can be proven that one can choose the number $\zeta = (s_2 - s_1)/\alpha$ so small that equation (5.34) becomes an equation with the contraction mapping operator, which, therefore, can be solved iteratively. Of course, the number ζ should not be too small since, otherwise, the resulting solution would be too close to the initial guess $\varepsilon_r^{(0)}$. So, one should choose optimal parameters s_1, s_2, α.

Temporary denote $\mathbf{x} = (x, y, z)$. When applying the modified gradient method (5.34) to the experimental data, our starting point for iterations was $\varepsilon_r^{(0)} \equiv 1$. In other words, since any gradient-like method is a locally convergent one, we have assumed that we know the background medium in the domain Ω. This is unlike the approximately globally convergent method. We have observed that the function $\lambda\left(\mathbf{x}, s; \varepsilon_r^{(0)}\right) = \lambda(\mathbf{x}, s; 1) < 0$. At the same time, by Theorem 2.7.2, $w\left(\mathbf{x}, s; \varepsilon_r^{(0)}\right) = w(\mathbf{x}, s; 1) > 0$, and we have also observed this inequality computationally. Hence, it follows from (5.34) that $\varepsilon_r^{(1)} < 1$, where $\varepsilon_r^{(1)}$ is the result of the first iteration of the solution of the problem (5.34) with the contraction mapping operator. We have tried a variety of numbers s_1, s_2, α in (5.34), some of which have ensured the contraction mapping property. Still, with all these parameters, we have obtained functions $\varepsilon_r^{(n)} < 1$ for all iteration numbers n. However, by (5.4), we should have $\varepsilon_r(x) \geq 1$.

We have a close to rigorous explanation of the negative values of the function $\lambda(\mathbf{x}, s; 1)$. Consider, for example, the case when the domain Ω is the half space, $\Omega = \{z > -2.4\}$ (see (5.8)). Changing variables $z' := z + 2.4$ and leaving the same notation for the new variable as for the old one (for brevity), we obtain $\Omega = \{z > 0\}$. In addition, assume that the condition $\lim_{|x|\to\infty} \lambda(\mathbf{x}, s; 1) = 0$ is imposed and also that $\lim_{|\mathbf{x}|\to\infty} (w|_{z=0} - \tilde{g}) = 0$. Consider the function $Q(\mathbf{x}, \boldsymbol{\xi})$:

$$Q(\mathbf{x}, \boldsymbol{\xi}) = \frac{\exp(-s|\mathbf{x} - \boldsymbol{\xi}|)}{4\pi|\mathbf{x} - \boldsymbol{\xi}|} + \frac{\exp\left(-s\left|\mathbf{x} - \boldsymbol{\xi}'\right|\right)}{4\pi\left|\mathbf{x} - \boldsymbol{\xi}'\right|}, \boldsymbol{\xi}' = (\xi_1, \xi_2, -\xi_3).$$

It can be easily verified that $Q(\mathbf{x}, \boldsymbol{\xi})$ is the Green's function with the Neumann boundary condition in the half space $\{z > 0\}$ for the operator $\Delta - s^2$. Hence, by (5.31),

$$\lambda(\mathbf{x}, s, 1) = \int_{\mathbb{R}^2} Q(\mathbf{x}, \xi_1, \xi_2, 0)\left[w((\xi_1, \xi_2, 0), s; 1) - \tilde{g}(\xi_1, \xi_2, s)\right] d\xi_1 d\xi_2.$$

We have observed computationally that $w((\xi_1, \xi_2, 0), s; 1) - \tilde{g}(\xi_1, \xi_2, s) \leq 0$ for all reasonable values of ξ_1, ξ_2, s. Hence, $\lambda(\mathbf{x}, s; 1) \leq 0$.

In addition, we have observed computationally that for all reasonable values of the pseudo frequency s maximal absolute values of functions w and λ were too small. So that

$$\max_{x \in \overline{\Omega}} \left[s^2 \left| w\lambda \right| (x, s) \right] \leq 3 \cdot 10^{-4}.$$

By (5.34), this means, however, that in order for the function ε_r to be rather significantly different from $\varepsilon_r^{(0)} \equiv 1$, i.e., in order to obtain above inclusion/background contrasts, one should choose a very small regularization parameter α. For example, to get $\varepsilon_r^f = 4.66$ within the imaged inclusion (Table 5.3), one should have $\alpha \approx 8 \cdot 10^{-5}$. It is well known, however, that exceedingly small values of regularization parameters affect results quite negatively.

We, therefore conclude that the modified gradient method (5.34) is inapplicable here. However, since any version of the gradient method should still use the gradient $E'(\varepsilon_r)$, then it is unlikely that other versions of the gradient method are applicable here. This likely means that locally convergent numerical methods are inapplicable in the pseudo frequency domain. Thus, it seems to be that our approximately globally convergent technique is the *single* choice for this kind of experimental data.

5.9 Performance of the Two-Stage Numerical Procedure

We show in this section how the two-stage numerical procedure works for the above experimental data. Recall that the first stage has provided us with accurate images of two components of dielectric abnormalities: locations and refractive indices; see Figure 5.6 as well as Tables 5.4 and 5.5. We now want to add the third component: the shape.

5.9.1 The First Stage

We have recomputed images for two cases using the algorithm of the first stage. More precisely, those were cases which are listed on Table 5.2 as 5.1(1) and 5.2. For the convenience of the reader, we list these two cases in Table 5.7 again. Since parameters in computations for these two cases were a little bit different from those used in Sect. 5.8, our images were a little bit different also, although we have used the same stopping rule (5.26) as in Sect. 5.8. Figures 5.7 and 5.8 show how images were changing with iterations, which is similar with Figs. 5.5, 5.7c and 5.8c display final images for two cases of Table 5.7. Table 5.8 shows reconstructed refractive indices for these two cases as well as their comparisons with results of direct measurements by the wave guide method. One can again observe an excellent accuracy of the reconstruction of refractive indices.

Table 5.7 Cases considered in the two-stage numerical procedure

Cube number	Case number	Center
1	1.1(1)	(0,0,−1.2)
2	2.2	(0.2,0,−1.2)

Source: L. Beilina and M.V. Klibanov, Reconstruction of dielectrics from experimental data via a hybrid globally convergent/adaptive inverse algorithm, *Inverse Problems*, 26, 125009, doi:10.1088/0266-5611/26/12/125009, 2010.

5.9.2 The Third Stage of Data Immersing

It is evident from Fig. 5.4a that the function $u_{\text{incl}}(x_m, t)$ is very noisy with respect to the positions of the detector $x_m \in P$. While the second stage of data immersing has worked in the "Laplace transform domain" (Sect. 5.6.2), we apply the adaptivity in the time domain. Hence, we now need to smooth somehow the function $u_{\text{incl}}(x_m, t)$. Although this smoothing can be done similarly with Sect. 5.6.2, this would not address the problem we face now. Indeed, it follows from (5.13) to (5.16) that we need to somehow obtain the proper data for the function $u(x,t)$ for $(x,t) \in P_{\text{obs}} \times (0,T)$ while having the data $u_{\text{incl}}(x_m, t)$ only for $x_m \in P$, where the rectangle P is narrower than the rectangle:

$$P_{\text{obs}} = \{(x,y,z) : (x,y) \in (-3,3) \times (-2,2), z = -2.4\}.$$

This extension from P in P_{obs} is the subject of our third stage of data immersing.

Let $\varepsilon_r^{\text{glob}}(x)$ be the solution obtained on the first stage. Let $U(x,t)$ be the solution of the problem (5.11) for the case $\varepsilon_r(x) := \varepsilon_r^{\text{glob}}(x)$. Let $u_{\text{incl}}(x,t)$, $(x,t) \in P \times (0,T)$ be the standard linear interpolation of the discrete function $u_{\text{incl}}(x_m, t)$. Our third stage of data immersing consists in defining the function $u_{\text{immers}}(x,t)$ for $(x,t) \in P_{\text{obs}} \times (0,T)$ as

$$u_{\text{immers}}(x,t) = \begin{cases} u_{\text{incl}}(x,t), \text{ if } x \in P \text{ and } u_{\text{incl}}(x,t) \geq \beta \max_{\overline{P}} u_{\text{incl}}(x,t), \\ U(x,t), \text{ otherwise.} \end{cases} \tag{5.35}$$

The parameter $\beta \in (0,1)$ in (5.35) should be chosen in numerical experiments. In particular, it follows from (5.35) that

$$u_{\text{immers}}(x,t) = U(x,t) \text{ for } x \in P_{\text{obs}} \setminus P. \tag{5.36}$$

Taking into account (5.13), we set in (5.15) and (5.16)

$$g(x,t) := u_{\text{immers}}(x,t) \text{ for } (x,t) \in S'_T = P_{\text{obs}} \times (0,T). \tag{5.37}$$

Comparison of Fig. 5.9a, c, e with Fig. 5.9b, d, f shows that the third stage of data immersing not only allows to extend the data from P to P_{obs} but also significantly

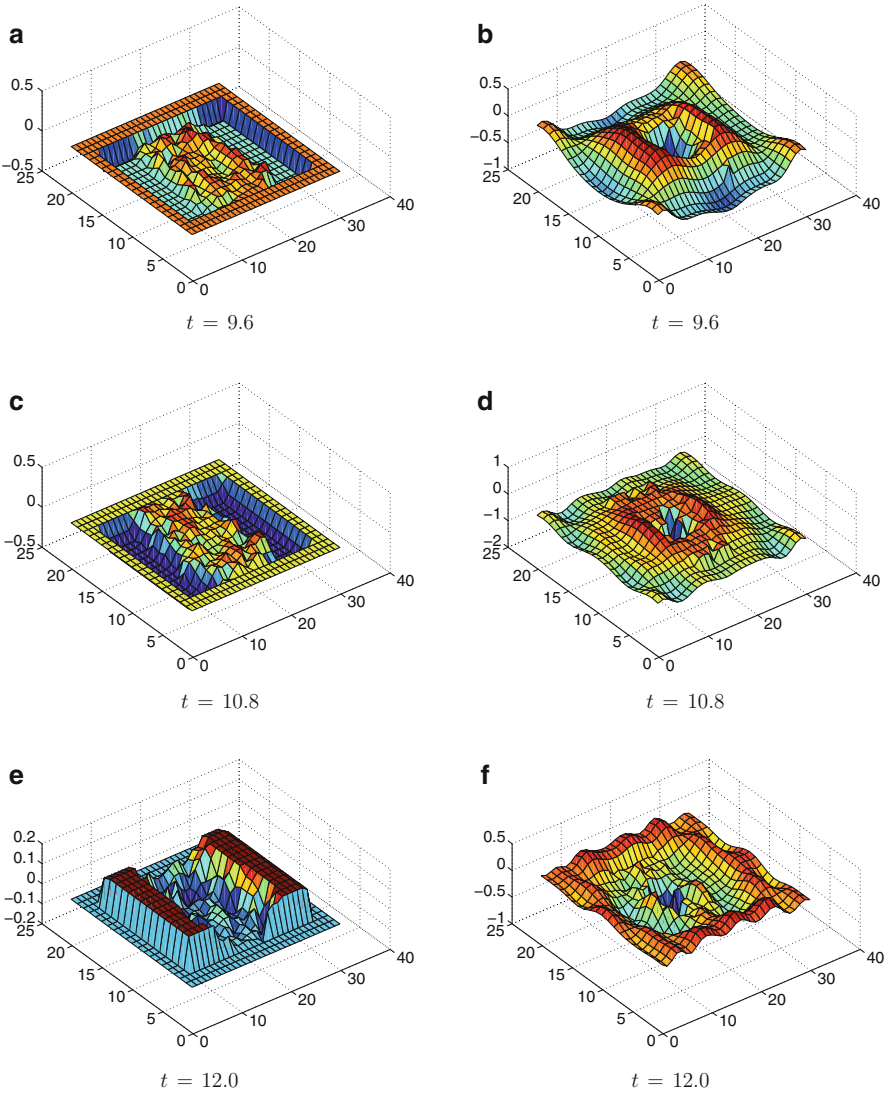

Fig. 5.7 (**a**),(**c**),(**e**) The function $g(x,t), x \in P$ for cube No.1 (Table 5.1). This is the function $u_{\text{incl}}(x,t), x \in P$. However, to solve the adjoint problem (5.15) in the adaptivity, we need to know this function at a wider rectangle $x \in P_{\text{obs}}$; see Sect. 5.6. So, since $P \subset\subset P_{\text{obs}}$, we need to extend somehow the function $g(x,t)$ from P to P_{obs}. This extension is carried out via the third stage of our data immersing procedure; see Sect. 5.6. (**b**),(**d**),(**f**) present the resulting immersed data with $\beta = 0.1$. Source: L. Beilina and M.V. Klibanov, Reconstruction of dielectrics from experimental data via a hybrid globally convergent/adaptive inverse algorithm, *Inverse Problems*, 26, 125009, doi:10.1088/0266-5611/26/12/125009, 2010. © IOP Publishing. Reprinted with permission

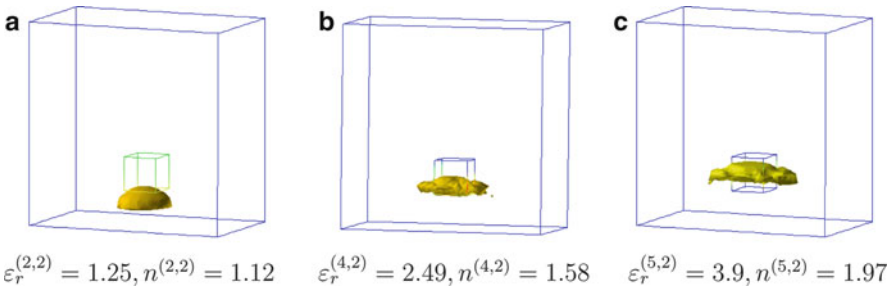

Fig. 5.8 Spatial distributions of iteratively computed dielectric constants $\varepsilon_r^{(n,k)}$ and refractive indexes $n^{(n,k)} = \sqrt{\varepsilon_r^{(n,k)}}$ for the cube number 1 (Table 5.7). The final image corresponds to $n^{(5,2)} := n_{\text{glob}} = 1.97$. See Table 5.8 for the reconstruction accuracy. Recall that refractive indices rather than dielectric constants are actually measured experimentally. Source: L. Beilina and M.V. Klibanov, Reconstruction of dielectrics from experimental data via a hybrid globally convergent/adaptive inverse algorithm, *Inverse Problems*, 26, 125009, doi:10.1088/0266-5611/26/12/125009, 2010. © IOP Publishing. Reprinted with permission

Table 5.8 Computed refractive indices on the first stage of the two-stage numerical procedure (second column). The third and fourth column show directly measured indices by the wave guide method and computational errors respectively

Cube Number	Computed n	Measured n, error (%)	Imaging error (%)
1	1.97	2.17, 11	9.2
2	1.79	1.78, 3.5	0.5

Source: L. Beilina and M.V. Klibanov, Reconstruction of dielectrics from experimental data via a hybrid globally convergent/adaptive inverse algorithm, *Inverse Problems*, 26, 125009, doi:10.1088/0266-5611/26/12/125009, 2010. © IOP Publishing. Reprinted with permission

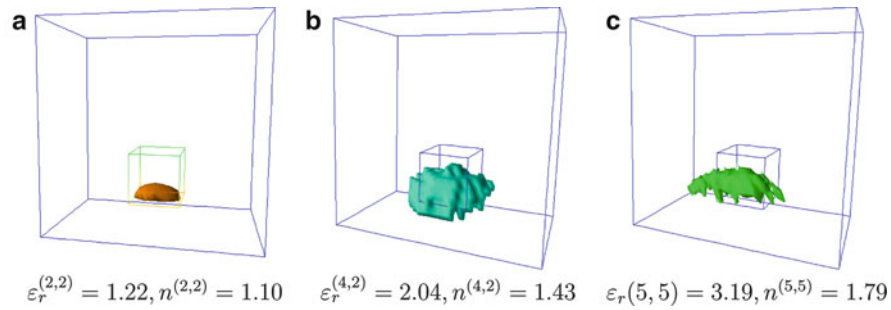

Fig. 5.9 Spatial distributions of iteratively computed dielectric constants $\varepsilon_r^{(n,k)}$ and refractive indexes $n^{(n,k)} = \sqrt{\varepsilon_r^{(n,k)}}$ for the cube number 2 (Table 5.7). The final image corresponds to $n^{(5,5)} := n_{\text{glob}} = 1.79$, which is only 3.5% error compared with the experiment; see Table 5.8. Recall that refractive indices rather than dielectric constants are actually measured experimentally. Source: L. Beilina and M.V. Klibanov, Reconstruction of dielectrics from experimental data via a hybrid globally convergent/adaptive inverse algorithm, *Inverse Problems*, 26, 125009, doi:10.1088/0266-5611/26/12/125009, 2010. © IOP Publishing. Reprinted with permission

decreases the noise in the data compared with the function $u_{\text{incl}}(x,t)$ which was the result of the first immersing stage. Another important point here is that variations of the parameter β in a wide range $\beta \in (0.1, 0.985)$ do not significantly affect results; see Fig. 5.15.

5.9.3 Some Details of the Numerical Implementation of the Adaptivity

The adaptivity in this case consists of two stages of mesh refinement:

Stage 1. On this stage, we use both first and second mesh refinement recommendations (5.17) and (5.18) of Sect. 5.5. In doing so, we use the same parameters β_1, β_2, α as ones in (5.19).

Stage 2. On this stage, we use only the second mesh refinement recommendation (5.18) with parameters β_2, α listed in (5.19).

Just as in Sect. 4.16.2, we use a cut-off parameter B_{cut}. In other words, we set

$$\varepsilon_{r,h}(x) = \begin{cases} \varepsilon_{r,h}(x), \text{ if } |\varepsilon_{r,h}(x) - \varepsilon_r^{\text{glob}}(x)| \geq B_{\text{cut}}, \\ \varepsilon_r^{\text{glob}}(x), \text{ elsewhere.} \end{cases} \tag{5.38}$$

Specific values of the parameter B_{cut} are given below.

In addition, we impose the upper bound d on functions $\varepsilon_{r,h}(x)$; see (5.4). In other words, we enforce that

$$\varepsilon_{r,h}(x) \in C_M = \{1 \leq \varepsilon_{r,h}(x) \leq d\}.$$

We find good estimates for the number d from results of the first stage since approximate global convergence Theorems 2.8.2 and 2.9.4 guarantee that the function $\varepsilon_r^{\text{glob}}(x)$ is close to the correct solution. Concrete values of d are given below.

5.9.4 Reconstruction Results for Cube Number 1

We have used the function $\varepsilon_r^{\text{glob}}(x)$ as the starting point for iterations; see Fig. 5.7c for the image of this function. Also, in addition to (5.17), we took the following values of parameters d in (5.4), β in (5.35) and B_{cut} in (5.38):

$$d = 4.4, \ \beta = 0.985, \ B_{\text{cut}} = 2.$$

We have chosen $d = 4.4$ since by Table 5.8, $\max \varepsilon_r^{\text{glob}}(x) = (1.97)^2 \approx 3.9$. Hence, the admissible set of parameters in this case is

$$\varepsilon_r(x) \in C_M = \{1 \leq \varepsilon_r(x) \leq 4\}.$$

As to the parameters α, β_1, β_2, see (5.19).

5.9.4.1 The First Stage of Mesh Refinements

First, using the same coarse mesh as the one on the first stage, we have not observed any image improvement, which is similar with numerical results of Sects. 4.15.3 and 4.16.2. To figure out when we should stop mesh refinements, we proceed similarly with Sects. 4.15.3 and 4.16.2. Namely, we analyze norms

$$\|g - u\|_{L_2(S'_T)} = \|u_{\text{immers}} - u\|_{L_2(S'_T)}; \tag{5.39}$$

see (5.37). These norms decrease with the number of mesh refinements up to the third mesh refinement. Next, on the fourth mesh refinement, the norm (5.39) slightly increases. Hence, similarly with Sects. 4.15.3 and 4.16.2, relaxation Theorems 4.9.3 and 4.11.4 tell us that the third mesh refinement should be the final one.

The resulting image is displayed on Fig. 5.10. Comparison of Figs. 5.10 and 5.7c shows that the adaptivity has improved the image of the shape. Also, refractive indices on both figures are the same. However, the shape of the abnormality is not yet imaged well.

5.9.4.2 The Second Stage of Mesh Refinements

Let $\overline{\varepsilon}_r(x)$ be the coefficient reconstructed on the first stage of mesh refinements. The image of $\overline{\varepsilon}_r(x)$ is depicted on Fig. 5.10. Analyzing the image of Fig. 5.10 computationally, we have observed that the imaged inclusion of this figure is contained in the subdomain $\tilde{\Omega} \subset \Omega$, where

$$\tilde{\Omega} = \{(x, y, z) \in [-0.5, 0.5] \times [-0.6, 0.6] \times [-1.4, -0.5]\}.$$

On this stage of mesh refinements, we use only the second mesh refinement recommendation and refine the mesh in neighborhoods of all such points x that

$$x \in \left\{\overline{\varepsilon}_r(x) \geq 0.2 \max_{\overline{\Omega}} \overline{\varepsilon}_r(x)\right\} \cap \tilde{\Omega}.$$

The same stopping criterion as the one in Sects. 4.15.3 and 4.16.2 was used again. Recall that relaxation Theorems 4.9.3 and 4.11.4 help in this case.

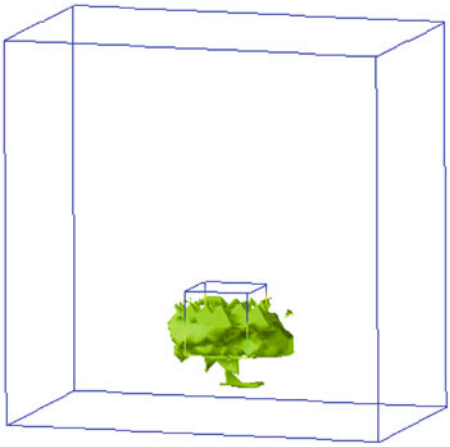

Fig. 5.10 The reconstruction result for the first stage of the adaptivity for the cube number 1. Maximal values of the imaged coefficient are shown for the third refined mesh. The shape is not yet well reconstructed, although a comparison with Fig. 5.8c shows an improvement. The refractive index is reconstructed accurately (Table 5.8). Source: L. Beilina and M.V. Klibanov, Reconstruction of dielectrics from experimental data via a hybrid globally convergent/adaptive inverse algorithm, *Inverse Problems*, 26, 125009, doi:10.1088/0266-5611/26/12/125009, 2010. © IOP Publishing. Reprinted with permission

Figure 5.12 displays the final image. Comparison of this figure with Fig. 5.10 shows an improvement of the image of the shape of the cube Number 1. Refractive indices are the same in both cases and are equal to the one computed by the approximately globally convergent algorithm.

5.9.5 *Reconstruction Results for the Cube Number 2*

Just as above, we took the function $\varepsilon_r^{glob}(x)$ as the starting point for iterations. The image of this function is displayed on on Fig. 5.8c. See (5.19) for parameters α, β_1, β_2. Since by the second line of Table 5.7 $\max \varepsilon_r^{glob}(x) = (1.79)^2 \approx 3.2$, then we took $d = 3.4$ in (5.4). Thus,

$$d = 3.4, \ \beta = 0.985,$$

where the number β is defined in (5.35). Hence, the admissible set of parameters is:

$$\varepsilon_r(x) \in C_M = \{1 \leq \varepsilon_r(x) \leq 4\}.$$

We now give the values of the parameter B_{cut} in (5.38). Let k be the number of the mesh refinement. We took

$$B_{\text{cut}} := B_{\text{cut}}(k) = \begin{cases} 0.91, \text{ for } k = 1, 2, \\ 1.1 \text{ for } k = 3, \\ 2 \text{ for } k > 3. \end{cases}$$

The stopping criterion for mesh refinements was the same as the one in Sect. 5.9.4.

5.9.5.1 The First Stage

Because of the above criterion, we have stopped on the third mesh refinement. The corresponding image is displayed on Fig. 5.12. Comparing with Fig. 5.8c, one can observe an improvement of the shape of the image. However, one can also see two disconnected inclusions on Fig. 5.12 instead of just one on Fig. 5.8c. In addition, the value of the refractive index is now $n = 1.59$, which is 12% less than the value of 1.79 listed in Table 5.7.

5.9.5.2 The Second Stage

We know from the image of Fig. 5.8c, which is obtained by the approximately globally convergent numerical method, that we have only one inclusion rather than two disconnected as ones on Fig. 5.12. In addition, we also know from Fig. 5.8c that this inclusion is located below the small upper inclusion imaged on Fig. 5.12. Hence, we have decided to refine mesh in the intersections of two subdomains $\Omega_1, \Omega_2 \subset \Omega$. The subdomain Ω_1 is defined as usual when the second mesh refinement recommendation is used:

$$\Omega_1 = \left\{ x \in \Omega : \overline{\varepsilon}_r(x) \geq 0.2 \max_{\overline{\Omega}} \overline{\varepsilon}_r(x) \right\}.$$

As to the subdomain Ω_2, this is a rectangular prism whose upper boundary is slightly below the lower boundary of the small inclusion imaged on Fig. 5.12. And the lower boundary of Ω_2 is slightly below the lower boundary of the larger inclusion imaged on Fig. 5.12.

Let $\Omega_3 = \Omega_1 \cap \Omega_2$. Then, our calculations show that

$$\Omega_3 = \{(x, y, z) \in [-0.6, 0.6] \times [-0.6, 0.6] \times [-1.8, -0.8]\}.$$

Thus, we refine mesh in neighborhoods of all points of the rectangular prism $\Omega_3 \subset \Omega$. The final image is displayed on Fig. 5.13. It is obtained after the third mesh refinement.

An excellent accuracy of the reconstruction of all three components for cube number 2 is evident from Fig. 5.13. These three components are location, shape, and refractive index.

5.9.6 Sensitivity to the Parameters α and β

We have tested the sensitivity of the image of Cube No. 2 to the choice of the regularization parameter $\alpha \in (0,1)$ in the Tikhonov functional (5.16) as well as to the choice of the parameter $\beta \in (0,1)$ on the third stage of data immersing. We have performed the following tests:

$$\beta = 0.985;\ \alpha = 0.001, 0.01, 0.1; \tag{5.40}$$

$$\beta = 0.5;\ \alpha = 0.001, 0.01, 0.1; \tag{5.41}$$

$$\beta = 0.1; \alpha = 0.001, 0.01, 0.1. \tag{5.42}$$

Results of these tests are displayed on Fig. 5.14. One can observe that, for any given value of β, the change of the regularization parameter α by the factor of 100 causes almost no change in imaging results. In addition, the change of the parameter β by the factor of $1.97 = 0.985/0.5$ affects results very insignificantly. Surprisingly, even for $\beta = 0.1$, we got almost the same visual quality of images as ones for $\beta = 0.5, 0.985$. However, the value of the imaged refractive index became 1.55 instead of the correct value of 1.78.

We conclude, therefore, that our procedure is quite stable with respect to changes of parameters α and β.

5.9.7 Additional Effort for Cube Number 1

We undertook an additional effort for cube number 1 on the adaptivity stage. Recall that the adaptivity requires solutions of state and adjoint problems on each iteration. Also, it was stated in Sect. 5.5 that in the case of these experimental data, our state problem is the problem (5.11). The main new element of this additional effort is that we use in (5.10) and (5.11) a higher frequency $\omega = 14$ instead of the previous one of $\omega = 7$. This is because $\omega = 14$ corresponds to the twice smaller dimensionless wavelength $2\pi/\omega \approx 0.45$. Indeed, the dimensionless size of cube number 1 is $0.8 \times 0.8 \times 0.8$ and $0.8/0.45 \approx 1.78 > 1$. On the other hand, $2\pi/7 \approx 0.897$ and $0.8/0.897 \approx 0.89 < 1$. In other words, we had less than one dimensionless wavelength per the side of cube number 1. However, in the new test, we have almost two wavelengths are per the side of this cube. Thus, we have conjectured that this new value of $\omega = 14$ might provide an image whose quality would be better than the one on Fig. 5.11.

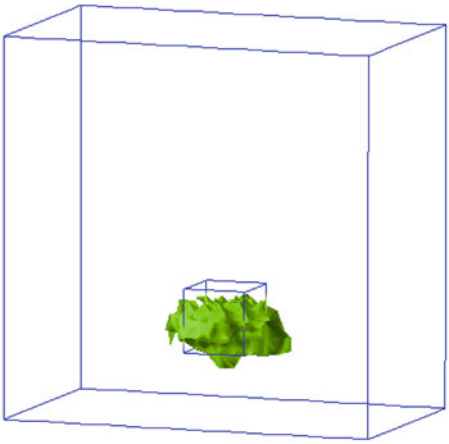

$$\varepsilon_{r,h} \approx 3.9, n_{glob} = \sqrt{\varepsilon_{r,h}} \approx 1.97$$

Fig. 5.11 The reconstruction result for the second stage of the adaptivity for the cube number 1. *Thin lines* (*blue*) indicate the correct cubical shape. Comparison with Fig. 5.10 shows an improvement of the image. The refractive index is reconstructed accurately (Table 5.8). Source: L. Beilina and M.V. Klibanov, Reconstruction of dielectrics from experimental data via a hybrid globally convergent/adaptive inverse algorithm, *Inverse Problems*, 26, 125009, doi:10.1088/0266-5611/26/12/125009, 2010. © IOP Publishing. Reprinted with permission

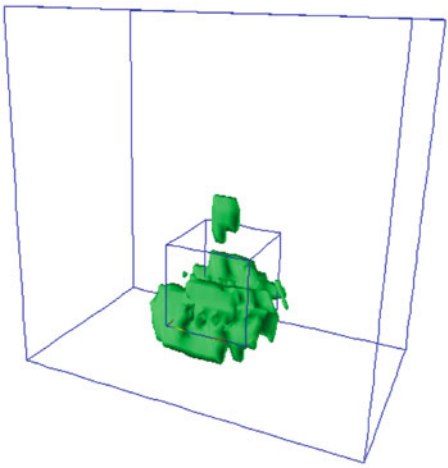

$$\varepsilon_{r,h} \approx 2.52, n_{glob} = \sqrt{\varepsilon_{r,h}} \approx 1.59$$

Fig. 5.12 The reconstruction result for the first stage of the adaptivity for the cube number 2. Only maximal values of the imaged coefficient are shown for the third refined mesh. The shape of the final imaged coefficient is better than one on Fig. 5.9c. However, the imaged refractive index is lowered by about 19% compared with the imaged on the globally convergent stage. Source: L. Beilina and M.V. Klibanov, Reconstruction of dielectrics from experimental data via a hybrid globally convergent/adaptive inverse algorithm, *Inverse Problems*, 26, 125009, doi:10.1088/0266-5611/26/12/125009, 2010. © IOP Publishing. Reprinted with permission

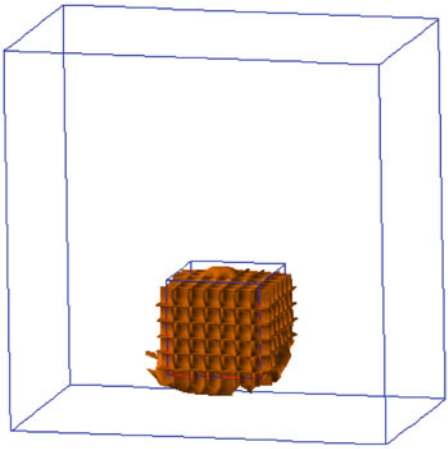

Fig. 5.13 The final reconstruction result for the cube number 2. Only the final, third mesh refinement, is shown. The imaged coefficient $\varepsilon_r(x) = 1$ outside of these images. All three components: shape, location, and refractive index are imaged with a very good accuracy. Source: L. Beilina and M.V. Klibanov, Reconstruction of dielectrics from experimental data via a hybrid globally convergent/adaptive inverse algorithm, *Inverse Problems*, 26, 125009, doi:10.1088/0266-5611/26/12/125009, 2010. © IOP Publishing. Reprinted with permission

First, we have simulated the data for the same inclusion as cube number1 is. In other words, we took the same location and size as ones listed in Table 5.7. Also, we took $\varepsilon_r = 4$ inside this inclusion and $\varepsilon_r = 1$ everywhere else. We have applied the same procedure as above to these computationally simulated data, starting from the approximately globally convergent method. The resulting image is displayed on Fig. 5.16a. A very good accuracy of reconstruction of location, shape, and refractive index is evident from Fig. 5.16a.

Next, we have applied the entire above procedure to the experimental data for cube number 1 with the new value of $\omega = 14$ in (5.10). Figure 5.16b displays the final resulting image of cube number 1. One can observe a significant improvement compared with Fig. 5.11.

Still, the image of Fig. 5.16b is not as perfect as the one of Fig. 5.13. We attribute this to the sizes of cubes 1 and 2. Indeed, the original wavelength of the signal in the experimental data was $\lambda = 3$ centimeters (cm). Hence, since the size of the side of cube number 1 is 4 cm, then its side is 1.33λ. On the other hand, the side of cube number 2 is 6 cm, which is 2λ. wavelengths. We conjecture that it is this difference of sizes which led to the difference of the quality of images of these two cubes.

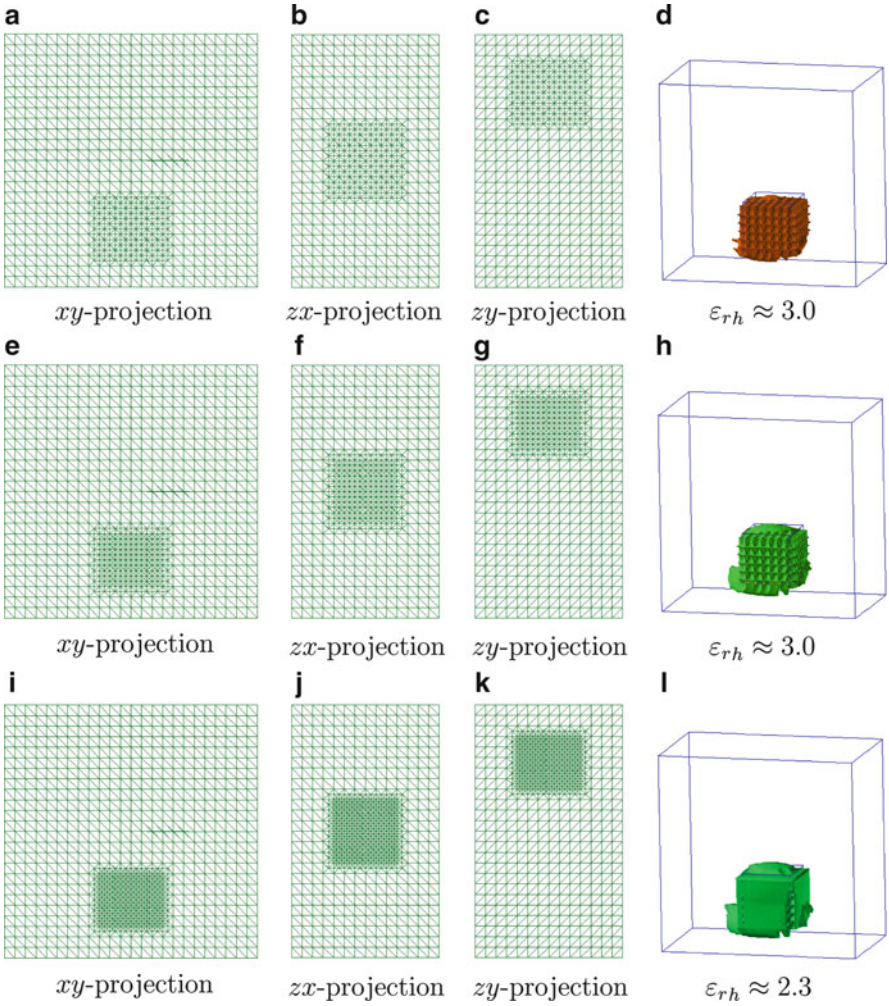

Fig. 5.14 Adaptively refined computational meshes in different projections and reconstruction results for cube number 2 with parameters $\beta = 0.985$ and $\alpha = 0.001$. *Lines* (*blue*) indicate the correct *cubical shape*. Maximal values of the imaged coefficient are displayed. The computed value of the coefficient outside of imaged inclusions is 1. We observe that a very good reconstruction is achieved on (**d**). The image on (**d**) is the same as the image on Fig. 5.13. This image is obtained after three mesh refinements. The same stopping criterion as the one in Sects. 4.15.3 and 4.16.2 was used. Relaxation Theorems 4.9.3 and 4.11.4 help in this case. On the other hand, (**h**) shows that reconstruction is stabilized, and (**l**) shows that the image deteriorates if one uses more mesh refinements than necessary, i.e., if one ignores that stopping criterion. Thus, (**d**) is our final image. Source: L. Beilina and M.V. Klibanov, Reconstruction of dielectrics from experimental data via a hybrid globally convergent/adaptive inverse algorithm, *Inverse Problems*, 26, 125009, doi:10.1088/0266-5611/26/12/125009, 2010.

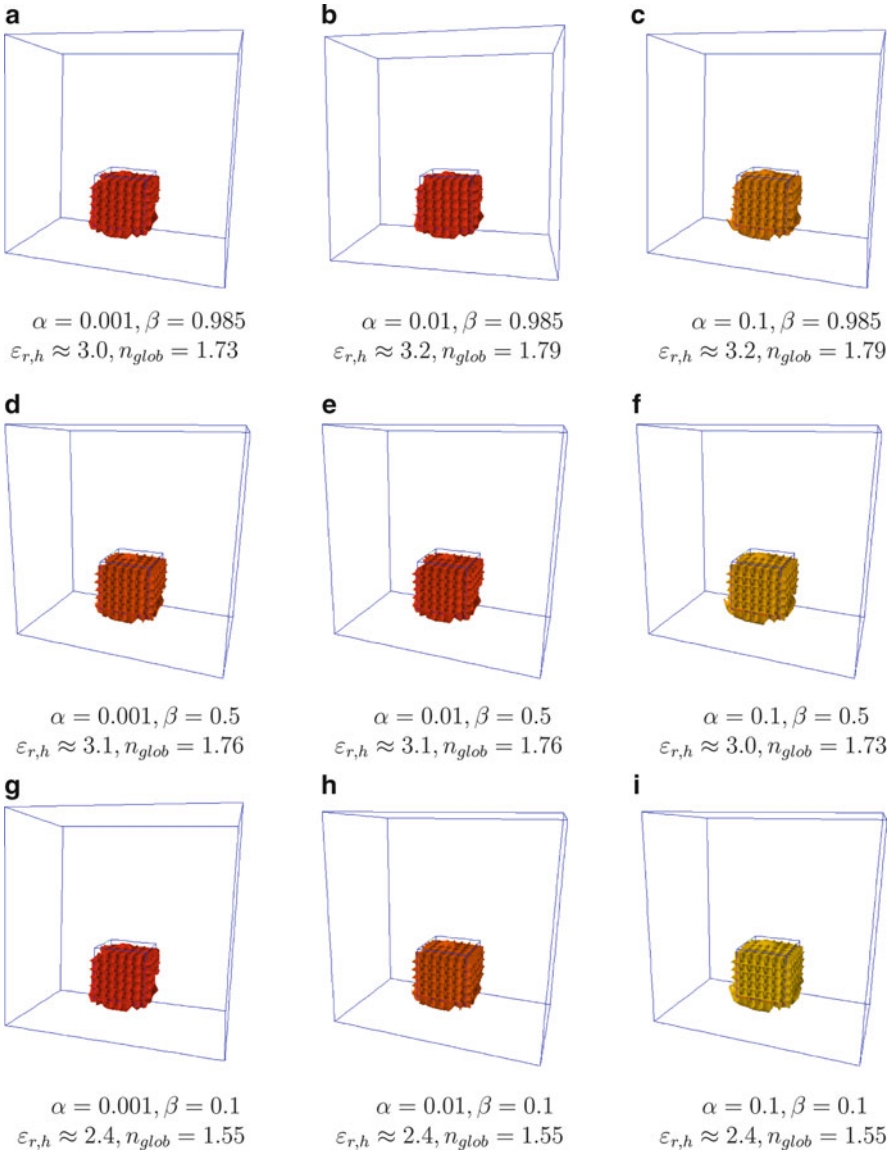

Fig. 5.15 Final reconstruction results for cube number 2 with varying parameters β and α. *Lines* (*blue*) indicate the correct cubical shape. Maximal values of the imaged coefficient are displayed. The computed value of the coefficient outside of imaged inclusions is 1. Source: L. Beilina and M.V. Klibanov, Reconstruction of dielectrics from experimental data via a hybrid globally convergent/adaptive inverse algorithm, *Inverse Problems*, 26, 125009, doi:10.1088/0266-5611/26/12/125009, 2010.

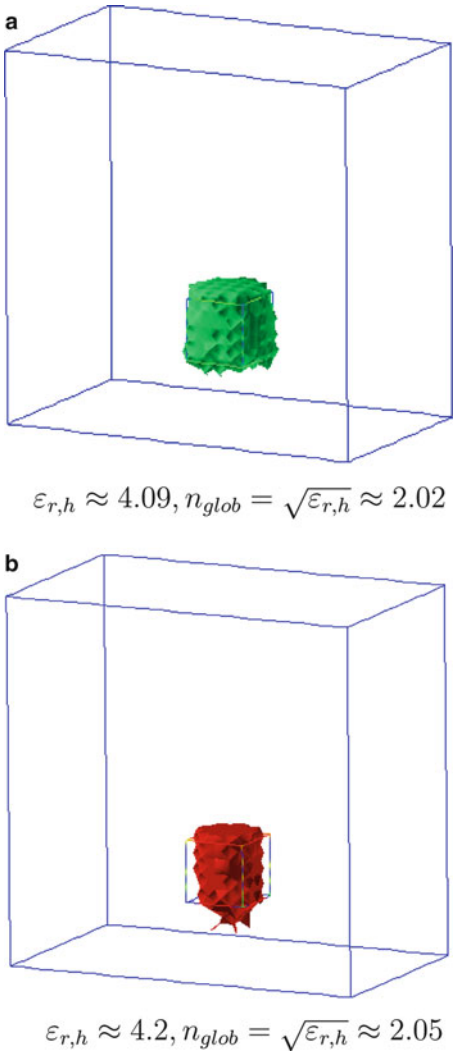

Fig. 5.16 (**a**) The image of computationally simulated cube number 1 from computationally simulated data with $\omega = 14$ in (5.10) and (5.11). (**b**) The image of cube number 1 from experimental data with $\omega = 14$ in (5.10) and (5.11). The same imaging procedure as above was applied. Compared with Fig. 5.11, a significant improvement is observed. Still, however, the image of the shape is not as good as the one for Cube number 2 on Fig. 5.13. Source: L. Beilina and M.V. Klibanov, Reconstruction of dielectrics from experimental data via a hybrid globally convergent/adaptive inverse algorithm, *Inverse Problems*, 26, 125009, doi:10.1088/0266-5611/26/12/125009, 2010. © IOP Publishing. Reprinted with permission

5.10 Summary

In this chapter, we have presented our work on experimental data of [28, 109]. The main difficulty of this work was caused by a **huge discrepancy** between experimentally measured and computationally simulated data. This discrepancy is not only due to the noise component, which is always present in any experimental data, but also due to a highly oscillatory behavior of experimentally measured curves, even for the case of the free space. On the other hand, computational simulations for the free space case do not show high oscillations. Thus, it is unclear

what kind of a PDE, if any, governs this process. We attribute this discrepancy to very small times at which experimental data were collected. Indeed, the time step between two consecutive readings was only $20\,\text{ps} = 2 \times 10^{-11}\,\text{s}$.

We have modeled this process by a single hyperbolic PDE (5.1), which is the same as (2.1). The Maxwell's system was not used. We believe that modeling by this system might lead to a better accuracy of results. Still, however, an analog of the above data pre-processing procedure should be used. Since only a single component of the electric field was measured and since the approximately globally convergent numerical method is not yet developed for CIPs for the Maxwell's system, then the above question should be left for future studies.

To handle the above huge discrepancy, a **crucial** step was a **radically new** data pre-processing procedure. This procedure consists in immersing the data in the mathematical model we are working with. We point out that the immersing procedure was **unbiased**. This is because our approximately globally convergent algorithm has worked with the most challenging case of **blind** experimental data, i.e., we did not know the answer in advance. The immersing procedure makes the data suitable to work with. This procedure consists of three stages. First two immersing stages were applied to work with the algorithm of Sect. 2.6.1. And the third stage was applied to make the data suitable for the adaptivity technique.

We had at least five (5) sources of error:

1. The natural noise in the experimental data.
2. The modeling noise, since it was unclear from the data analysis what kind of PDE, if any, governs the process.
3. The data pre-processing has contributed even more to the modeling noise.
4. In our theory, the coefficient $\varepsilon_r(x)$ should be sufficiently smooth. However, this function obviously had a discontinuity at the inclusion/medium interface.
5. The Maxwell's system was not used.

Nevertheless, we have consistently obtained an excellent accuracy of the reconstruction of both locations and refractive indices of dielectric inclusions in blind testing by the first stage of our two-stage numerical procedure. We point out that when applying the algorithm of Sect. 2.6.1, we were unbiased; see beginning of Sect. 5.7. The second stage has also resulted in an excellent reconstruction accuracy of locations and refractive indices of both cubes. In addition, the second stage has led to reconstructions of shapes of these cubes. The shape reconstruction accuracy was excellent for cube number 2, and it was very good for cube number 1. We conjecture that this difference of qualities is due to the difference of sizes of those cubes versus the wavelength λ of the EM wave we were operating with. Indeed, the size of the side of for 1 was 1.33λ versus to 2λ of cube number 2.

With reference to the two-stage numerical procedure, we have shown how important it is to use the approximately globally convergent algorithm on the first stage. Indeed, first, we have demonstrated that a modified gradient method of the minimization of the Tikhonov functional does not produce meaningful results, if it is taken alone, i.e., without the first stage algorithm of Sect. 2.6.1. Next, it is important for the third stage of data immersing to use the result obtained by the algorithm of

Sect. 2.6.1. In addition, we have shown that our adaptivity technique, being applied to these experimental data, is very stable with respect to the large changes of two key parameters: the regularization parameter α of the Tikhonov functional and the parameter β of the third stage of data immersing.

In summary, we repeat one thought of Sect. 5.1. Namely, it is quite surprising that, despite all these sources of error and especially despite the abovementioned huge misfit between experimentally measured and computationally simulated data, such a very good reconstruction accuracy was consistently observed. Finally, another interesting feature of results of this chapter is that this accuracy was obtained for the case when measurements were taken for a narrow view angle; see Fig. 5.1. We believe, therefore, that these results indicate a good degree of robustness of our algorithms. Finally, we believe that these results completely validate both first and second approximate mathematical models.

Chapter 6
Backscattering Data

In Sects. 6.1–6.8 we describe results of [115]. As to the numerical results of Sect. 6.8, Figs. 6.2a, b were published in *Methods and Applications of Analysis* [116] and are reprinted with permission. Other figures of this chapter were not published elsewhere.

6.1 Introduction

In Chaps. 2–5 we have considered the case of the so-called "complete data". In other words, the data were given at the entire boundary of the domain of interest. In the case of the experimental data of Chap. 5 only transmitted data were given, although they were measured on the transmitted side only and only for a very narrow view angle. Thus, we have worked with incomplete data in Chap. 5. However, the most interesting case of incomplete data is the case when they are given at the backscattering side of the medium. The case of the backscattering data is especially interesting in military applications. In this chapter we model the most suitable arrangement for this case, which is to use a single position of the point source and to measure only the backscattering signal. The target application of this chapter is in imaging of plastic antipersonnel land mines.

In the case of backscattering data, we have both Dirichlet and Neumann boundary conditions at the backscattering part of the boundary. These are informative conditions, since they depend on the unknown coefficient. The Dirichlet boundary condition models the result of measurements. The Neumann boundary condition can be calculated, as soon as the Dirichlet condition is known. As to the rest of the boundary, we have only the radiation condition. This one is a noninformative boundary condition since it is independent on the unknown coefficient. Hence, we use this noninformative condition only for a better stability of our algorithm.

Because of the overdetermination in the boundary conditions on the backscattering side, the idea is to use the quasi-reversibility method (QRM). Hence, the major part of this chapter is devoted to the version of the approximately globally

L. Beilina and M.V. Klibanov, *Approximate Global Convergence and Adaptivity for Coefficient Inverse Problems*, DOI 10.1007/978-1-4419-7805-9_6,

convergent method for the case when the QRM solves (2.49) for functions $q_{n,i}$ (Sect. 2.6.1). Theorem 6.7 is the central theorem of this chapter. Remarks 2.9.4 can be reformulated for this case. In addition, we present in this chapter our most recent computational result. In this result, only the Dirichlet boundary condition is used on the backscattering side of the boundary, and the zero Dirichlet boundary condition for functions $q_{n,i}$ is assigned on the rest of the boundary. With reference to the QRM, we present analytical results of [115] as well as some numerical results in 2D and 3D cases. In particular, the 2D computational result was published in [116]. The 3D result of this chapter was not published before. Computations in 2D were carried out by Dr. Andrey V. Kuzhuget with a help from both authors of this book, and the 3D result was computed by Dr. Natee Pantong with a help from both A.V. Kuzhuget and the second author.

In Sect. 6.9, we present results of our work with **blind** experimental data, which were collected by a forward looking radar of the US Army Research Laboratory (ARL); see [126] for a description of this radar. The ARL data were kindly provided to us, along with the permission to use in this book, by Drs. Lam Nguyen and Anders Sullivan, who work for ARL. The corresponding joint work is [117]. The ARL data were collected in the field, unlike the experimental data of Chap. 5, which were collected in a laboratory. Computations for this case were performed by Dr. A. V. Kuzhuget with a help from the authors of this book.

Because of the structure of these experimental data, only 1D inverse algorithms have a chance to succeed in this case; see Sect. 6.9.2. Thus, we have applied the 1D version of our algorithm [114]. The 1D version of our approximately globally convergent numerical method was initially considered in [114] "only as a preliminary step before applying similar ideas to 2D and 3D cases" (see p. 125 of [114]). This version is based on some approximations, similar with ones of Sect. 6.6.2. On the other hand, 1D numerical methods of [40, 47, 51, 56, 90] do not use approximations like ours, and they also do not need a priori given good first guess for the solution. Our experimental data have a number of uncertainties listed in Sect. 6.9.4. One of examples of such an uncertainty is the 1D modeling of the 3D process. Hence, because of these uncertainties, it is yet unclear how techniques of [40, 47, 51, 56, 90] would perform for these experimental data. The question of comparison of the performance of some of these algorithms with ours for our experimental data is outside of the scope of the current book.

The QRM was first proposed by R. Lattes and J.-L. Lions in their joint book [121]. Carleman estimates were not used for the convergence analysis in this book. It was shown later in [105] that the tool of Carleman estimates is a quite suitable one for proofs of convergence theorems for the QRM. The latter tool was used in a number of publications since then, where analytical results for the QRM were combined with computational ones; see, for example, [49, 59, 102, 106–108].

The QRM is designed to find approximate solutions of ill-posed problems for PDEs, for example, Cauchy problem for the Laplace equation. In particular, it can handle boundary value problems for PDEs with overdetermined boundary conditions, and the backscattering data indeed generate this problem for each

function $q_{n,i}$ in (2.49). The QRM minimizes the Tikhonov functional. However, instead of the traditionally case of a continuous operator, the Tikhonov functional for the QRM is generated by the linear operator of the corresponding PDE, and this operator is unbounded of course. A good feature of the QRM is that the uniqueness and existence of the minimizer (i.e., the regularized solution) for this case follows immediately from the Riesz theorem. However, the question of convergence of regularized solutions to the exact one is much more delicate, and it is usually addressed via a Carleman estimate.

While the QRM was applied only to linear problems in [49,59,102,106–108], our CIP is nonlinear. This causes the major difficulty, compared with previous works. Indeed, the QRM is applied only once in the linear case. Unlike this, we need to apply the QRM on each iteration. However, these iterations cause significant new difficulties in the convergence analysis. Addressing these difficulties is the major new point of the convergence analysis of this chapter.

6.2 Forward and Inverse Problems

First, we pose the forward and inverse problems. Below, $x = (x_1, x_2, x_3) \in \mathbb{R}^3$. The forward problem is the same as the problem (2.1) and (2.2) in Sect. 2.1:

$$c(x) u_{tt} = \Delta u \text{ in } \mathbb{R}^3 \times (0, \infty), \tag{6.1}$$

$$u(x, 0) = 0, u_t(x, 0) = \delta(x - x_0). \tag{6.2}$$

We impose the same conditions on the coefficient $c(x)$ as (2.3), (2.4) in Sect. 2.1, except that we require a little bit higher smoothness. Let $\Omega \subset \mathbb{R}^3$ be a convex bounded domain with the piecewise smooth boundary $\partial\Omega$. We assume that

$$c(x) \in [1, d], \ c(x) = 1 \text{ for } x \in \mathbb{R}^3 \backslash \Omega, \tag{6.3}$$

$$c(x) \in C^4\left(\mathbb{R}^3\right). \tag{6.4}$$

Everywhere below, $\alpha = \text{const.} \in (0, 1)$. It is convenient for our derivations to introduce the following set $\mathbb{M}$ of functions:

$$\mathbb{M} = \left\{c \in C^{\alpha}\left(\mathbb{R}^3\right) : \text{conditions (6.3) hold}\right\}. \tag{6.5}$$

To simplify the presentation and also because of our target application, we now specify the domain $\Omega \subset \mathbb{R}^3$ as follows; see Fig. 6.1. Let $P > 0$ be a constant. Below,

$$\Omega = \{x : -P < x_1, x_2 < P, x_3 \in (0, 2P)\}, \partial\Omega = \cup_{i=1}^{3} \Gamma_i, \tag{6.6}$$

$$\Gamma_1 = \{x : -P < x_1, x_2 < P, x_3 = 0\}, \tag{6.7}$$

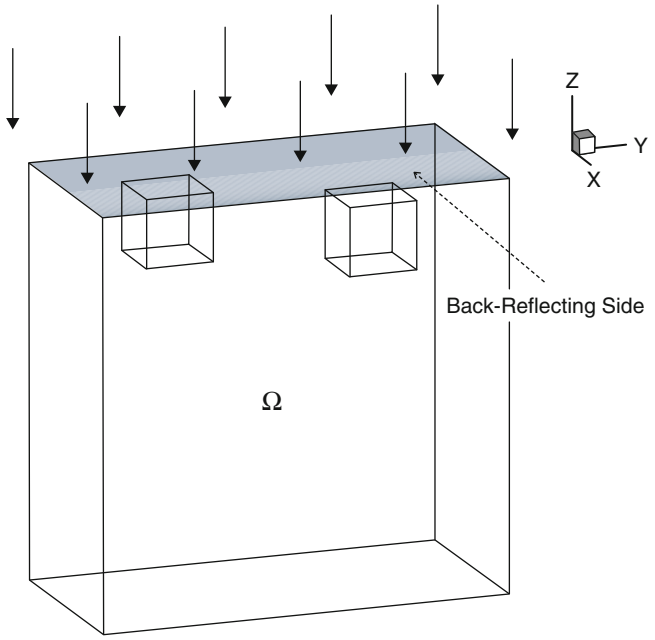

Fig. 6.1 Schematic diagram of data collection in the backscattering case. The incident plane wave falls from the top, and the back reflected data are collected on the top boundary as well

$$\Gamma_2 = \{x : x_1, x_2 = \pm P, x_3 \in (0, 2P)\}, \tag{6.8}$$

$$\Gamma_3 = \{x : -P < x_1, x_2 < P, x_3 = 2P\}. \tag{6.9}$$

Coefficient Inverse Problem 6.2. *Suppose that the coefficient $c(x)$ in (6.1) satisfies conditions (6.3), (6.4) and is unknown in the domain Ω. Determine the coefficient $c(x)$ for $x \in \Omega$, assuming that the following functions $g_0(x,t)$ and $g_1(x,t)$ are known for a single source position $x_0 \in \{x_3 < 0\}$:*

$$u(x,t)|_{\Gamma_1} = g_0(x,t),\ u_{x_3}(x,t)|_{\Gamma_1} = g_1(x,t), t \in (0,\infty). \tag{6.10}$$

Since $x_0 \in \{x_3 < 0\}$, then it follows from (6.6), (6.7), (6.8), and (6.9) that Γ_1 is the backscattering side. Hence, (6.10) models measurements of the backscattering data. In experiments, usually only the function $g_0(x,t)$ is measured. One can approximately assume that this function is known at the entire plane $\{x_3 = 0\}$. Next, since by (6.3) and (6.6) the coefficient $c(x) = 1$ for $x_3 < 0$, then solving the forward problem (6.1), (6.2) in the half space $\{z < 0\}$ with the boundary condition $u(x,t)\ |_{x_3=0} = g_0(x,t)$, one can uniquely determine the function $u(x,t)$ for $x_3 < 0, t > 0$, which gives the function $g_1(x,t)$.

6.3 Laplace Transform

In the case of the backscattering data, we work with an analog of the algorithm of Sect. 2.6.1. An essential difference, however, is that two boundary conditions (6.10) generate overdetermined boundary conditions for functions $q_{n,i}$ in (2.49). This overdetermination, in turn leads to the QRM. To derive (2.49), we have performed in Sect. 2.3 the Laplace transform (2.10) first. Thus, consider the function w defined by

$$w(x,s) = \int_0^\infty u(x,t)\mathrm{e}^{-st}\mathrm{d}t, \text{ for } s \geq \underline{s} = \text{const.} > 0, \tag{6.11}$$

where $\underline{s} > 0$ is a certain number. In our numerical studies, we choose $\underline{s}$ experimentally. We call the parameter s *pseudo-frequency*. The function w satisfies the following conditions:

$$\Delta w - s^2 c(x) w = -\delta(x - x_0), \ x \in \mathbb{R}^3, \forall s \geq \underline{s}, \tag{6.12}$$

$$\lim_{|x|\to\infty} w(x,s) = 0, \forall s \geq \underline{s}. \tag{6.13}$$

The condition (6.13) for sufficiently large $\underline{s} = \underline{s}(c)$ was established in Theorem 2.7.1 Theorem 2.7.2 provides more properties of the solution of the problem (6.12), (6.13). In particular, it follows from this theorem that if $c \in \mathbb{M}$, where the set $\mathbb{M}$ is defined in (6.5), then for every $s > 0$, there exists unique solution w of the problem (6.12), (6.13) of the form

$$w = w_1 + \overline{w}, \text{ where } \overline{w} \in C^{2+\gamma}\left(\mathbb{R}^3\right), \tag{6.14}$$

$$w_1(x,s) = \frac{\exp(-s|x - x_0|)}{4\pi|x - x_0|}. \tag{6.15}$$

The function w_1 solves the problem (6.12), (6.13) for the case $c(x) \equiv 1$.

Having the data at only one side Γ_1 of the cube Ω is not sufficient for a good stability of the numerical solution. To provide a better stability, we now derive an approximate boundary condition for the function $\ln w$ at the rest $\Gamma_2 \cup \Gamma_3$ of the boundary $\partial\Omega$. It follows from (6.15) and (2.101) that the function w satisfies the radiation condition at the infinity, $\lim_{|x|\to\infty}\left(\partial_{|x|}w + sw\right)(x) = 0$, where $\partial_{|x|}w := \partial_r w$ is understood in terms of spherical coordinates with the radius $r := |x - x_0|$. Hence, assuming that the number P in (6.6)–(6.9) is sufficiently large, we impose the following *approximate* boundary condition at $\Gamma_2 \cup \Gamma_3$L:

$$(\partial_n w + sw)|_{\Gamma_2\cup\Gamma_3} = 0. \tag{6.16}$$

It follows from (6.16) that

$$\partial_n(\ln w(x,s))|_{\Gamma_2\cup\Gamma_3} = -s. \tag{6.17}$$

Actually, condition (6.17) is not an informative one. This is because it is independent on the target coefficient $c(x)$. Hence, it is logical to use (6.17) only for a better stability of the algorithm.

We have verified the *approximate* boundary condition (6.16) computationally, both in 3D and 2D cases, as follows. For a variety of cases modeling our target application to imaging of antipersonnel plastic land mines (Sect. 6.1), we have computationally solved the forward problem for (6.12) in a domain $\widehat{\Omega}$, which was much larger than the domain Ω in (6.6), $\Omega \subset \widehat{\Omega}, \partial\Omega \cap \partial\widehat{\Omega} = \varnothing$. Because of (6.13), we have imposed the zero Dirichlet boundary condition at $\partial\widehat{\Omega}$. Next, we have solved (6.12) in the domain Ω with the boundary condition (6.16) at $\Gamma_2 \cup \Gamma_3$. As to Γ_1, we have used the Dirichlet boundary condition, which was calculated from the above solution of the forward problem in $\widehat{\Omega}$. When doing so, we have used the same values of the parameter s for which we have numerically solved our inverse problem. Comparison of these two solutions has consistently revealed that in a subdomain $\widetilde{\Omega} \subset \Omega$, whose boundary had a small distance from $\Gamma_2 \cup \Gamma_3$, these two solutions have almost coincided. Thus, the above provides a numerical justification for the approximation (6.16).

Remark 6.3. A heuristic explanation of a low sensitivity of the function $w(x,s)$ to the choice of boundary conditions at $\Gamma_2 \cup \Gamma_3$ is the following. Consider two arbitrary points $x_1 \neq x_0$ and $x_2 \neq x_0$ with $|x_2 - x_0| > |x_1 - x_0|$. Then, the function

$$f(x_2, s) = \frac{w_1(x_2, s)}{w_1(x_1, s)}$$

decays exponentially as $|x_2 - x_1| \to \infty$, and the point x_1 is fixed. In terms of practical computations of the CIP 6.2, this means that one can use such a boundary condition for the function w at $\Gamma_2 \cup \Gamma_3$ which provides best computational results. On the other hand, this condition will always be a noninformative one. We also refer to Chap. 5 for an analogy, since we have assigned in this chapter a noninformative boundary condition to those five sides of the prism Ω where experimental data were not collected.

6.4 The Algorithm

6.4.1 Preliminaries

The algorithm is similar with the algorithm of Sect. 2.6.1. Therefore, we are rather brief in Sects. 6.4.1 and 6.4.2. However, an essential difference is in the method of solving of (2.49). Indeed, while the problem (2.49), (2.50) is the Dirichlet boundary value problem, which we solve via the FEM, in the case of backscattering data,

(2.50) is replaced with overdetermined boundary conditions. The overdetermination is generated by two functions $g_0(x,t)$ and $g_1(x,t)$ instead of just one in (2.5) for the coefficient inverse problem 2.1.

Quite often, in applications, one can assume that actually, the coefficient $c(x) = 1$ for $x \in \mathbb{R}^3 \backslash G$ where $G \subset \Omega$ is such a subdomain of Ω which is a little bit smaller than the domain of interest Ω. We are doing this here for the sake of convenience of the convergence analysis. Let $P_2 = \text{const.} \in (0, P)$. Denote $\Omega_{P_2} = \Omega \cap \{x_3 \in (0, P_2)\}$. We assume below that $c(x) = 1$, $\forall x \in \mathbb{R}^3 \backslash \Omega_{P_2}$. Consider a subdomain $\Omega' \subset \Omega_{P_2}$ with $\partial\Omega' \cap \partial\Omega_{P_2} = \varnothing$. Choose a function $\chi_1(x) \in C^3\left(\mathbb{R}^3\right)$ such that

$$\chi_1(x) = \begin{cases} 1 \text{ in } \Omega', \\ \text{between 0 and 1 in } \Omega_{P_2} \backslash \Omega', \\ 0 \text{ outside of } \Omega_{P_2}. \end{cases}$$

Next, let $\chi_2(x)$ be the characteristic function of the domain Ω_{P_2}:

$$\chi_2(x) = \begin{cases} 1 \text{ in } \Omega_{P_2}, \\ 0 \text{ outside of } \Omega_{P_2}. \end{cases}$$

Let $c_{n,k}(x)$, $x \in \Omega$ be the function reconstructed by the algorithm described below. Then, by (6.34) and (6.35),

$$c_{n,k} \in [1, d], \ c_{n,k} \in C^{\gamma}\left(\overline{\Omega}\right). \tag{6.18}$$

Similarly with Sect. 2.6, we extend the function $c_{n,i}(x)$ in the entire space $\mathbb{R}^3$ as

$$\widehat{c}_{n,k}(x) := (1 - \chi_1(x)) + \chi_1(x)\, c_{n,k}(x), \forall x \in \mathbb{R}^3. \tag{6.19}$$

Then it follows from (6.5), (6.18), and (6.19) that

$$\widehat{c}_{n,k} \in \mathbb{M}. \tag{6.20}$$

We work below only with the function $w(x,s), s > 0$. Let in (6.12) the coefficient $c \in \mathbb{M}$. Then Theorem 2.7.2 implies that there exists unique solution $w(x,s)$ of the problem (6.12), (6.13) satisfying conditions (6.14) and (6.15). Furthermore, $w(x,s) > 0$ for $x \neq x_0$. Hence, similarly with Sect. 2.3, we consider functions $v(x,s), q(x,s)$ defined as

$$v(x,s) = \frac{\ln w(x,s)}{s^2}, \ q(x,s) = \frac{\partial v(x,s)}{\partial s}. \tag{6.21}$$

Hence,

$$\Delta v + s^2 (\nabla v)^2 = c(x), \ x \in \Omega. \tag{6.22}$$

Assume that we work on the interval $s \in [\underline{s}, \overline{s}]$. Hence,

$$v(x,s) = -\int_s^{\overline{s}} q(x,\tau)\, d\tau + V(x),$$

$$V(x) := V(x,\overline{s}) = \frac{\ln w(x,\overline{s})}{\overline{s}^2}, \tag{6.23}$$

where $V(x)$ is the tail function. Assuming that conditions of Lemma 2.3 hold, we have the asymptotic behavior similar with the one of Sect. 2.3:

$$\|V(x,\overline{s})\|_{C^{2+\gamma}(\overline{\Omega})} = O\left(\frac{1}{\overline{s}}\right), \ \overline{s} \to \infty, \tag{6.24}$$

$$\|q(x,\overline{s})\|_{C^{2+\gamma}(\overline{\Omega})} = O\left(\frac{1}{\overline{s}^2}\right), \ \overline{s} \to \infty. \tag{6.25}$$

6.4.2 The Sequence of Elliptic Equations

Considering the partition of the interval $[\underline{s}, \overline{s}]$ into N small subintervals of the length h,

$$\underline{s} = s_N < s_{N-1} < \ldots < s_0 = \overline{s}, \ s_{i-1} - s_i = h,$$

assuming that the function $q(x,s)$ is constant with respect to s in each of these subintervals, $q(x,s) := q_n(x)$, $s \in (s_n, s_{n-1}]$ and using the s-dependent CWF (2.38), we obtain similarly with Sect. 2.5 and 2.6.1 the following sequence of elliptic equations, which is similar with (2.49):

$$\Delta q_{n,k} - A_{1,n}\left(\chi_2(x)\, h \sum_{j=0}^{n-1} \nabla q_j - \nabla V_{n,k}\right) \nabla q_{n,k}$$

$$= -A_{2,n} h^2 \left(\sum_{j=0}^{n-1} \nabla q_j\right)^2 \chi_2(x) + 2A_{2,n} \nabla V_{n,k} \left(h \sum_{j=0}^{n-1} \nabla q_j\right) \chi_2(x)$$

$$-A_{2,n} (\nabla V_{n,k})^2, x \in \Omega, (n,k) \in [1,N] \times [1,m]. \tag{6.26}$$

Here,

$$q_0 := \equiv 0. \tag{6.27}$$

In (6.26), m is the number of iterations with respect to tails. We fix this number in the algorithm of this section. Boundary conditions for functions $q_{n,k}$ are

$$q_{n,k}|_{\Gamma_1} = \psi_{0,n}(x),\ \partial_{x_3} q_{n,k}|_{\Gamma_1} = \psi_{1,n}(x),\ \partial_n q_{n,k}|_{\Gamma_2 \cup \Gamma_3} = \frac{1}{s_n s_{n-1}}. \tag{6.28}$$

The third boundary condition (6.28) is obtained as follows. One can derive from (6.17) that

$$\partial_n q\,(x,s)\,|_{\Gamma_2 \cup \Gamma_3} = \frac{1}{s^2}. \tag{6.29}$$

Next, averaging over the interval (s_n, s_{n-1}) gives

$$\partial_n q_n|_{\Gamma_2 \cup \Gamma_3} = \frac{1}{h} \int\limits_{s_n}^{s_{n-1}} \frac{\mathrm{d}s}{s^2} = \frac{1}{s_n s_{n-1}}.$$

We assign then

$$\partial_n q_n|_{\Gamma_2 \cup \Gamma_3} := \frac{1}{s_n s_{n-1}}.$$

Functions $\psi_{0,n}(x)$ and $\psi_{1,n}(x)$ in (6.28) are obtained as follows. Let $\overline{g}_0(x,s)$ and $\overline{g}_1(x,s)$ be Laplace transforms (6.11) of functions $g_0(x,t)$ and $g_1(x,t)$, respectively. Then

$$w\,(x,s)\,|_{\Gamma_1} = \overline{g}_0\,(x,s)\,,\ \partial_n w\,(x,s)\,|_{\Gamma_1} = \overline{g}_1\,(x,s)\,.$$

Hence,

$$q\,(x,s)\,|_{\Gamma_1} = \frac{\partial}{\partial s}\left(\frac{\ln \overline{g}_0\,(x,s)}{s^2}\right) := \psi_0\,(x,s)\,, \tag{6.30}$$

$$\partial_n q\,(x,s)\,|_{\Gamma_1} = \frac{\partial}{\partial s}\left(\frac{\overline{g}_1\,(x,s)}{s^2 \overline{g}_0\,(x,s)}\right) = \psi_1\,(x,s)\,. \tag{6.31}$$

Thus, we set

$$\psi_{0,n}(x) = \frac{1}{h} \int\limits_{s_n}^{s_{n-1}} \psi_0\,(x,s)\,\mathrm{d}s,\ \psi_{1,n}(x) = \frac{1}{h} \int\limits_{s_n}^{s_{n-1}} \psi_1\,(x,s)\,\mathrm{d}s,\ x \in \Gamma_1.$$

In (6.26), $A_{1,n}, A_{2,n}$ are the same numbers as ones in Sect. 2.6.1.

There are three differences between (6.26) and (2.49). First, the nonlinear term $2\,(\nabla q_{n,k-1})^2\,(I_{1n}/I_0)$ is not present in (6.26), unlike (2.49). This is because this term is negligible for the case when in (2.38) $\lambda h \gg 1$; see (2.40). We have indeed discovered in our numerical studies that this term provides a very small impact in solutions of CIPs. We point out, however, that neglecting this term does not mean a linearization. Indeed, the nonlinear nature of the problem still surfaces in

terms containing ∇q_j as well as in gradients of tails $\nabla V_{n,k}$ in (6.26). Tails depend nonlinearly from functions $c_{n,k}$. The second difference between (6.26) and (2.49) is in the presence of the function $\chi_2(x)$ in (6.26), unlike (2.49). We need this presence for our convergence analysis. Finally, the third difference is in the absence of the term $-\varepsilon q_{n,k}$ in the left-hand side of (6.26), unlike (2.49).

6.4.3 The Iterative Process

First, we choose an initial tail function $V_{1,1}(x) \in C^{2+\gamma}\left(\overline{\Omega}\right)$. This can be either $V_{1,1}(x) \equiv 0$ or the function which corresponds to the solution of the problem (6.12), (6.13) for the case $c(x) \equiv 1$, which corresponds to the value of the function $c(x)$ outside the domain of interest Ω; see (6.3), or the choice described in Sect. 6.6.2; see (6.99), (6.100), and (6.101). These choice in our numerical studies are specified in Tests 1 and 2 of Sect. 6.8.4. Let $m \geq 1$ be an integer which we choose in numerical experiments. For each $n \in [1, N]$, we have m inner iterations with respect to the tails via computing functions $q_{n,k}, V_{n,k}, k \in [1, m]$.

Step n_k, where $n \in [1, N], k \in [1, m]$. Recall that by (6.27), $q_0 \equiv 0$. Suppose that functions $q_j \in H^5(\Omega), j \in [1, n-1]$ and tails $V_1, \ldots, V_{n-1}, V_{n,k} \in C^{2+\gamma}\left(\overline{\Omega}\right)$ are constructed. To construct the function $q_{n,k}$, we use the QRM described in Sect. 6.4.4. Hence, we obtain the function $q_{n,k} \in H^5(\Omega)$. To reconstruct an approximation $c_{n,k}(x)$ for the function $c(x)$, we first use the following discrete analogs of (6.22) and (6.23):

$$v_{n,k}(x, s_n) = -hq_{n,k}(x) - h\sum_{j=0}^{n-1} q_j(x) + V_{n,k}(x), x \in \Omega_{P_2}, \tag{6.32}$$

$$\overline{c}_{n,k}(x) = \Delta v_{n,k}(x, s_n) + s_n^2 \left|\nabla v_{n,k}(x, s_n)\right|^2, x \in \Omega_{P_2}. \tag{6.33}$$

Since we need (6.20), then, following (6.5), we set

$$c_{n,k}(x) = \begin{cases} \overline{c}_{n,k}(x), \text{ if } \overline{c}_{n,k}(x) \in [1, d], x \in \Omega_{P_2}, \\ 1, \text{ if } \overline{c}_{n,k}(x) < 1, x \in \Omega_{P_2}, \\ d, \text{ if } \overline{c}_{n,k}(x) > d, x \in \Omega_{P_2}. \end{cases} \tag{6.34}$$

Since functions $q_j, q_{n,k} \in H^5(\Omega)$, then the embedding theorem implies that $q_j, q_{n,k} \in C^3\left(\overline{\Omega}\right)$. In addition, the tail function $V_{n,k} \in C^{2+\gamma}\left(\overline{\Omega}\right)$. Hence, (6.32), (6.33), and (6.34) imply that

$$c_{n,k} \in C^{\gamma}\left(\overline{\Omega}_{P_2}\right). \tag{6.35}$$

Next, we construct the function $\widehat{c}_{n,k}(x)$ in (6.19). Hence, (6.34) and (6.35) imply (6.20).

Next, we solve the forward problem (6.12), (6.13) with $c(x) := \widehat{c}_{n,k}(x)$ for $s := \overline{s}$ and obtain the function $w_{n,k}(x,\overline{s})$. Both existence and uniqueness of the function $w_{n,k}(x,\overline{s})$ in the form (6.14), (6.15) are guaranteed by Theorem 2.7.2. We set for the new tail

$$V_{n,k+1}(x) = \frac{\ln w_{n,k}(x,\overline{s})}{\overline{s}^2} \in C^{2+\gamma}\left(\overline{\Omega}\right) \text{ if } k < m. \tag{6.36}$$

We also set

$$c_n(x) := c_{n,m}(x),\ q_n(x) := q_{n,m}(x),\ x \in \Omega, \tag{6.37}$$

$$V_n(x) := V_{n+1,1}(x) := V_{n,m+1}(x) := \tfrac{\ln w_{n,m}(x,\overline{s})}{\overline{s}^2},\ x \in \Omega. \tag{6.38}$$

6.4.4 The Quasi-Reversibility Method

Denote

$$a_{n,k}(x) = A_{1,n}\left(\chi_2(x)\, h \sum_{j=0}^{n-1} \nabla q_j - \nabla V_{n,k}\right), \tag{6.39}$$

$$H_{n,k}(x) = -A_{2,n}h^2\left(\sum_{j=0}^{n-1}\nabla q_j\right)^2 \chi_2(x) + 2A_{2,n}\nabla V_{n,k}\left(h\sum_{j=0}^{n-1}\nabla q_j\right)\chi_2(x)$$
$$-A_{2,n}\left(\nabla V_{n,k}\right)^2. \tag{6.40}$$

Note that the function $H_{n,k} \in L_2(\Omega)$. Because of (6.39), (6.40), the overdetermined boundary value problem (6.26), (6.28) can be rewritten as

$$\Delta q_{n,k} - a_{n,k}\nabla q_{n,k} = H_{n,k}, \tag{6.41}$$

$$q_{n,k}|_{\Gamma_1} = \psi_{0,n}(x),\ \partial_{x_3} q_{n,k}|_{\Gamma_1} = \psi_{1,n}(x),\ \partial_n q_{n,k}|_{\Gamma_2\cup\Gamma_3} = \tfrac{1}{s_n s_{n-1}}. \tag{6.42}$$

Since we have two boundary conditions rather then one at Γ_1, we find the "least squares" solution of the problem (6.41), (6.42) via the QRM. Specifically, we minimize the following Tikhonov functional

$$J^{\alpha}_{n,k}(u) = \frac{1}{2}\|\Delta u - a_{n,k}\nabla u - H_{n,k}\|^2_{L_2(\Omega)} + \frac{\alpha}{2}\|u\|^2_{H^5(\Omega)}, \tag{6.43}$$

subject to the boundary conditions (6.42). Here, $\alpha \in (0,1)$ is a small regularization parameter. Let $\overline{u}(x)$ be the unique minimizer of this functional, the existence of which is guaranteed by Lemma 6.5.2. Then we set $q_{n,k}(x) := \overline{u}(x)$. Local minima do not occur here since (6.43) is the sum of square norms of two expressions, both of which are linear with respect to u. The second term in the right-hand side of (6.43) is the Tikhonov regularization term. We use the $H^5(\Omega)$-norm here in order to ensure that the minimizer $u := q_{n,k} \in C^3\left(\overline{\Omega}\right)$. It was shown in Sect. 6.4.3 that the latter implies (6.35) and, therefore, (6.20). We call the minimizer $\overline{u}(x)$ of the functional $J^{\alpha}_{n,k}(u)$ *the QRM solution of the problem (6.41), (6.42).*

6.5 Estimates for the QRM

In this section, we temporary denote $x = (x,y,z)$. Although x denotes here both the vector and its first component, it will be always clear from the context what exactly x is in any particular place. It is convenient to scale variables in such a way that in (6.6)–(6.9) $P = 1/2$. Thus, in Sects. 6.5–6.7,

$$\Omega = \left\{x = (x,y,z) : (x,y) \in \left(-\frac{1}{4},\frac{1}{4}\right) \times \left(-\frac{1}{4},\frac{1}{4}\right),\ z \in \left(0,\frac{1}{2}\right)\right\}. \tag{6.44}$$

Below in Sects. 6.5–6.7, $C > 0$ denotes different generic constants which depend only on the domain Ω in (6.44), $(\cdot,\cdot)$ denotes the scalar product in $L_2(\Omega)$, and $[\cdot,\cdot]$ denotes the scalar product in $H^5(\Omega)$.

Let $\lambda, \nu > 2$ be two parameters. Introduce the z-dependent CWF $K(z)$:

$$K(z) := K_{\lambda,\nu}(z) = \exp(\lambda \rho^{-\nu}),\ \text{where } \rho(z) = z + \frac{1}{4},\ z > 0.$$

This CWF is different from the ones previously used for Carleman estimates for elliptic PDEs; see, for example, the function φ in (1.172) (Sect. 1.10.7) for the case when its dependence from t is dropped. Note that $\rho(z) \in (0,3/4)$ in Ω and $\rho(z)\mid_{\Gamma_3} = 3/4$. Let the number $\varkappa \in (1/3,1)$. Denote

$$\Omega_{\varkappa} = \left\{x \in \Omega : \rho(z) < \frac{3}{4}\varkappa\right\}.$$

Hence, if $\varkappa_1 < \varkappa_2$, then $\Omega_{\varkappa_1} \subset \Omega_{\varkappa_2}$. Also, $\Omega_1 = \Omega$ and $\Omega_{1/3} = \varnothing$. In addition,

$$K^2(z) \geq \exp\left[2\lambda\left(\frac{4}{3}\varkappa\right)^{\nu_0}\right] \text{ in } \Omega_{\varkappa}.$$

Lemma 6.5.1. *Fix the parameter $\nu > 2$. Consider an arbitrary function $u \in H^3(\Omega)$ such that*

$$u\mid_{\Gamma_1} = u_z\mid_{\Gamma_1} = \partial_n u\mid_{\Gamma_2} = 0. \tag{6.45}$$

Then there exists a constant $C > 0$ such that for all $\lambda > 2$ the following Carleman estimate is valid for all these functions u:

$$\int_\Omega (\Delta u)^2 K^2 \mathrm{d}x \geq \frac{C}{\lambda} \sum_{|\alpha|=2} \int_\Omega \left(D^\alpha u\right)^2 K^2 \mathrm{d}x + C \int_\Omega \left[\lambda \left(\nabla u\right)^2 + \lambda^3 u^2\right] K^2 \mathrm{d}x$$
$$-C\lambda^3 \|u\|^2_{H^3(\Omega)} \exp\left[2\lambda \left(\frac{4}{3}\right)^\nu\right].$$

Proof. We have

$$\begin{aligned}
\left(\Delta u\right)^2 K^2 &= \left(u_{xx}^2 + u_{yy}^2 + u_{zz}^2 + 2u_{xx}u_{zz} + 2u_{xx}u_{yy} + 2u_{yy}u_{zz}\right) K^2 \\
&= \left(u_{xx}^2 + u_{yy}^2 + u_{zz}^2\right) K^2 + \partial_x \left(2u_x u_{zz} K^2 + 2u_x u_{yy} K^2\right) \\
&\quad + \partial_y \left(2u_y u_{zz} K^2\right) - 2u_x u_{zzx} K^2 - 2u_x u_{yyx} K^2 - 2u_y u_{zzy} K^2 \\
&= \left(u_{xx}^2 + u_{yy}^2 + u_{zz}^2\right) K^2 + \partial_x \left(2u_x u_{zz} K^2 + 2u_x u_{yy} K^2\right) \\
&\quad + \partial_y \left(2u_y u_{zz} K^2\right) + \partial_y \left(-2u_x u_{xy} K^2\right) + 2u_{xy}^2 K^2 \\
&\quad + \partial_z \left(-2u_x u_{xz} K^2\right) + 2u_{xz}^2 K^2 - 4\lambda\nu\rho^{-\nu-1} u_x u_{xz} K^2 \\
&\quad + \partial_z \left(-2u_y u_{yz} K^2\right) + 2u_{yz}^2 K^2 - 4\lambda\nu\rho^{-\nu-1} u_y u_{yz} K^2.
\end{aligned}$$

Thus, we have obtained that

$$\begin{aligned}
\left(\Delta u\right)^2 K^2 &= \left(u_{xx}^2 + u_{yy}^2 + u_{zz}^2 + 2u_{xy}^2 + 2u_{xz}^2 + 2u_{yz}^2\right) K^2 \\
&\quad - 4\lambda\nu\rho^{-\nu-1} \left(u_x u_{xz} + u_y u_{yz}\right) K^2 + \partial_x \left[2\left(u_x u_{zz} + u_x u_{yy}\right) K^2\right] \\
&\quad + \partial_y \left[2\left(u_y u_{zz} - u_x u_{xy}\right) K^2\right] + \partial_z \left[-2\left(u_x u_{xz} + u_y u_{yz}\right) K^2\right].
\end{aligned} \tag{6.46}$$

Using the Cauchy–Schwarz inequality,

$$2ab \geq -\varepsilon a^2 - \frac{b^2}{\varepsilon},\ \forall \varepsilon > 0,$$

and taking $\varepsilon = 1/4$, we obtain

$$-4\lambda\nu\rho^{-\nu-1} \left(u_x u_{xz} + u_y u_{yz}\right) K^2 \geq -\left(u_{xz}^2 + u_{yz}^2\right) K^2 - 4\lambda^2\nu^2\rho^{-2\nu-2} \left(\nabla u\right)^2 K^2.$$

Hence, (6.46) implies that

$$(\Delta u)^2 K^2 \geq \sum_{|\alpha|=2} (D^\alpha u)^2 K^2 - 4\lambda^2 \nu^2 \rho^{-2\nu-2} (\nabla u)^2 K^2$$
$$+\partial_x \left[2u_x \left(u_{zz} + u_{yy}\right) K^2\right] + \partial_y \left[2 \left(u_y u_{zz} - u_x u_{xy}\right) K^2\right]$$
$$+\partial_z \left[-2 \left(u_x u_{xz} + u_y u_{yz}\right) K^2\right]. \tag{6.47}$$

Consider a new function $v = uK$. Substituting $u = vK^{-1}$, we obtain

$$(\Delta u)^2 \rho^{\nu+1} K^2 = (y_1 + y_2 + y_3)^2 \rho^{\nu+1} \geq 2y_2(y_1 + y_3)\rho^{\nu+1}, \tag{6.48}$$

$$y_1 = \Delta v,\ y_2 = 2\lambda\nu\rho^{-\nu-1} v_z,\ y_3 = (\lambda\nu)^2 \rho^{-2\nu-2}(1 - (\nu+1)(\lambda\nu)^{-1}\rho^\nu)v. \tag{6.49}$$

We have

$$2y_1 y_2 \rho^{\nu+1} = \partial_x \left(4\lambda\nu v_z v_x\right) + \partial_y \left(4\lambda\nu v_z v_y\right) + \partial_z \left[2\lambda\nu \left(v_z^2 - v_x^2 - v_y^2\right)\right]. \tag{6.50}$$

Next, by (6.48) and (6.49),

$$2y_2 y_3 \rho^{\nu+1} = 4(\lambda\nu)^3 \left(\rho^{-2\nu-2} - (\nu+1)(\lambda\nu)^{-1}\rho^{-\nu-2}\right) v_z v$$
$$= \partial_z \left[2(\lambda\nu)^3 \left(\rho^{-2\nu-2} - (\nu+1)(\lambda\nu)^{-1}\rho^{-\nu-2}\right) v^2\right]$$
$$+4(\lambda\nu)^3 (\nu+1)\rho^{-2\nu-3} \left(1 - (\nu+2)(2\lambda\nu)^{-1}\rho^\nu\right) v^2$$
$$\geq 2\lambda^3\nu^4\rho^{-2\nu-3}v^2 + \partial_z \left[2(\lambda\nu)^3 \left(\rho^{-2\nu-2} - (\nu+1)(\lambda\nu)^{-1}\rho^{-\nu-2}\right) v^2\right].$$

Hence,

$$2y_2 y_3 \rho^{\nu+1} \geq 2\lambda^3\nu^4\rho^{-2\nu-3}v^2 + \partial_z \left[2(\lambda\nu)^3 \left(\rho^{-2\nu-2} - (\nu+1)(\lambda\nu)^{-1}\rho^{-\nu-2}\right) v^2\right]. \tag{6.51}$$

Summing up (6.50) with (6.51), using (6.48) and the backward substitution $u = vK$, we obtain

$$(\Delta u)^2 \rho^{\nu+1} K^2 \geq 2\lambda^3\nu^4\rho^{-2\nu-3}u^2K^2 + \partial_x U_1 + \partial_y U_2 + \partial_z U_3, \tag{6.52}$$

where the following estimates are valid for functions U_1, U_2, U_3:

$$\begin{aligned} |U_1| &\leq C\lambda\nu \left|u_x\right| \left(\left|u_z\right| + \lambda\nu\rho^{-\nu-1}\left|u\right|\right) K^2, \\ |U_2| &\leq C\lambda\nu \left|u_y\right| \left(\left|u_z\right| + \lambda\nu\rho^{-\nu-1}\left|u\right|\right) K^2, \\ |U_3| &\leq C\lambda\nu \left(|\nabla u|^2 + \lambda^2\nu^2\rho^{-2\nu-2}u^2\right) K^2. \end{aligned} \tag{6.53}$$

We now need to incorporate the term $\lambda\left(\nabla u\right)^2 K^2$ in the right-hand side of the Carleman estimate. Hence, we continue as follows:

$$\begin{aligned} -\lambda\nu u\Delta u K^2 &= \partial_x\left(-\lambda\nu u u_x K^2\right) + \partial_y\left(-\lambda\nu u u_y K^2\right) + \partial_z\left(-\lambda\nu u u_z K^2\right) \\ &\quad +\lambda\nu\left(\nabla u\right)^2 K^2 - 2\lambda^2\nu^2\rho^{-\nu-1}u_z u K^2 \\ &= \lambda\nu\left(\nabla u\right)^2 K^2 - 2\lambda^3\nu^3\rho^{-2\nu-2}\left(1 + (\nu+1)\left(2\lambda\nu\right)^{-1}\rho^{\nu}\right)u^2 K^2 \\ &\quad +\partial_x U_4 + \partial_y U_5 + \partial_z U_6. \end{aligned}$$

Hence,

$$-\lambda\nu u\Delta u K^2 \geq \lambda\nu\left(\nabla u\right)^2 K^2 - 4\lambda^3\nu^3\rho^{-2\nu-2}u^2 K^2 + \partial_x U_4 + \partial_y U_5 + \partial_z U_6, \tag{6.54}$$

$$U_4 = -\lambda\nu u u_x K^2,\ U_5 = -\lambda\nu u u_y K^2, |U_6| \leq C\left(\lambda\nu u_z^2 + \lambda^2\nu^2\rho^{-\nu-1}u^2\right)K^2. \tag{6.55}$$

Summing up (6.52) and (6.54) and taking into account (6.53) and (6.55) as well as the fact that

$$2\lambda^3\nu^4\rho^{-2\nu-3} - 4\lambda^3\nu^3\rho^{-2\nu-2} = 2\lambda^3\nu^4\rho^{-2\nu-3}\left(1 - \rho\left(2\nu\right)^{-1}\right) > \lambda^3\nu^4\rho^{-2\nu-3},$$

we obtain

$$\begin{aligned} (\Delta u)^2 K^2 - \lambda\nu u\Delta u K^2 &\geq \lambda\nu\left(\nabla u\right)^2 K^2 + \lambda^3\nu^4\rho^{-2\nu-3}u^2 K^2 \\ &\quad +\partial_x U_7 + \partial_y U_8 + \partial_z U_9, \end{aligned} \tag{6.56}$$

$$|U_7| \leq C\lambda\nu\left|u_x\right|\left(\left|u_z\right| + \lambda\nu\rho^{-\nu-1}\left|u\right|\right)K^2, \tag{6.57}$$

$$|U_8| \leq C\lambda\nu\left|u_y\right|\left(\left|u_z\right| + \lambda\nu\rho^{-\nu-1}\left|u\right|\right)K^2, \tag{6.58}$$

$$|U_9| \leq C\lambda\nu\left(|\nabla u|^2 + \lambda^2\nu^2\rho^{-2\nu-2}u^2\right)K^2. \tag{6.59}$$

Since the number $\nu \geq 2$ is fixed, we can incorporate ν in C. Also, since $\rho^{\nu+1} < 1$, we can regard that $\rho^{\nu+1} < C$. By the Cauchy–Schwarz inequality,

$$-\lambda \nu u \Delta u K^2 \leq \frac{1}{2}(\Delta u)^2 \rho^{\nu+1} K^2 + \frac{1}{2}\lambda^2 \nu^2 \rho^{-\nu-1} u^2 K^2.$$

Hence, we obtain from (6.56), (6.57), (6.58), and (6.59)

$$(\Delta u)^2 K^2 \geq C\left[\lambda (\nabla u)^2 + \lambda^3 u^2\right] K^2 + \partial_x U_7 + \partial_y U_8 + \partial_z U_9. \tag{6.60}$$

We now divide (6.47) by λr with a constant $r = r(\nu) > 0$ such that $4\nu_0^2 \rho^{-2\nu_0-2}/r \leq C/2$, add the resulting inequality to (6.60), and take into account (6.57), (6.58), and (6.59). Then with a new constant C, we obtain the following pointwise Carleman estimate for the Laplace operator in the domain Ω:

$$(\Delta u)^2 K^2 \geq \frac{C}{\lambda} \sum_{|\alpha|=2} (D^\alpha u)^2 K^2 + C\left[\lambda (\nabla u)^2 + \lambda^3 u^2\right] K^2$$
$$+\partial_x U_{10} + \partial_y U_{11} + \partial_z U_{12}, \tag{6.61}$$

$$|U_{10}| \leq C\lambda |u_x| \left(|u_{zz}| + |u_{yy}| + |u_z| + \lambda |u|\right) K^2, \tag{6.62}$$

$$|U_{11}| \leq C\left[\lambda |u_y| \left(|u_{zz}| + |u_z| + \lambda |u|\right) + |u_{xy}| |u_x|\right] K^2, \tag{6.63}$$

$$|U_{12}| \leq C\lambda \left[|u_{xz}|^2 + |u_{yz}|^2 + |\nabla u|^2 + \lambda^2 u^2\right] K^2. \tag{6.64}$$

We now integrate both sides of formula (6.61) over the rectangle Ω using the Gauss' formula. It is *important* that because of (6.45) and estimates (6.62)–(6.64), each resulting boundary integral over Γ_1 and Γ_2 will turn out to be zero. We obtain

$$\int_\Omega (\Delta u)^2 K^2 \mathrm{d}x \geq \frac{C}{\lambda} \sum_{|\alpha|=2} \int_\Omega (D^\alpha u)^2 K^2 \mathrm{d}x + C \int_\Omega \left[\lambda (\nabla u)^2 + \lambda^3 u^2\right] K^2 \mathrm{d}x$$
$$-C\lambda \int_{\Gamma_3} \left[|u_{xz}|^2 + |u_{yz}|^2 + |\nabla u|^2 + \lambda^2 u^2\right] K^2 \mathrm{d}S. \tag{6.65}$$

Note that

$$K^2\left(\frac{1}{2}\right) = K^2(z)|_{\Gamma_3} = \min_{\overline{\Omega}} K^2(z) = \exp\left[2\lambda \left(\frac{4}{3}\right)^\nu\right].$$

Hence,

$$\int_{\Gamma_3} \lambda \left[|u_{xz}|^2 + |u_{yz}|^2 + |\nabla u|^2 + \lambda^2 u^2\right] K^2 \mathrm{d}x \leq C\lambda^3 \|u\|^2_{H^3(\Omega)} \exp\left[2\lambda \left(\frac{4}{3}\right)^\nu\right].$$

Substituting this in (6.65), we obtain the estimate of this lemma. □

We now establish both existence and uniqueness of the minimizer of the functional (6.43). Denote $a_{n,k}^{(i)}(x), i = 1,2,3$ components of the vector function $a_{n,k}(x)$ in (6.39). Let

$$\left\| a_{n,k}^{(i)} \right\|_{L_\infty(\Omega)} \leq M,\ M = \text{const.} > 0, i = 1,2,3. \tag{6.66}$$

Lemma 6.5.2. *Assume that there exists a function $\Phi \in H^5(\Omega)$ satisfying boundary conditions (6.42). Also, assume that condition (6.66) holds. Then there exists unique minimizer $u \in H^5(\Omega)$ of the functional (6.43). Furthermore, with a constant $C_1 = C_1(M) > 0$,*

$$\|u\|_{H^5(\Omega)} \leq \frac{C_1}{\sqrt{\alpha}} \left(\|H_{n,k}\|_{L_2(\Omega)} + \|\Phi\|_{H^5(\Omega)} \right).$$

Proof. Let $U = u - \Phi$. Then the function U satisfies boundary conditions (6.45). By the variational principle,

$$(G_{n,k}U, G_{n,k}v) + \alpha [U,v] = (H_{n,k} - G_{n,k}\Phi, G_{n,k}v) - \alpha [\Phi, v],$$

for all functions $v \in H^5(\Omega)$ satisfying boundary conditions (6.45). Here,

$$G_{n,k}U := \Delta U - a_{n,k}\nabla U. \tag{6.67}$$

The rest of the proof follows from the Riesz theorem. □

Lemma 6.5.3. *Let $G_{n,k}$ be the operator defined in (6.67). Let the function $u \in H^5(\Omega)$ satisfy boundary conditions (6.45) as well as the variational equality*

$$(G_{n,k}u, G_{n,k}v) + \alpha [u,v] = (H_{n,k}, G_{n,k}v) + \alpha [g,v] \tag{6.68}$$

for all functions $v \in H^5(\Omega)$ satisfying (6.45). Then

$$\|u\|_{H^5(\Omega)} \leq \frac{1}{\sqrt{\alpha}} \|H_{n,k}\|_{L_2(\Omega)} + \|g\|_{H^5(\Omega)}.$$

Proof. Set in (6.68) $v := u$ and use the Cauchy–Schwarz inequality. □

Theorem 6.5. *Let $G_{n,k}$ be the operator defined in (6.67). Assume that condition (6.66) holds. Let $g \in H^5(\Omega)$ be an arbitrary function. Let $u \in H^5(\Omega)$ be the function satisfying boundary conditions (6.45) as well as the variational equality (6.68) for all functions $v \in H^5(\Omega)$ satisfying (6.45). Let the number $\varkappa \in (1/3, 1)$ and the number $\beta \in (\varkappa, 1)$. Consider the numbers b_1, b_2,*

$$b_1 := b_1(\beta) = \frac{1}{2\left[1+(1-\beta^{\nu})(3\beta)^{-\nu}\right]} \in \left(0, \frac{1}{2}\right), \tag{6.69}$$

$$b_2 := b_2(\beta) = \frac{1}{2} - b_1 > 0, \tag{6.70}$$

where ν is the parameter of Lemma 6.5.1. Then there exists a sufficiently small number $\alpha_1 = \alpha_1(M,\beta) \in (0,1)$ such that for all $\alpha \in (0,\alpha_1)$ the following estimate holds with a constant $C_2 = C_2(M,\Omega) > 0$

$$\|u\|_{H^2(\Omega_x)} \leq C_2 \alpha^{-b_1} \|H_{n,k}\|_{L_2(\Omega)} + C_2 \alpha^{b_2} \|g\|_{H^5(\Omega)}. \tag{6.71}$$

Proof. In this proof, $C_2 = C_2(M,\Omega)$ denotes different constants depending only from M and Ω. Setting in (6.68) $v := u$ and using the Cauchy–Schwarz inequality, we obtain

$$\|G_{n,k}u\|^2_{L_2(\Omega)} \leq F^2 := \|H_{n,k}\|^2_{L_2(\Omega)} + \alpha \|g\|^2_{H^5(\Omega)}. \tag{6.72}$$

Note that

$$K^2(0) = \max_{\overline{\Omega}} K^2(z) = \exp(2\lambda \cdot 4^{\nu}).$$

Hence, we obtain from (6.72)

$$F^2 \geq \|G_{n,k}u\|^2_{L_2(\Omega)} = \left\|K^{-1}K \cdot G_{n,k}u\right\|^2_{L_2(\Omega)} \geq \frac{1}{K^2(0)} \|K \cdot G_{n,k}u\|^2_{L_2(\Omega)}$$
$$= \exp(-2\lambda \cdot 4^{\nu}) \|K \cdot G_{n,k}u\|^2_{L_2(\Omega)}.$$

Clearly

$$(G_{n,k}u)^2 K^2 \geq \frac{1}{2}(\Delta u)^2 K^2 - C_1 (\nabla u)^2 K^2.$$

Hence,

$$\int_{\Omega} (\Delta u)^2 K^2 \mathrm{d}x\mathrm{d}z \leq C_1 \int_{\Omega} (\nabla u)^2 K^2 \mathrm{d}x\mathrm{d}z + \exp(2\lambda \cdot 4^{\nu}) F^2. \tag{6.73}$$

Applying Lemma 6.5.1 to (6.73), choosing $\lambda > 1$ sufficiently large, and observing that the term with $(\nabla u)^2$ in (5.14) will be absorbed for such λ, we obtain

$$\lambda \exp(2\lambda \cdot 4^{\nu}) F^2 + C_2 \lambda^4 \|u\|^2_{H^3(\Omega)} \exp\left[2\lambda \left(\frac{4}{3}\right)^{\nu}\right]$$
$$\geq C_2 \sum_{|\alpha| \leq 2} \int_{\Omega} (D^{\alpha}u)^2 K^2 \mathrm{d}x$$

$$\geq C_2 \sum_{|\alpha|\leq 2} \int_{\Omega_\varkappa} (D^\alpha u)^2 \, K^2 \mathrm{d}x$$

$$\geq C_2 \exp\left[2\lambda \left(\frac{4}{3\varkappa}\right)^\nu\right] \|u\|^2_{H^2(\Omega)}.$$

Recalling that $\beta \in (\varkappa, 1)$, we obtain that the latter sequence of inequalities implies that

$$\lambda \exp\left(2\lambda \cdot 4^\nu\right) F^2 + C_2 \lambda^4 \|u\|^2_{H^3(\Omega)} \exp\left[2\lambda \left(\frac{4}{3}\right)^\nu\right]$$

$$\geq C_1 \exp\left[2\lambda \left(\frac{4}{3\varkappa}\right)^\nu\right] \|u\|^2_{H^2(\Omega)} \geq C_2 \exp\left[2\lambda \left(\frac{4}{3\beta}\right)^\nu\right] \|u\|^2_{H^2(\Omega)}.$$

Thus,

$$\lambda \exp\left(2\lambda \cdot 4^\nu\right) F^2 + C_2 \lambda^4 \|u\|^2_{H^3(\Omega)} \exp\left[2\lambda \left(\frac{4}{3}\right)^\nu\right]$$

$$\geq C_2 \exp\left[2\lambda \left(\frac{4}{3\beta}\right)^\nu\right] \|u\|^2_{H^2(\Omega)}.$$

Dividing this inequality by the exponential term in the right-hand side, we obtain a stronger estimate:

$$\|u\|^2_{H^2(\Omega_\varkappa)} \leq C_2 \exp\left(2\lambda \cdot 4^\nu\right) F^2 + C_2 \|u\|^2_{H^3(\Omega)} \exp\left[-2\lambda \left(\frac{4}{3\beta}\right)^\nu (1-\beta^\nu)\right]. \tag{6.74}$$

Applying Lemma 6.5.3 to $\|u\|^2_{H^3(\Omega)}$ in the right-hand side of (6.74), we obtain

$$\|u\|^2_{H^2(\Omega_\varkappa)} \leq C_2 F^2 \left\{\exp\left(2\lambda \cdot 4^\nu\right) + \frac{1}{\alpha} \exp\left[-2\lambda \left(\frac{4}{3\beta}\right)^\nu (1-\beta^\nu)\right]\right\}. \tag{6.75}$$

Since $\alpha \in (0, \alpha_0)$ and α_0 is sufficiently small, we can choose sufficiently large $\lambda = \lambda(\alpha)$ such that

$$\exp\left(2\lambda \cdot 4^\nu\right) = \alpha^{-1} \exp\left[-2\lambda \left(\frac{4}{3\beta}\right)^\nu (1-\beta^\nu)\right]. \tag{6.76}$$

We obtain from (6.76) that $2\lambda \cdot 4^\nu = \ln \alpha^{-2b_1}$. Hence, (6.74), (6.75), and (6.76) imply the validity of (6.71). □

6.6 The Third Approximate Mathematical Model

6.6.1 Exact Solution

First, we need to introduce the definition of the exact solution. Some aspects of this definition are different from the definition of Sect. 2.8.1. We assume that there exists a coefficient $c^*(x)$ which is the unique exact solution of coefficient inverse problem 6.2 with the exact data $g_0^*(x,t)$, $g_1^*(x,t)$ in (6.10). We assume that

$$c^* \in \mathbb{M} \cap C^4\left(\mathbb{R}^3\right), \tag{6.77}$$

where $\mathbb{M}$ was defined in (6.5). The assumption (6.77) is because of (6.3) and (6.4). Let $u^*(x,t)$ be the solution of the forward problem (6.1), (6.2) with $c := c^*$ and $w^*(x,s)$ be its Laplace transform (3.3) for $s > \underline{s} = \underline{s}(c^*) > 0$ (Theorem 2.7.1 Since the source $x_0 \notin \overline{\Omega}$, then it follows from (6.77) and Theorem 2.7.2 that $w^*(x,s) \in C^{5+\gamma}\left(\overline{\Omega}\right)$. Similarly with (6.21), let

$$v^*(x,s) = \frac{\ln w^*(x,s)}{s^2},\ q^*(x,s) = \frac{\partial v^*(x,s)}{\partial s}. \tag{6.78}$$

Let $[\underline{s}, \overline{s}]$ be the s-interval of Sect. 6.4 and $\underline{s} > \underline{s}(c^*)$. Since $w^*(x,s) \in C^{5+\gamma}\left(\overline{\Omega}\right)$, we assume that

$$q^* \in C^{5+\gamma}\left(\overline{\Omega}\right) \times C^1[\underline{s}, \overline{s}], \tag{6.79}$$

$$\|q^*(x,s)\|_{C^{5+\gamma}(\overline{\Omega}) \times C^1[\underline{s},\overline{s}]} \leq C^*, \tag{6.80}$$

$$C^* = \text{const.} \geq 2, \tag{6.81}$$

where the constant C^* is given. Consider the same partition of the interval $[\underline{s}, \overline{s}]$ into N small subintervals as one in Sect. 6.4.2. Let $q_n^*(x)$ be the average of the function $q^*(x,s)$ over the interval (s_n, s_{n-1}):

$$q_n^*(x) = \frac{1}{h} \int_{s_n}^{s_{n-1}} q^*(x,s)\, \mathrm{d}s.$$

Then (6.79) and (6.80) imply that

$$\max_{s \in [s_n, s_{n-1}]} \|q_n^*(x) - q^*(x,s)\|_{C^{5+\gamma}(\overline{\Omega})} \leq C^* h. \tag{6.82}$$

Hence, increasing, if necessary, the number C^*, we can assume that

$$\max_{1 \leq n \leq N} \|q_n^*\|_{H^5(\Omega)} \leq C^*. \tag{6.83}$$

Let

$$\psi_0^*(x,s) := q^*(x,s)\mid_{\Gamma_1},\ \psi_1^*(x,s) := \partial_{x_3} q^*(x,s)\mid_{\Gamma_1},\ s \in [\underline{s},\overline{s}]. \tag{6.84}$$

Given (6.84), let functions $\psi_{0,n}^*(x)$ and $\psi_{1,n}^*(x)$ be averages of functions $\psi_0^*(x,s)$ and $\psi_1^*(x,s)$ over the interval (s_n, s_{n-1}). Then boundary conditions for functions $q_n^*(x)$ at Γ_1 are

$$q_n^*|_{\Gamma_1} = \psi_{0,n}^*(x), \partial_{x_3} q_n^*|_{\Gamma_1} = \psi_{1,n}^*(x). \tag{6.85}$$

The exact tail function $V^*(x)$ is

$$V^*(x) = \frac{\ln w^*(x,\overline{s})}{\overline{s}^2}. \tag{6.86}$$

The function q_n^* satisfies the following analogue of (6.26):

$$\begin{aligned}
&\Delta q_n^* - A_{1,n}\left(h\sum_{j=0}^{n-1}\nabla q_j^*(x) - \nabla V^*\right)\nabla q_n^* \\
&= -A_{2,n}h^2\left(\sum_{j=0}^{n-1}\nabla q_j^*(x)\right)^2 + 2A_{2,n}\nabla V^*\left(h\sum_{j=0}^{n-1}\nabla q_j^*(x)\right) \\
&\quad -A_{2,n}\left(\nabla V^*\right)^2 + F_{1,n}(x,h,\lambda), \quad q_0^* :\equiv 0.
\end{aligned} \tag{6.87}$$

Similarly with (6.32) and (6.33),

$$v_n^*(x) := -hq_n^*(x) - h\sum_{j=0}^{n-1} q_j^*(x) + V^*(x) + F_{2,n}(x,h), x \in \Omega, \tag{6.88}$$

$$c^*(x) = \Delta v_n^*(x) + s_n^2\left|\nabla v_n^*(x)\right|^2 + F_{3,n}(x,h), x \in \Omega. \tag{6.89}$$

In (6.87)–(6.89) functions $F_{1,n}(x,h,\lambda), F_{2,n}(x,h), F_{3,n}(x,h)$ represent approximation errors. In particular, the nonlinear term $2(I_{1n}/I_0)\left(\nabla q_n^*\right)^2$, an analog of which was ignored in (6.26), is a part of $F_{1,n}$. Although we can prove an analog of Theorem 6.7 for the case

$$F_{1,n} \neq 0, F_{2,n} \neq 0, F_{3,n} \neq 0, \psi_{0,n}^* \neq \psi_{0,n}, \psi_{1,n}^* \neq \psi_{1,n},$$

this would require more space while the method of the proof would be almost the same. Hence, we "allow" now the error in the boundary data at Γ_1 to be present only at $s := \bar{s}$, see Lemma 6.7. Therefore, for *brevity only* we assume below that

$$F_{1,n} = F_{2,n} = F_{2,3} = 0, \psi_{0,n}^* = \psi_{0,n}, \psi_{1,n}^* = \psi_{1,n},\ n \in [1,N]. \tag{6.90}$$

Using, the idea of the proof of Theorem 2.7.2, it is possible to prove that not only the function $w^*(x,s) \in C^{5+\gamma}(\overline{\Omega})$ but also the functions $D_s^k w^*(x,s) \in C^{5+\gamma}(\overline{\Omega}), k = 1,2$. Since this implies that $q^*(x,s) \in C^{5+\gamma}(\overline{\Omega}) \times C^1[\underline{s},\overline{s}]$, then it is not necessary to impose this assumption in (6.79). However, we still prefer to use this assumption because the proof of (6.79) is not our main focus. The reason why we require the C^4-smoothness of c^* in (6.4) and (6.77) is to ensure that $V^* \in C^{5+\gamma}(\overline{\Omega})$. We need the latter to justify that the function $p^* \in H^5(\Omega)$ in (6.92).

6.6.2 The Third Approximate Mathematical Model

The third approximate mathematical model is similar with the second one of Sect. 2.9.2 Some differences with Sect. 2.9.2 are due to the fact that we use the backscattering data now, which was not the case of Sect. 2.9.2. Similarly with Sect. 2.9.2, Assumptions 1–3 below mean that we take into account only the first term of the asymptotic behavior of the function $s^{-2}\ln w^*(x,s)$ at $s \to \infty$ and ignore the rest. By (2.105) (Sect. 2.8.1), the equation for the function q^* is

$$\Delta q^* - 2s^2\nabla q^* \int_s^{\overline{s}} \nabla q^*(x,\tau)\,d\tau + 2s\left[\int_s^{\overline{s}} \nabla q^*(x,\tau)\,d\tau\right]^2 + 2s^2\nabla q^*\nabla V^*$$
$$- 2s\nabla V^* \int_s^{\overline{s}} \nabla q^*(x,\tau)\,d\tau + 2s\left(\nabla V^*\right)^2 = 0, \quad (x,s) \in \Omega \times [\underline{s},\overline{s}]. \tag{6.91}$$

The third approximate mathematical model consists of the following three **assumptions:**

1. There exists a function $p^*(x) \in H^5(\Omega)$ such that the exact tail function $V^*(x)$ has the form
$$V^*(x,s) = \frac{p^*(x)}{s}, \ \forall s \geq \overline{s}. \tag{6.92}$$
And also (see (6.86)),
$$\frac{p^*(x)}{\overline{s}} = \frac{\ln w^*(x,\overline{s})}{\overline{s}^2}. \tag{6.93}$$
2. There exists unique exact solution c^* of CIP 6.2 satisfying condition (6.77). For $\overline{s} > \underline{s} > \underline{s}(c^*) > 0$, the function $q^*(x,s), (x,s) \in \Omega \times [\underline{s},\overline{s}]$ defined in (6.78), satisfies conditions (6.79), (6.80).
3. For $s \in [\underline{s},\overline{s}]$, the function $q^*(x,s)$ satisfies boundary conditions (6.84) at Γ_1 as well as the boundary condition (6.29) at $\Gamma_2 \cup \Gamma_3$:

$$\partial_n q(x,s)\mid_{\Gamma_2\cup\Gamma_3} = \frac{1}{s^2}. \tag{6.94}$$

Since $q^*(x,s) = \partial_s V^*(x,s)$ for $s \geq \overline{s}$, we derive from (6.92) that

$$q^*(x,\overline{s}) = -\frac{p^*(x)}{\overline{s}^2}. \tag{6.95}$$

Recall that the boundary condition (6.29) is an approximate one and this is why we treat (6.94) as an assumption. It follows from (6.94) that

$$\partial_n q_n^*\mid_{\Gamma_2\cup\Gamma_3} = \frac{1}{s_n s_{n-1}}. \tag{6.96}$$

Set in (6.91) $s = \overline{s}$. Then, using (6.84) and (6.92), (6.95) and (6.94), we obtain the following *approximate* PDE and boundary conditions for the function $p^*(x)$:

$$\Delta p^* = 0 \text{ in } \Omega,\ p^* \in H^5(\Omega), \tag{6.97}$$

$$p^*|_{\Gamma_1} = -\overline{s}^2\psi_0^*(x,\overline{s}),\ \partial_n p^*|_{\Gamma_1} = -\overline{s}^2\psi_1^*(x,\overline{s}),\ \partial_n p^*\mid_{\Gamma_2\cup\Gamma_3} = -1. \tag{6.98}$$

The existence of the solution of the problem (6.97), (6.98) is assumed rather than proved because conditions (6.97) and (6.98) are derived from assumptions 1–3, and (6.94) is an approximate boundary condition. Let functions $\psi_0(x,s), \psi_1(x,s)$ be boundary conditions in (6.30), (6.31) (Sect. 6.4.2). Suppose that for each $\alpha \in (0,1)$, there exists the QRM solution $p = p(x;\alpha)$ of the following boundary value problem:

$$\Delta p = 0 \text{ in } \Omega,\ p(x) \in H^5(\Omega), \tag{6.99}$$

$$p|_{\Gamma_1} = -\overline{s}^2\psi_0(x,\overline{s}),\ \partial_n p|_{\Gamma_1} = -\overline{s}^2\psi_1(x,\overline{s}),\ \partial_n p\mid_{\Gamma_2\cup\Gamma_3} = -1; \tag{6.100}$$

see Lemma 6.7 for the existence and uniqueness of the function p. Then, we choose an appropriate $\alpha \in (0,1)$. Next, we set the first approximation for the tail function in the iterative process of Sect. 6.4.3 as (also, see Remarks 2.9.2)

$$V_{1,1}(x) := V_{1,1}(x;\alpha) := \frac{p(x;\alpha)}{\overline{s}}. \tag{6.101}$$

Remark 6.6.2. Analogs of Remarks 2.9.2 are valid here.

We now establish uniqueness within the framework of the third approximate mathematical model. Although uniqueness can be proven under less restrictive assumptions imposed on functions q^*, p^* than ones above, we are not doing this here for brevity.

Lemma 6.6.2. *Suppose that above Assumptions 1–3 hold. Then for* $(x,s) \in \Omega \times [\underline{s},\overline{s}]$, *there exists at most one function* $q^*(x,s)$ *satisfying conditions (6.79), (6.80) as well as (6.91). In addition, if assuming the continuous analog of (6.89),*

$$c^*(x) = \Delta v^*(x) + s^2 |\nabla v^*(x)|^2, (x,s) \in \Omega \times [\underline{s}, \overline{s}],$$

where the function v^* is the same as in (6.78), then there exists at most one function $c^*(x)$.

Brief Outline of the Proof. We outline the proof only briefly because it is simple. Uniqueness of the problem (6.97), (6.98) is obvious. Having uniquely determined the function p^*, we uniquely find the function $V^*(x,\overline{s})$ via (6.92). Substitute this function $V^*(x,\overline{s})$ in (6.91). Next, applying the Carleman estimate of Lemma 6.5.1, we obtain uniqueness of the function $q^*(x,s)$. The s integrals are not a problem, as it is clear from Sect. 1.10. □

6.7 The Third Approximate Global Convergence Theorem

Just as in (2.120) (Sect. 2.8.2), assume that

$$\overline{s} > 1, \ \lambda h \geq 1, \tag{6.102}$$

where $\lambda > 1$ is the parameter of the CWF (2.38). As in (2.121), we obtain from (6.102) that

$$\max_{1 \leq n \leq N} \{|A_{1,n}| + |A_{2,n}|\} \leq 8\overline{s}^2. \tag{6.103}$$

In general, embedding theorems are valid for domains with sufficiently smooth boundaries. It follows from Lemma 1 of §4 of Chap. 3 of the book [127] that if Q is a rectangular prism, then any function $f \in H^k(Q)$ can be extended in a bigger rectangular prism $Q_1 \supset Q$, $\partial Q \cap \partial Q_1 = \varnothing$ as the function $f_1 \in H^k(Q_1)$, $f_1(x) = f(x)$ in Q and $\|f_1\|_{H^k(Q_1)} \leq Z \|f\|_{H^k(Q)}$, where the constant $Z = Z(Q, Q_1) > 0$. Hence, embedding theorems are valid for rectangular prisms. Hence,

$$\|f\|_{C^3(\overline{\Omega})} \leq C \|f\|_{H^5(\Omega)}, \forall f \in H^5(\Omega). \tag{6.104}$$

Let the domain Ω be the same as in Sect. 6.5. Recall that $\Omega_\varkappa \subset \Omega$ for $\varkappa \in (1/3, 1)$ and $\Omega_1 = \Omega$. Following the construction of Sect. 6.4.1, we assume that

$$P_2 = \text{const.} \in \left(\frac{1}{3}, 1\right), \ c(x) = 1 \text{ for } x \in \mathbb{R}^3 \backslash \Omega_{P_2}, \tag{6.105}$$

$$\Omega' \subset \Omega_{P_2}, \ \partial\Omega' \cap \partial\Omega_{P_2} = \varnothing. \tag{6.106}$$

Recall that functions $\widehat{c}_{n,k}(x)$ are defined via (6.19). Since $\widehat{c}_{n,k}(x) \neq c_{n,k}(x)$ for $x \in \Omega_{P_2} \backslash \Omega'$, then the number $\text{meas}(\Omega_{P_2} \backslash \Omega')$ can be considered as a part of the error in the data. Hence, we assume that the domain Ω' is such that

$$\text{meas}\left(\Omega_{P_2} \backslash \Omega'\right) < \frac{\varepsilon}{2}, \tag{6.107}$$

where $\varepsilon \in (0,1)$ is sufficiently small. Since by construction $\widehat{c}_{n,k}(x), c^*(x) \in [1,d], \forall x \in \mathbb{R}^3$, and $\widehat{c}_{n,k}(x) = c_{n,k}(x), \forall x \in \Omega'$, then by (6.34), (6.105), and (6.107),

$$\|\widehat{c}_{n,k} - c^*\|_{L_2(\Omega)} \leq \|c_{n,k} - c^*\|_{L_2(\Omega')} + d\varepsilon \leq \|\overline{c}_{n,k} - c^*\|_{L_2(\Omega')} + d\varepsilon. \tag{6.108}$$

As it is always the case in the convergence analysis of ill-posed problems (see Chaps. 1, 2, and 4), we need to connect the regularization parameter α of the QRM in (6.43) with various approximation errors. Those errors are the level of the error σ in the data (Lemma 6.7), the grid step size h in the s-direction, and the number ε in (6.107).

As it was stated in Sect. 6.1, the major difficulty in applying the QRM to the nonlinear case is caused by many iterations rather than by a single iteration in the linear case. More precisely, to ensure the stability of our process, we need to iteratively "suppress" the large parameter α^{-b_1} in (6.71). In addition, we need to estimate tails. These are two reasons of imposing a smallness assumption on the length $\beta = \overline{s} - \underline{s} = Nh$, where $N \geq 1$ is an integer. The latter is similar with Theorems 2.8.2 and 2.9.4.

For a number $x > 0$, let $\{x\}^\circ$ denotes such an integer that $x - \{x\}^\circ \in [0,1)$. Thus, we impose the following conditions:

$$\sigma, \varepsilon \in \left(0, \sqrt{\alpha}\right), \tag{6.109}$$

$$h = \sqrt{\alpha},\ \beta := \beta(\alpha) = \sqrt{\alpha}\{f(\alpha)\}^\circ := \sqrt{\alpha}N, \tag{6.110}$$

where the function $f(\alpha)$ is monotonically decreasing for $\alpha \in (0,1)$,

$$f(\alpha) > 0 \text{ for } \alpha \in (0,1), \lim_{\alpha \to 0^+} f(\alpha) = \infty \text{ and } \lim_{\alpha \to 0^+} \frac{f(\alpha)}{\ln(\alpha^{-1})} = 0. \tag{6.111}$$

Two examples of the function $f(\alpha)$ are

$$f_1(\alpha) = \left[\ln\left(\alpha^{-1}\right)\right]^r, r = \text{const.} \in (0,1)$$

and

$$f_2(\alpha) = \ln\left(\ln\left(\alpha^{-1}\right)\right).$$

Recall that the number of iterations can be one of regularization parameters for an ill-posed problem. On the other hand, one might also have a vector of regularization parameters. Therefore, one can consider (6.109), (6.110), and (6.111) as the linkage between regularization parameters $(\alpha, N) := (\alpha, N(\alpha))$ between themselves as well as with "error" parameters (σ, ε, h).

Let $(q_{n,k}, \overline{c}_{n,k}, V_{n,k})$ be the triple computed on a certain step of our iterative process of Sect. 6.4.3. Denote

$$\widetilde{q}_{n,k} = q_{n,k} - q_n^*,\ \widetilde{c}_{n,k} = \overline{c}_{n,k} - c^*,\ \widetilde{V}_{n,k} = V_{n,k} - V^*.$$

Similarly for $\widetilde{q}_n, \widetilde{c}_n, \widetilde{V}_n$. Note that since the function $c^* \in [1,d]$, then (6.34) implies that

$$|c_{n,k}(x) - c^*(x)| \leq |\overline{c}_{n,k}(x) - c^*(x)| = |\widetilde{c}_{n,k}(x)|,\ x \in \Omega. \tag{6.112}$$

Even though we have assumed (for brevity only) that there is no error in functions of (6.90), Lemma 6.7 and Theorem 6.7 "allow" error to be present in functions $\psi_0^*(x,\overline{s}), \psi_1^*(x,\overline{s})$ in (6.98).

Lemma 6.7 (estimate of $\widetilde{\mathbf{V}}_{1,1}$). *Let the domain Ω be as in (6.44) and the source $x_0 \notin \overline{\Omega}$. Let assumptions 1–3 of Sect. 6.6.2 hold as well as (6.109). Let $\Psi^* \in H^5(\Omega)$ be a function satisfying boundary conditions (6.98). Suppose that there exists a function $\Psi \in H^5(\Omega)$ satisfying boundary conditions (6.80). Let the number $\sigma \in (0,1)$ be the level of the error in the function Ψ^* when it is replaced with the function Ψ, $B = B(\Omega, \overline{s}, d, x_0) > 2$ be the constant of Theorem 2.9.1.1 and*

$$\|\Psi - \Psi^*\|_{H^5(\Omega)} \leq \sigma \leq \sqrt{\alpha}, \tag{6.113}$$

$$\|p^*\|_{H^5(\Omega)} \leq B. \tag{6.114}$$

Let the function $p = p(x;\alpha) \in H^5(\Omega)$ be the unique QRM solution of the problem (6.99), (6.100) which is guaranteed by Lemma 6.5.2. Let the tail function $V_{1,1}(x) := V_{1,1}(x;\alpha)$ has the form (6.101). Then for every $\alpha \in (0,1)$,

$$\left\|\nabla \widetilde{V}_{1,1}\right\|_{L_2(\Omega)} + \left\|\Delta \widetilde{V}_{1,1}\right\|_{L_2(\Omega)} \leq B\sqrt{\alpha}, \tag{6.115}$$

$$\|\nabla V_{1,1}\|_{C(\overline{\Omega})} \leq B. \tag{6.116}$$

Proof. Note that the existence of the function Ψ^* follows from the assumed existence of the function p^* satisfying conditions (6.97), (6.98). Likewise the trace theorem, (6.113), (6.98), and (6.100) imply that

$$\|\psi_0^*(x,\overline{s}) - \psi_0(x,\overline{s})\|_{H^1(\Gamma_1)} + \|\psi_1^*(x,\overline{s}) - \psi_0(x,\overline{s})\|_{L_2(\Gamma_1)} \leq C\frac{\sigma}{\overline{s}^2},$$

where $C = C(\Omega) > 0$ is a constant. This means that the error is introduced in the boundary data $\psi_0^*(x,\overline{s}), \psi_1^*(x,\overline{s})$ and its level is proportional to $\sigma \in \left(0, \sqrt{\alpha}\right)$. For brevity, we do not put in this proof the dependence of the function p from α.

Denote

$$\widetilde{p}(x) = (p - \Psi)(x) - \left(p^* - \Psi^*\right)(x).$$

Then the function $\widetilde{p}(x)$ satisfies zero boundary conditions (6.100) and

$$(\Delta\widetilde{p}, \Delta v) + \alpha [\widetilde{p}, v] = \left(\Delta\Psi^* - \Delta\Psi, \Delta v\right) + \alpha \left[\Psi^* - \Psi, v\right] + \alpha \left[p^*, v\right],$$

for all functions $v \in H^5(\Omega)$ satisfying zero boundary conditions (6.100). Setting here $v := \widetilde{p}$, and using (6.109), (6.113), and (6.114), we obtain

$$\|\Delta\widetilde{p}\|^2_{L_2(\Omega)} + \alpha \|\widetilde{p}\|^2_{H^5(\Omega)} \leq \alpha B^2. \tag{6.117}$$

Estimate $\|\Delta\widetilde{p}\|^2_{L_2(\Omega)}$ in (6.117) from the below. We have

$$(\Delta\widetilde{p})^2 = \left(\widetilde{p}^2_{xx} + \widetilde{p}^2_{yy} + \widetilde{p}^2_{zz}\right) + 2\widetilde{p}_{xx}\widetilde{p}_{yy} + 2\widetilde{p}_{xx}\widetilde{p}_{zz} + 2\widetilde{p}_{yy}\widetilde{p}_{zz}, \tag{6.118}$$

$$2\widetilde{p}_{xx}\widetilde{p}_{yy} = \partial_x\left(2\widetilde{p}_x\widetilde{p}_{yy}\right) - 2\widetilde{p}_x\widetilde{p}_{yyx} = \partial_x\left(2\widetilde{p}_x\widetilde{p}_{yy}\right) + \partial_y\left(-2\widetilde{p}_x\widetilde{p}_{xy}\right) + 2\widetilde{p}^2_{xy},$$

$$2\widetilde{p}_{xx}\widetilde{p}_{zz} = \partial_x\left(2\widetilde{p}_x\widetilde{p}_{zz}\right) - 2\widetilde{p}_x\widetilde{p}_{zzx} = \partial_x\left(2\widetilde{p}_x\widetilde{p}_{zz}\right) + \partial_z\left(-2\widetilde{p}_x\widetilde{p}_{xz}\right) + 2\widetilde{p}^2_{xz},$$

and similarly for $2\widetilde{p}_{yy}\widetilde{p}_{zz}$. Integrate (6.118) over Ω using these formulas for products. Since by (6.98) and (6.100) $\partial_n\widetilde{p}\ |_{\partial\Omega} = 0$, then boundary integrals will be equal zero. Next, use

$$\widetilde{p}_x(x, y, z) = \int\limits_{-1/4}^{x} \widetilde{p}_{xx}(\xi, y, z)\, d\xi$$

and similar formulas for $\widetilde{p}_y, \widetilde{p}_z$. Using (6.117), we obtain

$$\alpha B^2 \geq \|\Delta\widetilde{p}\|^2_{L_2(\Omega)} \geq \sum_{|\alpha|=2} \|D^\alpha\widetilde{p}\|^2_{L_2(\Omega)} \geq C \|\nabla\widetilde{p}\|^2_{L_2(\Omega)}.$$

This, (6.92), (6.101), (6.113), and (6.114) imply (6.115). Next, by (6.104), (6.109), (6.113) (6.114), and (6.117) $\|\nabla p\|_{C(\overline{\Omega})} \leq C \|p\|_{H^5(\Omega)} \leq B$. This estimate combined with (6.101) imply (6.116). □

Theorem 6.7 claims approximate global convergence property of the algorithm of Sects. 6.4.3 and 6.4.4 in the framework of the third approximate mathematical model.

Theorem 6.7. *Let the following conditions hold: ones of Sect. (6.81), (6.90), ones of Lemma 6.7, as well as (6.102), (6.105), (6.106),(6.107), (6.109), (6.110), and (6.111). Let the number $\beta \in (P_2, 1)$, m be the number of inner iterations for functions $q_{n,k}$, $k \in [1, m]$ and f be the function in (6.110), (6.111). Then there exists a constant $D = D(\overline{s}, d, x_0, C^*, f, P_2, \beta) > 1$, numbers*

$$b_1 = b_1\left(\overline{s}, d, x_0, C^*, f, P_2, \beta\right) \in \left(0, \frac{1}{2}\right),\ b_2 = \frac{1}{2} - b_1$$

defined in (6.69) and (6.70) and a sufficiently small $\alpha_0 = \alpha_0(\overline{s}, d, x_0, C^*, f, P_2, \beta, m, N) \in (0,1)$ *such that the following estimates are valid:*

$$\|c_n - c^*\|_{L_2(\Omega_1)} \leq \alpha^{b_2/2}, \ \forall (n,\alpha) \in [1,N] \times (0,\alpha_0). \tag{6.119}$$

Thus, the iterative process of Sects. 6.4.3 and 6.4.4 is approximately globally convergent of the level $\alpha^{b_2/2}$ *in the framework of the third approximate mathematical model.*

Proof. In this proof, $B = B(\Omega, \overline{s}, d, x_0) > 2$ is the constant of Theorem 2.9.1.1. A combination of Theorem 2.7.2 with (6.5), (6.18), (6.19), (6.20), (6.34), (6.35), (6.36), and (6.37) guarantees the existence and uniqueness of tails $V_{n,k}$. Note that because of (6.79) and (6.80), the estimate (6.82) does not change when the number N of subintervals of the interval $[\underline{s}, \overline{s}]$ increases with the decrease of the parameter α. Let $(n,k) \in [1,N] \times [1,m]$.

Assuming that the constant D is found, we first estimate the number $D^{2Nm+4}\alpha^{b_2}$. Using (6.110) and (6.111), we obtain that there exists a sufficiently small number

$$\alpha_0 = \alpha_0\left(\overline{s}, d, x_0, C^*, f, P_2, \beta, m, N\right) \in (0,1),$$

such that for all $\alpha \in (0, \alpha_0)$,

$$D^{2Nm+4}\alpha^{b_2} \leq D^4 \exp\left\{-\ln\left(\alpha^{-1}\right)\left[b_2 - 2m \ln D \frac{f(\alpha)}{\ln(\alpha^{-1})}\right]\right\} < \alpha^{b_2/2}. \tag{6.120}$$

Below, in this proof, $\alpha \in (0, \alpha_0)$. It follows from (6.120) that it is sufficient to prove that

$$\|c_n - c^*\|_{L_2(\Omega')} \leq D^{2nm}\alpha^{b_2}, \ \forall (n,\alpha) \in [1,N] \times (0,\alpha_0). \tag{6.121}$$

By (6.26), (6.28), (6.40), (6.85), (6.87), (6.90), and (6.96), the function $\widetilde{q}_{n,k}$ is the QRM solution of the following problem:

$$\Delta \widetilde{q}_{n,k} - A_{1,n}\left(\chi_2(x) h \sum_{j=0}^{n-1} \nabla q_j - \nabla V_{n,k}\right) \nabla \widetilde{q}_{n,k} = \widetilde{H}_{n,k}, \tag{6.122}$$

$$\widetilde{q}_{n,k}\,|_{\Gamma_1} = \partial_{x_3}\widetilde{q}_{n,k}\,|_{\Gamma_1} = \partial_n \widetilde{q}_{n,k}\,|_{\Gamma_2 \cup \Gamma_3} = 0, \tag{6.123}$$

where

$$\widetilde{H}_{n,k}(x) = -A_{1,n}\left(\chi_2(x) h \sum_{j=0}^{n-1} \nabla \widetilde{q}_j - \nabla \widetilde{V}_{n,k}\right) \nabla q_n^*$$

$$-A_{2,n}\left(\chi_2(x) h \sum_{j=0}^{n-1} \nabla \widetilde{q}_j\right)\left(h \sum_{j=0}^{n-1}\left(\nabla q_j + \nabla q_j^*\right) - 2\nabla V_{n,k}\right)$$

$$+A_{2,n}\nabla\widetilde{V}_{n,k}\left(2\chi_2(x)\,h\sum_{j=0}^{n-1}\nabla q_j^* - \left(\nabla V_{n,k}+\nabla V^*\right)\right)$$
$$-(1-\chi_2(x))\,h\sum_{j=0}^{n-1}\nabla q_j^*\left(-A_{1,n}\nabla q_n^* + A_{2,n}h\sum_{j=0}^{n-1}\nabla q_j^* - 2A_{2,n}\nabla V_{n,k}^*\right). \tag{6.124}$$

Let $Q_n(x)$ be the last line of (6.124). We now estimate this function using Theorem 2.9.1.1, (6.81), (6.83), (6.103), (6.110), (6.111), and (6.116):

$$\|Q_n\|_{L_2(\Omega)} \le 8\overline{s}^2 C^*\sqrt{\alpha}\,f(\alpha)\left(C^*+\sqrt{\alpha}\,f(\alpha)+B\right) \le \alpha^{b_2},\ n\in[1,N]. \tag{6.125}$$

First, we estimate $\widetilde{q}_{1,1}$. Denote

$$G_{1,1}\widetilde{q}_{1,1} := \Delta\widetilde{q}_{1,1} + A_{1,1}\nabla V_{1,1}\nabla\widetilde{q}_{n,k}.$$

The function $\widetilde{q}_{1,1}$ satisfies boundary conditions (6.123). In addition, since $\widetilde{q}_{1,1}$ is the QRM solution of the problem (6.122), (6.123), (6.124) for $(n,k)=(1,1)$, then the following integral identity holds for all functions $v\in H^5(\Omega)$ satisfying (6.123):

$$(G_{1,1}\widetilde{q}_{1,1}, G_{1,1}v) + \alpha\left[\widetilde{q}_{1,1}, v\right] = \left(\widetilde{H}_{1,1}, G_{1,1}v\right) - \alpha\left[q_1^*, v\right],$$
$$\widetilde{H}_{1,1} := A_{1,1}\nabla\widetilde{V}_{1,1}\nabla q_n^* - A_{2,n}\nabla\widetilde{V}_{1,1}\left(\nabla V_{1,1}+\nabla V^*\right) + Q_1. \tag{6.126}$$

By (2.195), (Theorem 2.9.1.1), and (6.103), $\|A_{1,1}\nabla V_{1,1}\|_{C(\overline{\Omega})} \le 8B\overline{s}^2$. Hence, using Lemma 6.5.3, Theorem 6.5, and (6.83), we obtain

$$\|\widetilde{q}_{1,1}\|_{H^5(\Omega)} \le D\left(\alpha^{-1/2}\left\|\widetilde{H}_{1,1}\right\|_{L_2(\Omega)}+1\right), \tag{6.127}$$

$$\|\widetilde{q}_{1,1}\|_{H^2(\Omega_{P_2})} \le D\left(\alpha^{-b_1}\left\|\widetilde{H}_{1,1}\right\|_{L_2(\Omega)}+\alpha^{b_2}\right). \tag{6.128}$$

Estimate now the norm $\left\|\widetilde{H}_{1,1}\right\|_{L_2(\Omega)}$. By (2.195), (Theorem 2.9.1.1), (6.83), (6.103), (6.115), (6.116), (6.125), and (6.126),

$$\left\|\widetilde{H}_{1,1}\right\|_{L_2(\Omega)} \le 8\overline{s}^2 C^* B\alpha^{b_2} + 16\overline{s}^2 B\alpha^{b_2} + \alpha^{b_2} \le 8\overline{s}^2 B\left(C^*+3\right)\alpha^{b_2}.$$

We choose such a constant D that

$$D \ge 8\overline{s}^2 B\left(C^*+6\right). \tag{6.129}$$

Hence,

$$\left\|\widetilde{H}_{1,1}\right\|_{L_2(\Omega)} \le D\alpha^{b_2}.$$

Hence, using (6.127), (6.128). (6.129), and $b_2 = 1/2 - b_1$, we obtain

$$\|\widetilde{q}_{1,1}\|_{H^5(\Omega)} \leq D^2\left(\alpha^{-b_1}+1\right), \tag{6.130}$$

$$\|\widetilde{q}_{1,1}\|_{H^2(\Omega_{P_2})} \leq D^2\left(\alpha^{1/2-2b_1}+\alpha^{b_2}\right). \tag{6.131}$$

Since $q_{1,1} = \widetilde{q}_{1,1} + q_1^*$, then (6.83), (6.104), and (6.130) lead to

$$\|q_{1,1}\|_{C^1(\overline{\Omega})} \leq D^3\left(\alpha^{-b_1}+2\right). \tag{6.132}$$

We now estimate $\|\widetilde{c}_{1,1}\|_{L_2(\Omega')}$. It follows from (6.32), (6.33), (6.88), (6.89), and (6.90) that

$$\begin{aligned}\widetilde{c}_{1,1} = &\left(-h\Delta\widetilde{q}_{1,1} + \Delta\widetilde{V}_{1,1}\right)\\ &+s_1^2\left(-h\nabla\widetilde{q}_{1,1} + \nabla\widetilde{V}_{1,1}\right)\left[-h\nabla\left(q_{11}+q_1^*\right) + \nabla\left(V_{11}+V^*\right)\right].\end{aligned} \tag{6.133}$$

By (6.120),

$$D^{2Nm+4}\alpha^{b_2} < N^{-1}. \tag{6.134}$$

Hence, (6.83), (6.104), (6.110), (6.129), (6.130), (6.131), (6.132), and (6.134) imply that

$$h\left\|\Delta\widetilde{q}_{1,1}\right\|_{L_2(\Omega_{P_2})}, h\left\|\nabla\widetilde{q}_{1,1}\right\|_{L_2(\Omega_{P_2})} \leq 2D^2\alpha^{2b_2} \leq D^3\alpha^{2b_2} \leq \alpha^{b_2}N^{-1}, \tag{6.135}$$

$$h\left(\|\nabla q_{1,1}\|_{C(\overline{\Omega})} + 2\left\|\nabla q_1^*\right\|_{C(\overline{\Omega})}\right) \leq D^3\left(\alpha^{b_2}+4\alpha^{1/2}\right) \leq N^{-1}. \tag{6.136}$$

Next, by (2.195), (Theorem 2.9.1.1), and (6.116), $\|\nabla\left(V_{11}+V^*\right)\|_{C(\overline{\Omega})} \leq 2B$. Hence, using (6.129) and (6.136), we obtain

$$s_1^2\left\|-h\nabla\left(q_{1,1}+q_1^*\right) + \nabla\left(V_{1,1}+V^*\right)\right\|_{C(\overline{\Omega})} \leq D.$$

Hence, (6.115), (6.129), (6.133), and (6.135) imply that

$$\|\widetilde{c}_{1,1}\|_{L_2(\Omega')} \leq \|\widetilde{c}_{1,1}\|_{L_2(\Omega_{P_2})} \leq \left(B+N^{-1}\right)(D+1)\alpha^{b_2} \leq D^2\alpha^{b_2}. \tag{6.137}$$

Hence, (2.196), (Theorem 2.9.1.1), (6.108), (6.109), (6.129), and (6.137) lead to

$$\left\|\nabla\widetilde{V}_{1,2}\right\|_{L_2(\Omega)} + \left\|\Delta\widetilde{V}_{1,2}\right\|_{L_2(\Omega)} \leq D^3\alpha^{b_2}. \tag{6.138}$$

We have obtained estimates (6.130)–(6.132), (6.135), (6.136), (6.137) and (6.138) starting from the estimates (6.115), and (6.116) for functions $\widetilde{V}_{1,1}, V_{1,1}, V^*$. Hence, continuing this process m times, using $q_1 = q_{1,m}, c_1 = c_{1,m}$, and keeping in mind that by (6.38) $V_{2,1} = V_{1,m+1}$, we obtain similarly with (6.135)–(6.138)

$$h\left\|\nabla\widetilde{q}_1\right\|_{L_2(\Omega_{P_2})}, h\left\|\Delta\widetilde{q}_1\right\|_{L_2(\Omega_{P_2})} \leq \alpha^{b_2}N^{-1}, \tag{6.139}$$

$$h\left(\left\|\nabla q_1\right\|_{C(\overline{\Omega})} + 2\left\|\nabla q_1^*\right\|_{C(\overline{\Omega})}\right) \leq N^{-1}, \tag{6.140}$$

$$\left\|c_1 - c^*\right\|_{L_2(\Omega')} \leq \left\|\widetilde{c}_{1,m}\right\|_{L_2(\Omega')} \leq D^{2m}\alpha^{b_2}, \tag{6.141}$$

$$\left\|\nabla\widetilde{V}_{2,1}\right\|_{L_2(\Omega)} + \left\|\Delta\widetilde{V}_{2,1}\right\|_{L_2(\Omega)} \leq D^{2m+1}\alpha^{b_2}. \tag{6.142}$$

To obtain (6.141) from (6.137), we have used (6.112). Note that the estimate (6.141) is the estimate (6.121) for $n = 1$. Thus, Theorem 6.7 is proved for $N = 1$. Suppose now that $N \geq 2$ Without loss of generality, it is convenient to assume that $N > 2$. Let $n \in [2, N)$. Because of (6.139), (6.140), (6.141), and (6.142), we assume that

$$h\sum_{j=0}^{n-1}\left\|\nabla\widetilde{q}_j\right\|_{L_2(\Omega_{P_2})}, h\sum_{j=0}^{n-1}\left\|\Delta\widetilde{q}_j\right\|_{L_2(\Omega_{P_2})} \leq \frac{n-1}{N}\alpha^{b_2}, \tag{6.143}$$

$$h\sum_{j=0}^{n-1}\left(\left\|\nabla q_j\right\|_{C(\overline{\Omega})} + 2\left\|\nabla q_j^*\right\|_{C(\overline{\Omega})}\right) \leq \frac{n-1}{N}, \tag{6.144}$$

$$\left\|\nabla\widetilde{V}_{n,1}\right\|_{L_2(\Omega_{P_2})} + \left\|\Delta\widetilde{V}_{n,1}\right\|_{L_2(\Omega_{P_2})} \leq D^{2(n-1)m+1}\alpha^{b_2}, \tag{6.145}$$

$$\left\|c_{n-1} - c^*\right\|_{L_2(\Omega')} \leq \left\|\widetilde{c}_{n-1,m}\right\|_{L_2(\Omega_{P_2})} \leq D^{2(n-1)m}\alpha^{b_2}. \tag{6.146}$$

Denote

$$D^{2(n-1)m+1}\alpha^{b_2} := D_{n-1}\alpha^{b_2}. \tag{6.147}$$

We are going to prove now (6.143), (6.144), (6.145), (6.146), and (6.121) for $n := n + 1$. Because of (6.122), denote

$$G_{n,1}\widetilde{q}_{n,1} = \Delta\widetilde{q}_{n,1} - A_{1,n}\left(\chi_2(x)\, h\sum_{j=0}^{n-1}\nabla q_j - \nabla V_{n,1}\right)\nabla\widetilde{q}_{n,1}. \tag{6.148}$$

The function $\widetilde{q}_{n,1}$ satisfies boundary conditions (6.123) as well as the following integral identity for all functions $v \in H^5(\Omega)$ satisfying boundary conditions (6.123):

$$\left(G_{n,1}\widetilde{q}_{n,1}, G_{n,1}v\right) + \alpha\left[\widetilde{q}_{n,1}, v\right] = \left(\widetilde{H}_{n,1}, G_{n,1}v\right) - \alpha\left[q_n^*, v\right]. \tag{6.149}$$

Estimate the coefficient at $\nabla\widetilde{q}_{n,1}$ in (6.148). Using (2.195), (Theorem 2.9.1.1), (6.103), and (6.144), we obtain:

$$\left|A_{1,n}\left(\chi_2(x)\, h\sum_{j=0}^{n-1}\nabla q_j - \nabla V_{n,1}\right)\right| \leq 16B\overline{s}^2. \tag{6.150}$$

In terms of Theorem 6.5, an important feature of (6.150) is that this estimate is independent on n. Hence, the same constants $D, b_1, b_2 = 1/2 - b_1$ can be used in (6.151), (6.152) for all $n \in [2, N)$. Thus, using Lemma 6.5.3, Theorem 6.5, (6.129), (6.149), and (6.150), we obtain

$$\|\widetilde{q}_{n,1}\|_{H^5(\Omega)} \leq D\left(\alpha^{-1/2}\left\|\widetilde{H}_{n,1}\right\|_{L_2(\Omega)} + 1\right), \tag{6.151}$$

$$\|\widetilde{q}_{n,1}\|_{H^2(\Omega_{P_2})} \leq D\left(\alpha^{-b_1}\left\|\widetilde{H}_{n,1}\right\|_{L_2(\Omega)} + \alpha^{b_2}\right). \tag{6.152}$$

Hence, using (6.79), (6.80), (6.103), (6.104), (6.124), (6.125), (6.129), (6.143)–(6.147), Theorem 2.9.1.1, and that $B > 2$, we obtain

$$\begin{aligned}\left\|\widetilde{H}_{n,1}\right\|_{L_2(\Omega)} &\leq 8\overline{s}^2\left(\frac{n-1}{N}\alpha^{b_2} + D_{n-1}\alpha^{b_2}\right)C^* + 8\overline{s}^2\frac{n-1}{N}\alpha^{b_2}\left(\frac{n-1}{N} + 2B\right)\\ &\quad + 8\overline{s}^2 D_{n-1}\alpha^{b_2}\left(2\frac{n-1}{N} + 2B\right) + \alpha^{b_2}\\ &\leq 8\overline{s}^2 D_{n-1}\alpha^{b_2}\left(3 + 4B + \frac{3}{2}C^*\right) \leq DD_{n-1}\alpha^{b_2}.\end{aligned}$$

Hence, (6.104), (6.134), (6.145), (6.151), and (6.152) imply that

$$h\left(\|\nabla q_{n,1}\|_{C(\overline{\Omega})} + 2\left\|\nabla q^*_{n,1}\right\|_{C(\overline{\Omega})}\right) \leq D^3 D_{n-1}\alpha^{b_2} \leq D^{2Nm+4}\alpha^{b_2} \leq N^{-1}, \tag{6.153}$$

$$h\,\|\widetilde{q}_{n,1}\|_{H^2(\Omega_{P_2})} \leq D\left(DD_{n-1}\alpha^{2b_2} + \alpha^{b_2+1/2}\right) \leq D^{2Nm+4}\alpha^{2b_2} \leq \alpha^{b_2}N^{-1}. \tag{6.154}$$

We obtain similarly with (6.133)

$$\begin{aligned}\widetilde{c}_{n,1} &= -h\Delta\widetilde{q}_{n,1} - h\sum_{j=0}^{n-1}\Delta\widetilde{q}_j + \Delta\widetilde{V}_{n,1}\\ &\quad + s_n^2\left(-h\nabla\widetilde{q}_{n,1} - h\sum_{j=0}^{n-1}\nabla\widetilde{q}_j + \nabla\widetilde{V}_{n,1}\right)\\ &\quad \cdot\left(-h\nabla\left(q_{n,1} + q_n^*\right) - h\sum_{j=0}^{n-1}\nabla\left(q_j + q_j^*\right) + \nabla\left(V_{n,1} + V^*\right)\right).\end{aligned}$$

Hence, using (6.129), (6.143)–(6.145), (6.153), and (6.154), we obtain

$$\|\widetilde{c}_{n,1}\|_{L_2(\Omega_{P_2})} \leq \left(\frac{n}{N}\alpha^{b_2} + D_{n-1}\alpha^{b_2}\right)\left[1 + \overline{s}^2\left(\frac{n}{N} + B\right)\right] \leq DD_{n-1}\alpha^{b_2}.$$

Hence, (2.196), (Theorem 2.9.1.1), (6.108), and (6.109) imply that

$$\left\|\nabla \widetilde{V}_{n,2}\right\|_{L_2(\Omega)} + \left\|\Delta \widetilde{V}_{n,2}\right\|_{L_2(\Omega)} \leq D^2 D_{n-1}\alpha^{b_2}.$$

Similarly for $k = 1, \ldots, m$,

$$\|\widetilde{c}_{n,k}\|_{L_2(\Omega_{P_2})} \leq D^{2k-1} D_{n-1}\alpha^{b_2},$$

$$\left\|\nabla \widetilde{V}_{n,k+1}\right\|_{L_2(\Omega)} + \left\|\Delta \widetilde{V}_{n,k+1}\right\|_{L_2(\Omega)} \leq D^{2k} D_{n-1}\alpha^{b_2}.$$

Hence, similarly with the above, we obtain that estimates (6.153), (6.154) are valid for functions $q_{n,k}, \widetilde{q}_{n,k}$.This implies the validity of (6.143) and (6.144) for $n := n + 1$. Similarly,

$$\|c_{n,k} - c^*\|_{L_2(\Omega')} \leq \|\widetilde{c}_{n,k}\|_{L_2(\Omega_{P_2})} \leq D^{2k} D_{n-1}\alpha^{b_2} = D^{2(n-1)m+2k}\alpha^{b_2}, k \in [1, m],$$

$$\left\|\nabla \widetilde{V}_{n,m+1}\right\|_{L_2(\Omega)} + \left\|\Delta \widetilde{V}_{n,m}\right\|_{L_2(\Omega)} \leq D^{2m} D_{n-1}\alpha^{b_2} = D^{2nm+1}\alpha^{b_2}.$$

The last two estimates establish (6.145) and (6.146) for $n := n + 1$. □

6.8 Numerical Studies

6.8.1 *Main Discrepancies Between Convergence Analysis and Numerical Implementation*

It is well known that some discrepancies between the convergence analysis and numerical implementations are almost inevitable for both well-posed and ill-posed problems. The main reason is that because of the complicated structure of those problems, the theory usually can grasp only a part of numerical studies rather than all aspects. For example, as it was pointed out in Sect. 2.10, constants in convergence theorems usually are significantly overestimated (maybe with the only exception of a few very simple linear problems).

We now list main discrepancies between the above convergence analysis of this chapter and the numerical implementation for our specific case. Some of these discrepancies are the same as ones named in Sect. 3.1.2. The *first* main discrepancy is with regard to Lemma 2.3 about a sufficient condition of the regularity of geodesic lines. In general, an easily verifiable condition of this sort is unknown, except of the trivial case when the function $c(x)$ is close to a constant. On the other hand, the authors are unaware about any reasonable results for CIPs for hyperbolic PDEs without either the assumption of the regularity of geodesic lines or a somewhat close assumption. We verify the asymptotic behavior of Lemma 2.3 computationally; see Sect. 3.1.2.

The *second* main discrepancy is that we replace in our computations $\alpha \|u\|^2_{H^5(\Omega)}$ in (6.43) with $\alpha \|u\|^2_{H^2(\Omega)}$, because the latter is simpler to implement numerically. One of the reasons why this works computationally is that we deal with finite dimensional spaces whose dimensions are not exceedingly large. Recall that all norms are equivalent in such spaces.

The *third* main discrepancy is that we conduct computations for the case when the point source in (6.2) is replaced with the plane wave. This is because the case of the plane wave is reasonable for our target application to imaging of plastic land mines, since the wave radiated by a point source effectively becomes a pane wave when that source is located far from the domain of interest. We have chosen the point source in (6.2) only because we wanted to use Lemma 2.3. Other than this, the above technique can be easily extended to the case of the plane wave.

The *fourth* main discrepancy is that we have ignored in our computations the function $\chi_2(x)$ in Sects. 6.4.2 and 6.4.3. Indeed, this function was introduced only for the sake of the convergence analysis.

6.8.2 A Simplified Mathematical Model of Imaging of Plastic Land Mines

The first main simplification of our model is that we consider the 2D case instead of 3D, although a 3D numerical test is also presented below. Second, we ignore the air/ground interface, assuming that the governing PDE is valid on the entire 2D plane. Results of Sect. 6.9 indicate that the influence of the air/ground interface can be handled via a data pre-processing procedure.

Let the ground be $\{\mathbf{x} = (x, z) : z > 0\} \subset \mathbb{R}^2$. Suppose that a polarized electric field is generated by a plane wave, which is initialized at the line $\left\{z = z^0 < 0, x \in \mathbb{R}\right\}$ at the moment of time $t = 0$. The following hyperbolic equation can be derived from the Maxwell's equations in the 2D case:

$$\varepsilon_r(\mathbf{x}) u_{tt} = \Delta u, \ (\mathbf{x}, t) \in \mathbb{R}^2 \times (0, \infty), \tag{6.155}$$

$$u(\mathbf{x}, 0) = 0, \ u_t(\mathbf{x}, 0) = \delta\left(z - z^0\right), \tag{6.156}$$

where the function $u(\mathbf{x}, t)$ is a component of the electric field and $\varepsilon_r(\mathbf{x})$ is the spatially distributed dielectric constant. We assume that the function $\varepsilon_r(\mathbf{x})$ satisfies conditions (6.3) and (6.4) in 2D. Let the function $w_0(z, s)$,

$$w_0(z, s) = \frac{\exp\left(-s|z - z_0|\right)}{2s}, \tag{6.157}$$

be the one which corresponds to the Laplace transform (6.11) of the incident plane wave with $\varepsilon_r(\mathbf{x}) \equiv 1$. Applying the Laplace transform (6.11) to the function u in (6.155), we obtain the following analog of the problem (6.12), (6.13)

$$\Delta w - s^2 \varepsilon_r(\mathbf{x}) w = -\delta\left(z - z^0\right),\ s \geq \underline{s} = \text{const.} > 0, \mathbf{x} \in \mathbb{R}^2, \tag{6.158}$$

$$\lim_{|\mathbf{x}| \to \infty} (w - w_0)(\mathbf{x}, s) = 0. \tag{6.159}$$

It is well known that the maximal depth of an antipersonnel land mine does not exceed about 10 centimeters (cm) = 0.1 meter (m). So, we model these mines as small squares with the 0.1 m length of sides, and their centers are at the depth of 0.1 m or less. We set

$$\widetilde{\Omega} = \{\mathbf{x} = (x, z) \in (-0.3, 0.3)\ \text{m} \times (0, 0.6)\ \text{m}\}.$$

Introducing dimensionless spatial variables $\mathbf{x}' = \mathbf{x}/(0.1m)$ without changing notations, we obtain that the domain $\widetilde{\Omega}$ is transformed in the dimensionless domain:

$$\Omega = (-3, 3) \times (0, 6).$$

6.8.3 Some Details of the Numerical Implementation

To simulate the data for our CIP, we have solved (6.158) in the truncated domain

$$G = (-4, 4) \times (-2, 8).$$

We have used the FDM to solve this forward problem. The boundary condition (6.159) was replaced with

$$(w - w_0)(\mathbf{x}, s)\ |_{\partial G} = 0. \tag{6.160}$$

In principle, one might impose radiation boundary conditions at the top and bottom sides of the rectangle G. However, our computational experience shows that this would not bring much change for the function $w(x, s)$ inside the domain Ω, since this function decays exponentially with $|\mathbf{x}| \to \infty$; also see Remark 6.3 for a relevant statement. To compare, we have also solved once the problem (6.155), (6.156) and have applied the Laplace transform (6.11) then. Imaging results were almost the same. To avoid using the δ-function numerically, we have solved the problem (6.158), (6.160) for the function $\overline{w} = w - w_0$.

We assume the knowledge of functions $\varphi_0(x, s), \varphi_1(x, s)$:

$$w\ |_{\Gamma_1} = \varphi_0(x, s), \partial_n w\ |_{\Gamma_1} = \varphi_1(x, s),\ s \in [\underline{s}, \overline{s}],$$

$$\partial_n (\ln w(x, s))\ |_{\Gamma_2 \cup \Gamma_3} = -s,\ s \in [\underline{s}, \overline{s}],$$

$$\Gamma_1 = \{\mathbf{x} = (x, z) : x \in (-3, 3), z = 0\},\ \Gamma_2 \cup \Gamma_3 = \partial\Omega \backslash \Gamma_1;$$

see (6.17) for the boundary condition at $\Gamma_2 \cup \Gamma_3$. Functions $\varphi_0(x,s)$, $\varphi_1(x,s)$ were obtained in numerical simulations when the above forward problem was solved. We have added the random noise of the 5% level to the function $\varphi_0(x,s)$ via

$$\varphi_{0,\sigma}(x_i,0,s_n) = \varphi_0(x_i,0,s_n)(1+\sigma\omega_n), \sigma = 0.05,$$

where $\{x_i\}$ are grid points of the FDM for the forward problem solution and $\omega \in (-1,1)$ is a random variable. To calculate the derivative $\partial_s\left[s^{-2}\ln\left(\varphi_{0,\sigma}/w_0\right)(x_i,0,s_n)\right]$ (to obtain the boundary data for $\widehat{q}(x_i,s_n)$), we have smoothed first values of $\overline{\varphi}_{0,\sigma}(x_i,0,s_n)$ with respect to s via cubic B-splines similarly with, for example, [73]. Next, we have used finite differences to calculate the desired derivative.

We model land mines as squares with the dimensionless length of the side 1, which means 10 cm in real dimensions. Centers of those squares are located at the depths of $z = 0.6$ and $z = 1$, which means depths of 6 cm and 10 cm in variables with dimensions. We took $\Omega_{P_2} = (-3,3)\times(0,3)$ (Sect. 6.4.1).

Tables of dielectric constants [151] show that in the dry sand $\varepsilon_r = 5$ and $\varepsilon_r = 22$ in the trinitrotoluene (TNT). Hence, the mine/background contrast is $\approx 22/5 = 4.4$. Hence, considering new parameters

$$\varepsilon_r' = \frac{\varepsilon_r}{5},\ s' = s\cdot 0.1\cdot\sqrt{5}$$

and not changing notations, we obtain

$$\varepsilon_r(\text{dry sand}) = 1,\ \varepsilon_r(\text{TNT}) = 4.4. \tag{6.161}$$

Because of (6.161), we impose $\varepsilon_r(\mathbf{x}) \in [1,8]$, $\varepsilon_r(\mathbf{x}) = 1$ outside of the rectangle Ω_{P_2}. We have modified our algorithm of Sect. 6.4 via considering functions

$$\widehat{v}(\mathbf{x},s) = \frac{1}{s^2}\ln\left[\frac{w}{w_0}(\mathbf{x},s)\right],\ \widehat{q}(\mathbf{x},s) = \partial_s\widehat{v}(\mathbf{x},s) \tag{6.162}$$

instead of

$$v(\mathbf{x},s) = \frac{\ln(w(\mathbf{x},s))}{s^2},\ q(\mathbf{x},s) = \partial_s v(\mathbf{x},s),$$

where the function $w_0(z,s)$ is the same as in (6.157). This has resulted in obvious modifications of equations of Sect. 6.4. A slight modification of Theorem 6.7 can be proved for this case.

We have observed in our computations that at the backscattering side Γ_1 of the above square Ω the ratio $(w/w_0)(x,0,s) \approx 1$ for $s > 1.2$. This means a poor sensitivity of the backscattering data to the presence of abnormalities for values of the pseudo-frequency $s > 1.2$. The best sensitivity was for $s \in [0.5, 1.2]$. Hence, one should expect that the modified tail function

$$\widehat{V}(\mathbf{x},\overline{s}) = V(\mathbf{x},\overline{s}) - \frac{\ln w_0(z,\overline{s})}{\overline{s}^2} \approx 0$$

for $\overline{s} > 1.2$, at least for those points $\mathbf{x}$ which are located close to Γ_1. Hence, we have chosen $\overline{s} = 1.2$ and $s \in [0.5, 1.2] := [\underline{s}, \overline{s}]$.

We note that if we would work in the original domain $\widetilde{\Omega}$ making spatial variables dimensionless as $\mathbf{x}'' = \mathbf{x}/(1m)$, then $s'' = \sqrt{5}s$ implying that $\overline{s}'' = 12 (= 1.2/0.1)$, which can be considered as a large pseudo-frequency. The latter shows that in practical computations, the above notion of sufficiently large $\overline{s}$ is actually a conditional one and depends on particular ranges of parameters at hands.

The modified QRM functional (6.43) was written in the FDM form. Its minimization was performed with respect to the values of the function $u(x)$ at grid points via the conjugate gradient method. Our regularization term was

$$\frac{\alpha}{2}\left[\|u\|^2_{H^1(\Omega)} + \|u_{xx}\|^2_{L_2(\Omega)} + \|u_{zz}\|^2_{L_2(\Omega)}\right].$$

We have chosen the regularization parameter $\alpha = 0.08$ and the spatial grid step size $h_{sp} = 0.122$. First, we have solved the problem (6.99), (6.100) via the QRM and thus have calculated the first tail $V_{1,1}(x)$ in (6.101). Next, we have continued as in Sect. 6.4 with $m := 10$. We have used the spatial grid step size $h_{sp} = 0.122$ to minimize the QRM functional (6.43) via the FDM. However, our attempt to decrease it by the factor of 2 to $h_{sp} = 0.061$ has led to a significant deterioration of computational results.

We took the grid step size in the s-direction as $h = 0.1$ and have made several sweeps over the interval $s \in [0.5, 1.2]$ as follows. Let the function $\varepsilon_r^{(1)}(\mathbf{x})$ be the approximation for the function $\varepsilon_r(\mathbf{x})$ computed on the first sweep for $[s_N, s_{N-1}] = [0.5, 0.6]$. We compute the tail function

$$V^{(1)}(\mathbf{x}) = \frac{\ln w\left(\mathbf{x},\overline{s};\varepsilon_r^{(1)}\right) - \ln w_0(z,s)}{\overline{s}^2},\ \overline{s} = 1.2,$$

where $w\left(\mathbf{x},\overline{s};\varepsilon_r^{(1)}\right)$ is the solution of the problem (6.158), (6.160) with $\varepsilon_r := \varepsilon_r^{(1)}(x)$. Next, we set $V_{1,1}^{(2)}(x) := V^{(1)}(x)$ and repeat the algorithm of Sect. 6.4. We have made these sweeps until either

$$\left\|\varepsilon_r^{(p)} - \varepsilon_r^{(p-1)}\right\|_{L_2(\Omega_{P_2})} \leq 10^{-5}$$

or the gradient of the QRM functional has "exploded," i.e., when

$$\left\|\nabla J^{\alpha}_{n,k}\left(q^{(p)}_{n,k}\right)\right\|_{L_2(\Omega_{P_2})} \geq 10^5$$

for any appropriate indices n, k, p. Here, we use the discrete $L_2(\Omega_{P_2})$ norm. Tails were computed via solving the problem (6.158), (6.160) for $s := \overline{s}$.

The above algorithm has provided us with the function $\overline{\varepsilon}_{r,\text{glob}}(\mathbf{x})$. Next, we have found points $\{a_i\}$ of local maxima of this function and truncated the threshold as

$$\varepsilon_{r,\text{glob}}(\mathbf{x}) = \begin{cases} \overline{\varepsilon}_{r,\text{glob}}(\mathbf{x}), & \text{if } \overline{\varepsilon}_{r,\text{glob}}(\mathbf{x}) \geq 0.85\overline{\varepsilon}_{r,\text{glob}}(a_i), \\ 1 & \text{otherwise.} \end{cases} \tag{6.163}$$

This truncation was done in neighborhoods of points $\{a_i\}$. We note that such truncations are quite common in the image processing.

We have observed in our computations that the above algorithm can accurately image locations of mine-like targets. However, values of the function $\varepsilon_{r,\text{glob}}(\mathbf{x})$ near points of local maxima were not imaged accurately. Thus, we have applied a two-stage numerical procedure. While the first stage was the one described above, on the second stage, we have minimized the Tikhonov regularization functional via the gradient method taking the function $\varepsilon_{r,\text{glob}}(\mathbf{x})$ as the starting point. This was done similarly with Sect. 5.8.4. However, while in Sect. 5.8.4, we have applied the gradient method alone and were not successful, now we have applied it on the second stage only. Hence, unlike Sect. 5.8.4, we were successful this time. The latter indicates the importance of the first stage. When applying the gradient method, we have truncated as threshold 87.5% of maximal values on each iteration of the gradient method in a neighborhood of each point of local maxima $\{a_i\}$ of the function $\varepsilon_{r,\text{glob}}(\mathbf{x})$, similarly with (6.163).

6.8.4 Numerical Results

We refer to Fig. 6.1 for the schematic diagram of data collection. In both tests below, the incident plane wave falls from the top, and measurement data are also collected on the top side of this rectangular prism. Although only the 3D case is depicted on Fig. 6.1, the 2D case is similar.

Test 1. We test our numerical method for the case of two squares with the same size $p = 1$ of their sides. In the left square $\varepsilon_r = 6$, in the right one $\varepsilon_r = 4$, and $\varepsilon_r = 1$ everywhere else; see (6.161). Centers of these squares are at points $(-1.5, 0.6)$ and $(1.5, 1)$. However, we do not assume a priori in our algorithm neither the presence of these squares nor a knowledge of $\varepsilon_r(\mathbf{x})$ at any point of the square Ω. We took the initial tail for the function $\widehat{v}(\mathbf{x}, s)$ in (6.162) as $\widehat{V}_{1,1}(\mathbf{x}, s) \equiv 0$. Figures 6.2a and 6.2b display correct and computed images, respectively. Locations of both mine-like targets are images accurately. The computed function $\varepsilon_{r,\text{comp}}(\mathbf{x}) = 1$ outside of imaged inclusions. Next,

$$\max\left[\varepsilon_{r,\text{comp}}(\mathbf{x})\right] = \begin{cases} 6 \text{ in the left inclusion,} \\ 4.3 \text{ in the right inclusion.} \end{cases}$$

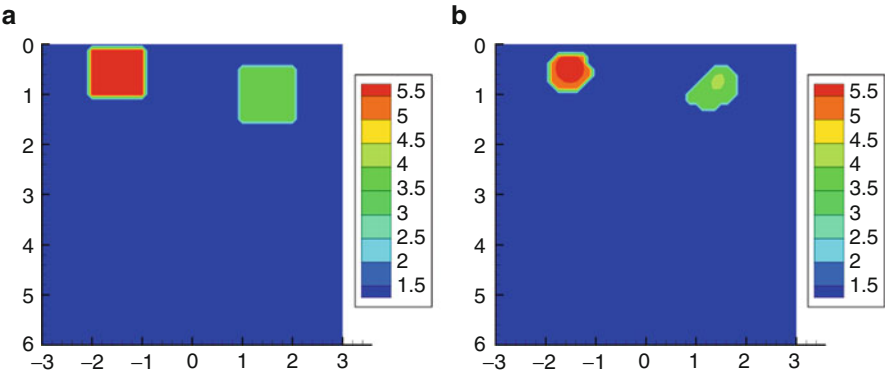

Fig. 6.2 Test 1. (**a**) Correct image. (**b**) Computed image. Locations of both mine-like targets are accurately imaged. The computed function $\varepsilon_{r,\text{comp}}(\mathbf{x}) = 1$ outside of imaged inclusions. The maximal value $\max \varepsilon_{r,\text{comp}}(\mathbf{x}) = 6$ in the left and $\max \varepsilon_{r,\text{comp}}(\mathbf{x}) = 4.3$ in the right imaged inclusion. Thus, the error in the inlcusion/background contrast is 0% in the left and 7% in the right imaged inclusion. The noise in the data was 5%. Source: A.V. Kuzhuget, N. Pantong and M.V. Klibanov, A globally convergent numerical method for a coefficient inverse problem with backscattering data, *Methods and Applications of Analysis*, 18, 47–68, 2011. Reprinted with permission

The error in the computed contrast in the right inclusion is 7%. Recall that the noise in the data was 5%. Therefore, inclusions/background contrasts are imaged accurately.

Test 2. The 3D Case. We have used 3D analogs of mine-like targets of Test 1. The size of the side of each of small cubes of Fig. 6.3a is $p = 1$. In the left cube, $\varepsilon_r = 6$, and in the right cube, $\varepsilon_r = 4$. Also, $\varepsilon_r = 1$ everywhere else. The distances between the centers and the upper side of the rectangular prism Ω were 0.6 in the left cube and 1 in the right cube. An obvious 3D analog of the problem (6.158), (6.160) was solved to simulate the backscattering data on the upper side $\{z = 0\}$ of the rectangular prism Ω of Fig. 6.3a:

$$\Omega = (-1.5, 1.5) \times (-3, 3) \times (0, 6).$$

The 5% noise in the data was introduced then, as in Sect. 6.8.3 . Although the data were simulated in 3D, when solving the inverse problem, we have solved twenty-three (23) 2D inverse problems in twenty-three (23) uniformly distributed vertical 2D cross-sections $\{x_i = b_i\}_{i=1}^{23}$ of the prism Ω.

We have solved them simultaneously on twenty-three (23) processors. We have done so because the QRM works slower in the 3D case than in the 2D case. In each 2D cross-section, the initial tail function was computed using the QRM solution of the problem (6.99), (6.100) and formula (6.101). We again have used (6.162). The above two-stage numerical method was applied. On the first stage, the approximately globally convergent numerical method of this chapter was applied. On the second stage, the gradient method of the minimization of the Tikhonov

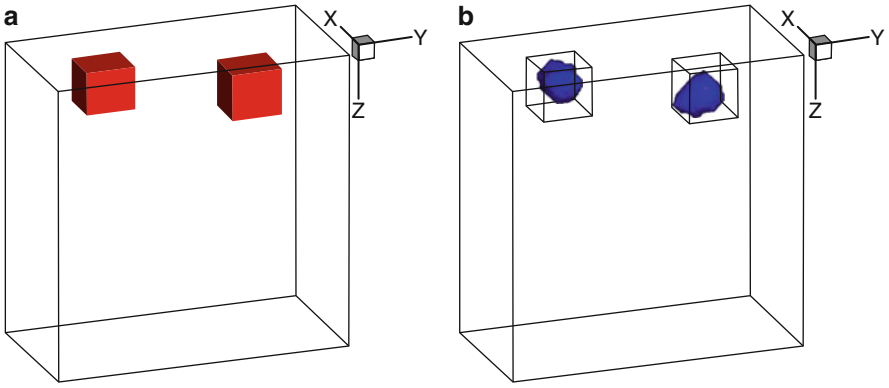

Fig. 6.3 Test 2. 3D case. (**a**) Correct image. (**b**) Computed image. Locations of both mine-like targets are accurately imaged. The computed function $\varepsilon_{r,\text{comp}}(\mathbf{x}) = 1$ outside of imaged inclusions. The maximal value $\max \varepsilon_{r,\text{comp}}(\mathbf{x}) = 6$ in the left and $\max \varepsilon_{r,\text{comp}}(\mathbf{x}) = 4$ in the right inclusion. Hence, the inclusion/background contrast is imaged very accurately for both inclusions

functional was used (Sect. 5.8.4). Having images in those 2D cross-sections, we have formed the 3D image then; see Fig. 6.3b. Locations of both inclusions are imaged accurately on this figure. The computed function $\varepsilon_{r,\text{comp}}(x) = 1$ outside of imaged inclusions. Also,

$$\max\left[\varepsilon_{r,\text{comp}}(x)\right] = \begin{cases} 6 \text{ in the left inclusion,} \\ 4 \text{ in the right inclusion.} \end{cases}$$

Therefore, inclusions/background contrasts are imaged very accurately.

6.8.5 *Backscattering Without the QRM*

A natural question to pose is *can the coefficient inverse problem 6.2 with the backscattering data (6.10) be solved by the approximately globally convergent algorithm of Sect. 2.6.1?* We now briefly describe in Test 3 one numerical example indicating that the answer on this question might be positive. This example was obtained just before submission of the text of this book to the publisher. Hence, although this example is promising, the corresponding study is not complete yet.

Test 3. In this test, the 2D analog of the coefficient inverse problem 6.2 is considered. However, the Neumann boundary condition $g_1(x,t)$ in (6.10) is not used. The data for the CIP were computationally simulated via solving the problem (6.155), (6.156) in a truncated domain, similarly with solving such problem in Sect. 4.17.1. To solve the forward problem (6.155), (6.156), we use the hybrid FEM/FDM method as in above chapters. The computational domain for the forward problem

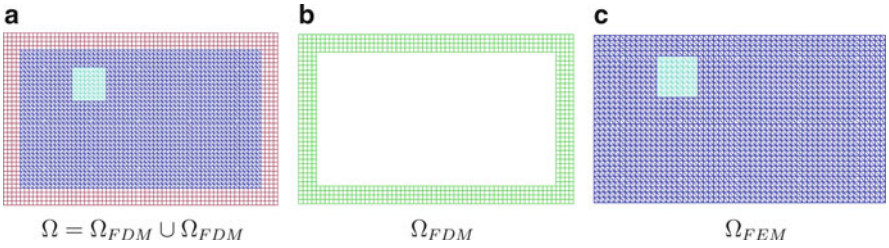

Fig. 6.4 (**a**) Geometry of the hybrid mesh. This is a combination of the quadrilateral mesh in the subdomain Ω_{FDM} (**b**), where we apply FDM, and the finite element mesh in the inner domain Ω_{FEM} (**c**), where we use FEM. The solution of the inverse problem is computed in Ω_{FEM}. The trace of the solution of the forward problem (6.155)–(6.156) is recorded at the top boundary Γ_1 of the finite element domain Ω_{FEM}

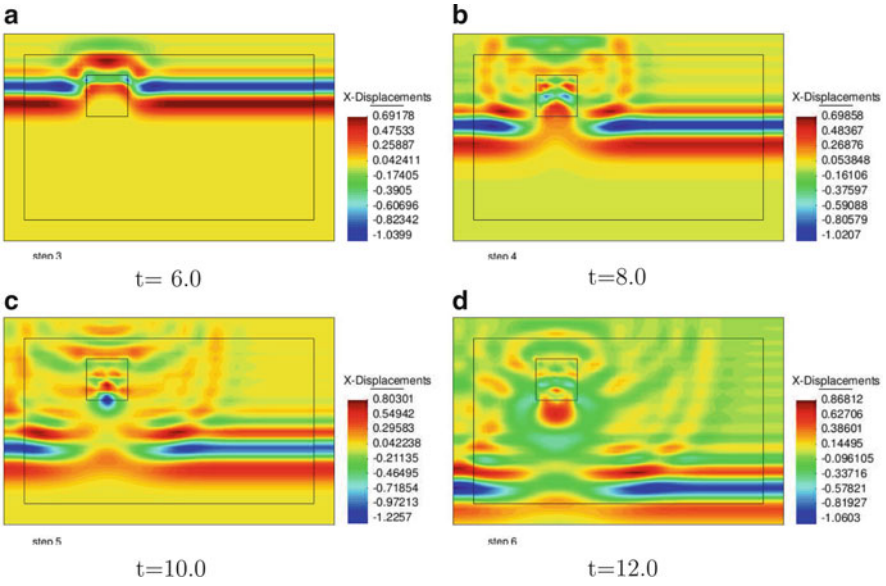

Fig. 6.5 Isosurfaces of the simulated exact solution for the forward problem (6.155)–(6.156) at different times with a plane wave initialized at the top boundary

is $\Omega = [-4, 4] \times [-1, 4]$; see Figs. 6.4 and 6.5. This domain is split into a finite element subdomain $\Omega_{\text{FEM}} := [-3.5, 3.5] \times [-0.5, 3.5]$ and a surrounding region Ω_{FDM} with a structured mesh such that $\Omega_{\text{FEM}} \cup \Omega_{\text{FDM}}$. The spatial mesh in Ω_{FEM} consists of triangles, and the mesh in Ω_{FDM} consists of squares. In the overlapping regions, the mesh size is $\widetilde{h} = 0.125$. The trace of the solution of the forward problem is recorded at the top boundary Γ_1 of Ω_{FEM}. This represents the backscattering data in space and time, and our goal is to reconstruct the unknown coefficient $\varepsilon_r(x)$ in (6.155) from these data inside the domain Ω_{FEM}.

In this test, when solving (6.26) for functions $q_{n,k}$, the function $\chi_2(x)$ was not used, and boundary conditions (6.28) were replaced with the following Dirichlet boundary conditions:

$$q_{n,k}|_{\Gamma_1} = \tilde{\psi}_{0,n}(x),\ q_{n,k}|_{\Gamma_2 \cup \Gamma_3} = \psi_{0,n}^{unif}(x). \tag{6.164}$$

Here functions $\tilde{\psi}_{0,n}(x)$ are obtained from functions $\psi_{0,n}(x)$ by setting them to zero outside of dents depicted on Figs. 6.6a, b. The functions $\psi_{0,n}^{unif}(x)$ are the ones which correspond to the case of the uniform background outside of the domain Ω_{FEM}. Recall that by (6.3) $c(x) = 1$ outside of Ω. Indeed, we have observed in our computational simulations that values of the function $\psi_0(x)$ on lateral sides of the rectangle Ω_{FEM} are only very slightly influenced by the presence of inclusions. And values of $\psi_0(x)$ on the bottom side of Ω_{FEM} are very close to zero.

Figure 6.6 displays the computed function $q(x,s), x \in \Gamma_1$ for different values of the pseudo-frequency s. We have started computations of the function $q(x)$ from very large values of the pseudo frequency $s = 18$ and finished with small values $s = 2$. We have observed numerically that the behavior of the function $|q(x,s)|$ for $x \in \Gamma_1$ is similar for all pseudo frequencies $s \leq 5$. Namely, this function is close to its maximal value only on a small part of the backscattering side Γ_1; see Fig. 6.4. This part of the boundary corresponds to the backscatered data from the inhomogeneity which should be reconstructed. However, all values of the function $|q(x)|$ for $s > 5$ are very close to zero; see Fig. 6.4e, f. Based on Fig. 6.7a–f, we have chosen the pseudo frequency interval for solving the inverse problem as $s \in [2,3]$. The grid step size with respect to s was $h = 0.05$. Just as in Sect. 5.7, we have used derivatives of tails $\partial_{\overline{s}} V_{n,k}(x,\overline{s})$ instead of tails themselves when computing functions $q_{n,k}$; see (2.182), (5.23), and Sect. 2.8.4 for explanations.

The algorithm of Sect. 2.6.1 was used to calculate the images of Fig. 6.7. Unlike Tests 1 and 2 in Sect. 6.8.4, the gradient method of the minimization of the Tikhonov functional was not used here. In other words, only the first stage of our two stage numerical procedure was used here. Location of the mine-like target is imaged accurately. Also, $\varepsilon_{r,\text{comp}}(x) = 1$ outside of the imaged inclusion, which is the correct value. Finally, $\max\left[\varepsilon_{r,\text{comp}}(x)\right] = 4$, which is the correct value. In other words, the inclusion/background 4 : 1 contrast is also accurately imaged.

6.9 Blind Experimental Data Collected in the Field

In this section, we present results which were obtained for the case of **blind** experimental data collected by the forward looking radar of US ARL [126]. We have obtained five (5) pieces of experimental data. Two of them are described here, and three more will be described in the paper [117]. All five cases were treated by exactly the same technique and accurate solutions were obtained for all of them.

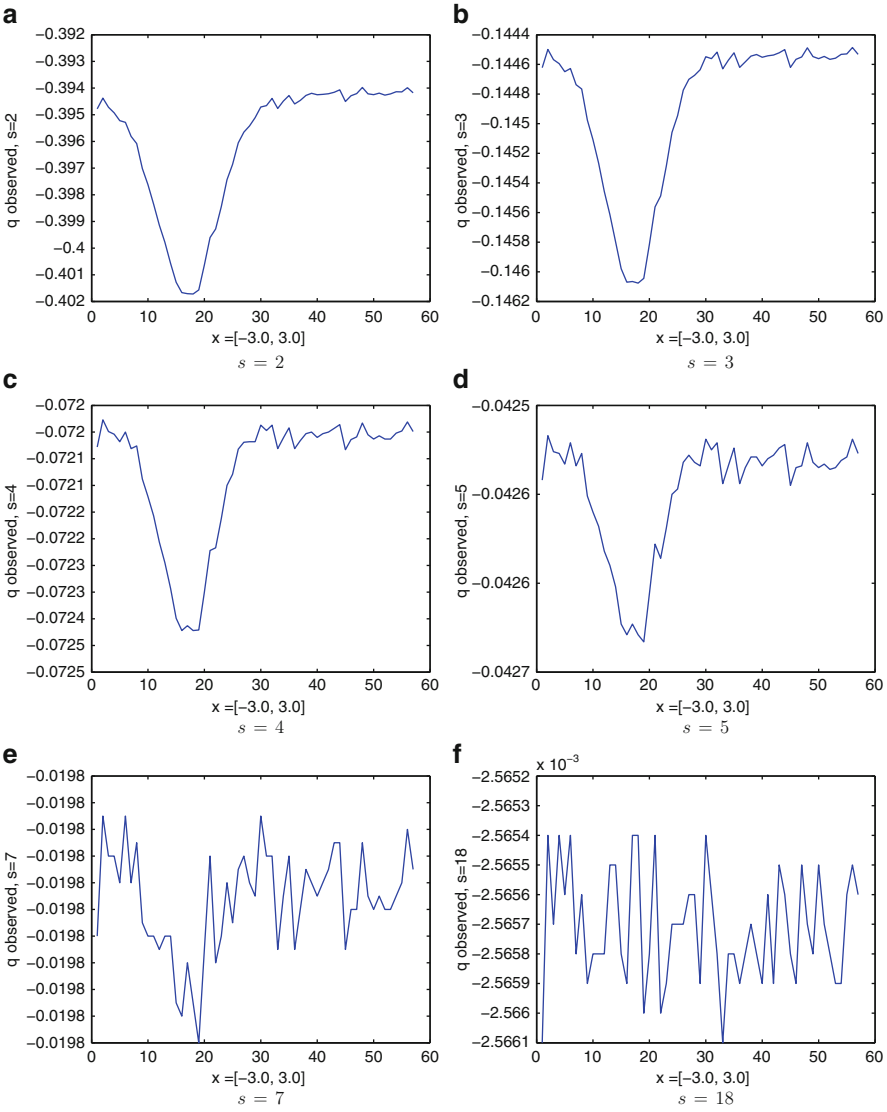

Fig. 6.6 Backscattered data for the function q at the top boundary Γ_1 of the computational domain Ω_{FEM} computed for the different values of the pseudo frequency s. We observe that for all pseudo frequencies $s \leq 5$, the values of the function $|q(x,s)|$ are close to its maximal value only on a small part of the boundary Γ_1. Values of the function $q(x,s)$ at the rest of Γ_1 are close to a constant. At the same time, $|q(x,s)| \approx 0, x \in \Gamma_1$ for $s > 5$. Computations were peformed with the software package WavES [148]

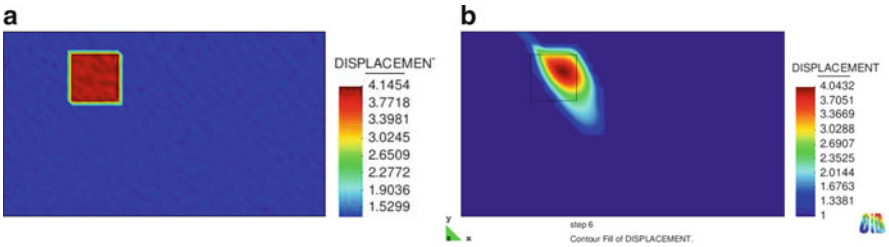

Fig. 6.7 (**a**) The computed image of the function $\varepsilon_{1,1}$ using backscattered data obtained from the geometry presented on Fig. 6.4a. Here, we used the exact tail and the variational formulation (3.14) for computing the function $\varepsilon_{1,1}$. (**b**) Computed image using backscattered data obtained from the geometry presented on Fig. 6.4a. Both location and contrast of the inclusion are accurately imaged. The computed function $\varepsilon_r = 1$ outside of imaged inclusions. The noise level in data is 5%

6.9.1 Introduction

The term "**blind**" means here that the mathematical sub-team of the authors of [117] (A.V. Kuzhuget, L. Beilina and M.V. Klibanov) had only two pieces of information when computing. The first piece was that only one target per data set was in place. And the second piece was where that target was located: below or above the ground. However, the mathematical team did not know neither constituent materials of targets, their sizes and locations, their dielectric constants nor soil. The engineering sub-team of the authors of [117] (L. Nguyen and A. Sullivan) knew the complete information about both the background medium and the targets. However, they have revealed this information to mathematicians only after computational results were presented to that team. In particular, it was revealed that the ground was always the dry sand with the dielectric constant in it:

$$\varepsilon_r \text{ (ground)} \approx 3; \tag{6.165}$$

see [151] as well as Figs. 6.14a and 6.16a. However, this dielectric constant was not measured directly, but rather was taken from tables [151].

Since dielectric constants of both targets and soil were not measured at the time when experimental data were collected, computed dielectric constants were a posteriori compared with tabulated values for constituent materials of those targets [151]. This comparison has revealed a good accuracy of computational results; see below.

A peculiar question is *how to interpret the dielectric constant of a metallic target*? This question is addressed on Figs. 6.8a, b, which were computed by Dr. Michael A. Fiddy. Comparison of these two figures shows that metallic targets can be viewed as dielectric targets with large values of dielectric constants. Hence, we choose

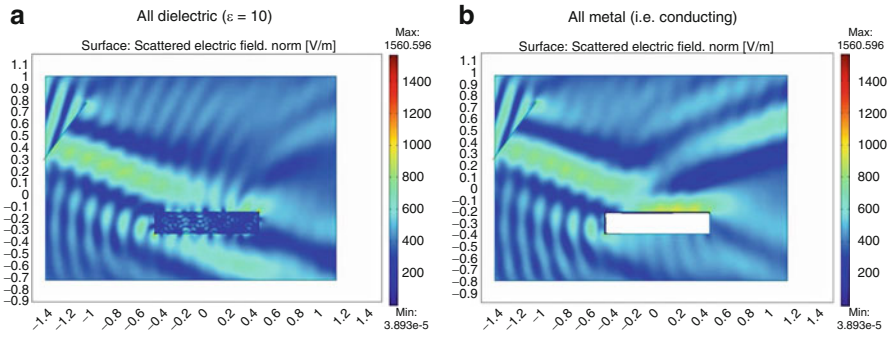

Fig. 6.8 Comparison of the reflected electric waves from a piece of metal and from a piece of dielectric with a large value of the dielectric constant. Only a single frequency is used. On (**a**) dielectric target with $\varepsilon_r = 10$ and on (**b**) metallic target are shown. Comparison of these two figures shows that reflected fields are very similar. Therefore, a metallic target can be viewed as a dielectric target with a large value of the dielectric constant ε_r

the following interpretation, which is only a conditional one and has no physical meaning:

$$\varepsilon_r(\text{metal}) \geq 10. \tag{6.166}$$

We call this *conditional dielectric constants* for metals. Furthermore, our computational simulations (not shown here) have demonstrated that values of the backscattering data $\varphi(s) := w(0, s)$ in (6.179) were changing only slightly when the value of ε_r (target) has increased larger than 10. Therefore, it is unlikely that target/background contrasts exceeding 10 can be accurately imaged.

6.9.2 *Data Collection and Imaging Goal*

The schematic diagram of data collection by the forward looking radar is depicted on Figs. 6.9 and 6.10. The goal of this radar is to detect and possibly identify shallow mine-like targets under the ground (a few centimeters depth) as well as those lying on the ground. The signals are originated by electric pulses emitted by two sources installed on the radar with 2 meters distance between sources. Only one component of the electric field is originated by these pulses. The time dependence of that component of the electric field is measured in the backscattering regime. Measurements are performed by sixteen (16) detectors with the step size in time of 0.133 nanosecond. For any target of interest, the radar/target distance is provided by the ground positioning system (GPS) in real time with only a few centimeters error.

For a shallow target which is located either above the ground or a few centimeters deep under the ground, the GPS provides the distance between the radar and a point on the ground located above that target. Resulting time-dependent curves are

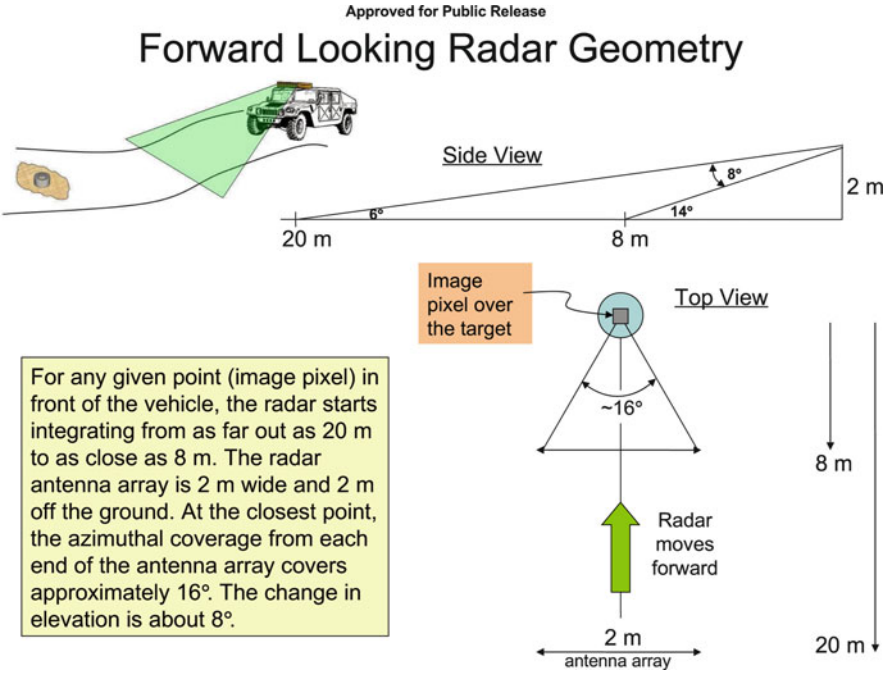

Fig. 6.9 The schematic diagram of data collection by the forward looking radar of US Army Research Laboratory

integrated over radar/target distances between 20 meters and 8 meters. In addition, readings of all sixteen (16) detectors are averaged. Hence, for any target of interest, only a single time dependent curve, which was approximately "responsible" for this target, was given to us. This means in turn that only a 1D CIP can be solved.

Since the radar/target distance is provided by GPS with a good accuracy, geometrical parameters of targets, including their depths, are not of an interest here. On the other hand, the available data processing procedure of this radar delivers only the energy information. Hence, the *main goal* of our work was to provide an additional imaging capability for this radar via imaging ratios R of dielectric constants:

$$R = \frac{\varepsilon_r(\text{target})}{\varepsilon_r(\text{background})}. \tag{6.167}$$

Using (6.165) and the value of R in (6.167), one can easily calculate ε_r(target) for targets located under the ground. In the case when the target is located above the ground, we have

$$\varepsilon_r\ (\text{background}) = \varepsilon_r\ (\text{air}) = 1.$$

Hence, $R = \varepsilon_r$(target) for targets located above the ground. Since targets can be mixtures of constituent materials, then ε_r(target) is a certain weighted average of dielectric constants of these materials.

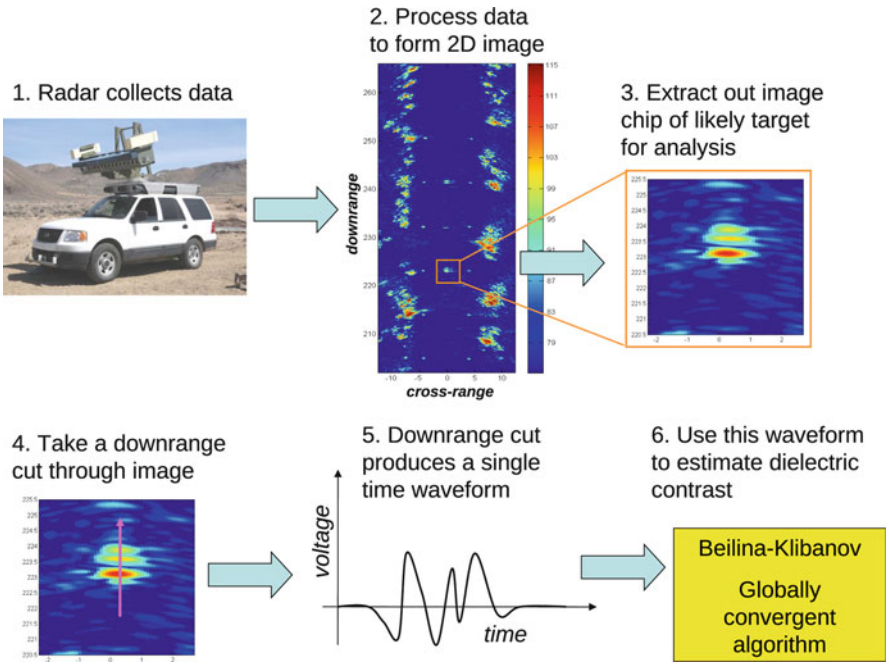

Fig. 6.10 The experimental setup for backscattered data collected in the field by a radar of the US Army Research Laboratory

We have imaged the ratio (6.167) rather than the function $\varepsilon_r(x)$ itself because one of conditions of our theory is that the unknown coefficient should have a known constant value outside of the domain of interest Ω; see (6.3). In our mathematical model, $\Omega = (0,1)$, where "1" stands for 1 meter. The point $x = 0$ corresponds to the ground, and $\{x < 0\}$ corresponds to the air in our mathematical model. We have assumed that $\varepsilon_r(x) = 1$ for $x \notin \Omega$. However, since the sand is not dry on the depth exceeding one meter, then (6.165) is invalid for $x > 1$. Also, values of ε_r(background) were not measured, but rather were taken from tables [151]. Hence, computing the ratio R in (6.167) was preferable.

6.9.3 The Mathematical Model and the Approximately Globally Convergent Algorithm

Since we were given only one time resolved curve for each target, we had no choice but to solve a 1D CIP. We have modeled the process by the 1D analog of the forward problem (6.1), (6.2). Following (6.167), let

$$\overline{\varepsilon}_r(x) := R(x) = \frac{\varepsilon_r(\text{target})}{\varepsilon_r(\text{background})}(x), \ x \in \mathbb{R}, \tag{6.168}$$

meaning that $R(x)$ is a function. The forward problem is

$$\overline{\varepsilon}_r(x) u_{tt} = u_{xx}, \ x \in \mathbb{R}, \ t \in (0, \infty), \tag{6.169}$$

$$u(x,0) = 0, u_t(x,0) = \delta(x - x_0), \ x_0 = \text{const.} < 0. \tag{6.170}$$

We assume that

$$\overline{\varepsilon}_r(x) \geq \varepsilon^0 = \text{const.} 0, \forall x \in \mathbb{R}, \tag{6.171}$$

$$\overline{\varepsilon}_r(x) \in \left[\varepsilon^0, d\right], \tag{6.172}$$

where $d = \text{const.} > 1$. Also, we assume that

$$\overline{\varepsilon}_r(x) = 1, x \notin (0,1). \tag{6.173}$$

Thus, the interval $\Omega := (0,1)$ is our domain of interest. One of complicating factors was that neither the "zero time" nor the source/medium distance were not given to us, i.e., the source position x_0 in (6.170) was not given. Indeed, it is unclear from Fig. 6.9 what kind of the distance is between the source and the domain of interest. We purely intuitively set in (6.170)

$$x_0 := -1. \tag{6.174}$$

Hence, we have assumed that the source is 1 meter away from the domain of interest. As always, we use the source position outside of the interval of interest $(0,1)$ because our technique works only with this case. We consider the following:

Coefficient Inverse Problem 6.9.3. *Suppose that the following function $\varphi(t)$ is known*:

$$u(0,t) = g(t), t \in (0, \infty). \tag{6.175}$$

Given conditions (6.169), (6.170), (6.171), (6.172), (6.173), and (6.174), determine the function $\overline{\varepsilon}_r(x)$ for $x \in (0,1)$.

Hence, the function $g(t)$ models the backscattering data measured by the forward looking radar. To solve this inverse problem, we have applied the 1D version of the approximate globally convergent method of this chapter. Thus, the 1D version of the QRM was applied. Since the convergence analysis in 3D was done above, we do not present it here. We refer to [114] for details of both the convergence analysis in the 1D case and for the numerical implementation.

As it was mentioned in Sect. 6.8.3, in 2D and 3D cases, we have applied the two-stage numerical procedure. On the second stage, the Tikhonov functional was minimized as described in Sect. 5.8.4. However, we have observed that the

application of the second stage to these experimental data has resulted in rather small changes of solutions. Hence, we have used only the first stage.

In terms of the above notations, we have in the 1D case

$$\Gamma_1 = \{x = 0\}, \ \Gamma_2 = \varnothing, \ \Gamma_3 = \{x = 1\}.$$

Hence, it seems to be that each boundary value problem (6.26), (6.28) can be treated in the 1D case as the conventional Sturm–Liouville problem for the function $q_{n,k}$. To do this, one needs to ignore in (6.28) either Dirichlet or Neumann boundary condition at Γ_1 and use two remaining boundary conditions (6.28): one at Γ_1 and the second one at Γ_3. However, our attempt to follow this path did not lead to acceptable quality solutions for computationally simulated data; see p. 126 of [114]. This indicates that the QRM is probably the optimal choice for the 1D case.

Just as above, consider the Laplace transform:

$$w(x,s) = \int_0^\infty u(x,t)\, e^{-st} dt, \ s \geq \underline{s} = \text{const.} > 0, \tag{6.176}$$

where $u(x,t)$ is the solution of the problem (6.169), (6.170). Then

$$w_{xx} - s^2 \overline{\varepsilon}_r(x)\, w = -\delta(x - x_0), \ x \in \mathbb{R}, \tag{6.177}$$

$$\lim_{|x| \to \infty} w(x,s) = 0. \tag{6.178}$$

In addition, by (6.175) and (6.176),

$$w(0,s) = \varphi(s), \tag{6.179}$$

where $\varphi(s)$ is the Laplace transform of the function $g(t)$. However, to apply the QRM, we also need to know the derivative:

$$w_x(0,s) = \rho(s). \tag{6.180}$$

To find the function $\rho(s)$, consider first the function $w_0(x,s)$ which is the solution of the problem (6.177), (6.178) for the case $\overline{\varepsilon}_r(x) \equiv 1$:

$$w_0(x,s) = \frac{\exp(-s|x - x_0|)}{2s}.$$

Let $\overline{w}(x,s) = w(x,s) - w_0(x,s)$. Then (6.177)–(6.179) imply that

$$\overline{w}_{xx} - s^2 \overline{\varepsilon}_r(x)\, \overline{w} = s^2 (\overline{\varepsilon}_r(x) - 1) w_0, \ x \in \mathbb{R}, \tag{6.181}$$

$$\lim_{|x| \to \infty} \overline{w}(x,s) = 0, \tag{6.182}$$

$$\overline{w}(0,s) = \overline{\varphi}(s) := \varphi(s) - \frac{\exp(-s|x_0|)}{2s}. \tag{6.183}$$

Since by (6.173) $\overline{\varepsilon}_r(x) = 1$ for $x < 0$, then (6.181), (6.182), and (6.183) become for $x < 0$:

$$\overline{w}_{xx} - s^2\overline{w} = 0, \ x < 0, \tag{6.184}$$

$$\lim_{x\to-\infty} \overline{w}(x,s) = 0, \tag{6.185}$$

$$\overline{w}(0,s) = \overline{\varphi}(s). \tag{6.186}$$

We can consider (6.184), (6.185), and (6.186) as the boundary value problem on the half line $\{x < 0\}$. Obviously, the unique solution of this problem is

$$\overline{w}(x,s) = \overline{\varphi}(s) e^{sx}, \ x < 0.$$

Hence,

$$\overline{w}_x(0,s) = s\overline{\varphi}(s).$$

Next, $w_x(0,s) = \overline{w}_x(0,s) + w_{0x}(0,s)$. Since by (6.174) $x_0 < 0$, then by (6.180),

$$w_x(0,s) := \rho(s) = s\varphi(s) - \exp(-s|x_0|). \tag{6.187}$$

Therefore, both functions $w(0,s)$ and $w_x(0,s)$ are known, which are required by the QRM. Also, since $\overline{\varepsilon}_r(x) = 1$ for $x > 1$, then (6.177) and (6.178) imply that

$$w(x,s) = C(s) e^{-sx}, x > 1,$$

where $C(s)$ is a certain function of s. Using

$$q(x,s) = \frac{\partial}{\partial s}\left(\frac{\ln w(x,s)}{s^2}\right),$$

we obtain the following analog of the boundary condition (6.29):

$$q_x(1,s) = \frac{1}{s^2}. \tag{6.188}$$

Boundary conditions (6.180), (6.187), and (6.188) were used to obtain 1D analogs of boundary conditions (6.28).

Just as in (6.162), we have replaced functions $v(x,s)$, $q(x,s)$,

$$v(x,s) = \frac{\ln[w(x,s)]}{s^2}, \ q(x,s) = \partial_s v(x,s),$$

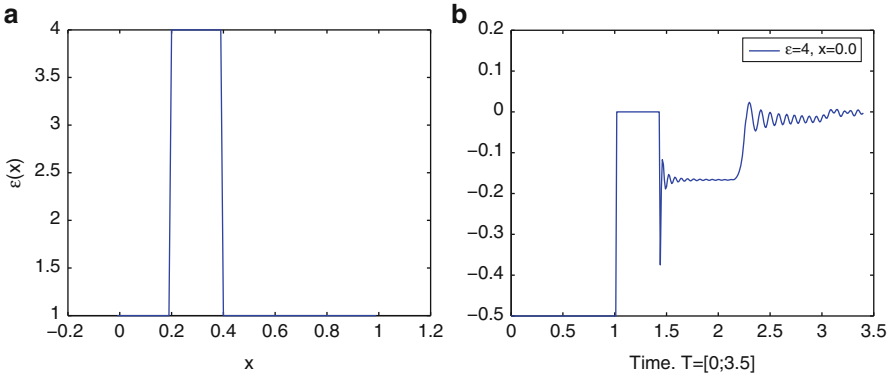

Fig. 6.11 (**a**) The medium with a single target and $\overline{\varepsilon}_r(x) = 4 > 1$ within this target. (**b**) The computed function $g(t) = u(0,t) - u_0(0,t)$ for a). Here, $u(x,t)$ is the solution of the problem (6.169), (6.170) for the function $\overline{\varepsilon}_r(x)$ depicted on (a), and $u_0(x,t)$ is the solution of the problem (6.169), (6.170) for the case $\overline{\varepsilon}_r(x) \equiv 1$

with functions $\widehat{v}(x,s)$, $\widehat{q}(x,s)$, where

$$\widehat{v}(x,s) = \frac{1}{s^2} \ln\left[\frac{w}{w_0}(x,s)\right], \ \widehat{q}(x,s) = \partial_s \widehat{v}(x,s). \tag{6.189}$$

This led to obvious modifications of (6.26) and (6.28).

To approximate tails, one should solve the problem (6.181), (6.182) at $s := \overline{s}$. Using (6.182), one can prove that the function $\overline{w}(x,s)$ decays exponentially as $|x| \to \infty$. Hence, we have solved the Sturm–Liouville problem for (6.181) in the interval $x \in (-4,6)$ with the boundary conditions

$$\overline{w}(-4,s) = \overline{w}(6,s) = 0.$$

6.9.4 Uncertainties

Similarly with the experimental data of Chap. 5, the data from the forward looking radar have **huge misfits** with computational simulations: Compare Fig. 6.12b with Fig. 6.13a as well as Fig. 6.11b with Fig. 6.15a. In addition, there are some other significant uncertainties here, which were not presented in experimental data of Chap. 5. These difficulties are basically caused by the fact that experimental data were collected in the field rather than in the controlled environment of a laboratory of Chap. 5. We now list those factors:

1. We did not have the reference signal for comparison.
2. The direction of the incident plane wave was oblique to the ground rather than orthogonal; see Figs. 6.14a and 6.16a.

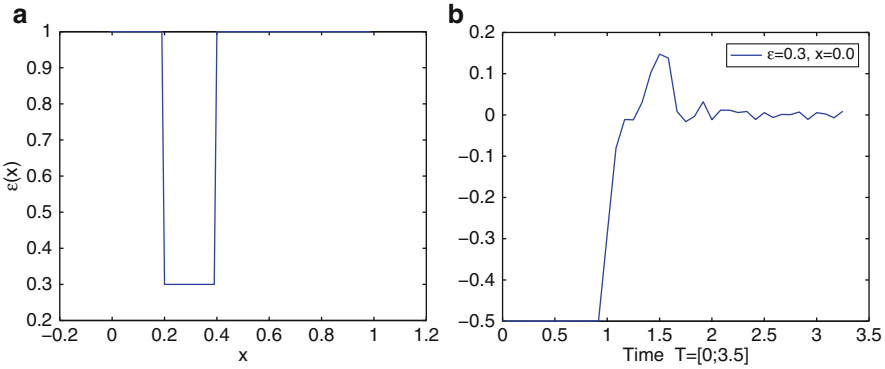

Fig. 6.12 (**a**) The medium with a single target and $\overline{\varepsilon}_r(x) = 0.3 < 1$ within this target. (**b**) The computed function $g(t) = u(0,t) - u_0(0,t)$ for (a). Here, $u(x,t)$ is the solution of the problem (6.169), (6.170) for the function $\overline{\varepsilon}_r(x)$ depicted on (a), and $u_0(x,t)$ is the solution of the problem (6.169), (6.170) for the case $\overline{\varepsilon}_r(x) \equiv 1$

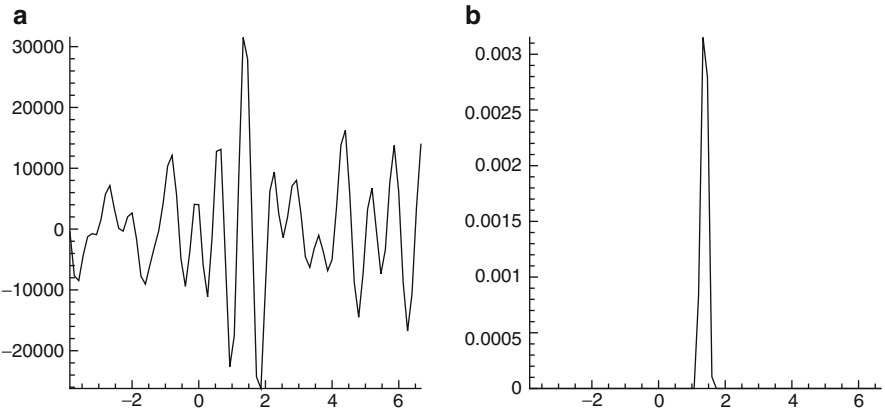

Fig. 6.13 Test 1. (**a**) A sample of the experimentally measured signal for a buried object depicted on Fig. 6.14a. It is unclear which part of this curve is responsible for this object and which part is responsible for the rest of the measured signal. Horizontal axis is time in nanoseconds. It is unclear where the time $t = 0$ is. It is also unclear which units are displayed on the vertical axis. (**b**) Pre-processed signal of (a). First, we have multiplied the amplitude of (a) by 10^{-7}. This multiplier was chosen to have about the same values of functions $w(0,s)$ in (6.179) for both simulated and experimental data. Next, we have selected the peak with the largest absolute value and have set the rest of the curve to zero. We set zero time $t = 0$ being 1 nanosecond to the left from the beginning of the selected peak. We apply our algorithm only to the data of (b)

3. We did not know the units for the amplitude of experimental data. These amplitudes were about $3 \cdot 10^4$, which is too large.
4. We did not know the source location. Thus, we have just intuitively assigned by (6.174) $x_0 := -1$.
5. We did not know where the time $t = 0$ was on the data.

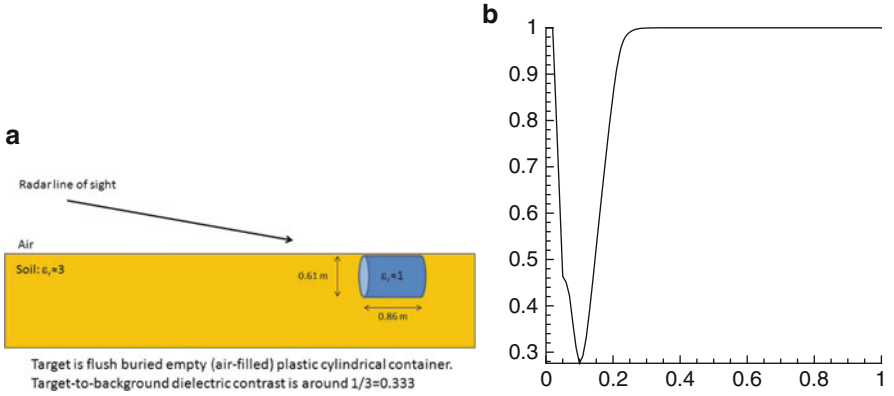

Fig. 6.14 Test 1. (**a**) The real image from which the data of Fig. 6.13a were collected. This is a buried plastic cylinder with $\varepsilon_r \approx 1$ in it; see [151]. (**b**) Computed 1D image of (a). Most importantly, $\min \overline{\varepsilon}_r = 0.28$, whereas the true value $\overline{\varepsilon}_r \approx 0.33$. Thus, a good accuracy in this blind imaging was achieved

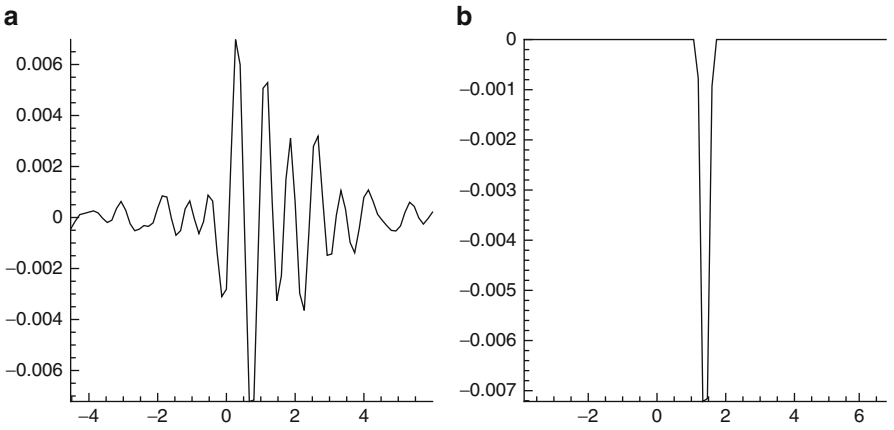

Fig. 6.15 Test 2. (**a**) The real signal. The amplitude was multiplied by 10^{-7}; see Sect. 6.9.4 for the data pre-processing procedure. (**b**) The pre-processed signal of (a)

6. We had only one time resolved curve for each target, whereas the reality is 3D.
7. We did not have a reference signal, unlike Chap. 5.
8. Since targets were surrounded by clutter, then the background was inhomogeneous. Targets might be heterogeneous ones as well. We remind that a knowledge of the background is not assumed in the approximately globally convergent method of this book.

At the same time, we had the following two simplifying factors:

A. We knew that the target is present and that we should work only with one target for each data set. In addition, we knew whether the target is located above the ground or buried in the ground.

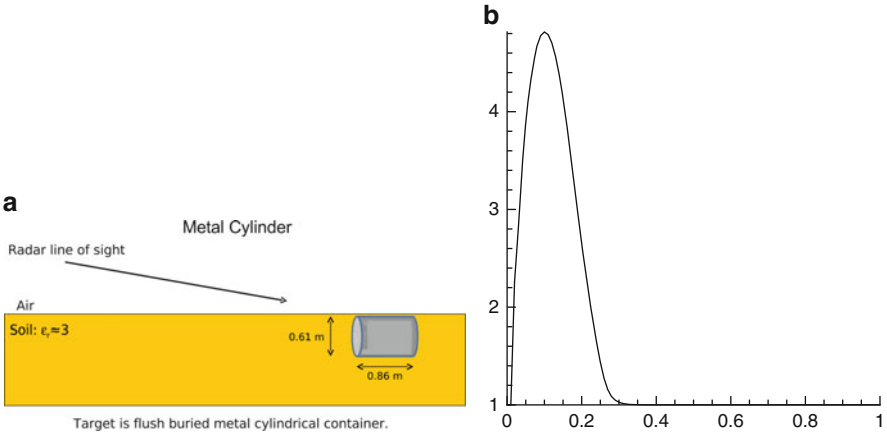

Fig. 6.16 Test 2. (**a**) The real image from which the data on Fig. 6.15a were collected. This is a buried metal box. (**b**) The computed 1D image of (a). Here, the maximal value of the target/background ratio of dielectric constants is $\max \overline{\varepsilon}_r = 4.8$. Hence, the computed value of the dielectric constant of this target is $\varepsilon_r = 4.8 \cdot 3 = 14.4$ which is about the right value of the apparent dielectric constants of metals; see Sect. 6.9.1. Therefore, a good accuracy in this blind imaging was achieved

B. We were not interested to image locations of targets. Furthermore, it was impossible to image locations accurately, since both the source position and the zero time were unknown. Rather, all what we wanted was to accurately compute either $\max \overline{\varepsilon}_r(x)$ or $\min \overline{\varepsilon}_r(x)$ within the target.

6.9.5 Data Pre-processing

As it was demonstrated in Chap. 5, it is crucial to pre-process experimental data in order to handle the abovementioned huge misfit between experimental and computationally simulated data. The idea of the data pre-processing procedure is similar with the idea of Chap. 5: basically, we immerse the experimental data in computationally simulated ones by using only one peak of the largest amplitude.

To figure out what kind of ideal data one should expect, we have performed computational simulations via solving the forward problem (6.169), (6.170), (6.174) for the case of one target. In data simulations, we have replaced $\mathbb{R}$ in (6.169) with the interval $x \in (-6, 6)$ and have set

$$u(-6, t) = u(6, t) = 0, t \in (0, 4). \tag{6.190}$$

Because of the structure of the medium, the signal did not yet reach points $x = \pm 6$ for $t \in (0, 4)$. This justifies boundary conditions (6.190). Figures 6.11 and 6.12

display two structures of the medium we have tested as well as the computed functions functions $g(t) = u(0,t) - u_0(0,t)$ for them. Here, $u_0(x,t)$ is the fundamental solution of the equation $v_{tt} = v_{xx}$,

$$u_0(x,t) = \frac{1}{2} H(t - |x - x_0|),$$

where H is the Heaviside function,

$$H(x) = \begin{cases} 1 \text{ if } x \geq 0, \\ 0 \text{ if } x < 0. \end{cases}$$

One can see from Figs. 6.11 and 6.12 that when working with one target only, one should anticipate only one peak in the backscattering data. We use this observation in our data pre-processing procedure.

Scaling

Figure 6.13a displays a typical sample of the experimental data we have worked with. First of all, the amplitude of the signal is too large, since its maximal value is $3 \cdot 10^4$. This is well above amplitudes of Figs. 6.11 and 6.12. Hence, we need to scale this signal via multiplying these data by a small number. A natural question is about the value of this number. We have multiplied all experimental data by 10^{-7}. In this case, the magnitudes of the values of the function $w(0,s)$ in the experimental data were about the same as ones in computational simulations for small inclusions with reasonable contrasts.

The Largest Peak

It is unclear from Fig. 6.13a which part of the signal is responsible for reflections from the clutter, including the air/ground interface. On the other hand, we need to select such a part of the signal, which is responsible for reflections from the target. In other words, we now have the same problem as the one we have faced in Chap. 5. We knew that the target might well be a heterogeneous one, especially since it is mixed with the ground. Nevertheless, one can hope to obtain only an average value of the function $\overline{\varepsilon}_r(x)$ within the target.

Based on Figs. 6.11 and 6.12, we have decided to select the peak of the largest amplitude out of all other peaks of Fig. 6.13a and set the rest of the curve to zero. We have done this for all five pieces of experimental data we had. Now, if the target is located above the ground, then $\overline{\varepsilon}_r(\text{target}) = \varepsilon_r(\text{target}) > 1$, since $\varepsilon_r(\text{air}) = 1$. Figure 6.11b tells one that the selected peak should look downward in this case.

Hence, our selection of the single peak was as follows: This should be the earliest peak of the largest amplitude:

$$\text{out of all} \begin{cases} \text{peaks for an underground target,} \\ \text{downward looking peaks for an above the ground target.} \end{cases} \tag{6.191}$$

Next, we regard the time zero: $\{t = 0\}$ as the point on the time axis, which is 1 nanosecond to the left from the beginning of the selected peak.

The Laplace Transform of the Pre-processed Data

To apply our algorithm, the Laplace transform (6.176) was calculated for the pre-processed time resolved data. It is clear from Fig. 6.13b that only the integration over a finite time interval is needed in this case. Since we also need to calculate the s-derivative of this transform, then we have used the formula

$$\varphi'(s) = -\int_0^\infty g(t)\, t e^{-st} \mathrm{d}t, \tag{6.192}$$

where $g(t)$ is pre-processed data and $\varphi(s)$ is its Laplace transform.

Just as in Sect. 6.8.3, we have observed in computational simulations of Figs. 6.11 and 6.12 that the function $\varphi(s)$ in (6.179) has the best sensitivity to the presence of inclusions for $s \in [0.5, 1.2]$. Still, we have discovered in our computational simulations that better to work on a larger interval $s \in [0.5, 12]$. However, in the case of the pre-processed experimental data, the function $q(0, s)$ was highly oscillatory for $s \in [5, 12]$.

Hence, we have pre-processed the function $\widehat{q}(0, s)$ in (6.189) as follows. First, we have calculated the function $\widehat{q}(0, s)$ for $s \in [0.5, 2.5]$ for the pre-processed experimental data using (6.192). Next, we have assigned

$$\widehat{q}(0, 12) := 0.025 \cdot \widehat{q}(0, 2.5).$$

Next, we have linearly interpolated in the plane $(s, \widehat{q})$ between points $(s_1, \widehat{q}_1)$ and $(s_2, \widehat{q}_2)$, where

$$(s_1, \widehat{q}_1) := (2.5, \widehat{q}(0, 2.5)), \quad (s_2, \widehat{q}_2) := (12, \widehat{q}(0, 12)).$$

Next, we have assigned to the function $\widehat{q}(0, s)$ those values for $s \in [2.5, 12]$, which were taken on this line after the linear interpolation. We have done the same to the function $\widehat{q}_x(0, s)$. For $s \in [0.5, 2.5]$, the function $\widehat{q}_x(0, s)$ was calculated using (6.179), (6.187), and (6.189). Derivatives with respect to s were calculated via finite differences. Thus, these values of functions $\widehat{q}(0, s)$, $\partial_x \widehat{q}(0, s)$ were used

to calculate 1D analogs of boundary conditions $\psi_{0,n}, \psi_{1,n}$ in (6.28):

$$\widehat{q}_n(0) = \widehat{\psi}_{0,n}, \ \partial_x \widehat{q}_n(0) = \widehat{\psi}_{1,n}.$$

Next, the 1D analog [114] of the algorithm of Sects. 6.4.3 and 6.4.4 was applied, and functions $\widehat{\psi}_{0,n}, \widehat{\psi}_{1,n}$ were the input data for this algorithm. The grid step size in the s-direction was $h = 0.5$.

6.9.6 *Results of Blind Imaging*

Test 1. The data are depicted on Fig. 6.13a and the pre-processed data are displayed on Fig. 6.13b. We only knew a priori that this was a target buried in the ground; see (6.191). Other features of this target were unknown to us when computing. Figure 6.14b displays our computed image. After this image was computed, Drs. L. Nguyen and A. Sullivan have compared our result with the reality and have sent Fig. 6.14a to us. The target was an empty plastic cylinder buried in the ground with the dielectric constant ε_r(plastic)≈ 1 [151]. The dielectric constant of the ground (dry sand) was as in (6.191), ε_r(background)≈ 3. We remind that this value was unknown to the mathematical team when computations were performed. One can see that our computed $\min \overline{\varepsilon}_{r,\text{comp}}(x) = 0.28$. At the same time, the real value was $\overline{\varepsilon}_r \approx 0.33$. Thus, our blindly computed result is quite accurate.

Test 2. The data, which were multiplied by 10^{-7} first (for scaling, see above), are depicted on Fig. 6.15a. We only knew a priori that this was a target buried in the ground. Other characteristics of this target were unknown to us at the time when computations were performed. Hence, following (6.191), we have selected on Fig. 6.15a the peak of the largest amplitude. Figure 6.16b displays our 1D computed image. Figure 6.16a depicts the real image, which was revealed to us by Drs. L. Nguyen and A. Sullivan only after the computational result was sent to ARL. The target was a metal box. One can see that our computed $\max \overline{\varepsilon}_r(x) = 4.8$. Since ε_r(ground)≈ 3, then the computed $\max \varepsilon_{r,\text{comp}}$(target)$\approx 3 \cdot 4.8 = 14.4$. This is the conditional dielectric constant of the metal box of Fig. 6.16b, see Sect. 6.9.1 for the definition of the conditional dielectric constant of metals. Hence, this result matches well Figs. 6.8a, b and (6.166).

Remark 6.9.6.

1. The sign "$\approx$" is used in this table instead of "$=$" because the values of the dielectric constant of the ground were only approximate ones, since they were not measured in experiments.
2. The value $\varepsilon_r = 0.84$ in Table 6.1 does not match physics well since $0.84 < 1$. However, the value ε_r(ground)≈ 3 is only an approximate one. If, for example, the real value was ε_r(ground)≥ 3.58, then the computed value ε_r of the target

Table 6.1 Summary of results of blind imaging of the data collected by the forward looking radar

Test number	Computed ε_r of the target	Tabulated ε_r
1 (buried plastic cylinder)	≈ 0.84	≈ 1
2 (buried metal cylinder)	≈ 14.4	≥ 10
3 (buried metal box)	≈ 11.4	≥ 10
4 (wood stake in air)	3.8	from 2 to 6
5 (bush: clutter in air)	6.4	from 3 to 20

was exceeding 1. Note that in tables [151], the dielectric constant of the dry sand is listed as being between 3 and 5. Hence, the most important point of the result of Test 1 is that the computed ratio $\min \overline{\varepsilon}_r(x) = 0.28$, which is quite close to the real value of about 0.33.

3. The computed conditional dielectric constant $\varepsilon_r \approx 14.4$ of the metal box is close to (6.166).

We had the blind data for five targets. Dielectric constants were not measured in experiments. Therefore, we had no choice but to compare our calculated values of dielectric constants of targets with tabulated ones [151]. In the case of bush we use the reference [52]. In the case of two metallic targets we use inequality (6.166). Table 6.1 summarizes our results.

6.9.7 Summary of Blind Imaging

It can be seen from the above description of complicating factors that we have worked with the case of a severely limited information caused by many uncertainties in the experimental data. Furthermore, we have worked with the most challenging case of blind experimental data. Nevertheless, above results demonstrate a surprisingly good accuracy. This is consistent with results of Chap. 5. Studies on larger sets of experimental data are necessary to figure out accuracy constraints of this algorithm.

References

1. M. Abramowitz and I.A. Stegun, *Handbook of Mathematical Functions*, National Bureau of Standards, Washington, DC, 1964.
2. M. Ainsworth and J.T. Oden, *A Posteriori Error Estimation in Finite Element Analysis*. New York, Wiley, 2000.
3. N.V. Alexeenko, V.A. Burov and O.D. Rumyantseva, Solution of three-dimensional acoustical inverse problem: II. Modified Novikov algorithm, *Acoust. Phys*., 54, 407–419, 2008.
4. H. Ammari, E. Iakovleva and S. Moskow, Recovery of small inhomogeneities from the scattering amplitude at a fixed frequency, *SIAM J. Math. Anal*., 34, 882–900, 2003.
5. H. Ammari and H. Kang, *Reconstruction of Small Inhomogeneities from Boundary Measurements*, Lecture Notes in Mathematics, 1846, Springer-Verlag, Berlin, 2004.
6. H. Ammari, E. Iakovleva, G. Perruson and D. Lesselier, Music-type electromagnetic imaging of a collection of small three dimensional inclusions, *SIAM J. Sci.Comp.,* 29, 674–709, 2007.
7. Iu. E. Anikonov and E. Anikonov, *Inverse Problems of Kinetic and Other Evolution Equations*, VSP, Utrecht, 2001.
8. S. Arridge, Optical tomography in medical imaging, *Inverse Problems*, 15, 841–893, 1999.
9. M. Asadzadeh and L. Beilina, *A posteriori* error analysis in a globally convergent numerical method for a hyperbolic coefficient inverse problem, *Inverse Problems*, 26, 115007, 2010.
10. A.B. Bakushinsky and M.Yu. Kokurin, *Iterative Methods for Approximate Solution of Inverse Problems*, Springer, New York, 2004.
11. A.B. Bakushinsky, *A posteriori* error estimates for approximate solutions of irregular operator equations, *Doklady Mathematics*, 83, 1-2, 2011.
12. W. Bangerth and A. Joshi, Adaptive finite element methods for the solution of inverse problems in optical tomography, *Inverse Problems* 24, 034011, 2008.
13. H. Bateman and A. Erdelyi, *Tables of Integral Transforms*, Vol. 1, McGrawHill, New York, 1954.
14. L. Baudonin and J.-P. Puel, Uniqueness and stability in an inverse problem for the Schrödinger equation, *Inverse Problems*, 18, 1537–1554, 2002.
15. R. Becker and R. Rannacher, An optimal control approach to *a posteriori* error estimation in finite element method, *Acta Numerica*, 10, 1–102, 2001.
16. L. Beilina and C. Johnson, A hybrid FEM/FDM method for an inverse scattering problem. In *Numerical Mathematics and Advanced Applications, ENUMATH 2001*, Springer-Verlag, Berlin, 2001.
17. L. Beilina, Adaptive hybrid FEM/FDM methods for inverse scattering problems, *J. Inverse Problems and Information Technologies*, 1, 73–116, 2002.
18. L. Beilina, Adaptive finite element/difference method for inverse elastic scattering waves, *Applied and Computational Mathematics*, 2, 119–134, 2003.

L. Beilina and M.V. Klibanov, *Approximate Global Convergence and Adaptivity for Coefficient Inverse Problems*, DOI 10.1007/978-1-4419-7805-9,

19. L. Beilina, Efficiency of a Hybrid FEM/FDM methods for elastic waves, *Applied and Computational Mathematics*, 2(1), 13–29, 2003.
20. L. Beilina and C. Johnson, *A posteriori* error estimation in computational inverse scattering, *Mathematical Models and Methods in Applied Sciences*, 15, 23–37, 2005.
21. L. Beilina and C. Clason, An adaptive hybrid FEM/FDM method for an inverse scattering problem in scanning acoustic microscopy, *SIAM J. Sci. Comp.,* 28, 382–402, 2006.
22. L. Beilina, M. Hatlo and H. Krogstad, Adaptive algorithm for an inverse electromagnetic scattering problem, *Applicable Analysis*, 1, 15–28, 2009.
23. L. Beilina, Adaptive finite element method for a coefficient inverse problem for the Maxwell's system, *Applicable Analysis*, 90:10, 1461–1479, 2011.
24. L. Beilina and M.V. Klibanov, A globally convergent numerical method for a coefficient inverse problem, *SIAM J. Sci. Comp.,* 31, 478–509, 2008.
25. L. Beilina and M.V. Klibanov, Synthesis of global convergence and adaptivity for a hyperbolic coefficient inverse problem in 3D, *J. Inverse and Ill-posed Problems,* 18, 85–132, 2010.
26. L. Beilina and M.V. Klibanov, *A posteriori* error estimates for the adaptivity technique for the Tikhonov functional and global convergence for a coefficient inverse problem, *Inverse Problems,* 26**,** 045012, 2010.
27. L. Beilina, M.V. Klibanov and A. Kuzhuget, New a posteriori error estimates for adaptivity technique and global convergence for a hyperbolic coefficient inverse problem, *Journal of Mathematical Sciences,* 172, 449–476, 2011.
28. L. Beilina and M.V. Klibanov, Reconstruction of dielectrics from experimental data via a hybrid globally convergent/adaptive inverse algorithm, *Inverse Problems*, 26, 125009, 2010.
29. L. Beilina, M.V. Klibanov and M.Yu Kokurin, Adaptivity with relaxation for ill-posed problems and global convergence for a coefficient inverse problem, *Journal of Mathematical Sciences,* 167, 279–325, 2010.
30. L. Beilina, K. Samuelsson and K. Åhlander, Efficiency of a hybrid method for the wave equation. In *International Conference on Finite Element Methods*, Gakuto International Series Mathematical Sciences and Applications. Gakkotosho CO., LTD, 2001.
31. M. Bellassoued, Global logarithmic stability in determining the speed of propagation of second-order hyperbolic equation with variable coefficients, *Inverse Problems*, 20, 1033–1052, 2004.
32. M. Bellassoued and M. Yamamoto, Carleman estimates and an inverse heat source problem for the thermoelasticity system, *Inverse Problems*, 27, 015006, 2011.
33. A. Benabdallah, M. Cristofol, P. Gaitan and M. Yamamoto, Inverse problem for a parabolic system with two components by measurements of one component, *Applicable Analysis*, 88, 683–709, 2009.
34. Ju. M. Berezanskii, The uniqueness theorem in the inverse problem of spectral analysis for the Schrödinger equation, *Proceedings of The Moscow Mathematical Society*, 7, 1–62, 1958 (in Russian). English translation in: *American Mathematical Society Translations*, Series 2, V. 35, 137–235, 1964.
35. J. Bikowski, K. Knudsen and J.L. Mueller, Direct numerical reconstruction of conductivities in three dimensions using scattering transforms, *Inverse Problems*, 27, 015002, 2011.
36. M. Born and E. Wolf, *Principles of Optics : Electromagnetic Theory of Propagation, Interference and Diffraction of Light*, Cambridge University Press, Cambridge, 1970.
37. F. Boyer, F. Hubert and J. Le Rousseau, Discrete Carleman estimates for elliptic operators in arbitrary dimension and applications, *SIAM J. Control Optim.*, 48, 5357–5397, 2010.
38. F. Boyer, F. Hubert and J. Le Rousseau, Discrete Carleman estimates for elliptic operators and uniform controllability of semi-discretized parabolic equations, *J. Math. Pures Appl.*, 93, 240–276, 2010.
39. A. Briggs, *Acoustic Microscopy*, Clarendon Press, Oxford, 1992.
40. K. Bube, Convergence of difference methods for one dimensional inverse problems, *IEEE Trans. Geoscience and Remote Sensing*, GE22, 674–682, 1984.
41. J.L. Buchanan, R.P. Gilbert, A. Wirgin and Y.S. Xu, *Marine Acoustics: Direct and Inverse Problems,* SIAM Publications, Philadelphia, 2003.

42. B.M. Budak, A.A. Samarskii and A.N. Tikhonov, *Collection of Problems in Mathematical Physics*, Dover Publications, New York, 1988.
43. A.L. Bukhgeim and M.V. Klibanov, Uniqueness in the large of a class of multidimensional inverse problems, *Soviet Math. Doklady*, 17, 244–247, 1981.
44. A.L. Bukhgeim, Carleman estimates for Volterra operators and uniqueness of inverse problems, in *Non-Classical Problems of Mathematical Physics*, pages 54–64, published by Computing Center of the Siberian Branch of USSR Academy of Science, Novosibirsk, 1981 (in Russian).
45. A.L. Bukhgeim, *Introduction In The Theory of Inverse Problems*, VSP, Utrecht, The Netherlands, 2000.
46. V.A. Burov, S.A. Morozov and O.D. Rumyantseva, Reconstruction of fine-scale structure of acoustical scatterers on large-scale contrast background, *Acoust. Imaging,* 26, 231–238, 2002.
47. R. Burridge, The Gelfand-Levitan, the Marchenko, and the Gopinath-Sondhi integral equations of inverse scattering theory, regarded in the context of inverse impulse response problems, *Wave Motion*, 2, 305–323, 1980.
48. F. Cakoni and D. Colton, *Qualitative Methods in Inverse Scattering Theory*, Springer, New York, 2006.
49. H. Cao, M.V. Klibanov and S.V. Pereverzev, A Carleman estimate and the balancing principle in the quasi-reversibility method for solving the Cauchy problem for the Laplace equation, *Inverse Problems*, 25, 35005, 2009.
50. T. Carleman, Sur un proble′me d'unicite′ pur les systee′mes d'équations aux dériveés partielles a′ deux varibales indépendantes, *Ark. Mat. Astr. Fys*, 26B, No. 17, 1–9, 1939.
51. K. Chadan and P. Sabatier, Inverse Problems in Quantum Scattering Theory, Springer, New York, 1989.
52. H.T. Chuah, K.Y. Lee and T.W. Lau, Dielectric constants of rubber and oil palm leaf samples at X-band, *IEEE Trans. on Geoscience and Remote Sensing*, 33, 221–223, 1995.
53. G. Chavent, Deux résultats sur le probléme inverse dans les équations aux dérivées partielles du deuxième ordre an tet sur l'unicit de la solution du problème inverse de la diffusion, *C.R. Acad. Sc. Paris*, 270, 25–28, 1970.
54. G. Chavent, *Nonlinear Least Squares for Inverse Problems: Theoretical Foundations and Step-by-Step Guide for Applications (Scientific Computation)*, Springer, New York, 2009.
55. Y. Chen, Inverse scattering via Heisenberg uncertainty principle, *Inverse Problems*, 13, 253–282, 1997.
56. Y. Chen, R. Duan and V. Rokhlin, On the inverse scattering problem in the acoustic environment, *J. Computational Physics*, 228, 3209–3231, 2009.
57. M. Cheney and D. Isaacson, Inverse problems for a perturbed dissipative half-space, *Inverse Problems*, 11, 865–888, 1995.
58. R. Cipolatti and M.Yamamoto, An inverse problem for a wave equation with arbitrary initial values and a finite time of observation, *Inverse Problems*, 27, 095006, 2011.
59. C. Clason and M.V. Klibanov, The quasi-reversibility method for thermoacoustic tomography in a heterogeneous medium, *SIAM J. Sci. Comp*., 30, 1–23, 2007.
60. D. Colton and R. Kress, *Inverse Acoustic and Electromagnetic Scattering Theory*, Springer-Verlag, New York, 1992.
61. G. C. Cohen, *Higher order numerical methods for transient wave equations*, Springer-Verlag, Berlin, 2002.
62. M. Cristofol, P. Gaitan and H. Ramoul, Inverse problems for a 2×2 reaction–diffusion system using a Carleman estimate with one observation, *Inverse Problems*, 22, 1561–1573, 2006.
63. M. DeAngelo and J.L. Mueller, 2D d-bar reconstructions of human chest and tank using an improved approximation to the scattering transform, *Physiological Measurement*, 31, 221–232, 2010.
64. C. Draft, G. Briggs, The elastic microstructure of various tissues, *J. Acoust. Soc. Am*., 85, 416–422, 1989.
65. H.W. Engl, M. Hanke and A. Neubauer 2000 *Regularization of Inverse Problems*, Kluwer Academic Publishers, Boston, 2000.

66. B. Engquist and A. Majda, Absorbing boundary conditions for the numerical simulation of waves *Math. Comp.* 31, 629–651, 1977.
67. K. Eriksson, D. Estep and C. Johnson, *Calculus in Several Dimensions*, Springer, Berlin, 2004.
68. T. Feng, N. Yan and W. Liu, Adaptive finite element methods for the identification of distributed parameters in elliptic equation, *Advances in Computational Mathematics*, 29, 27–53, 2008.
69. A. Friedman, *Partial Differential Equations of Parabolic Type*, Prentice Hall, Inc., Englewood Cliffs, N.J., 1964.
70. T. Gardner, J. Elliott, Z. Sklar, G. Briggs, Acoustic microscope study of the elastic properties of fluorapatite and hydroxyapatite, tooth enamel and bone, *J. Biomech.,* 25, 1265–1277, 1992.
71. H.H. Gerrish, W.E. Jr. Dugger and R.M. Robert, *Electricity and Electronics*, Merseyside, UK: Goodheart-Willcox Co. Inc., 2004.
72. D. Gilbarg and N.S. Trudinger, *Elliptic Partial Differential Equations of Second Order*, Springer-Verlag, Berlin, 1983.
73. Yu. A. Grayzin, M.V. Klibanov and T.R. Lucas, Numerical solution of a subsurface inverse imaging problem, *SIAM J. Appl. Math*., 62, 664–683, 2001.
74. A. Griesbaum, B. Kaltenbacher and B. Vexler, Efficient computation of the Tikhonov regularization parameter by goal-oriented adaptive discretization *Inverse Problems* 24, 025025, 2008.
75. P.G. Grinevich, The scattering transform for the two-dimensional operator with a potential that decreases at infinity at fixed nonzero energy *Russ. Math. Surv.,* 55, 3–70, 2000.
76. D. Grosenick, H. Wabnitz, H.R. Rinneberg, K.T. Moesta and P.M. Schlag, Development of a time-domain optical mammograph and first *in vivo* applications, *Applied Optics*, 38, 2927–2943, 1999.
77. A. Hasanov, Simultaneous determination of the source terms in a linear hyperbolic problem from the final overdetermination: weak solution approach, *IMA J. Appl. Math*., 74, 1–19, 2009.
78. T.J.R. Hughes, *The finite element method*, Prentice Hall, Englewood Cliffs, New Jersey, 1987.
79. O.Yu. Imanuvilov and M. Yamamoto, Lipschitz stability in inverse parabolic problems by the Carleman estimate, *Inverse Problems*, 14, 1229–1245, 1998.
80. O.Yu. Imanuvilov and M. Yamamoto, Global Lipschitz stability in an inverse hyperbolic problem by interior observations, *Inverse Problems*, 17, 717–728, 2001.
81. O.Yu. Imanuvilov and M. Yamamoto, Determination of a coefficient in an acoustic equation with a single measurement, *Inverse Problems*, 19, 157–171, 2003.
82. D. Isaacson, J.L. Mueller, J.C. Newell and S. Siltanen, Imaging cardiac activity by the D-bar methods for electrical impedance tomography, *Physiological Measurements*, 27, S43-S50, 2006.
83. V. Isakov, *Inverse Source Problems*, AMS, Providence, R.I., 1990.
84. V. Isakov, *Inverse Problems for Partial Differential Equations*, Springer, New York, 2005.
85. V. K. Ivanov, On ill-posed problems, *Mat. USSR Sb*., 61, 211–223, 1963.
86. V.K. Ivanov, V.V. Vasin and V.P. Tanana, *Theory Of Linear Ill-posed Problems And Its Applications*, VSP, Utrecht, 2002.
87. C. Johnson, *Numerical solution of partial differential equations by the finite element method*, Cambridge University Press, Cambridge, 1987.
88. C. Johnson and A. Szepessy, Adaptive finite element methods for conservation laws based on a posteriori error estimation, *Comm. Pure Appl. Math*., 48, 199–234, 1995.
89. P. Joly, (2003), Variational methods for time-dependent wave propagation problems, Lecture Notes in Computational Science and Engineering, Springer.
90. S.I. Kabanikhin, A.D. Satybaev and M.A. Shishlenin, *Direct Methods of Solving Multidimensional Inverse Hyperbolic Problems*, VSP, Utrecht, 2004.
91. S.I. Kabanikhin, A. Hasanov and A.V. Penenko, A gradient descent method for solving an inverse coefficient heat conduction problem, *Numerical Anal. Appl*., 1, 34–45, 2008.

92. S.I. Kabanikhin and M.A. Shishlenin, Numerical algorithm for two-dimensional inverse acoustic problem based on Gel'fand-Levitan-Krein equation, *J. Inverse and Ill-Posed Problems*, 18, 979–995, 2011.
93. B. Kaltenbacher, A. Neubauer and O. Scherzer, *Iterative Regularization Methods for Nonlinear Ill-Posed Problems*, de Gruyter, New York, 2008.
94. A. Kirsch, *An Introduction To the Mathematical Theory of Inverse Problems*, Springer, New York, 2011.
95. M.V. Klibanov, Uniqueness of solutions in the 'large' of some multidimensional inverse problems, in *Non-Classical Problems of Mathematical Physics*, 101–114, 1981, published by Computing Center of the Siberian Branch of the USSR Academy of Science, Novosibirsk (in Russian).
96. M.V. Klibanov, On a class of inverse problems, *Soviet Math. Doklady*, 26, 248–250, 1982.
97. M.V. Klibanov, Inverse problems in the 'large' and Carleman bounds, *Differential Equations*, 20, 755–760, 1984.
98. M.V. Klibanov, Uniqueness of the solution of two inverse problems for the Maxwell's system, *Computational Mathematics and Mathematical Physics*, 26, 1063–1071, 1986.
99. M.V. Klibanov, Inverse problems and Carleman estimates, *Inverse Problems*, 8, 575–596, 1992.
100. M.V. Klibanov and A. Timonov, A sequential minimization algorithm based on the convexification approach, *Inverse Problems*, 19, 331–354, 2003.
101. M.V. Klibanov and A. Timonov, A unified framework for constructing the globally convergent algorithms for multidimensional coefficient inverse problems, *Applicable Analysis*, 83, 933–955, 2004.
102. M.V. Klibanov and A. Timonov, *Carleman Estimates for Coefficient Inverse Problems and Numerical Applications*, VSP, Utrecht, 2004.
103. M.V. Klibanov and A. Timonov, Global uniqueness for a 3D/2D inverse conductivity problem via the modified method of Carleman estimates, *J. Inverse and Ill-Posed Problems*, 13, 149–174, 2005.
104. M.V. Klibanov and M. Yamamoto, Lipschitz stability estimate of an inverse problem for an acoustic equation, *Applicable Analysis*, 85, 515–538, 2006.
105. M.V. Klibanov and F. Santosa, A computational quasi-reversibility method for Cauchy problems for Laplace's equation, *SIAM J. Appl. Math.*, 51, 1653–1675, 1991.
106. M.V. Klibanov and Rakesh, Numerical solution of a timelike Cauchy problem for the wave equation, *Mathematical Methods in Applied Sciences*, 15, 559–570, 1992.
107. M.V. Klibanov, Estimates of initial conditions of parabolic equations and inequalities via lateral Cauchy data, *Inverse Problems*, 22, 495–514, 2006.
108. M.V. Klibanov, A.V. Kuzhuget, S.I. Kabanikhin and D.V. Nechaev, A new version of the quasi-reversibility method for the thermoacoustic tomography and a coefficient inverse problem, *Applicable Analysis*, 87, 1227–1254, 2008.
109. M.V. Klibanov, M. A. Fiddy, L. Beilina, N. Pantong and J. Schenk, Picosecond scale experimental verification of a globally convergent numerical method for a coefficient inverse problem, *Inverse Problems*, 26, 045003, 2010.
110. M.V. Klibanov, J. Su, N. Pantong, H. Shan and H. Liu, A globally convergent numerical method for an inverse elliptic problem of optical tomography, *Applicable Analysis*, 6, 861–891, 2010.
111. M.V. Klibanov, A.B. Bakushinsky and L. Beilina, Why a minimizer of the Tikhonov functional is closer to the exact solution than the first guess, *J. Inverse and Ill-Posed Problems*, 19, 83–105, 2011.
112. M.V. Klibanov, Uniqueness of an inverse problem with single measurement data generated by a plane wave in partial finite differences, *Inverse Problems*, 27, 115005, 2011.
113. A.N. Kolmogorov and S.V. Fomin, *Elements of the Theory of Functions and Functional Analysis*, Graylock Press, Albany, NY, 1957.
114. A.V. Kuzhuget and M.V. Klibanov, Global convergence for a 1-D inverse problem with application to imaging of land mines, *Applicable Analysis*, 89, 125–157, 2010.

115. A.V. Kuzhuget, N. Pantong and M.V. Klibanov, A globally convergent numerical method for a coefficient inverse problem with backscattering data, *Methods and Applications of Analysis*, 18, 47–68, 2011.
116. A.V. Kuzhuget, L. Beilina and M.V. Klibanov, Approximate global convergence and quasi-reversibility for a coefficient inverse problem with backscattering data, *Journal of Mathematical Sciences*, 181, 19–49, 2012.
117. A.V. Kuzhuget, L. Beilina, M.V. Klibanov, A Sullivan, L. Nguyen and M.A. Fiddy, Blind experimental data collected in the field and an approximately globally convergent inverse algorithm, http://www.ma.utexas.edu/mparc/.
118. O. A. Ladyzhenskaya and N. N. Uralceva, *Linear and Quasilinear Elliptic Equations*, Academic Press, New York, 1969.
119. O. A. Ladyzhenskaya, *Boundary Value Problems of Mathematical Physics*, Springer Verlag, Berlin, 1985.
120. O.A. Ladyzhenskaya, V.A. Solonnikov and N.N. Uralceva, *Linear and Quasilinear Equations of Parabolic Type*, AMS, Providence, R.I., 1968.
121. R. Lattes and J.-L. Lions, *The Method of Quasireversibility: Applications to Partial Differential Equation*s, Elsevier, New York, 1969.
122. M.M. Lavrentiev, *Some Improperly Posed Problems of Mathematical Physics*, Springer, New York, 1967.
123. M.M. Lavrentiev, K.G. Reznitckaya and V.G. Yakhno, *One-Dimensional Inverse Problems of Mathematical Physics*, AMS, Providence, RI, 1986
124. M.M. Lavrentiev, V.G. Romanov and S.P. Shishatskii, *Ill-Posed Problems of Mathematical Physics and Analysis*, AMS, Providence, R.I., 1986.
125. J. Li, J. Xie and J. Zou, An adaptive finite element reconstruction of distributed fluxes, *Inverse Problems*, 27, 075009, 2011.
126. L. Nguyen, D. Wong, M. Ressler, F. Koenig, B. Stanton, G. Smith, J. Sichina and K. Kappra, Obstacle avolidance and concealed target detection using the Army Research Lab ultra-wideband synchronous impulse Reconstruction (UWB SIRE) forward imaging radar, *Proc. SPIE*, 6553, pages 65530H (1)-65530H (8), 2007.
127. V.P. Mikhailov, *Partial Differential Equations,* imprint, Moscow: Mir Publishers, 1978.
128. M. Minoux, *Mathematical Programming: Theory and Algorithms*, Wiley and Sons, Chichester, 1986.
129. J. Mueller and S. Siltanen. Direct reconstructions of conductivities from boundary measurements, *SIAM J. Sci. Comp.*, 24, 1232–1266, 2003.
130. R.G. Novikov, Multidimensional inverse spectral problem for the equation $-\Delta\psi + (v(x) - Eu(x))\psi = 0$ *Functional Analysis and Its Applications,* 22**,** 11–22, 1988.
131. R.G. Novikov, The inverse scattering problem on a fixed energy level for the two-dimensional Schrödinger operator, *J. Func. Anal. and Its Applications,* 103**,** 409–463, 1992.
132. R.G. Novikov, The ∂—bar approach to approximate inverse scattering at fixed energy in three dimensions, *Int. Math. Res. Reports*, 6, 287–349, 2005.
133. J.R. Reitz, F.J. Milford, and R.W. Christy, *Foundations of Electromagnetic Theory*, Reading, Mass.: Addison-Wesley, 1980.
134. J. Nocedal, Updating quasi-Newton matrices with limited storage, *Mathematics of Comp.*, V.35, N.151, 773–782, 1991.
135. N. Pantong, J. Su, H. Shan, M.V. Klibanov and H. Liu, A globally accelerated reconstruction algorithm for diffusion tomography with continuous-wave source in arbitrary convex shape domain, *J. of the Optical Society of America, A*, 26, 456–472, 2009.
136. O. Poisson, Uniqueness and Hölder stability of discontinuous diffusion coefficients in three related inverse problems for the heat equation, *Inverse Problems*, 24, 025012, 2008.
137. B.T. Polyak, *Introduction to Optimization (Translations Series in Mathematics and Engineering)*, New York: Optimization Software, Publications Division, 1987
138. A.I. Prilepko, D.G. Orlovskii and I.A. Vasin, *Methods For Solving Inverse Problems In Mathematical Physics*, Marcel Dekker, Inc., New York, 2000.
139. R. Ramlau, A steepest descent algorithm for the global minimization of the Tikhonov functional, *Inverse Problems*, 18, 381–405, 2002.

140. R. Ramlau, TIGRA- an iterative algorithm for regularizing nonlinear ill-posed problems, *Inverse Problems*, 19, 433–465, 2003.
141. S.I. Repin, *A Posteriori Estimates for Partial Differential Equations*, de Gruyter, Berlin, 2008.
142. K.G. Reznitckaya, Connection between solutions of different types of Cauchy problems and inverse problems, in *Mathematical Problems of Geophysics*, issue 5, part 1, 55–62, 1974, published by Computing Center of the Siberian Branch of the USSR Academy of Science, Novosibirsk (in Russian).
143. V.G. Romanov, *Integral Geometry and Inverse Problems for Hyperbolic Equations*, Springer-Verlag, Berlin, 1974.
144. V.G. Romanov 1986 *Inverse Problems of Mathematical Physics* (Utrecht, The Netherlands: VNU).
145. V.G. Romanov, On smoothness of a fundamental solution to a second order hyperbolic equation, *Siberian Math. J.,* 50, 700–705, 2009.
146. A.A. Samarskii, *The Theory of Difference Schemes*, Marcel Dekker, New York, 2001.
147. H. Shan, M.V. Klibanov, J. Su, N. Pantong and H. Liu, A globally accelerated numerical method for optical tomography with continuous wave source, *J. Inverse and Ill-Posed Problems,* 16, 765–792, 2008.
148. Software package Wave Equations Solutions at http://www.waves24.com/.
149. J. Su, H. Shan, H. Liu and M.V. Klibanov, Reconstruction method from a multiplesite continuous-wave source for three-dimensional optical tomography, *J. Optical Society of America A,* 23, 2388–2395, 2006.
150. J. Su, M. V. Klibanov, Y. Liu, Z. Lin, N. Pantong, and H. Liu, An inverse elliptic problem of medical optics with experimental data, available on-line at http://www.ma.utexas.edu/mp_arc/.
151. Tables of dielectric constants at http://www.asiinstr.com/technical/Dielectric%20Constants.htm.
152. A. N. Tikhonov, On the stability of inverse problems, *Doklady of the USSR Academy of Science*, 39, 195–198, 1943 (in Russian).
153. A. N. Tikhonov and V. Y. Arsenin. *Solutions of Ill-Posed Problems,* Winston and Sons, Washington, DC, 1977.
154. A.N. Tikhonov, A.V. Goncharsky, V.V. Stepanov and A.G. Yagola, *Numerical Methods for the Solution of Ill-Posed Problems*, London: Kluwer, London, 1995.
155. J. Su, H. Shan, H. Liu and M. V. Klibanov, Reconstruction method from a multiple-site continuous-wave source for three-dimensional optical tomography, *J. Optical Society of America*, 23, 2388–2395, 2006.
156. B. J. Tromberg, O. Coquoz, H. B. Fishkin, T. Pham, E. R. Anderson, J. Bytler, M. Cahn, J. D. Gross, V. Venugopalan and D. Pham, Non-invasive measurements of breast tissue optical properties using frequency-domain photon migration, *Proc. Trans. R. Sosciety, London*, 352, 661–668, 1997.
157. J. Xin, M. V. Klibanov, Comparative studies of the globally convergent convexification algorithm with application to imaging of antipersonnel land mines, *Applicable Analysis*, 86, 1147–1176, 2007.
158. J. Xin and M. V. Klibanov, Numerical solution of an inverse problem of imaging of antipersonnel land mines by the globally convergent convexification algorithm, *SIAM J. Sci. Comp*., 30, 3170–3196, 2008.
159. J. Xin and M. V. Klibanov, High speed imaging of antipersonnel land mines by the convexification algorithm for a simplified mathematical model in two dimensions, *J. Inverse and Ill-Posed Problems*, 17, 187–207, 2009.
160. J. Xin, L. Beilina and M. V. Klibanov, Globally convergent numerical methods for coefficient inverse problems for imaging inhomogeneities, *IEEE J. Computing in Science and Engineering*, 12, 64–77, 2010.
161. M. Yamamoto, Carleman estimates for parabolic equations and applications, *Inverse Problems,* 25**,** 123013, 2009.

Index

L. Beilina and M.V. Klibanov, *Approximate Global Convergence and Adaptivity for Coefficient Inverse Problems*, DOI 10.1007/978-1-4419-7805-9,